The Dissertation Committee for Maedeh Faraji Certifies that this is the approved version of the following dissertation:

Evaluating Photochemical Mechanisms for Use in Southeast Texas

Committee:

David T. Allen, Supervisor

Richard Corsi

Howard Liljestrand

Elena McDonald-Buller

Jeffrey Siegel

Evaluating Photochemical Mechanisms for Use in Southeast Texas

by

Maedeh Faraji, B.Sc.; M.S.E.

Dissertation

Presented to the Faculty of the Graduate School of

The University of Texas at Austin

in Partial Fulfillment

of the Requirements

for the Degree of

Doctor of Philosophy

The University of Texas at Austin

December 2007

Dedication

This dissertation is dedicated to my mother, Marzieh.

Acknowledgments

I am grateful to my advisor, Professor David T. Allen, for making this dissertation possible through his continued support and careful guidance. Dr. Yosuke Kimura has been instrumental and no less than a dedicated teacher throughout my research career as a student. No words can sufficiently express the extent of my gratitude towards him. I thank Professor Richard Corsi, Dr. Elena McDonald-Buller, and Dr. Neil Crain for their encouragement and mentorship. I also respectfully thank Professor Liljestrand and Dr. Siegel for their contributions as instructors and committee members. Thanks to Professor Harvey Jeffries, Dr. Greg Yarwood, Dr. Gary Whitten, and Professor Bill Carter for their training and guidance. My thank also goes to Jan DeCabooter, Dori Eubank, MaryAnn Foran, Gwen Desilva, Terri Mulvey, and all the other wonderful staff at CEER for making the working environment a warm and joyful one. I am also indebted to Dave Sullivan, Alba Webb, Steve Orwick, and other CEER professional and technical staff for their unconditional support. Furthermore, thanks to my present and past colleagues at CEER for their generosity in sharing their skills and knowledge. Thanks to Mrs. Sanchez, Tim, and "Mickey" (may he rest in peace) for their warm late night company.

I express my deepest gratitude towards my family: my mother, Marzieh, my father, Hassan, my brother, Ehssan, and my dearest husband, Ali-Akbar. Their unconditional love, sacrifice, emotional, mental, and spiritual support makes my growth possible. I owe my personal and professional progress to their careful guidance, continued encouragement, and prayers.

I thank God for answering my prayers and for all His blessings. I hope to remain subservient to Him throughout my life and fulfill what He has decreed for me.

Evaluating Photochemical Mechanisms for Use in Southeast Texas

Publication No._____

Maedeh Faraji, Ph.D.

The University of Texas at Austin, 2007

Supervisor: David T. Allen

Gridded, regional photochemical models use simplified photochemical reaction mechanisms, and two commonly used mechanisms are the [California] Statewide Air Pollution Research Center (SAPRC) mechanism and the Carbon Bond (CB) mechanism. Versions of the mechanisms currently in use include SAPRC99 and the CB-IV version from 1996. For the modeling done of the summer of 2000 in southeast Texas, the SAPRC99 mechanism leads to concentrations of ozone that are 30-45 ppb higher than with CB-IV, and is more sensitive to reductions in NOx emissions. Differences between the mechanisms could have significant consequences for determining the levels of emission reductions that will be required to demonstrate attainment with the National Ambient Air Quality Standard (NAAQS) for ozone, with concentrations averaged over 8 hours. Therefore, various modeling tools, together with chamber experiments were used to diagnose the differences between the mechanisms. These differences are due to differences in both reaction rate parameters/stoichiometry and the condensation methods in the mechanisms. Major reasons for the differences are differences in aromatics and

free radicals chemistries, which lead to higher radical concentrations in the SAPRC formulation.

Table of Contents

List of Tables

List of Figures

Chapter 1: Introduction

1.1 Air Quality Chemical Mechanisms

Air quality chemical mechanisms are a component of regional air quality models which attempt to reproduce the major features of the complex chemical processes that occur in the atmosphere. Due to the large number of compounds emitted or formed in the troposphere and the large number of reactions of those compounds and their reactive products, chemical mechanisms include various types of parameterizations, approximations, and condensations. In the past, the predominant factor limiting the size and level of detail of chemical mechanisms has been their computational burden. However, with the emergence of powerful computers and capable and flexible software used to implement the chemical mechanisms, an additional factor restricting the level of complexity of chemical mechanisms is our understanding of the processes that must be represented. Thus, representations of urban tropospheric chemistry in regional photochemical models are evolving and mechanism developers must use different assumptions and extrapolation methods to accommodate additional reacting species and reaction pathways (National Research Council, 1999). Two of the approaches to mechanism development are manifest in the mechanism developed by Carter (1990) at the Statewide Air Pollution Research Center (SAPRC) and the Carbon Bond (CB) (Gery *et al.*, 1989) mechanism.

1.2 SAPRC and CB Chemical Mechanisms

Two of the most commonly employed chemical mechanisms currently used to describe urban atmospheric chemistry, and in particular, ozone formation and accumulation, are the SAPRC and CB mechanisms. The SAPRC mechanism has been

specifically designed for Volatile Organic Compound (VOC) reactivity assessment and has been employed to generate VOC reactivity scales used in regulatory applications (Carter, 1994). This mechanism uses the lumped molecule approach in condensing VOCs in which a generalized ("lumped") or surrogate species is used to represent similar organic compounds. For example, ARO1 is used as a surrogate species broadly representing mono-substituted aromatic compounds, and ARO2 is used to represent di-substituted aromatics in the chemical mechanism (Carter, 1990).

The CB mechanism is widely used in models of regional air quality, employed in regulatory applications. Unlike the SAPRC mechanism, the CB mechanism uses both lumped molecule and lumped structure techniques to condense the reactions of individual VOCs. In the lumped structure technique, organic compounds are grouped according to bond type. For example, most single-bonded carbon atoms are represented using a one carbon atom alkane surrogate, denoted PAR, regardless of the molecule in which they appear and most carbon-carbon double bonds are represented using a two carbon atom surrogate, OLE. Therefore, propene, for example, which contains one alkane group and one terminal carbon-carbon double bond group, is represented as one PAR and one OLE in the mechanism. For other types of species, the CB mechanism uses a lumped molecule approach, like that of SAPRC. For example, just as in SAPRC, a surrogate species (TOL) is used in the CB mechanism to broadly represent mono-substituted aromatic compounds and XYL is used to represent di-substituted aromatics in the chemical mechanism (Gery *et al.*, 1989).

Both SAPRC and CB have been evaluated against results of a large number of chamber experiments and are reasonably successful in predicting ozone formation from complex mixtures in a "typical" urban atmosphere (Carter 1990; Gery *et al.*, 1989). Specifically, the SAPRC mechanism has been evaluated against environmental chamber

experiments conducted at the University of California at Riverside (UCR), and the CB mechanism has been evaluated against environmental chamber experiments conducted at the University of North Carolina at Chapel Hill (UNC). The SAPRC mechanism contains more than three times the number of organic species than the current version of the CB mechanism, but the inorganic chemistry is similar for the two mechanisms. Both mechanisms are updated periodically to incorporate new experimental findings. Therefore, more than one version exists for the SAPRC and CB mechanisms. A brief history of the evolution of the mechanisms is provided in the next chapter.

1.3 COMPARISONS OF SAPRC AND CB UNDER DIFFERENT ATMOSPHERIC CONDITIONS

The atmospheric conditions under which the SAPRC and CB mechanisms have been developed are for a "typical" urban atmosphere. Therefore, not all the approximations and condensations incorporated these chemical mechanisms may be appropriate for the atmospheric conditions of the particular urban environment for which the mechanism is implemented. Furthermore, the environmental chamber experiments used to develop these mechanisms have systemic differences. For example, the mechanisms use different sets of reactions to characterize the chamber wall effects. Several studies have compared the performance of the SAPRC and CB mechanisms in air quality simulations under different atmospheric conditions. While photochemical mechanisms track the formation and reaction of a variety of chemical species, much of the focus in mechanism comparisons and evaluations is on ozone concentrations. Findings from studies comparing the predictions of ozone concentrations generated in photochemical simulations by the SAPRC and CB mechanisms under different atmospheric conditions are presented in Chapter 2.

1.4 ATMOSPHERIC CONDITIONS UNIQUE TO HOUSTON-GALVESTON

Most of the Houston area exhibits concentrations of ozone precursors, ozone production rates, and other atmospheric conditions that are comparable to other urban areas. In the highly industrialized Houston Ship Channel region, however, distinctive chemistry is observed. The Houston Ship Channel region encompasses one of the largest petrochemical complexes in the world. In this region, elevated concentrations of reactive hydrocarbons are co-emitted with NOx from industrial facilities. This combination leads to substantial and rapid ozone production in a few hours to a single day relative to a slower accumulation of ozone over a period of an entire day to several days typically observed in other urban areas in the U.S.. In fact, this area is marked by some of the highest ozone mixing ratios routinely encountered in the U.S.. The rate of ozone production observed in this area is 2-5 times greater than other less industrialized cities and can exceed 100 ppb/hr (Kleinman *et al.*, 2002). Furthermore, ozone production can vary significantly over spatial scales smaller than other urban areas. Specifically, ozone concentrations may vary by 50 ppb or more over length scales as small as a few kilometers (Kleinman *et al.*, 2002; Ryerson *et al.*, 2003). The unique ozone formation chemistry of the Houston atmosphere, specifically in the Ship Channel region, places demands on chemical mechanisms not encountered in other regions.

1.5 MOTIVATION OF STUDY

A preliminary assessment of ozone concentrations predicted by the SAPRC99 and CB-IV mechanisms under Houston-Galveston conditions revealed a significant difference between the mechanisms. The comparisons were performed using the Comprehensive Air Quality Model with extensions (CAMx, ENVIRON, 2004), which is described in detail at the model web site (www.camx.com). As shown in Figure 1-1, the maximum difference in predicted ozone concentrations between SAPRC99 and CB-IV is nearly 45

ppb for an air pollution episode that occurred on August 30th, 2000. This finding is similar to that obtained by Byun (2002). The simulation employing SAPRC99 predicted an area-wide maximum ozone concentration of 155 ppb while CB-IV predicted a maximum ozone concentration of 124 ppb. Similar percentage differences in maximum ozone concentrations were observed for other days in the modeled episode. These differences are large relative to differences observed in other regions, as documented in Chapter 2.

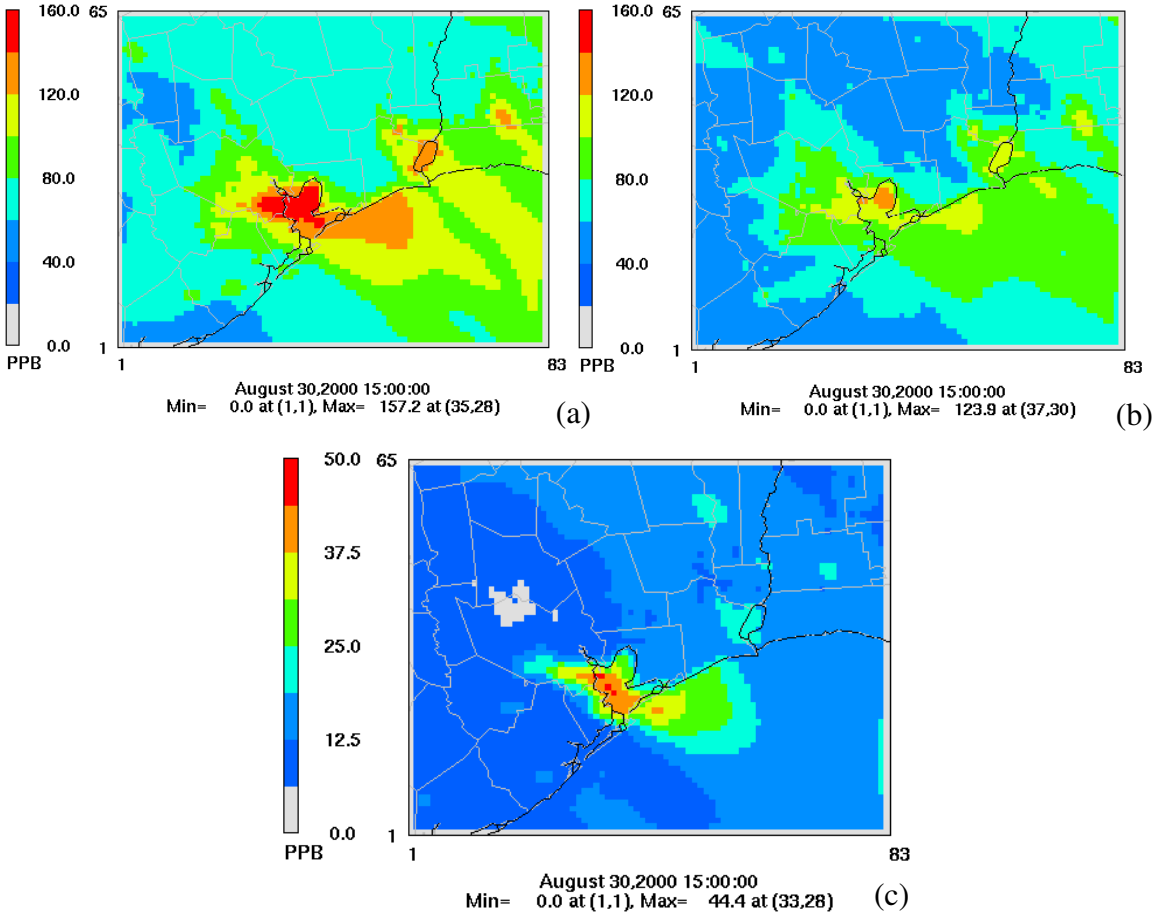

Figure 1-1 Predictions of domain-wide maximum ozone concentrations in CAMx on August 30, 2000, hour 15:00, in (a) SAPRC99, (b) CB-IV96, and (c) SAPRC99 minus CB-IV96.

While previous studies have identified and quantified the magnitude of these differences, the focus in this work will be to use a variety of tools to investigate the causes of the differences. The policy implications of these differences are discussed below.

1.6 POLICY IMPLICATIONS

The differences in O_3 concentrations predicted by the SAPRC and CB-IV mechanisms have significant policy implications. In Houston, significant NOx and VOC emission reductions have been proposed and under the proposed controls, SAPRC and CB-IV predict similar absolute ozone concentrations as illustrated in subsequent chapters. Since reducing predicted ozone concentrations to a target absolute level is how attainment is demonstrated for the National Ambient Air Quality Standard (NAAQS) for ozone, with concentrations averaged over 1-hour, the two mechanisms are largely equivalent in demonstrating attainment with the NAAQS for ozone, with one-hour averaged concentrations. However, when demonstrating attainment with the NAAQS for ozone with concentrations averaged over 8 hours, relative reductions in ozone predicted by the model are used. Houston is required to demonstrate attainment with both of these NAAQS for ozone. SAPRC predicts consistently larger relative reductions in ozone, in response to control strategies, than CB-IV. In particular, SAPRC is more sensitive to NOx emission reductions than CB-IV. The magnitude of the difference varies from day to day. For demonstrating attainment with the NAAQS for ozone, with concentrations averaged over 8 hours, these differences in NOx sensitivities may lead to different evaluations of proposed control strategies, depending on the mechanism chosen.

1.7 SCOPE AND OBJECTIVES OF STUDY

This work compares the SAPRC and CB mechanisms under conditions relevant to the Houston-Galveston area. The first objective of this work is to identify the differences between the SAPRC and CB mechanisms that cause the mechanisms to predict different ozone concentrations, under conditions relevant to the Houston-Galveston area. In this initial evaluation, three mechanisms are used: the 1999 version of SAPRC (SAPRC99), the 1996 version of the CB mechanism used by the Texas Commission on Environmental Quality (TCEQ) in its photochemical modeling (CB-IV96), and CB-IV with an extended inorganic chemistry (CB-IVxi). Three main hypotheses for causes of differences between the SAPRC99 and CB-IV96 mechanisms are investigated:

- Differences in aromatics chemistry.
- Differences in $OH+NO_2$ termination rates.
- Differences in free radical source terms.

Next, the ability of the mechanisms to replicate ozone concentrations in environmental chamber data is assessed. Again, three mechanisms are evaluated: SAPRC99, CB-IV96, and the newly developed CB mechanism (CB05). In addition to the hypotheses investigated for identifying causes of differences between the mechanisms, the effect of de-lumping is evaluated using environmental chamber data.

The overall objectives of the assessment are to provide guidance to the Texas Commission on Environmental Quality (TCEQ) in their selection of chemical mechanisms to be used in regional air quality modeling, and to suggest modifications for a next generation of mechanisms.

1.8 STRUCTURE OF THE DISSERTATION

Chapter 2 provides a brief overview of the mechanisms' features and summarizes the previous work on comparisons of the SAPRC and CB mechanisms documented in the

literature. The differences between the predictions of the mechanisms under Houston-Galveston conditions are presented in Chapter 3, followed by the underlying reasons for those differences. Chapter 4 describes the environmental chamber experiments and simulation software used in the analyses, and the approach that was used in evaluating the chamber experiments. Chapter 5 describes the effects of wall mechanisms used in modeling the chamber experiments. Chapters 5 and 6 describe experiments involving olefins and aromatics, respectively. Finally, Chapter 7 summarizes the findings and provides recommendations for future work.

1.9 REFERENCES

Byun, D. W. (2002, October). *A study of photochemical processes of the Houston-Galveston metropolitan airshed with EPA CMAQ 2002*. Paper presented at the Model-3 User's Workshop, EPA, Research Triangle Park, NC.

Carter, W. P. L. (1990). A detailed mechanism for the gas-phase atmospheric reactions of organic compounds. *Atmospheric Environment*, 24A, 481-518.

Carter, W. P. L. (1994). Development of ozone reactivity scales for Volatile Organic Compounds. *Journal of Air* and *Waste Management Association*, 44, 881-899.

ENVIRON International Corporation. (2004). *Users Guide to the Comprehensive Air Quality Model with Extensions (CAMx) version 4.03*. Available at http://www.camx.com.

Gery, M. W., Whitten, G. Z., and Killus, J. P. (1989). A photochemical kinetics mechanism for urban and regional scale computer modeling. *Journal of Geophysical Research*, 20, 12,925-12,956.

Kleinman, L. I., Daum, P. H., Imre D., Lee Y., Nunnermacker, L. J., and Springston, S. R. (2002). Ozone production and hydrocarbon reactivity in 5 urban areas: A cause of high ozone concentration in Houston, 2002. *Geophysical Research Letters*, 30 (12), 1639-1642.

National Research Council. (1999). *Ozone-forming potential of reformulated gasoline*. Washington, DC: National Academy Press.

Ryerson, T. R., Trainer, M., Angevine, W. M., Brock, C. A., Dissly, R. W., Fehsenfeld, F. C., Frost, G. J., Goldan, P. D., Holloway, J. S., Hubler, G., Jakoubek, R. O., Kuster, W. C., Neuman, J. A., D.K. Nicks Jr., D. K., Parrish, D. D., Roberts, J. M., and Sueper, D.T. (2003). Effect of petrochemical industrial emissions of reactive alkenes and NOx on tropospheric ozone formation in Houston, Texas. Journal of *Geophysical Research*, 108, 4249.

Chapter 2: Literature Review

The SAPRC and CB chemical mechanisms have been continuously revised and updated since their inception in 1990 and 1980, respectively, in accordance with new data and evaluations. In this chapter, the evolution of the SAPRC and CB chemical mechanisms is traced from when they were first developed to the latest versions of the mechanisms. The major versions of the mechanisms released and the revisions involved are outlined in detail. Following an overview of the different versions of the mechanisms, results from studies comparing the SAPRC and CB mechanisms with respect to ozone prediction in different urban areas is presented.

2.1 Evolution of the SAPRC Chemical Mechanism

The SAPRC mechanism, initially designated as SAPRC90, was designed by Carter (1990) at the University of California at Riverside (UCR). It was developed for use in ozone modeling and control strategy applications and to quantify the reactivities of VOCs with respect to ozone formation for the California Air Resources Board (CARB) (Carter, 1990). A list of reactions and rate constants for the SAPRC90 mechanisms, followed by the species descriptions are provided in Tables A.1.1 and A.1.2 of Appendix A, respectively. In the SAPRC mechanism, a base mechanism represents the reactions of inorganic species, the common organic products, and the intermediate radicals leading to those products. VOCs that can be represented separately can be added to the base mechanism as either explicit reactions for individual species or as lumped model species. The lumped model species represent a mixture of "representative" VOCs whose parameters are derived by averaging rate constants and product yield parameters. Two condensation methods can be employed in the SAPRC mechanism to represent VOCs: variable lumped parameter and fixed parameter. The variable lumped parameter approach

is discussed in Carter (2000). In this work, the SAPRC mechanism employing the fixed parameter approach was primarily used. In this approach, the parameters for the lumped species are derived using a typical or representative ambient mixture or emissions profile and then used in all subsequent model applications. This approach is particularly useful if the emissions composition for a model application is uncertain (Carter, 2000). In some analyses performed in this study, selected compounds were un-lumped, and represented explicitly, effectively creating a new lumping scheme. These will be described in the Chapters in which the analyses are presented.

The SAPRC90 mechanism has been updated several times to incorporate new information concerning the reactions of individual VOCs and their impacts on ozone formation. The major documented updates are the SAPRC93, SAPRC97, SAPRC99, and SAPRC07 versions (Carter, 2000; Carter, 2007). The updates and modifications included in the SAPRC93 mechanism are indicated below (Carter, 1995):

- Updated formaldehyde absorption cross-sections.
- Updated kinetics for reactions involved in the formation and decomposition of PAN.
- Modified the reaction of OH radicals with acetone to form acetyl peroxy radicals and formaldehyde after one NO-NO_2 conversion instead of forming 80% methyl gyloxal.
- Updated reactions of ozone with alkenes.
- Modified the reaction of NO with peroxy radical formed in the reaction of OH radicals with isobutene to form the corresponding hydroxyalkyl nitrate 10% of the time.
- Modified representations of isobutane and isoctane to improve model simulations of their reactivities.

These changes are discussed in detail in Carter (1995).

In 1997, an update of the SAPRC93 mechanism, SAPRC97, was finalized. The major revisions incorporated in this version of the mechanism concern updates of the reactions of aromatics based on newer chamber data. The SAPRC97 mechanism accounts for differences observed in reactivities of aromatic isomers that were previously assumed to have similar mechanisms. For example, rather than assuming that ethylbenzene reacts like toluene as in the previous mechanism, the reaction parameters in the oxidation of ethylbenzene were updated to account for the much lower yields of photoreactive ring fragmentation products relative to that of toluene. Likewise, the yields of these products in the oxidation of p-xylene and 1,2,4-trimethylbenzene were adjusted to be lower than that of their isomers (Carter *et al.*, 1997).

Later, CARB contracted Carter to update SAPRC90 to calculate a reactivity scale appropriate for CARB's proposed reactivity-based consumer products regulation. This led to the emergence of SAPRC99, which included updated reactions and rate constants for most of the inorganic species and common organic products. Furthermore, it incorporated important new information concerning mechanisms and reactivities of many VOCs, particularly oxygenated VOCs not previously studied. The most important advancement in the SAPRC99 mechanism, however, was its use of a new mechanism generation and estimation software. This software allowed for the assignment or adjustment of rate constants or branching ratios for the atmospheric reactions of many classes of VOCs in the presence of NOx in cases where data are available or adjustments are necessary for consistency with experimental data. The capabilities of this software were extended from alkanes to include alkenes and many classes of oxygenates including alcohols, ethers, glycols, esters, aldehydes, ketones, glycol ethers, and carbonates. Therefore, it permitted estimation of detailed mechanisms for a greater array of

compounds than otherwise would be possible. The specific updates to the SAPRC99 mechanism since the development of SAPRC90 are as follows (Carter, 2000):

- Reduced OH + NO_2 rate constant by 30%.
- Represented methyl peroxy and acetyl peroxy radical model species explicitly.
- Lumped model species used to predict formation of low-reactivity C1-C3 organic nitrates in the reactions of peroxy radicals with NO, with model species used to predict formation of higher nitrates in these reactions.
- Lumped the PAN analogue from glyoxal, GPAN, with other PAN analogues.
- Included isoprene photoxidation products used in the "four-product" condensed isoprene mechanism of Carter (1996).
- Represented methacrolein, methyl vinyl ketone, lumped C5 unsaturated aldehyde products (ISOPROD), and methacrolein PAN analogue (MPAN) explicitly.

Carter (2000) provides a comprehensive documentation of the updates incorporated in the SAPRC99 mechanism. A list of reactions in the base mechanism of SAPRC99 and in the fixed parameter lumped mechanism of SAPRC99, followed by the species descriptions are provided in Tables A.1.3-A.1.5 of Appendix A. In this thesis, we use the SAPRC99 fixed parameter lumped mechanism.

Finally, in 2007, Carter (2007) updated the SAPRC99 mechanism. The latest SAPRC mechanism, designated SAPRC07, incorporates the following updates:

- Updated rate constants.
    - Increased OH+NO_2 rate constant by ~ 18%.
    - Photolysis rates for selected aromatic and isoprene oxidation products increased by ~ 40%.
- Reformulated the mechanisms for the aromatic ring fragmentation reactions to be more consistent with explicit mechanisms.

- Added the representation for chlorine chemistry as an optional capability.
- Enhanced the mechanism generation system which is used to generate fully explicit mechanisms for most of the non-aromatic VOCs.
    - Updated rate constants for primary reactions of individual VOCs with OH, O_3, NO_3, and O^3P.
    - Added capability of estimating and generating mechanisms for reactions of VOCs with chlorine atoms.
    - Expanded types of compounds and radicals whose reactions could be generated to include species with more than one ring (e.g., terpenes), species with more than one double bond, alkynes, some aromatics, and unsaturated aromatic ring opening products.
- Improved capability for adaptation to Secondary Organic Aerosol predictions.
    - Implemented an alternative chemical operator approach for peroxy radicals reactions that involves adding much smaller number of species and reactions.
    - Represented hydroperoxide formation more explicitly.
    - Represented separate representation of organic nitrates formed in peroxy+NO reactions based on reactivity and volatility.
- Added or improved mechanisms for many types of VOCs.
    - Increased number of types of VOCs with distinct mechanisms, especially for alkanes, alkenes, and oxygenates found in emission inventories, by 23%.
    - Corrected a factor of 10 error in the rate constant for 3-methyoxy-1-butanol.

The SAPRC07 mechanisms was evaluated against all the environmental chamber experiments used for SAPRC99, plus the results of more recent chamber experiments at UCR as well as UNC experiments. The results of these evaluations are detailed in Carter (2007). A list of reactions and rate parameters in the base SAPRC07 mechanism and for

the lumped model species in the fixed parameter version of SAPRC07, followed by the species descriptions are provided in Tables A.1.6-A.1.8 of Appendix A. This version of the SAPRC mechanism was not included in this study because it was not finalized at the time this study was initiated, and had not yet been implemented in regional models.

2.2 EVOLUTION OF THE CB CHEMICAL MECHANISM

The CB mechanism was released in a series of Environmental Protection Agency (EPA) reports by System Applications International, Inc. (SAI) throughout the 1980s. It was originally intended to simulate the formation of urban ozone from NOx and VOCs. The mechanism contains a semi-explicit set of inorganic reactions and an organic representation based on both explicit and structurally lumped species. Throughout the 1980's, the CB mechanisms were revised and updated by SAI, with the CBM-X version of the mechanism (Table 2-1) containing a semi-explicit representation of both the inorganic and organic chemistry. The potential use of the mechanisms in air quality models for applications beyond predicting ozone concentrations prompted revisions to CBM-X. The large number of reactions and species in CBM-X was impractical for use in large air quality models at the time it was developed. Therefore, the CBM-IV mechanism was created with the objective of providing a highly condensed representation of the chemistry while maintaining a reasonable level of performance in modeling experimental data relative to more explicit CB mechanisms (Adelman, 1999). The predominant modeling techniques that were employed in the condensation of the CBM-X mechanism are as follows (Gery *et al.*, 1989):

- Eliminated reactions and products insignificant for urban scale modeling.
- Created the universal peroxy operators, XO_2 and XO_2N, used to represent the majority of the organic peroxy radicals in their reactions with NO to yield alkoxy radicals and organic nitrates, respectively.

- Reduced the number of species using mathematic and algebraic manipulations.
- Lumped secondary reaction products.

The versions of the CB mechanisms released in the 1980s and the major revisions are listed in Table 2-1.

Table 2-1. Evolution of CB into CBM-IV: Versions, release years, and major revisions (Adelman, 1999).

Mechanism	Date	Revisions
CBM-I	1980	condensed explicit mechanisms from the period; no Arrehnius rates; 32 reactions.
CBM-II	1980	updated rate constants; represented Craigee intermediates from O_3-OLE reactions; represented addition products of OH to double bonds with surrogates; added new carbonyl chemistry; treated alkyl radicals as long-chain PAR's; added explicit ETH for ethylene; treated internal OLE's as carbonyls; added new aromatics chemistry; 65 reactions.
CBM-III	1981	added aromatic oxidation mechanisms; updated inorganic rate constants; added ring opening and aromatic products species; 74 reactions.
CBM-X	1985	implemented semi-explicit representation of inorganic and organic chemistry; 146 reactions.
CBM-XR	1985	modified CBM-X to be regional; added isoprene reaction subset.
CBM-RR	1985	lumped M and O_2 into rate constants; eliminated stable products; combined parallel reactions; eliminated oxidation intermediates; added peroxy radical and nitrate operator.
CBM-IV	1986	removed Craigee intermediate species; reduced O_3 chemistry through steady-state assumptions; used XO_2 and C_2O_3 to represent range of radical chemistry; condensed PAR chemistry; 70 reactions.

An updated version of CBM-X containing 170 reactions was released in 1988 and it was the direct predecessor of CB-IV. The revised CBM-X treated the reactions of four different classes of species (Gery *et al.*, 1989):

- Inorganic species represented explicitly.

- Organic species represented explicitly because of their unique chemistry or significance in the environment.
- Organic species represented by carbon-bond surrogates.
- Organic species represented by molecular surrogates.

The first version of CB-IV (CB-IV.1) was published by Atmospheric Research Associates (ARA) and SAI in 1989 (Gery *et al.*, 1989) for use in regulatory applications. It contains 81 reactions and 12 organic species. Throughout the 1990's, suggestions by different research groups led to changes that resulted in new versions of CB-IV, updating the science in the mechanism and tailoring it for specific applications. However, the 36 reaction, hybrid-explicit inorganic reaction set remains essentially the same up to the CB-IV.5 version of the mechanism (Table 2-2). The three major revisions that led to the different versions of the CB-IV mechanism are as follows (Adelman, 1999):

- Updated the peroxyacetyl nitrate (PAN) kinetics.
- Modified the radical-termination chemistry.
- Implemented a new isoprene reaction mechanism.

These revisions are included in the version of CB-IV released in 1996, which occurred when the Ozone Transport Assessment Group (OTAG) commenced modeling (Yarwood *et al*., 2005a). The 1996 version of CB-IV, referred to as the OTAG version of CB-IV, is the version of CB-IV used in this study and used by the Texas Commission on Environmental Quality (TCEQ) in its air quality planning activities. In this thesis, this version of the mechanism is termed CB-IV96. The list of reactions and rate constants for the 1996 version of CB-IV, followed by the species definitions, are provided in Tables A.2.1 and A.2.2 of Appendix A, respectively. The versions of CB-IV following its first version and the major revisions adopted are listed in Table 2-2.

Table 2-2. Different versions of CB-IV: Versions, release years, and major revisions. (Adelman, 1999).

Mechanism	Date	Revisions
CB-IV.1	1989	regulatory version of CB-IV (Gery *et al.*, 1989); 81 reactions.
CB-IV.2	1991	Modified PAN rates; added reaction for XO_2 termination by HO_2.
CB-IV.3	1992	modified XO_2N+NO rate and added XO_2N termination by HO_2, XO_2, and XO_2N; revised ethanol and methanol reactions and added MTBE; 85 reactions.
CB-IV.4	1996	added 1-product isoprene chemistry from Carter (1996); updated HCHO photolysis rates; added SOx chemistry; 94 reactions.
CB-IV.5	1999	updated kinetics and photolysis rates; added methane for chamber simulations; corrected aromatic photolysis rates.

Adelman (1999) provides a formal documentation of the various versions of the mechanisms as of 1999 and presents empirical verification for the major revisions.

In 2002, the research group at the University of North Carolina at Chapel Hill (UNC), led by Jeffries updated the CB-IV mechanism by retaining the overall structure of CB-IV but updating rate constants including the OH + NO_2 rate constant and product yields based on updated data (Jeffries *et al.*, 2002). The list of reactions and rate constants for the CB2002 mechanism is provided in Table A.2.3 in Appendix A. The main modifications incorporated in CB2002 are as follows (Yarwood *et al.*, 2005a):

- Updated rate constants for many inorganic reactions including pressure dependencies for some reactions.

- Added new inorganic reactions for NO_3 with OH, HO_2, and NO_2 and O_3 + O(3P).
- Added new HONO photolysis reaction for NO_2 + H.
- Modified rate expression for N_2O_5 + water.
- Reduced rate constants for radical-radical termination reactions (i.e., XO_2 and HO_2).
- Modified reaction rates for all olefins: ETH, OLE and ISOP.
- Added new reaction products for ETH and OLE.

The effects of these changes are discussed in detail by Yarwood *et al.* (2005a).

In 2005, Yarwood *et al*. (2005a), upon review of the CB-IV mechanism, added seventeen inorganic reactions in order to describe additional relevant aspects of tropospheric chemistry. Since the reactions mostly involved the inorganic reaction set, the modification was referred to as the extended inorganic chemistry (CB-IVxi). The reactions added in the CB-IVxi mechanism, followed by the rate constants for those reactions are included in Tables A.2.4 and A.2.5 of Appendix A, respectively. The extended inorganic reactions are as follows:

- Reactions of molecular hydrogen particularly relevant to very dry conditions in the upper troposphere.
- Odd-oxygen reactions potentially important for pristine conditions such as the upper troposphere.
- Additional NO_3 radical reactions relevant to nighttime chemistry.
- NOx recycling reactions to better represent the fate of NOx over timescales of multiple days.

The latest version of the CB mechanism, CB05, was developed in 2005. The core CB05 mechanism consists of 51 species and 156 reactions. The list of reactions in the CB05 core mechanism followed by the species descriptions are provided in Tables A.2.6

and A.2.7 of Appendix A, respectively. The updates in CB05 relative to earlier CB-IV mechanisms are as follows (Yarwood *et al.*, 2005b):

- Updated rate constants based on recent (2003 – 2005) IUPAC and NASA evaluations.
- Included an extended inorganic reaction set for urban to remote tropospheric conditions.
- Added NOx recycling reactions to represent the fate of NOx over multiple days.
- Represented the organic chemistry for methane and ethane explicitly.
- Represented methylperoxy radical, methyl hydroperoxide, and formic acid explicitly.
- Lumped higher organic peroxides, organic acids and peracids.
- Represented internal olefin (R-HC=CH-R) species by IOLE.
- Represented higher aldehyde species represented by ALDX, making ALD2 explicitly acetaldehyde.
- Represented higher peroxyacyl nitrate species from ALDX by PANX.
- Lumped terpene species into TERP.
- Added an optional mechanism extension for reactive chlorine chemistry.
- Added an optional mechanism extension with explicit reactions for air-toxics.

Luecken and Sarwar (2006) have reported on the effects of using the CB05 mechanism versus CB-IV on model predictions in regional photochemical modeling.

2.3 PREVIOUS STUDIES ON COMPARISONS OF THE SAPRC AND CB CHEMICAL MECHANISMS

A number of studies have compared different versions of the SAPRC and CB mechanisms within air quality models for various atmospheric conditions. Much of the focus in mechanism comparison and evaluations is on ozone concentrations. An overview of these studies is presented in this section.

Dodge (1989) conducted approximately 400 simulations in a one-cell moving box model using a condensed version of the SAPRC mechanism and the CB-IV mechanism over a range of initial conditions for a number of scenarios representative of urban and rural environments. The goal was to determine the degree to which the mechanisms predict comparable ozone predictions among other oxidants. Discrepancies occurred for predictions of the dicarbonyl species, including glyoxal, methylglyoxal, and unsaturated carbonyls, produced during oxidation of aromatic hydrocarbons. For base case Philadephia simulations with a VOC/NOx ratio of 9:1 ([VOC] = 0.54 and [NOx] = 0.06), the maximum concentrations of dicarbonyls as predicted by the CB-IV and SAPRC mechanisms were 0.7 ppb and 1.3 ppb, respectively. Also, the maximum concentration of cresols in CB-IV was 0.6 ppb relative to a concentration of 0.3 ppb in SAPRC. Differences were also noted for higher molecular weight aldehydes, with CB-IV predicting a maximum concentration of 5.4 ppm relative to a maximum concentration of 3.3 ppm with SAPRC. The maximum concentration of O_3 in this basecase simulation as predicted by SAPRC and CB-IV were 179 and 178 ppb, respectively. However, it was shown that the agreement among the SAPRC and CB-IV mechanisms is very sensitive to the VOC/NOx ratio of the mixture being simulated. At high NOx concentrations, SAPRC predicted O_3 concentrations that were as much as 14 ppb higher than that of CB-IV. Also, at high VOC/NOx ratios, due to differences in the treatment of organic peroxy radicals, SAPRC predicted H_2O_2 concentrations that were as much as 4 ppb higher than that of CB-IV. Furthermore, at low VOC/NOx ratios, CB-IV predicted HNO_3 that were nearly 3 ppb lower than that of SAPRC. Also, it was found that predictions were sensitive to the composition of the initial VOC mixture. In an organic mixture comprised of aromatics, disagreements between SAPRC and CB-IV were greater than in mixtures with no aromatics. These differences were largest at high VOC/NOx ratios, with SAPRC

predicting as much as 24 ppb more ozone than CB-IV. Finally, it was found that predictions were also sensitive to the temperature. Difference in the representation of PAN chemistry which is important for ozone formation at low temperatures caused an increase in PAN formation in CB-IV, inhibiting ozone formation in CB-IV relative to SAPRC at low temperatures by as much as 27 ppb.

Jeffries and Tonnesen (1994) compared the SAPRC90 and CB-IV mechanisms in a Lagrangian model for a Chicago scenario. While the two mechanisms were reported to exhibit similar ozone maxima and reactivity, there were differences for high VOC/NOx ratios: SAPRC90 exhibited a higher reactivity and produced a higher ozone maximum relative to CB-IV. For example, at an initial VOC mixing ratio of 767 ppb and a NOx mixing ratio of 40 ppb, the ozone concentration in SAPRC90 was 142.4 ppb compared to 131.7 ppb in CB-IV while the Ox production corresponding to total reactivity was 254.7 ppb in SAPRC90 compared to 235.2 ppb in CB-IV.

In a study by Yarwood et al. (2003), 1-hr averaged ozone concentrations, predicted using SAPRC99 and CB-IV in the Comprehensive Air Quality Model with extensions (CAMx), were compared for the Los Angeles (LA) area during the Southern California Ozone Study episode, August 3-7, 1997. The ozone concentrations predicted by SAPRC99 were higher than CB-IV throughout the modeling domain. For example, the predicted peak ozone concentrations with CB-IV and SAPRC99 on one day of the episode were 176 ppb and 208 ppb, respectively. On another day of the episode, CB-IV and SAPRC99 predicted peak ozone concentrations of 159 and 188 ppb, respectively. This episode had relatively high NOx emissions and exhibited a “weekend effect” where changing the timing and lowering the magnitude of NOx emissions led to increased peak ozone concentrations.

Also recently, Byun (2002) compared the SAPRC99 and CB-IV mechanisms in EPA's Community Multiscale Air Quality (CMAQ) model for the Houston-Galveston area during the Texas Air Quality Study (TexAQS) 2000 episode, August 23-September 1, 2000. The CMAQ simulations with SAPRC99 resulted in higher daily maximum 1-hr averaged ozone concentrations than CB-IV throughout the modeling episode. The comparisons showed differences of up to 46 ppb between the mechanisms for the heavily industrialized Ship Channel area, which contains high emissions of olefins from the petrochemical industries. The CMAQ simulations indicated that the differences between the ozone predictions of the mechanisms increase with increasing ozone concentration. Furthermore, the calculations of ozone production efficiency were higher with SAPRC99 than CB-IV.

Recently, Luecken *et al.* (2006) compared the predictions of the CB-IV, CB05, and SAPRC99 chemical mechanisms in the CMAQ for a 36-km resolution of the continental U.S. and a 12-km resolution of Eastern U.S. An analysis of the 8-hour daily ozone concentrations averaged over the month of July, 2001, showed that the ozone concentration and distribution is different between the three mechanisms. Over the entire continental U.S. region, SAPRC99 predicted the highest concentrations of ozone while CB-IV predicted the lowest concentrations. The largest differences in the July monthly average of 8-hour maximum ozone concentrations between SAPRC and CB-IV occurred in the central-southern part of the U.S. and reached a maximum of 10 ppb in the continental U.S. domain (36 km grid resolution). CB-IV predicted monthly average concentrations of hydrogen peroxide that were significantly higher than CB05 and SAPRC99: CB-IV predicted a maximum of 1.6 ppb, CB05 predicted a maximum of 1.2 ppb, and SAPRC99 predicted a maximum of 0.8 ppb. Furthermore, significant differences in the monthly average concentrations and distributions of PAN were

observed between the three mechanisms: CB05 predicted the highest concentrations of PAN, followed by SAPRC99 and CB-IV. Additionally, sensitivity studies were conducted in the 12-km Eastern U.S. domain to assess differences in the responses of the mechanisms to emission changes. It was found that in some urban areas, particularly Chicago and Houston, there are differences between the mechanisms in their sensitivity to emission reductions. For a 50% NOx and 25% VOC reduction, the ratio of ozone in the reduction scenario divided by the ozone in the basecase as predicted by SAPRC was 0.045 higher than CB-IV in those urban areas.

2.4 SUMMARY

As outlined in this chapter, the SAPRC and CB mechanisms have continuously undergone modifications and updates since they were first developed. One of the ways in which shortcomings of mechanisms are realized is by their application in various regions which exhibit different atmospheric conditions. Chemical mechanisms are designed to represent the ozone formation chemistry in "typical" urban settings. The atmospheric conditions in a particular region, however, may exhibit chemistry not previously encountered and therefore not considered in the formulation of the mechanisms. Furthermore, the availability of observational data is a limiting factor in designing mechanisms suitable for particular atmospheric conditions. As noted above, in studies comparing the performances of the SAPRC and CB mechanisms in different scenarios, SAPRC generally results in higher ozone concentrations relative to CB. Specifically, when the mechanisms are applied to regions characteristic of the highest annual ozone mixing ratios in the nation, namely Houston-Galveston and LA, the differences in ozone predictions between the mechanisms are reported to be as high as 30 ppb and 45 ppb in those regions, respectively. Similarly, in this study, comparisons of the SAPRC and CB mechanisms with applications in the highly industrialized Houston-Galveston region

results in differences in ozone predictions of up to 45 ppb. Due to the inconsistencies in predictions between the mechanisms, this study aims to identify the shortcomings in either or both of the mechanisms in representing the ozone formation chemistry in the Houston-Galveston region. This goal is executed by testing the mechanisms using various modeling tools as well as evaluating the mechanisms' ability to simulate environmental chamber data.

In Chapter 3, results of comparing the predictions of the SAPRC and CB mechanisms using different modeling tools under the Houston-Galveston conditions will be presented. Additionally, hypotheses for the underlying causes of those differences will be discussed.

2.5 REFERENCES

Adelman, Z. E. (1999). A *reevaluation of the carbon bond-IV photochemical mechan*ism. Master's Thesis, Department of Environmental Engineering, University of North Carolina at Chapel-Hill, NC.

Byun, D. W. (2002, October). *A study of photochemical processes of the Houston-Galveston metropolitan airshed with EPA CMAQ 2002*. Paper presented at the Model-3 User's Workshop, EPA, Research Triangle Park, NC.

Carter, W. P. L. (1990). A detailed mechanism for the gas-phase atmospheric reactions of organic compounds. Atmospheric Environment, 24A, 481-518.

Carter, W. P. L. (1995). Computer modeling of environmental chamber measurements of maximum incremental reactivities of Volatile Organic Compounds. *Atmospheric Environment*, 29, 2513-2517.

Carter, W. P. L. (1996). Condensed atmospheric photooxidation mechanism for isoprene. *Atmospheric Environment*, 30, 4275-4290.

Carter, W. P. L. (2007, May). *Documentation of the SAPRC-07 chemical mechanism and updated ozone reactivity scales.* Draft Final Report to the California Air Resources Board, Sacramento, CA.

Carter, W. P. L. (2000). *Documentation of the SAPRC-99 chemical mechanism for VOC reactivity assessment*. Air Pollution Research Center and College of Engineering, Center for Environmental Research and Technology, University of California at Riverside, CA.

Carter, W. P. L., Luo, D., and Malkina, I. L. (1997, November). *Environmental chamber studies for development of an updated photochemical mechanism for VOC reactivity assessment*. Report to the California Air Resources Board, Contract 92-345, Coordinating Research Council Project M-9, and National Renewable Energy Laboratory Contract ZF-2-12252-07.

Dodge, M. (1989). A comparison of three photochemical oxidant mechanisms. *Journal of Geophysical Research*, 95(D4), 5121–5136.

Gery, M. W., Whitten, G. Z., and Killus, J. P. (1989). A photochemical kinetics mechanism for urban and regional scale computer modeling. Journal of Geophysical Research, 20, 12,925-12,956.

Jeffries, H. E. and Tonnesen, S. (1994). A comparison of two photochemical reaction mechanisms using mass balance and process analysis. *Atmospheric Environment*, 28, 2991-3003.

Jeffries, H.J., Voicu, I., and Sexton, K. (2002, December). *Experimental Tests of Reactivity and Re-Evaluation of the Carbon Bond Four Photochemical Reaction Mechanism*. Report to the U.S. Environmental Protection Agency, Process Modeling Research Branch, Office of Research and Development, Research Triangle Park, NC.

Luecken, D., Phillips, S., Jang, C., and Possiel, N. (2006, December). *Effects of using the CB05 vs. SAPRC99 vs. CB4 chemical mechanisms on model predictions*. Presented at the International Conference on Chemical Mechanisms, The University of California at Davis, CA.

Luecken, D. and Sarwar, G. (2006). *Effects of using the CB05 versus the CB4 chemical mechanism on model predictions*. U.S. Environmental Protection Agency, Research Triangle Park, NC.

TexAQSI. *The Texas Air Quality Study 2000*. The University of Texas at Austin. Accessed 3 February 2002. <http://www.utexas.edu/research/ceer/texaqs/>.

Yarwood, G., Stoeckenius, T. E., Heiken, J. G., and Dunker, A. M. (2003). Modeling weekday/weekend ozone differences in the Los Angeles region for 1997. *Journal of Air and Waste Management Association*, 53, 864-875.

Yarwood, G. and Rao, S. (2005b). *Updates to the Carbon Bond chemical mechanism: CB05*. Report to the U.S Environmental Protection Agency, Research Triangle Park, NC.

Yarwood, G., Whitten, G. Z., and Rao, S. (2005a). *Updates to the Carbon Bond 4 photochemical mechanism*. ENVIRON International Corporation. Report to the Lake Michigan Air Directors Consortium.

Chapter 3: Comparison of the Carbon Bond and SAPRC photochemical mechanisms under conditions relevant to southeast Texas

While photochemical mechanisms track the formation and reaction of a variety of chemical species, much of the focus in mechanism comparisons and evaluations is on ozone concentrations. There have been a number of studies where different versions of the SAPRC and CB mechanisms have been compared in different air quality models and for various atmospheric conditions. These studies have been described in Chapter 2.

This chapter continues the comparisons of the SAPRC and CB-IV mechanisms by performing the comparisons under conditions relevant to the Houston-Galveston area. The atmospheric conditions unique to the Houston area, specifically the industrialized Houston Ship Channel region, have been described in Chapter 2.

3.2 METHODS

Two types of modeling tools were employed to investigate the sources of the differences in ozone predictions of the SAPRC and CB-IV mechanisms. These tools – the Comprehensive Air Quality Model with extensions and a box model – are briefly described here. More detailed descriptions are available in Faraji (2004).

3.2.1 CAMx Simulations

Model simulations were performed using the Comprehensive Air Quality Model, with extensions, version 4.03, referred to in this work as CAMx 4.03. CAMx is an U.S. EPA-approved Eulerian photochemical grid model that simulates emission, chemical transformation, horizontal advection and diffusion, vertical transport and diffusion, dry deposition, and wet deposition of species in the atmosphere. Although any comparable photochemical grid model could be used, CAMx was selected for this study because it is

currently being used by the State of Texas for attainment demonstrations in areas that have violated the National Ambient Air Quality Standards for ozone.

The State of Texas has developed an August 22 - September 6, 2000 photochemical modeling episode for evaluating its air quality management plans for southeast Texas. The modeling domain was a nested regional/urban scale 36-km/12-km/4-km grid, shown in Figure 3-1. Meteorological inputs required by the model were based on results from the Mesoscale Meteorological Model, version 5, MM5. The volatile organic compound (VOC) and NOx emission inventories used as input for the modeling episode were prepared by the Texas Commission on Environmental Quality (TCEQ) in accordance with U.S. EPA guidance. A MOBILE6-based inventory was developed for on-road mobile source emissions; emissions for non-road mobile and area sources were developed using emission factors and the U.S. EPA's NONROAD model, using local activity data when available. Biogenic emission inventories were estimated using the GLOBEIS emission model with locally developed landcover data. Point source emissions were developed through a special inventory survey and were also estimated based on ambient data collected in the source region. In this work, underestimation in the emission inventory for VOC point sources, reported by Ryerson, et al. (2003) and by Daum, et al. (2002), was addressed by adding a total of 100 tons per day of ethylene emissions at point sources that the TCEQ identified as having highly reactive hydrocarbon emissions. These emissions were added to the facilities in ratios based on their emissions of NOx, following a procedure established by the TCEQ for addressing the underestimation in the point source VOC inventory (Russell, 2003). Details of the meteorological modeling and the VOC and NOx emission inventory development are available at (http://www.tnrcc.state.tx.us/air/aqp/airquality_photomod.html#section4; http://www.tnrcc.state.tx.us/air/aqp/airquality_contracts.html#section3). Collectively,

the versions of the base case emission inventories used in this work are referred to as the Base 4a inventory (with 100 t/d of added ethylene emissions).

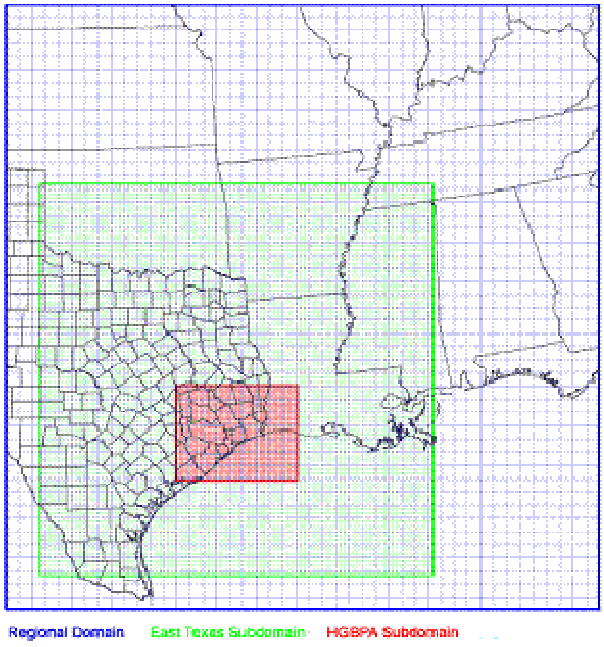

Figure 3-1. Modeling domain used in the study. The Regional, East Texas and Houston-Galveston-Beaumont-Port Arthur nested domains had 36, 12, 4 km resolution, respectively.

The emission inventories used in this work were originally processed by the TCEQ into CB-IV reactivity classes. In this work, the emission inventory information was processed as CB-IV reactivity classes, but was also processed into equivalent SAPRC99 reactivity classes. The inventories were developed by 1) speciating raw (total VOC) emissions to individual VOC compound emissions and 2) lumping VOC compounds to SAPRC99 or CB-IV model species. Raw emissions data were obtained from the Texas Commission on Environmental Quality (TCEQ) for all anthropogenic sources in the modeling domain and these emissions were speciated by applying speciation profiles (relative amounts of each compound in the total emissions) specific to

each emissions source. Speciation profiles for Texas point sources were derived directly from a detailed speciated inventory compiled by the TCEQ. (documentation and files downloaded from http://www.tnrcc.state.tx.us/air/aqp/airquality_photomod.html#ei3a.) Speciation profiles for Texas mobile sources were obtained from an emissions measurement study in a vehicular tunnel (McGaughey, 2004). Speciation profiles for all other anthropogenic sources were obtained from EPA's SPECIATE3.2 model (http://www.epa.gov/ttn).

Model simulations were performed using SAPRC99 (Carter, 2000) and the CB-IV mechanism. A version of the CB mechanism which corresponds to the Ozone Transport Assessment Group (OTAG) commencing modeling in 1996 is referred to as the OTAG version of CB-IV (Yarwood, 2005). This version of CB-IV is termed CB-IV96 in this study and is described by Adelman (1999) as CB-IV.4. CAMx 4.03 has the SAPRC99 and the OTAG version of CB-IV as built-in chemical mechanisms.

3.2.2 Box model simulations

In addition to CAMx modeling, a simple box model was also used to examine the sensitivities of predicted ozone concentrations to changes in the mechanisms. The box model assumed a well-mixed atmosphere, a fixed horizontal domain, and a vertical height that had the same temporal variability as the mixing height in Houston. This type of box model greatly simplifies the treatment of transport and diffusion, and thus cannot represent spatial variability. However, the box model has the advantage of being able to represent chemical mechanisms in great detail. In this work, this box model was used to assess the sensitivity of ozone predictions to changes in the chemical mechanisms and changes in the relative concentrations of various hydrocarbons. The goal of these box model analyses was to identify specific reaction pathways and classes of hydrocarbons that contribute to the discrepancies in the predicted magnitude of ozone formation

between the SAPRC99 and CB mechanisms. The conditions for the box model simulations were based on typical atmospheric conditions in Houston's industrial source region. Initial concentrations of volatile organic compounds (VOCs), NO, NO_2, O_3, peroxy acetyl nitrate (PAN), and its analogues were based on measurements made at LaPorte Texas during the Texas Air Quality Study (TexAQS), a large air quality field campaign conducted in Houston in August and September, 2000 (TexAQS I, 2002). The data on which the initial conditions are based are described by Faraji (2004). The initial conditions are summarized in Tables 3-1 and 3-2.

Emissions (VOC and NOx) were added continuously to the box model, based on typical emission inventory data for the industrial source region (Faraji, 2004). Emissions were assumed constant during the day, with the composition of VOC emissions assumed the same as the initial conditions. The mass of the daily emissions for both VOC and NOx were assumed to be three times the amount represented by the initial conditions (93.4 kg VOC in initial air, 280 kg per day of VOC emissions; 18.3 kg NOx in initial air, 54.9 kg per day of NOx emissions per 1 km^2 area). The ratio of NO to NO_2 in the emissions was assumed to be 9:1 on a molar basis. The SAPRC99 software was used for the box model simulations. The software suite implements chemical mechanisms and is designed so that the user can readily modify the mechanisms.

Table 3-1. Average morning concentrations at LaPorte airport site (August 25-September 2, 2000).

Species	Concentration (ppb)
O_3	6.3
NO	24
NO_2	21
PAN	0.065
PPN	0.0073
MPAN	0
PiBN	0

Table 3-2. Meteorological conditions used in the box model scenario.

Time	Mixing height (m)	Temperature (K)	Moisture content (%)
06:00	270	297	2.7
07:00	270		
08:00	360		
09:00	540	297	2.7
10:00	780		
11:00	960		
12:00	1180	300	2.3
13:00	1450		
14:00	1630		
15:00	1790	302	2.1
16:00	1870		
17:00	1870		
18:00	1870	302	2.2
19:00	1870		

3.3 RESULTS

A preliminary assessment of the ozone concentrations predicted by the SAPRC99 and CB-IV mechanisms under Houston conditions showed a significant difference in predictions of ozone between the mechanisms. The assessment was performed using the Comprehensive Air Quality Model with extensions (CAMx, ENVIRON, 2004), which is described in detail at the model web site (www.camx.com). Figure 3-2 illustrates ozone concentrations as predicted by the mechanisms for an air pollution episode that occurred on August 30, 2000, at the hour the maximum ozone concentrations throughout the modeling domain is reached. As shown in the figure, the maximum difference in predicted ozone concentrations between SAPRC99 and CB-IV was 44.4 ppb, similar to the finding by Byun (2002). The simulation employing SAPRC99 predicted a maximum ozone concentration of 157.2 ppb while CB-IV predicted a maximum ozone concentration of 123.9 ppb. Similar percentage differences in ozone concentrations were observed on other days in the modeled episode. As shown in Appendix B, Figures B-1 –

B-3, the differences in ozone predictions for CB-IV96 and SAPRC99 occur under a wide variety of conditions.

While previous studies have identified and quantified the magnitude of these differences, this work will be the first to use a variety of modeling tools to investigate the sources of the differences.

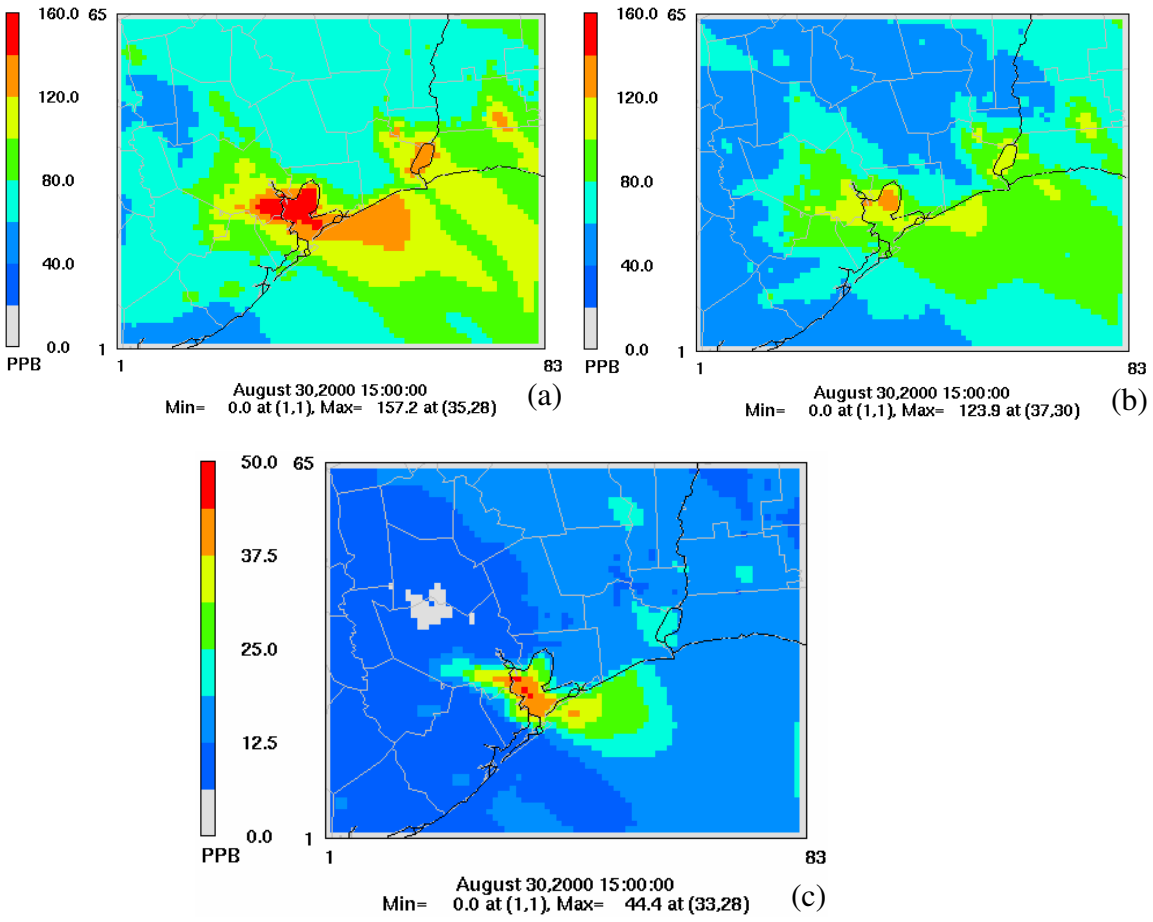

Figure 3-2. Ozone concentrations at the hour (15:00) the ozone maximum throughout the domain is reached in CAMx on August 30, 2000, in (a) SAPRC99, (b) CB-IV96, and (c) SAPRC99-CB-IV96.

Based on the assessment in CAMx, a number of box model simulations were performed to assess the sensitivity of the two mechanisms to the rates of specific

hydrocarbon reactions and the rates of reactions that control hydroxyl radical concentrations.

The ozone concentrations predicted by the box model using the SAPRC99 and CB-IV96 chemical mechanisms for the basecase box model scenario (described in Faraji, 2004) are shown in Figure 3-3. For these base case conditions, the SAPRC99 mechanism predicted a maximum ozone concentration of approximately l00 ppb while CB-IV96 predicted a maximum ozone concentration of approximately 60 ppb. These differences in maximum ozone concentration are comparable to maximum differences observed in the CAMx modeling (approximately 40 ppb).

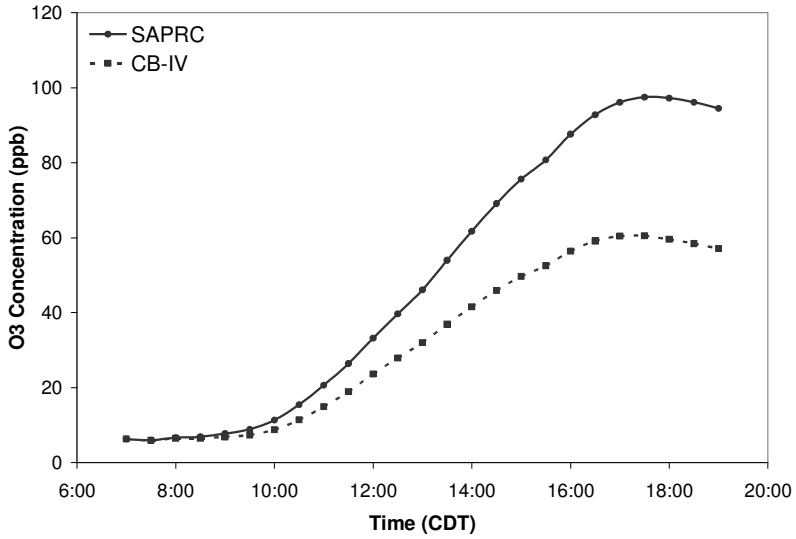

Figure 3-3. Comparison of predictions of ozone concentrations with SAPRC99 and CB-IV96 in the basecase of the box model under conditions of Houston's industrial source region.

The hypotheses that were examined using the box model postulated that differences in hydrocarbon chemistry were sources of the differences in the model predictions. The differences in hydrocarbon chemistries were explored by changing the composition of the VOCs emitted in the box model. The mixture of VOCs in the initial box model

formulation was changed, in a series of sensitivity studies, to a series of single chemical species. For example, in one simulation, the mixture of VOCs emitted into the box was replaced with emissions of ethylene only. In other simulations, the mixture of VOCs emitted into the box was substituted with other single hydrocarbons, listed in Table 3-3. These simulations were not meant to be representative of atmospheric conditions. Rather, they were used to identify potential differences in the mechanisms. Therefore, the results from the box model analyses were used as a qualitative rather than a quantitative evaluation of the differences between the mechanisms. The hydrocarbon species labeled as "explicit" in Table 3-3 are those that are represented individually in both SAPRC99 and CB-IV96 (ethylene, isoprene, and formaldehyde). For these species, VOC emissions into the box model were modified in exactly the same way for both SAPRC99 and CB-IV96 mechanisms. The VOC emissions were replaced by model species identified explicitly as ethylene, isoprene or formaldehyde. For the other chemical species listed in Table 3-3, the emissions in the box model were changed differently for the SAPRC99 and CB-IV96 mechanisms. For example, when the VOC emissions were changed to toluene emissions, the CB-IV96 mechanism modeled the toluene as the lumped chemical species TOL. SAPRC99 modeled the toluene as lumped chemical species ARO1.

Table 3-3. Single hydrocarbon species evaluated in the box model.

Compound Classes	Species	SAPRC99	CB-IV96
Explicit Species	Ethylene	ETHE	ETH
	Isoprene	ISOP	ISOP
	Formaldehyde	HCHO	FORM
Aromatics			
Mono-substituted	Toluene	ARO1	TOL
	Ethylbenzene	ARO1	1PAR; 1TOL
Di-substituted	Xylene	ARO2	1XYL
	Ethyltoluene	ARO2	1PAR; 1XYL
Tri-substituted	1,3,5-Trimethylbenzene	ARO2	1PAR; 1XYL
Alkanes	Ethane	ALK1	0.4PAR; 1.6UNR
	Propane	ALK2	1.5PAR; 1.5UNR
Alkenes	Propylene	OLE1	1PAR; 1OLE
	1-Butene	OLE1	2PAR; 1OLE
	cis-2-Butene	OLE2	2ALD2
	1,3-Butadiene	OLE2	2OLE
Aldehydes	Acetaldehyde	CCHO	ALD2

Figure 3-4 compares the ozone concentrations predicted by the box model for the two chemical mechanisms when VOC emissions are assumed to be single, explicitly represented species. For these simulations, the VOC emissions in the box model were changed to explicitly represented chemical species. These simulations were not intended to be representative of atmospheric conditions, but rather were used to test the consistency of the mechanisms. SAPRC99 and CB-IV96 yielded nearly identical predicted ozone concentrations for these explicitly represented species, as shown in Figure 3-4.

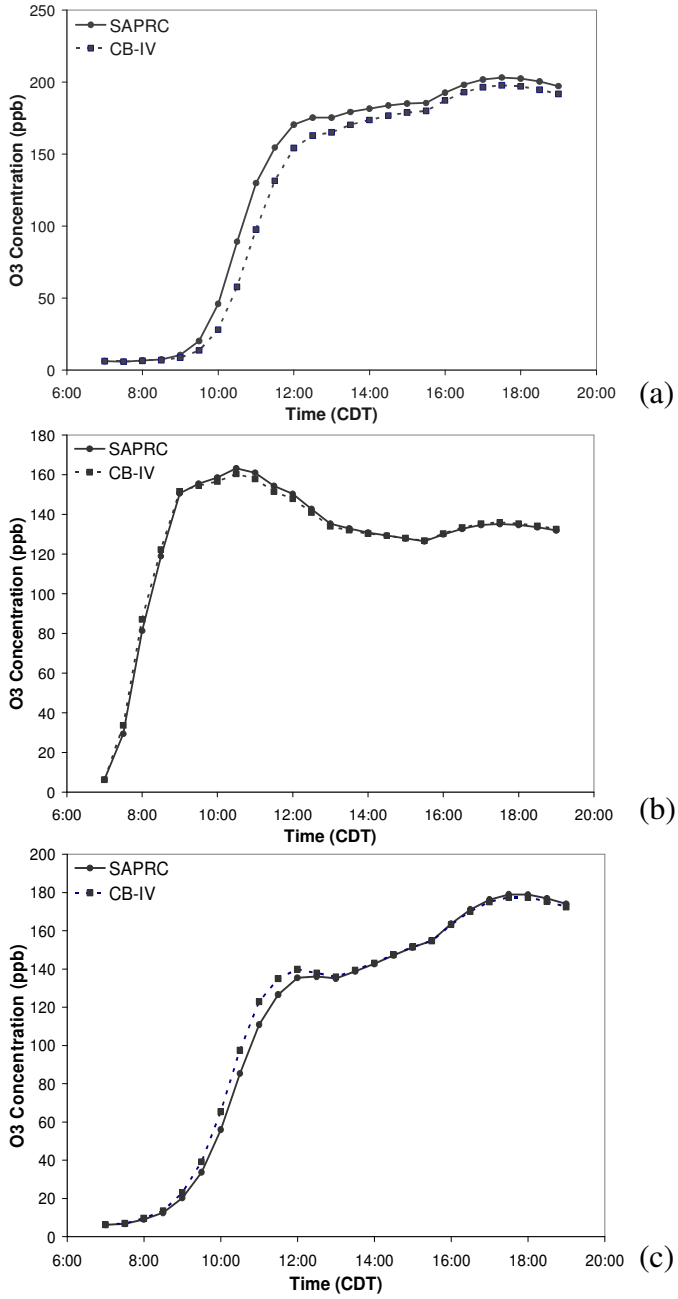

Figure 3-4. Comparisons of ozone concentrations predicted by the box model for the SAPRC99 and CB-IV96 chemical mechanisms when VOC emissions are assumed to be the explicitly-modeled species (a) ethylene, (b) formaldehyde and (c) isoprene.

The consistency in ozone predictions for the two mechanisms when only explicitly represented VOCs are emitted into the box suggests that the specific hydrocarbon chemistry and the inorganics chemistry in the two models at high hydrocarbon reactivity (ethylene, isoprene and formaldehyde are all highly reactive species) is consistent. When the same analysis was done for alkanes, alkenes, and aldehydes, the models again were reasonably consistent (Faraji, 2004). The simulations with mono-substituted aromatics, however, showed significant discrepancies between the two mechanisms as shown in Figure 3-5. Multiply substituted aromatics exhibited less of a discrepancy, but differences were still significant.

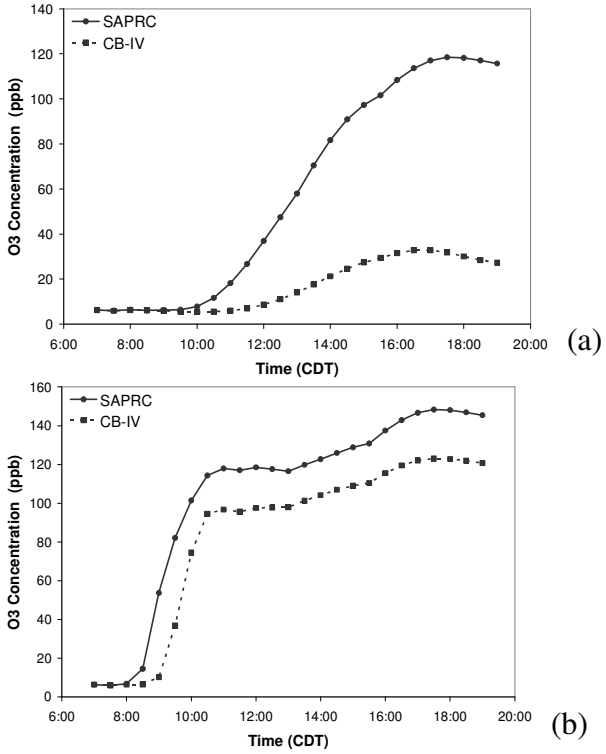

Figure 3-5. Comparisons of the ozone concentrations predicted by the box model for the SAPRC99 and CB-IV96 chemical mechanisms when VOC emissions are assumed to be the mono-substituted aromatic species (a) toluene and the multiply substituted aromatic species (b) xylene.

In the simulation with toluene emissions, CB-IV96 predicts a maximum ozone concentration of approximately 40 ppb while SAPRC99 predicts a maximum ozone concentration of approximately 120 ppb. Similarly, in the ethylbenzene simulation, the CB-IV96 and SAPRC99 ozone predictions are approximately 25 and 110 ppb, respectively. The significant discrepancy (80-85 ppb difference in predicted peak ozone concentration) between SAPRC99 and CB-IV96 for toluene and ethylbenzene are due to differences in chemistry between the TOL lumped species in CB-IV96 and the ARO1 lumped species in SAPRC99. When xylene was the only VOC emitted into the box, the maximum ozone prediction between the two mechanisms differed by 25 ppb, with CB-IV96 predicting approximately 123 ppb while SAPRC99 predicted a maximum ozone concentration of 148 ppb. This suggests that the differences in chemistry between the XYL species in CBIV96 and the ARO2 species in SAPRC99 are not as significant as for the TOL and ARO1 species.

The pathways used in SAPRC99 and CB-IV96 for the toluene and ethylbenzene reactions with hydroxyl radical species are shown in Table 3-4. The yield of the peroxy radical operators in SAPRC99, namely RO2-R and RO2-N, are larger than the yields of the XO2 and XO2N peroxy radical operators the CB-IV96 mechanism, leading to a higher production of ozone in the SAPRC99 mechanism. In addition to differences in the yields of peroxy radical operators, the two mechanisms make different assumptions about the importance of ring opening pathways. SAPRC99 assumes that the majority of the reaction products are highly reactive species associated with ring opening reactions (MGLY, GLY, DCB1 and DCB2), as opposed to the less reactive species associated with ring-addition products (CRES and BALD). In contrast, CB-IV96 has a high fraction of the ring-retaining products (CRES) and a different representation of potential ring opening products (TO2).

Estimated concentrations of mono-substituted aromatics in the Houston-Galveston area for the SAPRC99 and the CB-IV96 formulations of the emission inventory are consistent. However, Figure 3-6 illustrates that for consistent inventories of mono-substituted aromatics, on the same day and hour, the predicted concentrations of cresol in SAPRC99 are much lower than in CB-IV96. The higher branching ratio of the reactive ring-opening to ring-retaining products in SAPRC99, relative to CB-IV96, is one cause of the higher concentrations of ozone (and lower concentrations of cresol) in the SAPRC99 mechanism.

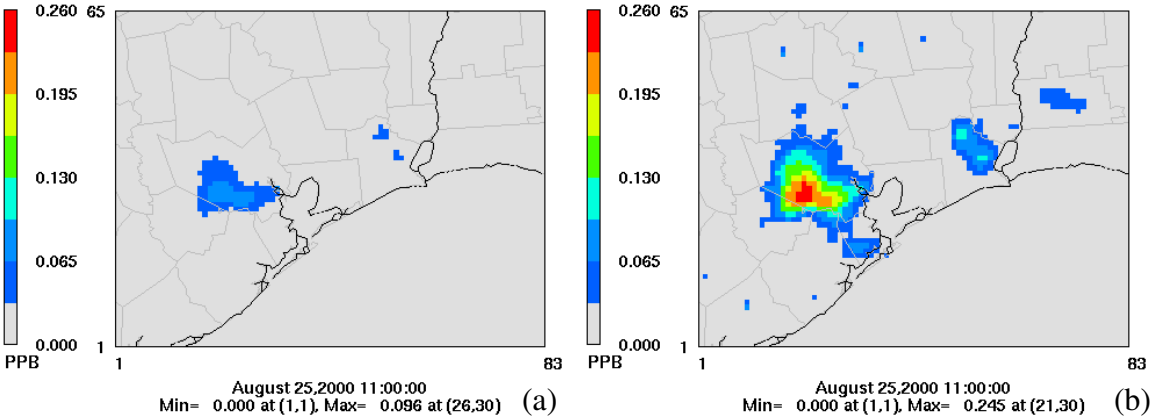

Figure 3-6. Predictions of cresol concentrations in (a) SAPRC99 and (b) CB-IV96 on August 25, 2000 at hour 11 in CAMx.

Table 3-4. Reactions of toluene and ethylbenzene with OH in SAPRC99 and CB-IV96.

Mechanism	Reactions
SAPRC99	ARO1 + OH = #0.224 HO2 + #.765 RO2-R. + #.011 RO2-N. + #.055 PROD2 + #.118 GLY + #.119 MGLY + #.017 PHEN + #.207 CRES + #.059 BALD + #.491 DCB1+ #.108 DCB2 + #.051 DCB3 + #1.288 XC
CB-IV96	TOL + OH = #.44 HO2 + #.08 XO2 + #.36 CRES + #.56 TO2 PAR + OH = #.87 XO2 + #.13 XO2N + #.11 HO2 + #.11 ALD2 + #-0.11 PAR + #.76 ROR

SAPRC99 species

Model Species	Description
ARO1	Aromatics with kOH < 2·104 ppm-1min-1
OH	hydroxyl radicals
HO2	hydroperoxide radicals
RO2-R	peroxy radical Operator representing NO to NO2 conversion with HO2 formation
RO2-N	peroxy radical operator representing NO consumption with organic nitrate formation
PROD2	ketones and other non-aldehyde oxygenated products which react with OH radicals faster than 5 x 10-12 cm3 molec-2 sec-1
GLY	Glyoxal
MGLY	methyl glyoxal
PHEN	Phenol
CRES	Cresols
BALD	aromatic aldehydes (e.g. benzaldehyde)
DCB1	reactive aromatic fragmentation products that do not undergo significant photodecomposition to radicals
DCB2	reactive aromatic fragmentation products which photolyze with alpha-dicarbonyl-like action spectrum
DCB3	reactive aromatic fragmentation products which photolyze with acrolein action spectrum
XC	lost carbon

CB-IV96 Species

Model Species	Description
TOL	mono-substituted benzenes
OH	hydroxyl radicals
HO2	hydroperoxide radicals
XO2	peroxy radical operator representing NO to NO2 conversion without O3 conversion
CRES	Cresols
TO2	OH-O2 adduct formed from aromatic oxidation
PAR	paraffinic carbon bond
XO2N	operator for NO consumption with organonitrate formation
ALD2	higher molecular weight aldehydes
ROR	representing ring cycling and isomerization of alkyl chain

The box model sensitivity analyses suggest that differences in the treatment of aromatics in the CB-IV96 and SAPRC99 mechanisms might account for much of the differences in ozone predictions between the two mechanisms. To test this hypothesis, a CAMx simulation was performed in which all of the aromatics emissions were eliminated. Specifically, a simulation was performed in which the CB-IV96 species TOL and XYL and the SAPRC99 species ARO1 and ARO2 were eliminated in the emissions for the basecase scenario. If the major cause of the differences between the two mechanisms was the aromatics chemistry, then, in principle, the predictions of the two mechanisms would converge for these simulations. This was not the case. The maximum predicted ozone concentrations for CB-IV96 and SAPRC99, along with the differences between the ozone concentration predictions from the two mechanisms are shown in Figures 3-7a-c. The figures indicate that large differences in the ozone concentrations predictions are still observed, even if all aromatics emissions are eliminated.

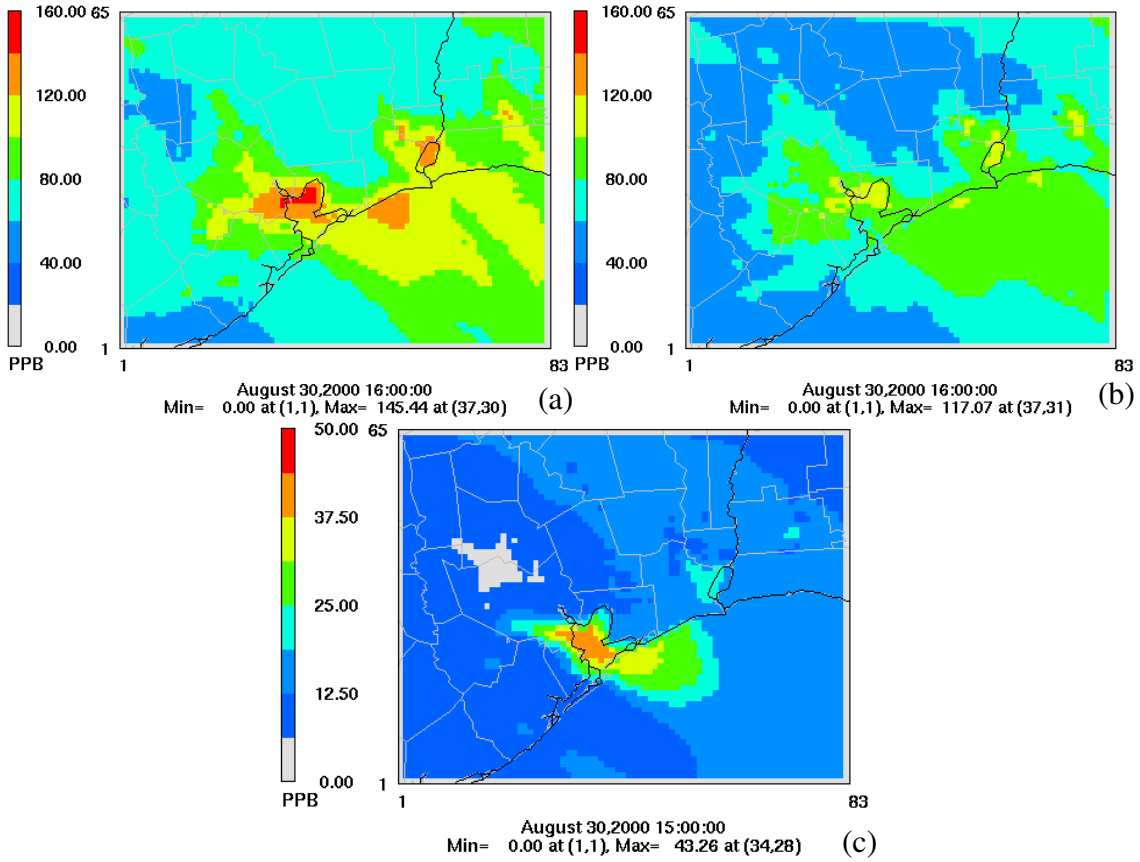

Figure 3-7. Ozone concentrations at the hour the ozone maximum throughout the domain is reached in CAMx on August 30, 2000, where all aromatic emissions were eliminated; (a) SAPRC99 mechanism; (b) CB-IV96 mechanism; (c) SAPRC99-CB-IV96.

In addition to differences in the chemistry of aromatics between the mechanisms, the chemistry of the termination of the hydroxyl radical and formation of nitric acid is different between the mechanisms. As shown in Table 3-5, the rate of the main radical termination process, the reaction of OH with NO_2, is greater in CB-IV96 relative to SAPRC99.

Table 3-5. Comparison of OH + NO_2 reaction rate constants in $ppm^{-1}min^{-1}$.

Temp (K)	298	273	298	Difference from CB-IV96
Pres (mbar)	1013	1013	491	
CB-IV96	1.68E+04	2.29E+04	8.15E+03	
SAPRC99	1.33E+04	1.80E+04	4.77E+03	-21% to -41%

Figures 3-8a and 3-8b show the concentration of the hydroxyl radical over the Houston Ship Channel area as predicted by SAPRC99 and CB-IV96, respectively, on August 30, 2000, at noon. As shown in the figures, although in some limited areas CB-IV96 predicts higher concentrations of the hydroxyl radical, the hydroxyl radicals predicted by SAPRC99 are generally higher relative to CB-IV96. The mechanisms predict similar NO_2 concentrations on this day and hour. In Figures 3-9a – 3-9d, the termination rate of the hydroxyl radical due to the OH+NO_2 reaction as predicted by the SAPRC99 and CB-IV96 mechanisms, respectively, are shown. Assuming that the reaction of OH with NO_2 is the dominant termination reaction for hydroxyl radicals, SAPRC99 predicts a higher termination rate of hydroxyl radicals relative to CB-IV96. Based on the pseudo-steady-state approximation for hydroxyl radicals, the rate of termination of hydroxyl radicals is equivalent to the rate of formation of hydroxyl radicals. Therefore, the higher termination rate of hydroxyl radicals in SAPRC99 relative to CB-IV96 is also indicative of a higher formation rate of hydroxyl radicals in SAPRC99 relative to CB-IV96. The dominant reaction pathways of radical formation are the photolysis of ozone and the photolysis of aldehydes. Figure 3-9 shows that the termination rate of hydroxyl radicals as predicted by SAPRC99 (Figure 3-9c) is greater than CB-IV96 (Figure 3-9d) in the morning, even when the concentrations of ozone are low. Therefore, differences in the chemistry of aldehydes were explored to evaluate the causes for a higher rate of radical formation in SAPRC99 relative to CB-IV96.

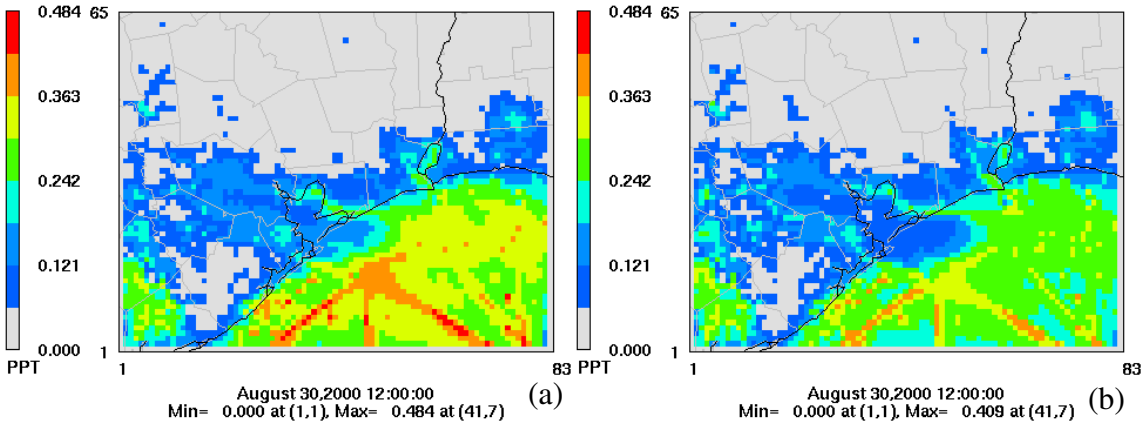

Figure 3-8. Hydroxyl radical concentrations at noon on August 30, 3000 as predicted by (a) SAPRC99 and (b) CB-IV96.

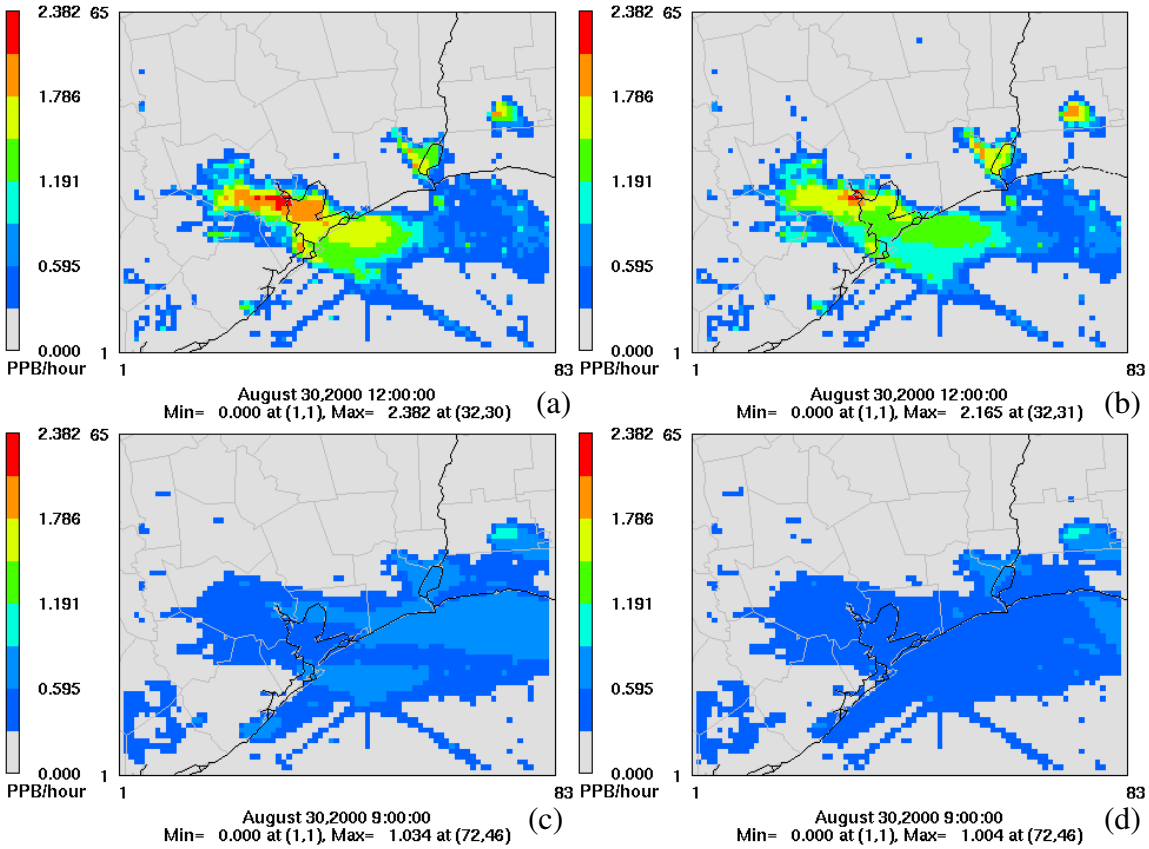

Figure 3-9. Termination rate of OH+NO2 on August 30, 2000, as predicted by (a) SAPRC99 at noon, (b) CB-IV96 at noon, (c) SAPRC99 in the morning, (d), CB-IV in the morning.

To evaluate differences in the chemistry of aldehydes in SAPRC99 and CB-IV96, ozone concentrations predicted by the mechanisms in CAMx on August 25, 2000 were compared at the hour when the ozone maximum throughout the modeling domain was reached. Figure 3-10 presents the concentration of C2 and higher molecular weight aldehydes (Species CCHO and RCHO in SAPRC99 and ALD2) as a function of time for a domain encompassing the maximum difference between the mechanisms on this day. As shown in the figure, the concentration of higher aldehydes in SAPRC99 is much higher than that of CB-IV96 between hours 9:00 and 19:00.

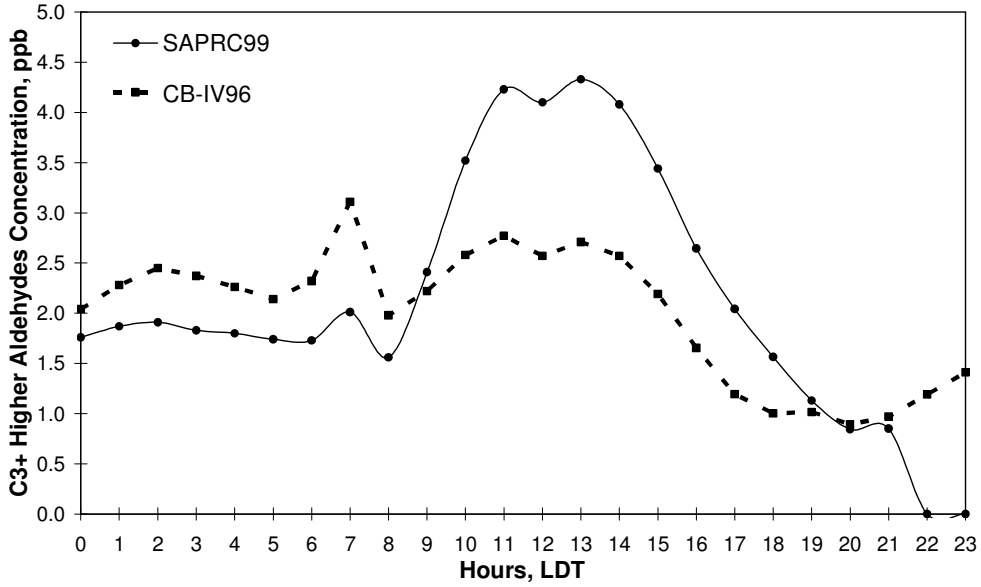

Figure 3-10. Concentration of higher molecular weight aldehydes (Species CCHO and RCHO in SAPRC99 and ALD2 in CB-IV96) as a function of time as predicted by SAPRC99 and CB-IV96 at the location of highest difference between the mechanisms on August 25, 2000.

Since the causes of the differences in higher aldehyde concentrations could be both differences in how emissions are modeled and differences in reaction rates and stoichiometry, a Process Analysis (PA) tool (Jeffries and Tonnesen, 1994) was applied to derive the contribution of each chemical pathway to the formation and sink of higher

aldehydes. The chemistry of the sink of higher molecular weight aldehydes is similar between the mechanisms. However, Figure 3-11 illustrates that with SAPRC99, there is a higher production of higher aldehydes relative to CB-IV96. As shown in the following photolysis reactions, these additional higher aldehydes are free radical sources which can contribute to the higher concentrations of ozone predicted by SAPRC99 relative to CB-IV96.

- SAPRC99: CCHO{+hν} = 1.0 CO+1.0 HO2+1.0 CXO2

  RCHO{+hν} = 1.0 CCHO+1.0 RO2-R+1.0 CO + 1.0 HO2
- CB-IV: ALD2{+hν} = FORM+2.0 HO2+CO+XO2

The dominant sources of higher aldehydes identified as leading to the higher production of higher aldehydes in SAPRC99 are as follows:

- RCO3+NO = NO2+CCHO+RO2-R
- PROD2+OH=0.379HO2+0.473RO2-R+0.070RO2-N+0.029CCO3+0.049 RCO3+0.213 HCHO+0.084 CCHO+0.558 RCHO+0.115 MEK+0.329 PROD2
- RNO3+OH = 0.338 NO2+0.113 HO2+0.376 RO2-R+0.173RO2N+0.596 R2O2+0.010 HCHO+0.439 CCHO+0.213 RCHO+0.020 ACET+0.243 MEK +0.435 PROD2

The chemical species represented by the SAPRC99 model species in the reactions above are described in Table 3-6.

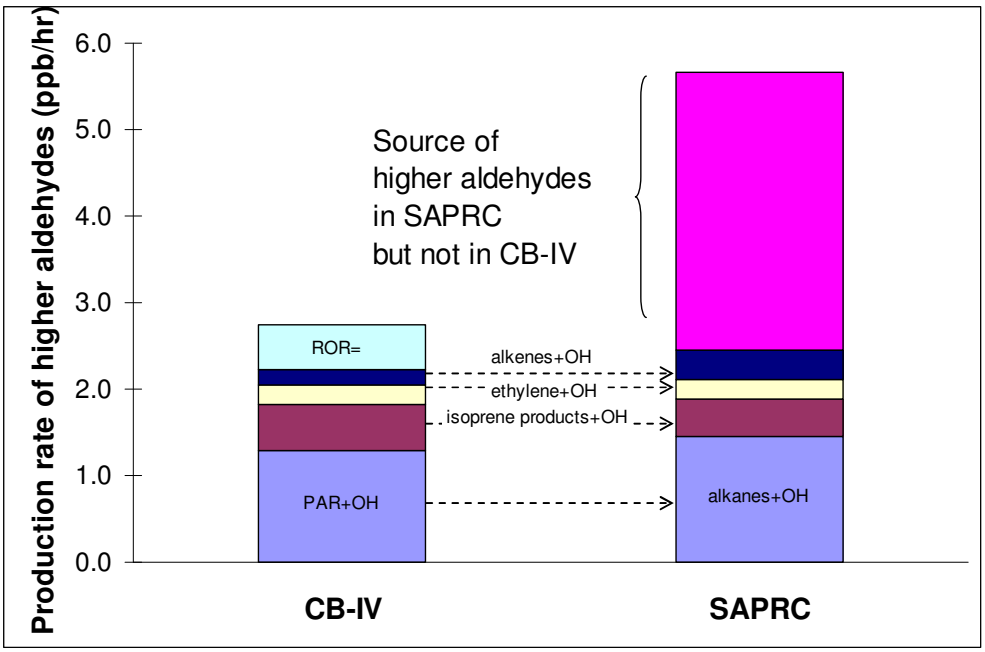

Figure 3-11. Relative production of higher aldehydes by SAPRC99 and CB-IV96 on August 25, 2000, 13:00 hr, when the difference in predicted ozone concentrations by the mechanisms is high.

Table 3-6. Species lumped into the SAPRC99 model species included in the dominant reactions contributing to higher aldehydes formation and photolysis of higher aldehydes.

SAPRC99 Model Species	Description
RCHO	propionaldehyde and higher aldehydes.
RCO3	peroxy propionly and higher peroxy acyl radicals, including the acyl peroxy radical formed from glyoxal.
PROD2	higher reactivity non-aldehyde oxygenates, specifically ketones, alcohols, and other reactive non-aromatic and non-double-bond-containing oxygenated products.
RNO3	organic nitrates with the exception of PAN or PAN analogues, primarily those formed in the reactions of peroxy radicals from NO.
CCHO	Acetaldehyde
HCHO	Formaldehyde
MEK	ketones and other non-aldehyde oxygenated products which react with OH radicals slower than 5E-12 cm3molec-2sec-1.
ACET	Acetone
CXO2	methylperoxy radical

In order to evaluate the role of the difference in the radicals chemistry on the discrepancy between SAPRC99 and CB-IV96, the rate of the reaction OH + NO_2 = HNO_3 in CB-IV96 was decreased to the rate in SAPRC99. Figure 3-12b compares the concentration of ozone over Galveston Bay on August 30, 2000 between the basecase CB-IV96 and CB-IV96 with the rate of OH+NO_2 modified. As a result of decreasing the rate, the maximum ozone concentration in CB-IV96 increases by approximately 3 ppb. Therefore, similar to the aromatics chemistry, the difference in the radical termination chemistry between SAPRC99 and CB-IV96 alone is not sufficient to account for the discrepancy in predictions of ozone concentrations between the mechanisms. The fact that the aromatics and hydroxyl chemistries in isolation do not have a major effect on the differences between the mechanisms might indicate a synergetic interaction between these two pathways.

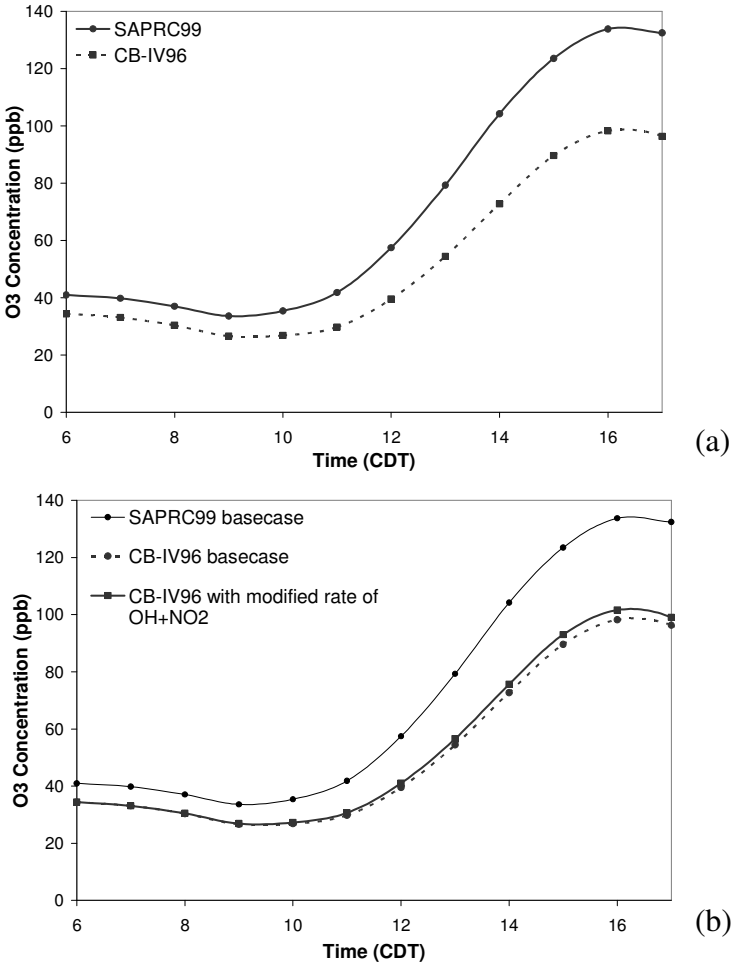

Figure 3-12. Timeseries of ozone in (a) basecase SAPRC99 and CB-IV96 and in (b) basecase CB-IV96, basecase SAPRC99, and CB-IV96 with modified $OH+NO_2=HNO_3$ reaction rate constant in CAMx over Galveston Bay on August 30, 2000.

In addition to assessing the effects of differences in the aromatics and free radicals chemistries independently, an additional simulation in CAMx was performed in order to investigate the combined effect of these two chemistries on the differences in ozone predictions between the mechanisms. In this simulation, in addition to eliminating the emissions of aromatics, the rate of the $OH+NO_2=HNO_3$ reaction in SAPRC99 was equated to the rate in CB-IV96. As a result of these modifications, as shown in Figure 3-

13a, on August 30, hour 1500, SAPRC99 predicts a maximum ozone concentration of approximately 128 ppb relative to a concentration of 145.4 ppb when only the aromatics emissions were eliminated. In the basecase scenario, Figure 3-13c, the difference between SAPRC99 and CB-IV96 is up to 12 ppb over a broad urban region, in addition to differences as high as 45 ppb over Galveston Bay. As shown in Figure 3-13b, when both changes are made, the differences between the mechanisms is reduced across the urban area and the maximum difference over Galveston Bay is nearly halved, converging from a difference of nearly 45 ppb to a maximum difference of approximately 23 ppb. Therefore, although the individual contribution of the aromatics and free radical chemistries to the differences between the mechanisms may not be significant, differences in these two chemistries combined can be considered as one of the main factors leading to differences in ozone concentrations between the mechanisms.

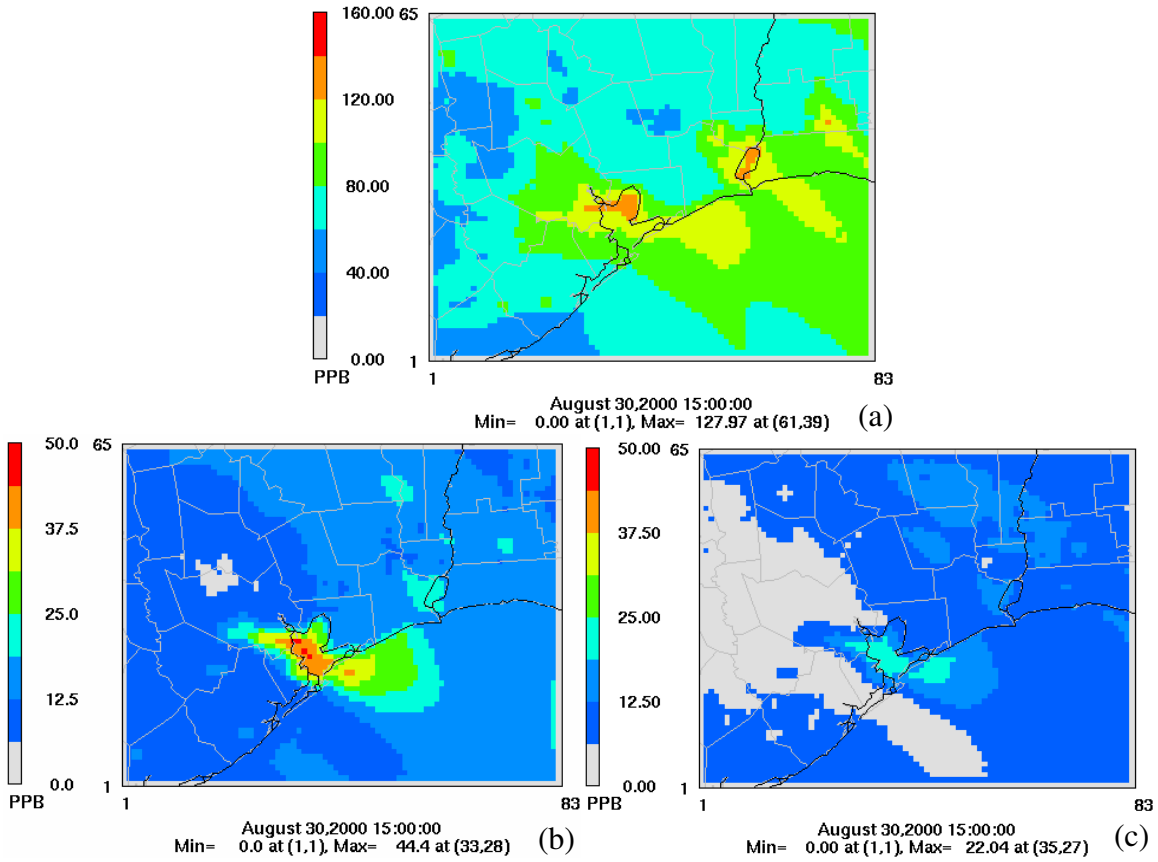

Figure 3-13. Ozone concentrations at the hour (15:00) the ozone maximum throughout the domain is reached in CAMx on August 30, 2000, for simulation where in addition to all aromatic emissions being eliminated, the rate of the $OH+NO_2=HNO_3$ reaction in SAPRC99 was equated to that of CB-IV96; (a) SAPRC99 without aromatic emissions and modified OH+NO2 rate; (b) SAPRC99 without aromatic emissions and modified OH+NO2 rate minus CB-IV96 without aromatic emissions; (c) SAPRC99 in basecase minus CB-IV96 in basecase.

3.4 POLICY IMPLICATIONS

Differences in the predictions of the SAPRC and CB-IV mechanisms have significant policy implications. When demonstrating attainment with the National Ambient Air Quality Standard (NAAQS) for ozone with concentrations averaged over 8 hours, relative reductions in ozone predicted by the model are used. SAPRC is more

sensitive to NOx emission reductions than CB-IV, and when NOx concentrations are reduced, as has been proposed in the Houston area, SAPRC predicts larger relative reductions in ozone concentrations than CB-IV (Appendix B). Therefore, identifying the causes for the different predictions of the mechanisms and choosing a mechanism that best represents atmospheric conditions in Houston is pertinent to the development of the State Implementation Plan in Texas.

3.5 CONCLUSIONS

For an air pollution episode that occurred during August 22-September 1, 2000 in the Houston-Galveston area, the SAPRC99 mechanism predicts ozone concentrations that are up to 45 ppb higher than CB-IV96. When aromatics emissions were eliminated and the rates of the $OH+NO_2$ rate constant in the two mechanisms were equated, the difference between the mechanisms converged from nearly 45 ppb to approximately 22 ppb. Therefore, the differences between SAPRC99 and CB-IV96 can be at least partially attributed to the combined effects of difference in the aromatics and free radicals chemistries. These differences are due to differences in both reaction rate parameters/stoichiometry and the condensation methods in the mechanisms. Additional causes of differences in the mechanisms remain to be identified, and will be explored in the remaining chapters of this thesis.

3.6 REFERENCES

Adelman, Z. E. (1999). A *reevaluation of the carbon bond-IV photochemical mechan*ism. Master's Thesis, Department of Environmental Engineering, University of North Carolina at Chapel-Hill, NC.

Byun, D. W. (2002, October). *A study of photochemical processes of the Houston-Galveston metropolitan airshed with EPA CMAQ 2002*. Paper presented at the Model-3 User's Workshop, EPA, Research Triangle Park, NC.

Carter, W. P. L. (2000). *Documentation of the SAPRC-99 chemical mechanism for VOC reactivity assessment*. Air Pollution Research Center and College of Engineering, Center for Environmental Research and Technology, University of California at Riverside, CA.

Daum, P., Meagher, J., Allen, D. T., Durrenberger, C. (2002, November). Accelerated Science Evaluation of ozone formation n the Houston-Galveston area. Available at <http://www.utexas.edu/research/ceer/texaqsarchive/accelerated.htm>.

ENVIRON International Corporation. (2004). *Users Guide to the Comprehensive Air Quality Model with Extensions (CAMx) version 4.03*. Available at http://www.camx.com.

Faraji, M. (2004). *Comparison of chemical mechanisms used in air quality models in Houston*. Master's Thesis, Department of Civil and Environmental Engineering, University of Texas at Austin, Austin, Texas.

Jeffries, H. E. and Tonnesen, S. (1994). A comparison of two photochemical reaction mechanisms using mass balance and process analysis. *Atmospheric Environment*, 28, 2991-3003.

McGaughey, G. R., Desai, N.R., Allen, D.T., Seila, R.L., Lonneman, W.A., Fraser, M.P., Harley, R.A., Ivy, J.M., and Price, J.H., 2004. Analysis of Motor Vehicle Emissions in a Houston Tunnel during the Texas Air Quality Study 2000. Atmospheric Environment 38, 3363-3372.

Ryerson, T. R., Trainer, M., Angevine, W. M., Brock, C. A., Dissly, R. W., Fehsenfeld, F. C., Frost, G. J., Goldan, P. D., Holloway, J. S., Hubler, G., Jakoubek, R. O., Kuster, W. C., Neuman, J. A., D.K. Nicks Jr., D. K., Parrish, D. D., Roberts, J. M., and Sueper, D.T. (2003). Effect of petrochemical industrial emissions of reactive alkenes and NOx on tropospheric ozone formation in Houston, Texas. Journal of *Geophysical Research*, 108, 4249.

Russell, M. M. (2003). *Predicting secondary organic aerosol formation rates and concentrations in southeast Texas*. Ph.D. Dissertation, Department of Civil Engineering, University of Texas at Austin, Austin, Texas. Available at

<http://www.lib.utexas.edu/etd/d/2003/russellmm039/russellmm039.pdf#page=3>
.

TexAQSI. *The Texas Air Quality Study 2000*. The University of Texas at Austin. Accessed 3 February 2002. <http://www.utexas.edu/research/ceer/texaqs/>.

Yarwood, G., Whitten, G. Z., and Rao, S. (2005). *Updates to the Carbon Bond 4 photochemical mechanism*. ENVIRON International Corporation. Report to the Lake Michigan Air Directors Consortium. Available at <http://www.camx.com/publ/pdfs/CB05_Final_Report_120805.pdf>.

Chapter 4: Environmental Chamber Experiments for Evaluating SAPRC99 and CB Mechanisms

The hypotheses for the causes of the differences in predictions for the SAPRC and CB mechanisms, described in Chapter 3, were tested by comparing the predictions of the mechanisms to environmental chamber experiments. Conditions in an environmental chamber are not necessarily representative of those in ambient air, and more specifically, actual atmospheric conditions in Houston, Texas. Factors such as surface effects, constant light intensity, unrealistic spectral distribution, constant temperature and relative humidity, static operating conditions, and reactant identity usually differ from actual urban air (Jeffries *et al*., 1975). Therefore, it can be difficult to directly extrapolate results obtained in environmental chamber experiments to the behavior of ambient air. Nevertheless, these experiments can serve as a guide and a means of testing the hypotheses in this study.

This Chapter will describe the environmental chambers, the software used in modeling the chamber experiments, and the strategy that will be employed for interpreting the comparisons between chamber observations and model predictions. As will be described in this chapter, the simulations of experiments in environmental chambers have large wall-effects corrections. Because these wall effects corrections are not used in regional air quality simulations, the overall magnitudes of the wall effect corrections and the chemical pathways most strongly affected by the wall chemistry will be probed. In addition, the sensitivity of predicted concentrations to the choice of wall mechanism will be examined.

4.1 UNC ENVIRONMENTAL CHAMBER

The environmental chamber at the University of North Carolina at Chapel Hill (UNC) was developed by Jeffries *et al*., (1975). The chamber was constructed outdoors in rural North Carolina, in one of the least industrialized counties in North Carolina. It is an A-frame structure covered with Teflon film and partitioned into two sections, each with a volume of 156 m^3. The dual compartment system allows for two experiments to be conducted simultaneously. The chamber utilized ambient conditions of solar radiation, temperature, and relative humidity in order to achieve a realistic simulation of urban ambient conditions. The background concentrations of NOx and nonmethane hydrocarbons in ambient air at the site were usually less than 0.025 ppm and 0.20 ppm, respectively, so that ambient air that leaked into the chamber was relatively clean, compared to the air inside the chamber. More importantly, the air exhibited very low reactivity in the chamber, but these background effects were still larger than those encountered in indoor chambers using purified air. Details of the design and construction of the chamber, experimental methods and procedures, and corrections in measurements are described in Jeffries *et al*., (1975).

4.1.1 Quality assurance in use of simulation software for UNC chamber experiments

The Morpho Photochemical Simulation software, developed at UNC (Sexton and Jeffries, 1999), was used in this study to simulate the chamber experiments at UNC with the SAPRC and CB chemical mechanisms. Yarwood at ENVIRON and Whitten at Smog Reyes who provided the software, implemented the CB05 mechanism within Morpho to test the performance of the latest CB mechanism against the UNC chamber experiments (Yarwood *et al*., 2005). In this study, ENVIRON's procedure for implementing the CB05 within the Morpho software was replicated and simulations of selected UNC chamber experiments using CB05 were compared against simulations using CB05 in

Morpho as conducted by ENVIRON in order to verify the procedure of implementing the mechanisms within the software. For example, in a chamber experiment conducted on September 23, 1996, one side of the dual chamber was injected with an initial formaldehyde concentration of 0.5 ppm while the other side of the chamber was injected with 1 ppm of formaldehyde. The predictions of O_3, NO, NO_2, CO, and HCHO, along with several environmental parameters were compared between the simulation of this experiment using CB05 by ENVIRON and simulation of the same experiment using CB05 in this study. As shown in Figures 4-1 and 4-2, for both sides of the experimental chamber, labeled in red and blue, the O_3 and NOx predictions as well as the CO and HCHO predictions simulated by ENVIRON with CB05 are identical with those simulated in this work by CB05. The same verification procedure was repeated for two other experiments in which CO was used as primary a reactant, and the outputs of the simulations obtained in this work using CB05 were identical to the simulation performed by ENVIRON as shown in Figures 4-3– 4-6. In the figures, the solid lines represent the simulations and the dashed lines represent the measurements.

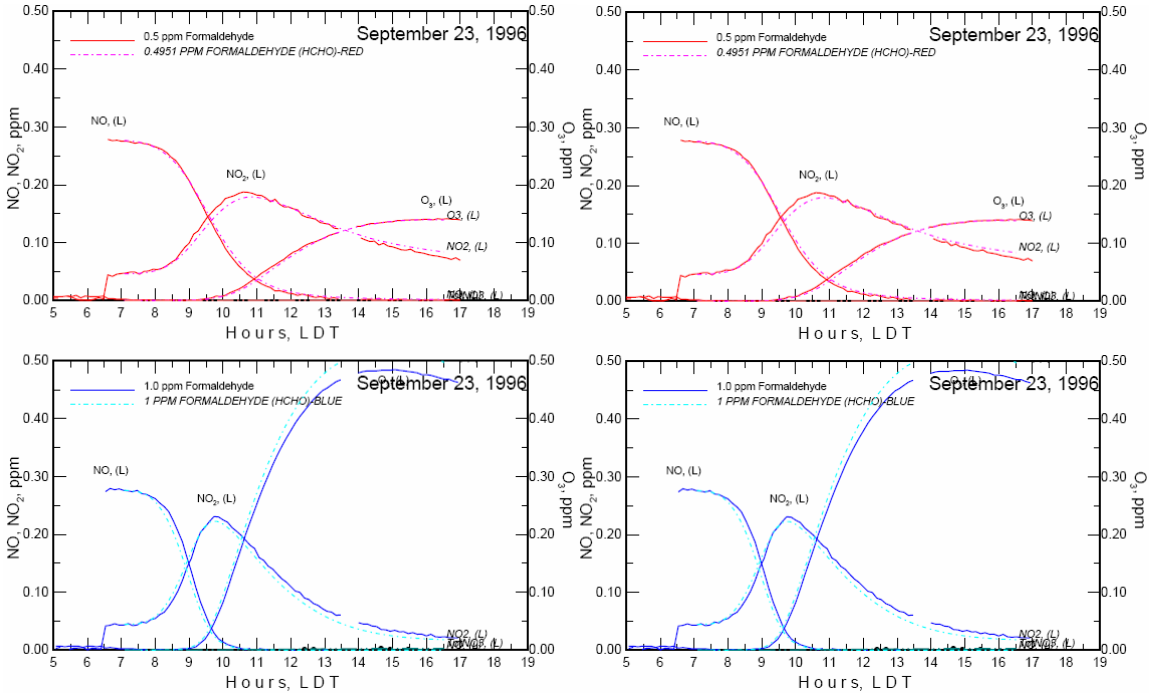

(a) (b)

Figure 4-1. Simulation of a UNC formaldehyde chamber experiment conducted on September 23, 1996 using the CB05 mechanism in Morpho by (a) ENVIRON and (b) in this study, comparing O_3 and NOx.

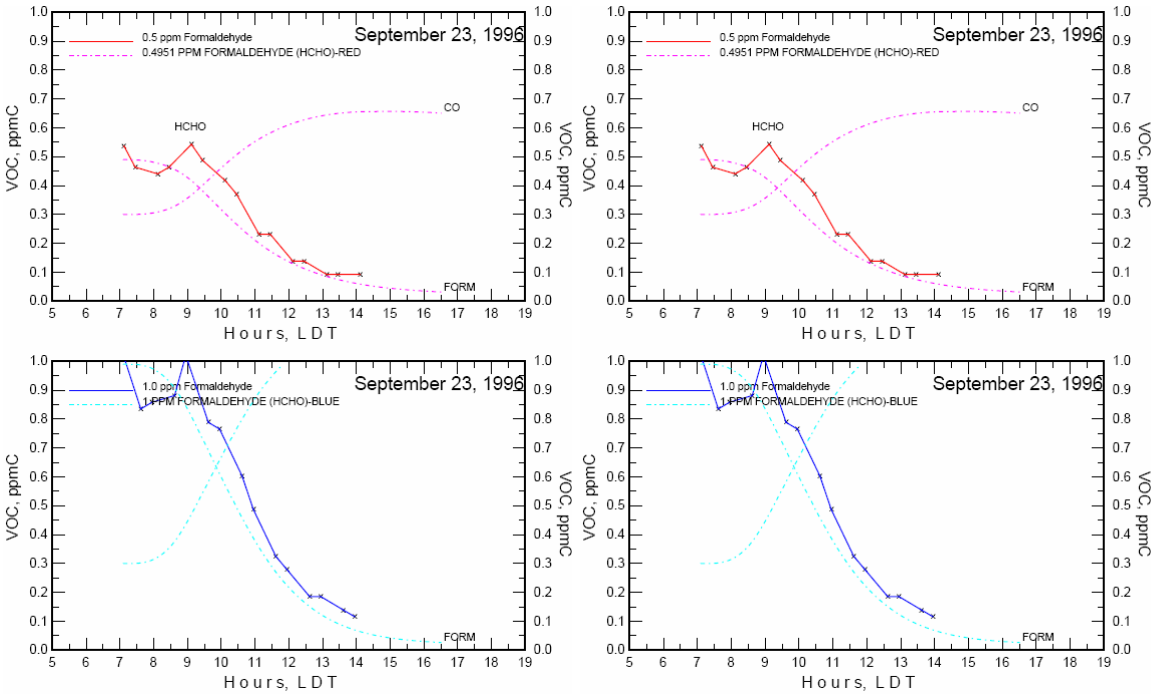

(a) (b)

Figure 4-2. Simulation of a UNC formaldehyde chamber experiment conducted on September 23, 1996 using the CB05 mechanism in Morpho by (a) ENVIRON and (b) in this study, comparing HCHO and CO.

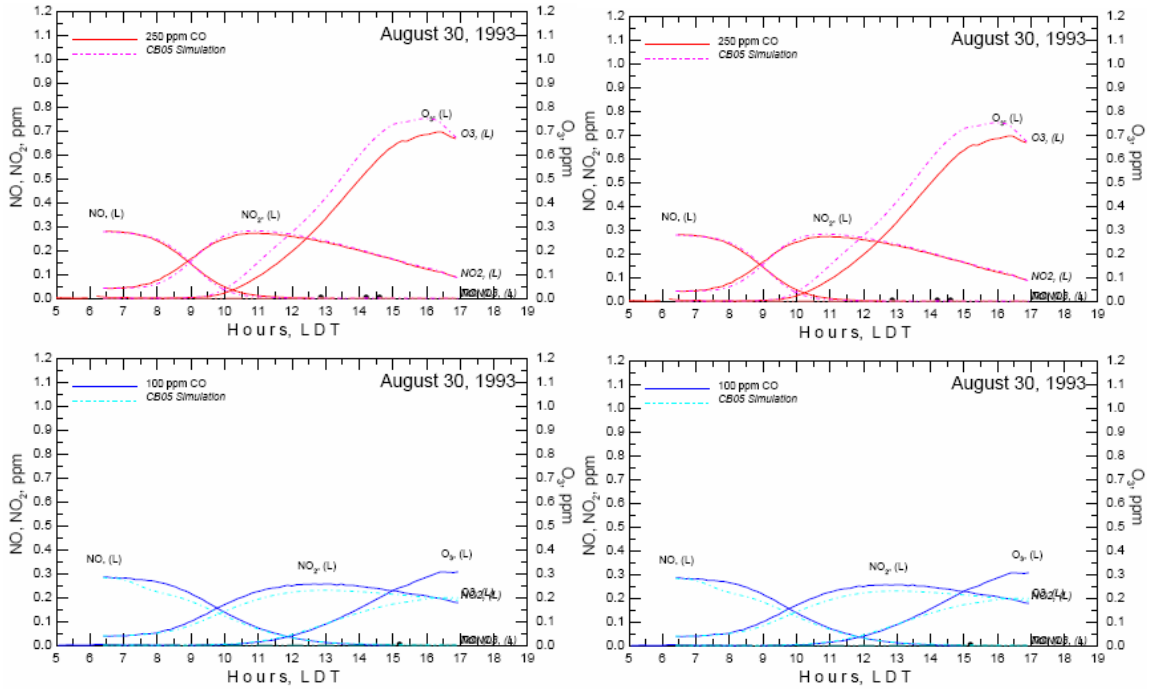

(a) (b)

Figure 4-3. Simulation of a UNC CO chamber experiment conducted on August 30, 1993 using the CB05 mechanism in Morpho by (a) ENVIRON and (b) in this study, comparing O_3 and NOx.

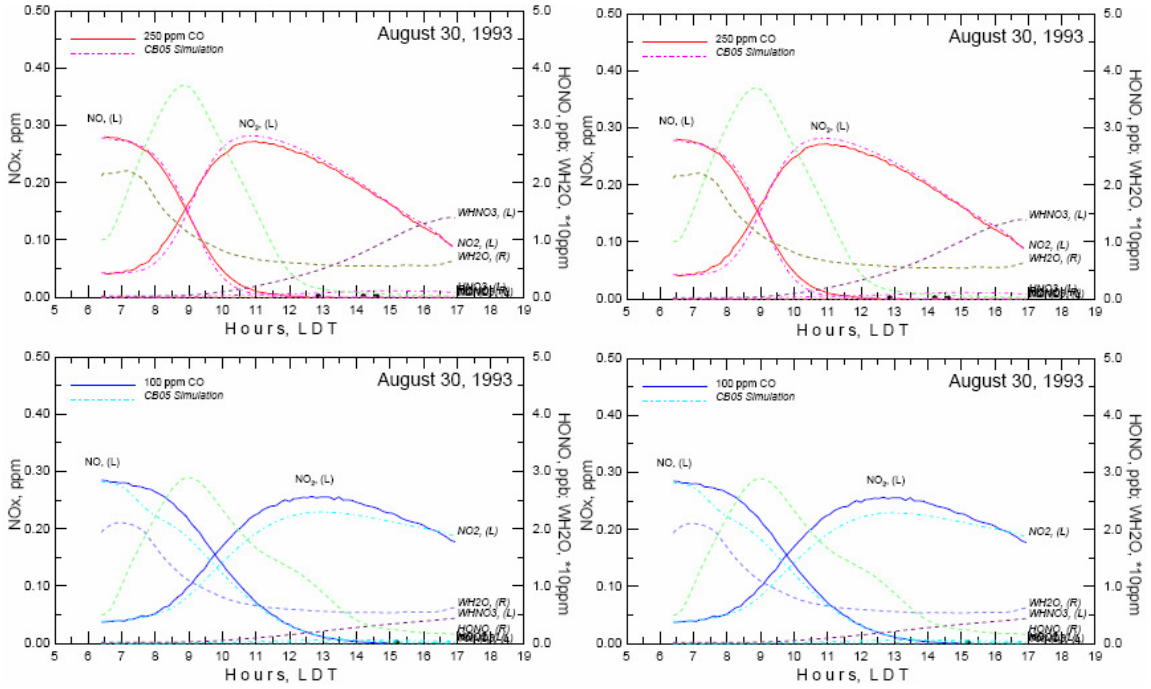

(a) (b)

Figure 4-4. Simulation of a UNC CO chamber experiment conducted on August 30, 1993 using the CB05 mechanism in Morpho by (a) ENVIRON and (b) in this study, comparing NOx and HONO.

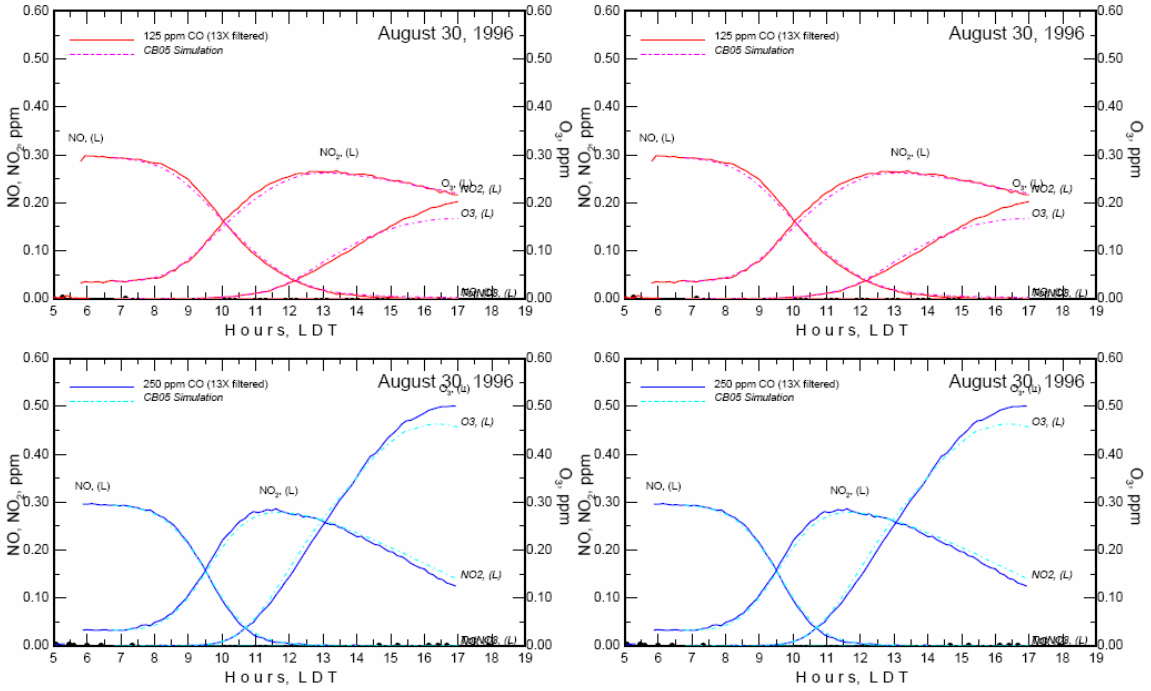

(a) (b)

Figure 4-5. Simulation of a UNC CO chamber experiment conducted on August 30, 1996 using the CB05 mechanism in Morpho by (a) ENVIRON and (b) in this study, comparing O_3 and NOx.

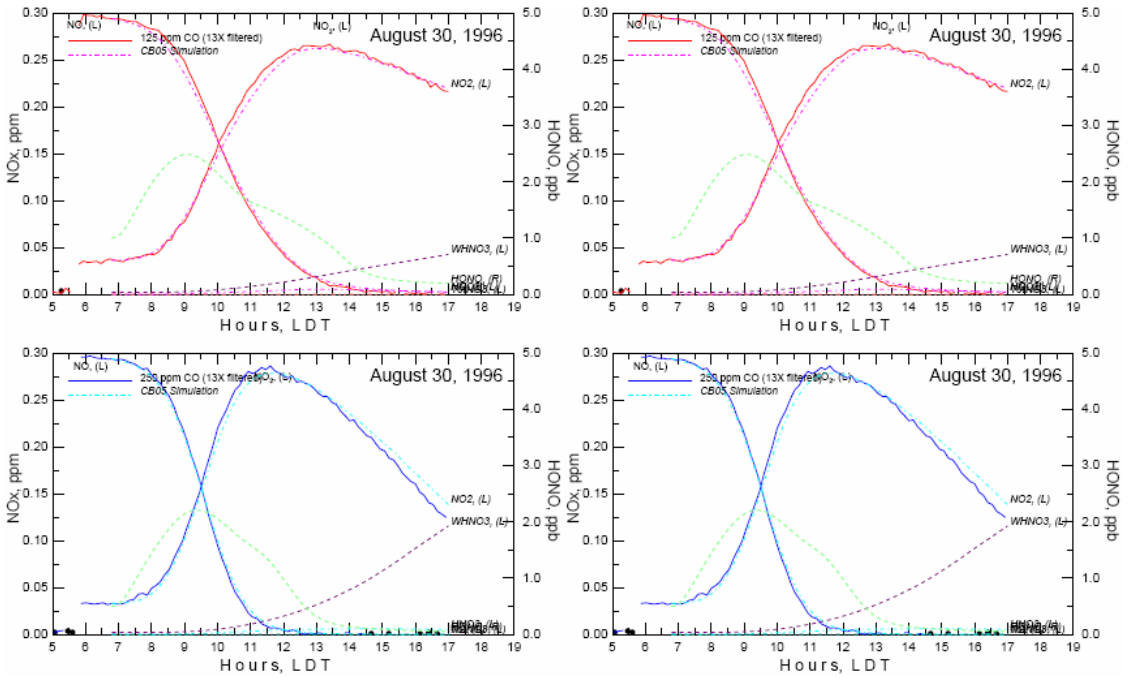

Figure 4-6. Simulation of a UNC CO chamber experiment conducted on August 30, 1996 using the CB05 mechanism in Morpho by (a) ENVIRON and (b) in this study, comparing NOx and HONO.

With the implementation of a chemical mechanism within the Morpho software verified for CB05, the CB-IV and SARC99 mechanisms were also implemented within the Morpho framework in this study.

With the collaboration of Yarwood and Whitten, various updates where made to the CB05 mechanism originally implemented in Morpho. These updates are consistent with the CB05 mechanism documented in the CB05 report. Therefore, the version of CB05 implemented in Morpho in this work was consistent with the CB05 mechanism released and documented in the CB05 report. As a result of these updates, the results of the September 23, 1996 chamber experiment shown in Figure 4-1 and Figure 4-2 were updated, as shown in Figures 4-7 and 4-8.

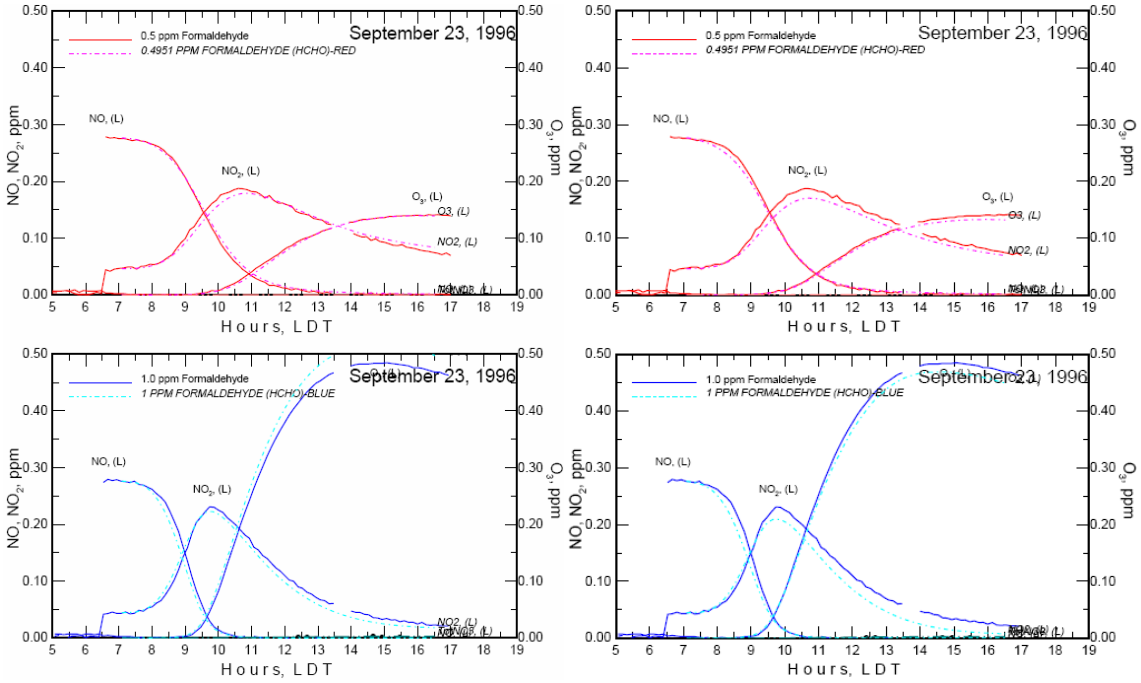

(a) (b)

Figure 4-7. Simulation of a formaldehyde CO chamber experiment conducted on September 23, 1996 using the CB05 mechanism in Morpho by (a) ENVIRON and (b) this work with updates to CB05, comparing O_3 and NOx.

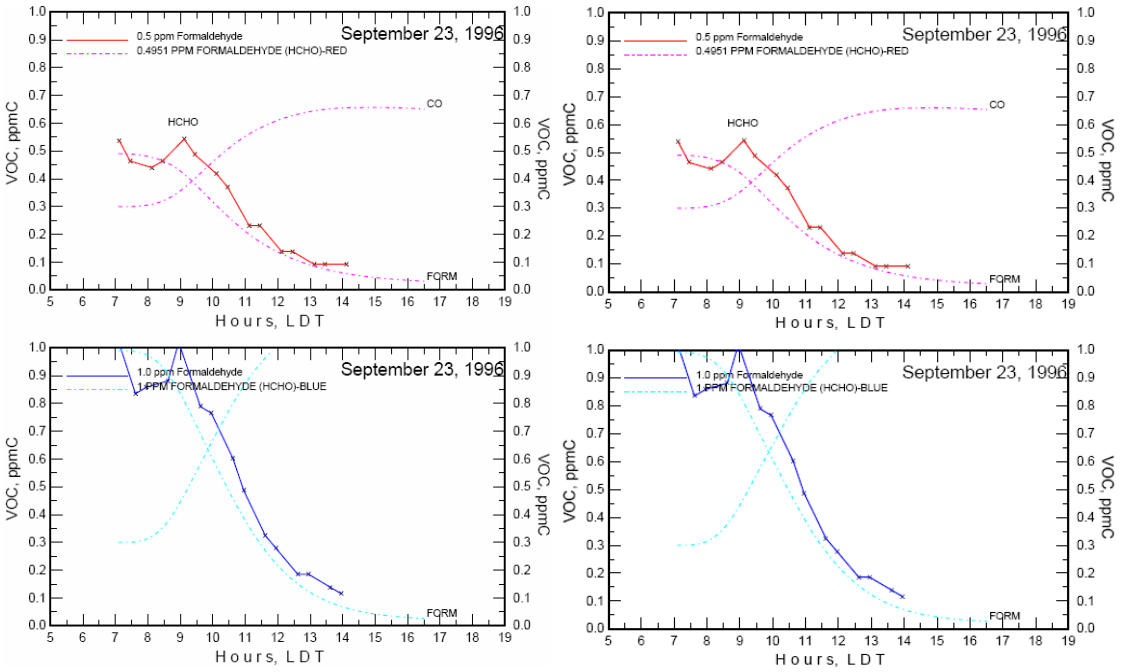

(a) (b)

Figure 4-8. Simulation of a UNC formaldehyde chamber experiment conducted on September 23, 1996 using the CB05 mechanism in Morpho by (a) ENVIRON and (b) this study, with updates to CB05, comparing HCHO and CO.

4.2 UCR AND TVA ENVIRONMENTAL CHAMBERS

A variety of environmental chambers at the University of California at Riverside (UCR) have provided data which that were also used for mechanism evaluation. These chambers are outlined below. Detailed descriptions of the chambers and measurement corrections are described in detail by Carter *et al*., (1993), Carter (2004), and Carter *et al*., (2005).

- Evacuable Chamber (EC): 5800-liter evacuable, thermostatted cylindrical chamber. FEP Teflon-coated aluminum walls. Quartz windows on both ends. 25 kW Xenon arc light "solar simulator" light source with pyrex filters to remove UV below ~ 290 nm. Generally operated at ~ 303 K and 50% relative humidity (RH).

- Indoor Teflon Chamber #1 (ITC): ~6000-liter FEP Teflon bag in aluminum frame with banks of blacklights on either side. Generally operated at room temperature and 50% RH.
- Indoor Telfon Chamber #2 (ETC): ~4000-liter FEP Teflon bag in an aluminum frame with banks of blacklights on the top and bottom. All runs at room temperature and < 5% RH.
- Dividable Teflon Chamber (DTC): Dual ~5000-liter FEP Teflon film bags with a blacklight light source. All runs at room temperature and generally <5% RH.
- Xenon Teflon Chamber (XTC): ~5000-liter FEP Teflon film bag with 4 6.5 kW xenon arc lights. All runs at room temperature and <5% RH.
- Outdoor Teflon Chamber (OTC): ~50,000-liter pillow-shaped FEP Teflon reaction bag located outdoors and irradiated with sunlight. Usually divided into two ~25,000-liter sides. All runs at somewhat higher than ambient temperature and <5% RH. Runs usually carried out in summer.
- CE-CERT Chamber (CTC): Two adjacent ~2,500-liter reactors constructed of FTP Teflon film held in a framework. Experiments used dry air at ~300°K and carried out in 1994 – 1995. The light source modeled after the XTC with the same xenon arc lighting system. This chamber no longer exists.
- EPA Chamber: Two 90 m^3 FEP Teflon film reactors enclosed within a 450 m^3 thermally insulated enclosure continually flushed with purified air at 1000 min^{-1}. The light source includes a 200 kW Argon arc lamp or a bank of 115 W blacklights, with the Argon Arc light being used for most EPA chamber experiments modeled in this study. Temperature in enclosure controlled with air-conditioner capable of producing a temperature range of 5-45 °C and <5% RH. This chamber was designed to carry out experiments at lower pollutant levels than previously possible for mechanism

evaluation, and consequently had the lowest chamber effects of the other chambers used (Carter *et al*, 2005). Generally, the experiments in this chamber were at much lower levels than in the other chambers, except for some experiments in the TVA chamber, discussed below.

In 1993 through 1995, Simonaitis and Bailey of the Tennessee Valley Authority (TVA) used a 28,000-liter indoor smog chamber to conduct a series of chamber experiments under lower NOx conditions than employed previously (Simonaitis *et al*., 1996). Although no longer operational, this chamber was used to carry out a number of reasonably well characterized experiments under relatively low NOx conditions that are potentially useful for mechanism evaluation. The TVA chamber was a ~28,000-liter indoor chamber constructed of 0.13 mm FEP Teflon film supported on an aluminum frame. Irradiation was provided using banks of blacklamps, Q-Panel 340s, and Phillips TL40W/O bulbs in 4:3:1 ratio, which results in a spectrum that gives a better simulation of the relative intensity of sunlight in the <325 , ~350, and 400-450 nm regions than blacklights alone. The chamber was purged with clear air with the lights on for at least two days before an experiment and the experiments were continuously diluted with purified air during the experiments. Temperature varied by as much as 20 °C during the experiments. The characterization of the input data for modeling as used by this project is described by Carter (2004). Because it was designed for mechanism evaluation at low NOx conditions, this chamber had relatively low chamber effects, comparable in most respects to the UCR EPA chamber. However, because of a contaminated humidification system it had a relatively high formaldehyde offgasing rate that had to be taken into account when modeling these runs (Carter, 2004, and references therein). This does not represent a large uncertainty when modeling these runs because the formaldehyde offgasing was fairly consistent from run to run, and could be determined based on the

experimental measurements of formaldehyde in experiments where this compound was not injected or formed in the gas-phase reactions.

4.2.1 Quality assurance in use of simulation software for UCR and TVA chamber experiments

The modeling programs and software necessary to conduct model simulations of the UCR and TVA chamber runs using the SAPRC and CB chemical mechanisms were provided by Carter and are distributed at http://www.cert.ucr.edu/~carter/SAPRC/. The program used to simulate the UCR chambers is referred to as the SAPRC software in this work. The SAPRC software was previously adopted for use in box model simulations in Chapter 3 and its application is extended for simulating UCR chamber experiments in this chapter. In order to verify the procedure of adapting the SAPRC software for chamber simulations, chamber simulations performed by Carter were replicated. As shown in Figure 4-9 for simulations of toluene experiments at UCR using the CB05 mechanism, the simulations performed for this study were identical to those performed by Carter.

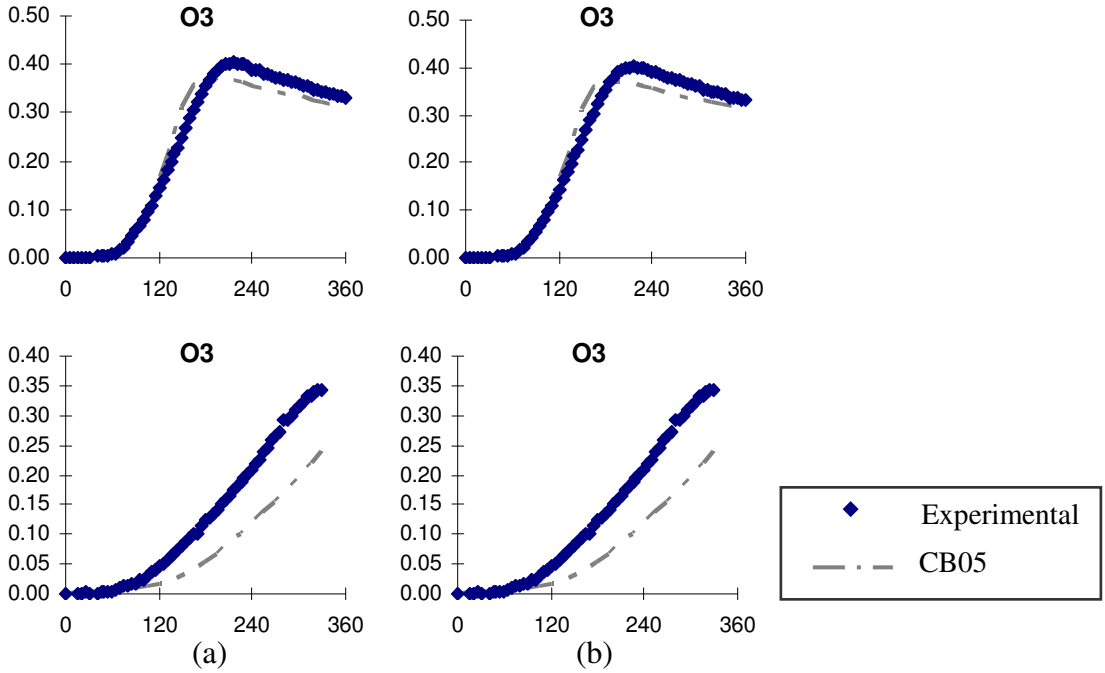

(a) (b)

Figure 4-9. Simulation of UCR toluene chamber experiments (EC266 and EC 340) conducted in the EC chamber using the CB05 mechanism in the SAPRC software by (a) Carter and (b) this study.

4.3 STRUCTURE OF ANALYZING CHAMBER DATA

Chemical mechanisms used in regional photochemical models have three primary elements to their structure: inorganic chemistry, organic chemistry and lumping strategies. The inorganic chemistry components of air quality mechanisms describe the cycling of free radicals, the cycling of oxides of nitrogen and the reactions of products of these reaction cycles. The organic chemistry components of air quality models describe the reactions of the thousands of organic species that are present in the atmosphere. The lumping strategies used by the mechanisms are necessary because not all of the thousands of chemically reacting species can be represented explicitly in the mechanisms. Species are placed into reactivity groups (or lumps) that are assumed to react in similar ways. This lumping is an approximation because most compounds making up a reactivity class have somewhat different reactivities.

In comparing the predictions of chemical mechanisms to chamber data, the concept of a hierarchy of species is used (Whitten, 1983). With this concept, species involved in photochemical oxidant formation are assigned a hierarchical level depending on the number of hydrocarbon/NOx systems in which the species participates. For example, acetaldehyde is a dominant product of the photochemical oxidation of butane/NOx systems. However, little or no butane is formed in the photochemical oxidation of acetaldehyde/NOx systems. Therefore, since acetaldehyde must be included in an explicit mechanism for butane but butane need not be incorporated in an explicit mechanism for acetaldehyde. With this logic, the most ubiquitous species, namely CO, CO_2, NO, NO_2, OH, HO_2, and O_3 are assigned to the lowest hierarchical level, and

species involving more reaction products are assigned higher hierarchical levels. The main advantage of the hierarchical approach to utilizing chamber experiments is that it clarifies the sources of uncertainty in simulations, beginning with simpler photochemical oxidation systems and proceeding to more complex systems.

One of the challenges associated with this hierarchical approach is that experiments at the lower hierarchical levels are not representative of atmospheric conditions, and the different chemical environments of experiments at higher hierarchal levels may change the relative importance of processes that occur at the lower hierarchal levels. For example, experiments without reactive organics (e.g., CO – NOx experiments) generally do not have sufficient reactivity to test portions of the inorganic mechanism that are important under conditions of high reactivity, such as those affecting NOx sinks. Thus, a hierarchical approach has both advantages and disadvantages, but there is likely no better alternative to systematically evaluating mechanisms. The hierarchical scheme used in this study, in order of lowest to highest hierarchical level is as follows (Whitten, 1983):

- Inorganics (e.g., OH+NO_2 in CO systems)
- Formaldehyde and other aldehydes
- Paraffins (e.g., methane)
- Olefins (including the lumping of olefins into compound classes)
- Aromatics (including the lumping of aromatics into compound classes)

4.4 Effect of Wall Mechanism on Simulated Environmental Chamber Experiments

As will be described in this section, the simulations of experiments in environmental chambers have wall-effects corrections. Various chemical species either adsorb to or react with the wall and species adsorbed on the wall. The rate parameters

and stoichiometry for these reactions have not been as extensively studied as homogeneous reactions, and vary from one chamber to another, and therefore the mechanisms are generally tuned to experimental data. These wall effect corrections address the well-established observation that environmental chamber walls can be a source of reactive species, particularly free radicals, as well as a sink for some species. Wall effects are most significant for experiments that have relatively few radical sources in the gas-phase reactions of the species present. These experiments are therefore highly sensitive to radical sources from chamber effects. Examples of such experiments are as alkane - NOx or CO - NOx irradiations. Therefore, mechanisms designed to account for wall effects are generally tuned based on experimental data obtained from low reactivity experiments with few internal radical sources (e.g., CO - NOx experiments).

In this study, the simulations of environmental chamber experiments will include the well-established wall effects corrections developed for each of the chambers from which experimental data are drawn. Comparisons between simulations of chamber experiments and chamber experiments will be done using the appropriate wall mechanisms. Otherwise, the conditions of the experiments are not appropriately simulated. It is important, however, to recognize that when chemical mechanisms are implemented in regional photochemical models, wall mechanisms are not included. Therefore, given that the objective of this study is to provide guidance in the selection of chemical mechanisms to be used in regional air quality modeling, it is important to characterize the effects that might be expected when a mechanism is used in CAMx simulations, without wall effects

This section examines the overall magnitudes of the wall effect corrections and the chemical pathways most strongly affected by the wall chemistry. In addition, the sensitivity of predicted concentrations to the choice of wall mechanism will be probed.

4.4.1 Effect of wall mechanism on chamber simulations: Overview

The latest version of the UNC wall mechanism provided by Whitten, available in Appendix C, requires the PNA (HNO_4) chemistry of SAPRC99, CB-IV, and CB05. This chemistry is deactivated by ENVIRON in the CAMx (Comprehensive Air Quality Model, with extensions, www.camx.com) version of the mechanisms due to its lack of significance in tropospheric chemistry as well as its computational burden. In order to utilize the wall mechanism for the UNC chamber simulations, however, the PNA chemistry in the three mechanisms must be activated. Therefore, in addition to evaluating the effect of the wall mechanism, the effect of separately activating the PNA chemistry was studied. The PNA chemistries activated for each mechanism for comparison with chamber experiments are listed in Appendix C.1. The PNA chemistry for CB05 was used for CB-IV. For SAPRC99, the PNA chemistry in the base mechanism of SAPRC99, listed in Appendix C, was used. The three scenarios evaluated in the simulation of these experiments are as follows:

- Active wall mechanism and PNA chemistry, labeled “wall on PNA on”.
- Inactive wall mechanism but active PNA chemistry, labeled “wall off PNA on”.
- Inactive wall mechanism and PNA chemistry, labeled “wall off PNA off”.

Characterization of wall effects for experiments using CO and formaldehyde as a reactant have been performed by other members of our research group, and are described in an Appendix to this Chapter (Appendix D). The chamber experiments involving CO have demonstrated that for low reactivity experiments, the effects of the wall mechanisms are large and that the wall mechanism corrects the predictions so that the agreement between simulation and experiment is reasonable.

4.4.2 Effect of wall mechanism on UNC chamber simulations: Olefin experiments

Since the conditions of most interest in CAMx simulations of the Houston region are those with high reactivity, the effect of wall mechanisms on simulation predictions was also examined for UNC chamber experiments with high reactivity, specifically, chamber experiments involving olefins. The chamber experiments considered are listed in Table 4-1.

Table 4-1. UNC ethylene and propylene environmental chamber experiments.

Experiment		VOC	NOx
AU2497	Red	3.84 ppmC Ethylene	0.321 ppm
	Blue	3.68 ppmC Ethylene	0.318 ppm
ST1995	Red	6.12 ppmC Propylene	0.67 ppm
JN2392	Red	0.908 ppmC Propylene	0.384 ppm
	Blue	0.907 ppmC Propylene	0.384 ppm
JN1798	Red	1.737 ppmC Propylene	0.492 ppm

For these experiments, the affect of the PNA chemistry on simulated species concentrations was examined by comparing the scenario in which the wall mechanism is deactivated, but the PNA chemistry is active, to the simulation in which the PNA chemistry and the wall mechanism are inactive. Additional comparisons were done between simulations in which the wall mechanism and PNA chemistry are activated, to the simulation in which the PNA chemistry and the wall mechanism are inactive. Results from ethylene and propylene simulations evaluating the effects of the wall mechanism and PNA chemistry are shown in Figures 4-10 – 4-15.

In the AU2497 ethylene experiments and the ST1995 propylene experiment, the affect of the PNA chemistry is by far dominated by the affect of the wall mechanism on

simulated ozone concentrations. In the JN2392 and JN1798 propylene experiments, the PNA chemistry alone does not affect the simulated ozone concentrations. Since for these ethylene and propylene chamber experiments, the effect of the PNA chemistry on the simulated ozone concentrations of the mechanisms is dominated by the effect of the wall mechanism, further analysis will focus on the affect of the wall mechanism. Specifically, further analysis focuses on the comparison of the two scenarios: when both the wall mechanism and PNA chemistry are active and when both the wall mechanism and PNA chemistry are deactivated.

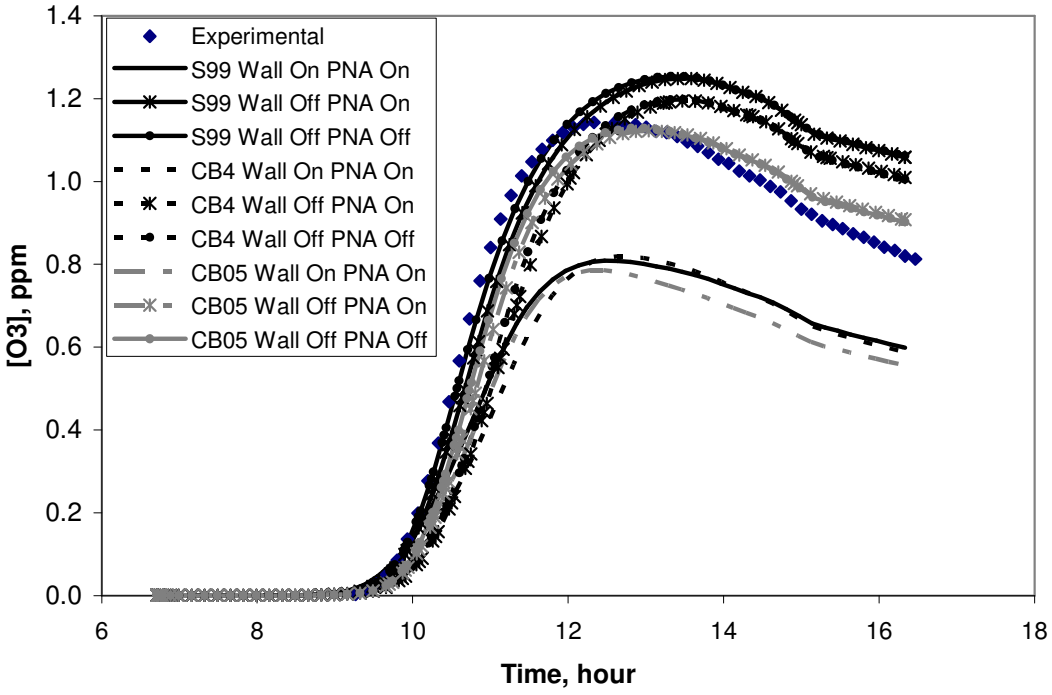

Figure 4-10. O_3 in AU2497 UNC red chamber experiment with 3.84 ppmC ethylene.

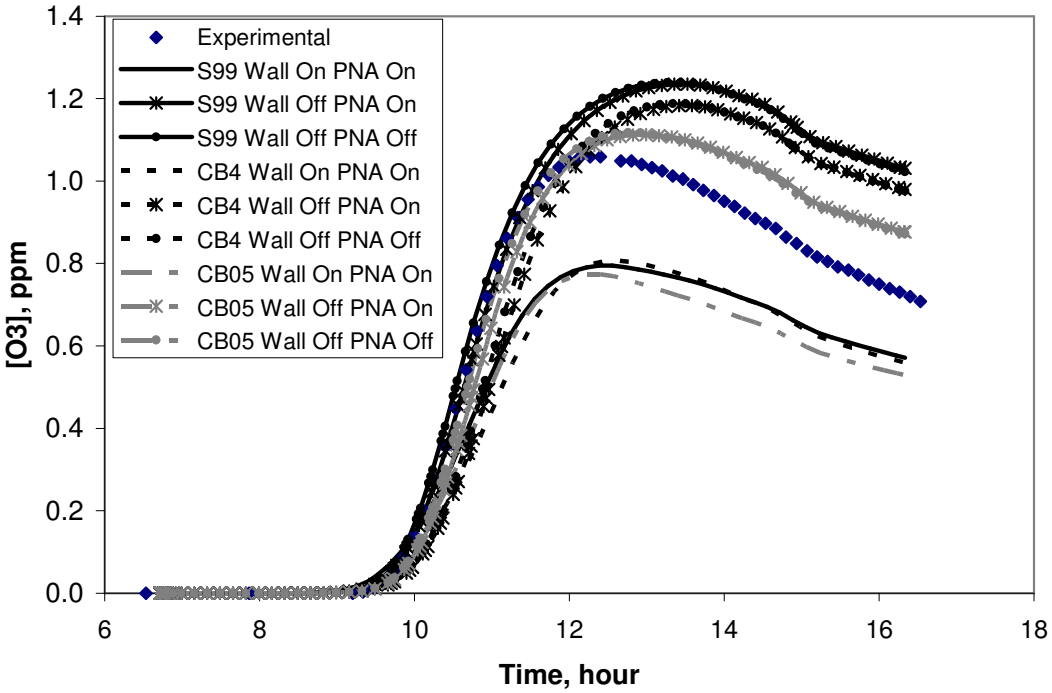

Figure 4-11. O_3 in AU2497 UNC blue chamber experiment with 3.68 ppmC ethylene.

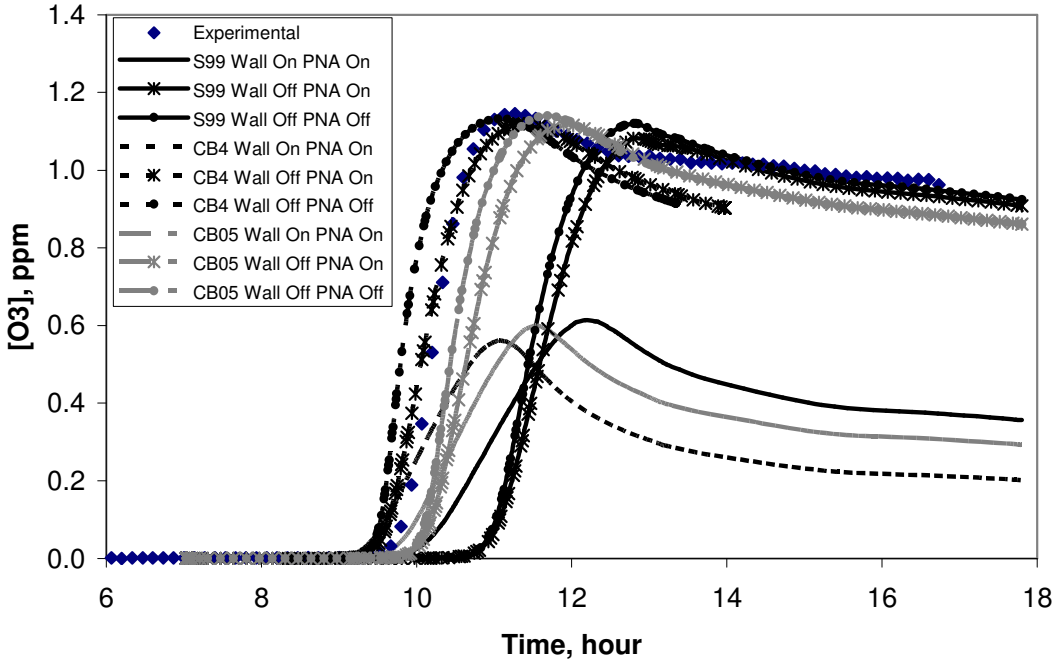

Figure 4-12. O_3 in ST1995 UNC red chamber experiment with 6.12 ppmC propylene.

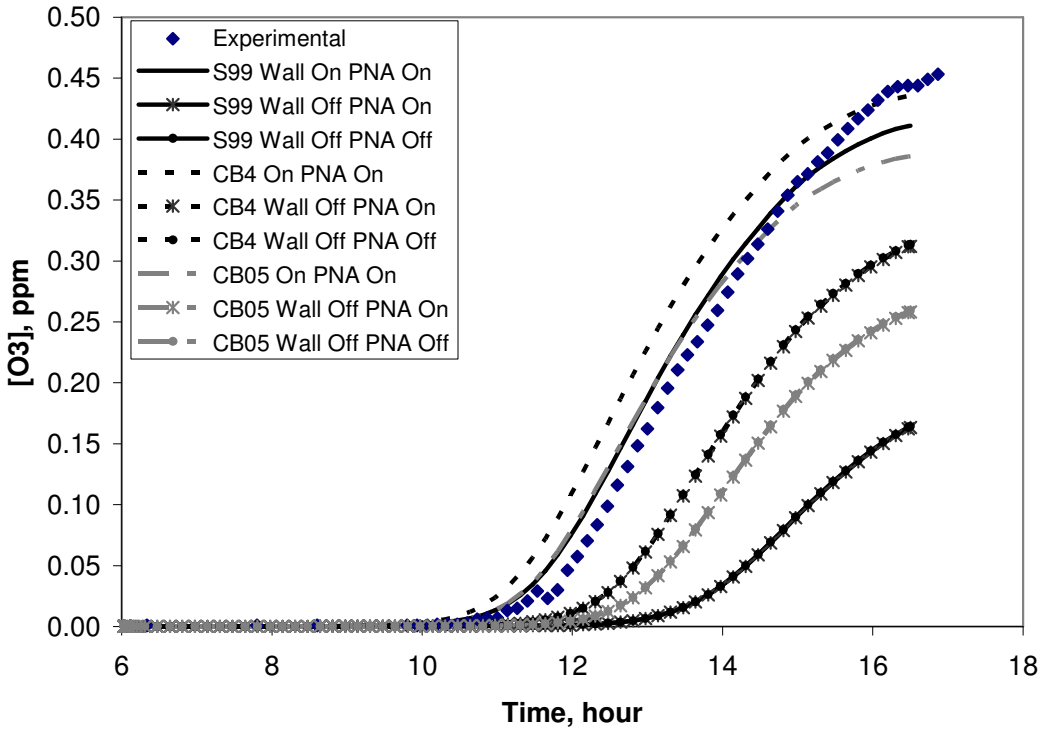

Figure 4-13. O_3 in JN2392 UNC red chamber experiment with 0.908 ppmC propylene.

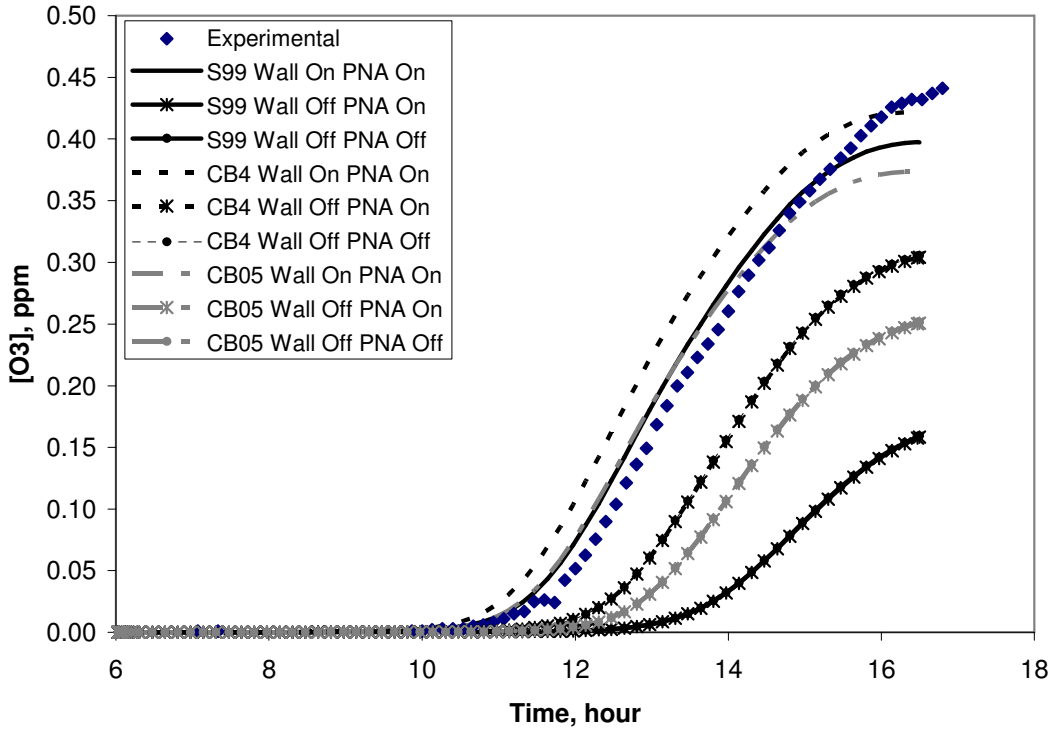

Figure 4-14. O_3 in JN2392 UNC blue chamber experiment with 0.907 ppmC propylene.

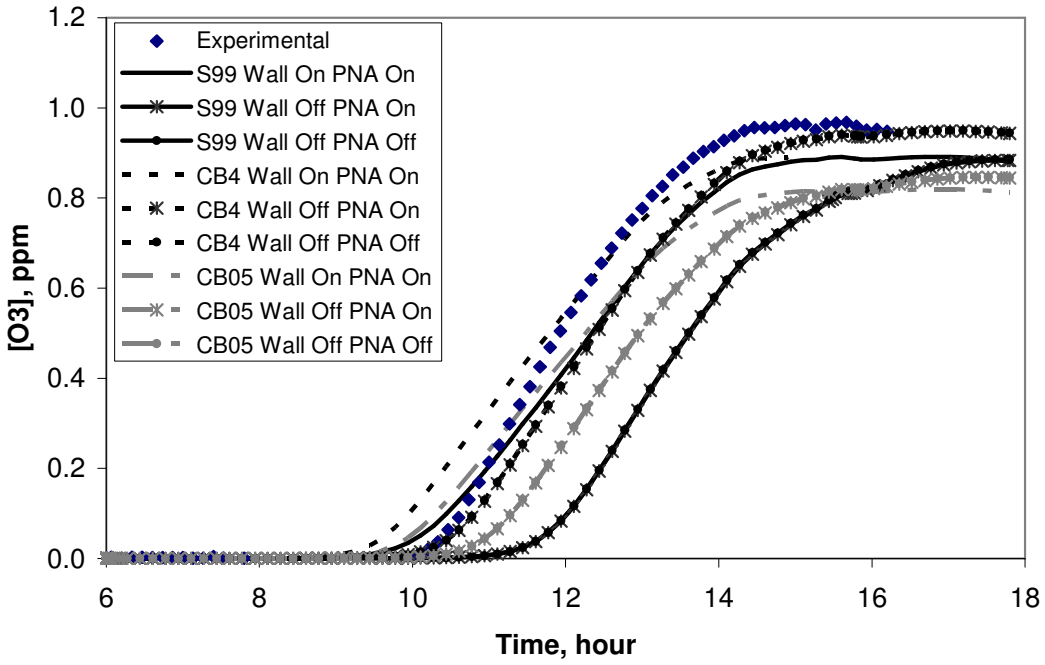

Figure 4-15. O_3 in JN1798 UNC red chamber experiment with 1.737 ppmC propylene.

Figures 4-10 and 4-11 illustrate that activating the wall mechanism reduces the simulated ozone concentrations relative to simulations with the wall mechanism off in the ethylene experiments. In the ST1995 propylene experiment in Figure 4-12, the wall mechanism reduces the ozone concentrations relative to simulations with the wall mechanism off. However, in the JN2392 and JN1798 propylene experiments (Figures 4-13, 4-14 and 4-15) the wall mechanism increases propylene concentrations. This decreases in ozone concentration in ST1995 are surprising, since generally the walls are viewed as regarded as a free radical source. A possible explanation of the behavior of the mechanisms was identified. Figures 4-16 – 4-19 and Figures 4-20 – 4-23 show the concentrations of measured and simulated NO and NO_2 concentrations, respectively, in the three propylene experiments. Activating the wall mechanism leads to a faster

depletion of NO and a faster production of NO_2 in all three propylene experiments relative to simulations with the wall mechanism deactivated. The concentration of NO in the beginning of the ST1995 experiment is higher, followed by faster depletion, relative to the other two propylene experiments. Similarly, the peak of NO_2 concentration is higher in the ST1995 experiment. So, the wall mechanism, as a NOx sink, may be causing the increases and decreases in ozone predictions in experiments with differing NOx availability.

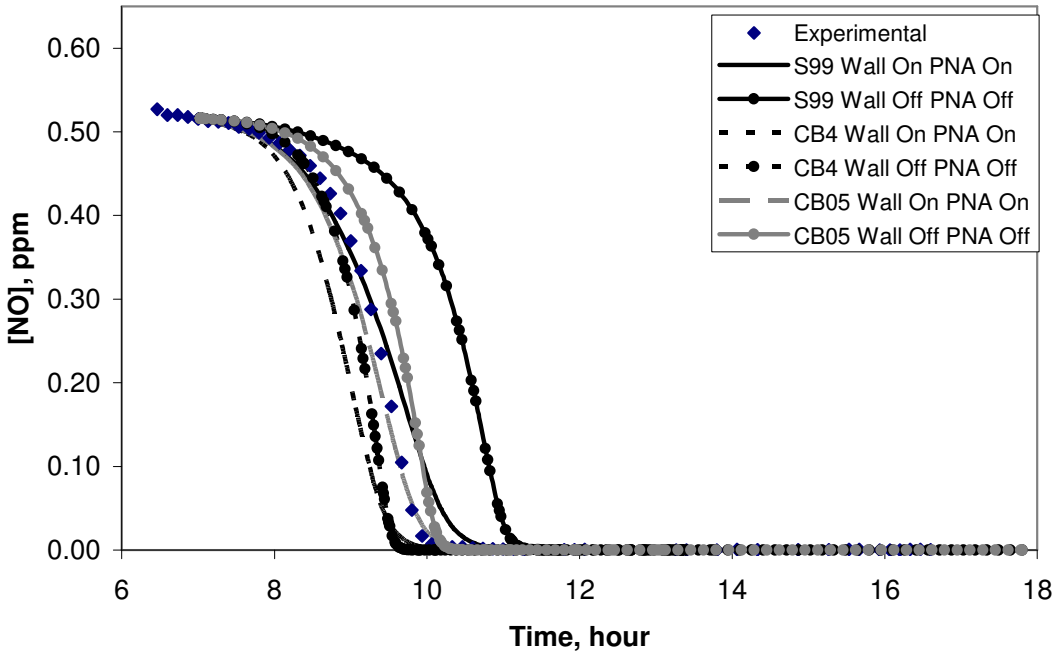

Figure 4-16. NO in ST1995 UNC red chamber experiment with 6.12 ppmC propylene.

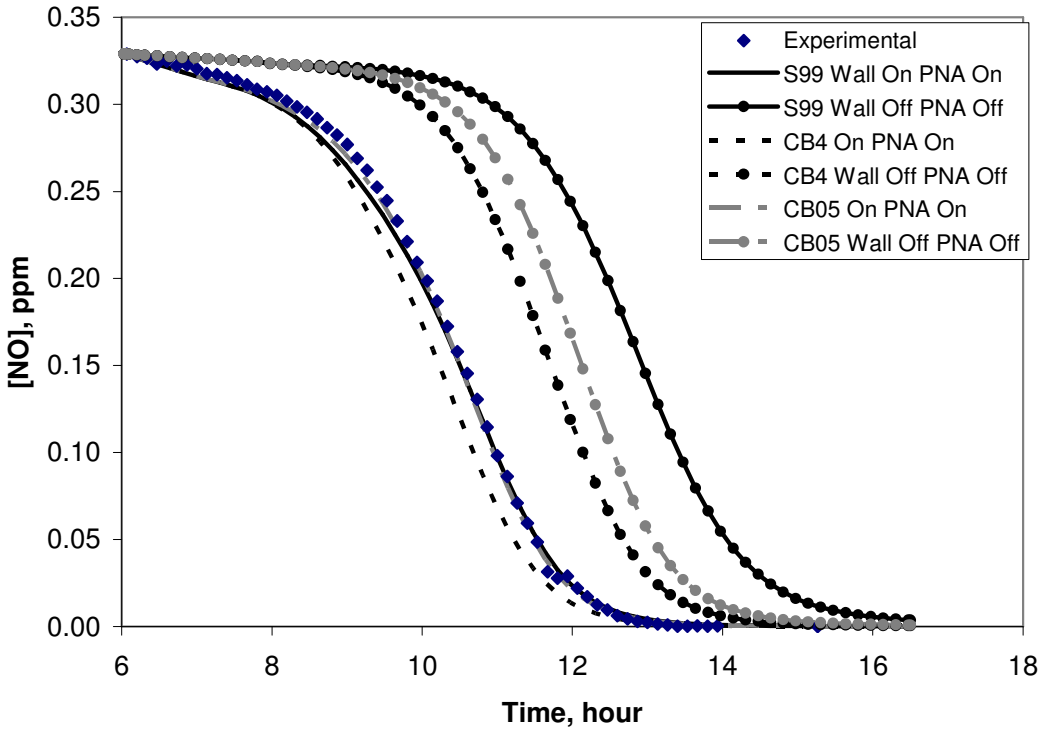

Figure 4-17. NO in JN2392 UNC red chamber experiment with 0.908 ppmC propylene.

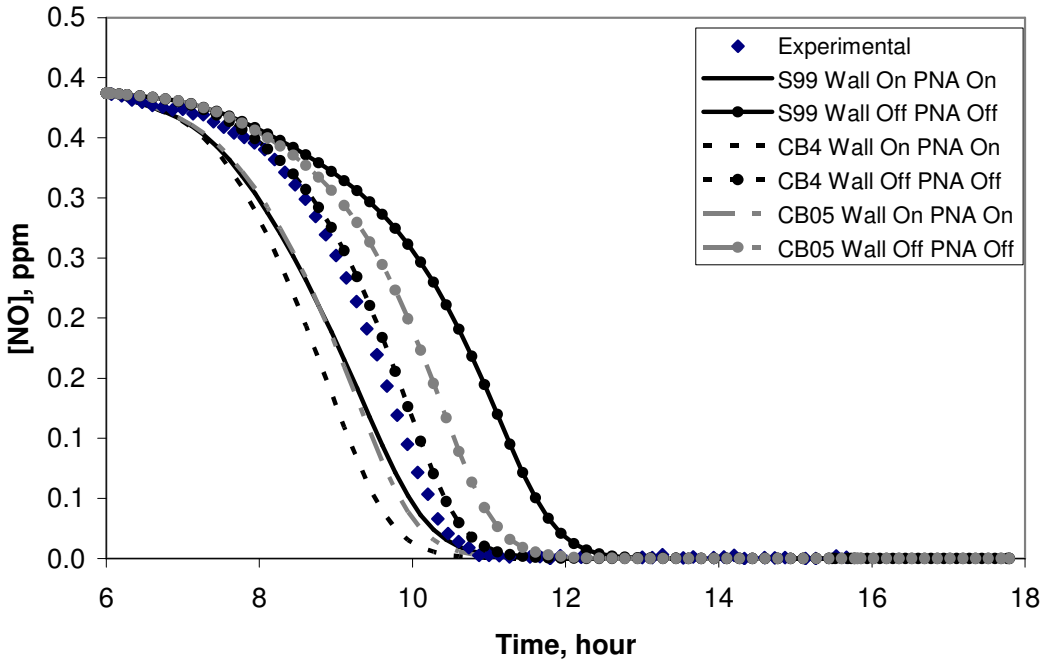

Figure 4-18. NO in JN1798 UNC red chamber experiment with 1.737 ppmC propylene.

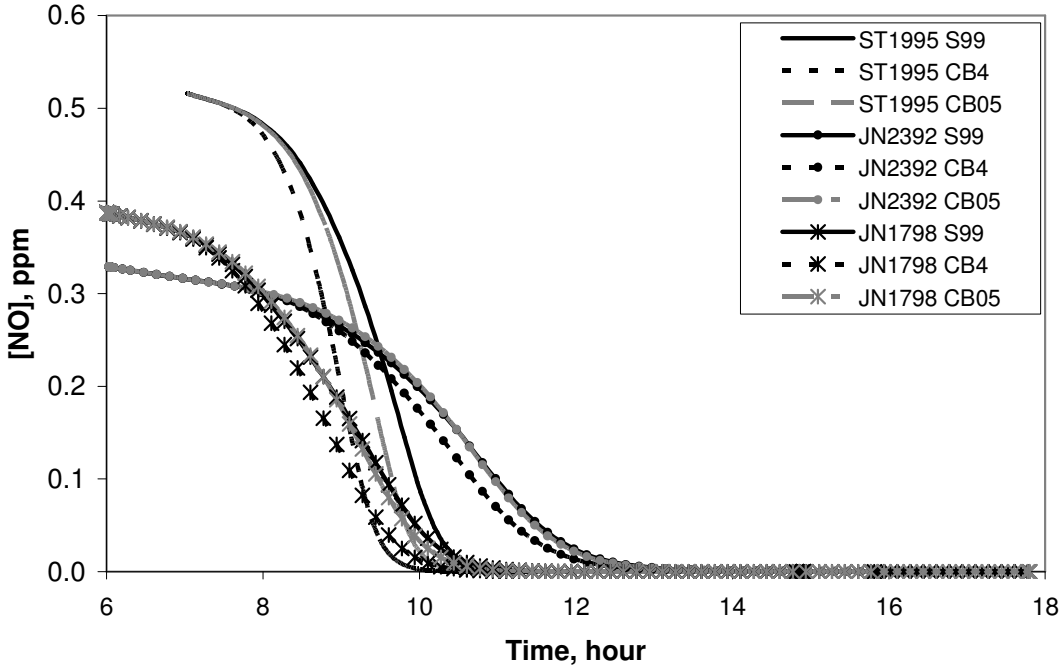

Figure 4-19. NO comparison among three propylene experiments with activated wall mechanism and PNA (HNO_4) chemistry.

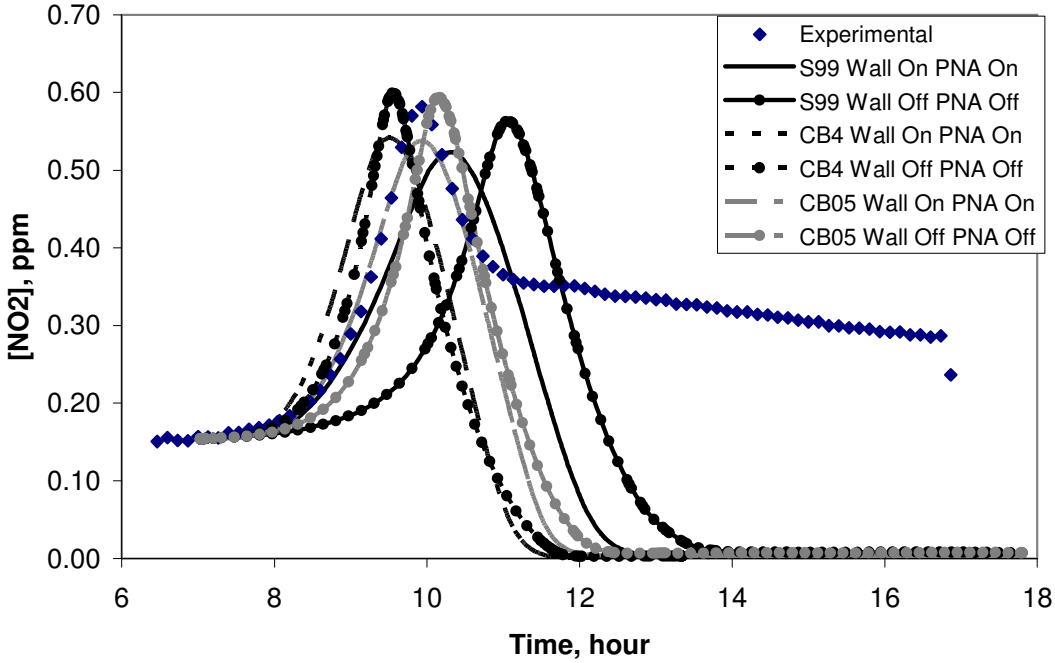

Figure 4-20. NO_2 in ST1995 UNC red chamber experiment with 6.12 ppmC propylene.

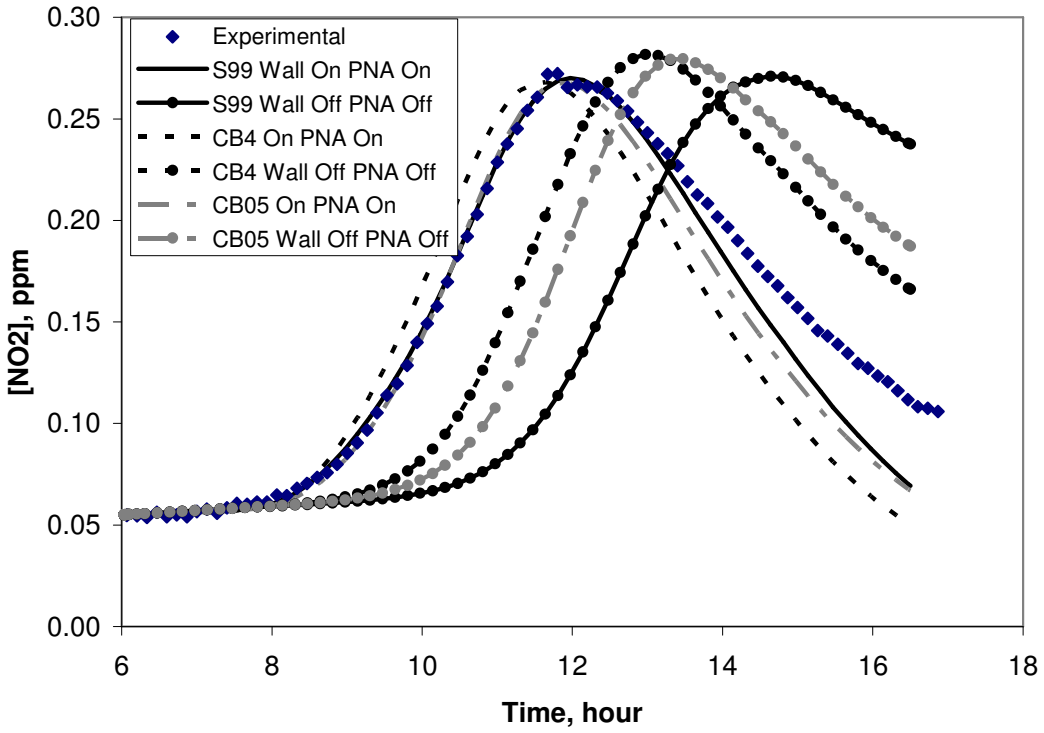

Figure 4-21. NO_2 in JN2392 UNC red chamber experiment with 0.908 ppmC propylene.

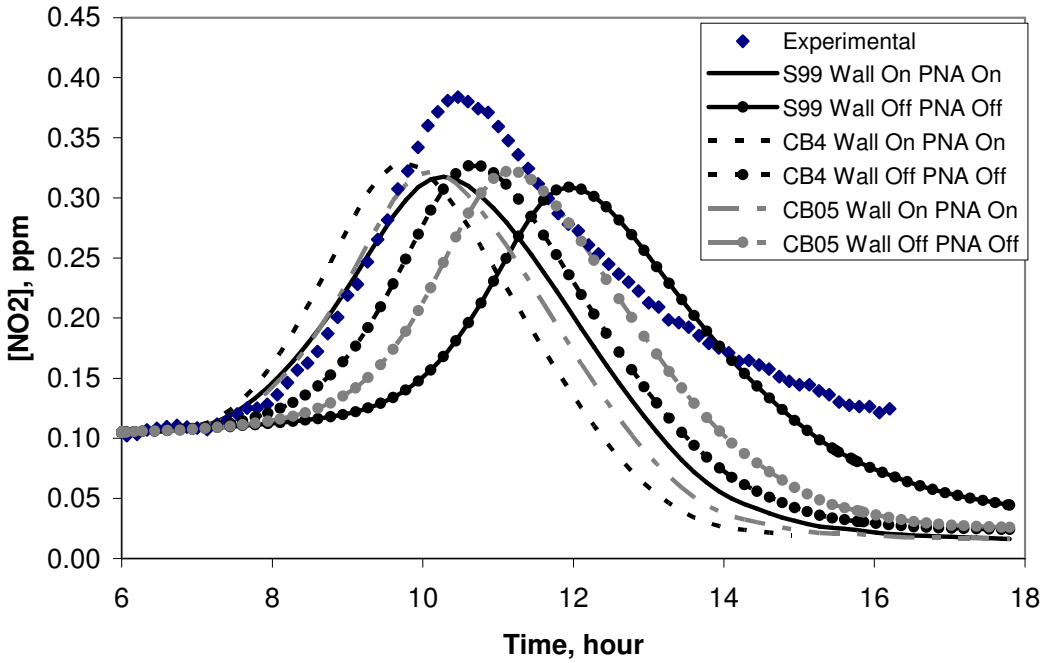

Figure 4-22. NO_2 in JN1798 UNC red chamber experiment with 1.737 ppmC propylene.

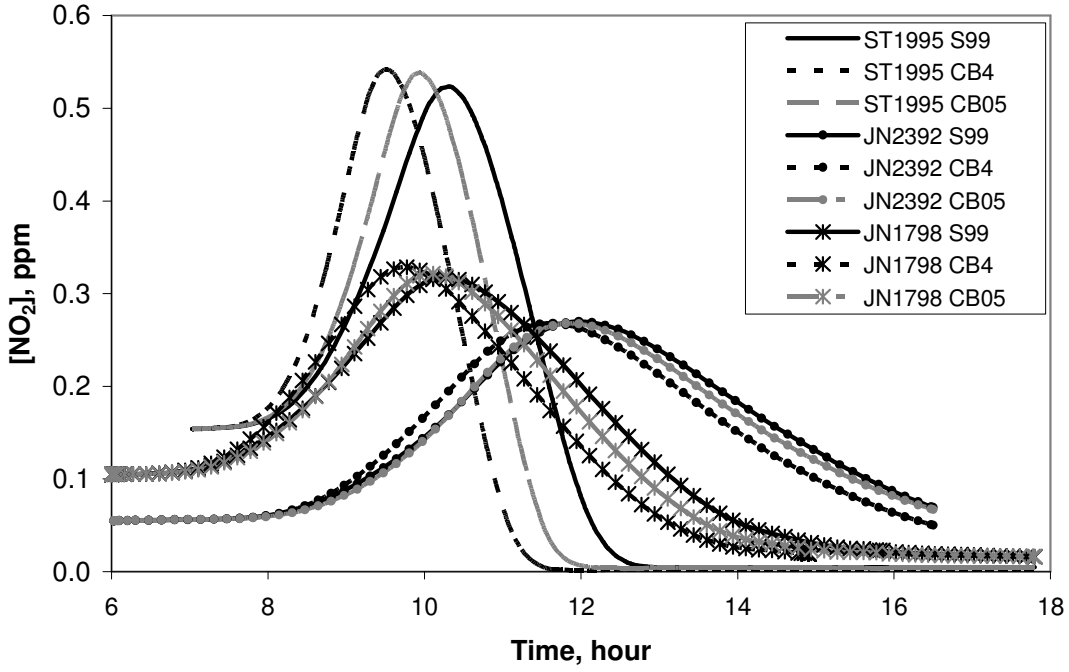

Figure 4-23. NO_2 comparison among three propylene experiments with activated wall mechanism and PNA (HNO4) chemistry.

In order to distinguish the depletion of NOx due to homogeneous chemistry losses from the depletion of NOx due to the wall mechanism, the evolution of total NOy, defined as the sum of NO, NO_2, and HNO_3, is presented in Figures 4-24 – 4-26. In the three propylene experiments, the predictions of NOy are lower when the wall mechanism (and PNA chemistry) is activated. Furthermore, as shown in Figure 4-27, the NOy in the ST1995 experiment is depleted at a faster rate relative to the other two propylene experiments. The ST1995 propylene experiment (6.12 ppmC Propylene and 0.67 ppm NOx) exhibits a high reactivity/NOx ratio, making the ozone formation chemistry NOx-limited. In comparison, the JN2392 and JN1798 propylene experiments are not inhibited

by NOx availability. The wall mechanism reduces the availability of NOx in these experiments, thereby inhibiting ozone formation in the ST1995 experiment.

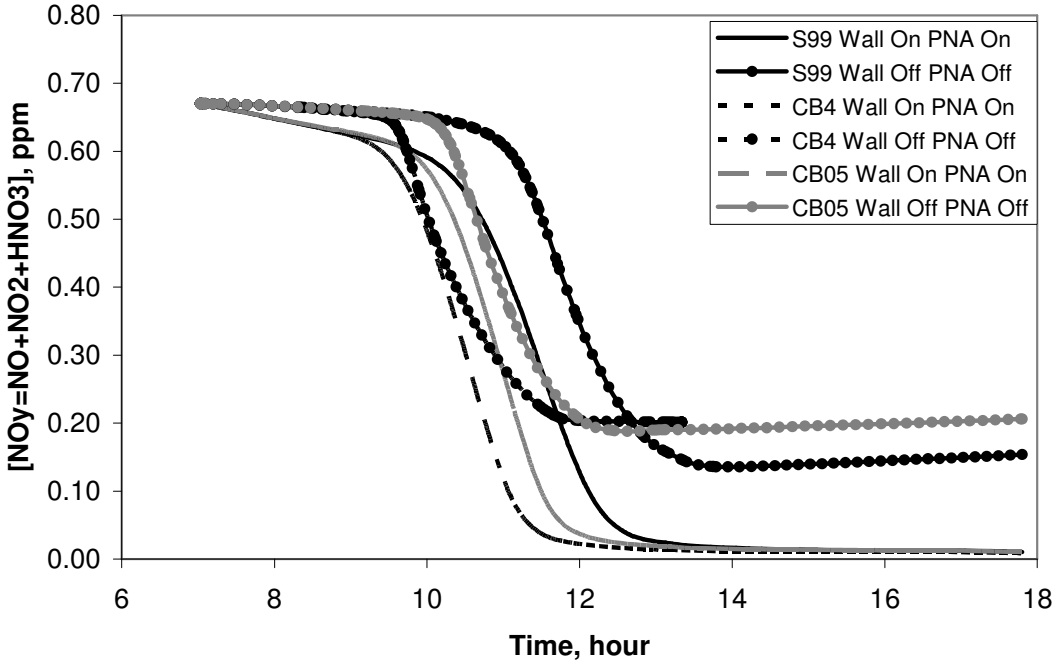

Figure 4-24. NOy in ST1995 UNC red chamber experiment with 6.12 ppmC propylene.

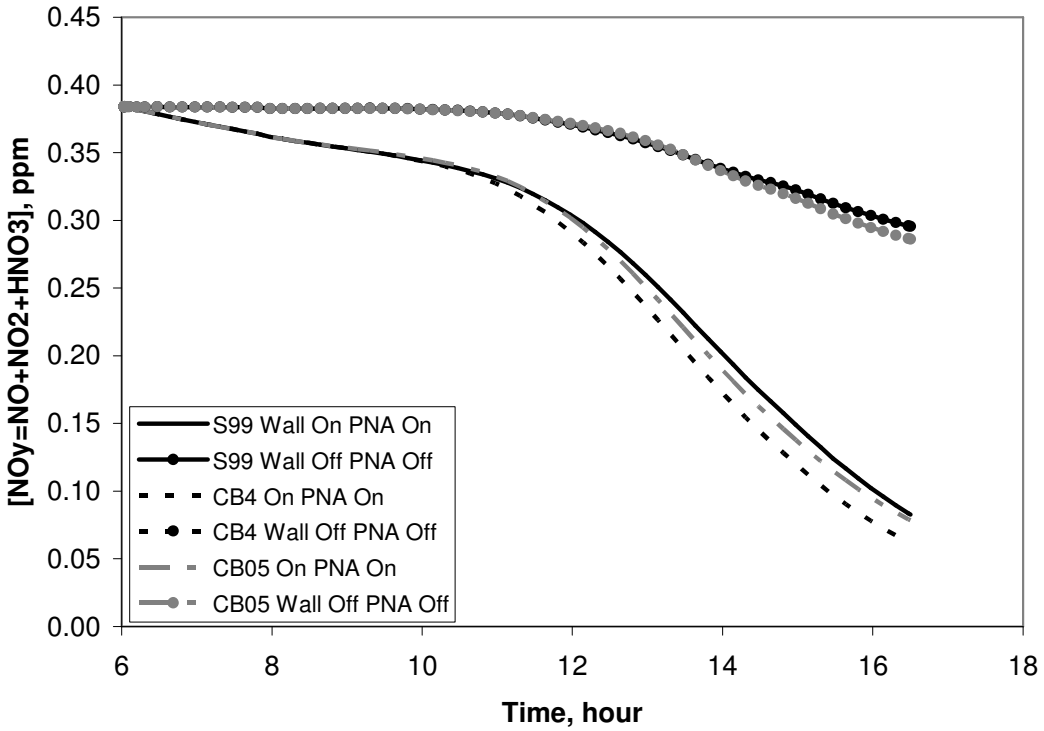

Figure 4-25. NOy in JN2392 UNC red chamber experiment with 0.908 ppmC propylene.

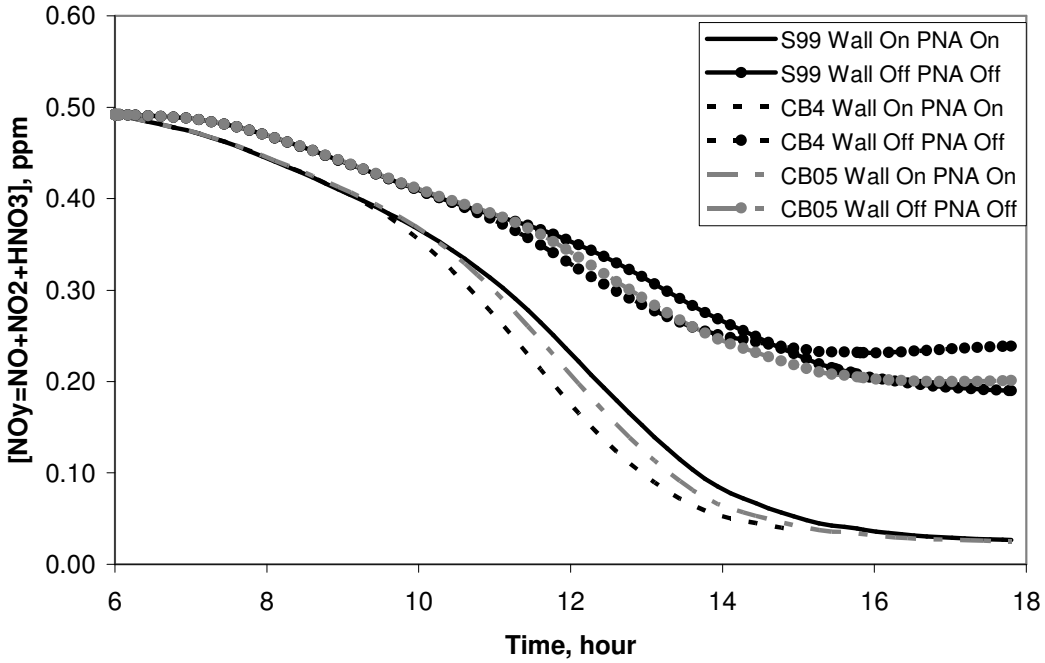

Figure 4-26. NOy in JN1798 UNC red chamber experiment with 1.737 ppmC propylene.

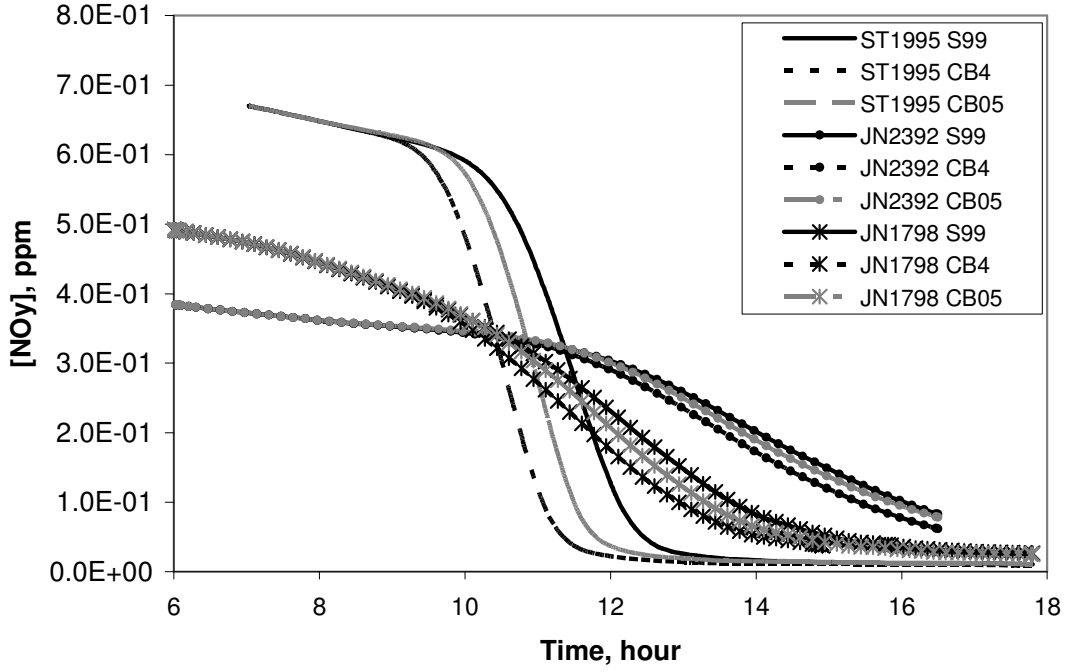

Figure 4-27. NOy comparison among three propylene experiments with activated wall mechanism and PNA (HNO4) chemistry.

In addition to ozone, propylene concentrations also respond differently to the wall mechanisms in the three propylene experiments. In the ST1995 propylene experiment, the response of the CB and SAPRC99 mechanisms vary, with the propylene concentrations increasing with the wall mechanism on in CB and decreasing with the wall mechanism on in SAPRC99. In the JN2392 and JN1798 experiments, however, the mechanisms predict consistently lower propylene concentrations with the wall mechanism activated. The concentrations of propylene in these experiments are shown in Figures 4-28 – 4-30. Concentrations of propylene among the three propylene experiments when the wall mechanism and PNA chemistry are activated are compared in Figure 4-31.

The consumption rate of propylene in the simulated ST1995 experiment is higher than in the other two simulated propylene experiments.

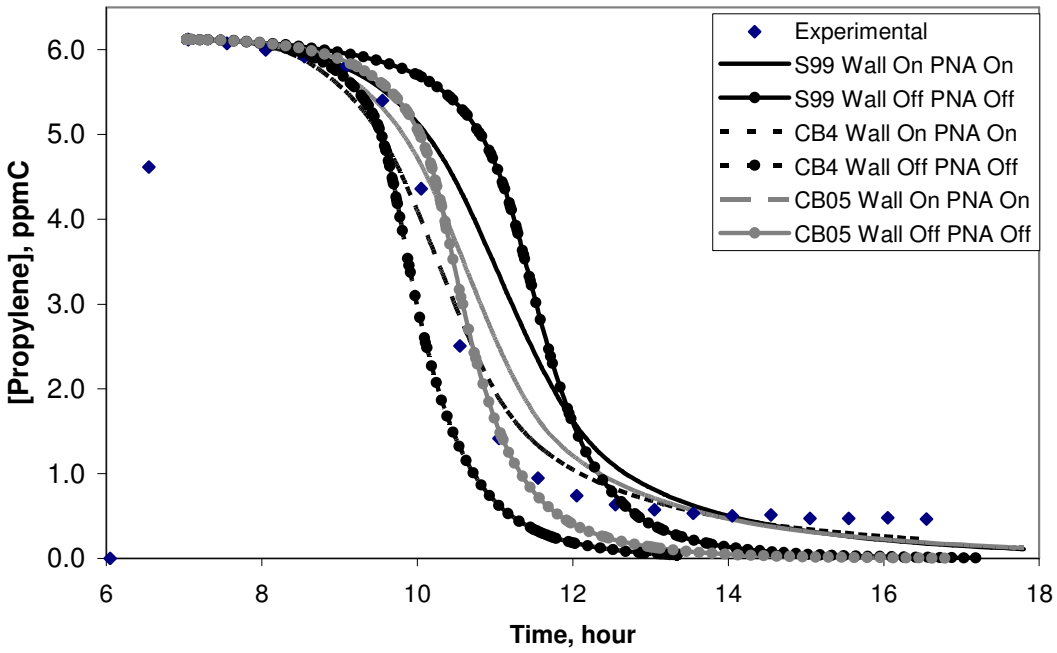

Figure 4-28. Propylene in ST1995 UNC red chamber experiment with 6.12 ppmC propylene.

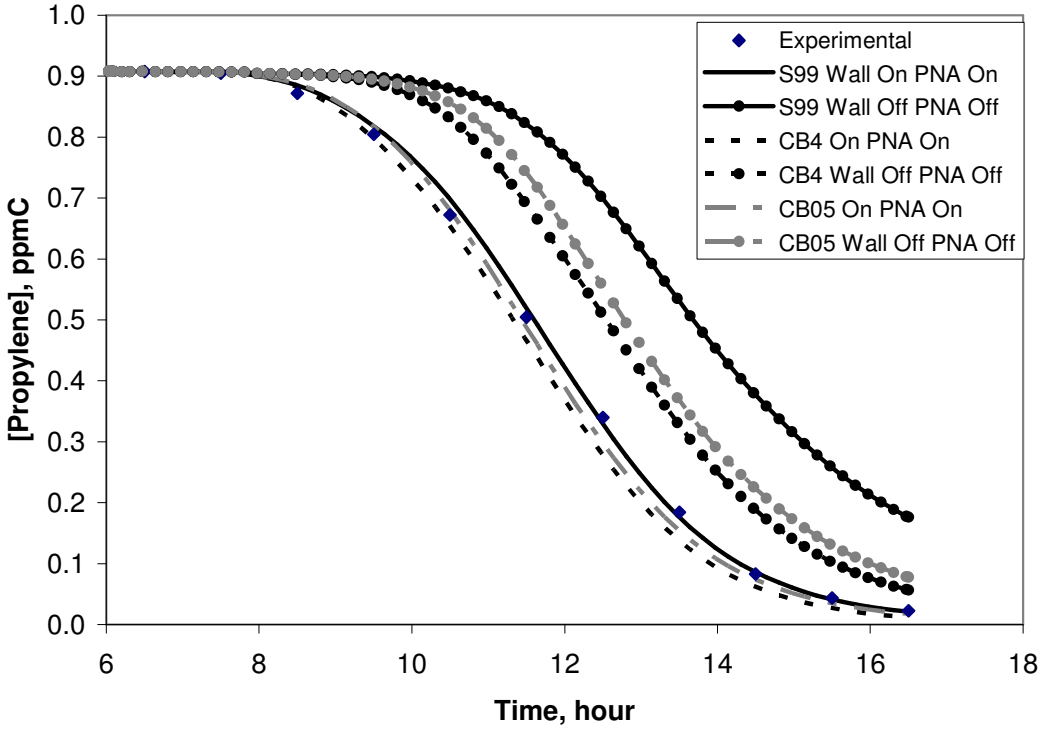

Figure 4-29. Propylene in JN2392 UNC red chamber experiment with 0.908 ppmC propylene.

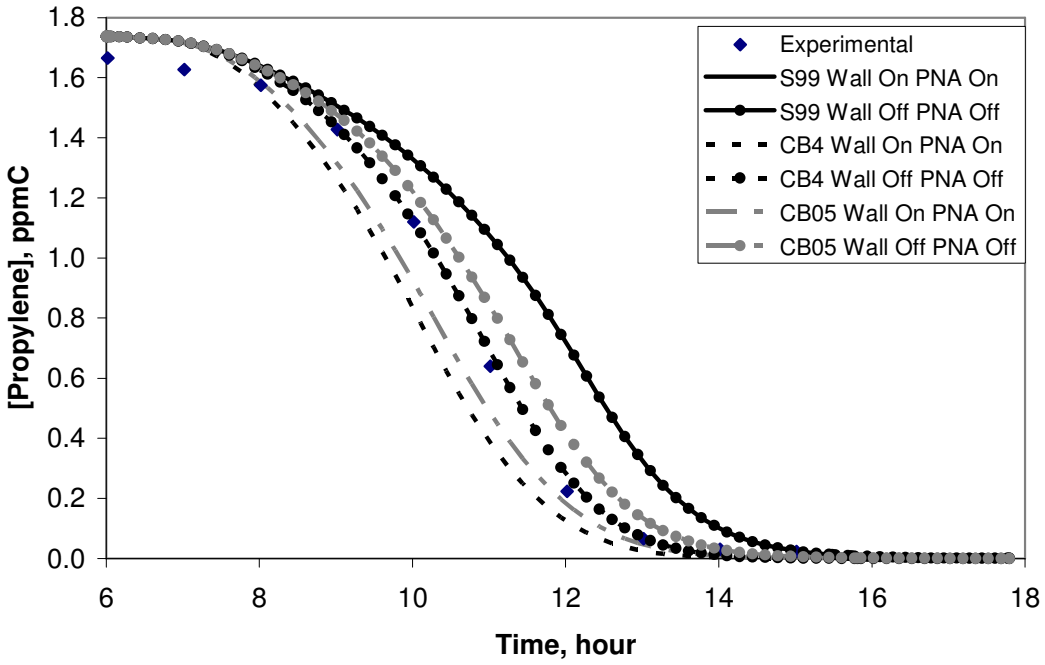

Figure 4-30. Propylene in JN1798 UNC red chamber experiment with 1.737 ppmC propylene.

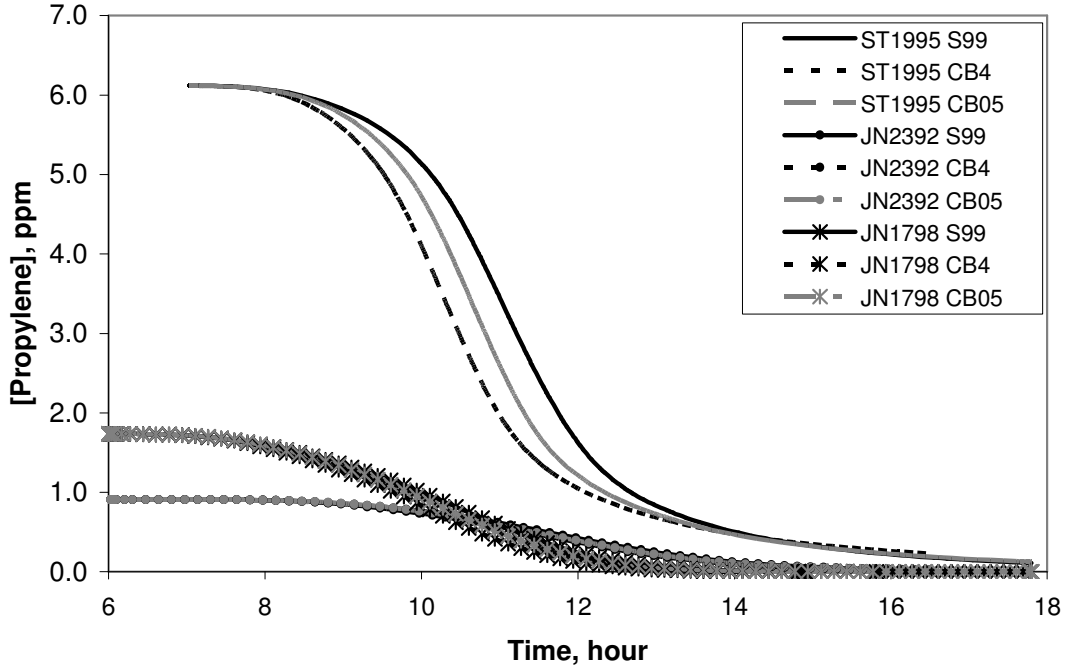

Figure 4-31. Propylene comparison among three propylene experiments with activated wall mechanism and PNA (HNO_4) chemistry.

Figures 4-32 and 4-33 compare the concentrations of OH and HO_2 among the three propylene experiments when the wall and PNA chemistry are activated. The high depletion rate of NOx species in the ST1995 experiment in turn reduces the OH availability in the ST1995 experiment. The HO_2 concentrations are higher in the ST1995 experiment relative to the other two propylene experiments. Furthermore, Figure 4-34 illustrates that the availability of NO_3 in the ST1995 is lower than the other two experiments when the wall mechanism is activated. The sudden drops and peaks in the radical concentrations in the figures may be due to sudden changes in sunlight.

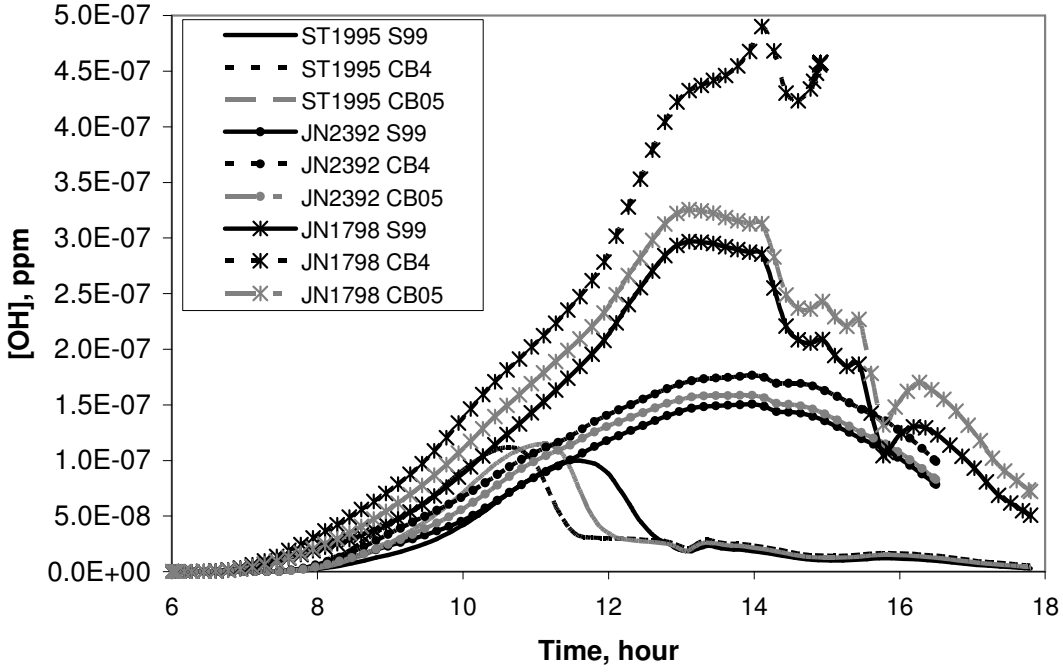

Figure 4-32. OH comparison among three propylene experiments with activated wall mechanism and PNA (HNO_4) chemistry.

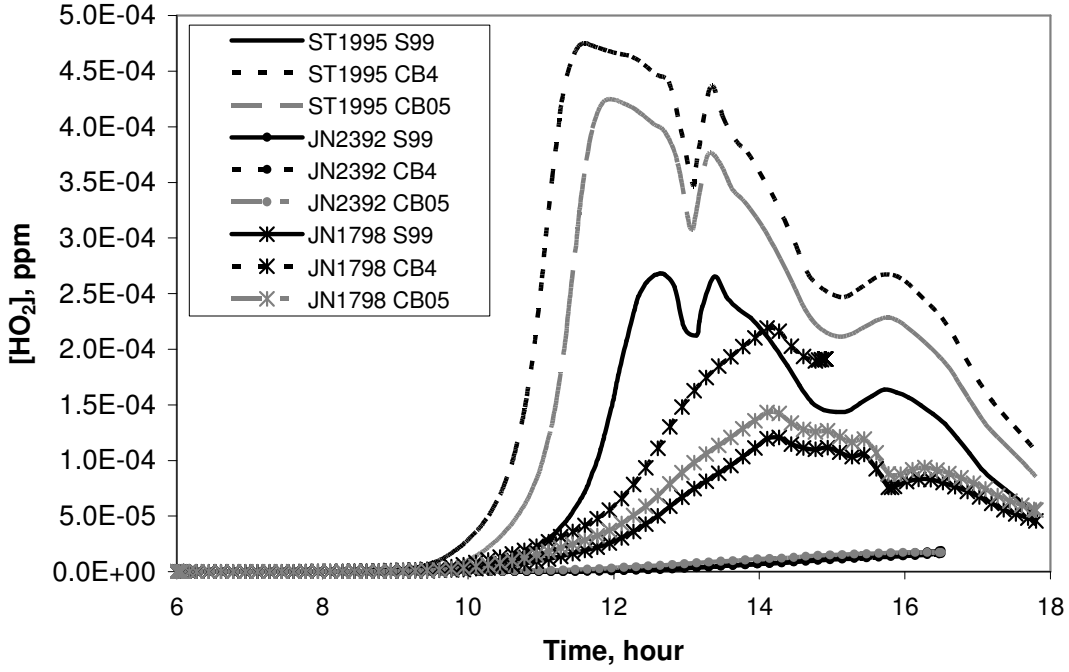

Figure 4-33. HO_2 comparison among three propylene experiments with activated wall mechanism and PNA (HNO_4) chemistry.

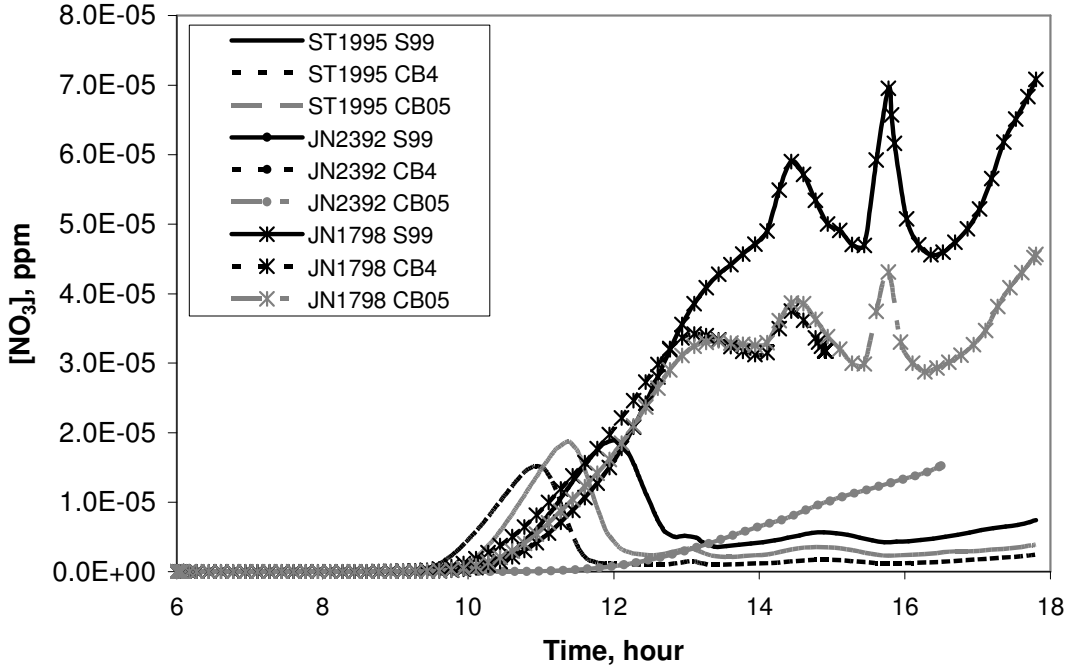

Figure 4-34. NO_3 comparison among three propylene experiments with activated wall mechanism and PNA (HNO_4) chemistry.

Figures 4-35 - 4-37 and Figures 4-39 - 4-41 show the concentrations of HONO and HNO_3 in the propylene experiments, respectively. In all three mechanisms, simulations with activated wall mechanism lead to higher concentrations of HONO and lower concentrations of HNO_3 relative to simulations with the wall mechanism deactivated. Furthermore, comparison among the three propylene experiments with the wall mechanism activated shows that a higher peak of HONO (Figure 4-38) and HNO_3 (Figure 4-42) is reached in the ST1995 experiment, followed by a faster consumption of these two species relative to the other two propylene experiments.

The higher levels of HONO in the simulations with the wall model is due to the wall model including sources of HONO from wall processes. This is included in the UCR

chamber wall models as well, because it is used to explain the chamber radical source. The lower levels of HNO_3 and its rapid consumption is due to the wall model including rapid losses of HNO_3 to the walls. However, the loss of HNO_3 to the walls does not, by itself, affect simulation results significantly because gas-phase HNO_3 is relatively unreactive.

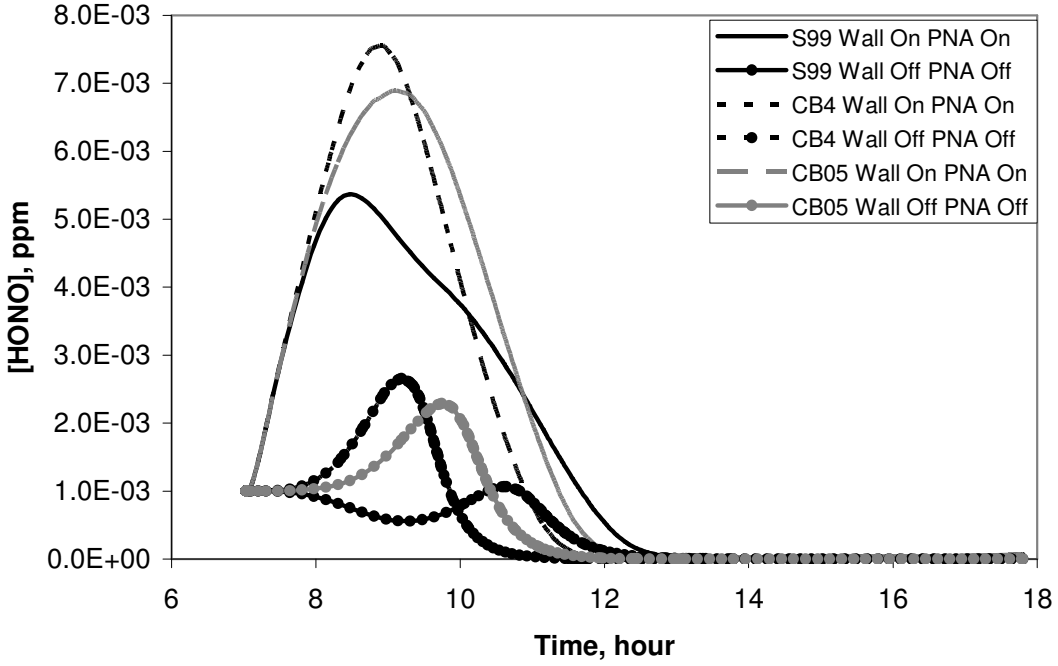

Figure 4-35. HONO in ST1995 UNC red chamber experiment with 6.12 ppmC propylene.

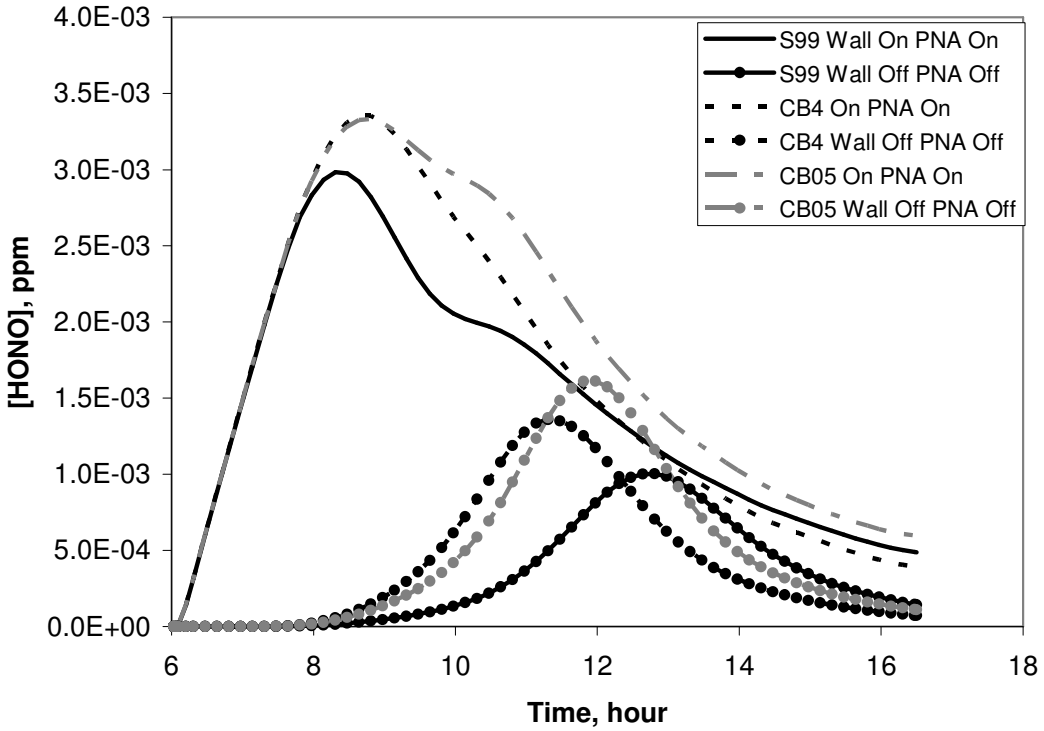

Figure 4-36. HONO in JN2392 UNC red chamber experiment with 0.908 ppmC propylene.

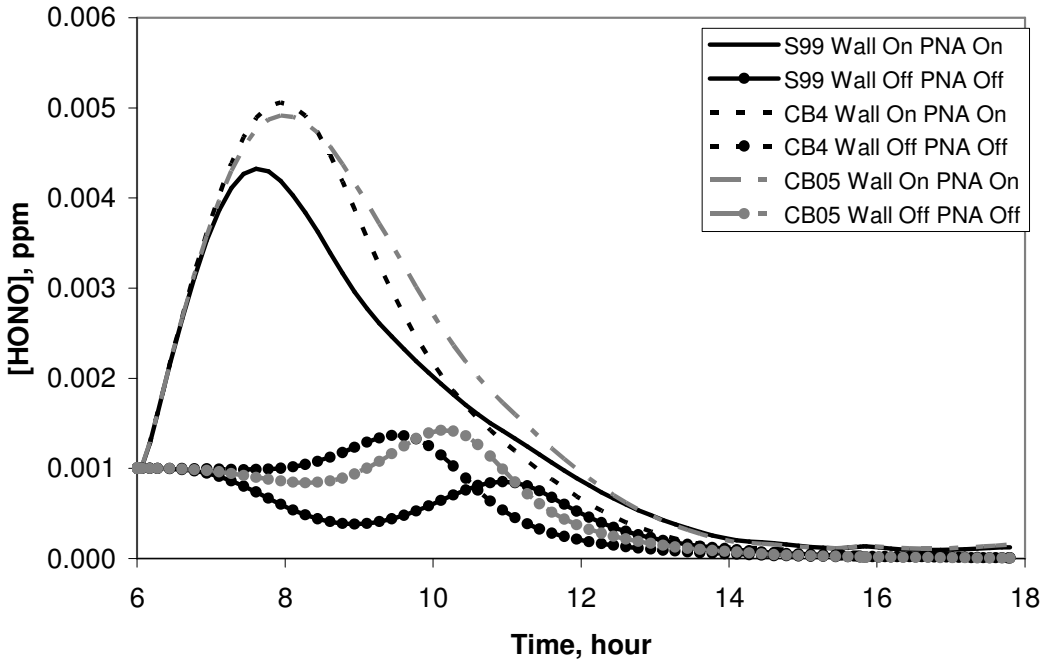

Figure 4-37. HONO in JN1798 UNC red chamber experiment with 1.737 ppmC propylene.

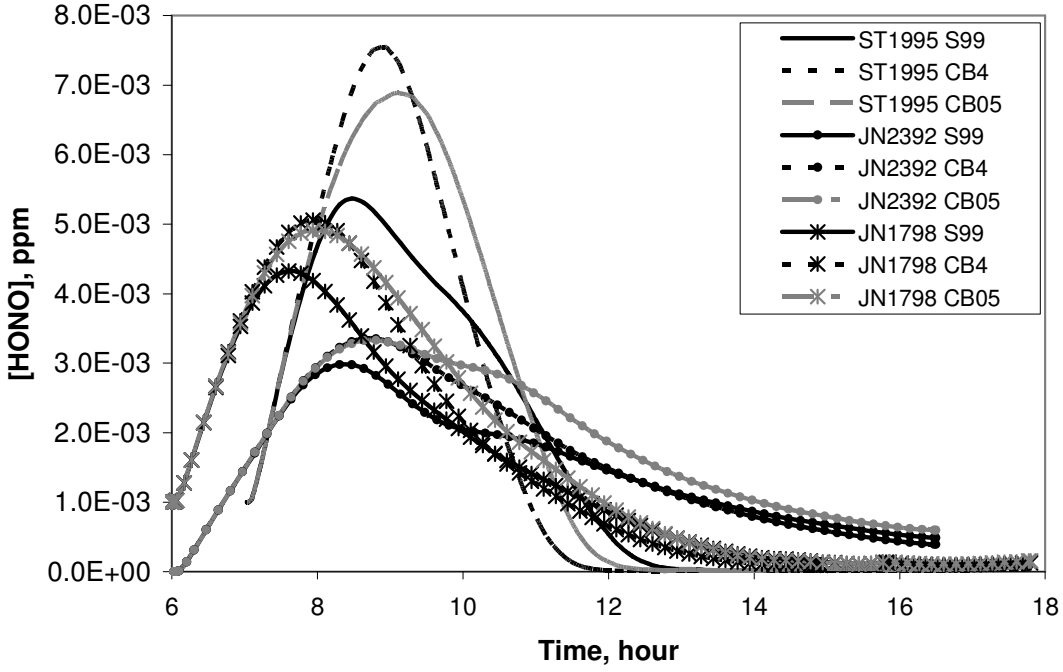

Figure 4-38. HONO comparison among three propylene experiments with activated wall mechanism and PNA (HNO4) chemistry.

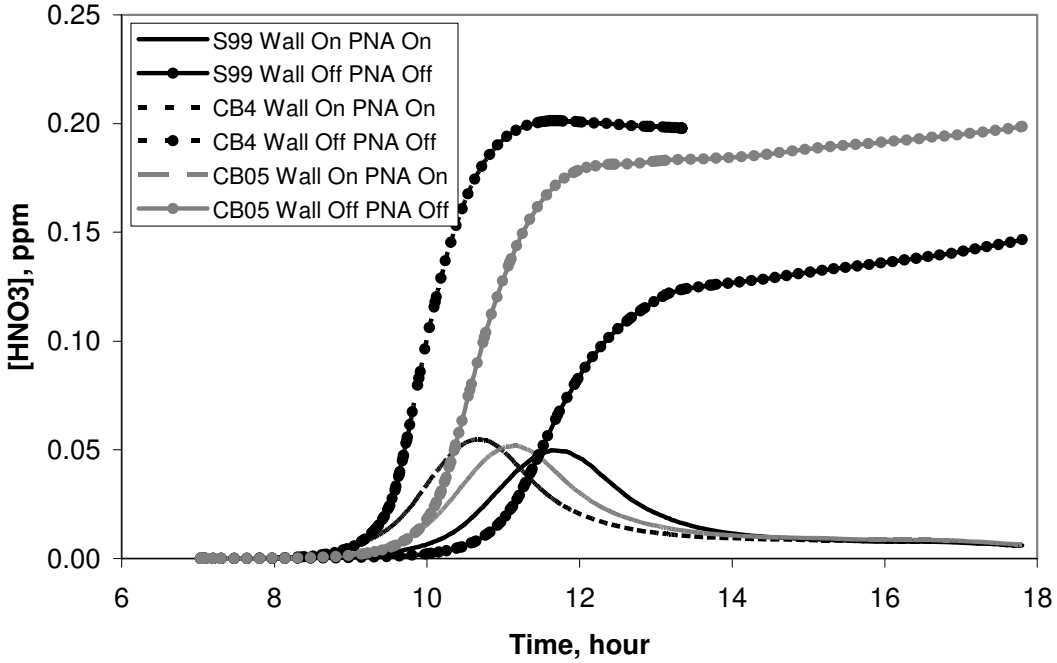

Figure 4-39. HNO_3 in ST1995 UNC red chamber experiment with 6.12 ppmC propylene.

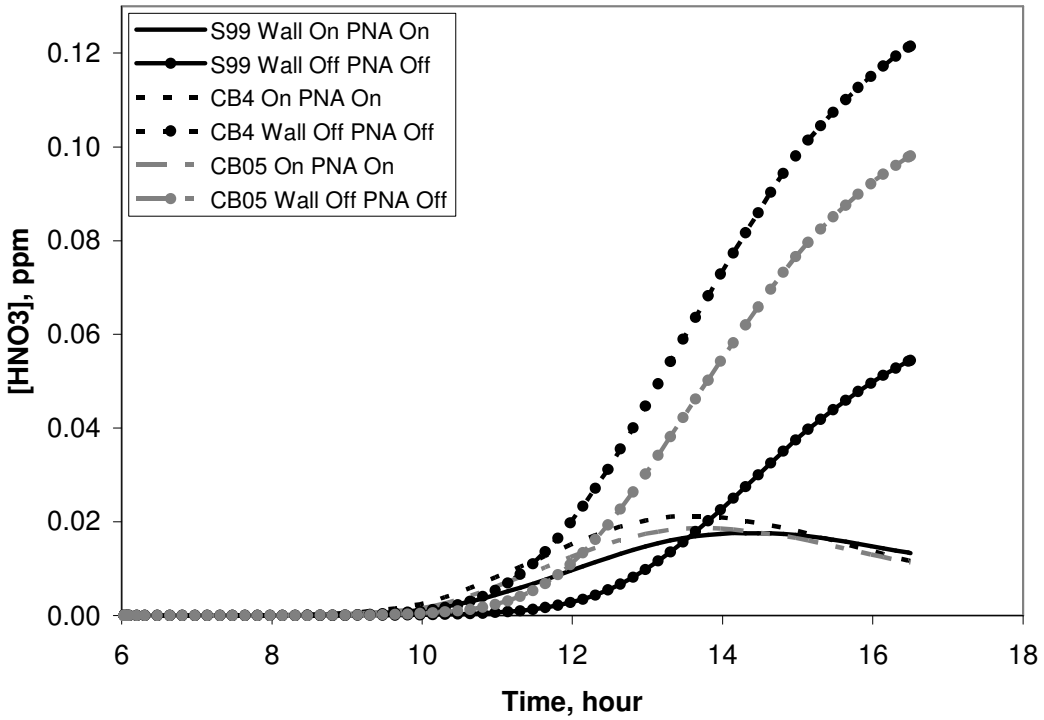

Figure 4-40. HNO_3 in JN2392 UNC red chamber experiment with 0.908 ppmC propylene.

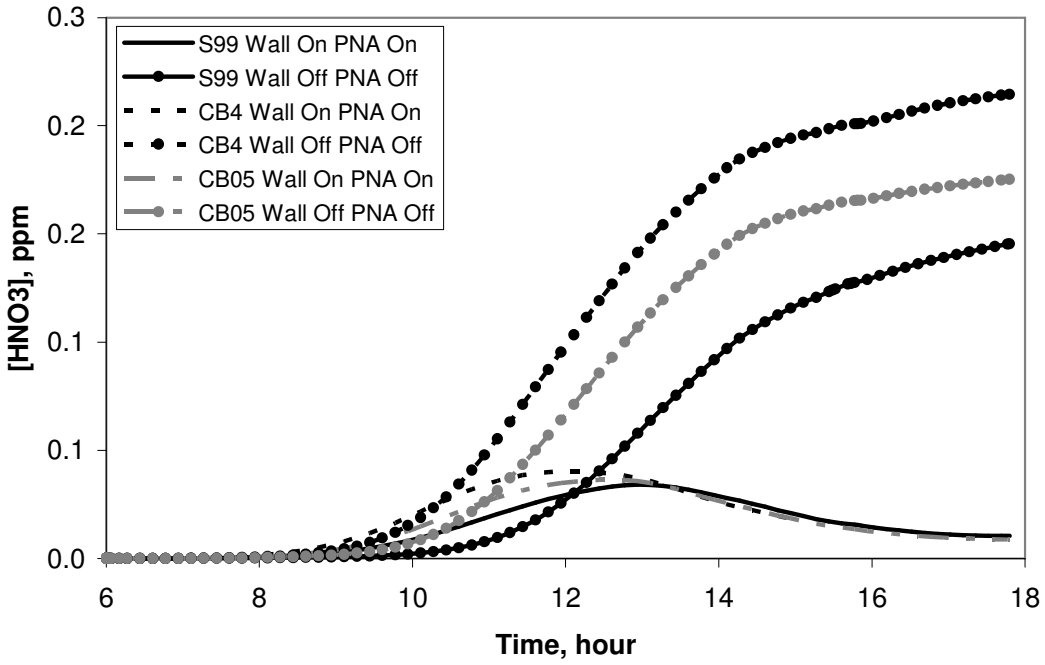

Figure 4-41. HNO_3 in JN1798 UNC red chamber experiment with 1.737 ppmC propylene.

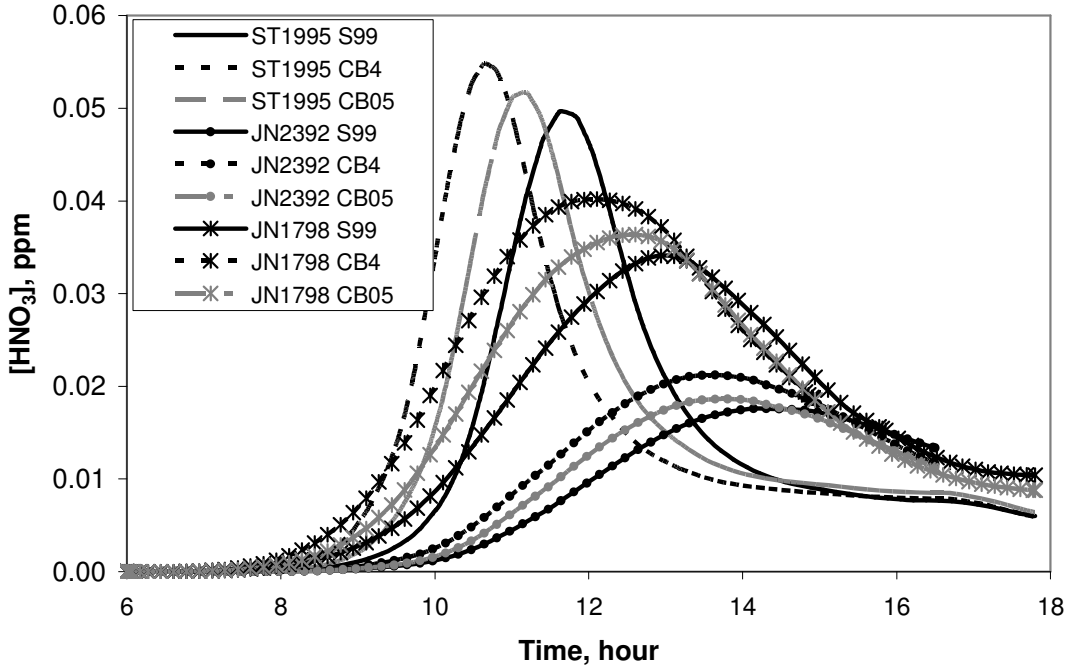

Figure 4-42. HNO_3 comparison among three propylene experiments with activated wall mechanism and PNA (HNO_4) chemistry.

Figures 4-43 – 4-45 show the concentrations of HCHO for the propylene experiments. In the ST1995 experiment, the affect of the wall mechanism on the HCHO predictions of the mechanisms varies. The wall mechanism leads to slower HCHO formation in the CB mechanisms while it leads to faster HCHO formation in the SAPRC99 mechanism. On the other hand, in the JN2392 and JN1798 propylene experiments, the wall mechanism leads to faster HCHO formation and this affect is consistent for the CB and SAPRC99 mechanisms. Figure 4-46 compares the concentration of HCHO among the three propylene experiments when the wall mechanism is activated. The higher formation of HCHO in the ST1995 experiment

corresponds to the higher rate of consumption of propylene in that experiment relative to the JN2392 and JN1798 experiments.

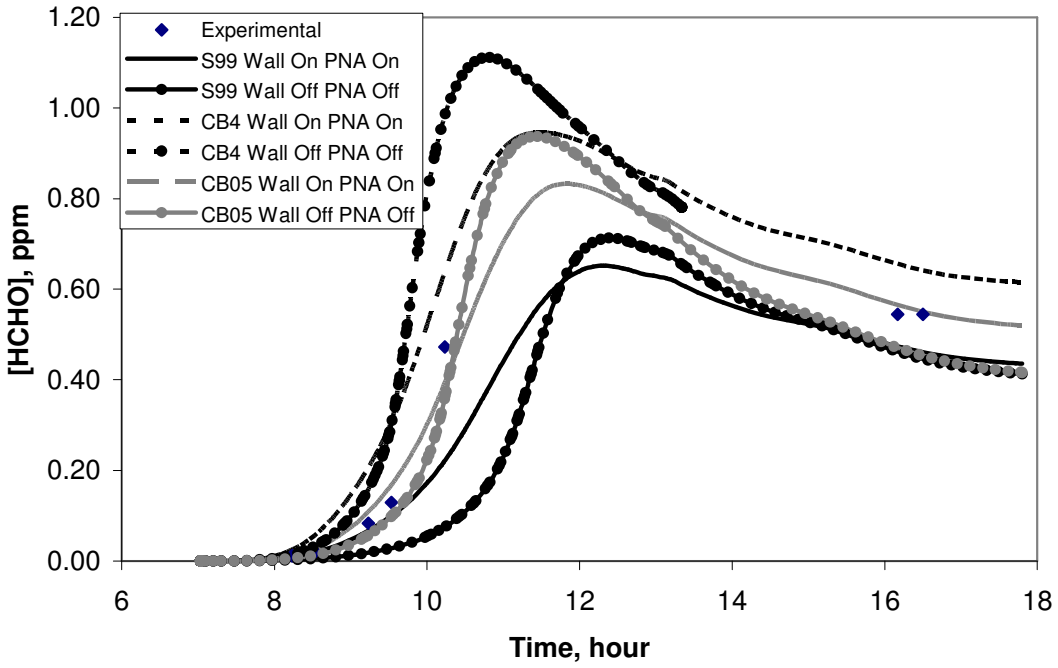

Figure 4-43. HCHO in ST1995 UNC red chamber experiment with 6.12 ppmC propylene.

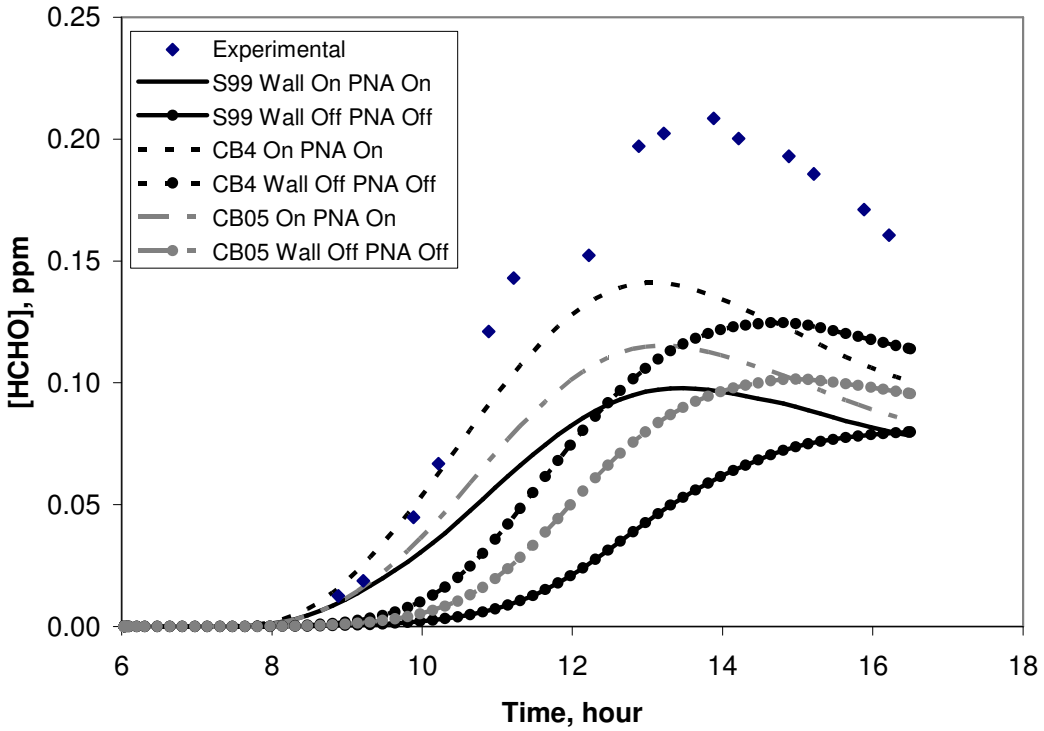

Figure 4-44. HCHO in JN2392 UNC red chamber experiment with 0.908 ppmC propylene.

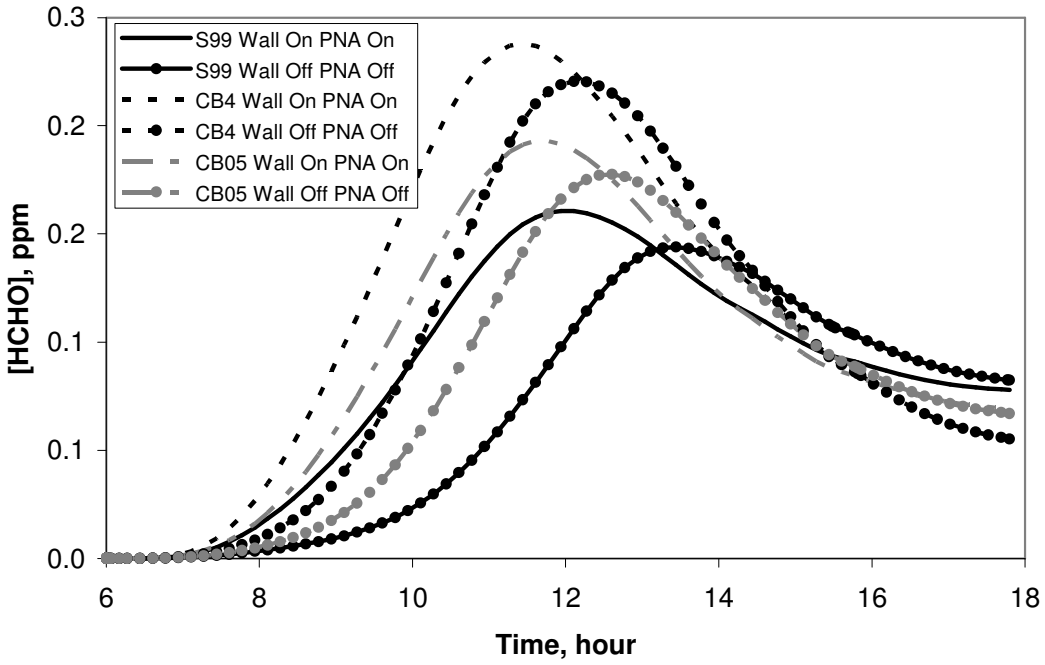

Figure 4-45. HCHO in JN1798 UNC red chamber experiment with 1.737 ppmC propylene.

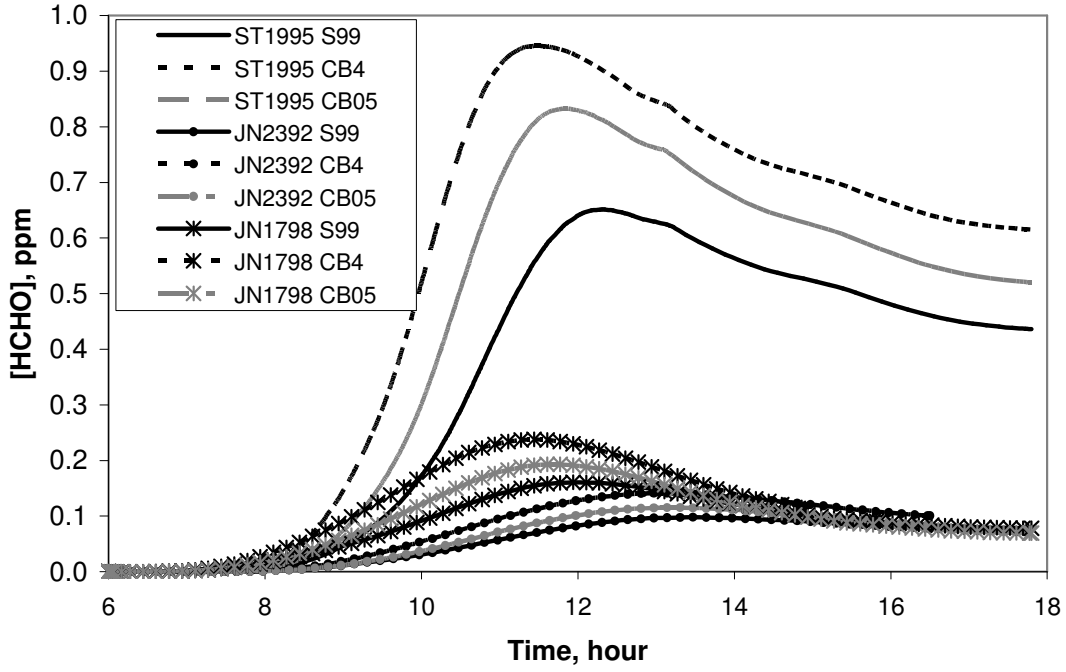

Figure 4-46. HCHO comparison among three propylene experiments with activated wall mechanism and PNA (HNO4) chemistry.

In addition to HCHO, the affect of the wall mechanism on ST1995 varies from the affect of the wall mechanism on the JN2392 and JN1798 experiments for PAN. The wall mechanism in ST1995 leads to less PAN whereas it leads to more PAN and faster PAN formation in the JN2392 and JN1798 experiments, respectively. The concentrations of PAN for the propylene experiments are shown in Figures 4-47 – 4-49. The evolution of PAN concentrations among the three propylene experiments are compared in Figure 4-50.

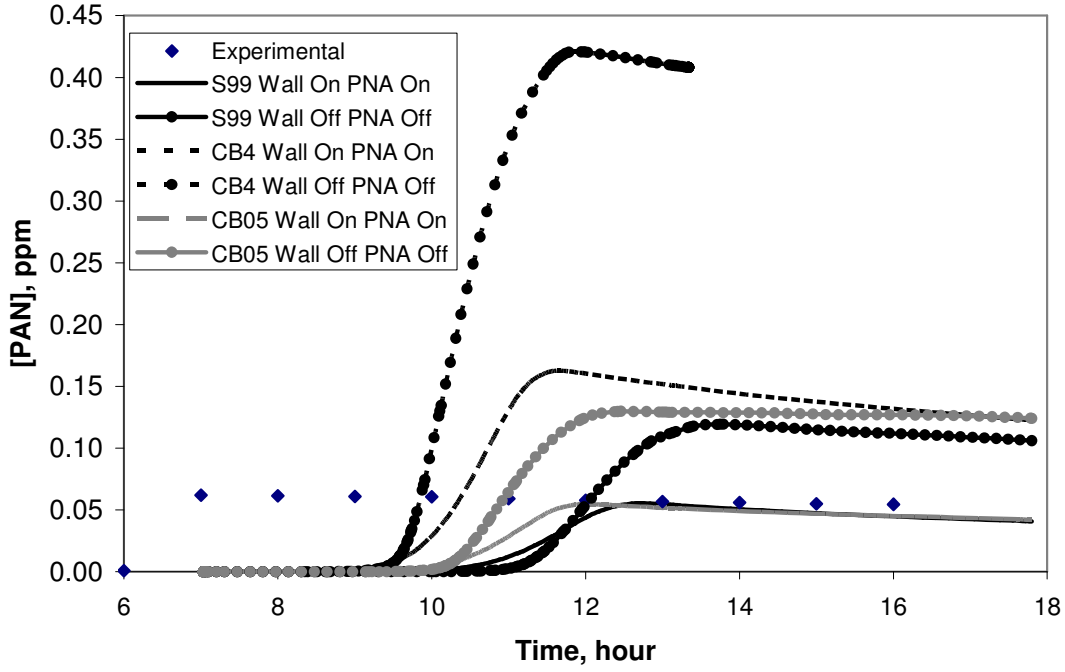

Figure 4-47. PAN in ST1995 UNC red chamber experiment with 6.12 ppmC propylene.

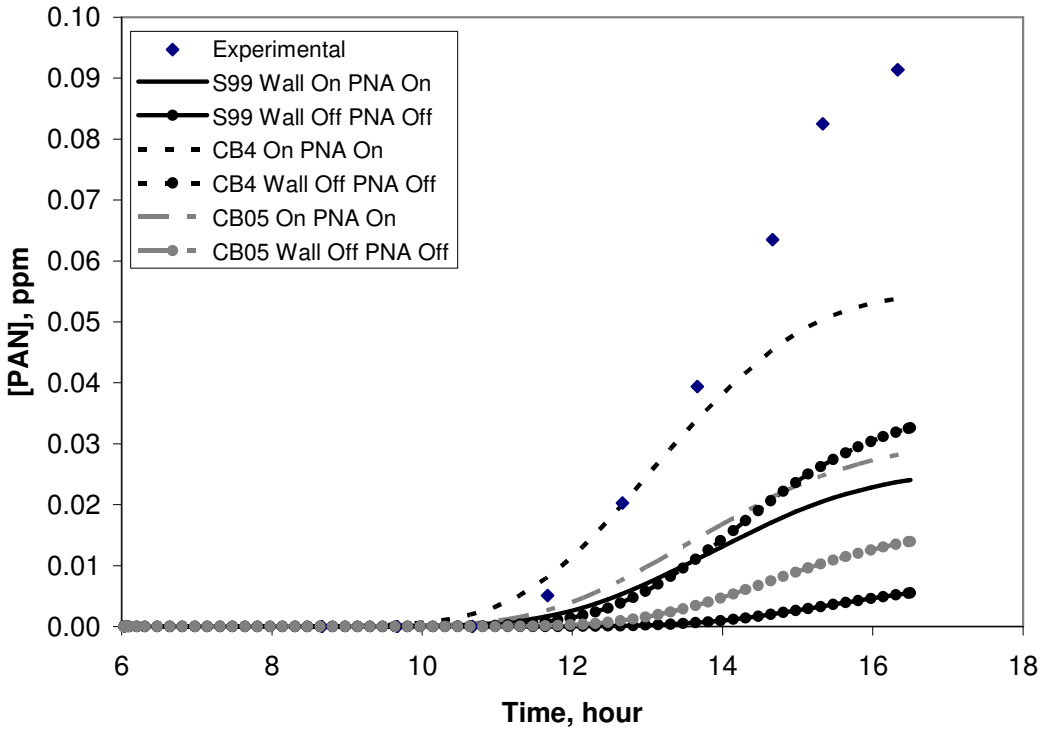

Figure 4-48. PAN in JN2392 UNC red chamber experiment with 0.908 ppmC propylene.

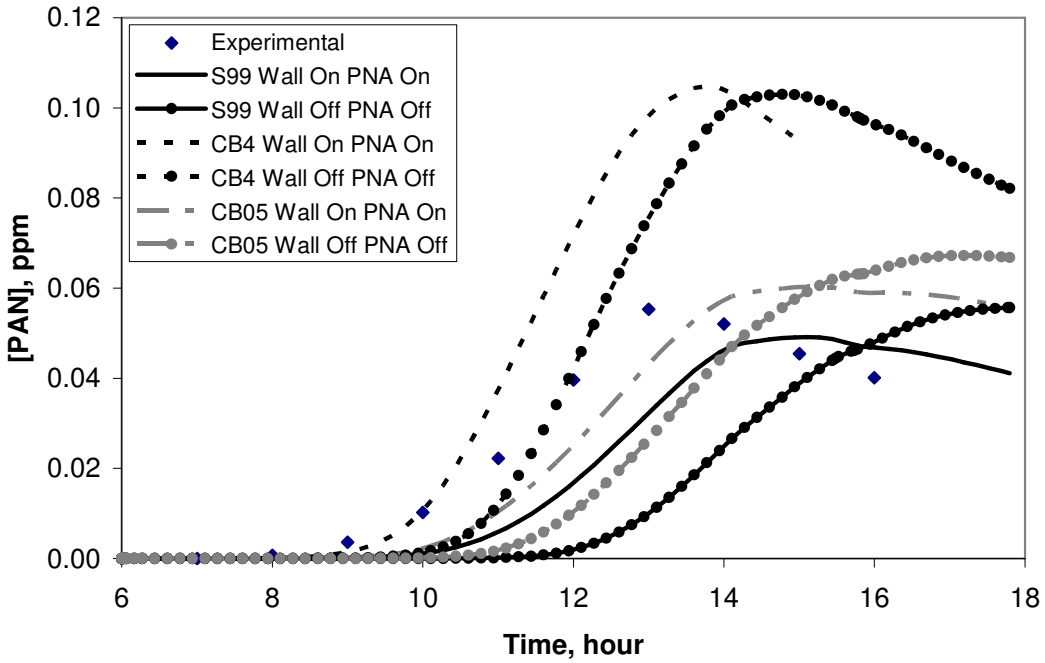

Figure 4-49. PAN in JN1798 UNC red chamber experiment with 1.737 ppmC propylene.

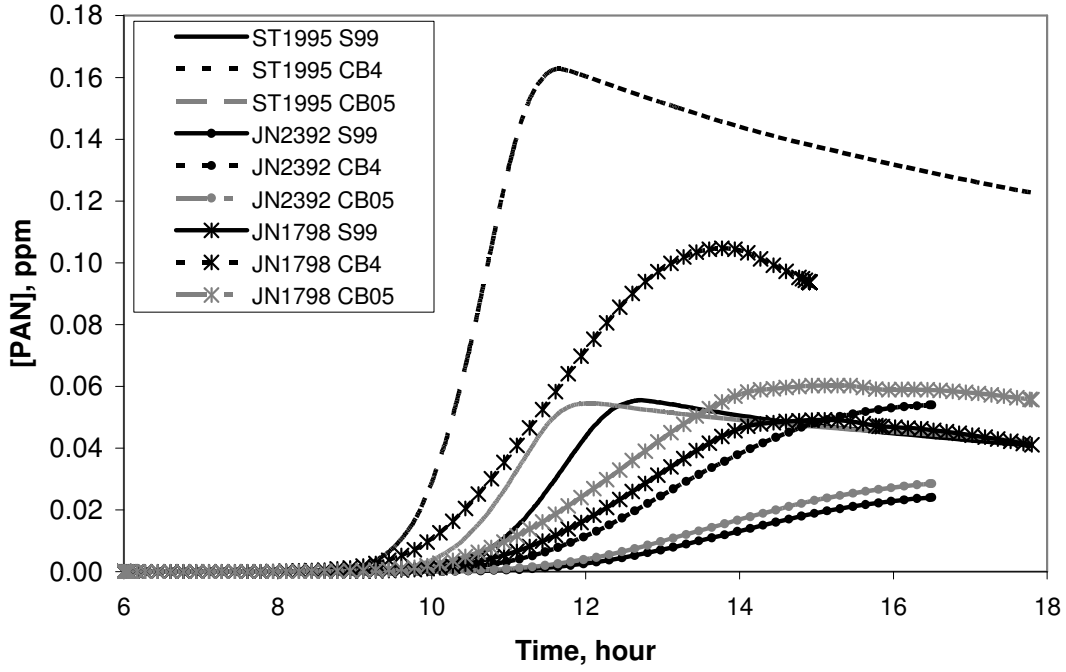

Figure 4-50. PAN comparison among three propylene experiments with activated wall mechanism and PNA (HNO_4) chemistry.

Figure 4-51 compares the concentration of N_2O_5 between the three experiments when the wall mechanism is activated. As shown, the concentration of N_2O_5 in the simulated ST1995 experiment is higher than the other two propylene experiments.

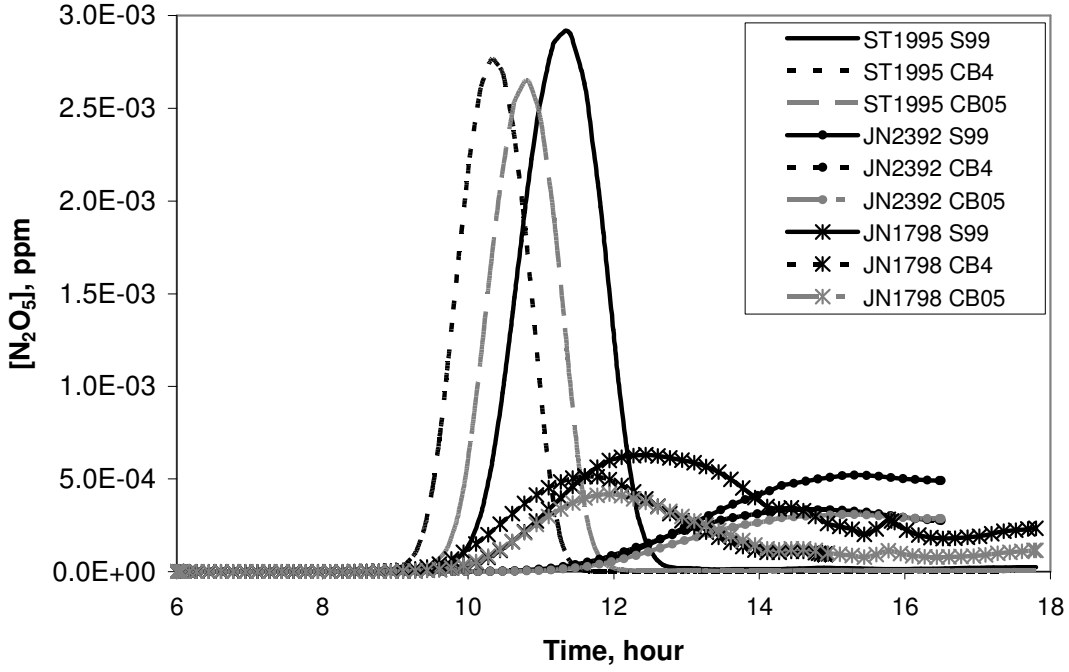

Figure 4-51. N_2O_5 comparison among three propylene experiments with activated wall mechanism and PNA (HNO_4) chemistry.

In order to further compare the effect of the wall mechanism among the three propylene mechanisms, the concentrations of species unique to the wall mechanism were compared. The concentration of the NO, NO_2, HNO_3, and HONO species used only in the wall mechanism, denoted WNO, WNO_2, $WHNO_3$, and WHONO, respectively, were compared between the three propylene experiments. These comparisons are illustrated in Figures 4-52 - 4-55. The peak of the HONO concentration as a result of the wall mechanism, WHONO, is higher in ST1995 versus the JN2392 and JN1798 propylene experiments. Furthermore, the concentration of the HNO_3 species as a result of the wall mechanism, $WHNO_3$, is higher in ST1995 versus the other two propylene experiments.

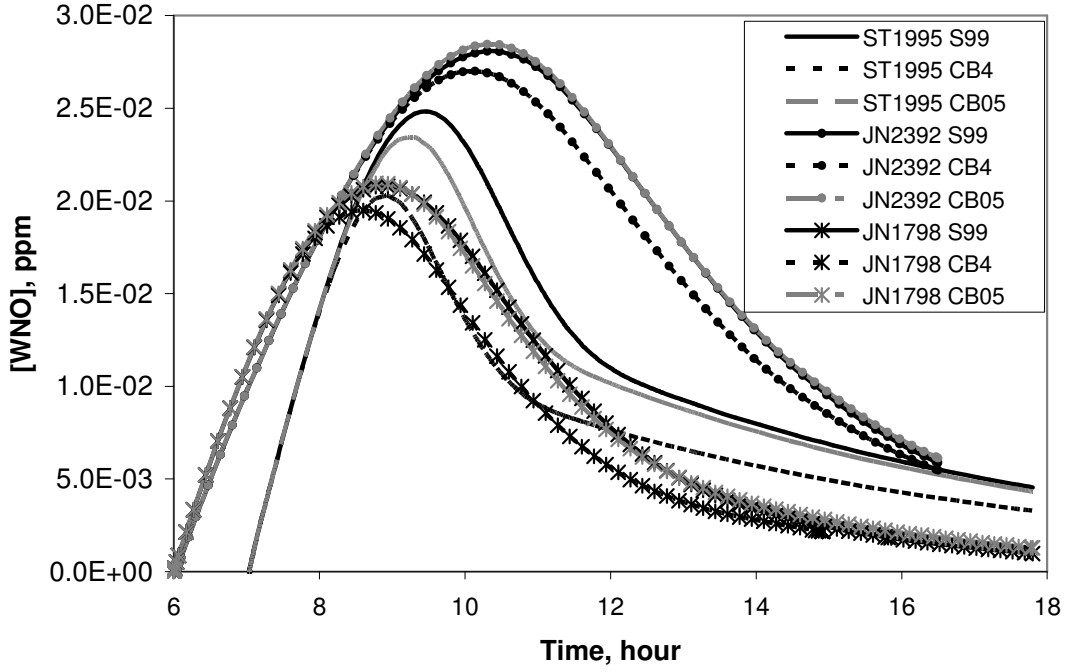

Figure 4-52. Comparison of the concentration of NO due to wall mechanism, [WNO], in UNC chamber between three propylene experiments.

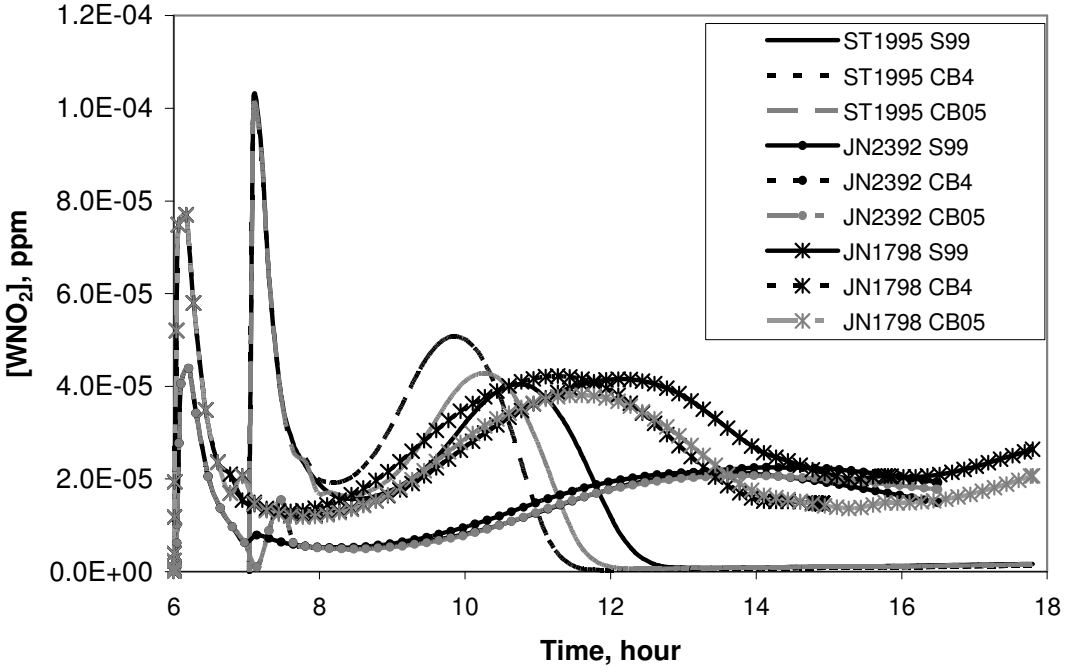

Figure 4-53. Comparison of the concentration of NO_2 due to wall mechanism, [WNO_2], in UNC chamber between three propylene experiments.

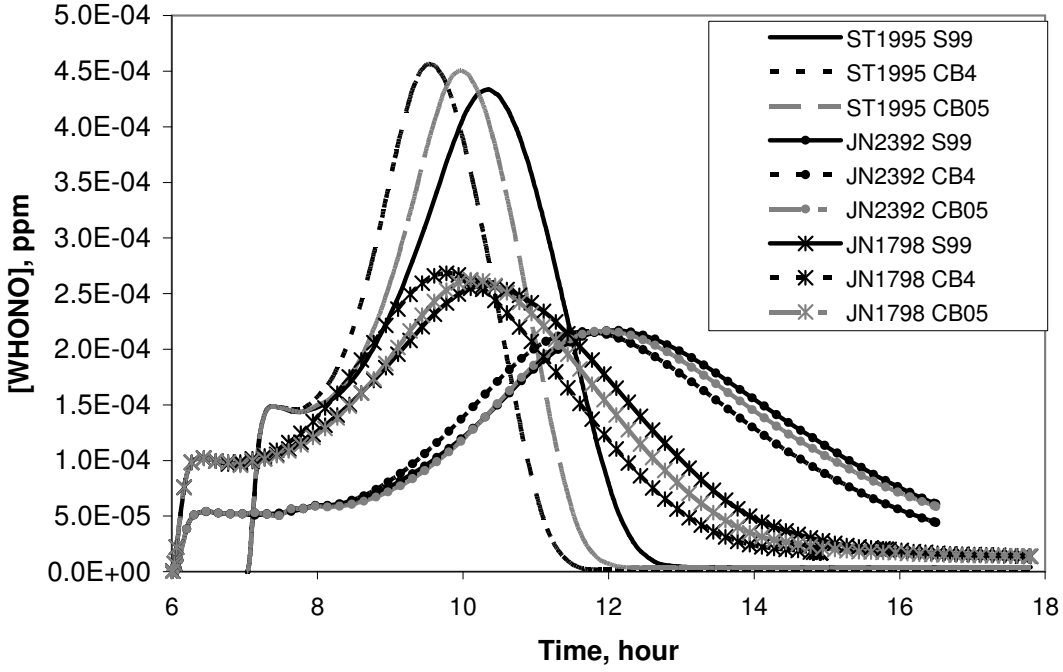

Figure 4-54. Comparison of the concentration of HONO due to wall mechanism, [WHONO], in UNC chamber between three propylene experiments.

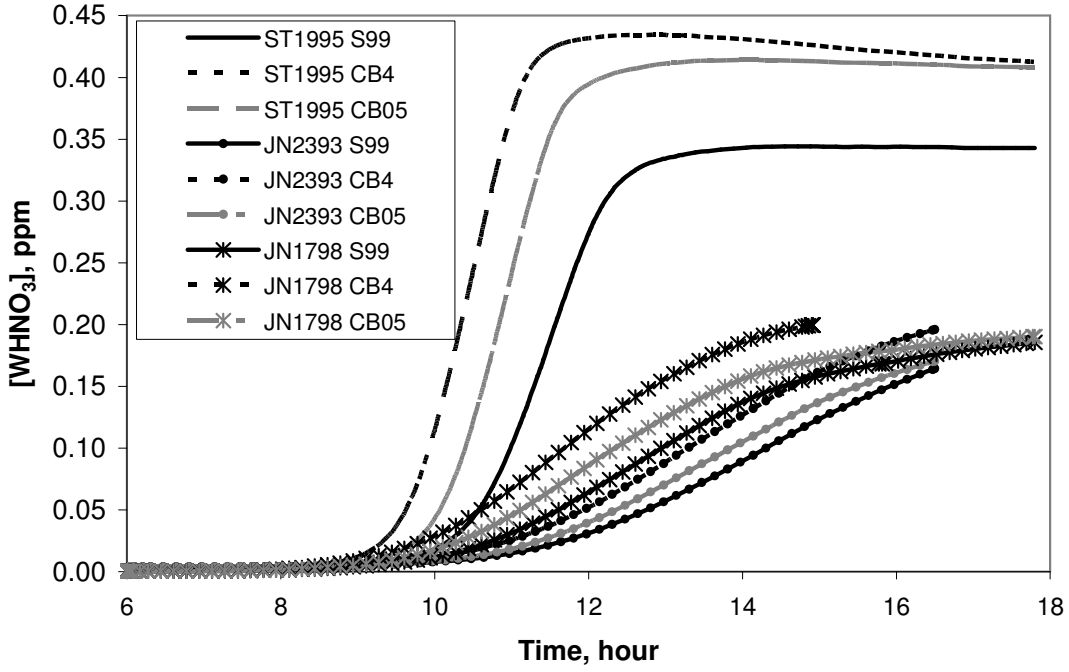

Figure 4-55. Comparison of the concentration of HNO_3 due to wall mechanism, [$WHNO_3$], in UNC chamber between three propylene experiments.

The differences in the direction of responses to the wall mechanism in the propylene experiments could also be due to the sensitivity of the wall mechanism to environmental conditions, for example temperature and radiation. In Figures 4-56 – 4-58, the time dependent temperature, ultraviolet radiation, and total solar radiation in the chamber for the three propylene experiments are compared. In the ST1995 experiment, in which the wall mechanism reduces the simulated ozone concentrations, the temperature and the radiation of the chamber are generally lower than the other two propylene experiments in which the wall mechanism increases the reactivity of the simulations.

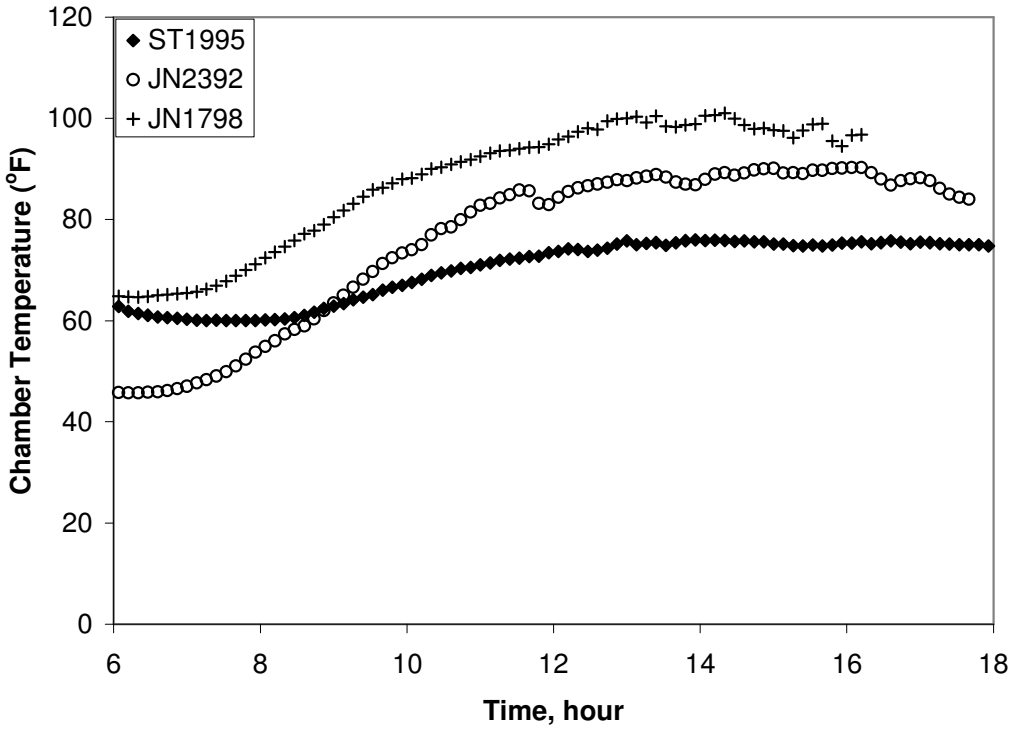

Figure 4-56. Measurements of temperature in the UNC environmental chambers.

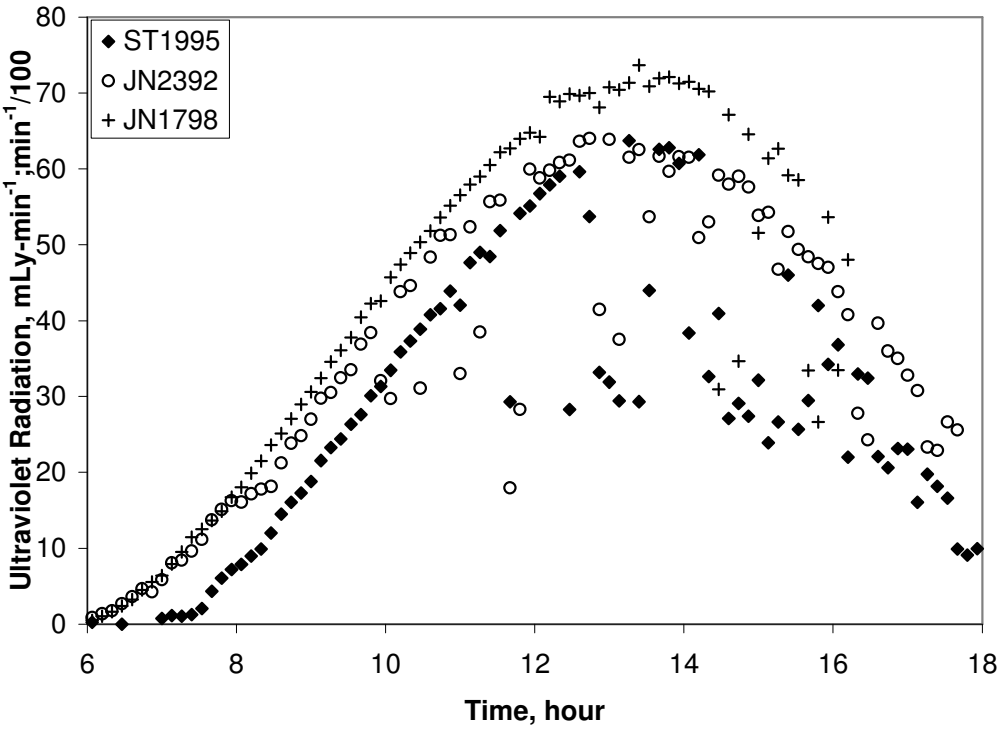

Figure 4-57. Measurements of ultraviolet radiation in the UNC environmental chambers.

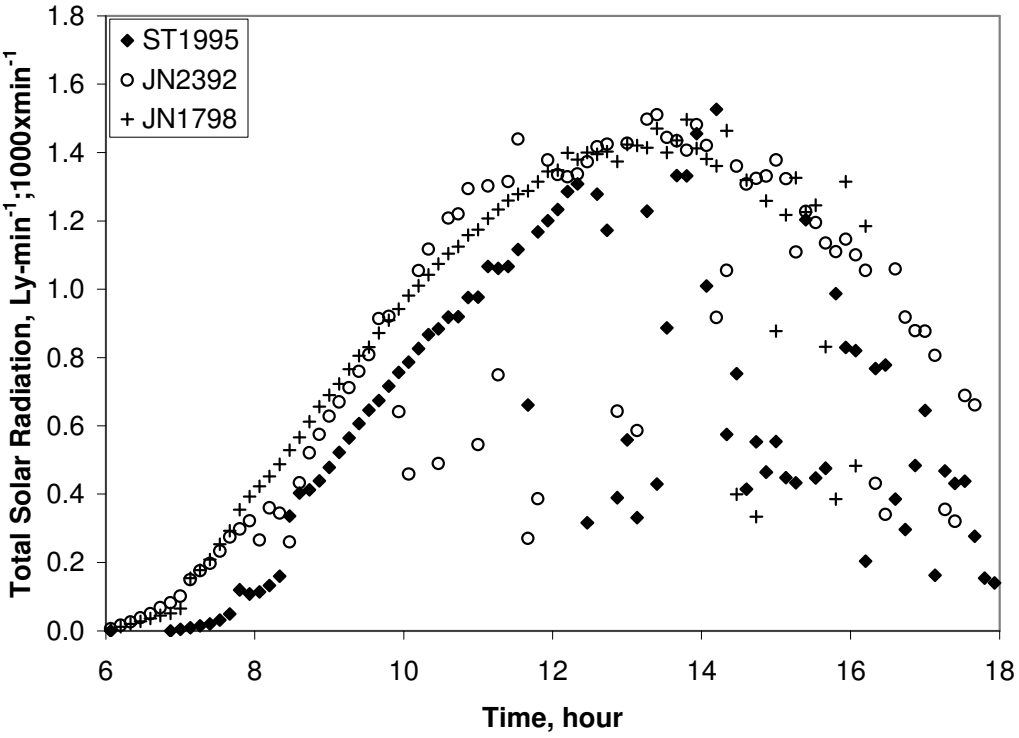

Figure 4-58. Measurements of total solar radiation in the UNC environmental chambers.

In order to test the sensitivity of the wall mechanism to the chamber temperature, an analysis was done in which the temperature in the ST1995 propylene experiment was elevated to the temperature in the JN1798 propylene experiment. The ST1995 simulation results with increased temperature in the two cases, activated wall mechanism and PNA and deactivated wall mechanism and PNA, are shown in Figure 4-59b. In comparison to Figure 4-59a which shows the simulations results for ST1995 with the original chamber temperature designated for that experiment, the effect of the wall mechanism is less significant when the chamber temperature is increased. Nevertheless, the direction of response to ozone is consistent with the ST1995 simulation with the lower temperature and is the opposite of the direction of ozone response in the JN2392 and JN1708 propylene experiments.

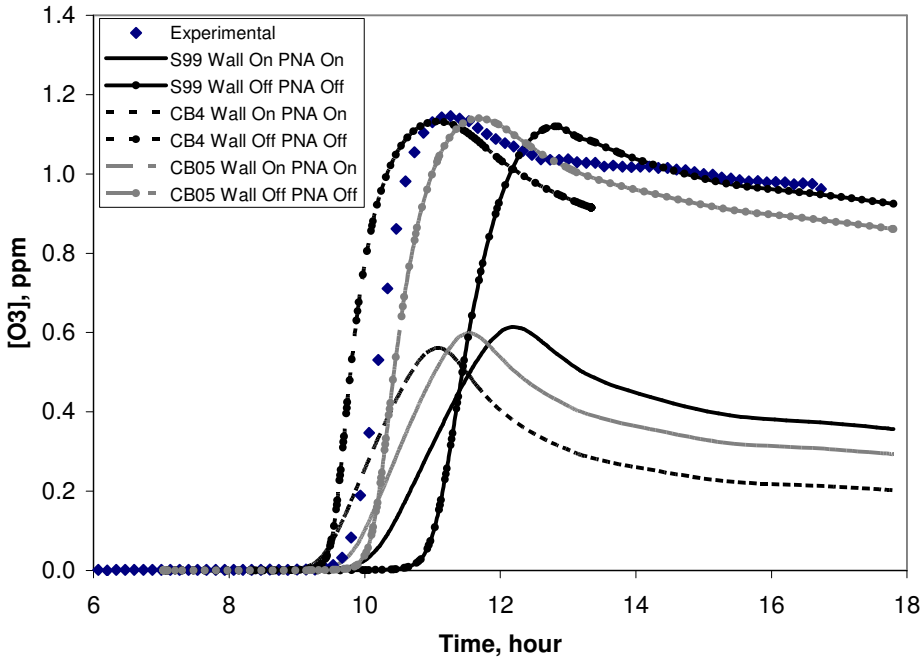

(a)

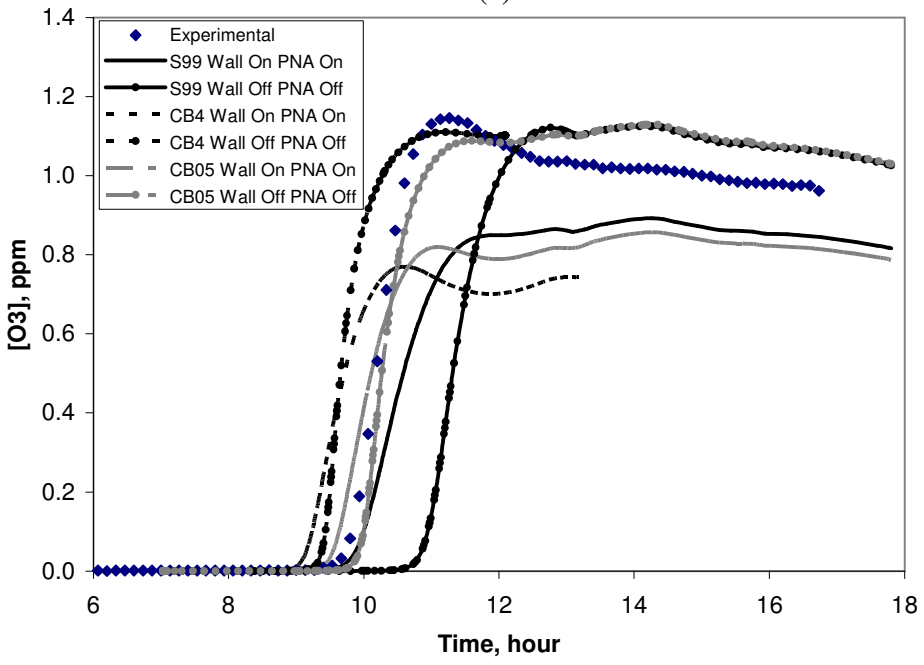

(b)

Figure 4-59. Comparison of the effect of the wall mechanism in (a) ST1995 propylene experiment and in (a) ST1995 propylene experiment with temperature increased to that of JN1798 experiment.

A summary of the assessment of the UNC wall mechanism for three propylene experiments is provided in Tables 4-3 and 4-4. The approximate factor of difference ("x value") is also provided.

Table 4-3. Concentration of species in three propylene experiments with the wall mechanism and PNA (HNO_4) chemistry activated relative to the wall mechanism and PNA chemistry deactivated.

Experiment	ST1995 Red	JN2392 Red	JN1798 Red
VOC	6.12 ppmC Propene (2.04 ppm)	0.908 ppmC Propene (0.303 ppm)	1.737 ppmC Propene (0.579 ppm)
NOx	0.67 ppm (NO=0.516; NO_2=0.154)	0.384 ppm (NO=0.329; NO_2=0.055)	0.492 ppm (NO=0.387; NO_2=0.105)
O_3	Lower (x2)	Higher (x2)	Higher (x2)
Propylene	CB: Higher (x4) S99: Lower (x1)	Lower (x1)	Lower (x2)
NO	Faster depletion (x2)	Faster depletion (x5)	Faster depletion (x7)
NO_2	Faster production (x1)	Faster production (x2)	Faster production (x1)
NOy	Lower (x6)	Lower (x4)	Lower (x8)
HONO	Higher (x3)	Higher (x2)	Higher (x4)
HNO3	Lower (x3)	Lower (x8)	Lower (x5)
HCHO	CB: Slower formation (x1) S99: Faster formation (x1)	Faster formation (x2)	Faster formation (x1)
PAN	Lower (x3)	Higher (x2)	Faster formation (x2)

Table 4-4. Concentration of species in the simulated ST1995 propylene experiment relative to the concentration of species in the simulated JN232 and JN1708 propylene experiments with the wall mechanism and PNA (HNO_4) chemistry activated.

Experiment	ST1995 Red
NO	Faster depletion
NO_2	Faster depletion
NOy	Faster depletion
OH	Lower availability
Propylene	Faster consumption
HO2	Higher
NO_3	Lower
HONO	Higher peak followed by faster depletion
HNO_3	Higher peak followed by faster depletion
HCHO	Higher
N_2O_5	Higher
WHONO	Higher peak
$WHNO_3$	Higher

4.5 Effect of Different UNC Wall Mechanisms on Olefin Experiments

The effect of the UNC wall mechanism was further evaluating by using an older and more complex version of the wall mechanism which was used in evaluating the CB05 mechanism against UNC chamber experiments in the CB05 report by Yarwood *et*

al. (2005). This version of the wall mechanism is provided in Appendix C.3. However, it should be noted that for certain experiments, the wall parameters were assigned values different from the "generalized" wall mechanism provided in Appendix C.3. For the olefins experiments, the values assigned to the wall parameters which supersede those assigned in the generalized wall mechanism are listed in Appendix C.4. Simulations of the olefins experiments with the older version of the UNC wall mechanism are compared to the newer version of the UNC wall mechanism in Figures 4-60 – 4-65. As shown in the figures, for the AU2497 ethylene and ST1995 propylene experiments, the older wall mechanism leads to higher ozone concentrations relative to the newer wall mechanism. For the JN2392 and JN1798 experiments, the effect is much less pronounced. These findings, summarized in Table 4-5, further characterize the different effects of the wall mechanisms which can be significant for some experiments.

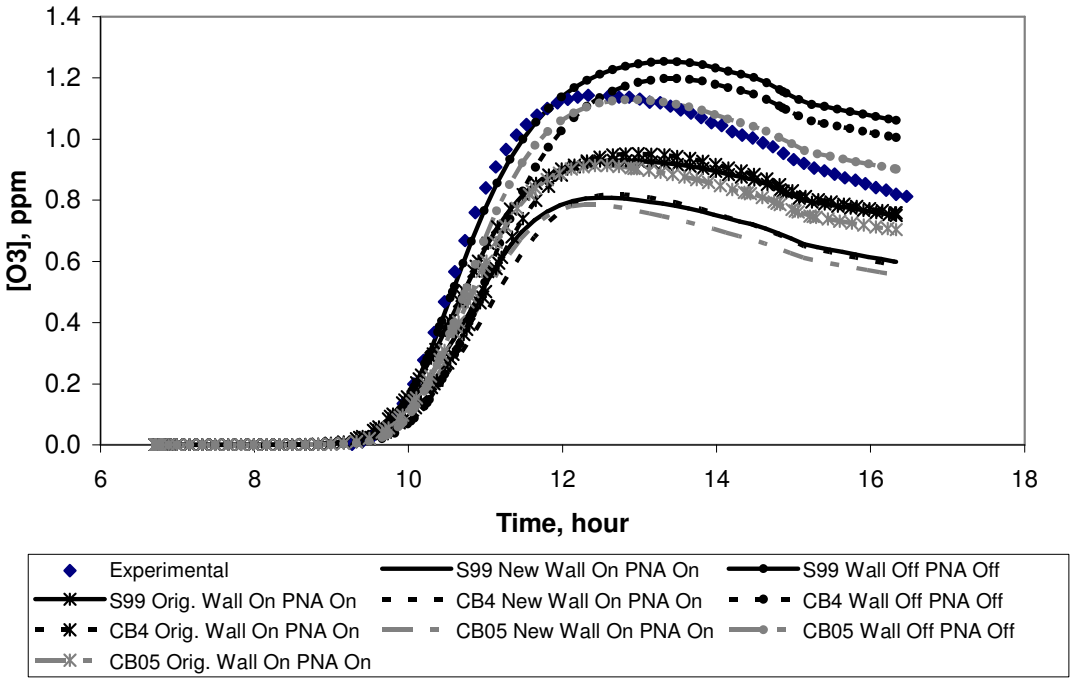

Figures 4-60. Simulation of AU2497 red ethylene experiment with two UNC wall mechanisms.

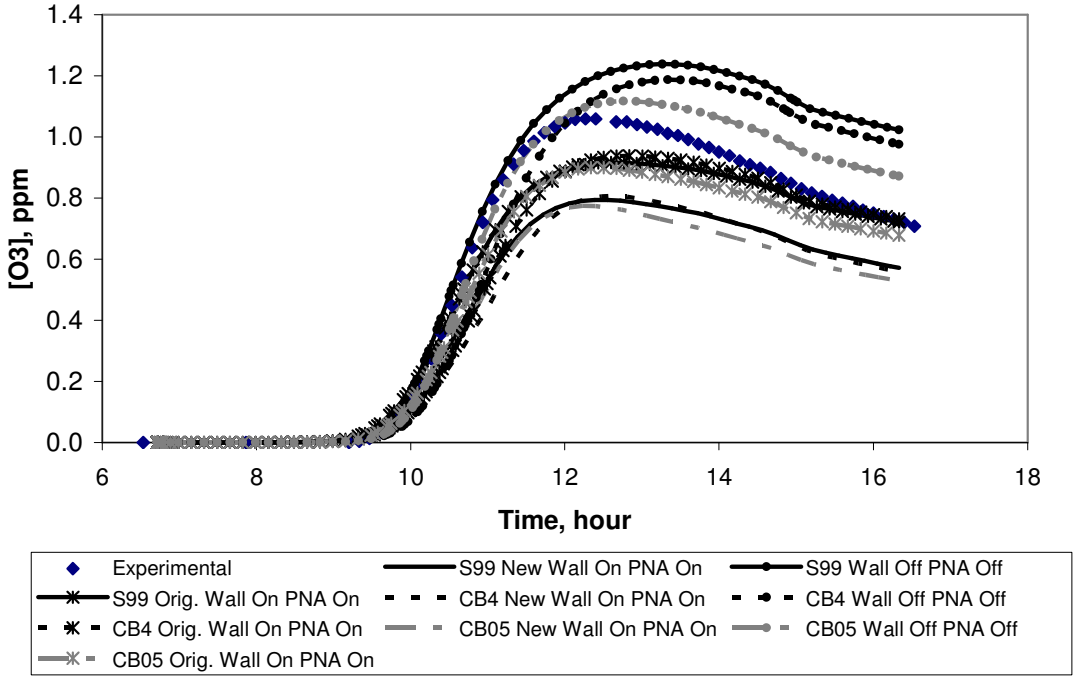

Figure 4-61. Simulation of AU2497 blue ethylene experiment with two UNC wall mechanisms.

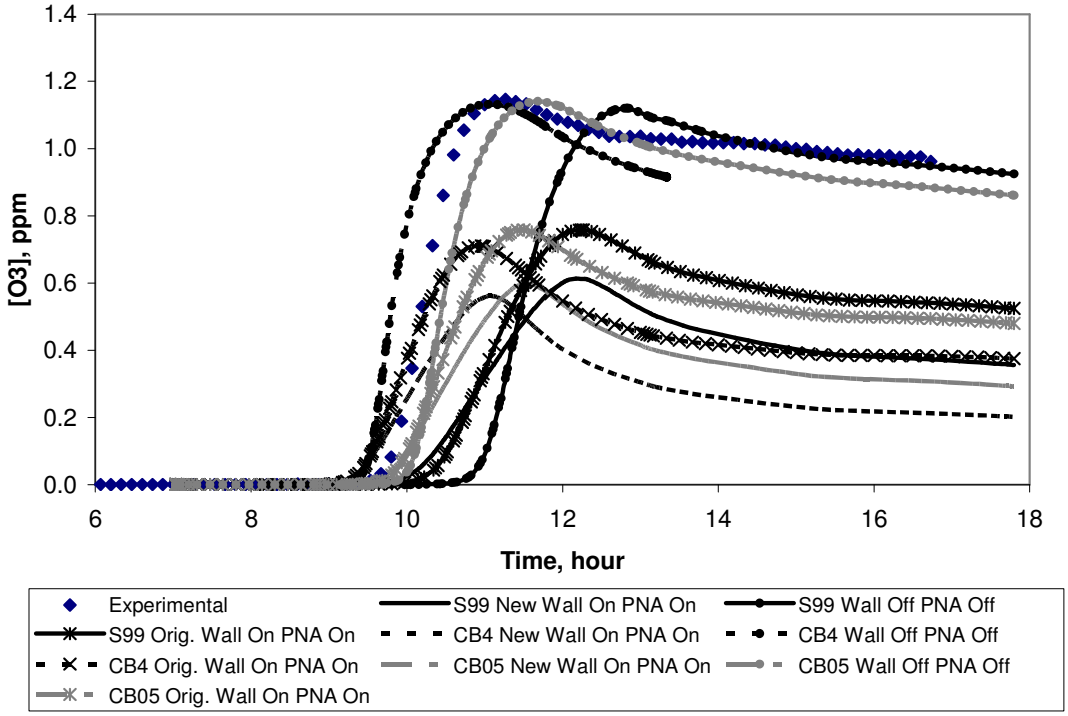

Figure 4-62. Simulation of ST1995 propylene experiment with two UNC wall mechanisms.

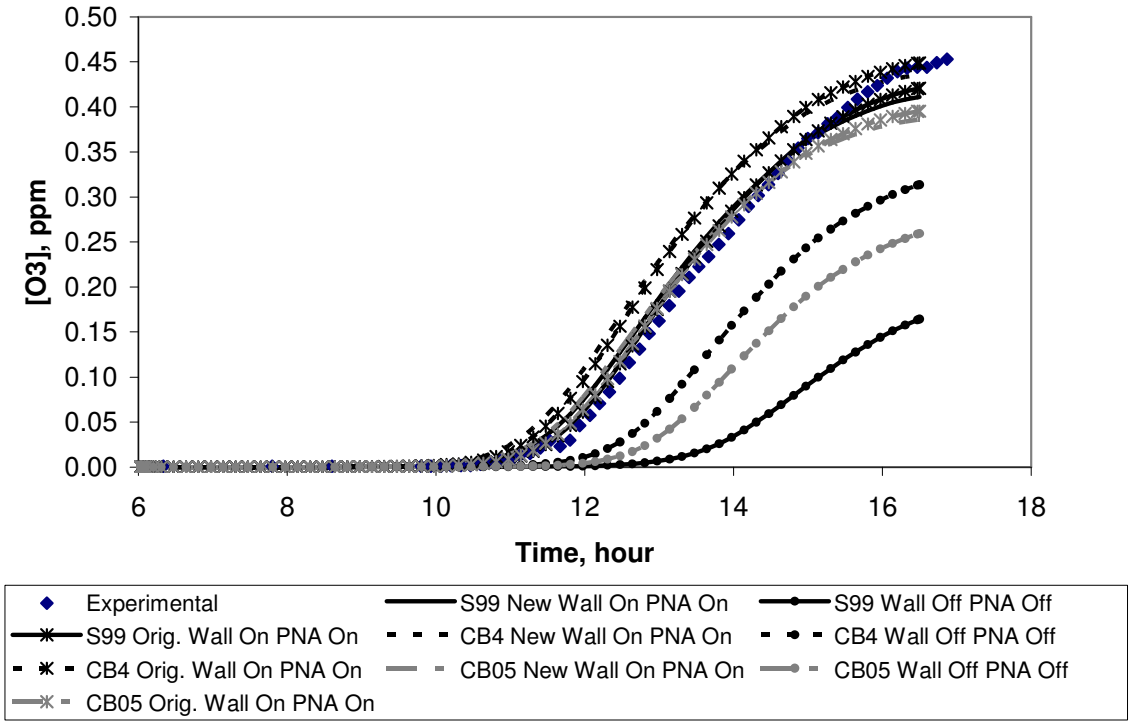

Figure 4-63. Simulation of JN2392 red propylene experiment with two UNC wall mechanisms.

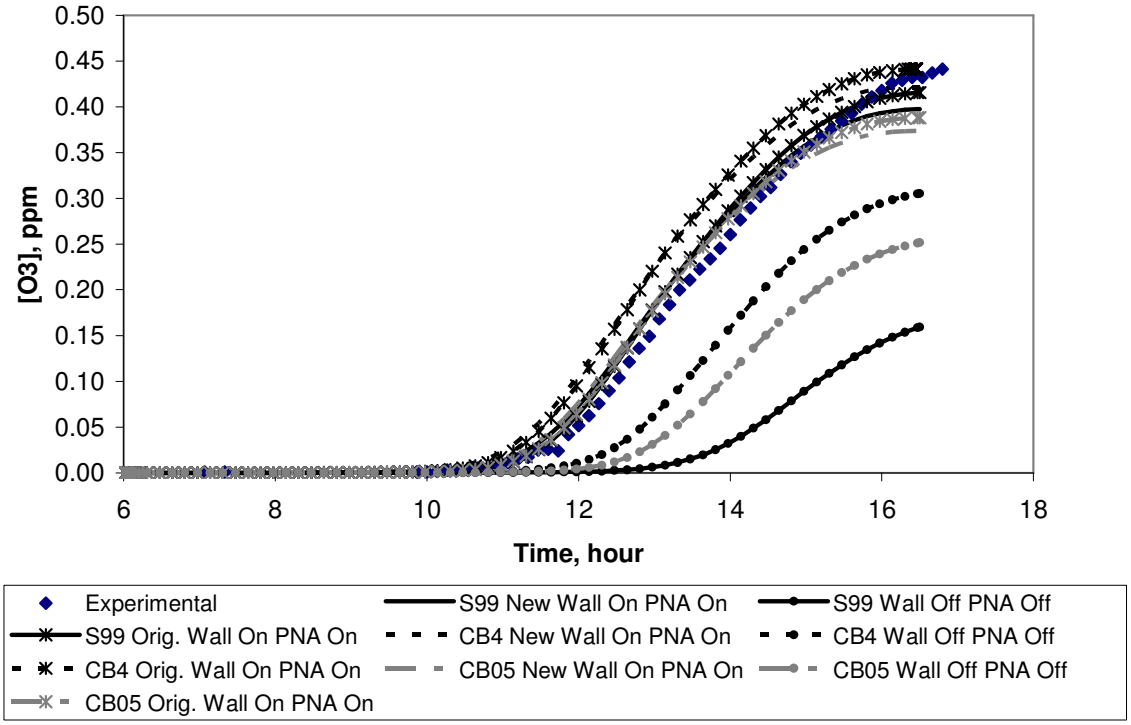

Figure 4-64. Simulation of JN2392 blue propylene experiment with two UNC wall mechanisms.

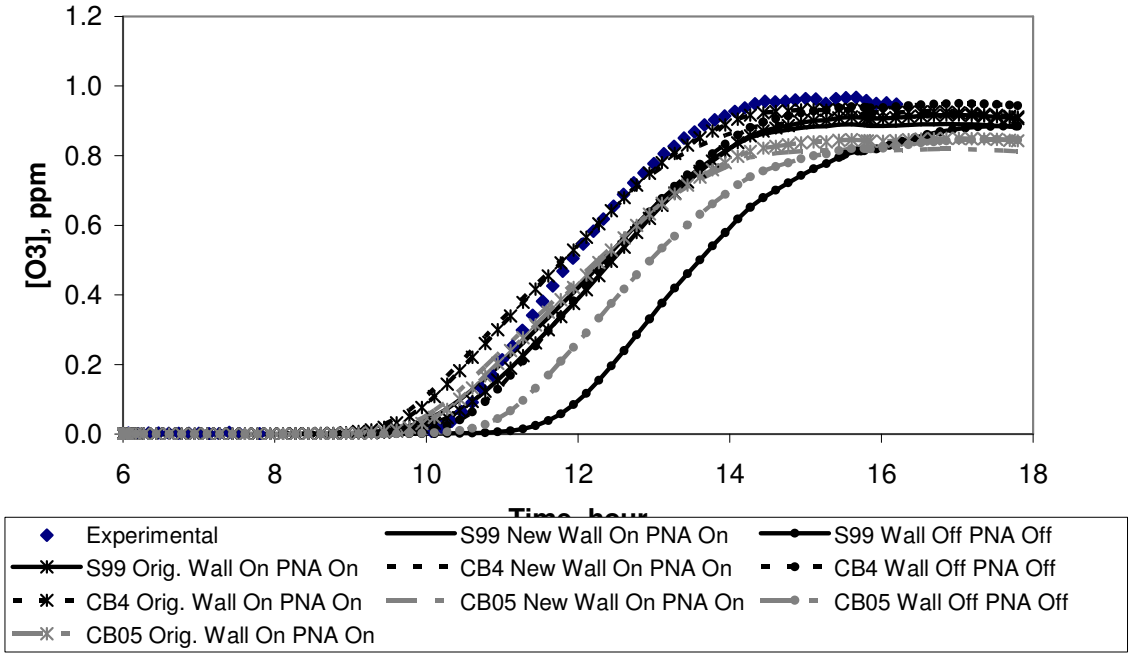

Figure 4-65. Simulation of JN1798 propylene experiment with two UNC wall mechanisms.

Table 2-5. Comparison of peak ozone predictions between two wall mechanisms in UNC olefin experiments.

		Peak O_3 Concentration (ppb)		
	Mechanism	New Wall Mechanism	Original Wall Mechanism	% Increase from New Wall
AU2497 Red	SAPRC99	0.809	0.930	15%
	CB-IV	0.815	0.953	17%
	CB05	0.786	0.913	16%
AU2497 Blue	SAPRC99	0.782	0.915	17%
	CB-IV	0.807	0.934	16%
	CB05	0.774	0.896	16%
ST1995 Red	SAPRC99	0.612	0.758	24%
	CB-IV	0.562	0.710	26%
	CB05	0.600	0.758	26%
JN2392 Red	SAPRC99	0.411	0.421	2%
	CB-IV	0.436	0.449	3%
	CB05	0.386	0.395	2%
JN2392 Blue	SAPRC99	0.400	0.416	4%
	CB-IV	0.422	0.441	5%
	CB05	0.374	0.388	4%
JN1798 Red	SAPRC99	0.880	0.923	5%
	CB-IV	0.890	0.932	5%
	CB05	0.837	0.844	1%

4.4.3 Effect of wall mechanism on UCR chamber simulations: Olefin experiments

The discussion above shows the effect of the chamber model on the simulations of the experiments in the chamber with the greatest wall effects. At the other end of the spectrum is the UCR EPA chamber, which was designed for low concentration experiments and found to have lower wall effects than other chambers (Carter *et al*, 2005). By contrast, Figure 4-67 shows the effects of removing the wall effects for three representative propene experiments in the UCR EPA Chamber, conducted by Carter. The initial conditions of these three experiments are as follows:

EOA341A: Propene 0.25 ppm, NOx: 13 ppb;

EPA417B: Propene 0.29 ppm, NOx 27 ppb;

EPA260B: Propene 0.53 ppm, NOx 28 ppb.

All runs were carried out using the arc light source and with low (<~5%) humidity. (Note that the worse model performance for SAPRC99 is due to lumping effects as discussed in the following chapter). It can be seen that for these runs the wall effects are small for all three mechanisms. This is contrast with the results for the UNC chamber experiments. The UCR EPA wall model incorporates a number of effects, but the most important in affecting simulation results is offgasing of HONO from the walls. Therefore, representative plots of HONO data are also shown on Figure 4-67, where it can be seen that the HONO is much higher with the wall model turned on. However, the HONO input and the radical input from this HONO is not large compared to the homogeneous radical sources from the propene reactions.

4.6 SUMMARY OF WALL EFFECTS

Simulations of experiments in environmental chambers have wall-effects corrections. These wall effect corrections address the well-established observation that environmental chamber walls can be a source of reactive species, particularly free radicals, as well as a sink for some species. The importance of these wall effects corrections depend on the type of experiment and the chamber employed. Some types of experiments, such as the CO - NOx experiments discussed in this chapter, are highly sensitive to wall effects and indeed are carried out primarily to determine which wall effects parameters to use for modeling. In addition, some chambers have much greater wall effects than others. Of the chambers used in this study, the UNC chamber has the greatest wall effects and the UCR EPA chamber has the least.

The propene experiments should have less wall effects than the CO - NOx experiments because of the homogeneous radical sources in the propene mechanisms.

However, simulations in this chapter show that, at least according to the UNC chamber wall model, the wall effects in that chamber are sufficiently large to significantly affect results of such experiments in that chamber. On the other hand, the wall effects model has a relatively small effect on propene - NOx runs in the UCR EPA chamber, which is believed to be the chamber with the lowest wall effects. Other chambers would have intermediate sensitivities to wall effects. This needs to be taken into account when assessing the importance of uncertainties related to chamber parameters when using chamber runs for mechanism evaluation. When wall effects are large, the wall mechanisms can have complex impacts on predicted peak concentrations of multiple pollutant concentrations. In the case of the UNC chamber, these impacts are not restricted to low-reactivity experiments, as demonstrated in the simulations of olefin experiments described in this Chapter. For other chambers and reactants, this would need to be examined on a case-by-case basis. With regard to effects of uncertainties in wall mechanisms and their impacts on chamber simulations, it is important to recognize that looking at effects of turning on or off the wall mechanisms will tend to overstate the importance of such uncertainties. Removing wall effects entirely is known to be well beyond the range of uncertainty of wall effects, because characterization results indicate that wall effects indeed occur, and chamber simulations must account for them. However, wall effects vary at least to some extent from run to run, and this introduces uncertainties in evaluations of chamber experiments. While the magnitude of these uncertainties will probably be less than the difference between wall and no-wall models, the sensitivity calculations presented above are useful in indicating the approximate magnitude and upper limit range of these uncertainties.

Comparisons between simulations of chamber experiments and chamber experiments, in subsequent chapters of this study, will be done using the appropriate wall

mechanisms. It is important, however, to recognize that when chemical mechanisms are implemented in regional photochemical models, wall mechanisms are not included. Therefore, given that the objective of this study is to provide guidance in the selection of chemical mechanisms to be used in regional air quality modeling, it is important to keep in mind how the mechanisms will behave when the wall mechanisms are not included in simulations. Mechanisms tuned to chambers with large wall effects at atmospheric conditions may have more uncertainty than mechanisms tuned to chamber experiments with small wall effects. The greatest source of uncertainty in the chamber experiments is the existence of chamber wall effects, for which the physical and chemical basis is not known. Wall effects can dominate certain types of experiments and can vary from one experiment to another in a manner which is not always successfully predicted. Other sources of uncertainty associated with measurements and knowledge of temperature and light intensity, for example, are generally dwarfed by the uncertainty in wall effects in the environmental chambers. This Chapter has demonstrated that wall effects are complex, vary from chamber to chamber, and can impact overall free radical cycling in the chambers. Further, the choice of a particular wall mechanism for the UNC chamber, from among well accepted choices, can lead to more than 20% differences in peak ozone concentrations for high reactivity experiments. As a consequence, subsequent chapters will focus on peak predicted concentrations in the chambers, rather than temporal evolution of concentrations, and will use a 20% prediction accuracy as a benchmark for acceptable performance.

4.7 REFERENCES

Carter,W.P.L. (2004, May). *Evaluation of a gas-phase atmospheric reaction mechanism for low NOx conditions*. Final Report to California Air Resources Board Contract No. 01-305. Available at http://www.cert.ucr.edu/□carter/absts.htm#lnoxrpt.

Carter, W. P. L, Crocker, D. R., Fitz, D. R., Malkina, I. L., Bumiller, K., Sauer, C. G., Pisano, J. T., Bufalino, C., and Song, C. (2005). A new environmental chamber for evaluation of gas-phase chemical mechanisms and secondary aerosol formation. *Atmospheric Environment*, 39, 7768-7788.

Carter, W. P. L., Luo, D., Malkina, I. L., and Fitz, D. (1993). *The University of California, Riverside environmental chamber data base for evaluating oxidant mechanisms: Indoor chamber experiments through 1993, Volumes I and II*. Report to the Environmental Protection Agency, Office of Research and Development, Research Triangle Park, NC.

Jeffries, H., Fox, D., and Kamens, R. (1975). *Outdoor smog chamber studies: Effects of hydrocarbon reduction on nitrogen dioxide*. Report to the U.S. Environmental Protection Agency, Office of Research and Development, Washington, D.C..

Sexton, K. and Jeffries, H. (1999, July). UNC chamber data and model simulations using Morpho. Report to the Environmental Protection Agency from the University of North Carolina at Chapel Hill, NC.

Simonaitis, R., Meagher, J. F., and Bailey, E. M (1996). Evaluation of the condensed carbon bond (CB-IV) mechanism against smog chamber data at low VOC and NOx concentrations. *Atmospheric Environment*, 31, 27-43.

Whitten, G. Z. (1983). The chemistry of smog formation: A review of current knowledge. *Environmental International*, 9, 447-463.

Yarwood, G., Whitten, G., and Rao, S. (2005, March). *Updates to the Carbon Bond 4 photochemical mechanism*. Prepared by ENVIRON International Corporation and Smog Reyes for the Lake Michigan Air Directors Consortium.

Chapter 5: Assessment of Olefins Chemistry in SAPRC99 and CB mechanisms using Environmental Chamber Experiments

As indicated in Chapter 4, in comparing predictions of chemical mechanisms to chamber data, the focus will be on peak concentrations rather than temporal evolution of concentrations. This approach is consistent with most mechanism evaluation studies as exemplified by the SAPRC-CB comparison studies summarized in Chapter 2. As discussed in Chapter 4, this is in part due to the complex impacts of the chamber wall mechanisms, particularly on the rates of formation and depletion of various species including olefins. In the UNC chamber simulations, the new wall mechanism and PNA chemistry referred to in Chapter 4 are used (Appendix C.1 and C.2). Appropriate representation of wall effects for the UCR chambers are discussed in detail by Carter (2000). Parameters used to model the chamber-dependent radical source and NOx offgasing in the UCR chambers were adjusted for each mechanism by Carter. The chamber effects characterization parameters employed when modeling the UCR chamber experiments are reported in Carter (2007).

This chapter examines chamber experiments involving terminal and internal olefins. Experiments for ethylene, propylene, and trans-2-butene are considered. Emission inventory analyses indicate that internal olefins account for approximately 30% of reported olefin emissions in Houston (Appendix E). Ethylene and propylene alone account for approximately a third of the olefin inventory. The reported olefins inventory may underestimate the fractions of ethylene, propylene and butenes that are actually emitted, however, based on imputed emissions data included in SIP analyses. Therefore, a focus on ethylene, propylene, and to a lesser extent butenes, is appropriate in this Chapter.

When evaluating mechanism performance for propylene and higher alkenes, it is important to recognize that the model species are being used to represent a group of compounds and not a single compound. For example, SAPRC-99 represents the propene and the higher 1- alkenes with the model species OLE1, whose mechanisms are derived based on explicit mechanisms for the mixture of 1-alkenes in a representative ambient mixture, which includes 1-butene and other higher 1-alkenes as well as propene. Because these higher alkenes have somewhat different mechanisms than propene in the SAPRC99 scheme, using OLE1 results in non-optimal fits to the propene experiments for this mechanism, compared to when the explicit propene mechanism is used (see results below). In the case of CB-IV and CB05, the mechanism for the OLE model species is based on the mechanism for propene (and modeling propene experiments), and in the case of CB05 the IOLE model species is based on the mechanism of trans-2-butene. Other compounds are represented using various approaches. Therefore, these mechanisms would be expected to give better performance in simulating experiments for propene and the 2-butenes (in the case of CB05) or for propene (in the case of CB-IV) than is the case for other compounds for which they were not explicitly designed. This needs to be taken into account when interpreting the applicable model performance results described in this chapter in terms of the suitability of the mechanisms for ambient simulations. This is not applicable to ethylene, however, since all three mechanisms represent this compound explicitly.

5.1 COMPARISON BETWEEN THE SAPRC99 AND CB SIMULATIONS OF THE UNC CHAMBER EXPERIMENTS FOR OLEFINS

The terminal olefin experiments in the UNC chamber used to evaluate the olefins chemistry in the three mechanisms are listed in Table 5-1. In this chapter, all the chamber simulations are carried out with the wall mechanism and PNA chemistry activated. In

addition, all SAPRC simulations for propylene use the lumped representation of propylene, unless otherwise noted.

Table 5-1. Terminal olefins experiments in UNC chamber.

Experiment		VOC	NOx
AU2497	Red	3.84 ppmC Ethylene	0.321 ppm
	Blue	3.68 ppmC Ethylene	0.318 ppm
ST1995	Red	6.120 ppmC Propylene	0.67 ppm
JN2392	Red	0.908 ppmC Propylene	0.384 ppm
	Blue	0.907 ppmC Propylene	0.384 ppm
JN1798	Red	1.737 ppmC Propylene	0.492 ppm

Figures 5-1 – 5-2 show the simulations of SAPRC99 and CB in the UNC ethylene experiments. As summarized in Table 5-5 in Section 5.3, there is a slight difference in peak ozone concentrations between the three mechanisms for the ethylene experiments. However, all three mechanisms underpredict the maximum ozone concentration measured in the chamber.

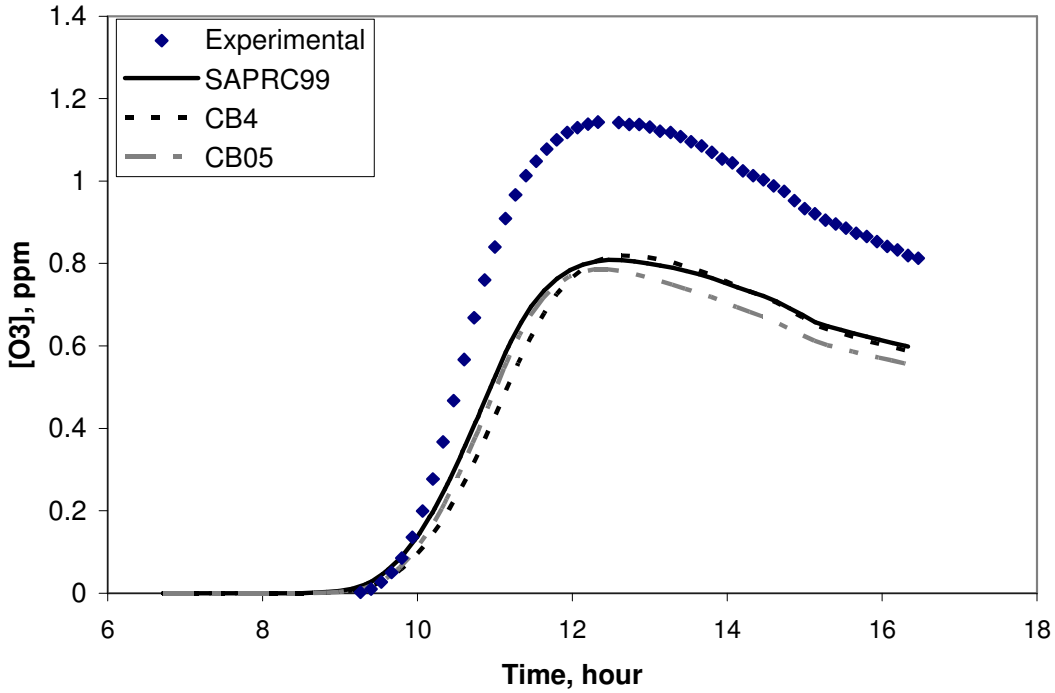

Figure 5-1. AU2497 UNC red chamber experiment with 3.84 ppmC ethylene; wall mechanism and PNA on.

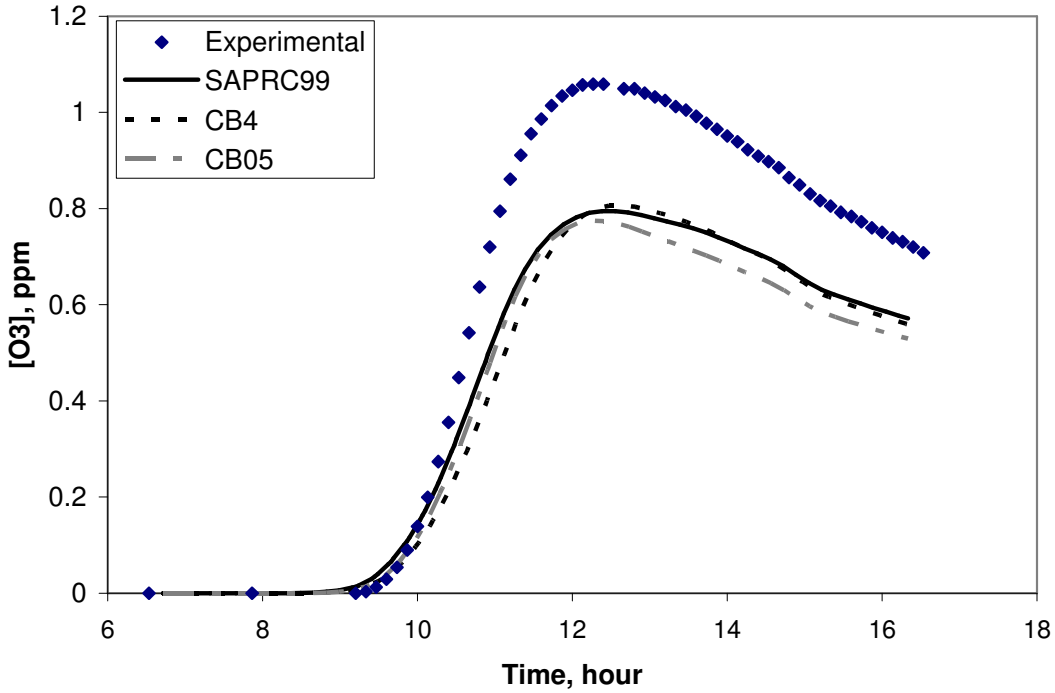

Figure 5-2. AU2497 UNC blue chamber experiment with 3.68 ppmC ethylene; wall mechanism and PNA on.

The UNC propylene experiments are shown in Figures 5-3 – 5-6. Table 5-6 in Section 5.3 summarizes the simulated and measured peak ozone concentrations in the UNC propylene experiments. Similar to the ethylene experiments, the simulated peak ozone concentrations are underpredicted relative to the measured peak ozone in the experiments. In the ST1995 experiment, SAPRC99 produces the highest peak; in JN2392, CB-IV produces the highest peak; and in JN1798, SAPRC99 and CB-IV yield similar ozone peaks which are greater than the ozone peak predicted with CB05.

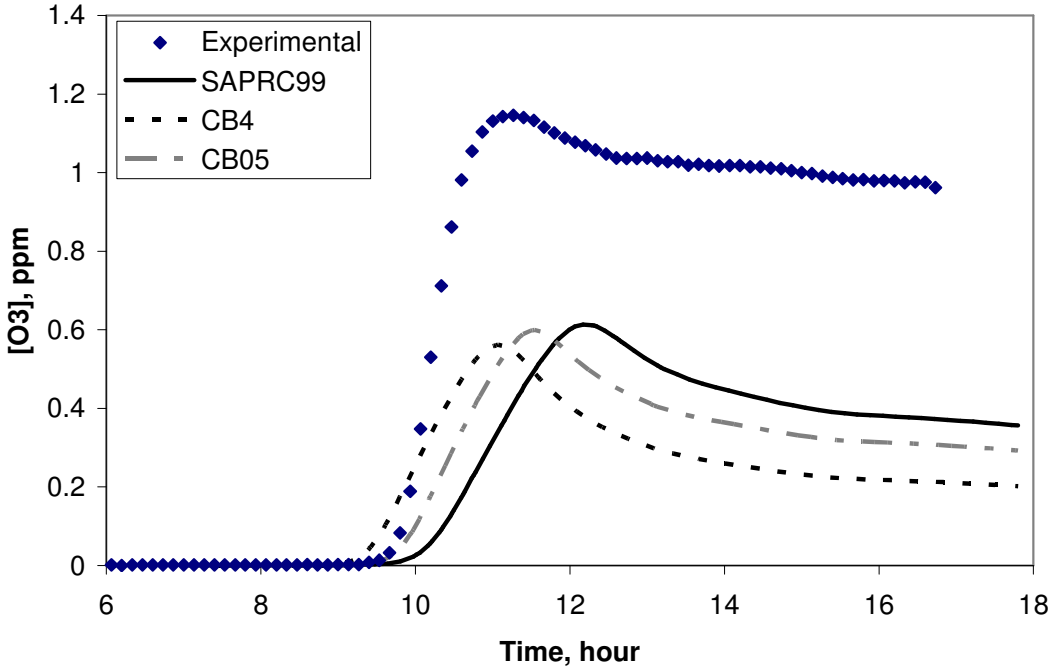

Figure 5-3. ST1995 UNC red chamber experiment with 6.12 ppmC propylene; wall mechanism and PNA on.

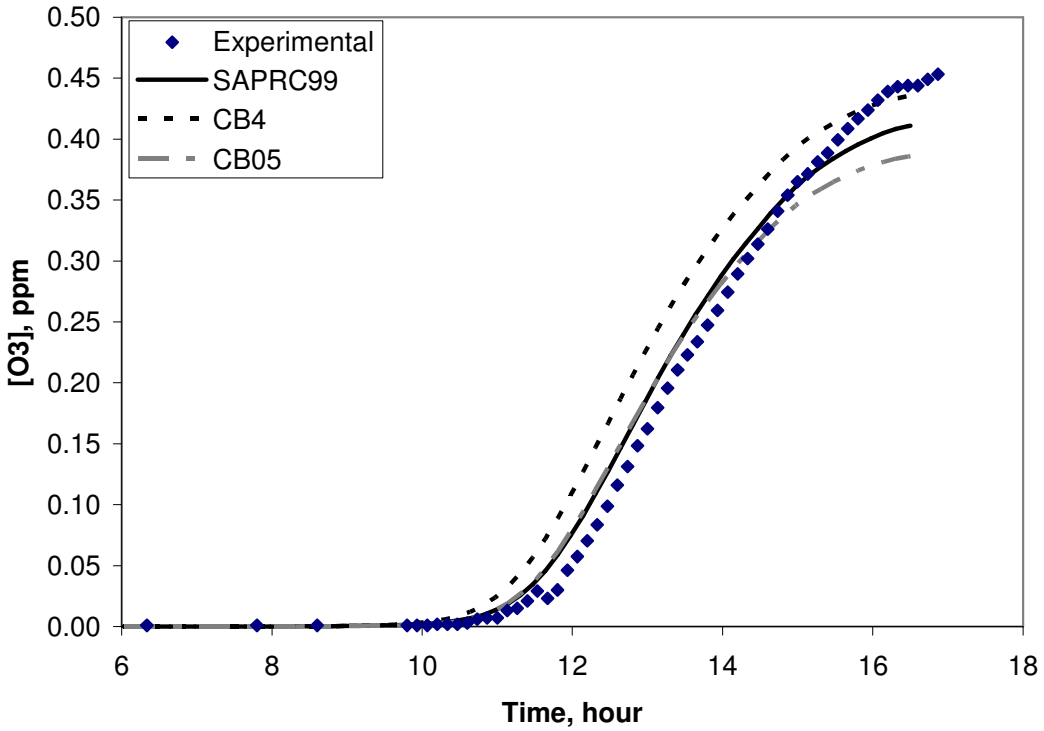

Figure 5-4. JN2392 UNC red chamber experiment with 0.908 ppmC propylene; wall mechanism and PNA on.

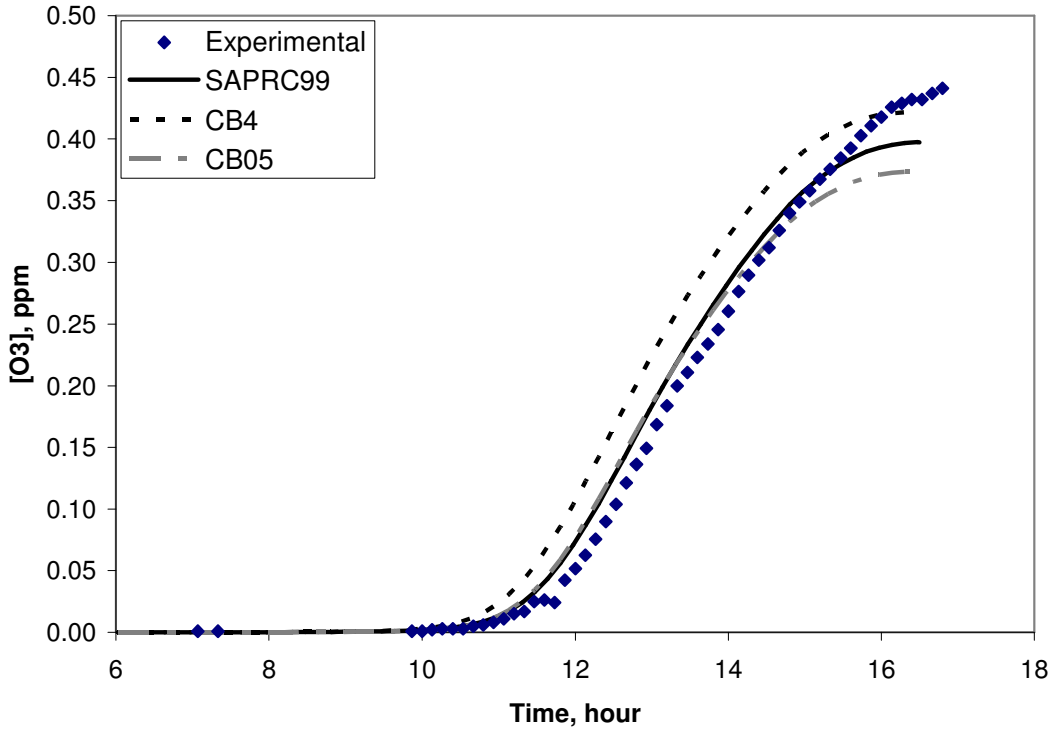

Figure 5-5. JN2392 UNC blue chamber experiment with 0.907 ppmC propylene; wall mechanism and PNA on.

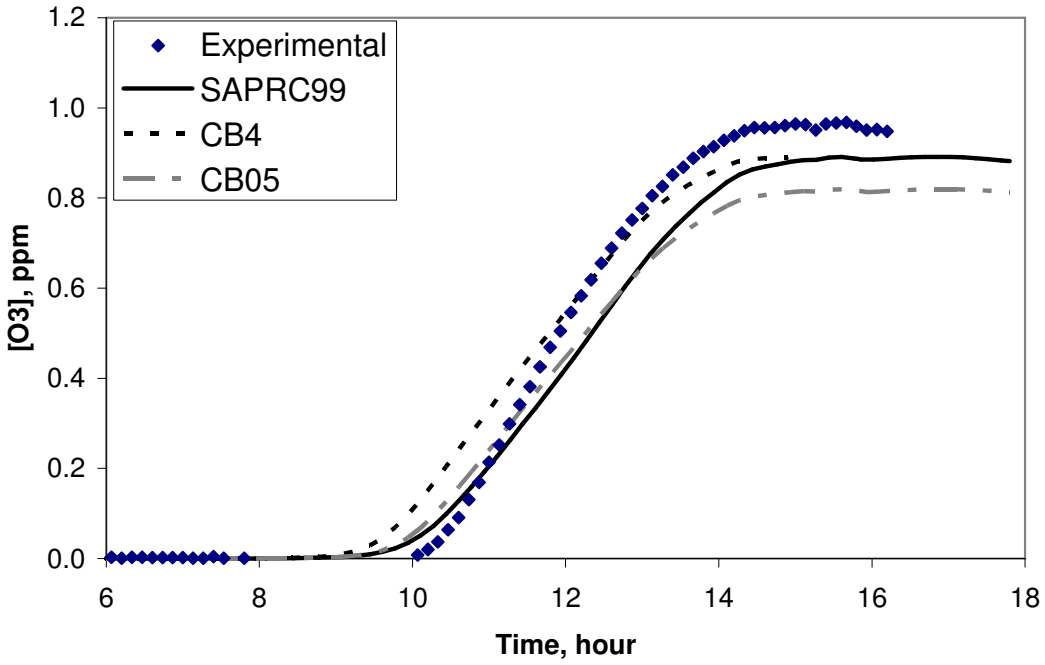

Figure 5-6. JN1798 UNC red chamber experiment with 1.737 ppmC propylene; wall mechanism and PNA on.

In Section 5.3, the results from the UNC propylene simulations are further analyzed. In the next section, the results of UCR chamber simulations for olefins are presented.

5.2 COMPARISON BETWEEN THE SAPRC99 AND CB SIMULATIONS OF THE UCR CHAMBER EXPERIMENTS FOR OLEFINS

The terminal olefin experiments in the UCR chambers used to evaluate the olefins chemistry are listed in Table 5-3 and Table 5-4.

Table 5-3. Ethylene experiments in the UCR chambers.

Experiment	VOC	NOx	Light Source
EPA073A	1.23 ppmC	25 ppb	Arc light solar simulator
XTC105	3.47 ppmC	241 ppb	Arc light solar simulator
XTC112	5.11 ppmC	518 ppb	Arc light solar simulator
EC285	3.90 ppmC	1014 ppb	Arc light solar simulator
EC287	7.99 ppmC	545 ppb	Arc light solar simulator
TVA008	0.50 ppmC	52 ppb	Blacklights + Sunlamps
OTC278B	1.25 ppmC	465 ppb	Sunlight
OTC279A	2.02 ppmC	531 ppb	Sunlight
OTC304B	2.00 ppmC	232 ppb	Sunlight

The ozone predictions in ppm as a function of time (minutes) for the UCR ethylene experiments in Table 5-3 are presented in Figure 5-7. The findings for these UCR ethylene experiments are summarized in Table 5-7 in Section 5.3. In all but the EC experiments, the experimental peak ozone concentrations exceed the simulated peak ozone concentrations. In the EPA experiment, the three mechanisms predict similar ozone peaks. In the XTC experiments, SAPRC99 and CB05 predict similar ozone peaks while CB-IV yields a lower maximum ozone concentration. In the OTC experiments, the ozone peaks predicted with SAPRC99 and CB05 are much higher the ozone peak predicted with CB05.

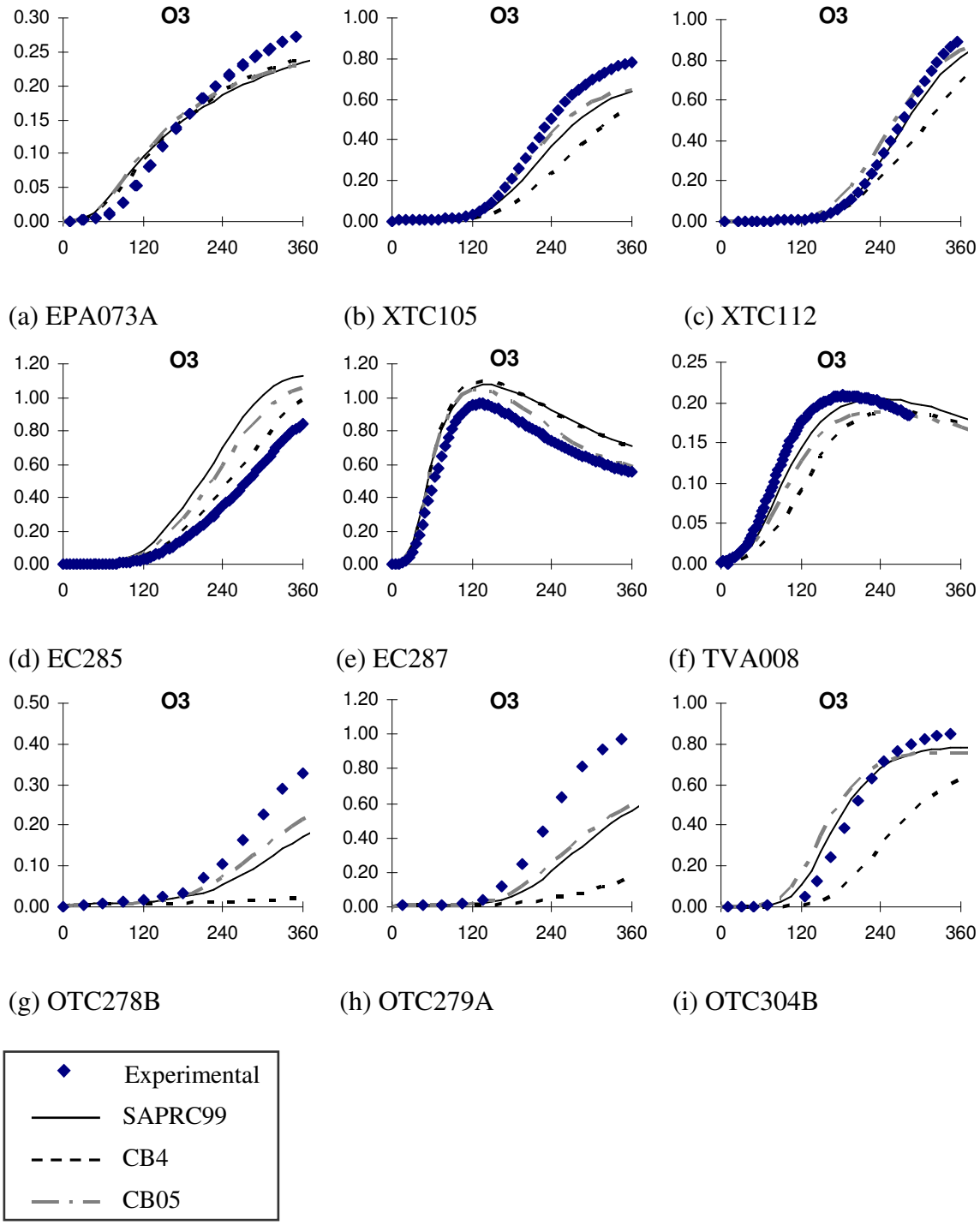

Figure 5-7. Ethylene experiments in UCR chambers: O_3 (ppm) as a function of time (min); wall mechanism and PNA on.

The UCR propylene experiments evaluated in this chapter are listed in Table 5-4.

Table 5-4. Propylene experiments in the UCR chambers.

Experiment	VOC	NOx	Light Source
EC216	1.51 ppmC	524 ppb	Arc light solar simulator
EC277	1.69 ppmC	114 ppb	Arc light solar simulator
EC314	3.19 ppmC	980 ppb	Arc light solar simulator
EC687	3.12 ppmC	470 ppb	Arc light solar simulator
EC899	3.18 ppmC	485 ppb	Arc light solar simulator
OTC272B	3.09 ppmC	530 ppb	Sunlight
OTC295A	4.37 ppmC	535 ppb	Sunlight
OTC295B	4.34 ppmC	520 ppb	Sunlight
OTC298A	3.75 ppmC	582 ppb	Sunlight

The ozone predictions in ppm as a function of time (minutes) for the propylene experiments in Table 5-4 are presented in Figure 5-8. The findings are summarized in Table 5-8 in Section 5.3. For all the propylene experiments in Figure 5-8, CB-IV predicts the highest peak ozone concentrations relative to the other mechanisms as well as the experiments.

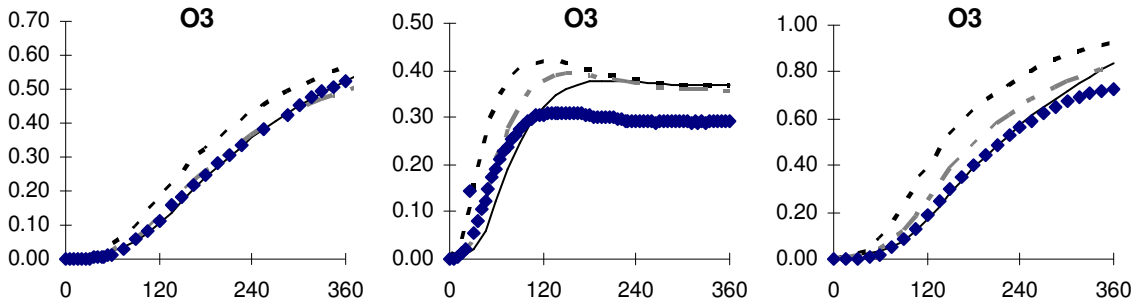

(a) EC216 (b) EC277 (c) EC314

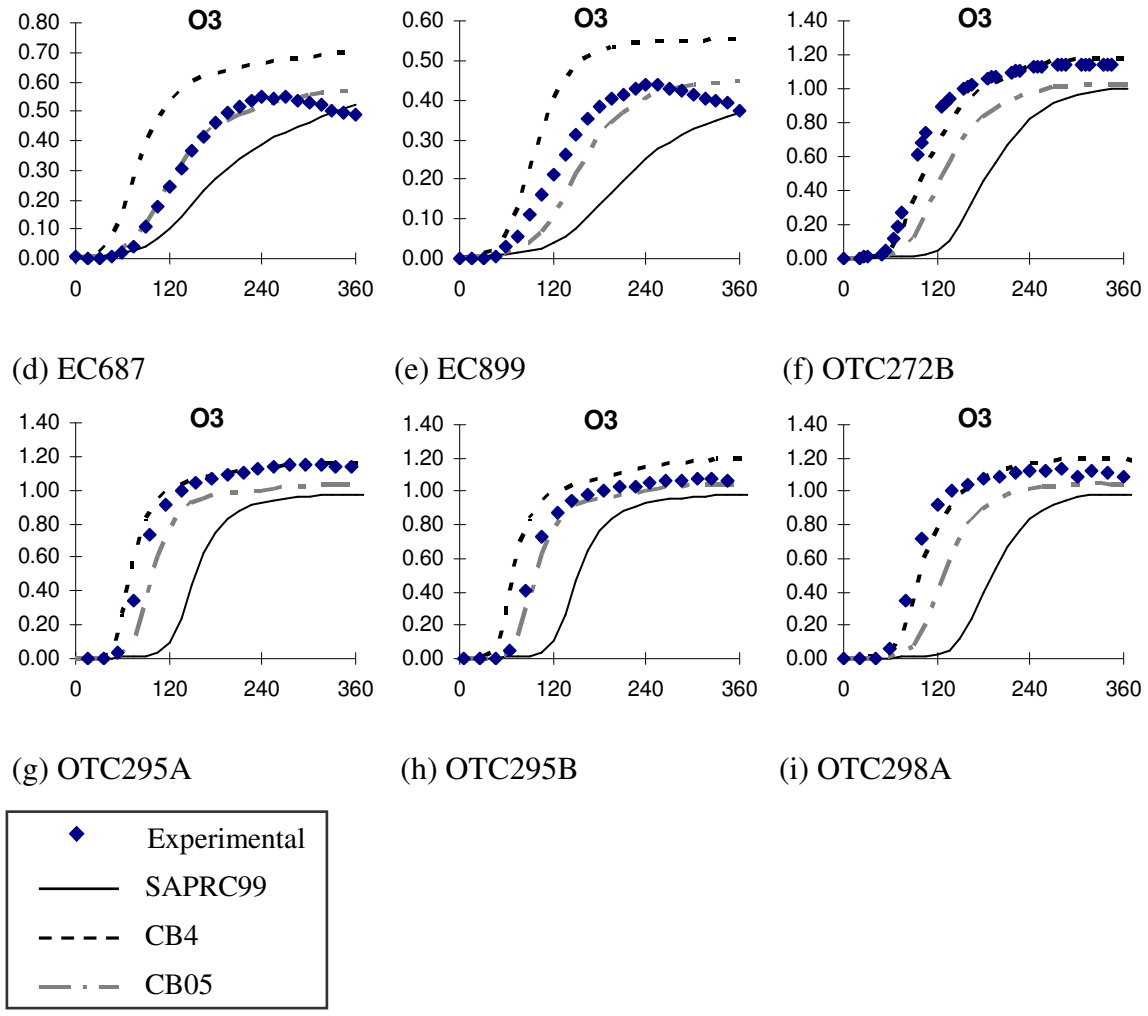

Figure 5-8. Propylene experiments in UCR chambers: O_3 (ppm) as a function of time (min); wall mechanism and PNA on.

The next section provides a more in depth analysis of the UCR olefins experiments and compares the findings to the UNC olefins experiments.

5.3 COMPARISON BETWEEN THE SAPRC99 AND CB SIMULATIONS AND UNC AND UCR CHAMBER DATA FOR OLEFINS

For a further inspection of the predictions of olefins in the UNC and UCR experiments, the underpredictions in peak ozone concentrations produced with the mechanisms relative to the measured ozone peaks in the chambers were evaluated as a

function of the VOC/NOx ratio of the experiments. The underprediction in predicted peak ozone concentrations relative to the experiments were calculated as follows:

(Experimental peak ozone – Model peak ozone)/(Experimental peak ozone)

The percentage of underprediction by each mechanism for the terminal olefins experiments in the UNC and UCR experiments are reported in Tables 5-5 – 5-8.

In order to consider the different reactivities of olefins with respect to ozone formation in this assessment, the Maximum Incremental ozone Reactivities (MIRs) of the different olefins were utilized. The MIR is a measure of effect of a VOC on ozone formation in a set of standard airshed scenarios that represent NOx conditions where ozone formation is most sensitive to VOCs (Carter, 1994a; Carter, 2000). Table 5-2 gives MIRs for ethylene and propylene retrieved from Carter (2000) in units of grams ozone per gram VOC emitted. The underprediction in simulated peak ozone concentrations were also plotted against values of (MIR*VOC)/NOx for the ethylene and propylene experiments in the UNC and UCR chambers. The underprediction error versus (MIR*VOC)/NOx in the UNC and UCR experiments for ethylene are presented in Figures 5-11 and 5-12, respectively, and for the propylene, in Figures 5-15 and 5-16, respectively.

Table 5-2. Maximum Incremental ozone Reactivities (MIRs) for ethylene and propylene in units of grams ozone per gram VOC emitted (Carter, 2000).

VOC	MIR (g/g)
Ethylene	9.08
Propylene	11.58

Table 5-5. Comparison between the SAPRC99 and CB simulations and UNC chamber data for ethylene.

	Experiment	AU2497 Red	AU2497 Blue
	VOC (ppmC)	3.840	3.680
	NOx (ppm)	0.321	0.318
	VOC/NOx	11.963	11.572
Peak Ozone (ppm)	SAPRC99	0.808	0.794
	CB-IV	0.819	0.807
	CB05	0.786	0.774
	Experiment	1.143	1.059
(Experimental-Model) /Experimental	SAPRC99	29.31%	25.02%
	CB-IV	28.35%	23.80%
	CB05	31.23%	26.91%
	MIR (g/g)	9.08	9.08
	MIR*VOC/NOx	108.6	105.1

Table 5-6. Comparison between the SAPRC99 and CB simulations and UNC chamber data for propylene.

	Experiment	ST1995 Red	JN2392 Red	JN2392 Blue	JN1798 Red
	VOC (ppmC)	6.120	0.908	0.907	1.737
	NOx (ppm)	0.670	0.384	0.384	0.492
	VOC/NOx	9.134	2.365	2.362	3.530
Peak Ozone (ppm)	SAPRC99	0.611	0.411	0.397	0.891
	CB-IV	0.562	0.436	0.422	0.890
	CB05	0.599	0.386	0.374	0.815
	Experiment	1.146	0.453	0.441	0.968
(Experimental-Model) /Experimental	SAPRC99	46.68%	9.27%	9.98%	7.95%
	CB-IV	50.96%	3.75%	4.31%	8.06%
	CB05	47.73%	14.79%	15.19%	15.81%
	MIR (g/g)	11.58	11.58	11.58	11.58
	MIR*VOC/NOx	105.8	27.4	27.4	40.9

Table 5-7. Comparison between the SAPRC99 and CB simulations and UCR chamber data for ethylene.

	Experiment	EPA073A	XTC105	XTC112	EC285	EC287	TVA008	OTC278B	OTC279A	OTC304B
	VOC (ppmC)	1.234	3.472	5.114	3.898	7.990	0.502	1.254	2.018	1.998
	NOx (ppm)	0.025	0.241	0.518	1.014	0.545	0.052	0.465	0.531	0.232
	VOC/NOx	49.376	14.407	9.873	3.844	14.661	9.662	2.698	3.800	8.610
Peak Ozone (ppm)	SAPRC99	0.237	0.639	0.844	1.129	1.073	0.205	0.187	0.590	0.780
	CB-IV	0.243	0.569	0.734	0.990	1.102	0.190	0.023	0.181	0.635
	CB05	0.234	0.650	0.863	1.053	1.050	0.189	0.229	0.608	0.760
	Experiment	0.281	0.781	0.934	0.837	0.961	0.209	0.387	0.984	0.845
(Experimental-Model) /Experimental	SAPRC99	15.73%	18.14%	9.59%	-34.89%	-11.65%	1.96%	51.73%	39.98%	24.84%
	CB-IV	13.59%	27.17%	21.47%	-18.24%	-14.67%	9.14%	94.19%	81.57%	10.02%
	CB05	16.90%	16.75%	7.59%	-25.81%	-9.26%	9.38%	40.88%	38.17%	10.02%
	MIR (g/g)	9.08	9.08	9.08	9.08	9.08	9.08	9.08	9.08	9.08
	MIR*VOC/NOx	448.33	130.81	89.64	34.91	133.12	87.73	24.49	34.51	78.18

Table 5-8. Comparison between the SAPRC99 and CB simulations and UCR chamber data for propylene.

	Experiment	EC216	EC277	EC314	EC687	EC899	OTC272B	OTC295A	OTC295B	OTC298A
	VOC (ppmC)	1.509	1.692	3.186	3.120	3.180	3.087	4.371	4.335	3.747
	NOx (ppm)	0.524	0.114	0.980	0.470	0.485	0.530	0.535	0.520	0.582
	VOC/NOx	2.879	14.845	3.251	6.638	6.557	5.825	8.170	8.337	6.438
Peak Ozone (ppm)	SAPRC99	0.630	0.378	0.835	0.521	0.370	0.999	0.977	0.981	0.986
	CB-IV	0.624	0.421	0.920	0.699	0.554	1.180	1.165	1.192	1.199
	CB05	0.558	0.393	0.823	0.577	0.450	1.028	1.032	1.045	1.048
	Experiment	0.563	0.299	0.725	0.547	0.440	1.145	1.147	1.079	1.134
(Experimental-Model) /Experimental	SAPRC99	-11.85%	-26.40%	-15.16%	4.68%	16.02%	12.76%	14.81%	9.05%	13.03%
	CB-IV	-10.83%	-40.57%	-26.92%	-27.84%	-25.93%	-3.06%	-1.57%	-10.47%	-5.73%
	CB05	0.83%	-31.32%	-13.52%	-5.45%	-2.36%	10.22%	10.03%	3.15%	7.58%
	MIR (g/g)	11.58	11.58	11.58	11.58	11.58	11.58	11.58	11.58	11.58
	MIR*VOC/NOx	33.34	171.90	37.65	76.87	75.93	67.45	94.61	96.54	74.55

The underprediction of the peak ozone concentrations in the mechanisms relative to the experimental peak ozone concentrations in the UNC ethylene experiments are presented in Figure 5-9. The three mechanisms all underpredict the experimental peak ozone concentrations for the ethylene experiments. The underprediction with the CB-IV mechanism is slightly less than the underprediction with the SAPRC99 mechanism. The CB05 mechanism shows the highest percentage of underprediction relative to the experimental peak ozone concentrations.

In the UCR ethylene experiments, with the exception of the EC experiments where the mechanisms overpredict peak ozone concentrations relative to measurements, the mechanisms underpredict peak ozone concentrations relative to experimental peak ozone. As reported in Table 5-7, in the OTC278B, and OTC279A experiments, the percentage underprediction with CB-IV is greater than 80%.

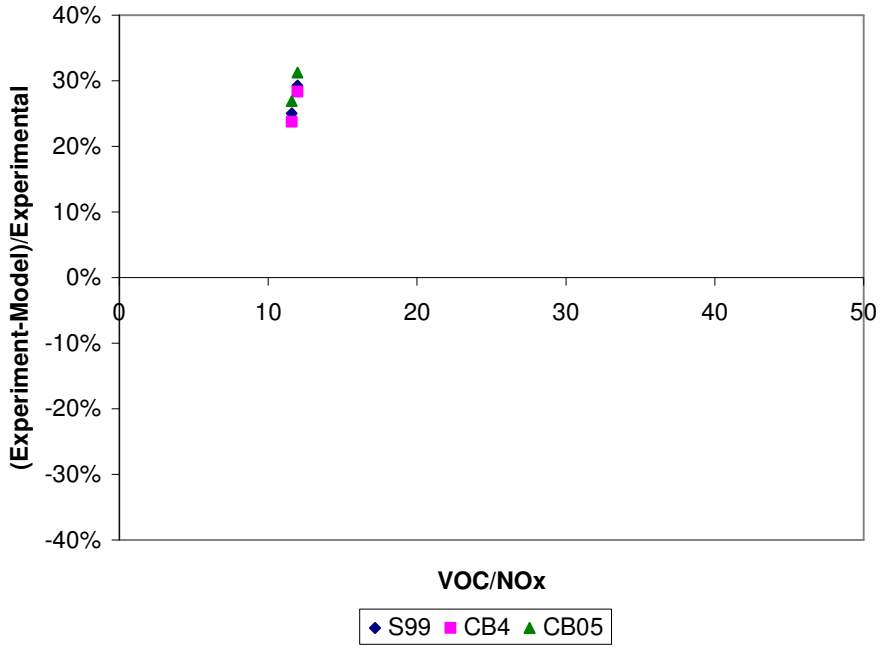

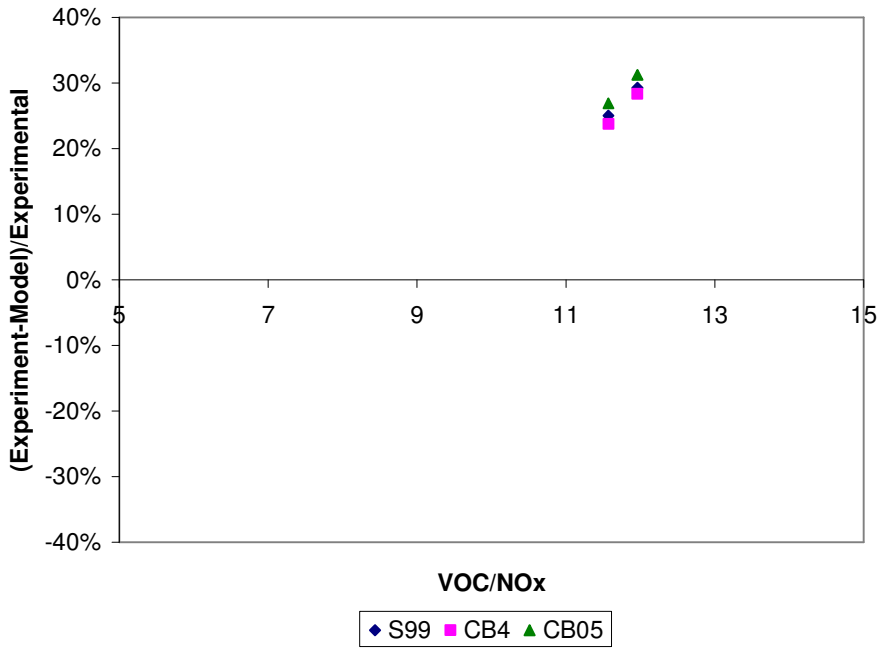

Figure 5-9. Model underprediction error for peak ozone in UNC chamber ethylene experiments against VOC/NOx ratio.

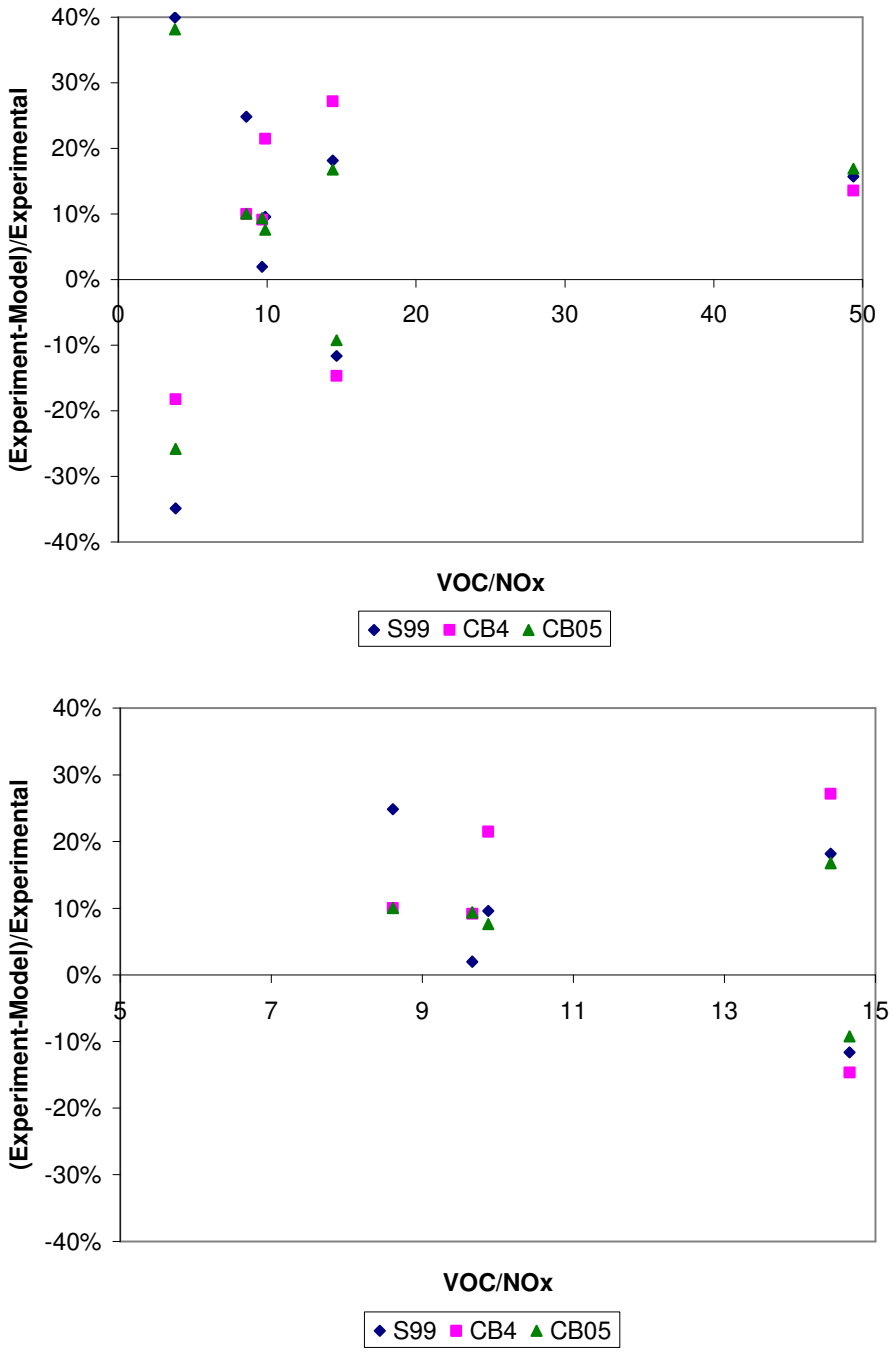

Figure 5-10. Model underprediction error for peak ozone in UCR chamber ethylene experiments against VOC/NOx ratio.

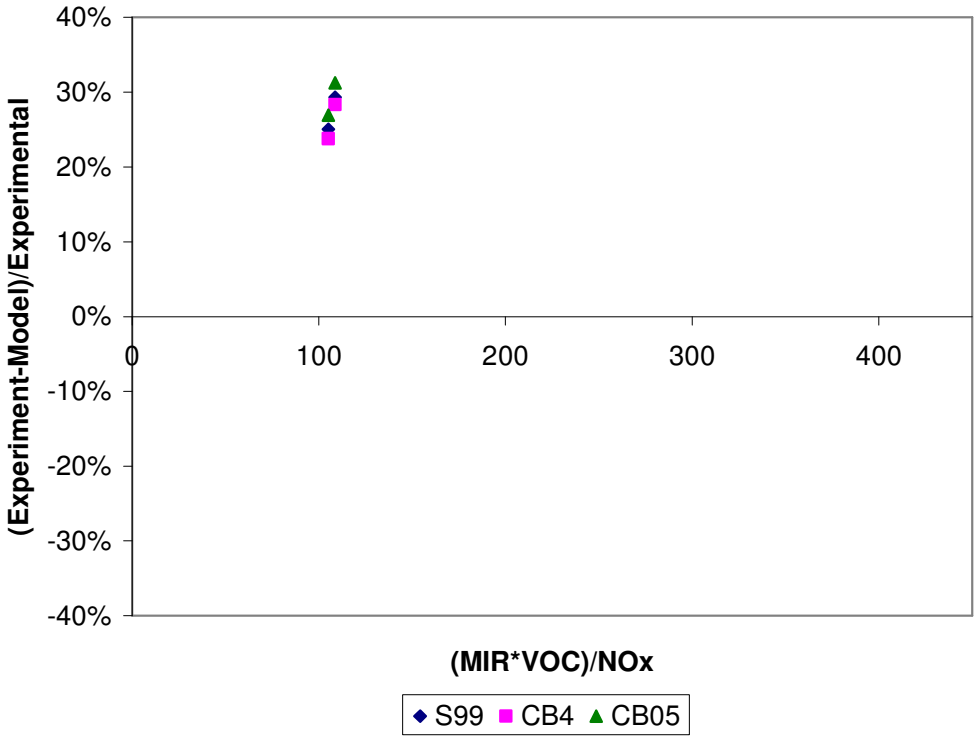

Figure 5-11. Model underprediction error for peak ozone in UNC chamber ethylene experiments against (MIR*VOC)/NOx ratio.

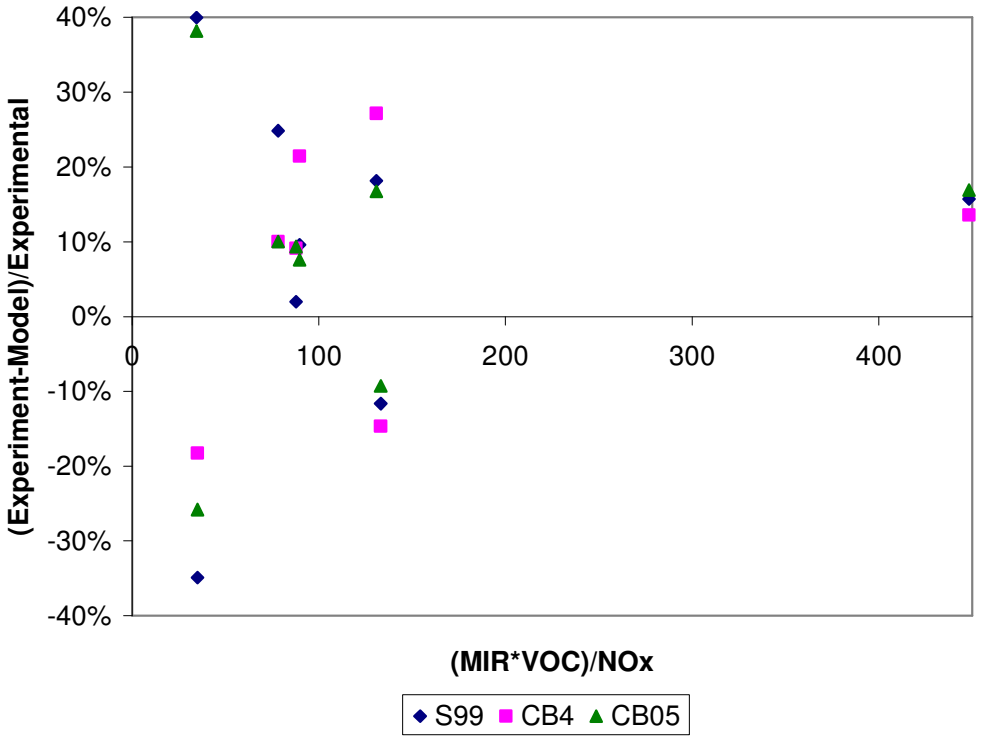

Figure 5-12. Model underprediction error for peak ozone in UCR chamber ethylene experiments against (MIR*VOC)/NOx ratio.

For the propylene experiments at UNC, as shown in Figure 5-13, as in the ethylene experiments, the mechanisms generally underpredict ozone concentrations relative to the experiments. As reported in Table 5-6, in the ST1995 propylene experiment, all three mechanisms show an underprediction of greater than 40% relative to the experimental peak ozone. In all but the ST1995 experiment, CB05 shows the greatest underprediction relative to the measured maximum ozone concentrations.

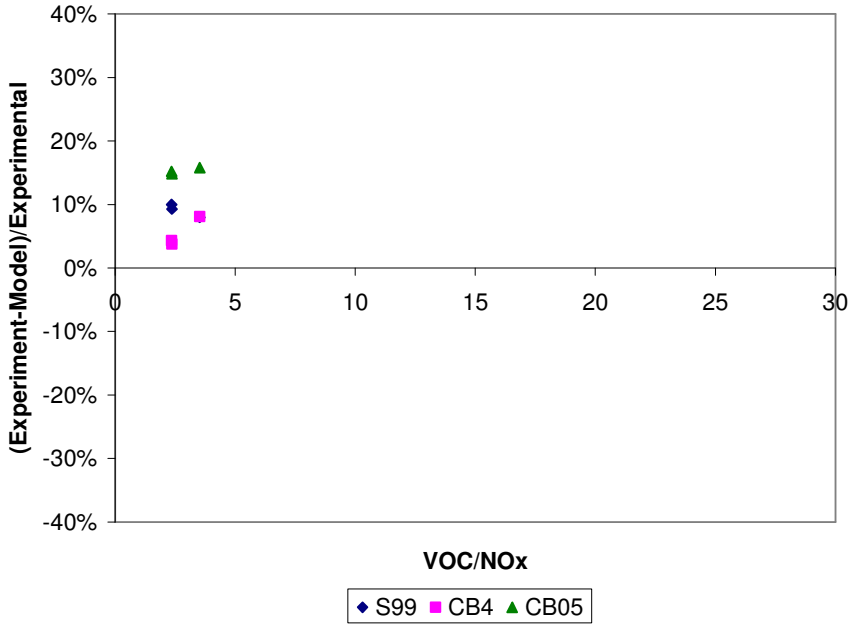

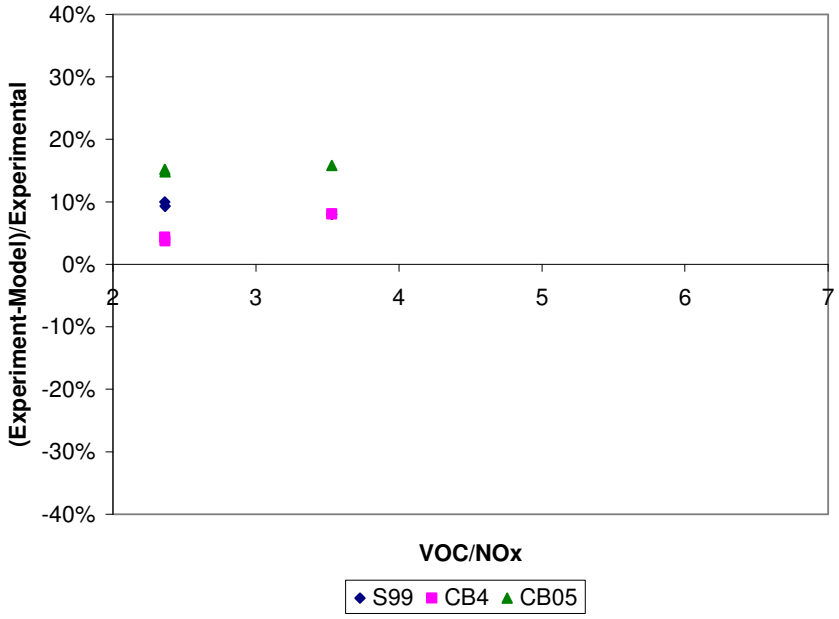

Figure 5-13. Model underprediction error for peak ozone in UNC chamber propylene experiments against VOC/NOx ratio.

The mechanism underpredictions for the UCR propylene experiments are shown in Figure 5-14. The mechanisms show both underpredictions and overpredictions of peak ozone relative to measured peak ozone in these experiments.

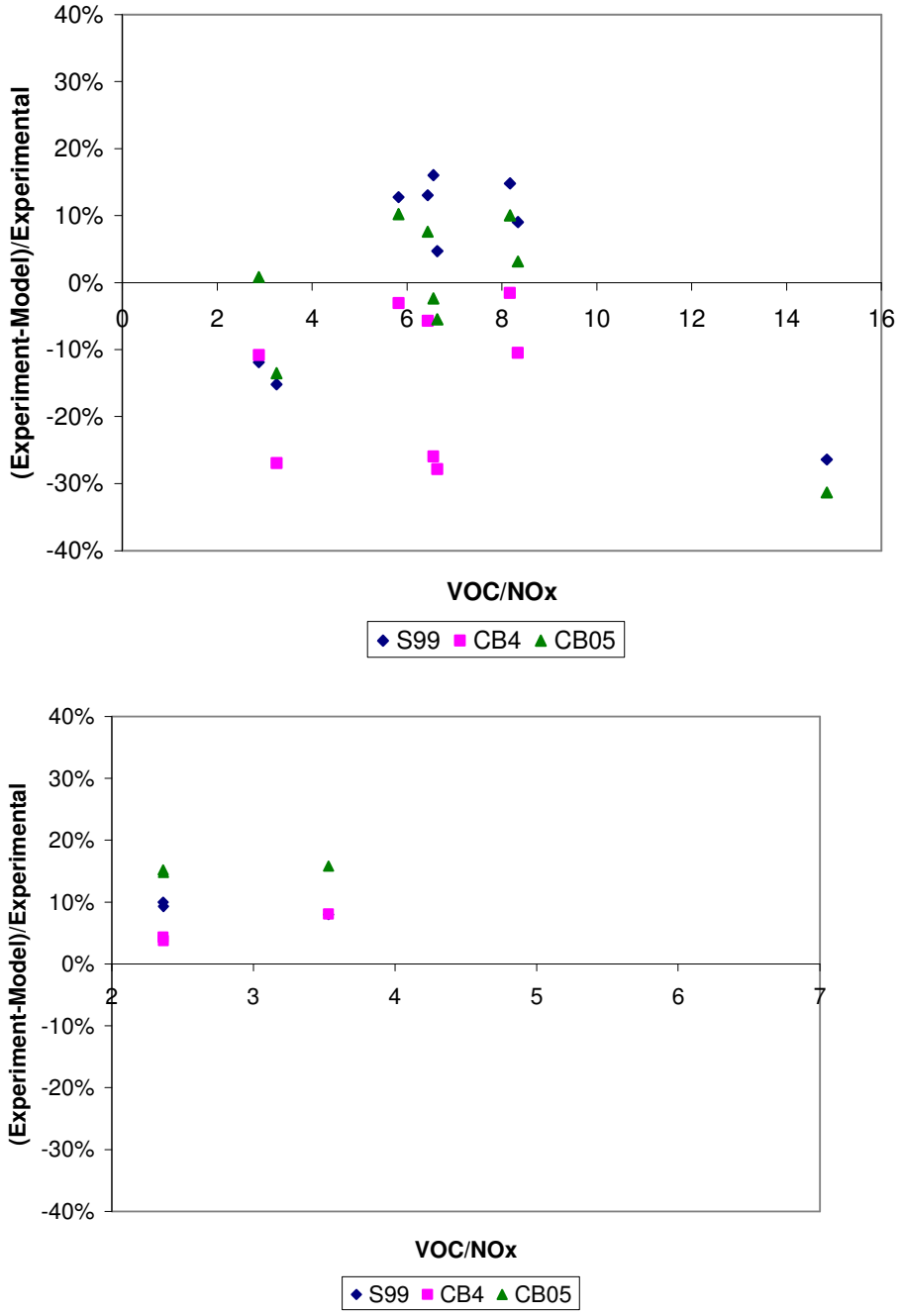

Figure 5-14. Model underprediction error for peak ozone in UCR chamber propylene experiments against VOC/NOx ratio.

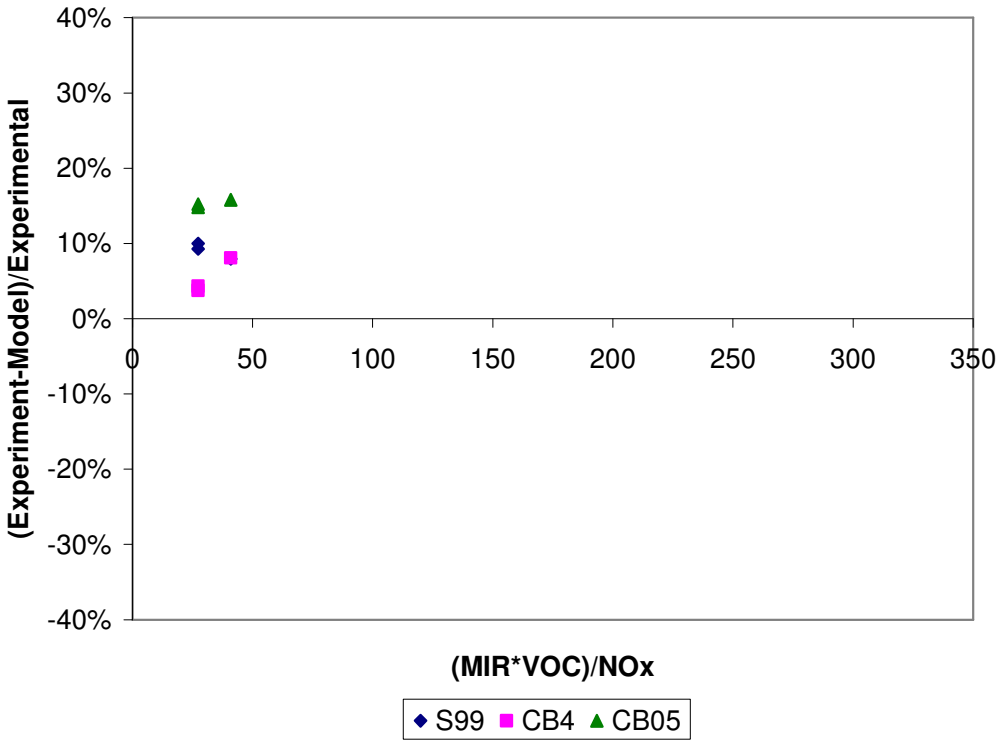

Figure 5-15. Model underprediction error for peak ozone in UNC chamber propylene experiments against (MIR*VOC)/NOx ratio.

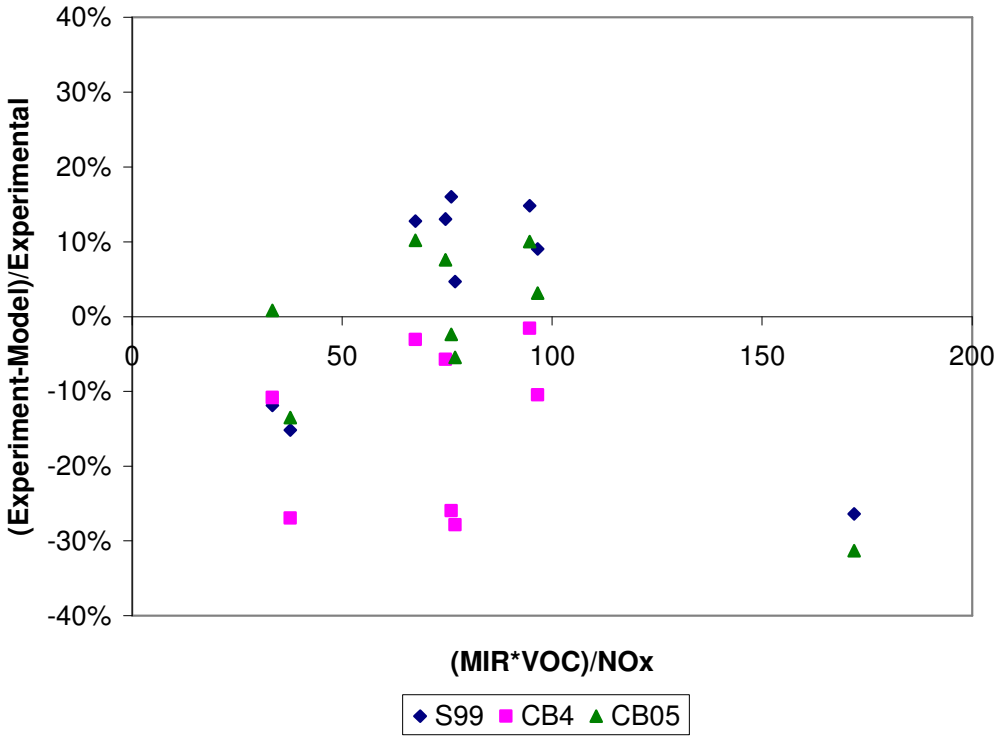

Figure 5-16. Model underprediction error for peak ozone in UCR chamber propylene experiments against (MIR*VOC)/NOx ratio.

5.4 Effect of the OH + NO_2 Rate Constant on Simulations of Olefins Chemistry

Other members of our research group investigated the sensitivity of the mechanism predictions in CO-NOx experiments to the OH+NO_2 rate constant. These results are provided in Appendix F. Equating the rate constant for the OH + NO_2 reaction in CB-IV, CB05, and SAPRC99 mechanisms led to convergence in the concentrations of O_3, OH, HO_2, NO and NO_2 with the wall mechanism turned off. This suggests that in photochemical modeling simulations, where wall reactions are not included, the major differences in the inorganic chemistry between the mechanisms are due to differences in the rate parameters of the OH + NO_2 reaction. However, since at least some of the

important parameters in the chamber wall models are derived by modeling chamber data that are sensitive to the OH + NO_2 rate constant, just changing the OH+NO_2 rate constant does not provide a straightforward comparison of the importance of this reaction when modeling experiments with the wall effects represented. In evaluating a single set of chamber data, the OH + NO_2 rate constant and the chamber effects parameters deriving from modeling experiments sensitive to it can be changed in a consistent manner when assessing the effects of this rate constant on model performance. But this linkage between wall mechanisms tuned to individual chambers and the OH + NO_2 rate constant make comparisons across chambers very difficult and make assessments of how the mechanism will perform in the absence of chamber effects (e.g., in regional photochemical models) very difficult.

In accordance with the hierarchical approach of evaluating chemical mechanisms, additional simulations were conducted for the olefin experiments in which the effect of interchanging the OH+NO_2 rate constants in the SAPRC99 and CB-IV experiments in the olefins experiments were studied. Specifically, the following simulations were added to the ethylene and propylene analyses:

- SAPRC99 with OH+NO_2=HNO_3 rate constant increased to equal the rate constant in CB-IV, labeled "S99 with CB4 HNO_3".
- CB-IV with OH+NO_2=HNO_3 rate constant decreased to equal the rate constant in SAPRC99, labeled "CB4 with S99 HNO_3".

5.4.1 Effect of the OH+NO_2 rate constant in the SAPRC99 and CB Simulations of the UNC Chamber Experiments for olefins

The results of simulations for the olefins experiments at UNC are presented in Figures 5-17 to 5-21. Also, the peak ozone concentrations predicted with SAPRC99 and

CB-IV with modified rates of $OH+NO_2$ for UNC ethylene and propylene experiments are reported in Tables 5-9 and 5-10, respectively.

In the ethylene experiments, increasing the $OH+NO_2$ rate constant in SAPRC99 to that of CB-IV slightly decreases the peak ozone concentrations predicted with SAPRC99. Decreasing the CB-IV $OH+NO_2$ rate constant to that of SAPRC99 increases the peak ozone predictions in CB-IV.

In the propylene experiments, the SAPRC99 mechanism predicts lower peak ozone concentrations with the $OH+NO_2$ rate constant increased to that of CB-IV in all but the ST1995 propylene experiment in which the peak ozone in SAPRC99 slightly increases with the increased rate of termination.

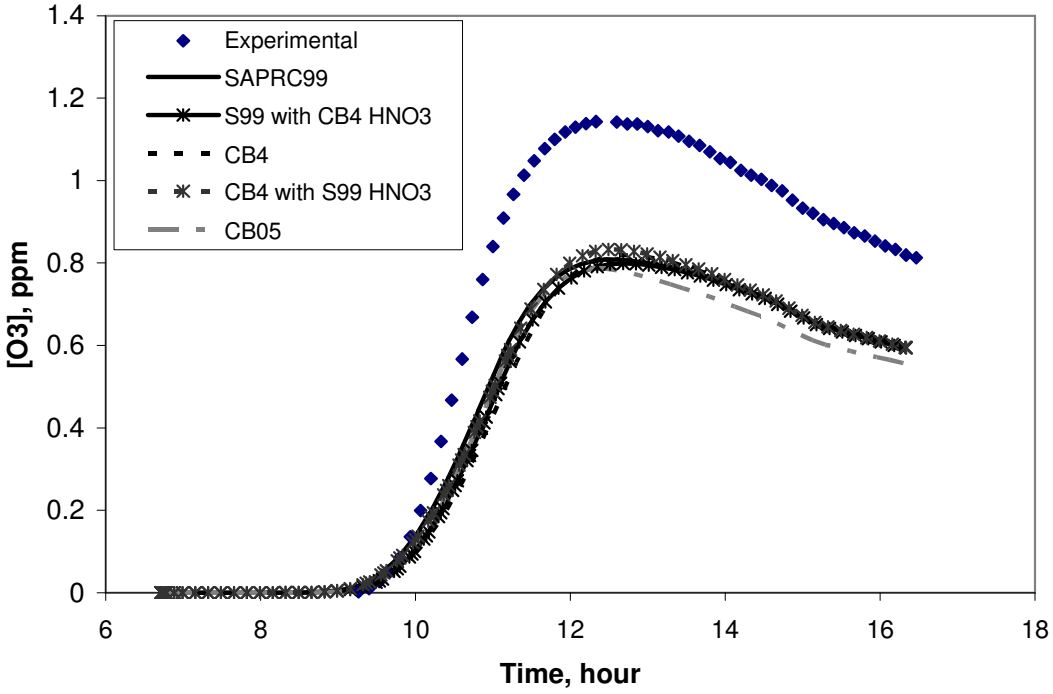

Figure 5-17. AU2497 UNC red chamber experiment with 3.84 ppmC ethylene; wall mechanism and PNA on; switched SAPRC99 and CB-IV $OH+NO_2$ rate constants.

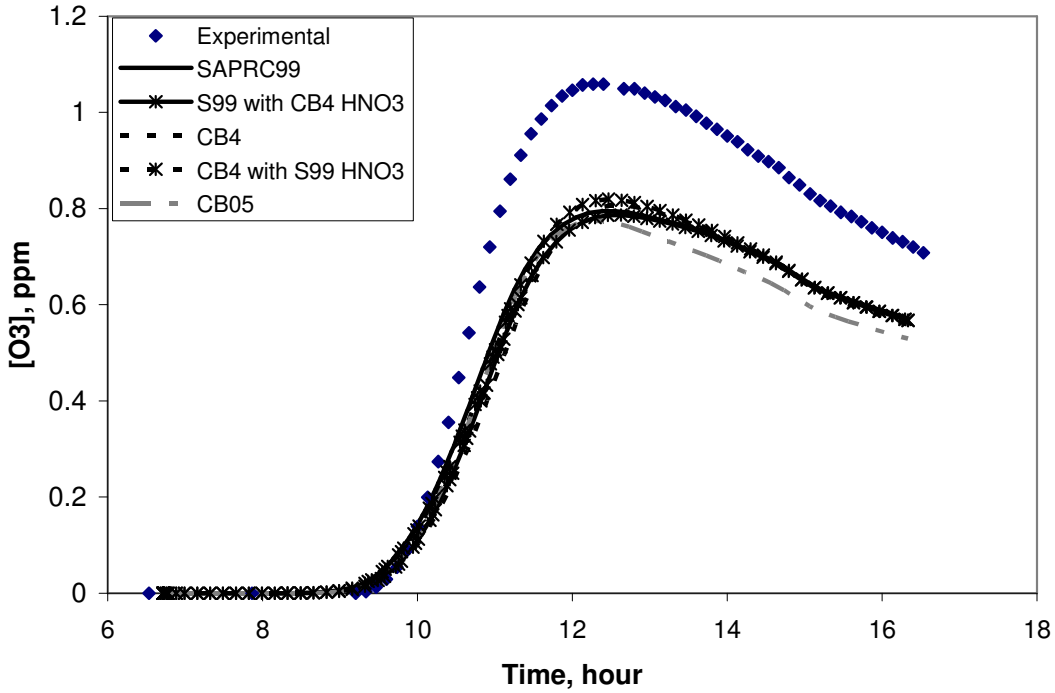

Figure 5-18. AU2497 UNC blue chamber experiment with 3.68 ppmC ethylene; wall mechanism and PNA on; switched SAPRC99 and CB-IV OH+NO_2 rate constants.

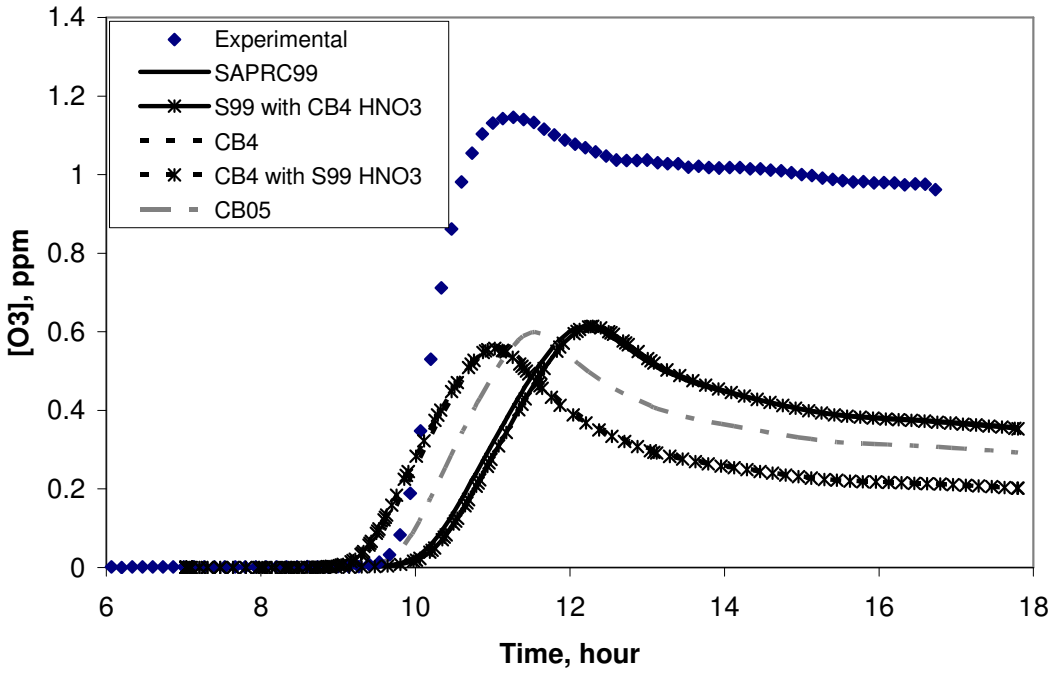

Figure 5-19. ST1995 UNC red chamber experiment with 6.12 ppmC propylene; wall mechanism and PNA on; switched SAPRC99 and CB-IV OH+NO_2 rate constants.

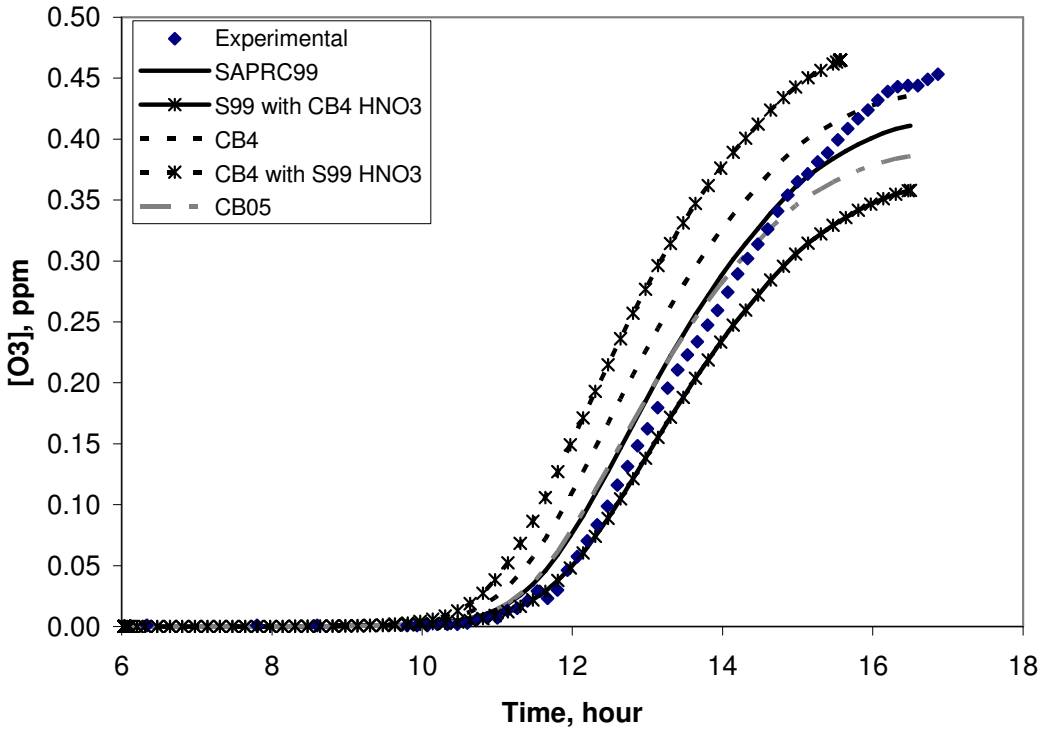

Figure 5-20. JN2392 UNC red chamber experiment with 0.908 ppmC propylene; wall mechanism and PNA on; switched SAPRC99 and CB-IV OH+NO_2 rate constants.

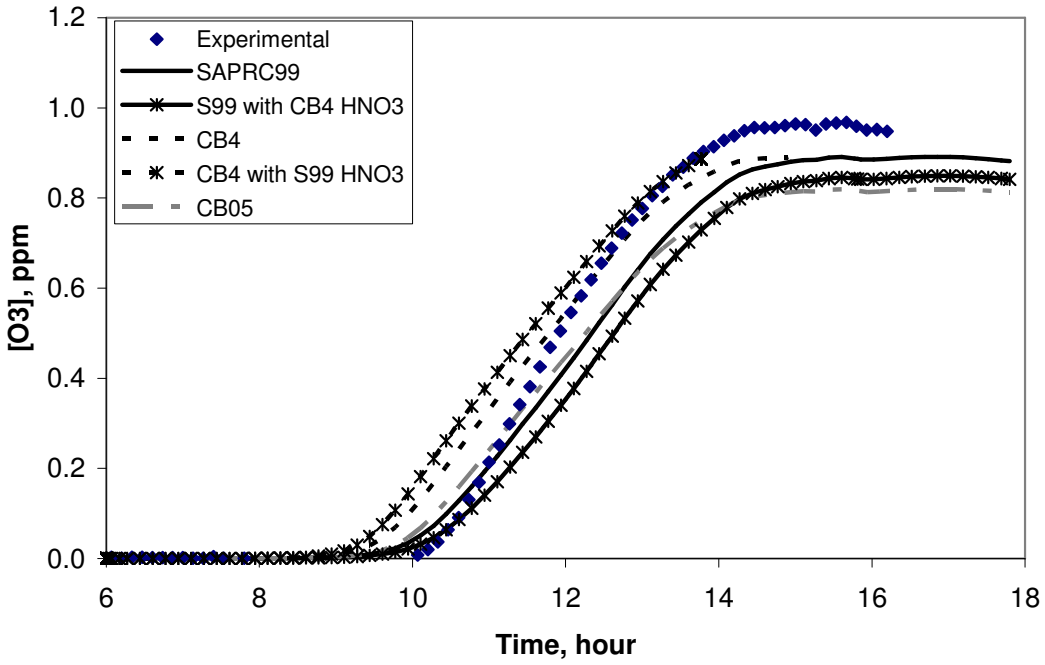

Figure 5-21. JN1798 UNC red chamber experiment with 1.737 ppmC propylene; wall mechanism and PNA on; switched SAPRC99 and CB-IV OH+NO_2 rate constants.

The effect of modifying the OH+NO_2 termination rates in the SAPRC99 and CB-IV mechanisms will be more quantitatively evaluated in Section 5.5.

5.4.2 Effect of the OH+NO_2 rate constant in the SAPRC99 and CB Simulations of the UCR Chamber Experiments for olefins

The sensitivity of the olefin experiments to the OH+NO_2 rate parameter was also studied in the UCR experiments. Figure 5-22 and 5-23 show the effect of increasing the OH+NO_2 rate constant in SAPRC99 to that of CB-IV in the UCR ethylene and propylene experiments, respectively. Figures 5-24 and 5-25 show the effect of decreasing the OH+NO_2 rate constant in CB-IV to that of SAPRC99 in the UCR ethylene and propylene

experiments, respectively. In Section 5.6, Tables 5-11 and 5-12 report the peak ozone concentrations in the UCR olefins experiments with modifications in the OH+NO_2 rate parameter. The increase in the termination rate in SAPRC99 consistently leads to a lower ozone peak relative to the basecase SAPRC99 in the UCR ethylene and propylene experiments. Likewise, decreasing the termination rate in CB-IV leads to higher ozone peak concentrations relative to basecase CB-IV in all the ethylene and propylene experiment except the OTC272B propylene experiment in which decreasing the rate leads to OTC295A propylene experiment.

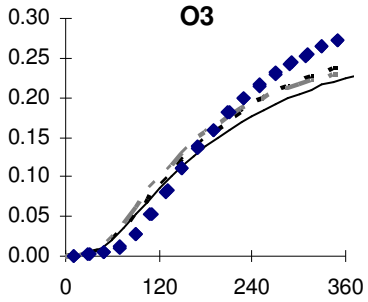

(a) EPA073A

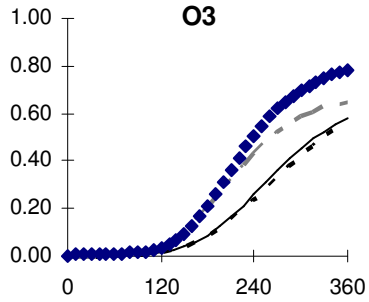

(b) XTC105

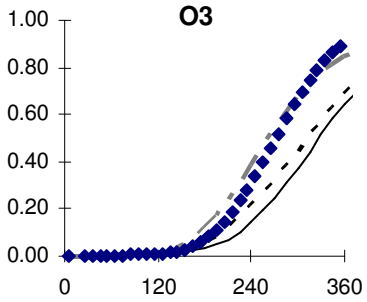

(c) XTC112

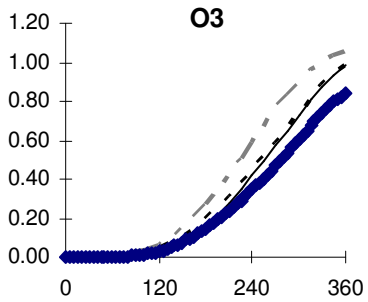

(d) EC285

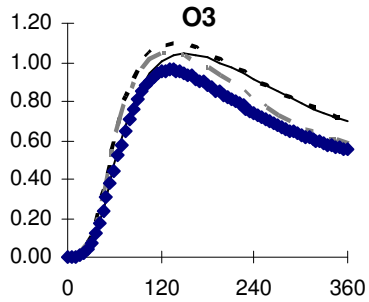

(e) EC287

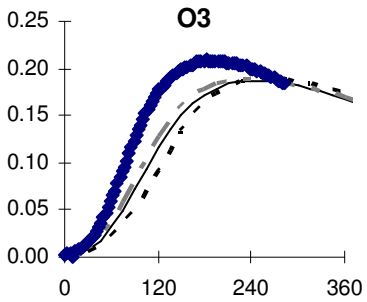

(f) TVA008

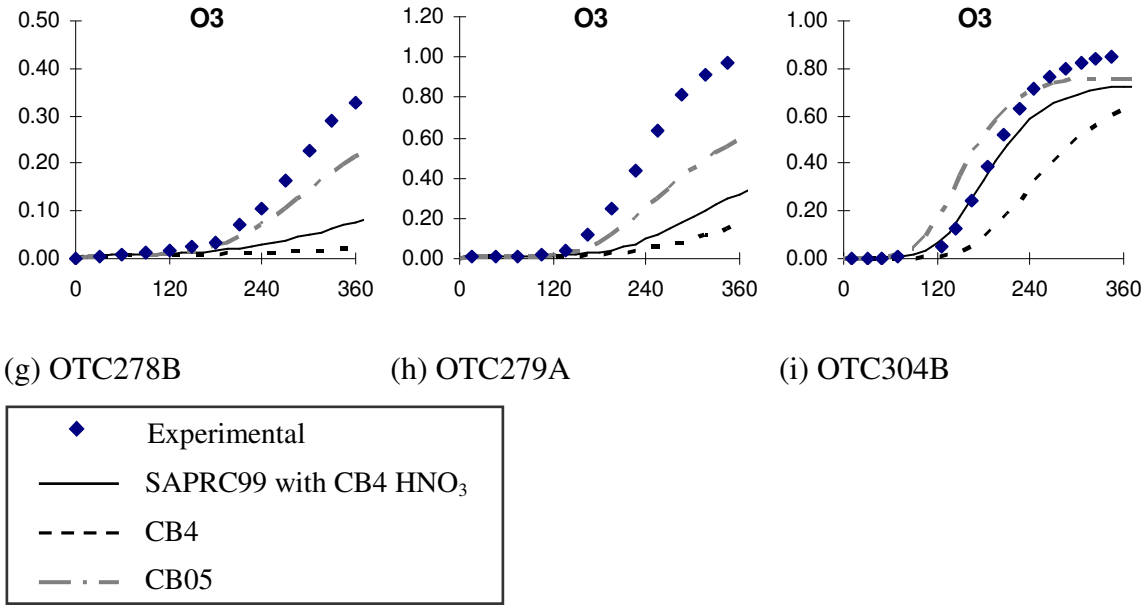

(g) OTC278B (h) OTC279A (i) OTC304B

Figure 5-22. Ethylene experiments in UCR chambers: O_3 (ppm) as a function of time (min); wall mechanism and PNA on; replaced SAPRC99 OH+NO_2 rate constant with CB-IV.

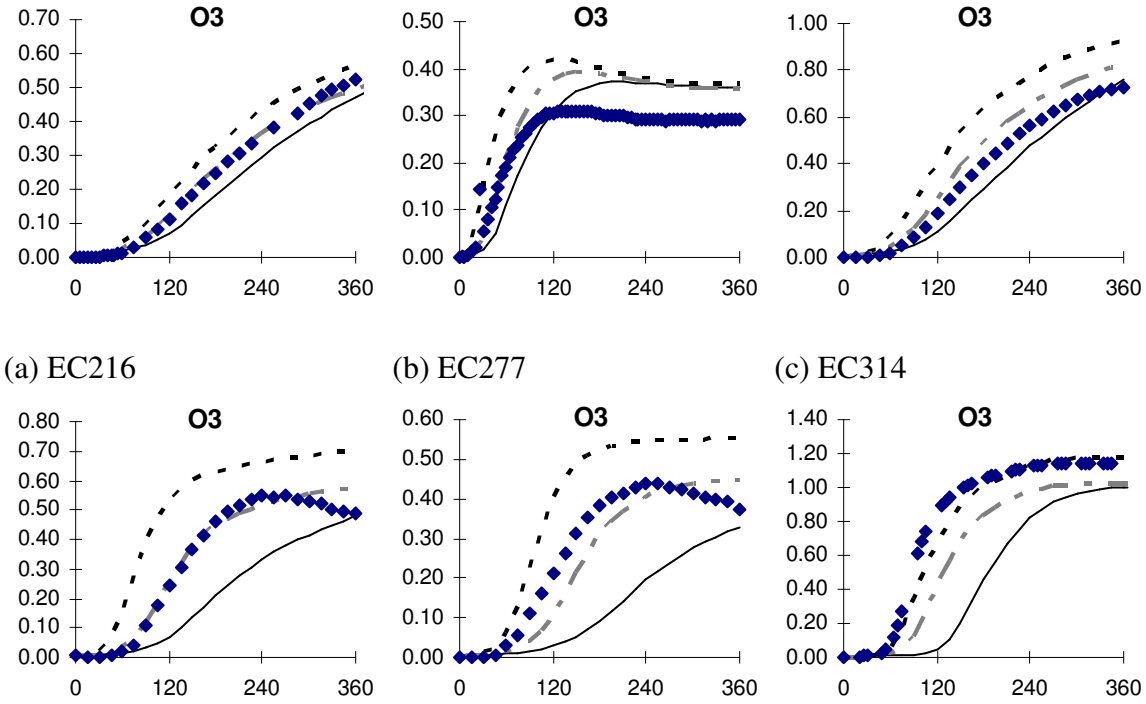

(a) EC216 (b) EC277 (c) EC314

(d) EC687 (e) EC899 (f) OTC272B

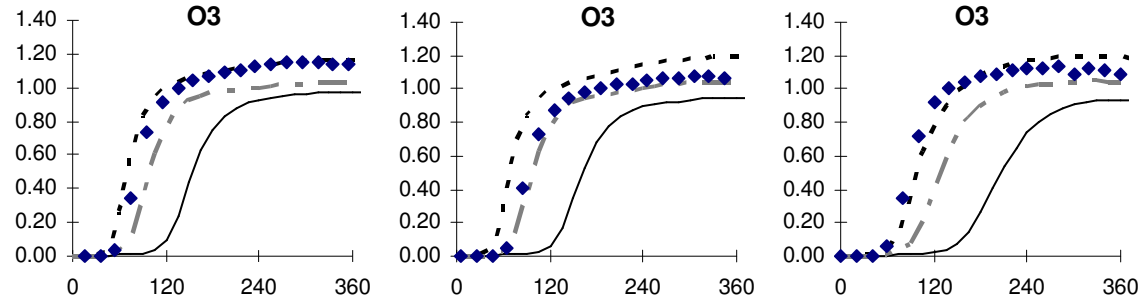

(g) OTC295A (h) OTC295B (i) OTC298A

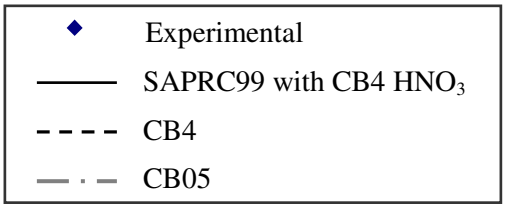

Figure 5-23. Propylene experiments in UCR chambers: O_3 (ppm) as a function of time (min); wall mechanism and PNA on; replaced SAPRC99 OH+NO_2 rate constant with CB-IV.

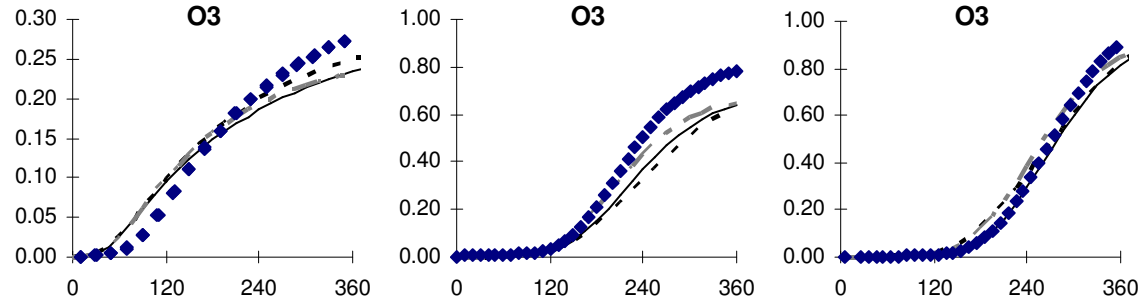

(a) EPA073A (b) XTC105 (c) XTC112

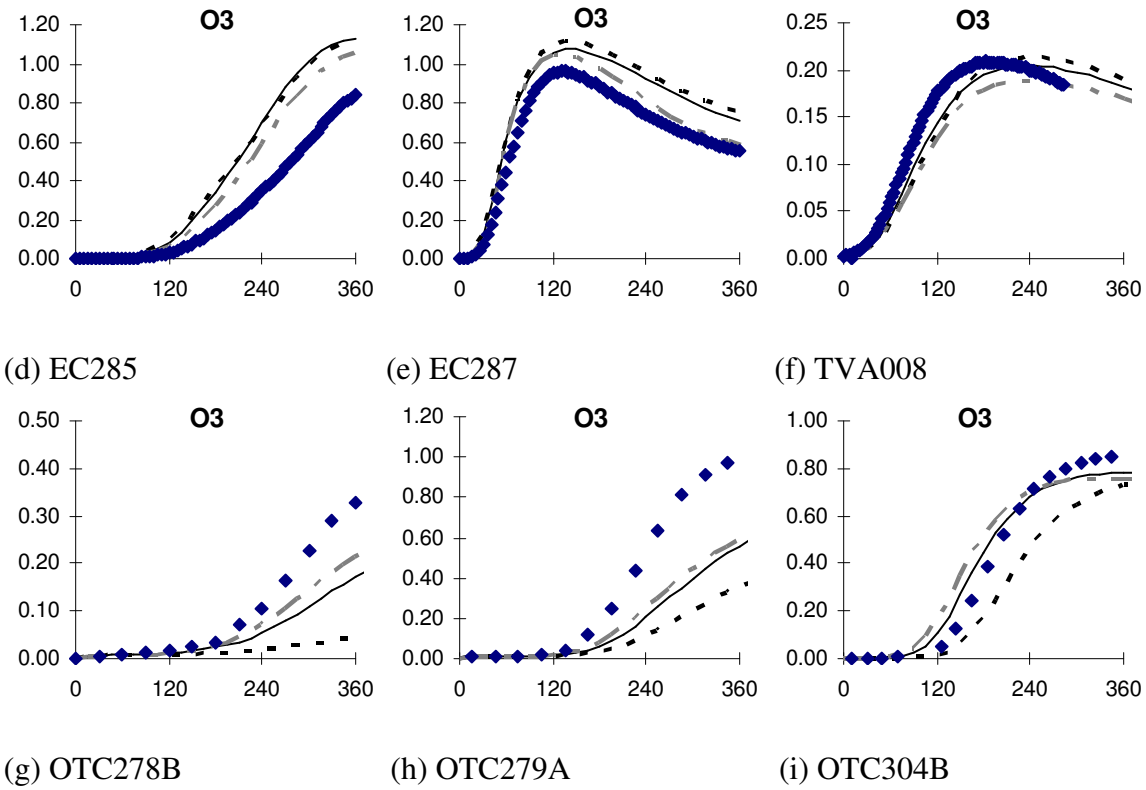

Figure 5-24. Ethylene experiments in UCR chambers: O_3 (ppm) as a function of time (min); wall mechanism and PNA on; replaced CB-IV OH+NO_2 rate constant with SAPRC99.

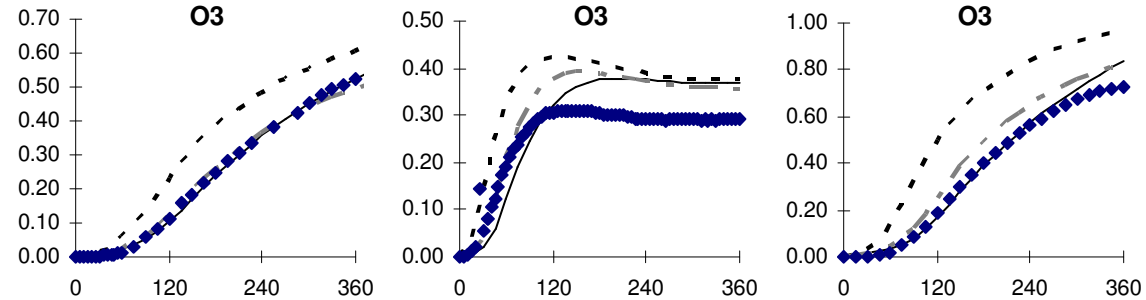

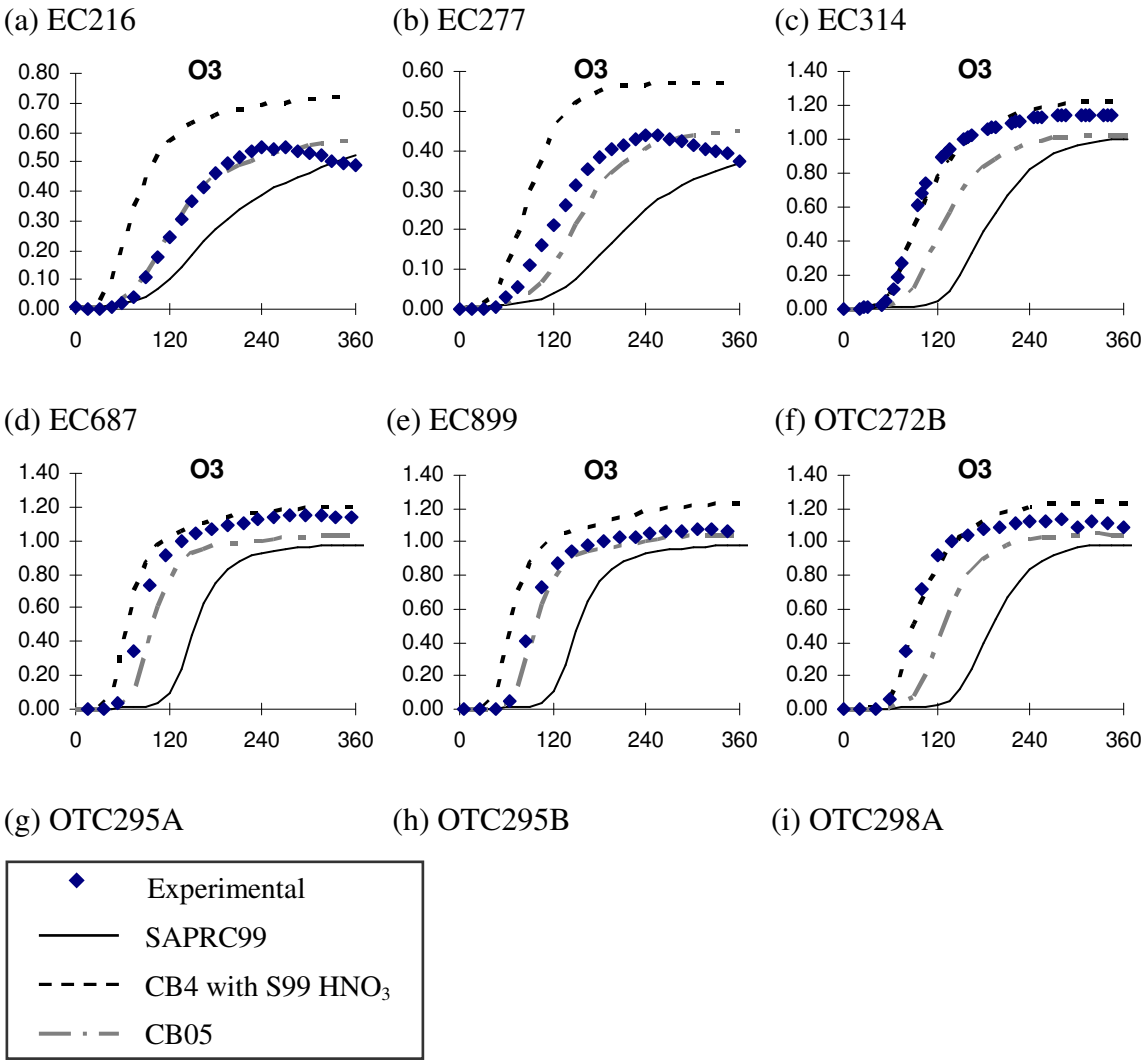

Figure 5-25. Propylene experiments in UCR chambers: O_3 (ppm) as a function of time (min); wall mechanism and PNA on; replaced CB-IV OH+NO_2 rate constant with SAPRC99.

5.6 COMPARISON BETWEEN THE SAPRC99 AND CB SIMULATIONS WITH MODIFIED OH+NO_2 RATE CONSTANTS AND UNC AND UCR CHAMBER DATA FOR OLEFINS

The effect of modifying the OH+NO_2 rate constant in the SAPRC99 and CB-IV simulations on the underprediction of the peak ozone concentrations are evaluated in this section. Tables 6-9 - 6-12 compare the underprediction of the mechanisms in the basecase and modified termination rate scenarios in the UNC and UCR propylene

experiments. In Figures 6-26 - 6-29, in addition to the basecase simulations, SAPRC99 and CB-IV simulations with modified OH+NO_2 rate constants were added. In the UNC ethylene experiments, increasing the termination rate in SAPRC99 slightly increases the underprediction error in SAPRC99 as compared to the basecase. Increasing the termination rate in CB-IV leads to a lower underprediction in peak ozone relative to the basecase scenario.

Table 5-9. Comparison between the SAPRC99 and CB simulations and UNC chamber data for ethylene with modified OH+NO_2 rate constants.

	Experiment	AU2497 Red	AU2497 Blue
	VOC (ppmC)	3.840	3.680
	NOx (ppm)	0.321	0.318
	VOC/NOx	11.963	11.572
Peak Ozone (ppm)	SAPRC99	0.808	0.794
	S99 w/ CB4 HNO_3	0.799	0.786
	CB-IV	0.819	0.807
	CB-IV w/ S99 HNO_3	0.832	0.820
	CB05	0.786	0.774
	Experiment	1.143	1.059
(Experimental-Model) /Experimental	SAPRC99	29.31%	25.02%
	S99 w/ CB4 HNO_3	30.10%	25.78%
	CB-IV	28.35%	23.80%
	CB-IV w/ S99 HNO_3	27.21%	22.57%
	CB05	31.23%	26.91%
	MIR (g/g)	9.08	9.08
	MIR*VOC/NOx	108.6	105.1

In the UNC propylene experiments, in all but the ST1995 propylene experiments, decreasing the $OH+NO_2$ rate in SAPRC99 to that of CB-IV leads to a slightly higher underprediction error of peak ozone. Increasing the termination rate in CB-IV causes a slightly higher underprediction in the ST1995 propylene experiment and an overprediction rather than an underprediction in peak ozone in the JN2392 propylene experiment.

Table 5-10. Comparison between the SAPRC99 and CB simulations and UNC chamber data for propylene with modified $OH+NO_2$ rate constants.

	Experiment	ST1995 Red	JN2392 Red	JN2392 Blue	JN1798 Red
	VOC (ppmC)	6.120	0.908	0.907	1.737
	NOx (ppm)	0.670	0.384	0.384	0.492
	VOC/NOx	9.134	2.365	2.362	3.530
Peak Ozone (ppm)	SAPRC99	0.611	0.411	0.397	0.891
	S99 w/ CB4 HNO_3	0.614	0.358	0.346	0.849
	CB-IV	0.562	0.436	0.422	0.890
	CB-IV w/ S99 HNO_3	0.559	0.465	-	-
	CB05	0.599	0.386	0.374	0.815
	Experiment	1.146	0.453	0.441	0.968
(Experimental-Model) /Experimental	SAPRC99	46.68%	9.27%	9.98%	7.95%
	S99 w/ CB4 HNO_3	46.42%	20.97%	21.54%	12.29%
	CB-IV	50.96%	3.75%	4.31%	8.06%
	CB-IV w/ S99 HNO_3	51.22%	-2.65%	-	-
	CB05	47.73%	14.79%	15.19%	15.81%
	MIR (g/g)	11.58	11.58	11.58	11.58
	MIR*VOC/NOx	105.8	27.4	27.4	40.9

In the UCR ethylene experiments, SAPRC99 shows a lower underprediction of peak ozone when the $OH+NO_2$ termination rate is increased to that of CB-IV. Except for

the EC experiments, there is a lower bias when the termination is decreased in the CB-IV mechanism.

Likewise, in the UCR propylene experiments, changing the main termination rate constant in SAPRC99 decreases the underprediction error relative to the basecase. Equating the termination rate in CB-IV to that of SAPRC99 increases the bias in CB-IV in the propylene experiments.

Table 5-11. Comparison between the SAPRC99 and CB simulations and UCR chamber data for ethylene with modified $OH+NO_2$ rate constants.

	Experiment	EPA073A	XTC105	XTC112	EC285	EC287	TVA008	OTC278B	OTC279A	OTC304B
	VOC (ppmC)	1.234	3.472	5.114	3.898	7.990	0.502	1.254	2.018	1.998
	NOx (ppm)	0.025	0.241	0.518	1.014	0.545	0.052	0.465	0.531	0.232
	VOC/NOx	49.376	14.407	9.873	3.844	14.661	9.662	2.698	3.800	8.610
Peak Ozone (ppm)	SAPRC99	0.237	0.639	0.844	1.129	1.073	0.205	0.187	0.590	0.780
	S99 w/ CB4 HNO_3	0.228	0.578	0.695	0.981	1.043	0.187	0.083	0.346	0.727
	CB-IV	0.243	0.569	0.734	0.990	1.102	0.190	0.023	0.181	0.635
	CB-IV w/ S99 HNO_3	0.251	0.631	0.855	1.130	1.115	0.214	0.052	0.378	0.741
	CB05	0.234	0.650	0.863	1.053	1.050	0.189	0.229	0.608	0.760
	Experiment	0.281	0.781	0.890	0.837	0.961	0.209	0.387	0.969	0.845
(Experimental-Model) /Experimental	SAPRC99	15.73%	18.14%	5.12%	-34.89%	-11.65%	1.96%	51.73%	39.08%	7.67%
	S99 w/ CB4 HNO_3	18.93%	26.06%	21.92%	-17.25%	-8.53%	10.53%	78.50%	64.27%	14.01%
	CB-IV	13.59%	27.17%	17.58%	-18.24%	-14.67%	9.14%	94.19%	81.29%	24.84%
	CB-IV w/ S99 HNO_3	10.68%	19.21%	3.93%	-35.01%	-16.02%	-2.20%	86.51%	61.04%	12.36%
	CB05	16.90%	16.75%	3.02%	-25.81%	-9.26%	9.38%	40.88%	37.24%	10.02%
	MIR (g/g)	9.08	9.08	9.08	9.08	9.08	9.08	9.08	9.08	9.08
	MIR*VOC/NOx	448.33	130.81	89.64	34.91	133.12	87.73	24.49	34.51	78.18

Table 5-12. Comparison between the SAPRC99 and CB simulations and UCR chamber data for propylene with modified $OH+NO_2$ rate constants.

	Experiment	EC216	EC277	EC314	EC687	EC899	OTC272B	OTC295A	OTC295B	OTC298A
	VOC (ppmC)	1.509	1.692	3.186	3.120	3.180	3.087	4.371	4.335	3.747
	NOx (ppm)	0.524	0.114	0.980	0.470	0.485	0.530	0.535	0.520	0.582
	VOC/NOx	2.879	14.845	3.251	6.638	6.557	5.825	8.170	8.337	6.438
Peak Ozone (ppm)	SAPRC99	0.630	0.378	0.835	0.521	0.370	0.999	0.977	0.981	0.986
	S99 w/ CB4 HNO_3	0.590	0.372	0.757	0.487	0.327	0.951	0.945	0.950	0.938
	CB-IV	0.624	0.421	0.920	0.699	0.554	1.180	1.165	1.192	1.199
	CB-IV w/ S99 HNO_3	0.657	0.425	0.959	0.721	0.571	1.226	1.200	1.228	1.240
	CB05	0.558	0.393	0.823	0.577	0.450	1.028	1.032	1.045	1.048
	Experiment	0.563	0.311	0.725	0.547	0.440	1.145	1.147	1.079	1.134
(Experimental-Model) /Experimental	SAPRC99	-11.85%	-21.49%	-15.16%	4.68%	16.02%	12.76%	14.81%	9.05%	13.03%
	S99 w/ CB4 HNO_3	-4.81%	-19.37%	-4.47%	10.97%	25.70%	16.99%	17.64%	11.98%	17.27%
	CB-IV	-10.83%	-35.11%	-26.92%	-27.84%	-25.93%	-3.06%	-1.57%	-10.47%	-5.73%
	CB-IV w/ S99 HNO_3	-16.66%	-36.62%	-32.28%	-31.81%	-29.77%	-7.07%	-4.62%	-13.81%	-9.35%
	CB05	0.83%	-26.21%	-13.52%	-5.45%	-2.36%	10.22%	10.03%	3.15%	7.58%
	MIR (g/g)	11.58	11.58	11.58	11.58	11.58	11.58	11.58	11.58	11.58
	MIR*VOC/NOx	33.34	171.90	37.65	76.87	75.93	67.45	94.61	96.54	74.55

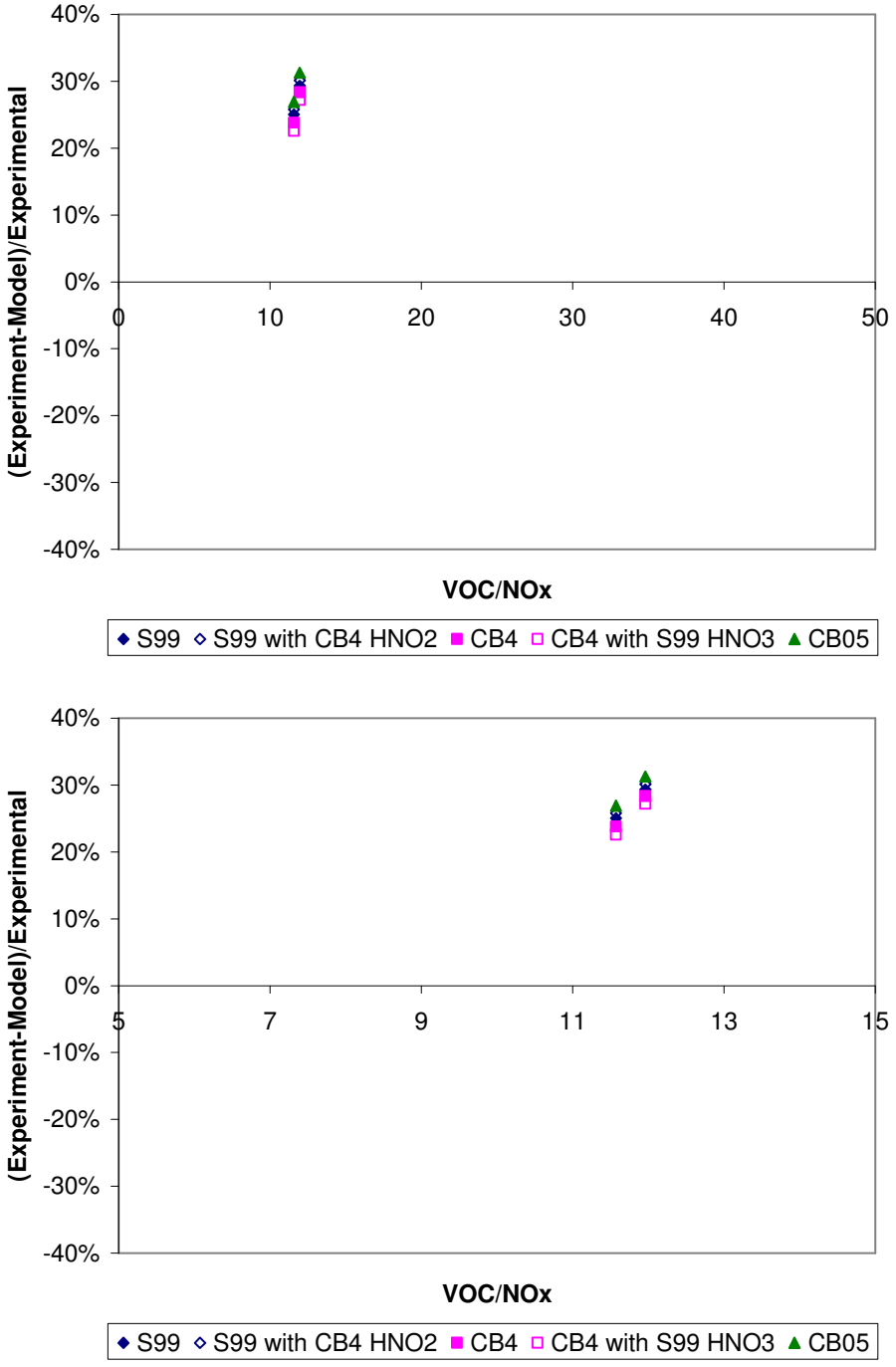

Figure 5-26. Model underprediction error for peak ozone in UNC chamber ethylene experiments against VOC/NOx ratio with modified OH+NO_2 rate constants.

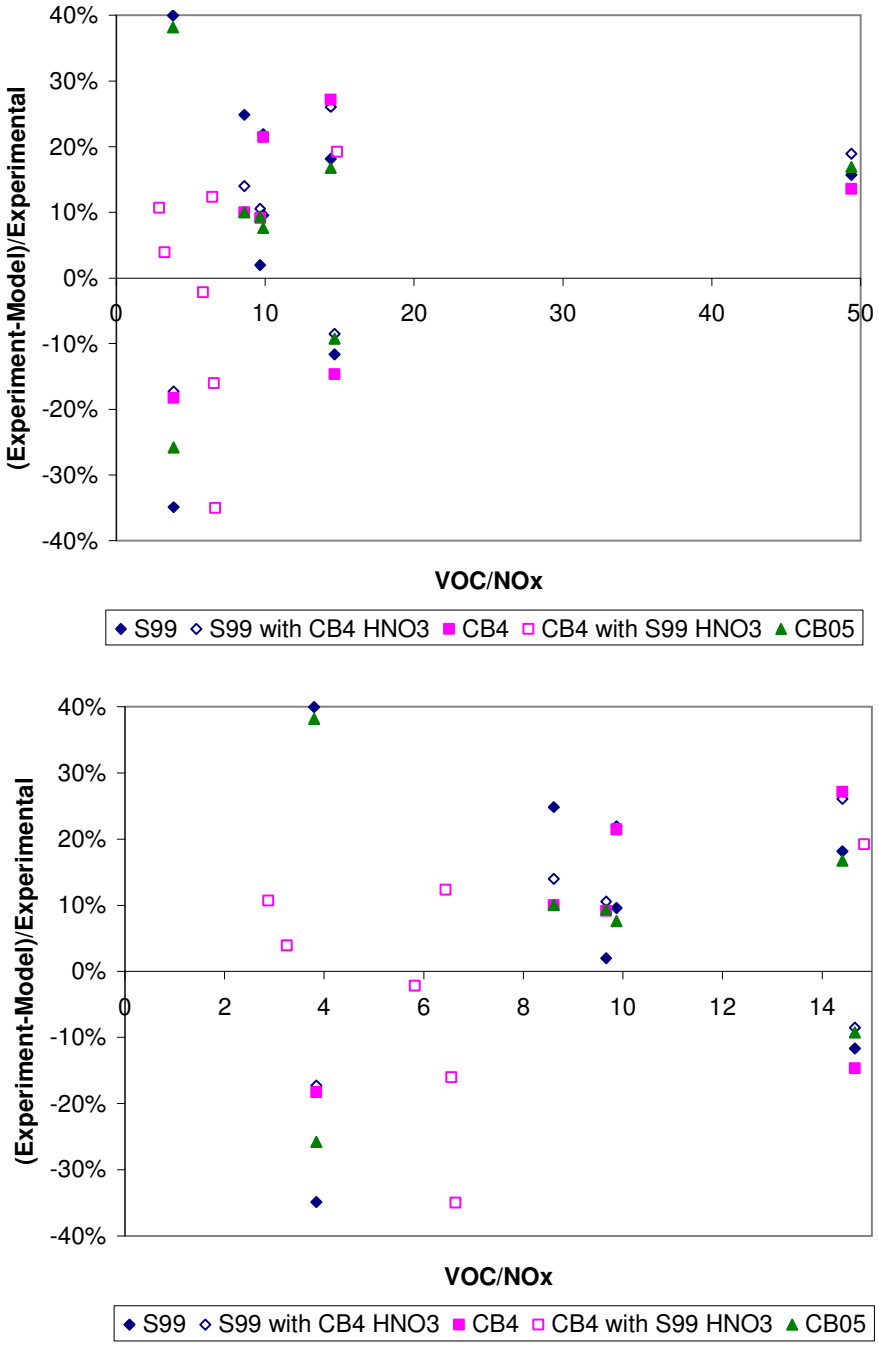

Figure 5-27. Model underprediction error for peak ozone in UCR chamber ethylene experiments against VOC/NOx ratio with modified OH+NO_2 rate constants.

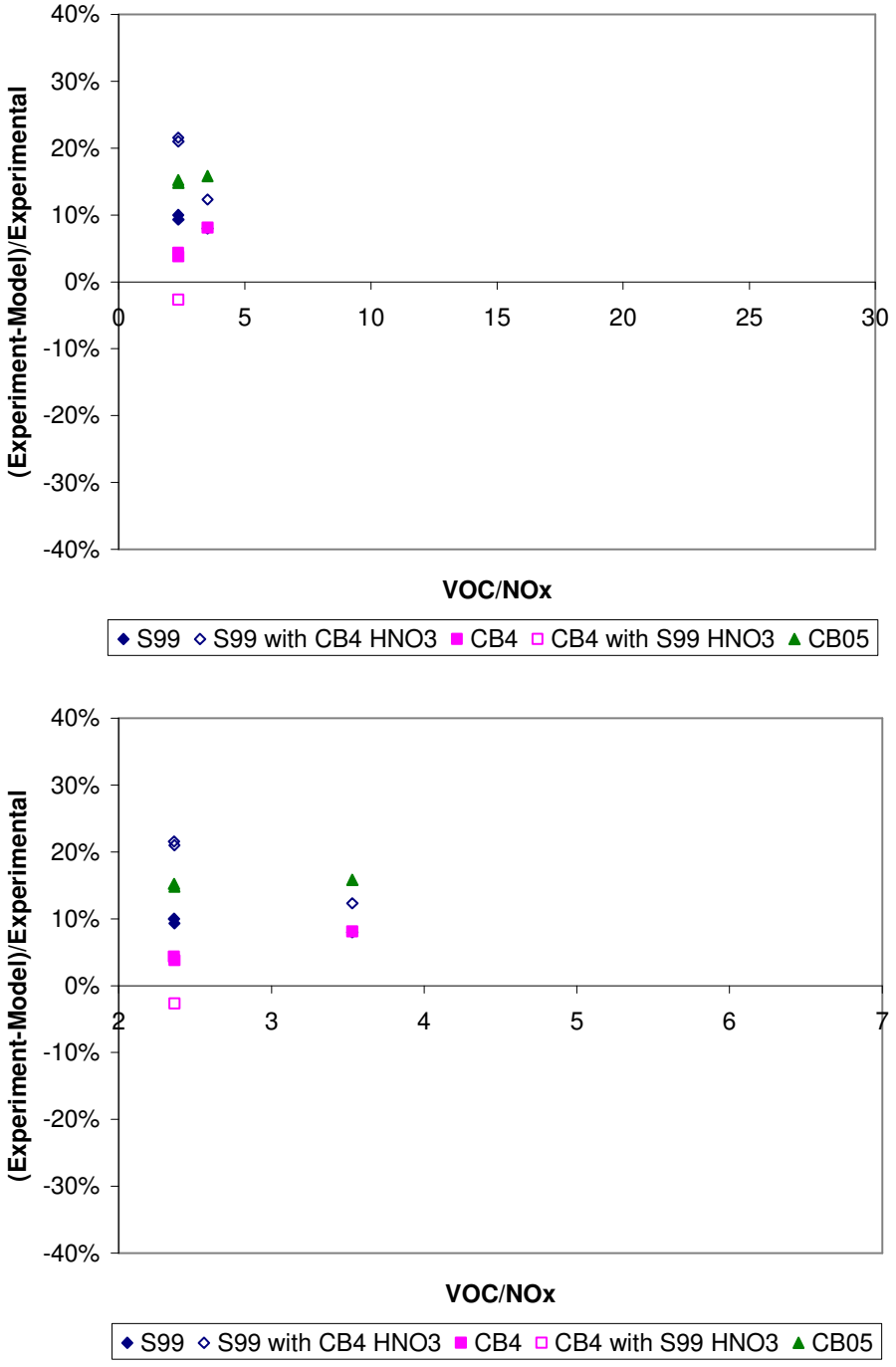

Figure 5-28. Model underprediction error for peak ozone in UNC chamber propylene experiments against VOC/NOx ratio with modified OH+NO_2 rate constants.

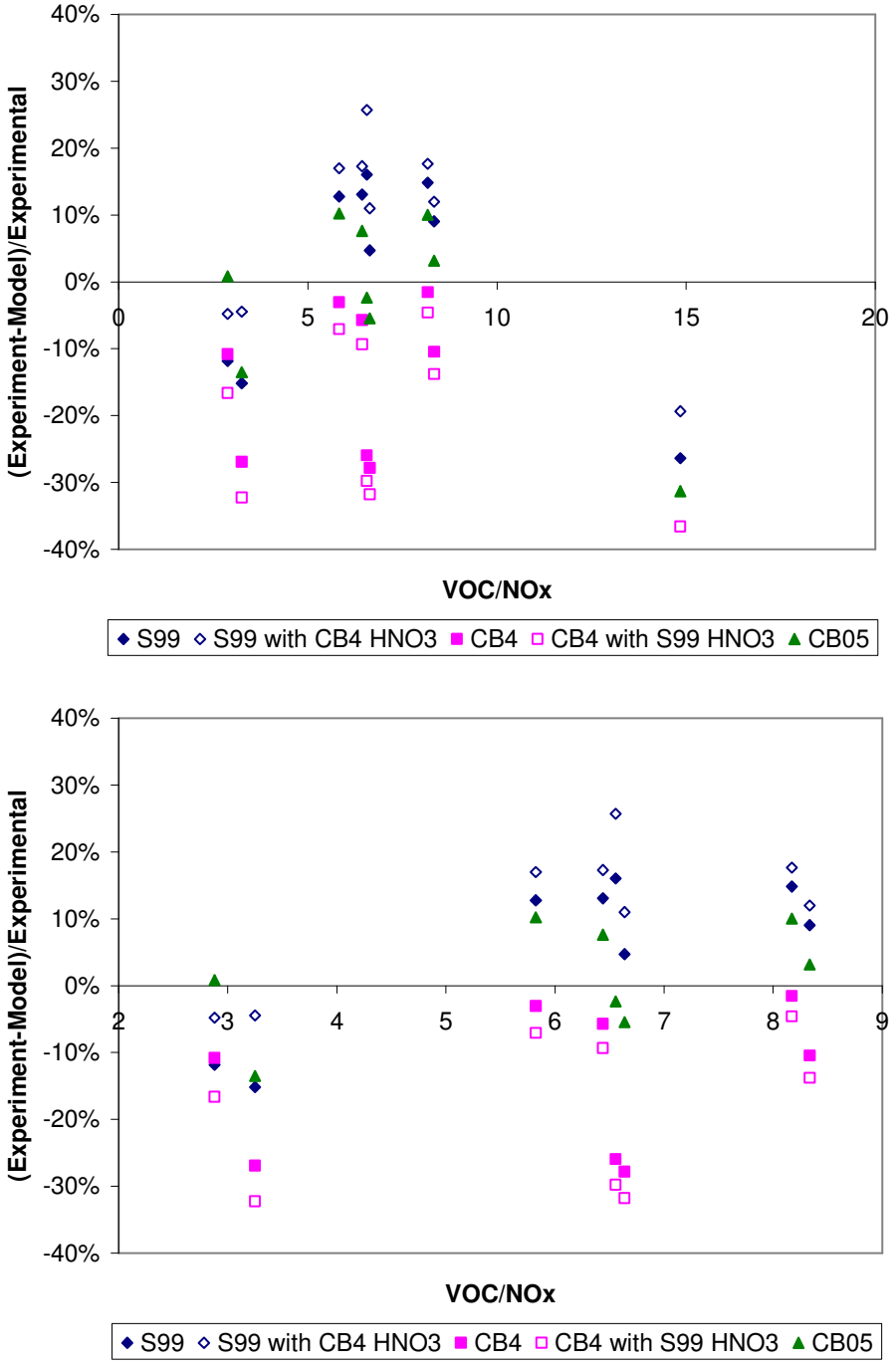

Figure 5-29. Model underprediction error for peak ozone in UCR chamber propylene experiments against VOC/NOx ratio modified OH+NO_2 rate constants.

In order to determine the effect of equating the $OH+NO_2$ rate parameters in the SAPRC99 and CB-IV mechanisms on differences in peak ozone concentrations between the mechanisms, the difference in peak ozone concentrations between the following SAPRC99 and CB-IV mechanisms were compared:

- basecase SAPRC99 minus basecase CB-IV, denoted "basecase S99 – basecase CB-IV"
- SAPRC99 with $OH+NO_2$ rate equated to rate in CB-IV minus basecase CB-IV, denoted "S99 with CB4 HNO_3 rate – basecase CB4"
- Basecase SAPRC99 minus CB-IV with $OH+NO_2$ rate equated to rate in SAPRC99, denoted "basecase S99 - CB4 with S99 HNO_3 rate"

Table 5-13 – 5-16 summarize the differences in peak ozone concentrations between SAPRC99 and CB-IV in the three scenarios above for the UNC and UCR ethylene and propylene chambers.

Table 5-13. Differences in peak ozone concentrations for UNC ethylene experiments.

	Difference in Peak Ozone (ppm)		
UNC Ethylene Experiment	S99 basecase - CB4 basecase	S99 w/ CB4 HNO_3 rate - CB4 basecase	S99 basecase - CB4 w/ S99 HNO_3 rate
AU2497 Red	-0.01100	-0.02000	-0.02400
AU2497 Blue	-0.01300	-0.02100	-0.02600

Table 5-14. Differences in peak ozone concentrations for UNC propylene experiments.

	Difference in Peak Ozone (ppm)		
UNC Propylene Experiment	S99 basecase - CB4 basecase	S99 w/ CB4 HNO_3 rate - CB4 basecase	S99 basecase - CB4 w/ S99 HNO_3 rate
ST1995 Red	0.04900	0.05200	0.05200
JN2392 Red	-0.02500	-0.07800	-0.05400

Table 5-15. Differences in peak ozone concentrations for UCR ethylene experiments.

	Difference in Peak Ozone (ppm)		
UCR Ethylene Experiment	S99 basecase - CB4 basecase	S99 w/ CB4 HNO_3 rate - CB4 basecase	S99 basecase - CB4 w/ S99 HNO_3 rate
EPA073A	-0.00600	-0.01500	-0.01420
XTC105	0.07050	0.00870	0.00830
XTC112	0.1109	-0.03860	-0.01060
EC285	0.1393	-0.0083	-0.00100
EC287	-0.029	-0.059	-0.04200
TVA008	0.015	-0.0029	-0.00870
OTC278B	0.1643	0.0607	0.13460
OTC279A	0.409	0.1649	0.21280
OTC304B	0.1451	0.0915	0.03960

Table 5-16. Differences in peak ozone concentrations for UCR propylene experiments.

	Difference in Peak Ozone (ppm)		
UCR Propylene Experiment	S99 basecase - CB4 basecase	S99 w/ CB4 HNO_3 rate - CB4 basecase	S99 basecase - CB4 w/ S99 HNO_3 rate
EC216	0.00570	-0.03390	-0.02710
EC277	-0.04240	-0.04900	-0.04710
EC314	-0.08530	-0.16280	-0.12410
EC687	-0.17790	-0.21230	-0.19960
EC899	-0.18460	-0.22720	-0.20150
OTC272B	-0.18110	-0.22950	-0.22710
OTC295A	-0.18790	-0.22030	-0.22290
OTC295B	-0.21060	-0.24230	-0.24660
OTC298A	-0.21280	-0.26080	-0.25380

Figures 5-30 – 5-33 correspond to the reported differences in peak ozone concentrations in Tables 5-13 – 5-16. In the UNC ethylene experiments, setting the $OH+NO_2$ rates in the SAPRC99 and CB-IV mechanisms increase the differences in peak ozone concentrations between SAPRRC and CB-IV. This is also the case in the UNC propylene experiments (Figure 5-31). In the UCR ethylene experiments, equating the main radical termination rates in SAPRC99 and CB-IV lead to lower differences in peak ozone concentrations in all but the EPA and EC experiments. In the UCR propylene

experiments, equating the $OH+NO_2$ rate constants in the mechanisms lead to larger discrepancies in predicted peak ozone concentrations between the mechanisms.

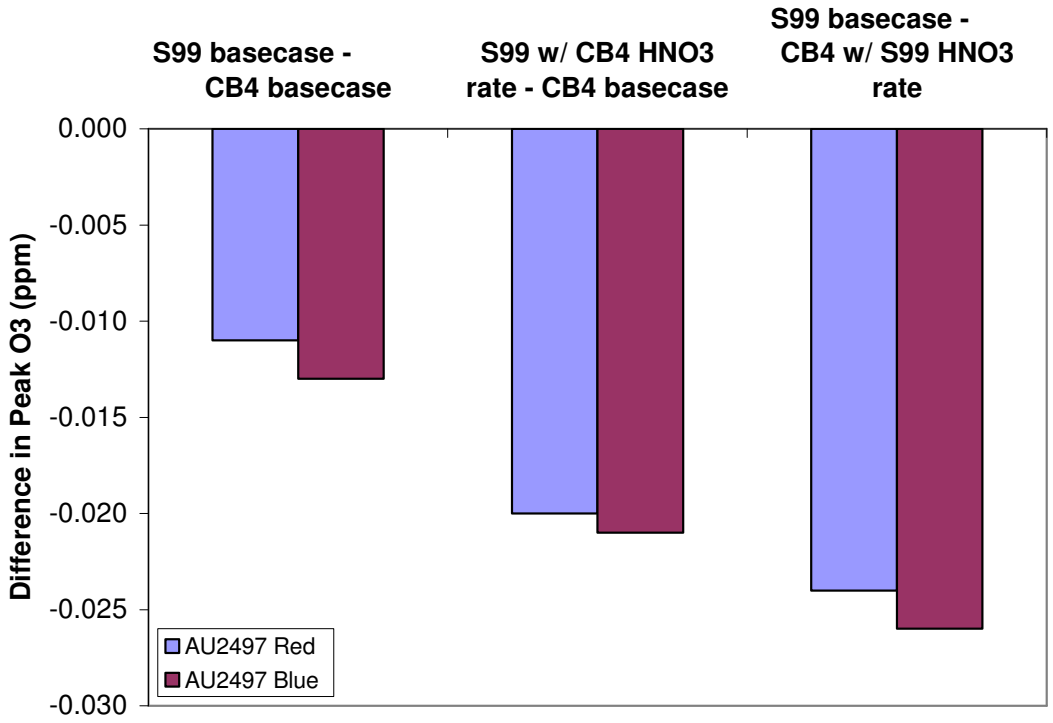

Figure 5-30. Differences in peak ozone concentrations for UNC ethylene experiments.

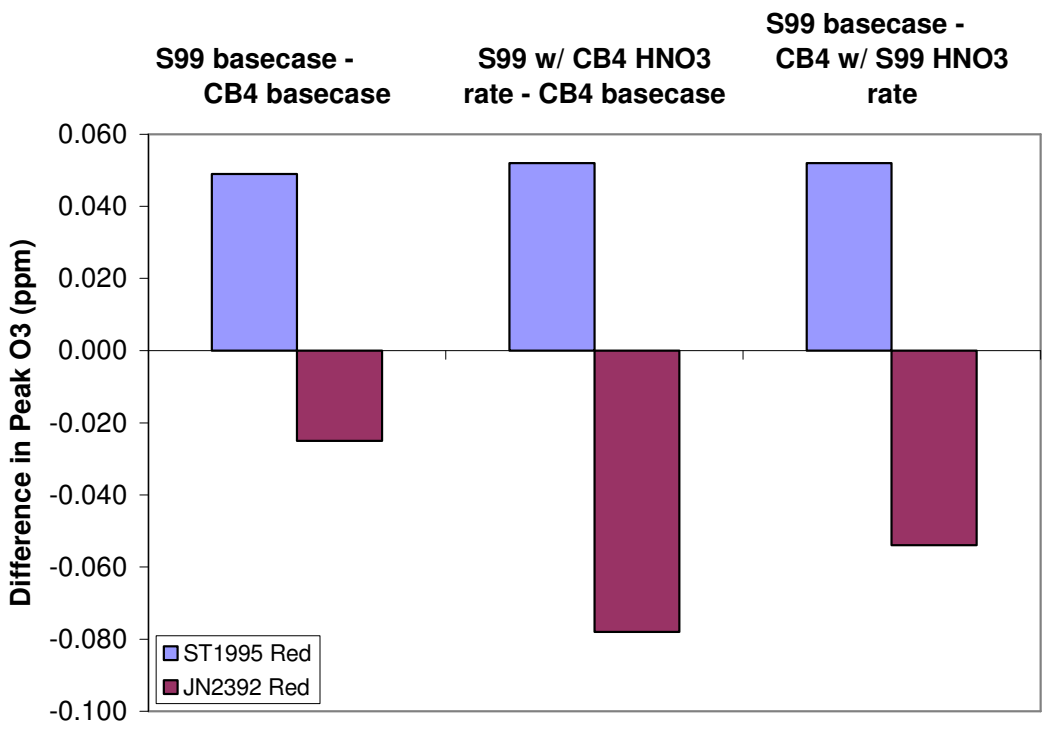

Figure 5-31. Differences in peak ozone concentrations for UNC propylene experiments.

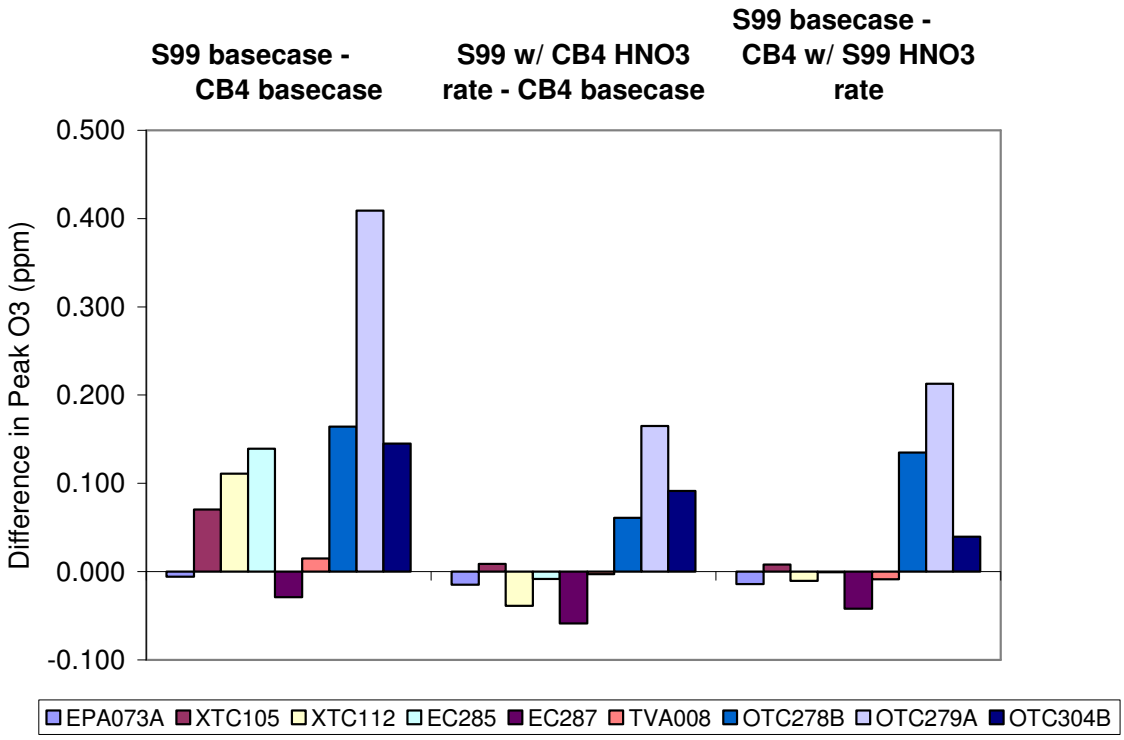

Figure 5-32. Differences in peak ozone concentrations for UCR ethylene experiments.

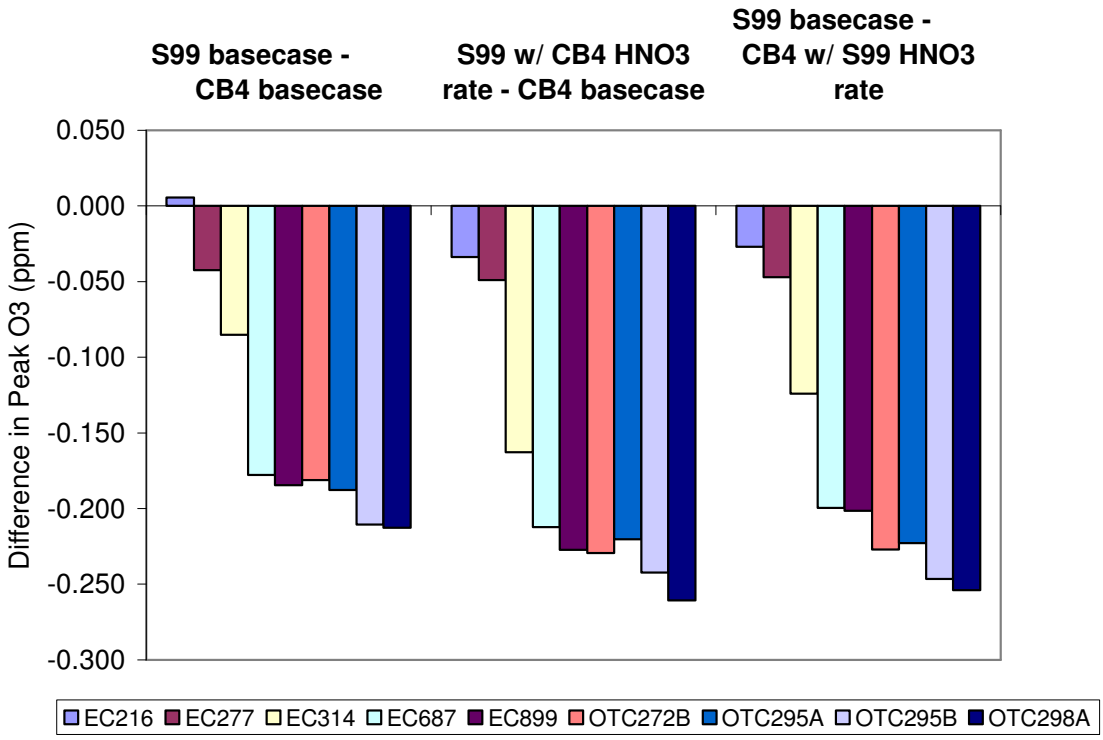

Figure 5-33. Differences in peak ozone concentrations for UCR propylene experiments.

Overall, altering the radical termination rate constant plays a relatively minor role in the predictions of the mechanisms for the ethylene and propylene experiments.

5.7 ASSESSMENT OF THE CHEMISTRY OF INTERNAL OLEFIN SPECIES

As part of the updates in CB05, a new four carbon species, IOLE, was added to explicitly represent olefins with internal double bonds which react very rapidly to produce photolytic products (aldehydes) (Yarwood, *et al.*, 2005). In CB-IV, internal olefins are represented by aldehyde species. For example, in CB-IV, 2-butene is represented by 2 ALD2. Relative to the CB-IV approach, the IOLE chemistry improves the representation of internal olefin reactions. Also, the IOLE chemistry includes both acetaldehyde (ALD2) and higher aldehydes (ALDX) as reaction products, which further

improves the chemistry of internal olefins relative to CB-IV. In SAPRC99, internal olefins are represented by the lumped species OLE2 which represents olefins with kOH > 7E+04 $ppm^{-1}min^{-1}$.

Figure 5-34 shows a simulation of an AU0180 UNC chamber experiment with VOC injections of 0.456 ppmC ethylene and 0.230 ppmC trans-2-butene and 0.58 ppm NOx. The SAPRC99 and CB05 mechanism predict similar O_3 concentrations while the CB-IV mechanism predicts lower peak O_3 concentration. Relative to the experiments, all three mechanisms underpredict O_3 concentrations.

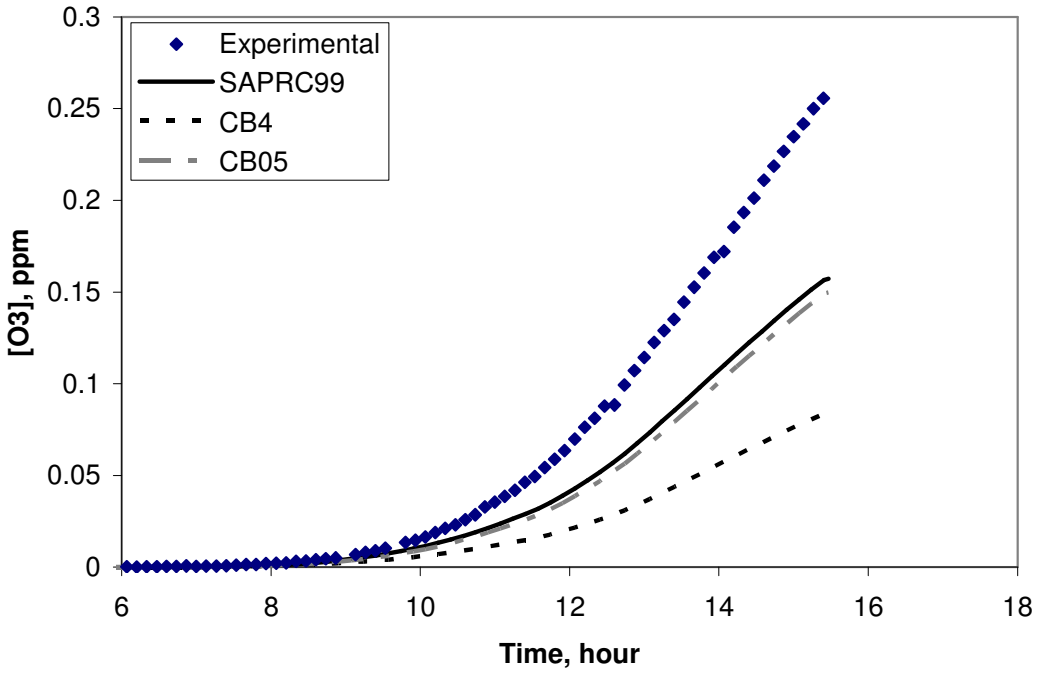

Figure 5-34. AU0180 UNC red chamber experiment with 0.456 ppmC ethylene and 0.230 ppmC trans-2-butene; wall mechanism and PNA on.

Table 5-17 lists the UCR chamber experiments available for the internal olefin species trans-2-butene. The ozone predictions in ppm as a function of time (min) for these experiments using the three chemical mechanisms are presented in Figure 5-35. In

TVA063, the SAPRC99 and CB-IV mechanisms predict nearly identical peak ozone concentrations while CB05 predicts higher maximum ozone. All three mechanisms overpredict the peak ozone relative to measurements. In TVA064, TVA065, and the EC experiments, CB05 predicts the highest maximum ozone concentration, followed by SAPRC99 and CB-IV. In EC146 and EC157, all three mechanisms underpredict the peak ozone relative to measurements. With the exception of the TVA063 experiments, CB-IV shows more of an underprediction relative to measured peak ozone as compared to the SAPRC99 and CB05 mechanisms. Furthermore, the performance with the SAPRC99 mechanism is more comparable with the CB05 mechanism versus the CB-IV mechanism. With the larger discrepancy in peak ozone concentrations between CB-IV and measurements, it can be concluded that the internal olefins chemistry in SAPRC99 and CB05 represent the chemistry in the UNC and UCR chambers better.

Table 5-17. Trans-2-butene experiments in UCR chamber.

Experiment	VOC	NOx	Light Source
TVA063	0.10 ppmC	20 ppb	Blacklights + Sunlamps
TVA064	0.10 ppmC	40 ppb	Blacklights + Sunlamps
TVA065	0.10 ppmC	41 ppb	Blacklights + Sunlamps
EC146	0.92 ppmC	512 ppb	Arc light solar simulator
EC147	1.67 ppmC	962 ppb	Arc light solar simulator
EC157	0.86 ppmC	557 ppb	Arc light solar simulator

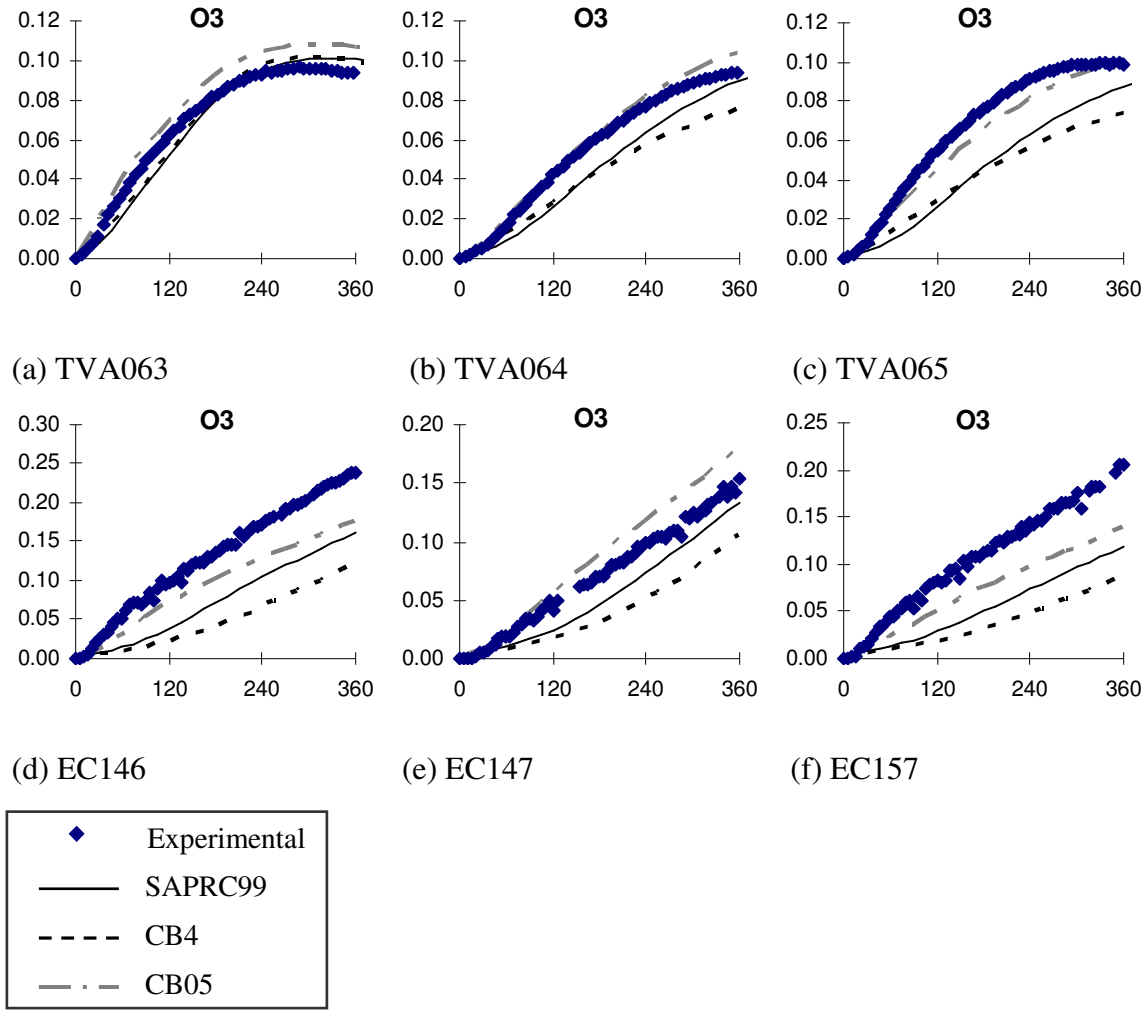

Figure 5-35. Trans-2-butene experiments in UCR chambers: O_3 (ppm) as a function of time (min); wall mechanism and PNA on.

5.8 SENSITIVITY OF HYDROXYL RADICAL YIELD OZONE-OLEFIN REACTIONS

The reactions of ozone with olefins lead to a direct production of OH radicals. Paulson *et al*. (1999) have used a new technique to measure the OH formation yields from the reaction of olefins with the goal of doing so with good precision. They report the OH formation yield for ethylene to be 0.18, which is higher than the OH yield currently used in the SAPRC99, CB-IV, and CB05 mechanisms. Therefore, a sensitivity

study was conducted to assess the effect of increasing the OH yield from the reaction of ethylene with O_3. The yield of OH from the reaction of ethylene with O_3 was increased from 0.12 in SAPRC99 and CB-IV and 0.13 in CB05 to 0.18. The reactions of ethylene + O_3 with the original stoichiometry used in the three mechanisms and the stoichiometry modified for the sensitivity analysis are shown below:

SAPRC99:

Original: ETHENE + O_3 = #.12 HO. + #.12 HO2. + #.5 CO + #.13 CO2 + HCHO + #.37 HCOOH

Modified: ETHENE + O3 = #.18 HO. + #.12 HO2. + #.5 CO + #.13 CO2 + HCHO + #.37 HCOOH

CB-IV:

Original: O3 + ETH = HCHO + #.42 CO + #.12 HO2

Modified: O3 + ETH = HCHO + #.42 CO + #.18 HO2

CB05:

Original: O3 + ETH = FORM + #0.63 CO + #0.13 HO2 +#0.13 OH + #0.37 FACD

Modified: O3 + ETH = FORM + #0.63 CO + #0.13 HO2 +#0.18 OH + #0.37 FACD

The increase in the OH yield from ethylene + O_3 leads to a slight increase in simulated ozone concentrations in the UCR chamber experiments for ethylene. This is shown for five ethylene experiments conducted in UCR chambers in Figure 5-36. As shown in Table 5-19, the increase in peak ozone generally leads to a lower underprediction with the three mechanisms relative to the experimental peak ozone.

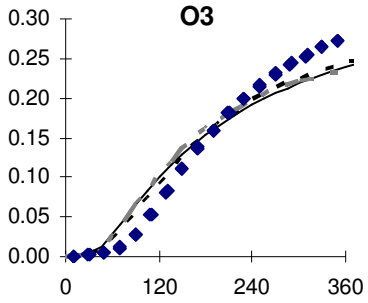

(a) EPA073A modified

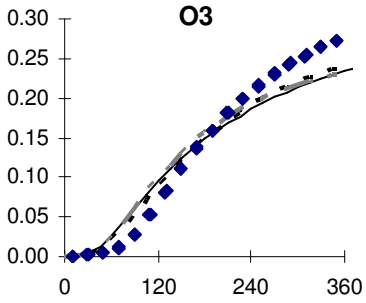

(a) EPA073A basecase

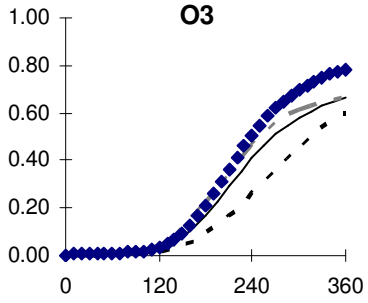

(b) XTC105 modified

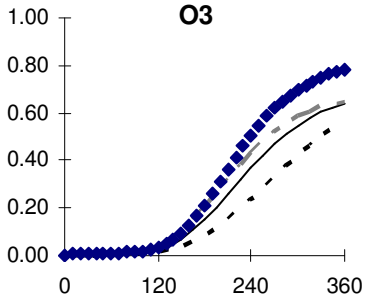

(b) XTC105 basecase

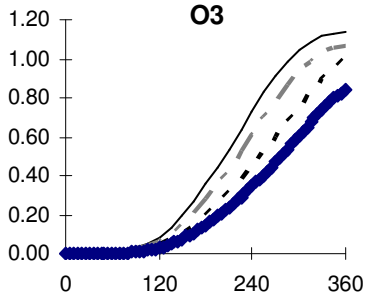

(c) EC285 modified

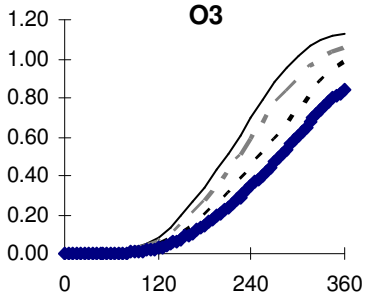

(d) EC285 basecase

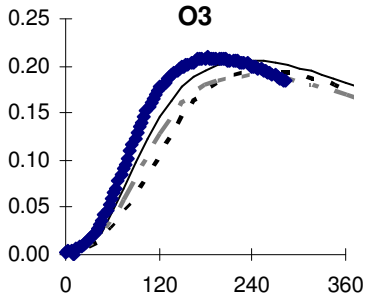

(d) TVA008 modified

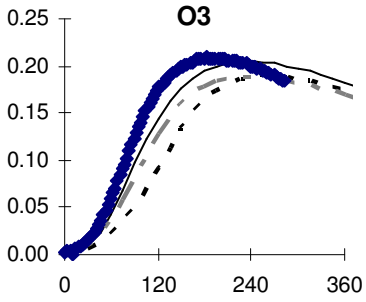

(d) TVA008 basecase

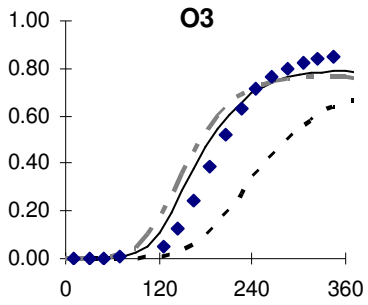

(e) OTC279A modified

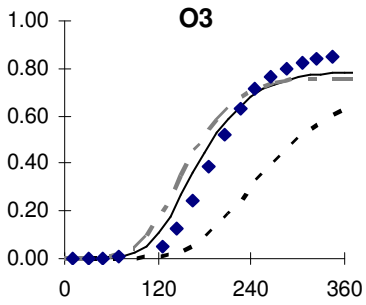

(e) OTC279A basecase

Figure 5-36. Ethylene experiments in UCR chambers: O_3 (ppm) as a function of time (min); wall mechanism and PNA on; increased OH yield from ethylene + O_3 in SAPRC99, CB-IV, and CB05.

Table 5-18. Comparison between the SAPRC99 and CB simulations and UCR chamber data for ethylene with modified yield of OH from ethylene +O_3.

	Experiment	EPA073A	XTC105	EC285	TVA008	OTC279A
	VOC (ppmC)	1.234	3.472	3.898	0.502	2.018
	NOx (ppm)	0.025	0.241	1.014	0.052	0.531
	VOC/NOx	49.376	14.407	3.844	9.662	3.800
Peak Ozone (ppm)	SAPRC99	0.237	0.639	1.129	0.205	0.590
	S99 w/ higher OH yield from ethene	0.241	0.662	1.141	0.205	0.625
	CB-IV	0.243	0.569	0.990	0.190	0.181
	CB4 w/ higher OH yield from ethene	0.247	0.599	1.003	0.195	0.200
	CB05	0.234	0.650	1.053	0.189	0.608
	CB05 w/ higher OH yield from ethene	0.236	0.663	1.066	0.190	0.632
	Experiment	0.281	0.781	0.837	0.209	0.984
(Experimental-Model)/Experimental	SAPRC99	15.73%	18.14%	-34.89%	1.96%	39.98%
	S99 w/ higher OH yield from ethene	14.16%	15.26%	-36.32%	1.77%	36.48%
	CB-IV	13.59%	27.17%	-18.24%	9.14%	81.57%
	CB4 w/ higher OH yield from ethene	12.24%	23.27%	-19.83%	6.79%	79.64%
	CB05	16.90%	16.75%	-25.81%	9.38%	38.17%
	CB05 w/ higher OH yield from ethene	16.05%	15.15%	-27.36%	9.19%	35.70%

5.9 EXPLICIT REPRESENTATION OF PROPYLENE

In the SAPRC99 mechanism, propylene is lumped into the surrogate species OLE1, which is also used to represent terminal olefins that exhibit different reactivity in producing O_3 than propylene. In CB, on the other hand, the basis for the surrogate OLE

species is the highly reactive propylene species. The SAPRC99 mechanism containing explicit representations of individual organic compounds includes an explicit chemistry for propylene, composed of four reactions and respective rate parameters (A, $cms^3molec^{-1}s^{-1}$; Ea/R, K; B), as follows:

4.850E-12 -504.2 0.00 ;PROPENE + HO. = #.984 RO2-R. + #.016 RO2-N. +
#.984 HCHO + #.984 CCHO + #-0.048 XC

5.510E-15 1878.0 0.00 ;PROPENE + O3 = #.32 HO. + #.06 HO2. +
#.26 C-O2. + #.51 CO + #.135 CO2 + #.5 HCHO +
#.5 CCHO + #.185 HCOOH + #.17 CCO-OH +
#.07 INERT + #.07 XC

4.590E-13 1156.0 0.00 ;PROPENE + NO3 = #.949 RO2-R. + #.051 RO2-N. +
#2.693 XC + XN

1.180E-11 324.1 0.00 ;PROPENE + O3P = #.45 RCHO + #.55 MEK +
#-0.55 XC

The lumped version of SAPRC99 lumps propylene into the OLE1 surrogate species which undergoes the following reactions with the respective rate parameters (A, $cms^3molec^{-1}s^{-1}$; Ea/R, K; B):

7.1020E-12 -451.39 0.00 ;OLE1 + HO. = #.91 RO2-R. + #.09 RO2-N. +
#.205 R2O2. + #.732 HCHO + #.294 CCHO +
#.497 RCHO + #.005 ACET + #.119 PROD2 + #.92 XC

2.6208E-15 1640.5 0.00 ;OLE1 + O3 = #.155 HO. + #.056 HO2. +
#.022 RO2-R. + #.001 RO2-N. + #.076 C-O2. +
#.345 CO + #.086 CO2 + #.5 HCHO + #.154 CCHO +
#.363 RCHO + #.001 ACET + #.215 PROD2 +
#.185 HCOOH + #.05 CCO-OH + #.119 RCO-OH +

```
                                #.654 XC
4.4513E-14 375.91 0.00  ;OLE1 + NO3 = #.824 RO2-R. + #.176 RO2-N. +
                                #.488 R2O2. + #.009 CCHO + #.037 RCHO +
                                #.024 ACET + #.511 RNO3 + #.677 XC + #.489 XN
1.0703E-11 234. 0.00   ;OLE1 + O3P = #.45 RCHO + #.437 MEK + #.113 PROD2 +
                                #1.224 XC
```

An analysis was done in which for the propylene chamber experiments, the chemistry for OLE1 in the lumped version of SAPRC99, including reactions and reaction rate constants, was substituted with the propylene chemistry from the explicit version of SAPRC99. The results of this analysis for the UNC propylene experiments are shown in Figures 5-37 to 5-40, comparing simulations of ozone with the explicit propylene chemistry and the lumped propylene chemistry. Tables 5-19 Figure 5-42 summarize the results from this analysis. Except for the ST1995 propylene experiment, the explicit propylene chemistry in SAPRC99 leads to higher peak ozone concentrations than SAPRC99 with the lumped propylene chemistry. Also, except for the ST1995 experiment, the bias for SAPRC99 with the explicit propylene chemistry is lower relative to SAPRC99 with the lumped propylene chemistry.

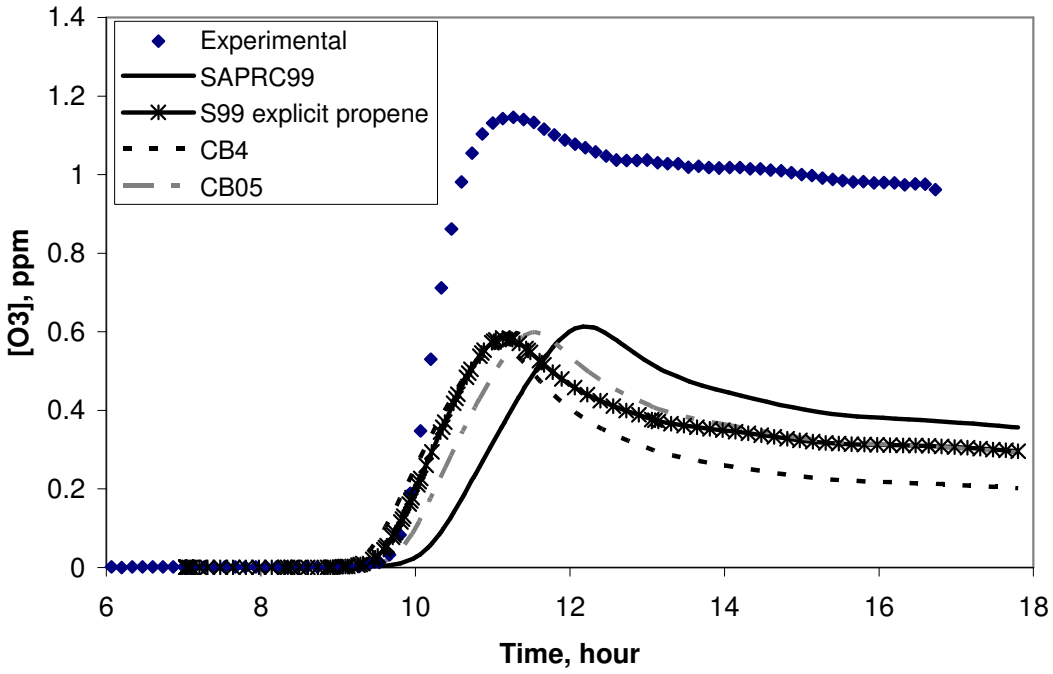

Figure 5-37. ST1995 UNC red chamber experiment with 6.12 ppmC propylene; wall mechanism and PNA on; comparing lumped and explicit propylene chemistries.

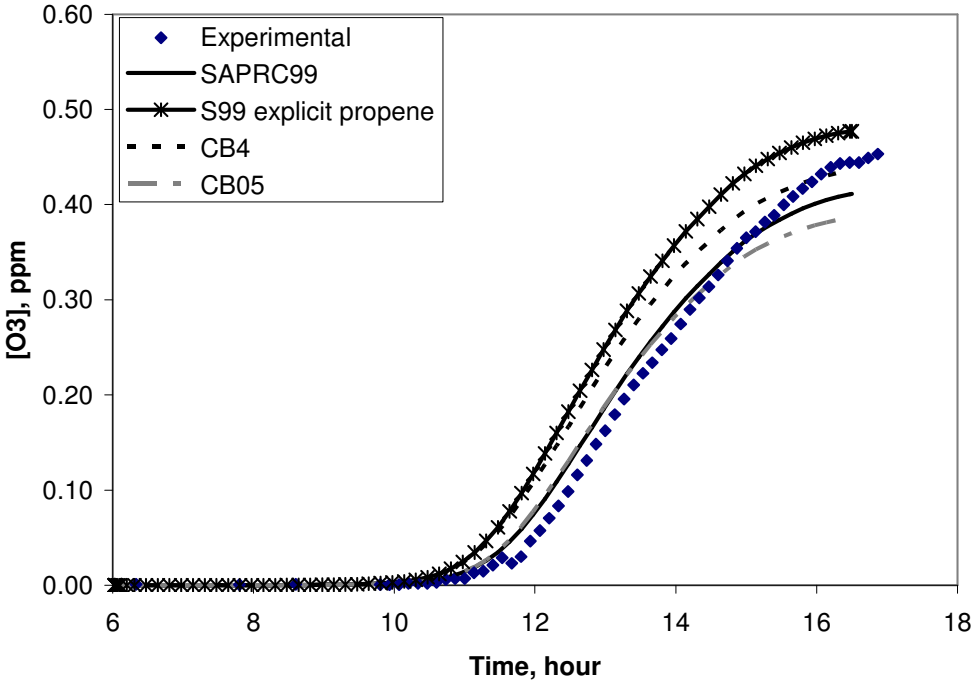

Figure 5-38. JN2392 UNC red chamber experiment with 0.908 ppmC propylene; wall mechanism and PNA on; comparing lumped and explicit propylene chemistries.

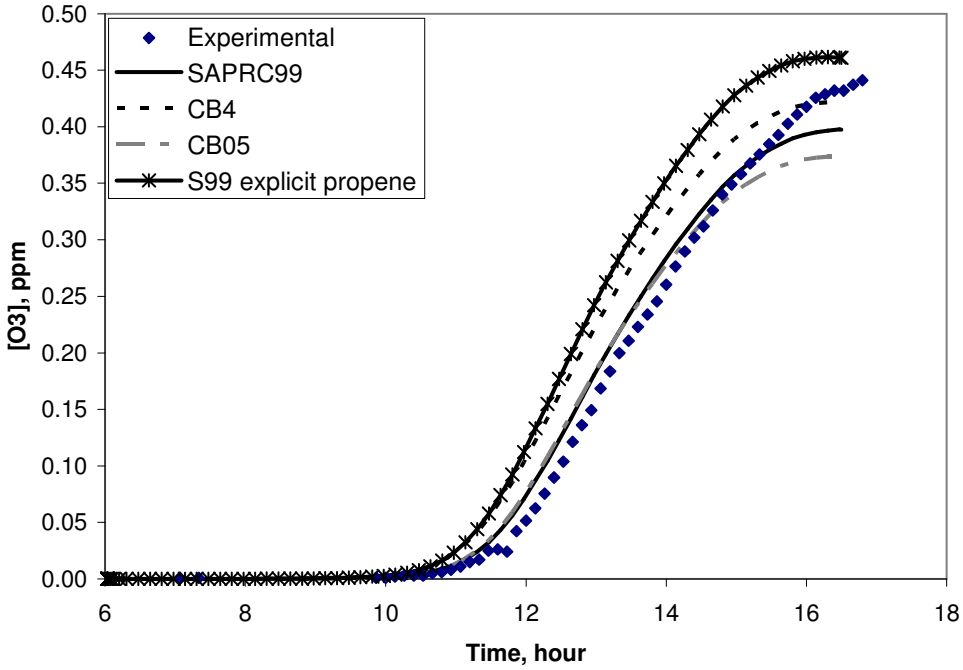

Figure 5-39. JN2392 UNC blue chamber experiment with 0.907 ppmC propylene; wall mechanism and PNA on; comparing lumped and explicit propylene chemistries.

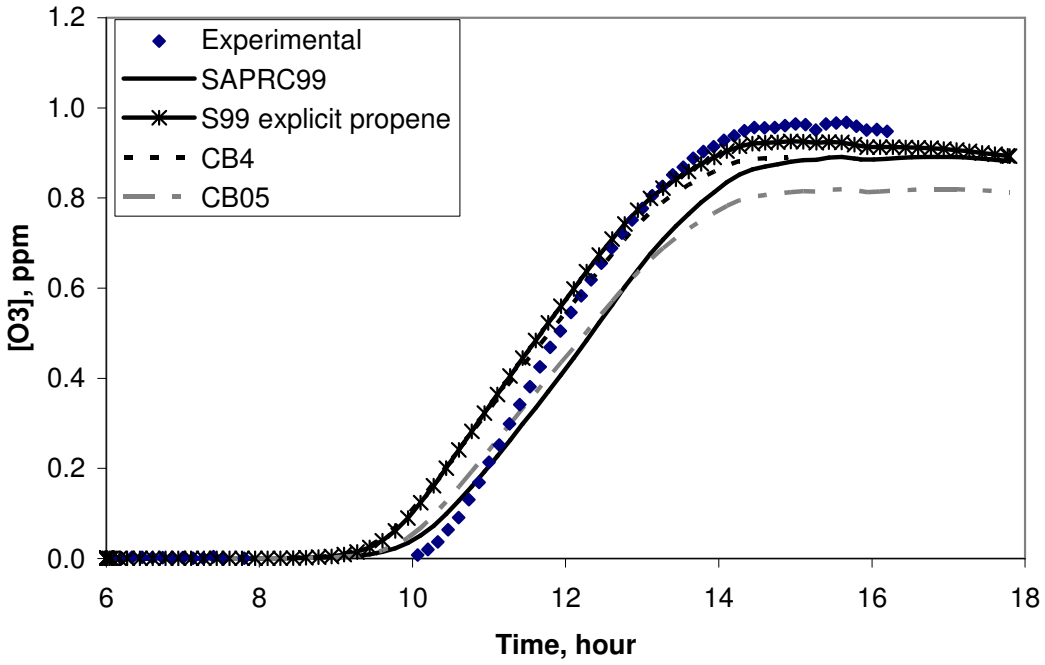

Figure 5-40. JN1798 UNC red chamber experiment with 1.737 ppmC propylene; wall mechanism and PNA on; comparing lumped and explicit propylene chemistries.

The results of this analysis for the UCR propylene experiments are shown in Figure 5-41. Tables 5-20 Figures 5-43 summarize the results from this analysis. The SAPRC99 mechanism with the explicit propylene chemistry leads to higher peak ozone concentrations relative to the SAPRC99 with the lumped propylene chemistry in all the UCR propylene experiments evaluated. The relative bias in predicted peak ozone concentrations for SAPRC99 with the explicit propylene chemistry is higher than that of SAPRC99 with the lumped propylene representation in the EC chamber experiments evaluated. On the other hand, in the OTC chamber, there is less of an underprediction in

peak ozone when the explicit chemistry for propylene is used than when the lumped propylene chemistry is used.

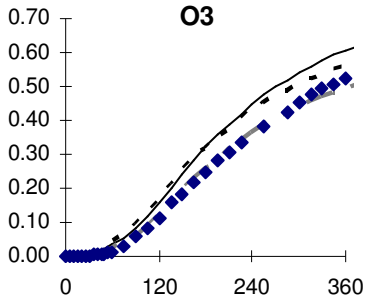

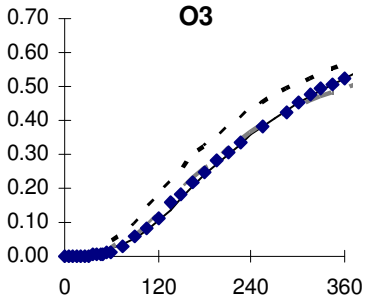

(a) EC216 explicit propene propene as OLE1

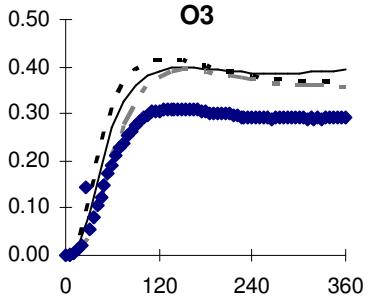

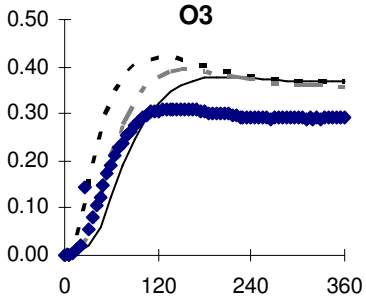

(b) EC277 explicit propene propene as OLE1

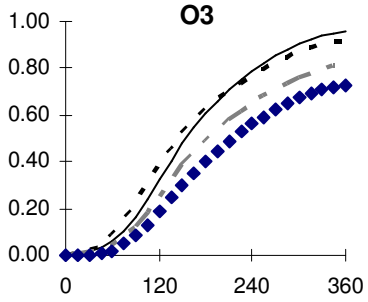

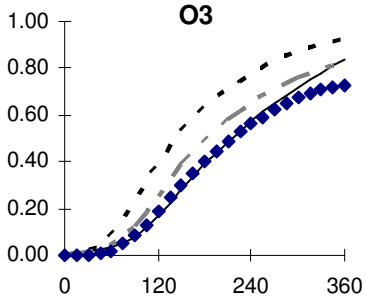

(c) EC314 explicit propene propene as OLE1

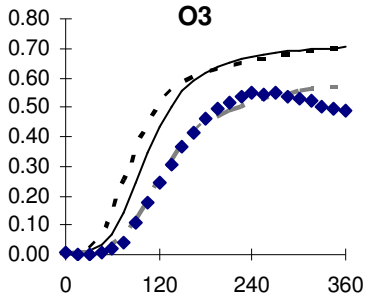

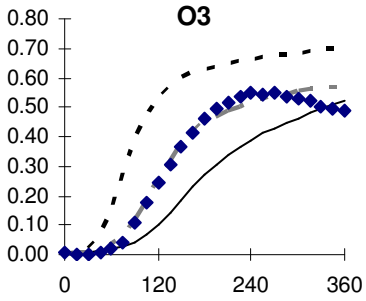

(d) EC687 explicit propene propene as OLE1

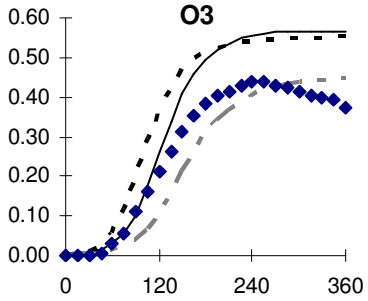

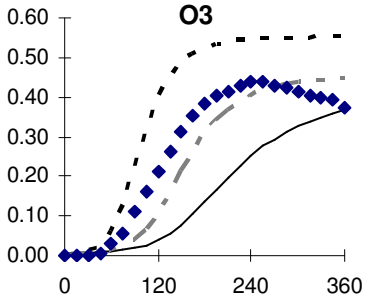

(e) EC899 explicit propene propene as OLE1

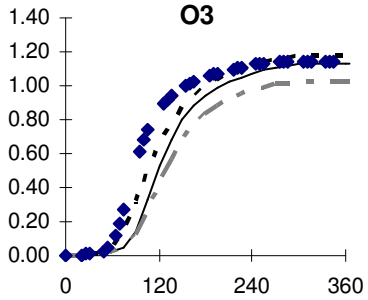

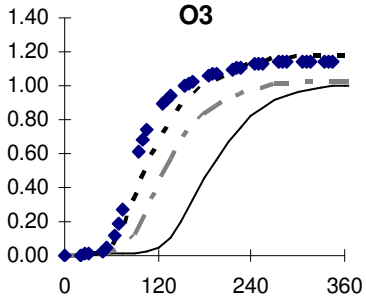

(f) OTC272B explicit propene propene as OLE1

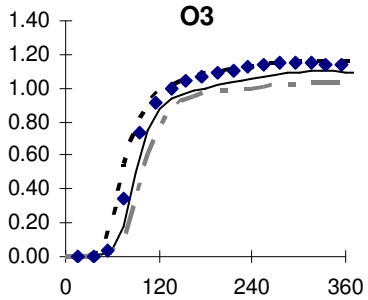

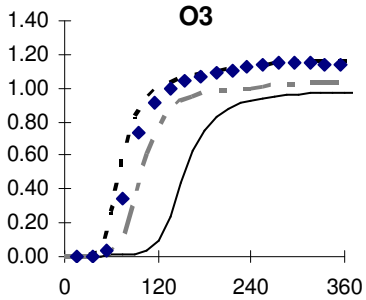

(g) OTC295A explicit propene propene as OLE1

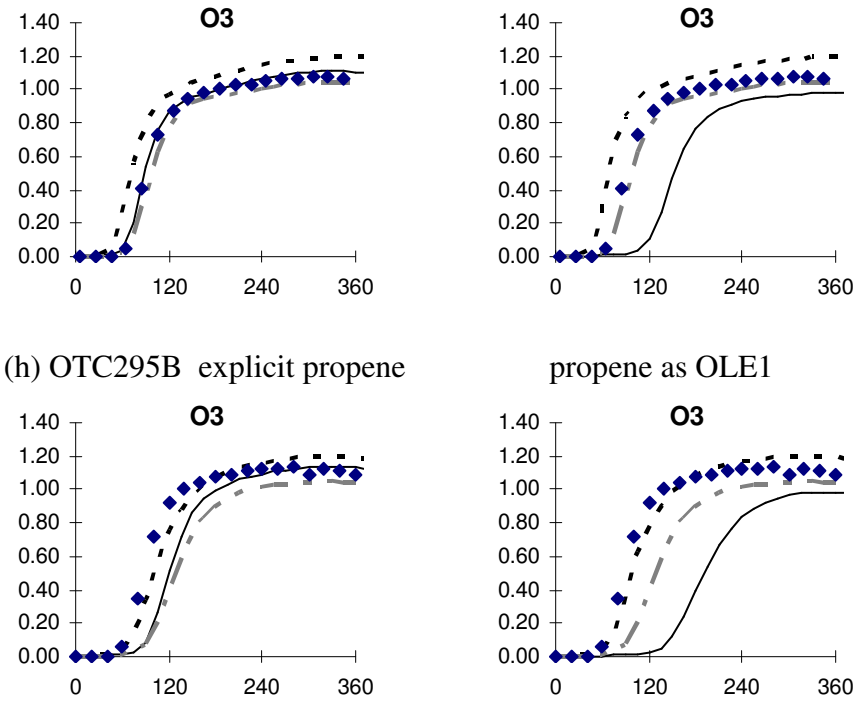

(h) OTC295B explicit propene propene as OLE1

(i) OTC298A explicit propene propene as OLE1

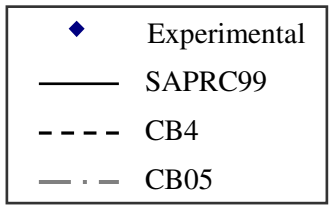

Figure 5-41. Propylene experiments in UCR chambers: O_3 (ppm) as a function of time (min); wall mechanism and PNA on; comparing lumped and explicit propylene chemistries.

Table 5-19. Comparison between the SAPRC99 and CB simulations and UNC chamber data for propylene: comparing lumped and explicit propylene chemistries.

	Experiment	ST1995 Red	JN2392 Red	JN2392 Blue	JN1798 Red
	VOC (ppmC)	6.120	0.908	0.907	1.737
	NOx (ppm)	0.670	0.384	0.384	0.492
	VOC/NOx	9.134	2.365	2.362	3.530
Peak Ozone (ppm)	SAPRC99	0.611	0.411	0.397	0.891
	SAPRC99 Explicit	0.584	0.477	0.462	0.925
	CB-IV	0.562	0.436	0.422	0.890
	CB05	0.599	0.386	0.374	0.815
	Experiment	1.146	0.453	0.441	0.968
(Experimental-Model) /Experimental	SAPRC99	46.68%	9.27%	9.98%	7.95%
	SAPRC99 Explicit	49.04%	-5.30%	-4.76%	4.44%
	CB-IV	50.96%	3.75%	4.31%	8.06%
	CB05	47.73%	14.79%	15.19%	15.81%
	MIR (g/g)	11.58	11.58	11.58	11.58
	MIR*VOC/NOx	105.8	27.4	27.4	40.9

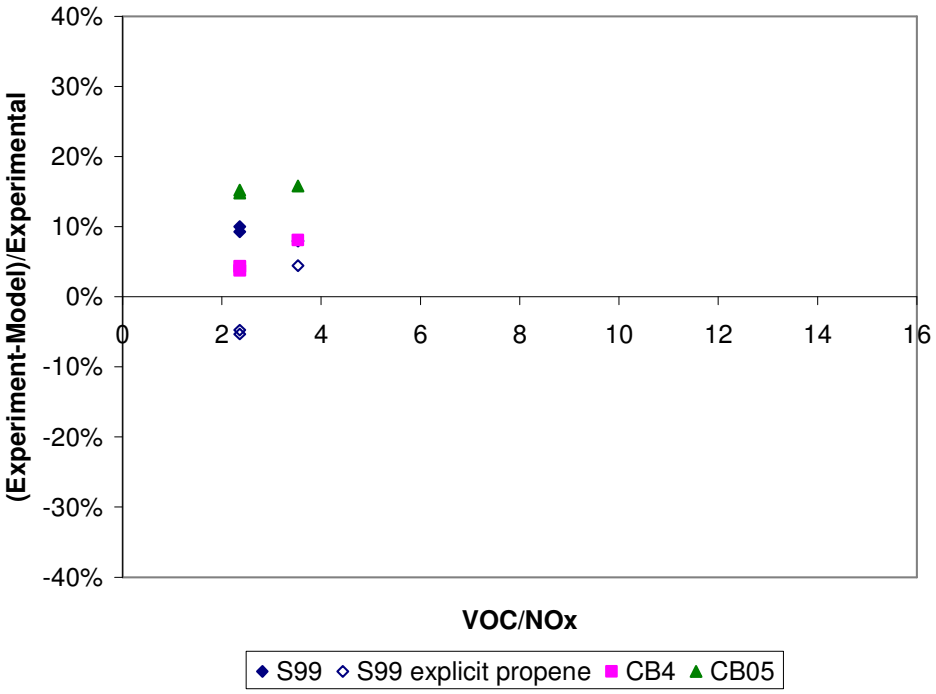

Figure 5-42. Model underprediction error for peak ozone in UNC chamber propylene experiments against VOC/NOx ratio modified: comparing lumped and explicit propylene chemistries.

Table 5-20. Comparison between the SAPRC99 and CB simulations and UCR chamber data for propylene: comparing lumped and explicit propylene chemistries.

	Experiment	EC216	EC277	EC314	EC687	EC899	OTC272B	OTC295A	OTC295B	OTC298A
	VOC (ppmC)	1.509	1.692	3.186	3.120	3.180	3.087	4.371	4.335	3.747
	NOx (ppm)	0.524	0.114	0.980	0.470	0.485	0.530	0.535	0.520	0.582
	VOC/NOx	2.879	14.845	3.251	6.638	6.557	5.825	8.170	8.337	6.438
Peak Ozone (ppm)	SAPRC99	0.630	0.378	0.835	0.521	0.370	0.999	0.977	0.981	0.986
	SAPRC99 Explicit	0.665	0.399	0.959	0.703	0.566	1.028	1.032	1.045	1.048
	CB-IV	0.624	0.421	0.920	0.699	0.554	1.180	1.165	1.192	1.199
	CB05	0.558	0.393	0.823	0.577	0.450	1.028	1.032	1.045	1.048
	Experiment	0.563	0.299	0.725	0.547	0.440	1.145	1.147	1.079	1.134
(Experimental-Model) /Experimental	SAPRC99	-11.85%	-26.40%	-15.16%	4.68%	16.02%	12.76%	14.81%	9.05%	13.03%
	SAPRC99 Explicit	-18.15%	-33.29%	-32.32%	-28.48%	-28.59%	10.22%	10.03%	3.15%	7.58%
	CB-IV	-10.83%	-40.57%	-26.92%	-27.84%	-25.93%	-3.06%	-1.57%	-10.47%	-5.73%
	CB05	0.83%	-31.32%	-13.52%	-5.45%	-2.36%	10.22%	10.03%	3.15%	7.58%
	MIR (g/g)	11.58	11.58	11.58	11.58	11.58	11.58	11.58	11.58	11.58
	MIR*VOC/NOx	33.34	171.90	37.65	76.87	75.93	67.45	94.61	96.54	74.55

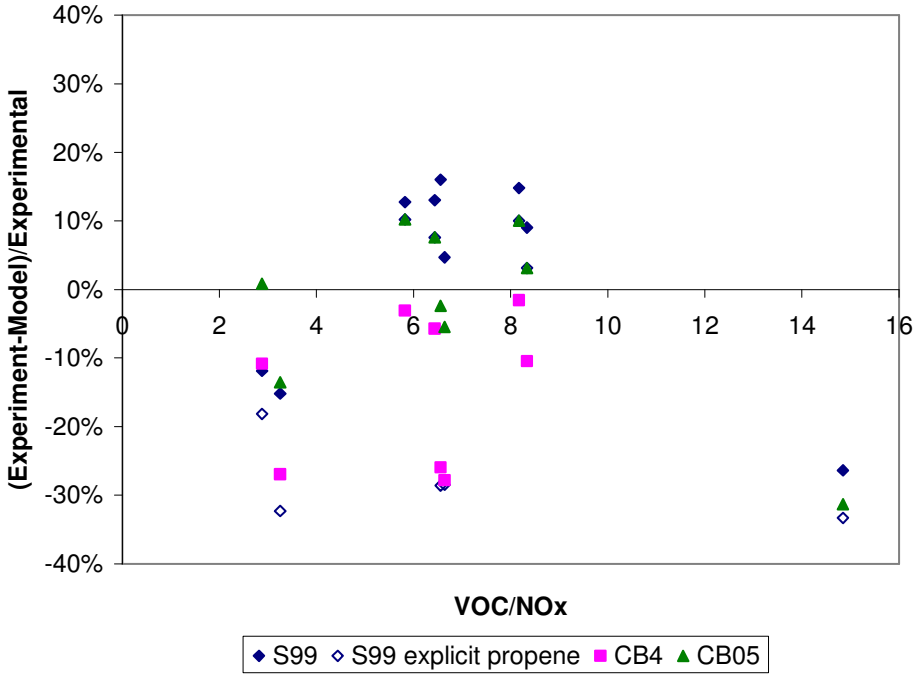

Figure 5-43. Model underprediction error for peak ozone in UCR chamber propylene experiments against VOC/NOx ratio modified: comparing lumped and explicit propylene chemistries.

As shown in Table 5-21 and Figure 5-44, in the UNC chamber propylene simulations, the difference in peak ozone concentrations between SAPRC99 and CB4 increases in all but the ST1995 experiment when the explicit chemistry for propylene is used rather than the lumped chemistry for propylene. In the UCR chamber simulations (Table 5-22 and Figure 5-45), the difference between SAPRC99 and CB-IV decreases for all the propylene experiments evaluated except EC216.

Table 5-21. Differences in peak ozone concentrations in UNC propylene experiments: comparing lumped and explicit propylene chemistries.

	Difference in Peak Ozone (ppm)	
UNC Propylene Experiment	S99 basecase - CB4 basecase	S99 explicit propene - CB4 basecase
ST1995 Red	0.04900	0.02200
JN2392 Red	-0.02500	0.04100
JN2392 Blue	-0.02500	0.04000
JN1798 Red	0.00100	0.03500

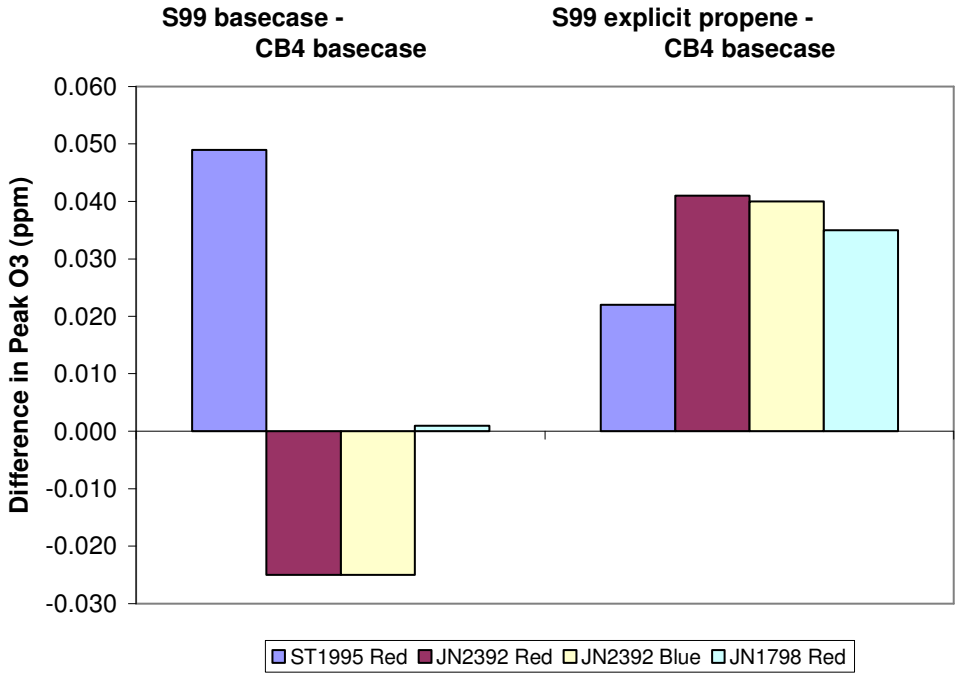

Figure 5-44. Differences in peak ozone concentrations in UNC propylene experiments: comparing lumped and explicit propylene chemistries.

Table 5-22. Differences in peak ozone concentrations in UCR propylene experiments: comparing lumped and explicit propylene chemistries.

	Difference in Peak Ozone (ppm)	
UCR Propylene Experiment	S99 basecase - CB4 basecase	S99 explicit propene - CB4 basecase
EC216	0.00570	0.04120
EC277	-0.04240	-0.02180
EC314	-0.08530	0.03910
EC687	-0.17790	0.00350
EC899	-0.18460	0.01170
OTC272B	-0.18110	-0.15200
OTC295A	-0.18790	-0.13300
OTC295B	-0.21060	-0.14700
OTC298A	-0.21280	-0.15100

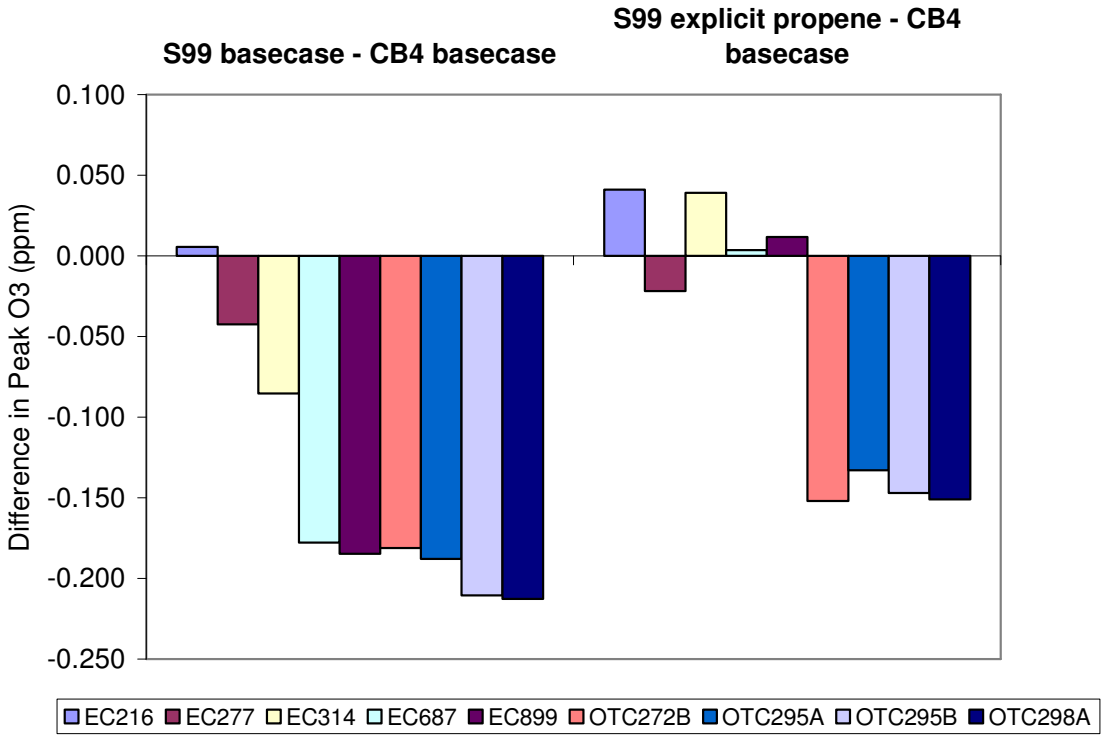

Figure 5-45. Differences in peak ozone concentrations in UCR propylene experiments: comparing lumped and explicit propylene chemistries.

5.10 SUMMARY

Predictions of SAPRC99, CB-IV and CB05 were compared to UNC and UCR environmental chamber experiments involving terminal and internal olefins. The simulations indicate that the performance of the mechanisms can be improved through more explicit representation of internal olefin chemistry (presently included in CB05 and SAPRC, but not in CB-IV). In addition, performance of the SAPRC mechanism for the propene experiments was improved for some experiments when propylene was modeled explicitly, as opposed to being represented by a lumped chemical species based on the mixture of terminal alkenes in ambient air. The better performances of CB05 and CB-IV in simulating the propene experiments is attributed to the fact that the lumped olefin species in these mechanisms are based on the chemistry of propene, without taking into account mechanisms of the higher 1-alkenes. The higher 1-alkenes are modeled using the olefin species with additional PAR species to model the additional carbons, based on the Carbon Bond lumping concept.

For high reactivity chamber experiments involving olefins, sensitivity analyses indicated that mechanism adjustments that would lead to increased radical concentrations (increasing the radical yield in olefin-ozone reactions and changing the $OH+NO_2$ termination rate constant) had little impact on predicted ozone concentrations. On the other hand, in the CO-NOx systems, equating the rate constant for the $OH + NO_2$ reaction in CB-IV, CB05, and SAPRC99 led to convergence in the concentrations of O_3 with the wall mechanism turned off. This suggests that in photochemical modeling simulations, where wall reactions are not included, the major differences in the inorganic chemistry between the mechanisms are due to differences in the rate parameters of the $OH + NO_2$ reaction.

5.11 REFERENCES

Carter, W. P. L. (1994). Development of ozone reactivity scales for Volatile Organic Compounds. *Journal of Air and Waste Management Association*, 44, 881-899.

Carter, W. P. L. (2007, May). *Documentation of the SAPRC-07 chemical mechanism and updated ozone reactivity scales*. Draft Final Report to the California Air Resources Board, Sacramento, CA.

Carter, W. P. L. (2000). *Documentation of the SAPRC-99 chemical mechanism for VOC reactivity assessment*. Air Pollution Research Center and College of Engineering, Center for Environmental Research and Technology, University of California at Riverside, CA.

Paulson, S., Chung, M.Y., and Hasson, A.S. (1999). OH radical formation from the gas-phase reaction of ozone with terminal alkenes and the relationship between structure and mechanism. *The Journal of Physical Chemistry A*, 103, 8125-8138.

Yarwood, G., Whitten, G., and Rao, S. (2005, March). *Updates to the Carbon Bond 4 photochemical mechanism*. Prepared by ENVIRON International Corporation and Smog Reyes for the Lake Michigan Air Directors Consortium.

Chapter 6: Assessment of Aromatics Chemistry in SAPRC99 and CB mechanisms using Environmental Chamber Experiments

Based on the box model and CAMx simulations in Chapter 3, one of the hypotheses for explaining the differences in predictions of ozone concentrations by SAPRC99 and CB-IV is the differences in the aromatics chemistry. This chapter examines the environmental chamber experiments involving singly and multiply substituted aromatics. The experiments include toluene, ethylbenzene, xylenes, and trimethylbenzenes as reactants. Emission inventory analyses performed (Appendix G.3) indicate that these species account for approximately three-quarters of the aromatics emissions in the Houston-Galveston area. Singly substituted aromatics, especially toluene, dominate the emissions. Therefore, a focus on toluene, ethylbenzene, xylenes, and trimethylbenzenes, with a particular focus on toluene is appropriate in this chapter.

As in Chapter 5, all the simulations in this chapter were conducted with the wall mechanism and PNA chemistry (Appendix C) activated. Unless otherwise noted, species in SAPRC99 are represented by their lumped species surrogates.

6.1 Comparison between the SAPRC99 and CB Simulations of the UNC Chamber Experiments for Aromatics

A summary of the UNC experiments considered in this chapter is provided in Table 6-1. The ozone concentrations simulated using the SAPRC99, CB-IV, and CB05, mechanisms as well as the measured concentrations of ozone in the UNC chamber for the toluene experiments are shown in Figure 6-1 – 6-4. For the toluene experiments, SAPRC99 consistently predicts maximum ozone concentrations that are significantly higher than peak ozone concentrations predicted with the CB mechanisms. This finding is in agreement with the findings from single-VOC box model simulations in Chapter 3 in

which SAPRC99 and CB-IV showed large discrepancies in ozone concentrations for mono-substituted aromatics. Comparisons between simulated and measured peak ozone concentrations for the UNC toluene experiments are made in Section 6.3.1.

Table 6-1. Aromatics experiments in UNC chamber.

Experiment		VOC	NOx
AU0183	Red	4.59 ppmC Toluene	0.395 ppm
	Blue	2.622 ppmC o-Xylene	0.373 ppm
AU1788	Red	4.93 ppmC Toluene	0.357 ppm
	Blue	1.715 ppmC m-Xylene	0.356 ppm
ST1393	Red	0.789 ppmC m-Xylene	0.321 ppm
	Blue	1.909 ppmC Toluene	0.324 ppm
AU0395	Red	8.00 ppmC p-Xylene	0.641 ppm
	Blue	7.21 ppmC 1,3,5-Trimethylbenzene	0.621 ppm
AU3095	Red	8.00 ppmC m-Xylene	0.622 ppm
	Blue	7.21 ppmC Toluene	0.618 ppm

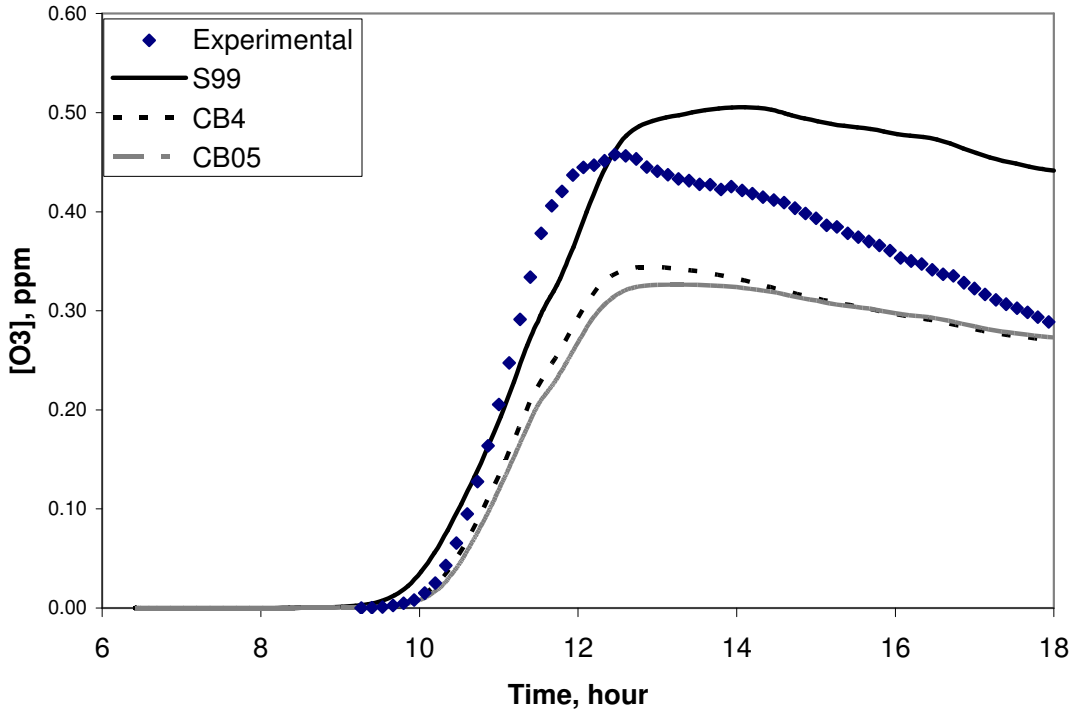

Figure 6-1. AU0183 UNC red chamber experiment with 4.59 ppmC toluene.

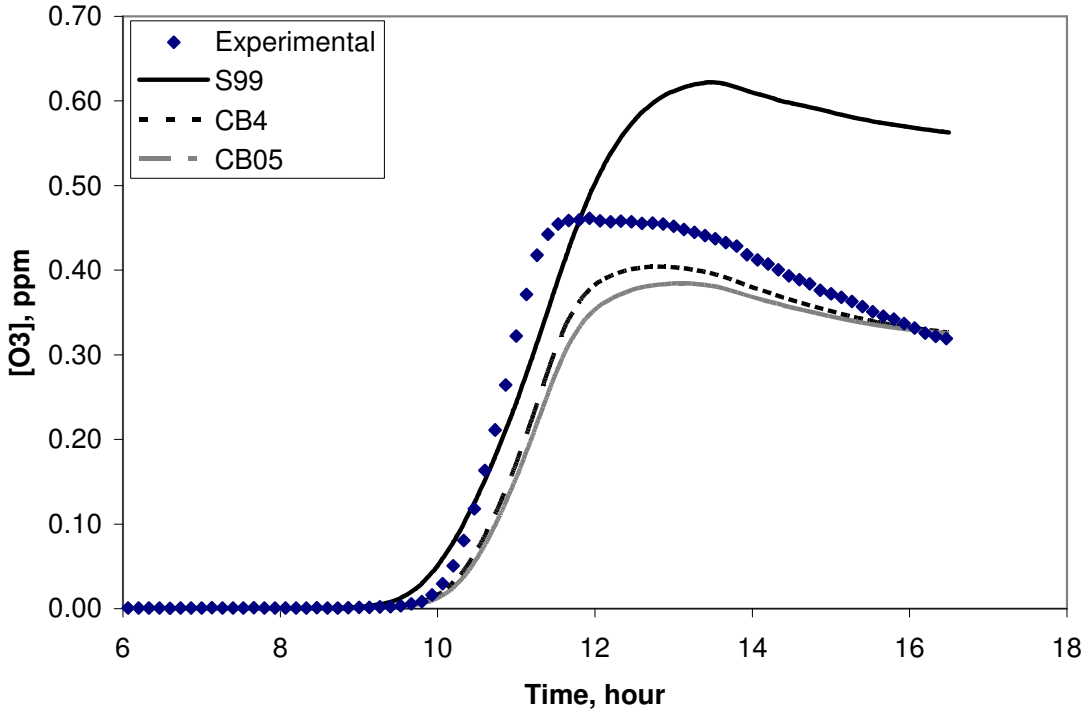

Figure 6-2. AU1788 UNC red chamber experiment with 4.93 ppmC toluene.

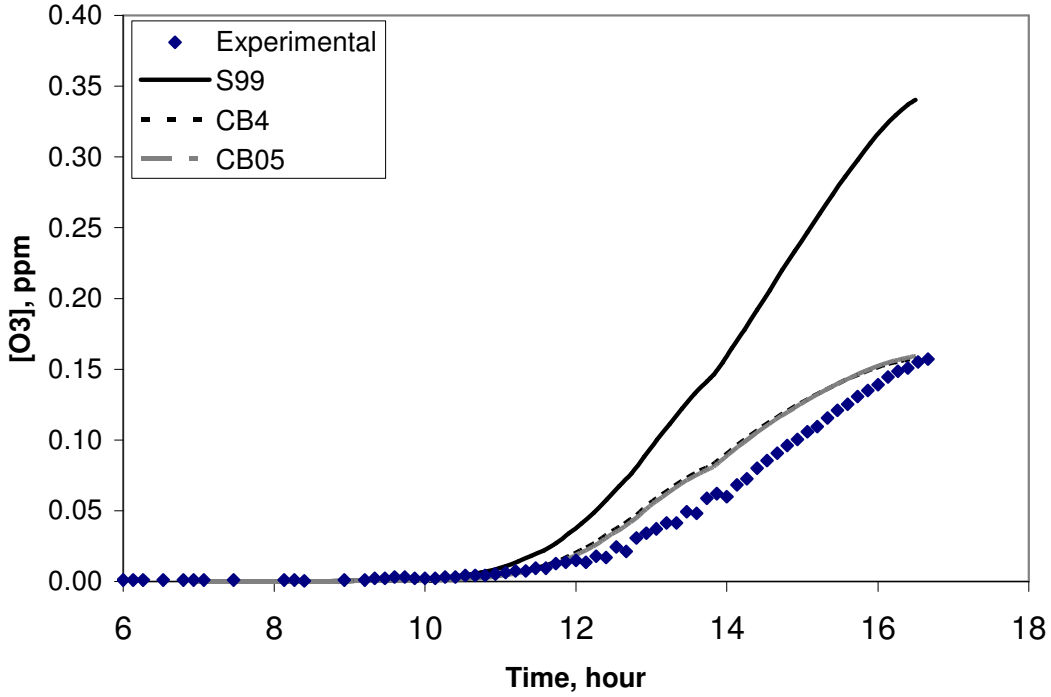

Figure 6-3 ST1393 UNC blue chamber experiment with 01.909 ppmC toluene.

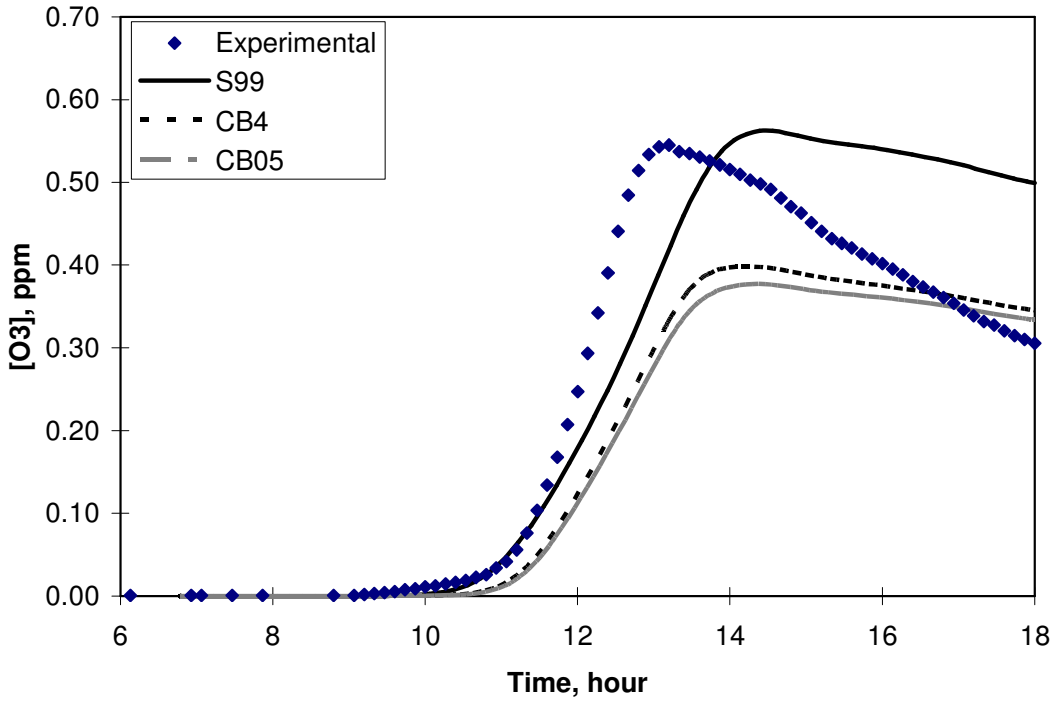

Figure 6-4. AU3095 UNC blue chamber experiment with 7.21 ppmC toluene.

Similar to the UNC toluene experiments, in the xylene and trimethylbenzene experiments in Figures 6-5 – 6-9, respectively, SAPRC99 predicts peak ozone concentrations that are consistently higher than the predictions by the CB mechanisms. However, the discrepancy between SAPRC99 and CB-IV for the toluene experiments is larger compared to the differences in the predictions of the mechanisms for xylenes and trimethylbenzenes. This is in agreement with findings from the single-VOC box model simulations in Chapter 3 in which the SAPRC99 and CB-IV mechanisms showed a larger discrepancy for the mono-substituted aromatics relative to the di- and multiply-substituted aromatics. Comparisons between predicted and measured ozone concentrations in UNC experiments of xylenes and trimethylbenzenes are made in Sections 6.3.3 and 6.3.4, respectively.

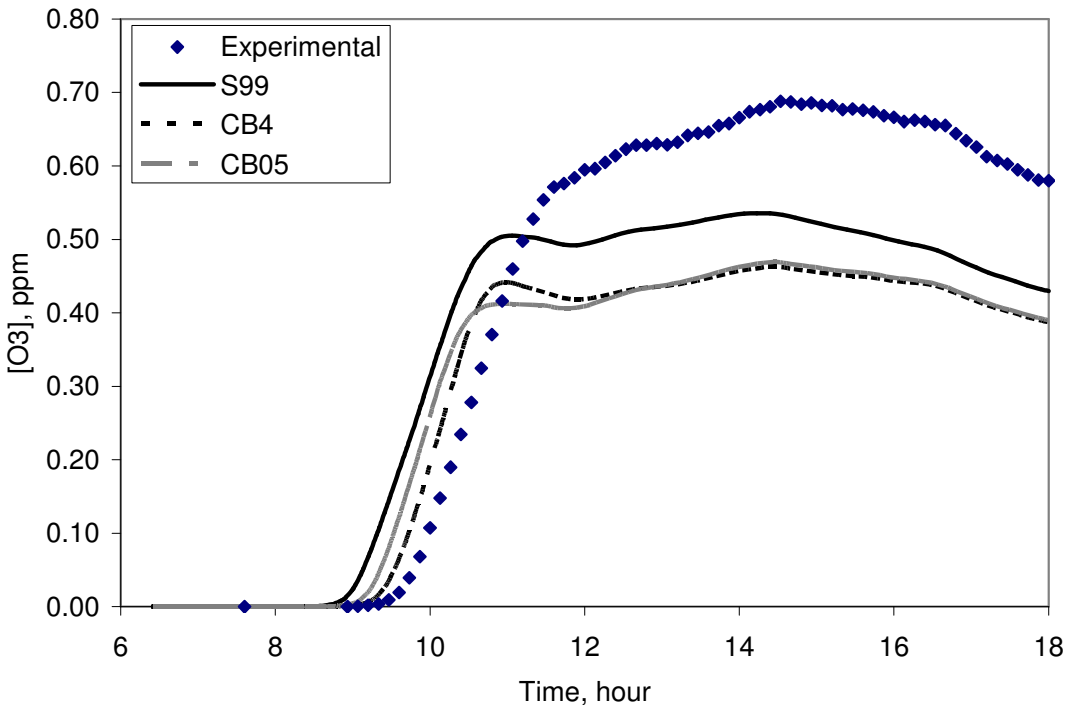

Figure 6-5. AU0183 UNC blue chamber experiment with 2.622 ppmC o-xylene.

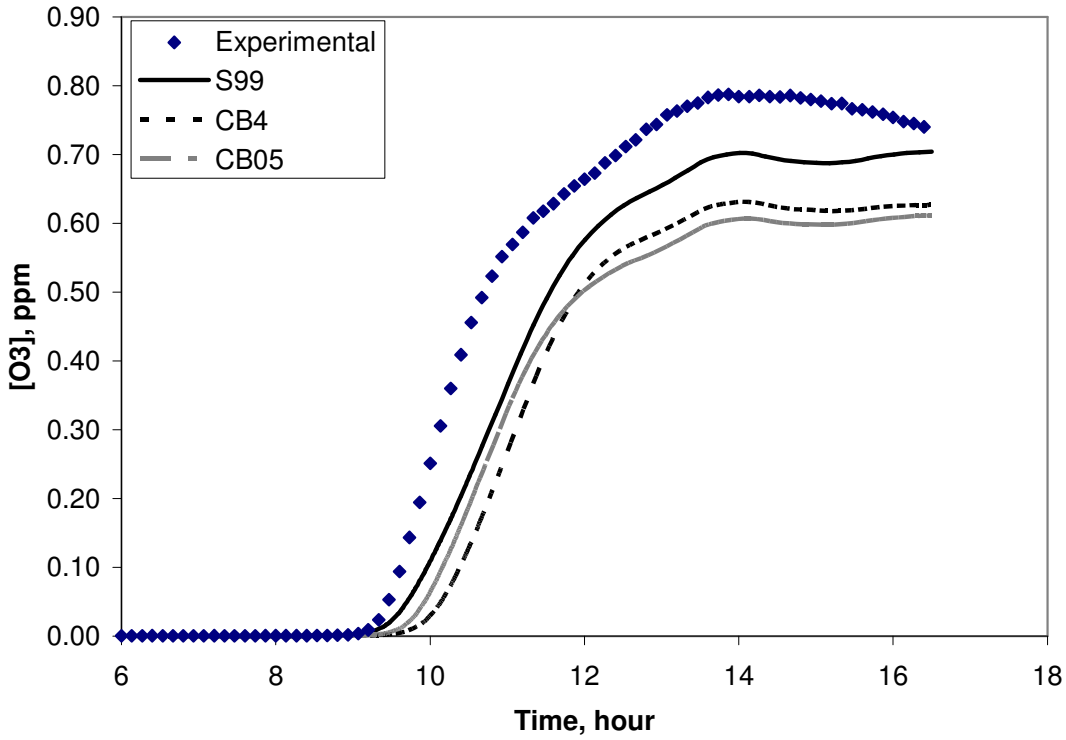

Figure 6-6. AU1788 UNC blue chamber experiment with 1.715 ppmC m-xylene.

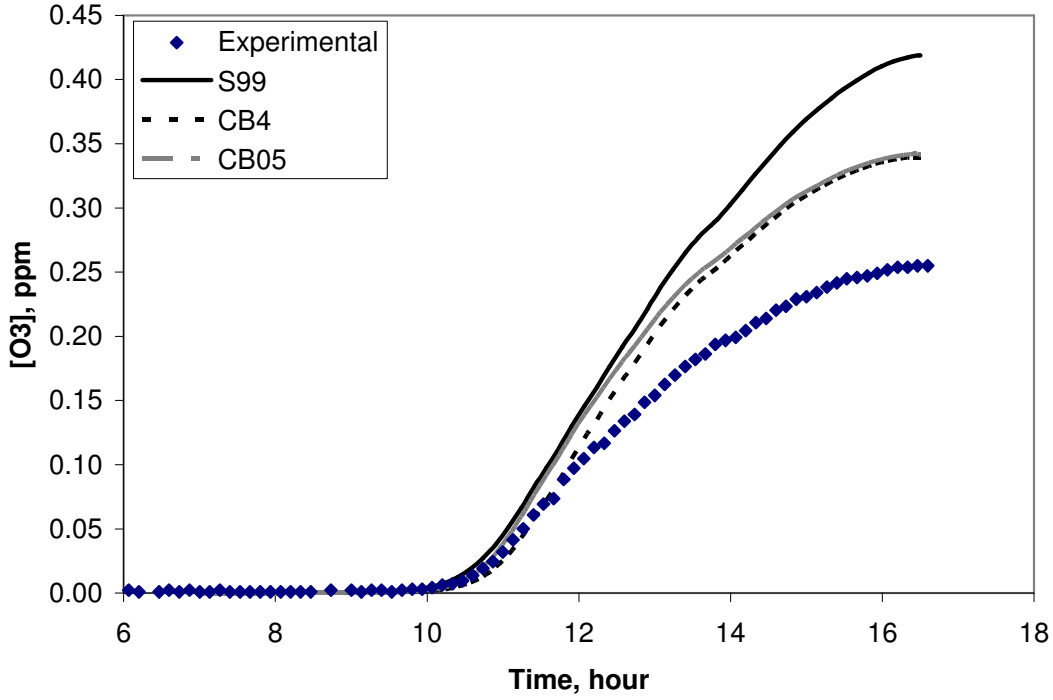

Figure 6-7. ST1393 UNC red chamber experiment with 0.789 ppmC m-xylene.

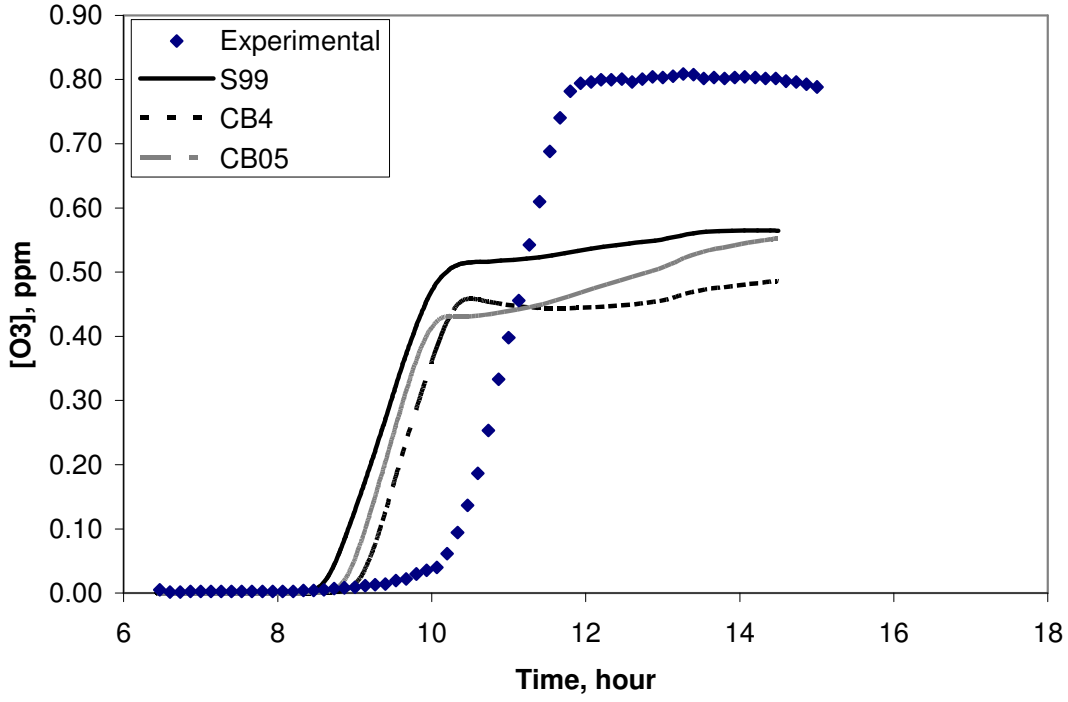

Figure 6-8. AU0395 UNC red chamber experiment with 1.00 ppm p-xylene.

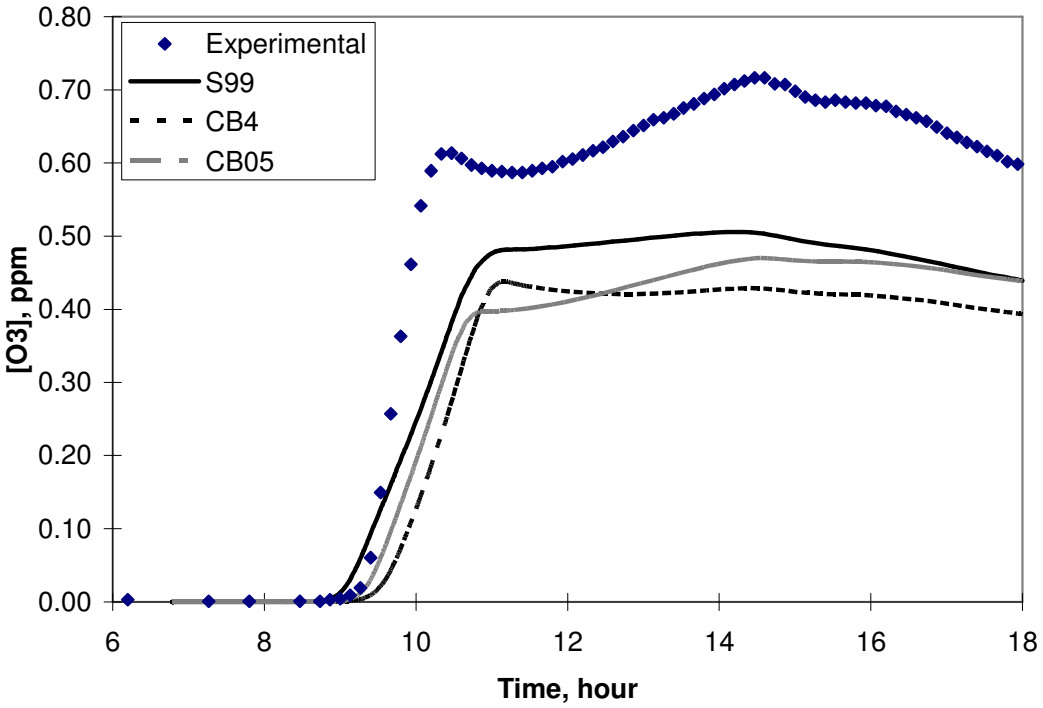

Figure 6-9. AU3095 UNC red chamber experiment with 8 ppmC m-xylene.

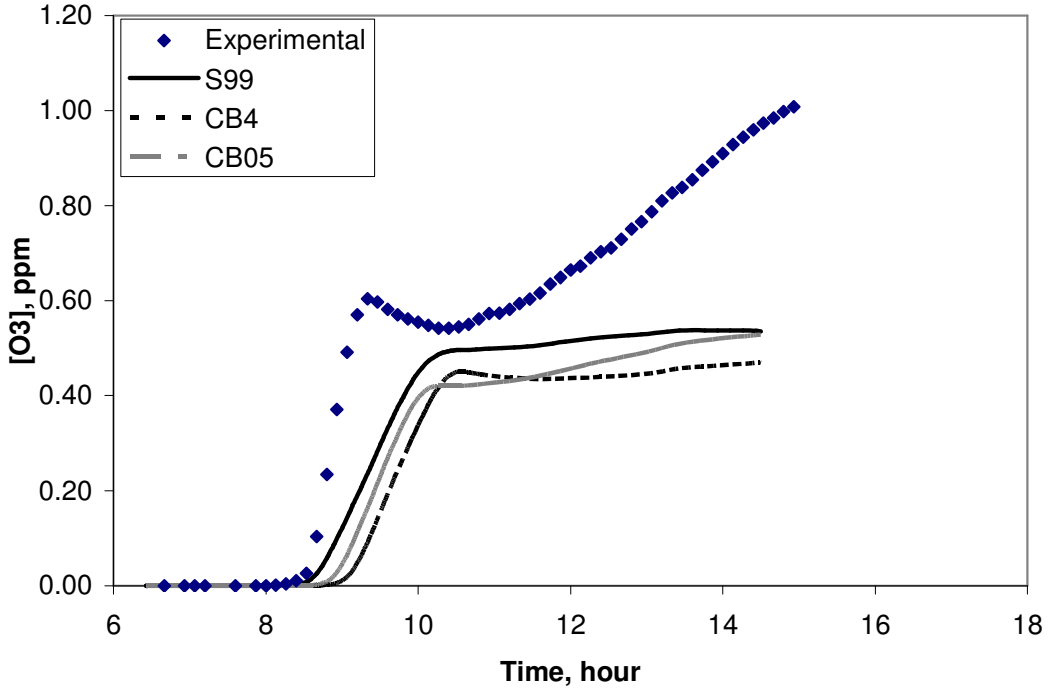

Figure 6-10. AU0395 UNC blue chamber experiment with 1.00 ppm 1,3,5-trimethylbenzene.

6.2 COMPARISON BETWEEN THE SAPRC99 AND CB SIMULATIONS OF THE UCR CHAMBER EXPERIMENTS FOR AROMATICS

In evaluating the performance of the mechanisms in simulating aromatics experiments conducted at UCR, chambers with blacklight sources (e.g., DTC, ITC, and ETC chambers) were not considered. This section includes two subsections in which experiments of mono-substituted aromatics and di- and multiply-substituted aromatics are presented.

6.2.1 Mono-substituted Aromatics: Toluene and Ethylbenzene

The UCR experiments of mono-substituted aromatics included those of toluene and ethylbenzene. The EC experiments included six toluene experiments in which

concentrations of cresols were among the species measured. A subset of these experiments, together with selected toluene experiments in the EPA, OTC and TVA chambers are listed in Table 6-2. The EPA chamber experiments are conducted at much lower levels of NOx relative to the experiments in the other chambers. A complete listing of toluene experiments conducted at UCR chambers, followed by the concentration of O_3 and other species are provided in Appendix G.1. Predictions of the SAPRC99, CB-IV, and CB05 mechanisms in simulating the experiments in Table 6-2 are shown in Figure 6-11. The x-axes are the concentrations of the designated species in ppm as a function of the simulation time in minutes.

Table 6-2 List of toluene experiments with cresol measurements in EC chamber at UCR.

Experiment ID	VOC	NOx	Light Source
EC271	8.02 ppmC Toluene	215 ppb	Arc light solar simulator
EC273	4.11 ppmC Toluene	112 ppb	Arc light solar simulator
EC340	3.76 ppmC Toluene	493 ppb	Arc light solar simulator

Figure 6-11 shows that the peak ozone concentrations predicted with SAPRC99 are consistently larger than the peak ozone concentrations predicted with the CB mechanisms. Figure 6-11 also reports CRES concentrations, which are compared to concentrations of cresols observed in the chambers. The available cresol measurements in the EC experiments show that the concentrations of the lumped cresol species predicted with SAPRC99 are in better agreement with the measurements relative to the lumped cresol species predicted with the CB mechanisms. These comparisons should be interpreted cautiously, however, especially for the CB mechanism. The CRES group in the CB mechanisms represents not only cresol production, but also other NOx sink reactions under NOx limited conditions. Killus and Whitten (1982 and 1983) noted that a

large NOx sink exists in toluene oxidation when a smog system approaches NOx-limited conditions. Cresol is a known major product of toluene decay via ring-retaining pathways (Calvert *et al*., 2002) and cresol reacts rapidly with the nitrate radical (NO_3) (Atkinson *et al*., 1992). Thus, cresol production introduces a strong NOx sink in toluene smog chemistry. However, Gery *et al*. (1989) found that the observed yields of cresol (recently summarized by Calvert *et a*l., 2002) were insufficient to fully account for the apparent NOx sink in toluene experiments that reach NOx-limited conditions. Cresol is a surrogate product in the Carbon Bond representation of toluene chemistry. The higher than observed yield of cresol acts as a surrogate for other products (such as unsaturated dicarbonyls) that would also react rapidly with the nitrate radical. Comparisons between predicted and measured peak ozone concentrations in the UCR toluene experiments are made in Section 6.3.1.

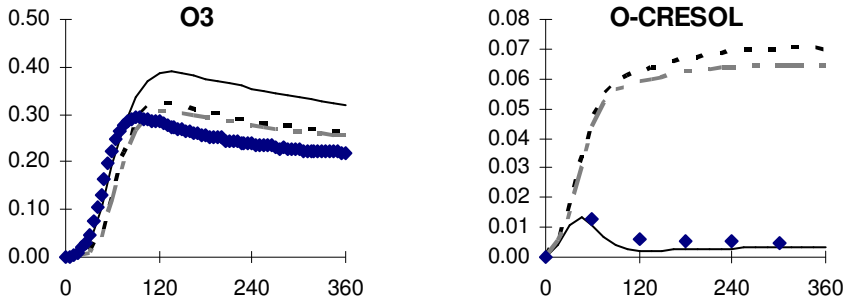

(a) EC271

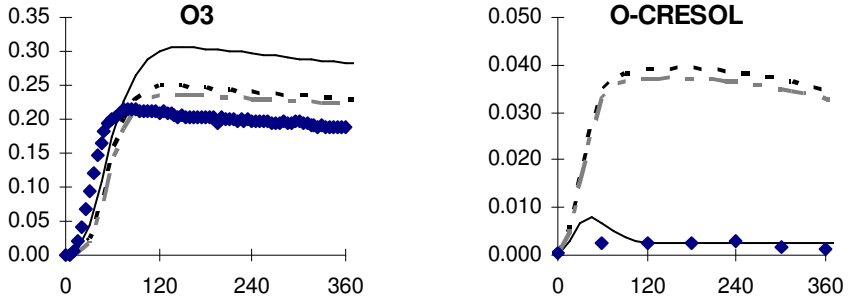

(b) EC273

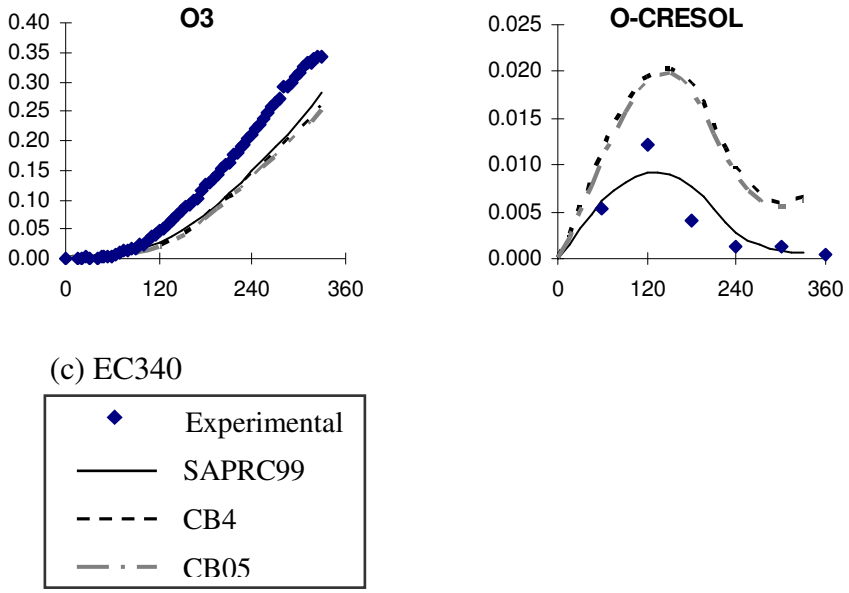

Figure 6-11. Concentrations of species in ppm as a function of time (minutes) in EC chamber toluene experiments at UCR.

A more comprehensive listing of toluene experiments available from the UCR and TVA chambers is provided in Table 6-3. Results, some of which were provided by Carter, are shown in Figure 6-12. These experiments include those used in the SAPRC07 mechanism evaluation (Carter, 2007) except that experiments using the blacklight light source (which is not a good representative of sunlight for aromatic product photolysis) are not included. As shown in Figure 6-12, the peak ozone concentrations predicted with SAPRC99 are consistently larger than the peak ozone concentrations predicted with the CB mechanisms. Table 6-9 and Figure 6-17 and 6-19 summarize the performance of the mechanisms in predicting peak ozone concentrations relative to the experimental data.

Table 6-3 Summary of UCR and TVA toluene experiments used in the mechanism evaluation.

Experiment ID	Toluene (ppm)	NOx (ppm)	Light Source
EC273	0.59	0.111	Arc light solar simulator
EC271	1.15	0.213	Arc light solar simulator
EC340	0.54	0.486	Arc light solar simulator
EC269	0.57	0.480	Arc light solar simulator
EC327	0.57	0.484	Arc light solar simulator
EC270	0.58	0.462	Arc light solar simulator
EC293	1.07	0.481	Arc light solar simulator
EC264	1.16	0.436	Arc light solar simulator
EC266	1.20	0.436	Arc light solar simulator
CTC079	0.50	0.256	Arc light solar simulator
CTC048	0.95	0.247	Arc light solar simulator
CTC026	2.01	0.270	Arc light solar simulator
CTC034	2.21	0.523	Arc light solar simulator
CTC065	0.97	0.656	Arc light solar simulator
XTC106	1.92	0.245	Arc light solar simulator
EPA066B	0.06	0.005	Arc light solar simulator
EPA077A	0.15	0.022	Arc light solar simulator
EPA074A	0.15	0.024	Arc light solar simulator
EPA443A	0.17	0.031	Arc light solar simulator
EPA210A	0.26	0.042	Arc light solar simulator
EPA210B	0.26	0.093	Arc light solar simulator
EPA443B	0.36	0.099	Arc light solar simulator
TVA080	0.06	0.054	Blacklights + Sunlamps
TVA047	0.07	0.104	Blacklights + Sunlamps
TVA071	0.35	0.265	Blacklights + Sunlamps
OTC300B	0.51	0.224	Sunlight
OTC300A	0.51	0.521	Sunlight
OTC299A	1.22	0.509	Sunlight

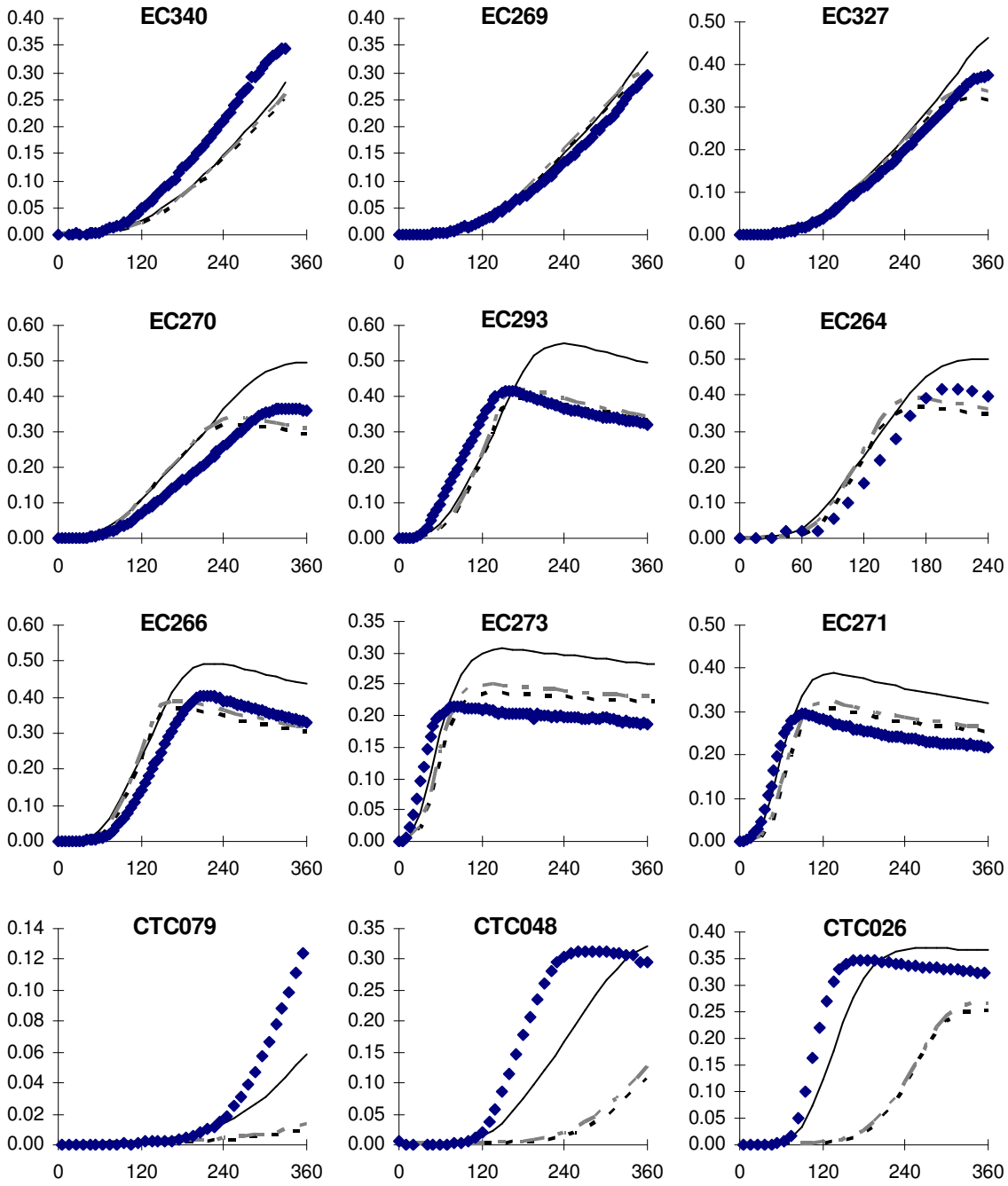
EC340
EC269
EC327
EC270
EC293
EC264
EC266
EC273
EC271
CTC079
CTC048
CTC026

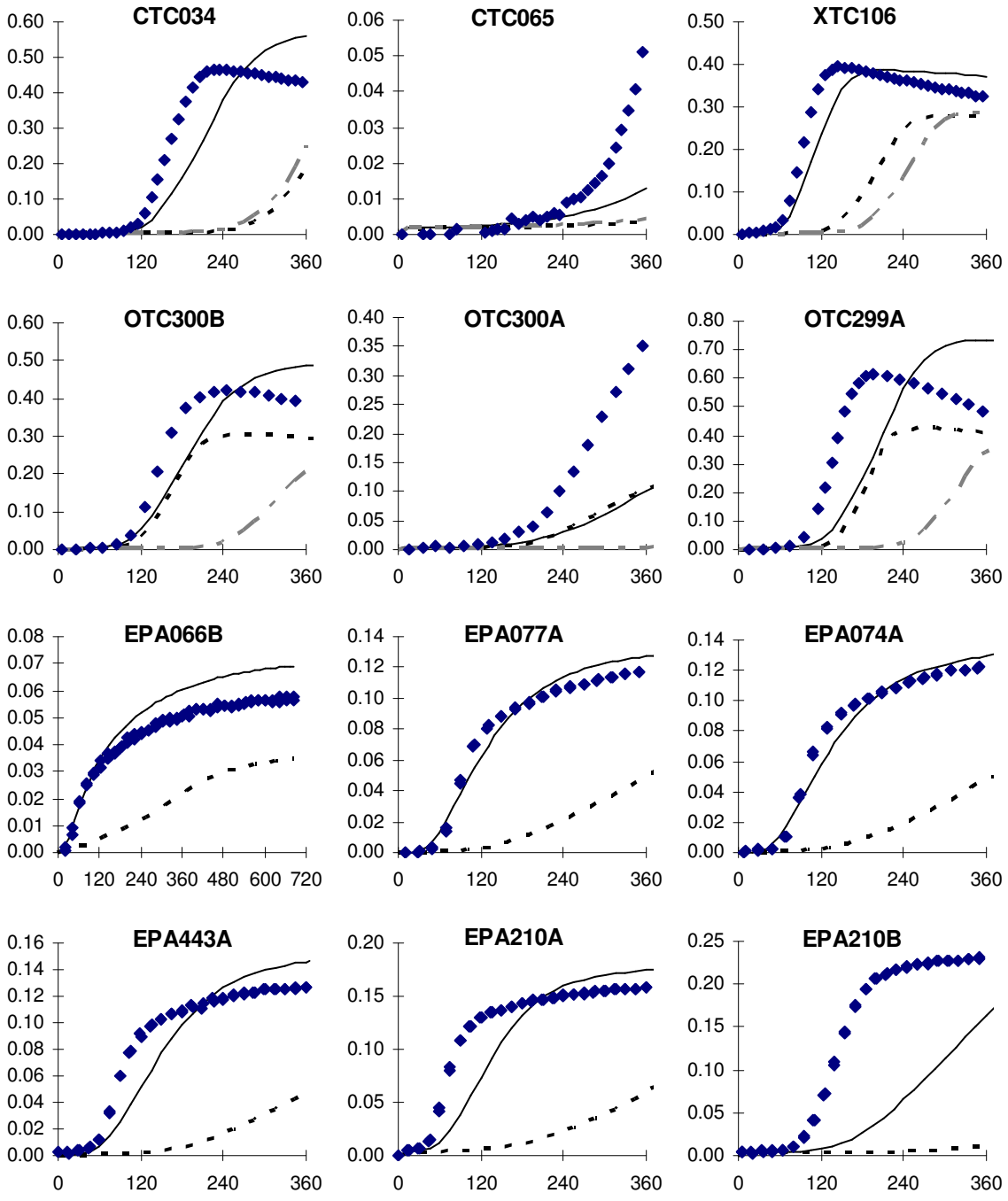
CTC034
CTC065
XTC106
OTC300B
OTC300A
OTC299A
EPA066B
EPA077A
EPA074A
EPA443A
EPA210A
EPA210B

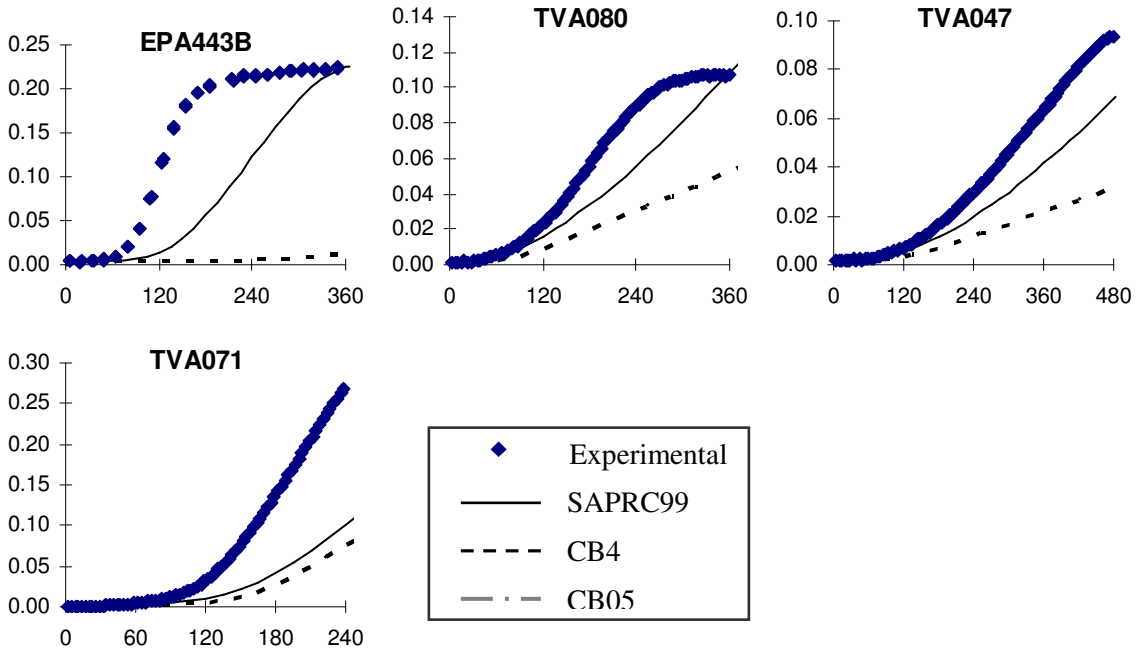

Figure 6-12. Concentrations of ozone in ppm as a function of irradiation time (minutes) in toluene experiment at UCR and TVA.

In addition to toluene experiments, Other UCR experiments are available for the mono-substituted aromatic ethylbenzene. Table 6-4 lists ethylbenzene experiments conducted in the CTC chamber, followed by the results in Figure 6-13. The maximum ozone concentrations predicted with SAPRC99 in these experiments greatly exceed that of the CB mechanisms. Comparisons between predicted and measured peak ozone concentrations in the ethylbenzene experiments are made in Section 6.3.1.

Table 6-4. List of ethylbenzene experiments in the CTC chambers at UCR.

Experiment ID	VOC	NOx	Light Source
CTC092A	8.22 ppmC Ethylbenzene	268 ppb	Arc light solar simulator
CTC092B	15.68 ppmC Ethylbenzene	270 ppb	Arc light solar simulator
CTC098B	15.01 ppmC Ethylbenzene	494 ppb	Arc light solar simulator
CTC057	16.22 ppmC Ethylbenzene	272 ppb	Arc light solar simulator

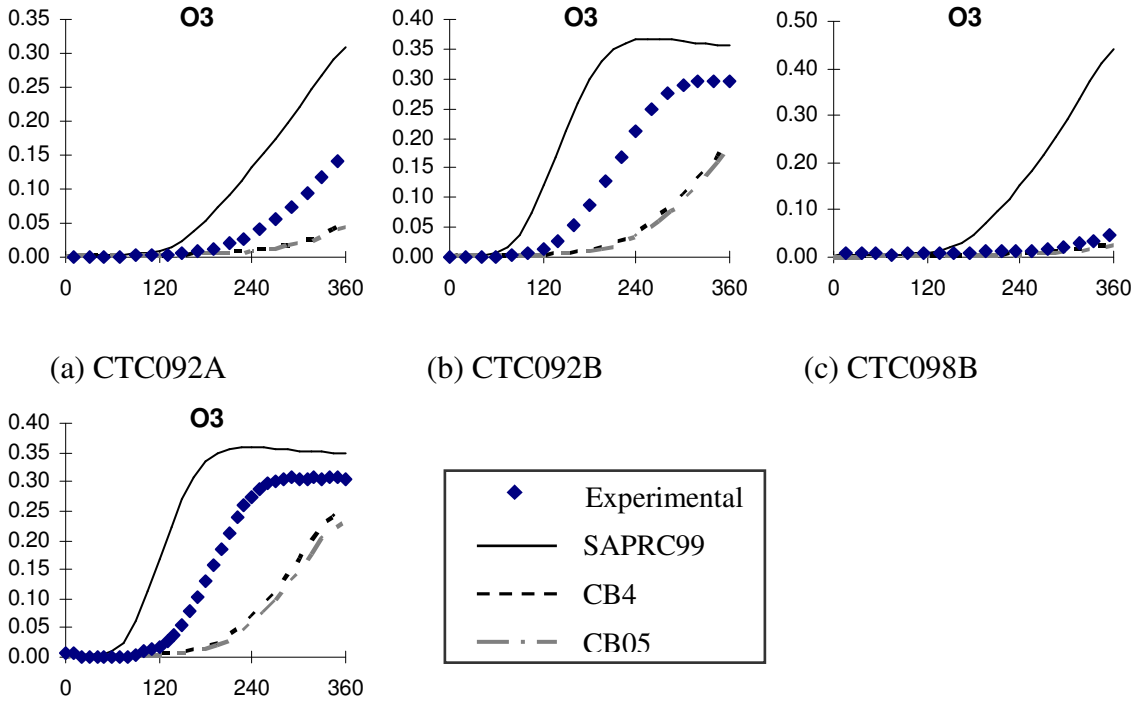

(a) CTC092A (b) CTC092B (c) CTC098B

(d) CTC057

Figure 6-13. Concentrations of species in ppm as a function of time (minutes) in ethylbenzene experiments at UCR.

6.2.2 Di- and multiply-substituted Aromatics: Xylenes and trimethylbenzenes

Selected experiments of xylenes and trimethylbenzenes conducted in UCR chambers are listed in Tables 6-5 and 6-6, respectively. Simulated and experimental

ozone concentrations for xylenes and trimethylbenzenes are presented in Figures 6-14 and 6-15, respectively. Similar to the UNC experiments, differences in peak ozone concentrations between SAPRC99 and CB-IV for these experiments are not as pronounced as the discrepancy found for the mono-substituted aromatics.

Table 6-5. Selected experiments of xylenes in UCR chambers.

Experiment ID	VOC	NOx	Light Source
EPA149B	1.31 ppmC m-Xylene	54 ppb	Arc light solar simulator
EPA556A	1.28 ppmC m-Xylene	78 ppb	Arc light solar simulator
CTC036	1.27 ppmC m-Xylene	509 ppb	Arc light solar simulator
CTC080	4.24 ppmC m-Xylene	507 ppb	Arc light solar simulator
CTC046	2.40 ppmC o-Xylene	503 ppb	Arc light solar simulator
EC288	1.44 ppmC o-Xylene	502 ppb	Arc light solar simulator
EC291	4.83 ppmC o-Xylene	495 ppb	Arc light solar simulator
CTC043	1.54 ppmC p-Xylene	250 ppb	Arc light solar simulator
CTC047	7.78 ppmC p-Xylene	276 ppb	Arc light solar simulator

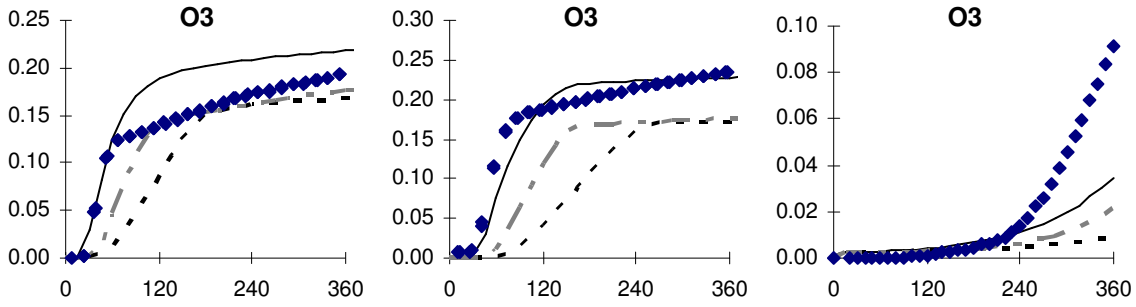

(a) EPA149B (b) EPA556A (c) CTC036

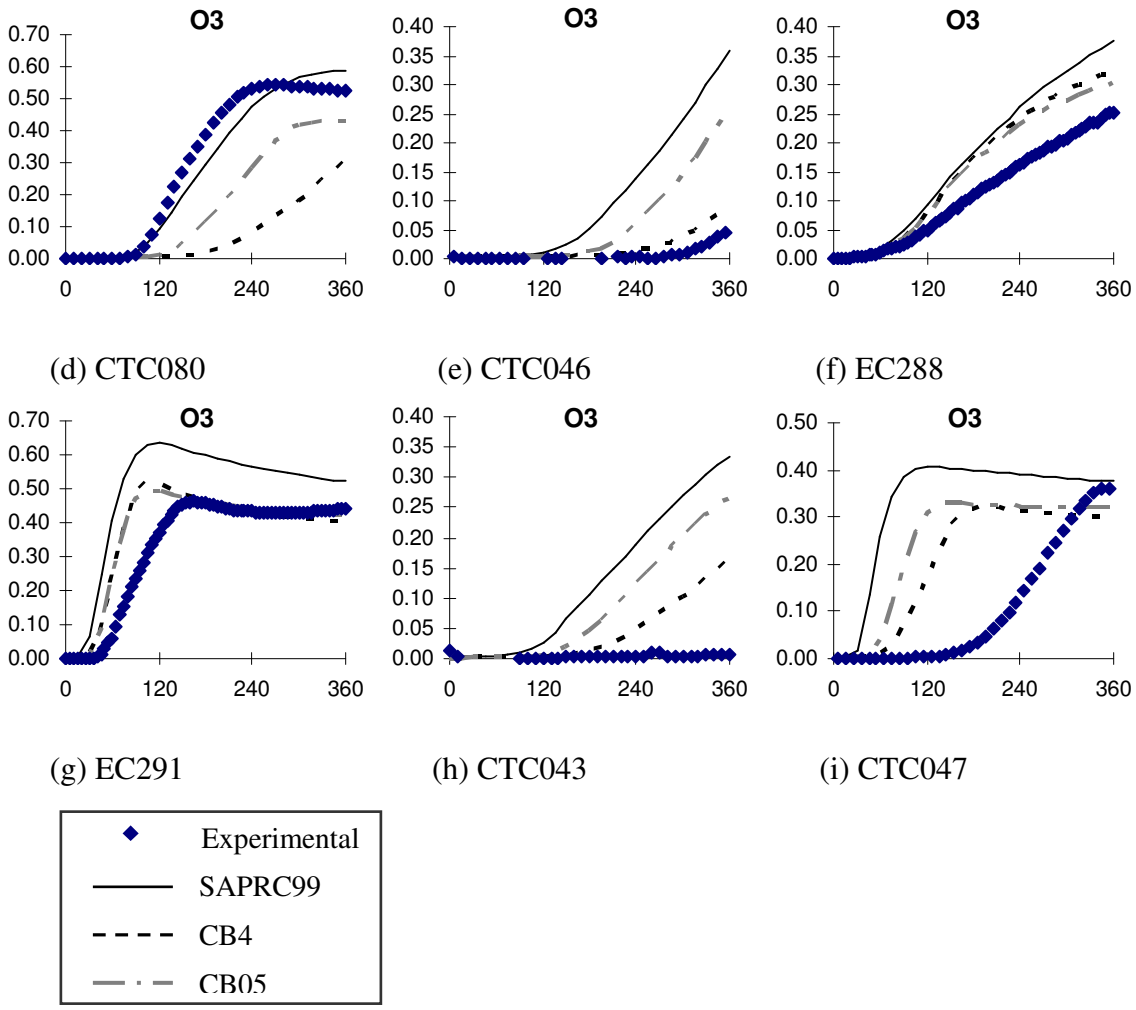

Figure 6-14. Concentrations of ozone in ppm as a function of time (minutes) in the experiments of xylenes at UCR.

Table 6-6. Selected experiments of trimethylbenzenes in UCR chambers.

Experiment ID	VOC	NOx	Light Source
CTC075	2.05 ppmC 1,2,3-Trimethylbenzene	520 ppb	Arc light solar simulator
CTC076	1.60 ppmC 1,2,3-Trimethylbenzene	258 ppb	Arc light solar simulator
CTC091B	4.17 ppmC 1,2,4-Trimethylbenzene	281 ppb	Arc light solar simulator
CTC093A	4.30 ppmC 1,2,4-Trimethylbenzene	482 ppb	Arc light solar simulator
CTC056	2.03 ppmC 1,2,4-Trimethylbenzene	254 ppb	Arc light solar simulator
CTC098A	1.78 ppmC 1,3,5-Trimethylbenzene	480 ppb	Arc light solar simulator
CTC071	2.96 ppmC 1,3,5-Trimethylbenzene	517 ppb	Arc light solar simulator
CTC073	1.57 ppmC 1,3,5-Trimethylbenzene	257 ppb	Arc light solar simulator
XTC103	2.68 ppmC 1,3,5-Trimethylbenzene	496 ppb	Arc light solar simulator

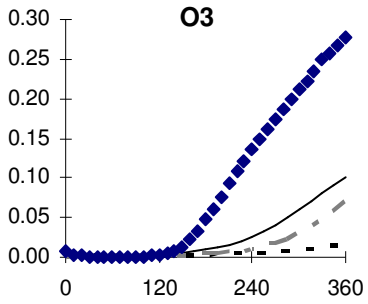

(a) CTC075

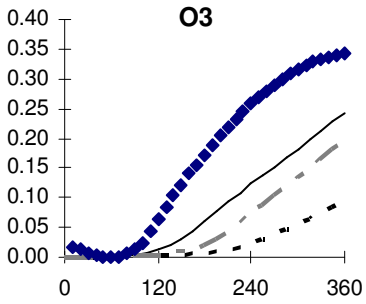

(b) CTC076

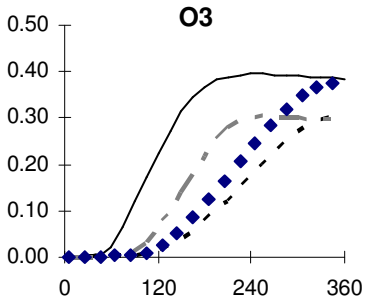

(c) CTC091B

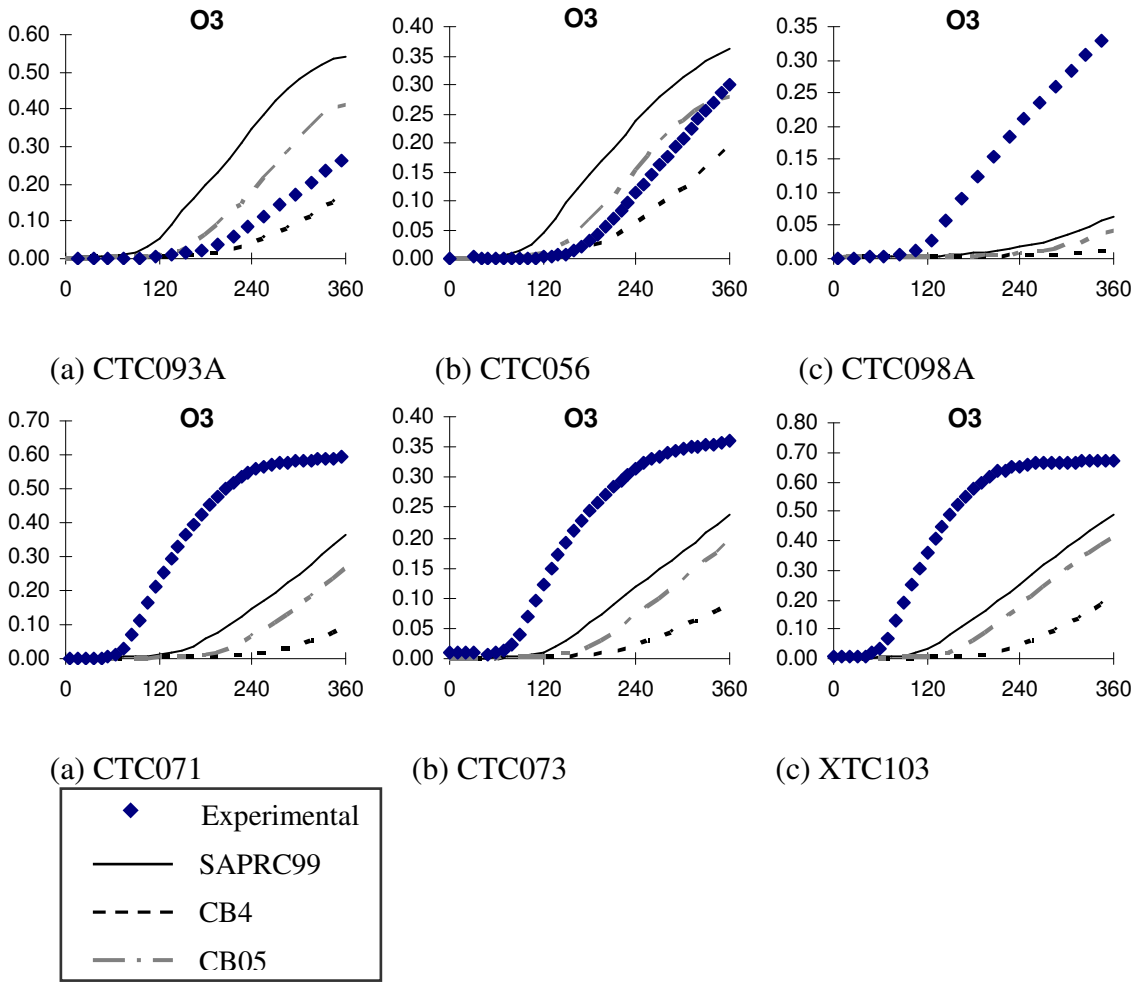

Figure 6-15. Concentrations of ozone in ppm as a function of time (minutes) in the experiments of trimethylbenzenes at UCR.

6.3 COMPARISON BETWEEN THE SAPRC99 AND CB SIMULATIONS AND UNC AND UCR CHAMBER DATA FOR AROMATICS

Underprediction in peak ozone concentrations simulated with the mechanisms relative to the measured ozone peaks in the chambers, {(Experimental peak ozone-Model peak ozone)/Experimental peak ozone}, as a function of VOC/NOx ratios and reactivity weighted VOC/NOx ratios are reported. Table 6-7 gives the MIRs for aromatics retrieved from Carter (2000) in units of grams ozone per gram VOC emitted. These

analyses were conducted separately for toluene, ethylbenzene, xylenes, and trimethylbenzenes in the following subsections.

Table 6-7. MIRs for aromatics in units of grams ozone per gram VOC emitted (Carter, 2000).

VOC	MIR (g/g)
Toluene	3.97
Ethylbenzene	2.79
m-xylene	10.61
o-xylene	7.49
p-xylene	4.25
1,2,3-trimethylbenzene	11.26
1,2,4-trimethylbenzene	7.18
1,3,5-trimethylbenzene	11.22

6.3.1 Comparison between the SAPRC99 and CB simulations and UNC and UCR chamber data for toluene

For the toluene experiments, prediction in peak ozone concentrations simulated with the mechanisms relative to the measured ozone peaks in the chambers, as a function of VOC/NOx ratios and reactivity weighted VOC/NOx ratios are reported in Tables 6-8 and 6-9 and Figures 6-16 to 6-19.

The Figures for the UNC experiments show that overall the SAPRC99 mechanism tends to be biased towards overpredicting O_3 in these experiments, while the CB mechanisms tend to underpredict O_3, though to a much lesser extent than observed for the UCR and TVA experiments. As with most UCR and TVA experiments (except OTC), the two CB mechanisms perform about the same in simulating these experiments. Although the SAPRC and CB mechanisms are quite different in simulating these

experiments, overall all three mechanisms simulate this UNC chamber dataset about equally well (or poorly).

In the UCR/TVA experiments, the earlier UCR arc light runs are summarized separately from the newer UCR EPA chamber experiments because the latter had lower reactant concentrations and generally lower chamber effects. It can be seen from the UCR/TVA experiments that the ability of the mechanisms to simulate these experiments varies from experiment to experiment, but overall the SAPRC99 mechanism has relatively little overall bias in simulating O_3 and O_3 formed and NO oxidized in these experiments, while both the CB mechanisms significantly underpredict O_3 and $\Delta([O_3]-[NO])$ in most experiments. Note that this is not a condensation issue because the CB TOL model species is intended to simulate primarily toluene, which is the major emitted compound that is represented by this lumped species. The performance of the CAMx SAPRC99 mechanism is only slightly different from that of the detailed SAPRC99 mechanism in simulating these runs (not shown).

Table 6-8. Comparison between the SAPRC99 and CB simulations and UNC chamber data for toluene.

	Experiment	AU0183 Red	AU1788 Red	ST1393 Blue	AU3095 Blue
	VOC (ppmC)	4.590	4.930	1.909	7.210
	NOx (ppm)	0.395	0.357	0.324	0.618
	VOC/NOx	11.620	13.810	5.892	11.667
Peak Ozone (ppm)	SAPRC99	0.506	0.622	0.340	0.562
	CB-IV	0.344	0.404	0.158	0.398
	CB05	0.326	0.384	0.159	0.377
	Experiment	0.458	0.460	0.157	0.545
(Experimental-Model) /Experimental	SAPRC99	-10.48%	-35.34%	-116.28%	-3.08%
	CB-IV	24.89%	12.10%	-0.51%	27.00%
	CB05	28.82%	16.45%	-1.15%	30.85%
	MIR (g/g)	3.97	3.97	3.97	3.97
	MIR*VOC/NOx	46.1	54.8	23.4	46.3

Table 6-9. Comparison between the SAPRC99 and CB simulations and UCR/TVA chamber data for toluene.

Experiment	Final O_3	Model Fit to $\Delta([O_3]-[NO])$		
	(ppm)	SAPRC99	CB05	CB4
EC273	0.187	36%	14%	17%
EC271	0.217	26%	10%	12%
EC340	0.317	-9%	-11%	-10%
EC269	0.297	8%	1%	4%
EC327	0.375	12%	-7%	-4%
EC270	0.360	16%	-9%	-8%
EC293	0.341	23%	1%	3%
EC264	0.393	13%	-7%	-5%
EC266	0.331	13%	-4%	-3%
CTC079	0.130	-24%	-64%	-60%
CTC048	0.297	7%	-38%	-34%
CTC026	0.324	8%	-17%	-15%
CTC034	0.430	10%	-53%	-48%
CTC065	0.058	-31%	-74%	-71%
XTC106	0.323	7%	-11%	-12%
	Average:	8%	-18%	-16%
EPA066B	0.050	14%	-55%	-55%
EPA077A	0.117	7%	-49%	-47%
EPA074A	0.123	6%	-51%	-49%
EPA443A	0.126	10%	-64%	-62%
EPA210A	0.158	9%	-54%	-52%
EPA210B	0.231	-22%	-85%	-84%
EPA443B	0.223	-2%	-84%	-84%
	Average:	3%	-63%	-62%
TVA080	0.107	1%	-36%	-36%
TVA047	0.063	-19%	-35%	-36%
TVA071	0.270	-37%	-42%	-42%
	Average:	-18%	-38%	-38%
OTC300B	0.385	8%	-19%	-55%
OTC300A	0.360	-37%	-33%	-91%
OTC299A	0.481	18%	-12%	-43%
	Average:	-4%	-21%	-63%

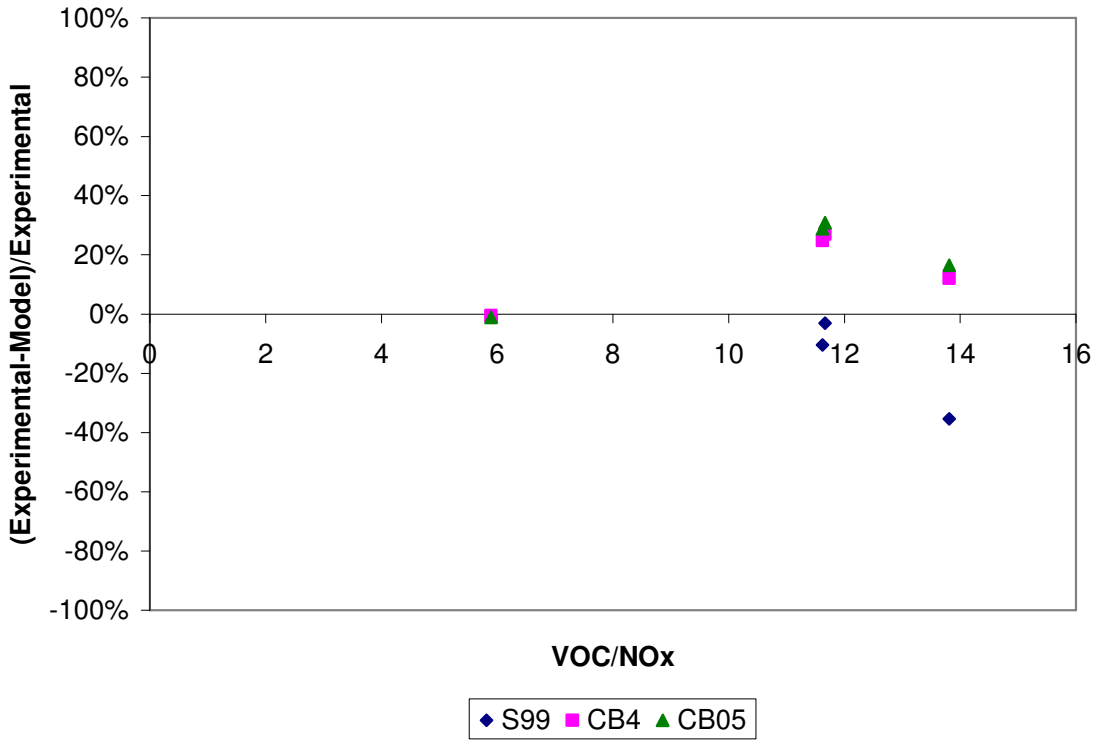

Figure 6-16. Model underprediction error for peak ozone in UNC chamber toluene experiments against VOC/NOx ratio.

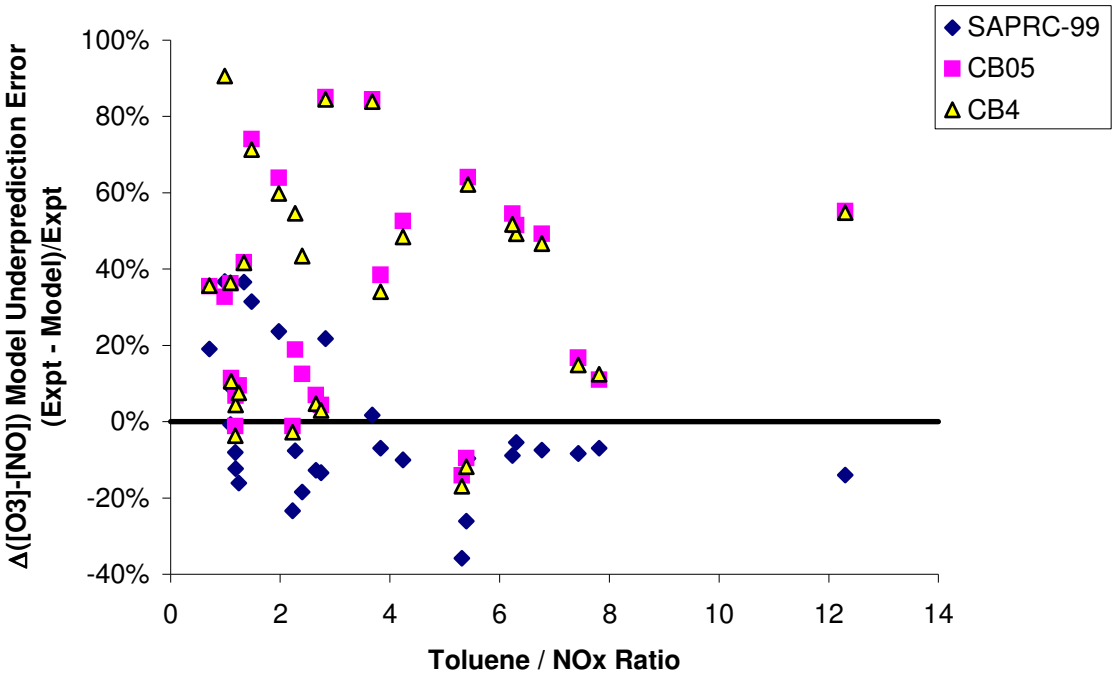

Figure 6-17. Model underprediction error for peak ozone in UCR chamber toluene experiments against VOC/NOx ratio.

The underprediction of the mechanisms as a function of (MIR*VOC)/NOx for the UNC and UCR toluene experiments are shown in Figures 6-18 and 6-19, respectively.

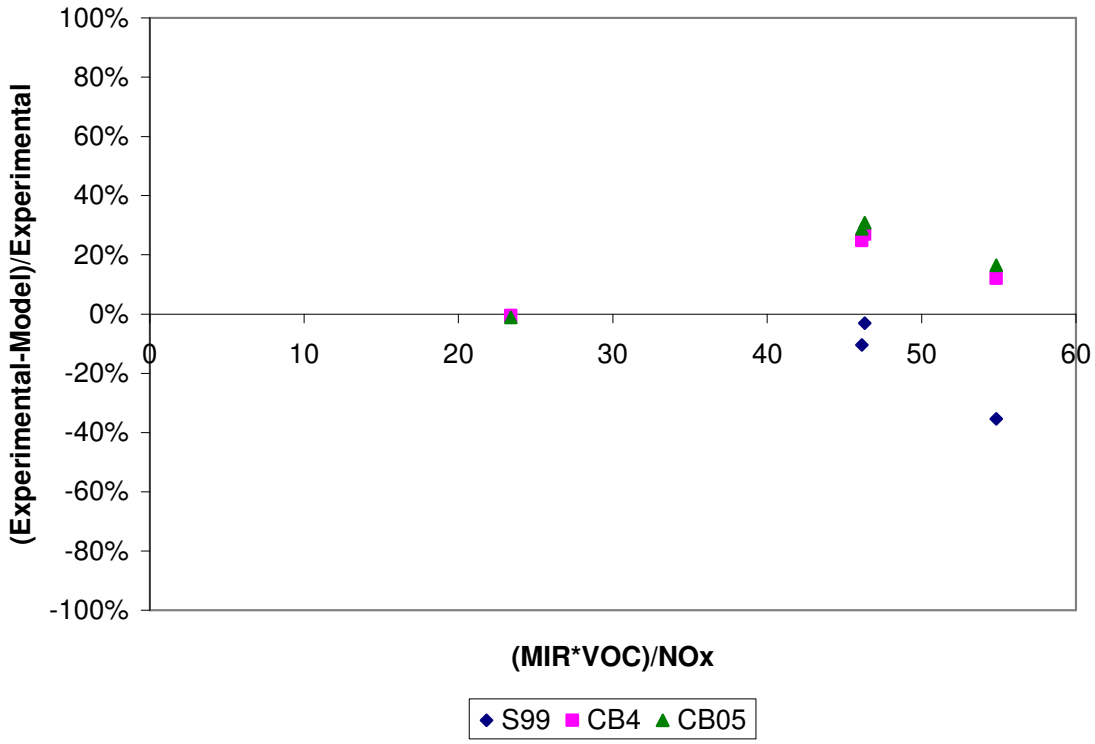

Figure 6-18. Model underprediction error for peak ozone in UNC chamber toluene experiments against (MIR*VOC)/NOx ratio.

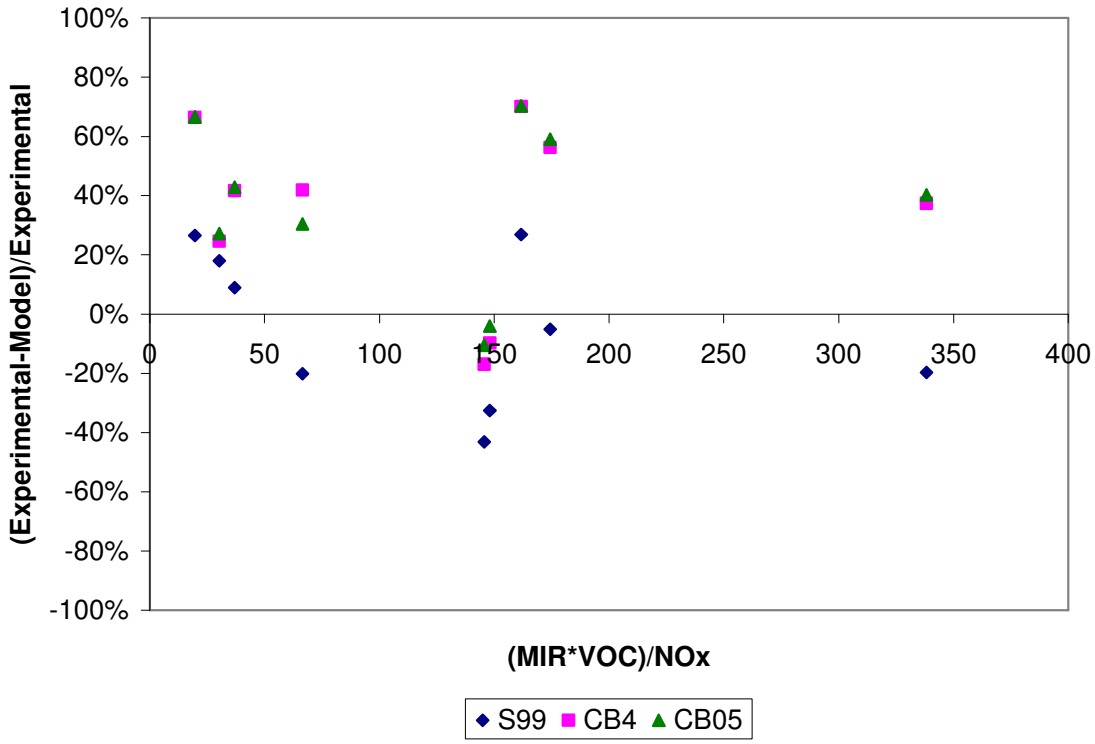

Figure 6-19. Model underprediction error for peak ozone in UCR chamber toluene experiments against (MIR*VOC)/NOx ratio.

6.3.2 Comparison between the SAPRC99 and CB simulations and UCR chamber data for ethylbenzene

Comparison between simulated and predicted peak ozone concentrations for the UCR ethylbenzene experiments are made in Table 6-9 and Figure 6-20. SAPRC99 consistently overpredicts peak ozone relative to the measurements while the CB mechanisms underpredict the peak ozone in these experiments. Furthermore, the extent of underprediction with CB05 is slightly greater than the extent of underprediction with CB-IV. Figure 6-21 shows the percent underprediction for each mechanism as a function of (MIR*VOC)/NOx.

Table 6-9. Comparison between the SAPRC99 and CB simulations and UCR chamber data toluene for ethylbenzene.

	Experiment	CTC092A	CTC092B	CTC098B	CTC057
	VOC (ppmC)	8.220	15.680	15.010	16.220
	NOx (ppm)	0.268	0.270	0.494	0.272
	VOC/NOx	30.672	58.074	30.385	59.632
Peak Ozone (ppm)	SAPRC99	0.308	0.367	0.441	0.358
	CB-IV	0.047	0.195	0.029	0.251
	CB05	0.044	0.183	0.025	0.233
	Experiment	0.142	0.296	0.046	0.307
(Experimental-Model) /Experimental	SAPRC99	-117.11%	-23.98%	-857.23%	-16.56%
	CB-IV	66.62%	34.28%	36.39%	18.38%
	CB05	69.01%	38.23%	44.85%	24.37%
	MIR (g/g)	2.79	2.79	2.79	2.79
	MIR*VOC/NOx	85.57	162.03	84.77	166.37

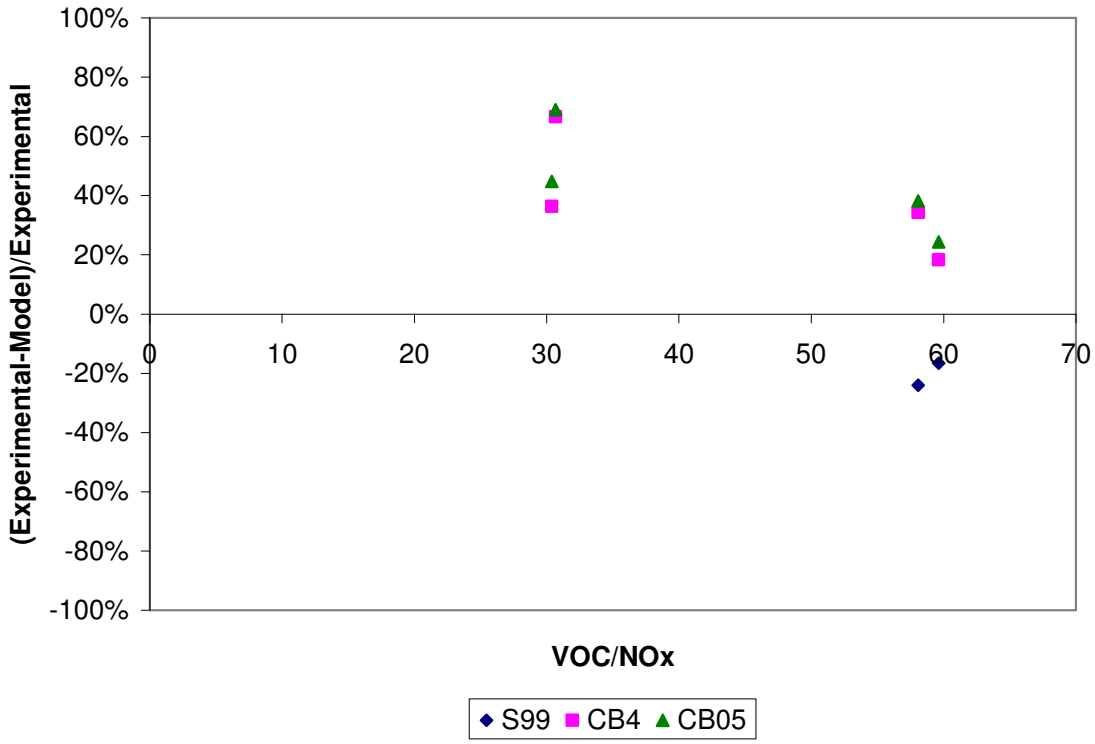

Figure 6-20. Model underprediction error for peak ozone in UCR chamber ethylbenzene experiments against VOC/NOx ratio.

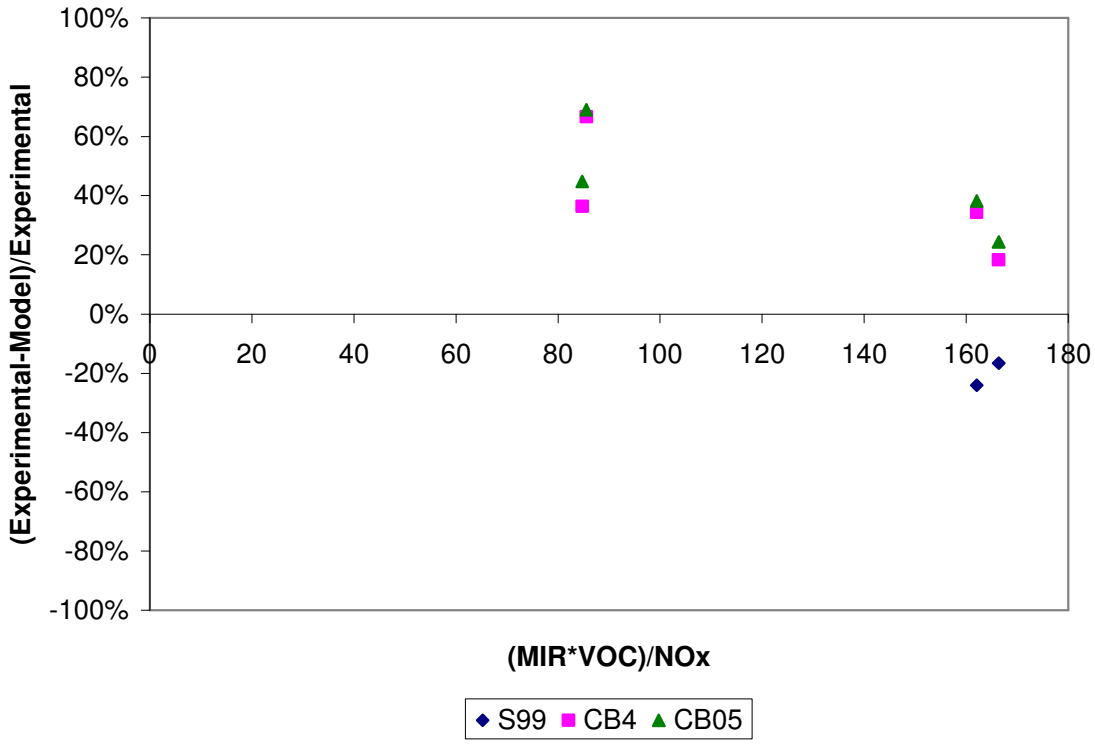

Figure 6-21. Model underprediction error for peak ozone in UCR chamber t ethylbenzene experiments against (MIR*VOC)/NOx ratio.

6.3.3 Comparison between the SAPRC99 and CB simulations and UNC and UCR chamber data for xylenes

For both the UNC and UCR chambers, the bias with SAPRC99 relative to the bias with CB mechanisms varies from one experiment to another; when the mechanisms show an underprediction, SAPRC99 exhibits a lower bias, whereas when there is an overprediction, SAPRC99 exhibits a greater bias. This is illustrated in Tables 6-10 and 6-11 and Figures 6-22 and 6-23. Figures 6-24 and 6-26 show the percent bias a function of (MIR*VOC)/NOx in the UNC and UCR chambers, respectively.

Table 6-10. Comparison between the SAPRC99 and CB simulations and UNC chamber data for xylenes.

	Experiment	AU0183 Blue	AU1788 Blue	ST1393 Red	AU0395 Red	AU3095 Red
	VOC (ppmC)	2.622	1.715	0.789	8.000	8.000
	NOx (ppm)	0.373	0.356	0.321	0.641	0.622
	VOC/NOx	7.029	4.817	2.458	12.480	12.862
Peak Ozone (ppm)	SAPRC99	0.536	0.702	0.419	0.564	0.505
	CB-IV	0.463	0.632	0.340	0.486	0.438
	CB05	0.469	0.607	0.342	0.552	0.470
	Experiment	0.688	0.788	0.255	0.809	0.717
(Experimental-Model)/Experimental	SAPRC99	22.09%	10.91%	-64.38%	30.28%	29.57%
	CB-IV	32.70%	19.80%	-33.39%	39.93%	38.91%
	CB05	31.83%	22.97%	-34.17%	31.77%	34.45%
	MIR (g/g)	7.49	10.61	10.61	4.25	10.61
	MIR*VOC/NOx	52.7	51.1	26.1	53.0	136.5

Table 6-11. Comparison between the SAPRC99 and CB simulations and UCR chamber data toluene for xylenes.

	Experiment	EPA149B	EPA556A	CTC036	CTC080	CTC046	EC288	EC291	CTC043	CTC047
	VOC (ppmC)	1.310	1.280	1.270	4.240	2.400	1.440	4.830	1.540	7.780
	NOx (ppm)	0.054	0.078	0.509	0.507	0.503	0.502	0.495	0.250	0.276
	VOC/NOx	24.259	16.410	2.495	8.363	4.771	2.869	9.758	6.160	28.188
Peak Ozone (ppm)	SAPRC99	0.221	0.236	0.035	0.587	0.357	0.374	0.634	0.333	0.406
	CB-IV	0.173	0.172	0.009	0.305	0.092	0.322	0.523	0.161	0.323
	CB05	0.184	0.191	0.022	0.432	0.254	0.302	0.498	0.266	0.331
	Experiment	0.204	0.278	0.092	0.543	0.044	0.263	0.462	0.013	0.359
(Experimental-Model) /Experimental	SAPRC99	-8.43%	15.34%	62.28%	-8.14%	-705.59%	-42.52%	-37.22%	-2375.13%	-12.94%
	CB-IV	15.34%	38.40%	89.97%	43.77%	-106.81%	-22.73%	-13.27%	-1096.73%	10.07%
	CB05	9.71%	31.39%	76.56%	20.38%	-472.17%	-15.00%	-7.79%	-1872.53%	7.85%
	MIR (g/g)	10.61	10.61	10.61	10.61	7.49	7.49	7.49	4.25	4.25
	MIR*VOC/NOx	257.39	174.11	26.47	88.73	35.74	21.49	73.08	26.18	119.80

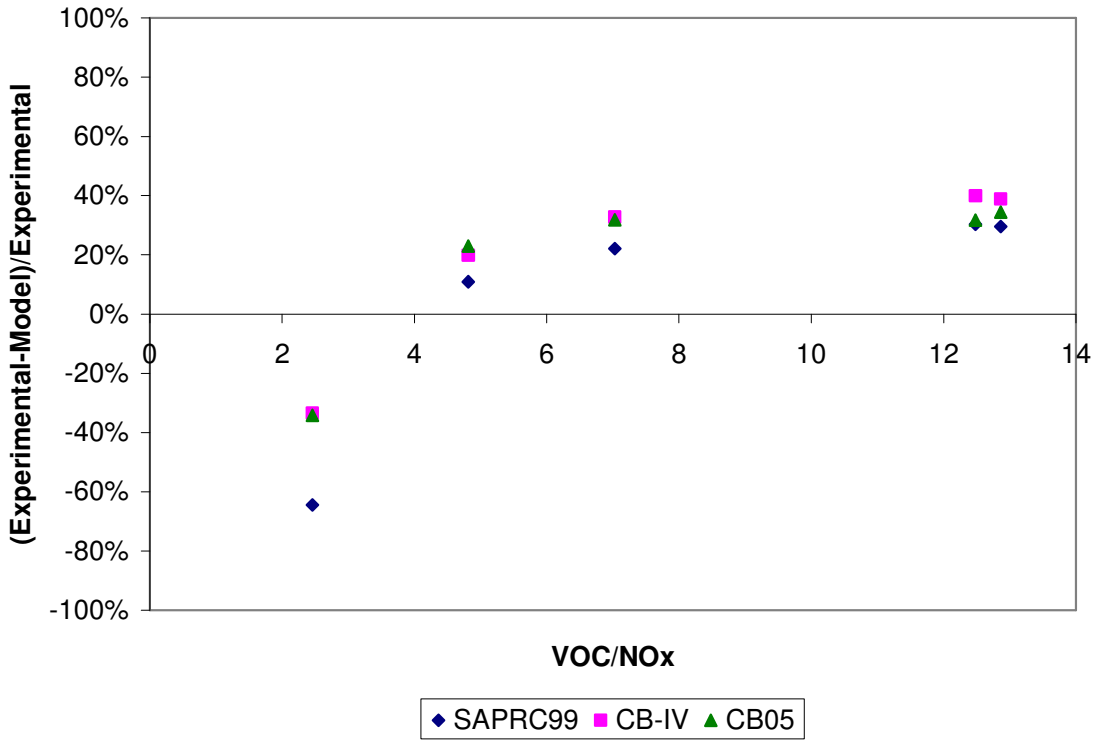

Figure 6-22. Model underprediction error for peak ozone in UNC chamber xylenes experiments against VOC/NOx ratio.

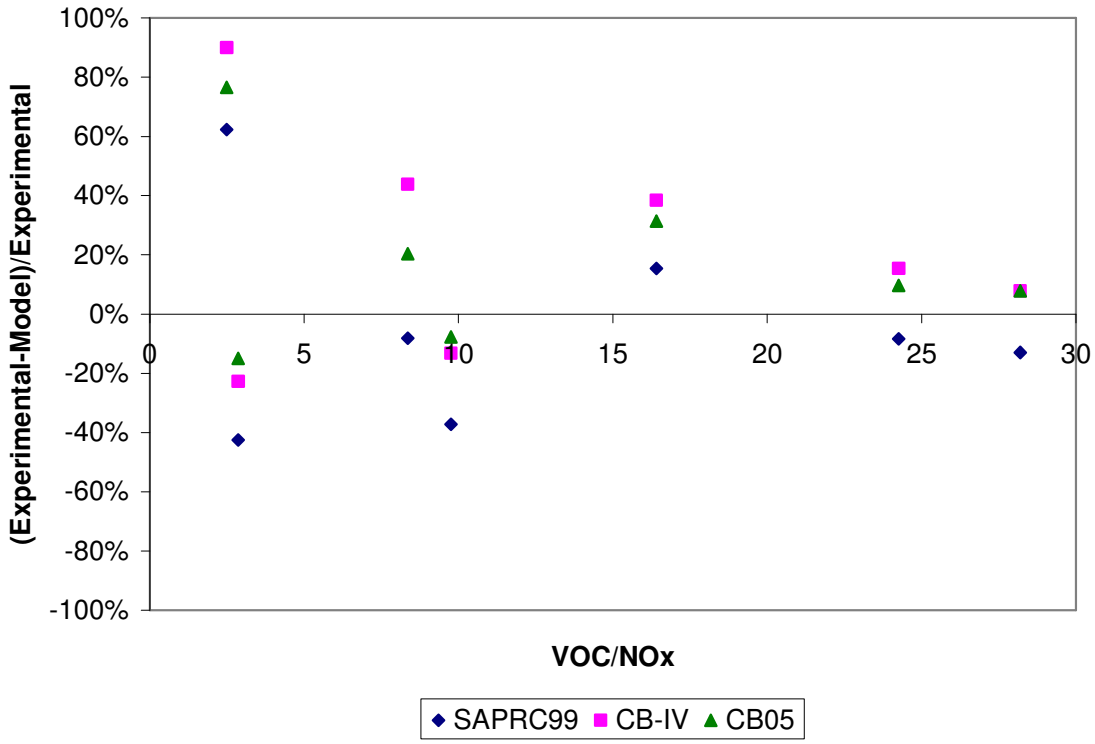

Figure 6-23. Model underprediction error for peak ozone in UCR chamber xylenes experiments against VOC/NOx ratio.

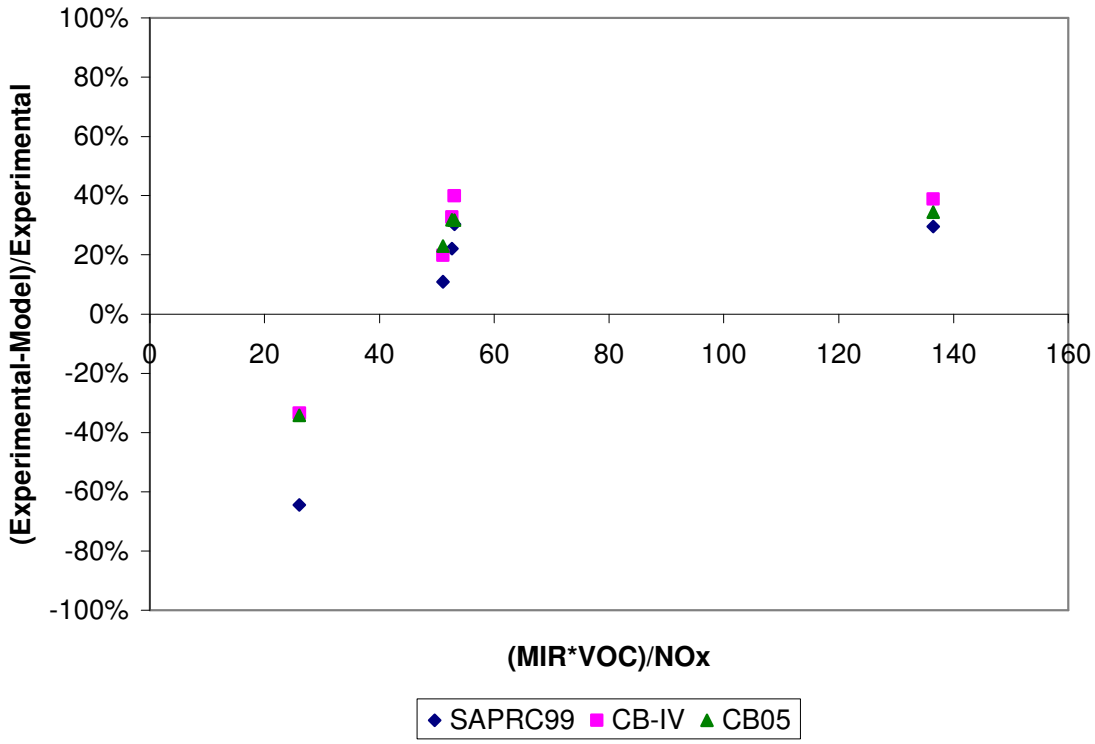

Figure 6-24. Model underprediction error for peak ozone in UNC chamber xylenes experiments against (MIR*VOC)/NOx ratio.

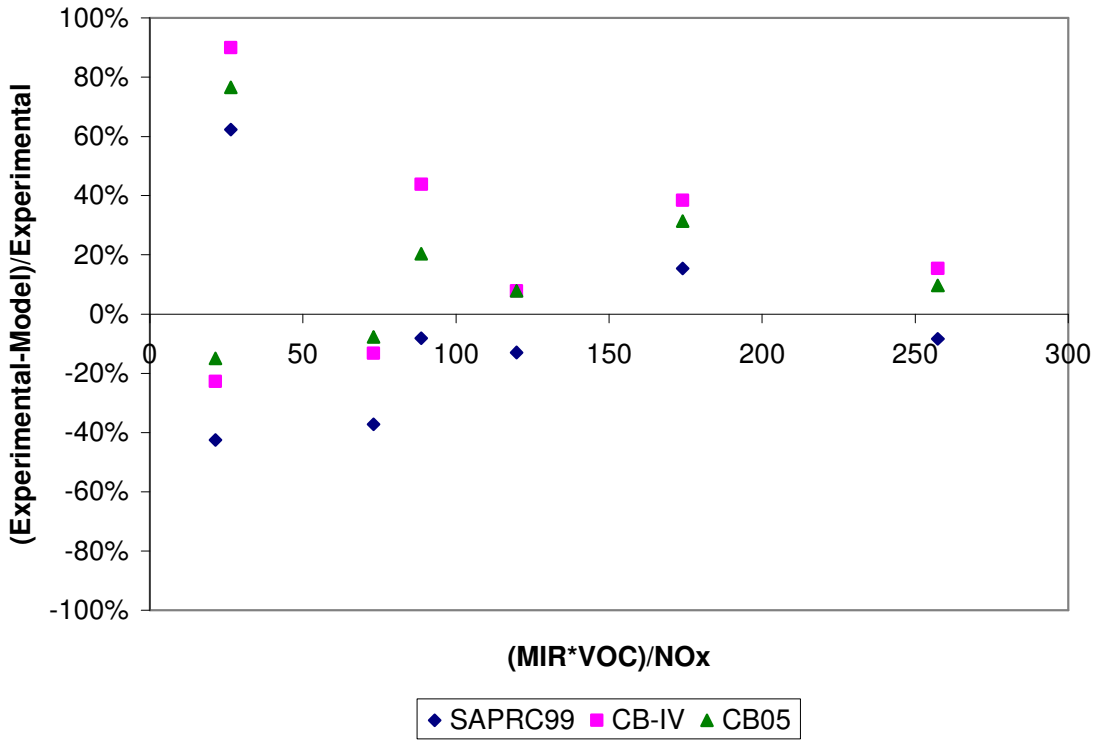

Figure 6-25. Model underprediction error for peak ozone in UCR chamber xylenes experiments against (MIR*VOC)/NOx ratio.

6.3.4 Comparison between the SAPRC99 and CB simulations and UNC and UCR chamber data for trimethylbenzenes

In the trimethylbenzene experiment in the UNC chamber, Table 6-12 and Figures 6-26 and 6-28, all three mechanisms underpredict the peak ozone relative to the measurements. The underprediction with SAPRC99 is lower than the CB mechanisms, but SAPRC99 and CB05 are more in agreement. In the UCR chambers, except for the XTC experiment in which SAPRC99 shows a greater underprediction relative to the CB mechanisms, SAPRC99 either overpredicts the ozone peak or shows a lower

underprediction relative to the CB mechanisms (Table 6-13 and Figures 6-27 and 6-29). The bias with CB05 is in closer agreement with the SAPRC99 mechanism.

Table 6-12. Comparison between the SAPRC99 and CB simulations and UNC chamber data for trimethylbenzenes.

	Experiment	AU0395 Blue
	VOC (ppmC)	7.210
	NOx (ppm)	0.621
	VOC/NOx	11.610
Peak Ozone (ppm)	SAPRC99	0.535
	CB-IV	0.469
	CB05	0.528
	Experiment	1.008
(Experimental-Model) /Experimental	SAPRC99	46.92%
	CB-IV	53.47%
	CB05	47.62%
	MIR (g/g)	11.22
	MIR*VOC/NOx	130.3

Table 6-13. Comparison between the SAPRC99 and CB simulations and UCR chamber data toluene for trimethylbenzenes.

	Experiment	CTC075	CTC076	CTC091B	CTC093A	CTC056	CTC098A	CTC071	CTC073	XTC103
	VOC (ppmC)	2.050	1.600	4.170	4.300	2.030	1.780	2.960	1.570	2.680
	NOx (ppm)	0.520	0.258	0.281	0.482	0.254	0.480	0.517	0.257	0.496
	VOC/NOx	3.942	6.202	14.840	8.921	7.992	3.708	5.725	6.109	5.403
Peak Ozone (ppm)	SAPRC99	0.102	0.243	0.395	0.543	0.361	0.063	0.362	0.236	0.489
	CB-IV	0.018	0.093	0.304	0.171	0.189	0.013	0.094	0.090	0.205
	CB05	0.070	0.195	0.304	0.413	0.281	0.042	0.262	0.191	0.410
	Experiment	0.277	0.344	0.374	0.265	0.300	0.328	0.591	0.359	0.671
(Experimental-Model) /Experimental	SAPRC99	65.34%	29.18%	-5.75%	-105.13%	-20.43%	80.65%	38.80%	34.10%	69.46%
	CB-IV	94.01%	73.06%	18.73%	35.56%	36.96%	96.12%	84.19%	74.85%	38.93%
	CB05	76.33%	43.15%	18.65%	-56.06%	6.28%	87.12%	55.66%	46.84%	38.93%
	MIR (g/g)	11.26	11.26	7.18	7.18	7.18	11.22	11.22	11.22	11.22
	MIR*VOC/NOx	44.39	69.83	106.55	64.05	57.38	41.61	64.24	68.54	60.62

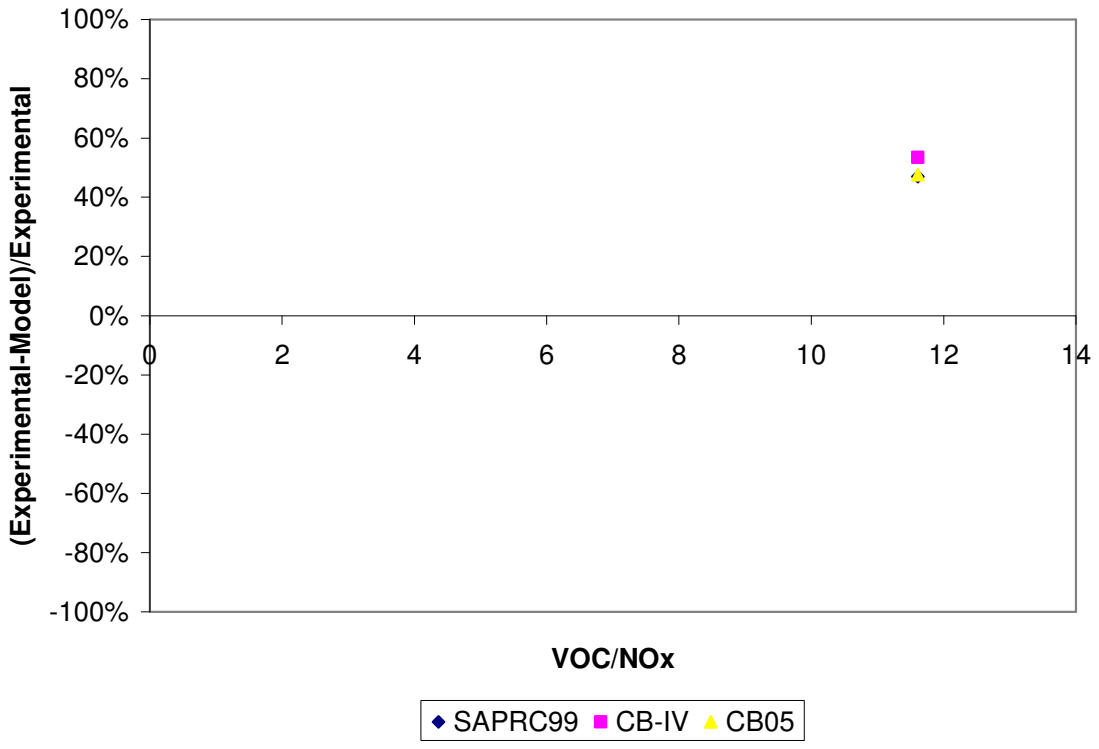

Figure 6-26. Model underprediction error for peak ozone in UNC chamber trimethylbenzenes experiments against VOC/NOx ratio.

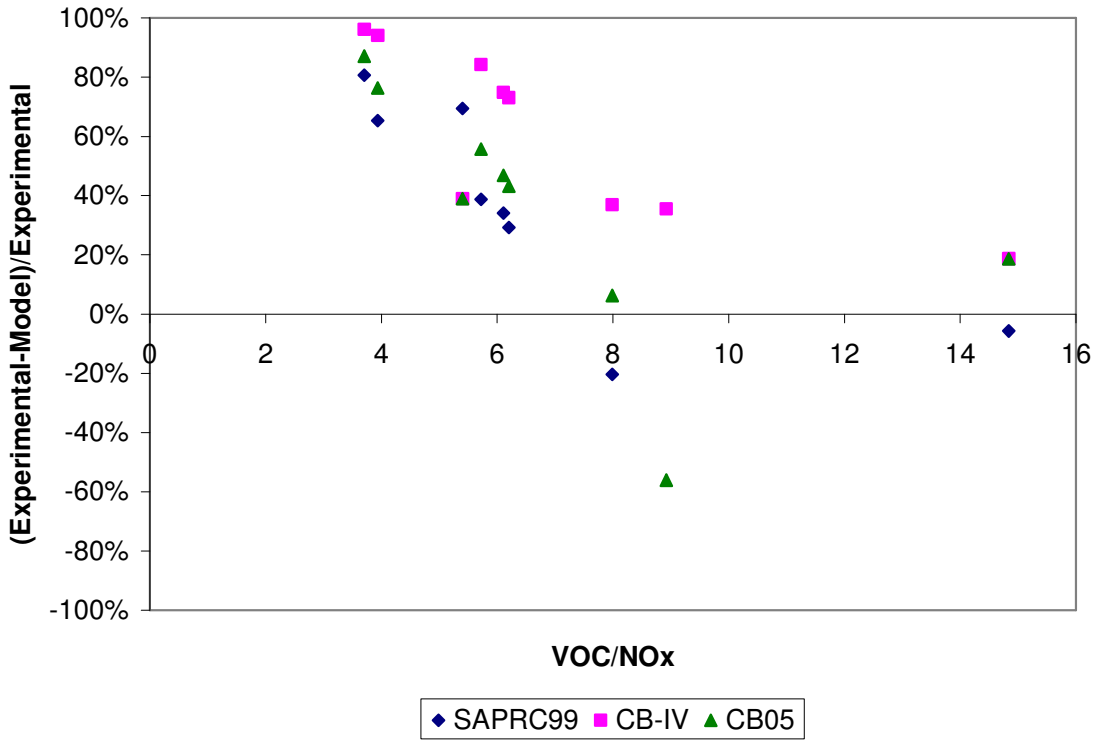

Figure 6-27. Model underprediction error for peak ozone in UCR chamber trimethylbenzenes experiments against VOC/NOx ratio.

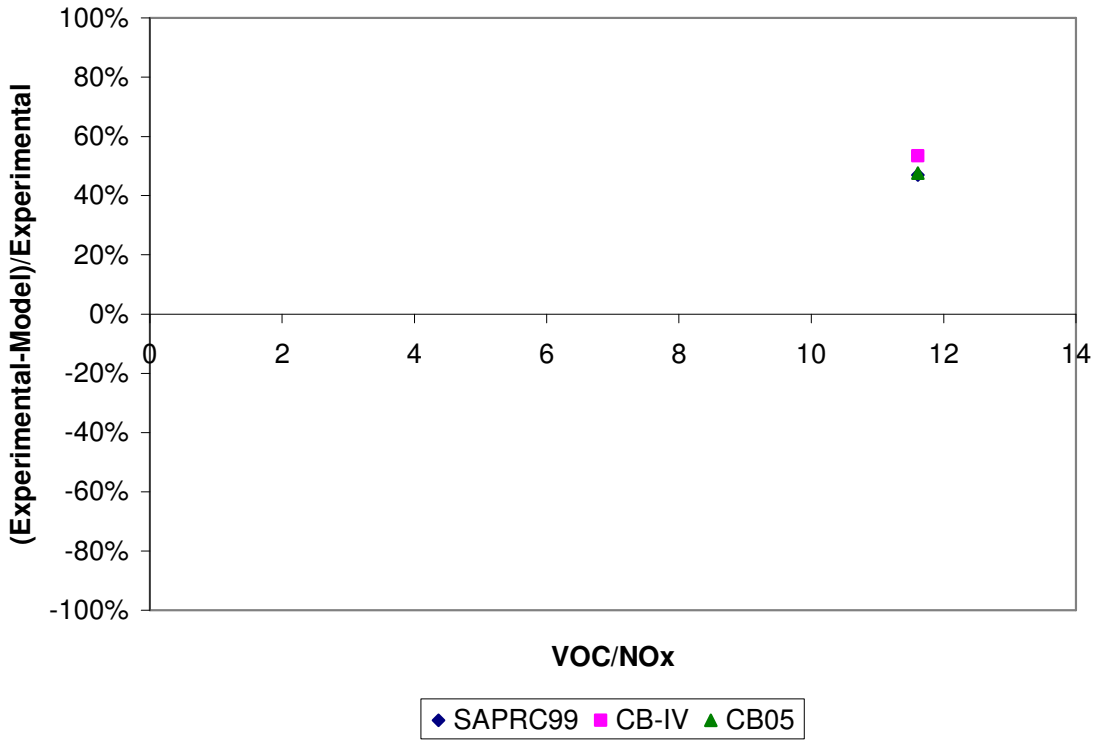

Figure 6-28. Model underprediction error for peak ozone in UNC chamber trimethylbenzenes experiments against (MIR*VOC)/NOx ratio.

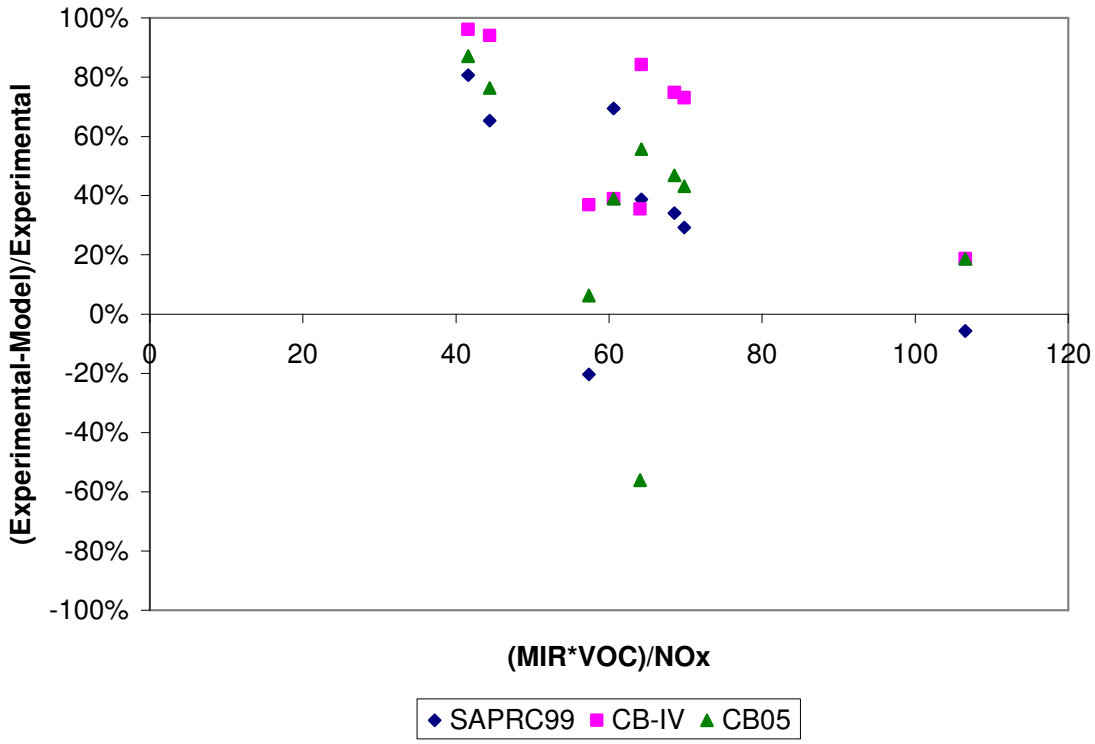

Figure 6-29. Model underprediction error for peak ozone in UCR chamber trimethylbenzenes experiments against (MIR*VOC)/NOx ratio.

6.4 Effect of the OH + NO_2 Rate Constant on Simulations of Aromatics Chemistry

In this section, the effect of the OH+NO_2 = HNO_3 rate parameter on predicted ozone concentrations in the SAPRC99 and CB-IV mechanisms were investigated. Upon equating the OH+NO_2 rate constant in SAPRC99 to the higher rate constant in CB-IV, and likewise the OH+NO_2 rate constant in CB-IV to the lower rate constant in SAPRC99, the difference in predicted ozone concentrations between the mechanisms converged, for simulations involving CO and no hydrocarbons. Therefore, in accordance with the hierarchical approach of evaluating chemical mechanisms, additional simulations were conducted for the toluene experiments in which the OH+NO_2 rate constant in the

SAPRC99 mechanism was increased to equal the rate constant in the CB-IV mechanism. The SAPRC99 simulations modified as such is labeled "S99 with CB05 HNO_3" in the following tables and figures.

6.4.1 Effect of the OH+NO_2 rate constant in simulations of the UNC Chamber Experiments for aromatics

Figures 6-30 – 6–33 show the effect of equating the OH+NO_2 rate constant in SAPRC99 to that of CB-IV for toluene experiments at UNC. The higher radical termination rate in SAPRC99 lowers the predicted ozone peak in SAPRC99. In general, however, the large discrepancy between the SAPRC99 and CB mechanisms remains. Comparisons between measured and predicted ozone peaks with the modified OH+NO_2 rate for the UNC chamber are made in Section 6.4.3.

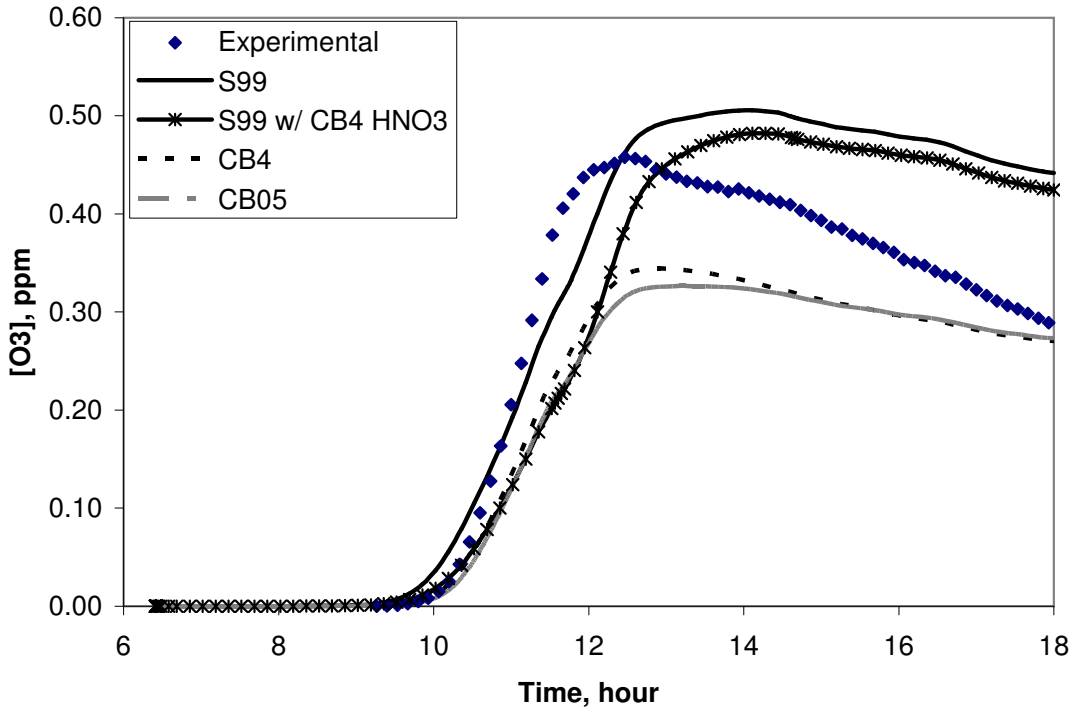

Figure 6-30. AU0183 UNC red chamber experiment with 4.59 ppmC toluene; increased OH+NO_2 rate constant in SAPRC99 to that of CB-IV.

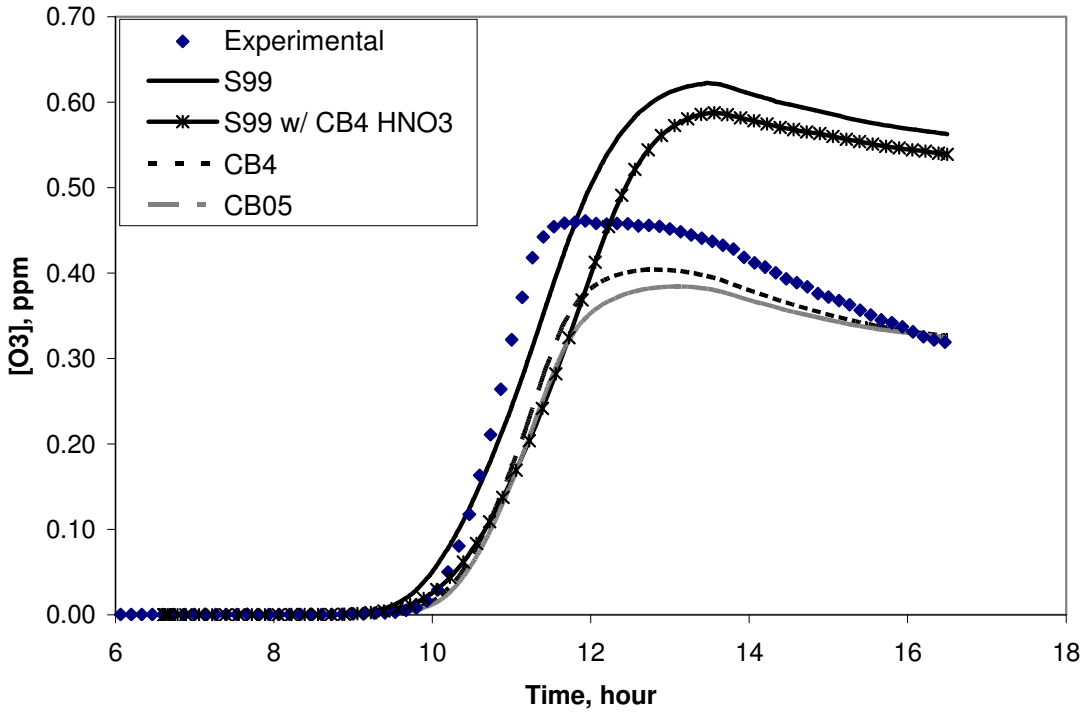

Figure 6-31. AU1788 UNC red chamber experiment with 4.93 ppmC toluene; increased OH+NO_2 rate constant in SAPRC99 to that of CB-IV.

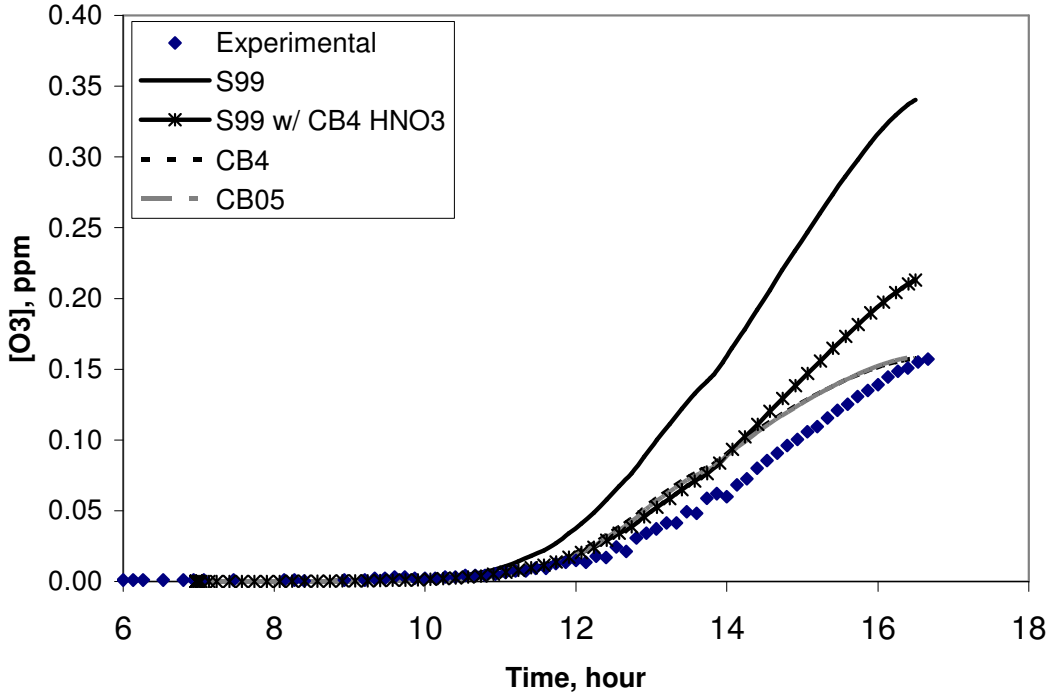

Figure 6-32 ST1393 UNC blue chamber experiment with 01.909 ppmC toluene; increased OH+NO_2 rate constant in SAPRC99 to that of CB-IV.

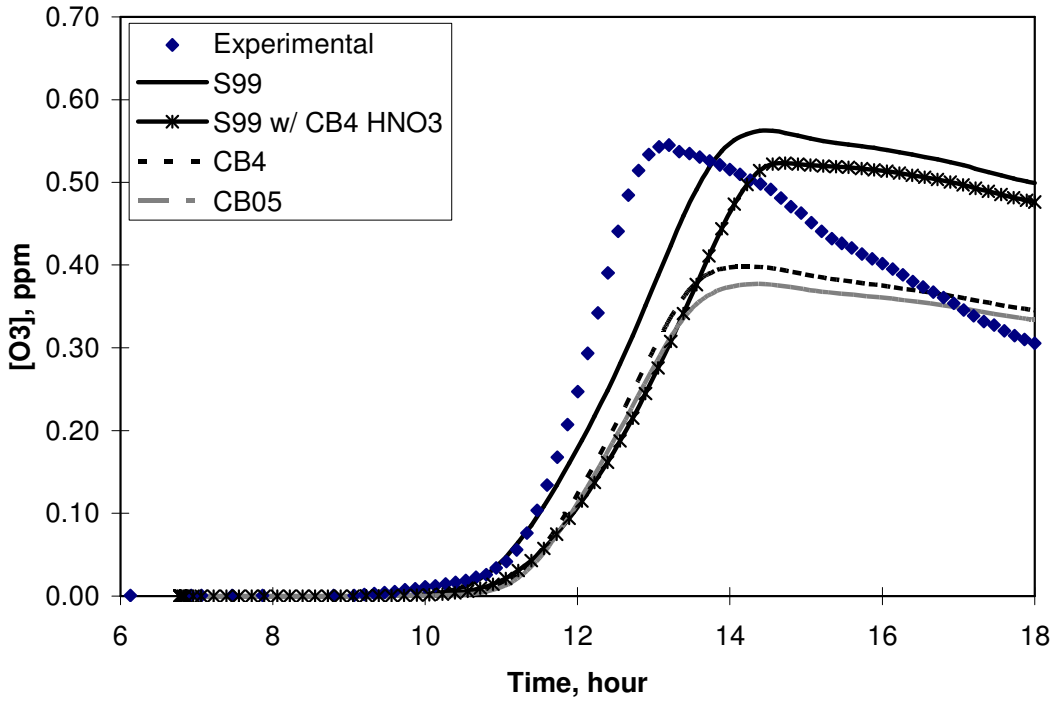

Figure 6-33. AU3095 UNC blue chamber experiment with 7.21 ppmC toluene; increased $OH+NO_2$ rate constant in SAPRC99 to that of CB-IV.

6.4.2 Effect of the $OH+NO_2$ rate constant in simulations of the UCR Chamber Experiments for aromatics

Comparing Figure 6-34 to Figure 6-12, in the UCR toluene experiments, the predicted ozone concentrations in SAPRC99 with a higher $OH+NO_2$ rate (Figure 6-34) is lower than the predicted ozone in basecase SAPRC99 (Figure 6-12). Comparisons between measured and predicted ozone peaks with the modified $OH+NO_2$ rate for the UCR chambers are made in Section 6.4.3.

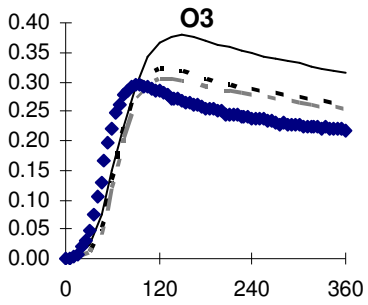

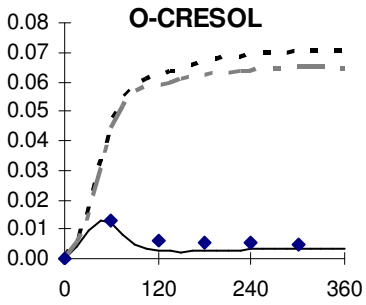

(a) EC271

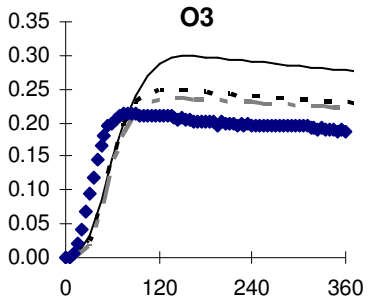

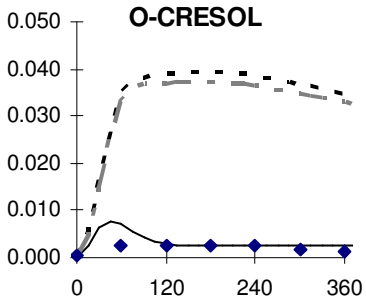

(b) EC273

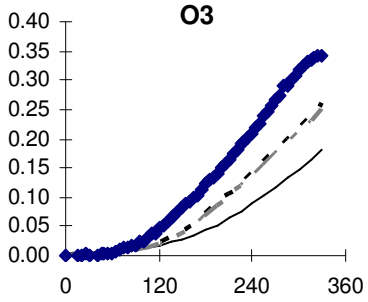

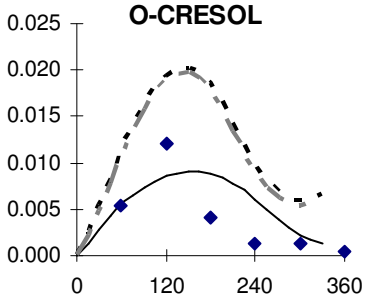

(c) EC340

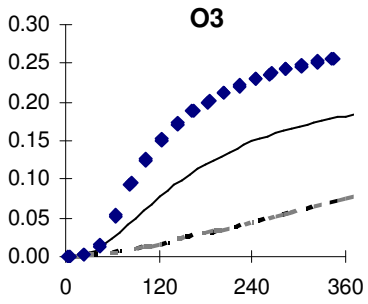

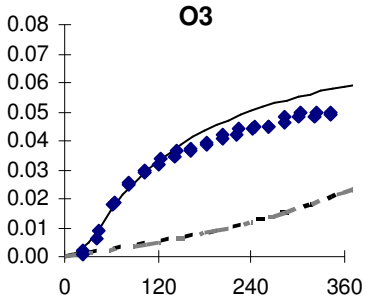

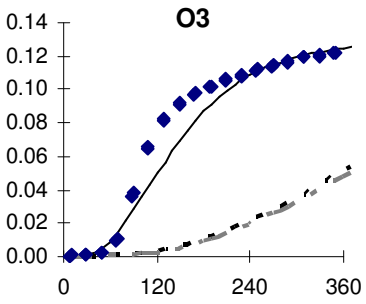

(d) EPA074B (e) EPA066B (f) EPA074A

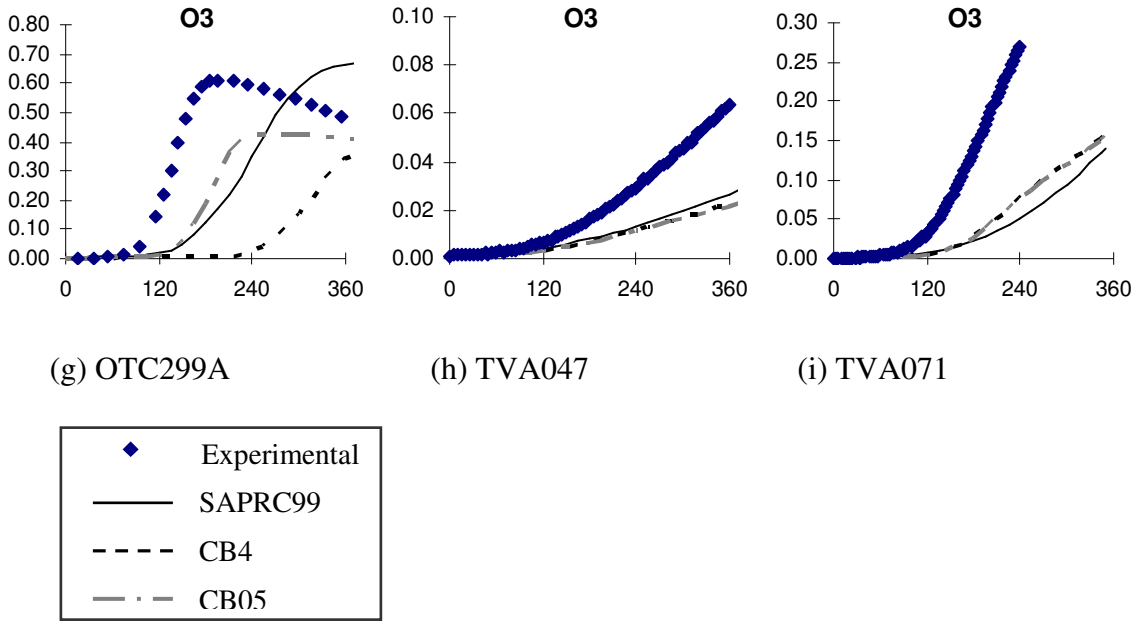

(g) OTC299A (h) TVA047 (i) TVA071

Figure 6-34. Concentrations of species in ppm as a function of time (minutes) in the toluene experiment at UCR; increased OH+NO_2 rate constant in SAPRC99 to that of CB-IV.

6.4.3 Comparison between Simulations with Modified OH+NO_2 rate constant and UNC and UCR Chamber data for aromatics

As shown in Table 6-14 and Figure 6-35, increasing the OH+NO_2 rate in SAPRC99 lowers the extent of overprediction of peak ozone relative to the basecase in the UNC chamber. In the UCR chambers, as shown in Table 6-15 and Figure 6-36, when basecase SAPRC99 shows an overprediction, this overprediction is lessened when the radical termination rate is increased relative to the basecase; when basecase SAPRC99 shows an underestimation, the extent of underestimation by SAPRC99 with the increased termination rate is heightened relative to the basecase SAPRC99.

Table 6-14. Comparison between the SAPRC99 and CB simulations and UNC chamber data for toluene.

	Experiment	AU0183 Red	AU1788 Red	ST1393 Blue	AU3095 Blue
	VOC (ppmC)	4.590	4.930	1.909	7.210
	NOx (ppm)	0.395	0.357	0.324	0.618
	VOC/NOx	11.620	13.810	5.892	11.667
Peak Ozone (ppm)	SAPRC99	0.506	0.622	0.340	0.562
	S99 w/ CB4 HNO_3	0.482	0.588	0.213	0.523
	CB-IV	0.344	0.404	0.158	0.398
	CB05	0.326	0.384	0.159	0.377
	Experiment	0.458	0.460	0.157	0.545
(Experimental-Model) /Experimental	SAPRC99	-10.48%	-35.34%	-116.28%	-3.08%
	S99 w/ CB4 HNO_3	-5.24%	-27.94%	-35.50%	4.07%
	CB-IV	24.89%	12.10%	-0.51%	27.00%
	CB05	28.82%	16.45%	-1.15%	30.85%
	MIR (g/g)	3.97	3.97	3.97	3.97
	MIR*VOC/NOx	46.1	54.8	23.4	46.3

Table 6-15. Comparison between the SAPRC99 and CB simulations and UCR chamber data toluene.

	Experiment	EC271	EC273	EC340	EPA074B	EPA066B	EPA074A	OTC299A	TVA047	TVA071
	VOC (ppmC)	8.020	4.110	3.760	1.100	0.426	1.054	8.530	0.520	2.480
	NOx (ppm)	0.215	0.112	0.493	0.027	0.005	0.024	0.509	0.105	0.266
	VOC/NOx	37.302	36.696	7.627	40.741	85.200	43.917	16.758	4.952	9.323
Peak Ozone (ppm)	SAPRC99	0.390	0.306	0.281	0.191	0.069	0.130	0.734	0.069	0.246
	S99 w/ CB4 HNO_3	0.378	0.298	0.183	0.184	0.067	0.126	0.671	0.045	0.140
	CB-IV	0.323	0.250	0.259	0.078	0.036	0.054	0.356	0.032	0.157
	CB05	0.306	0.237	0.250	0.078	0.035	0.051	0.426	0.031	0.154
	Experiment	0.294	0.214	0.343	0.261	0.058	0.124	0.611	0.094	0.270
(Experimental-Model) /Experimental	SAPRC99	-32.52%	-43.13%	18.01%	26.92%	-19.76%	-5.17%	-20.07%	26.50%	8.97%
	S99 w/ CB4 HNO3	-28.61%	-39.44%	46.79%	29.53%	-16.65%	-1.53%	-9.75%	52.24%	48.28%
	CB-IV	-9.80%	-16.92%	24.56%	70.13%	37.35%	56.22%	41.81%	66.35%	41.68%
	CB05	-4.05%	-10.51%	27.13%	70.24%	40.29%	59.05%	30.39%	66.56%	42.86%
	MIR (g/g)	3.97	3.97	3.97	3.97	3.97	3.97	3.97	3.97	3.97
	MIR*VOC/NOx	148.09	145.68	30.28	161.74	338.24	174.35	66.53	19.66	37.01

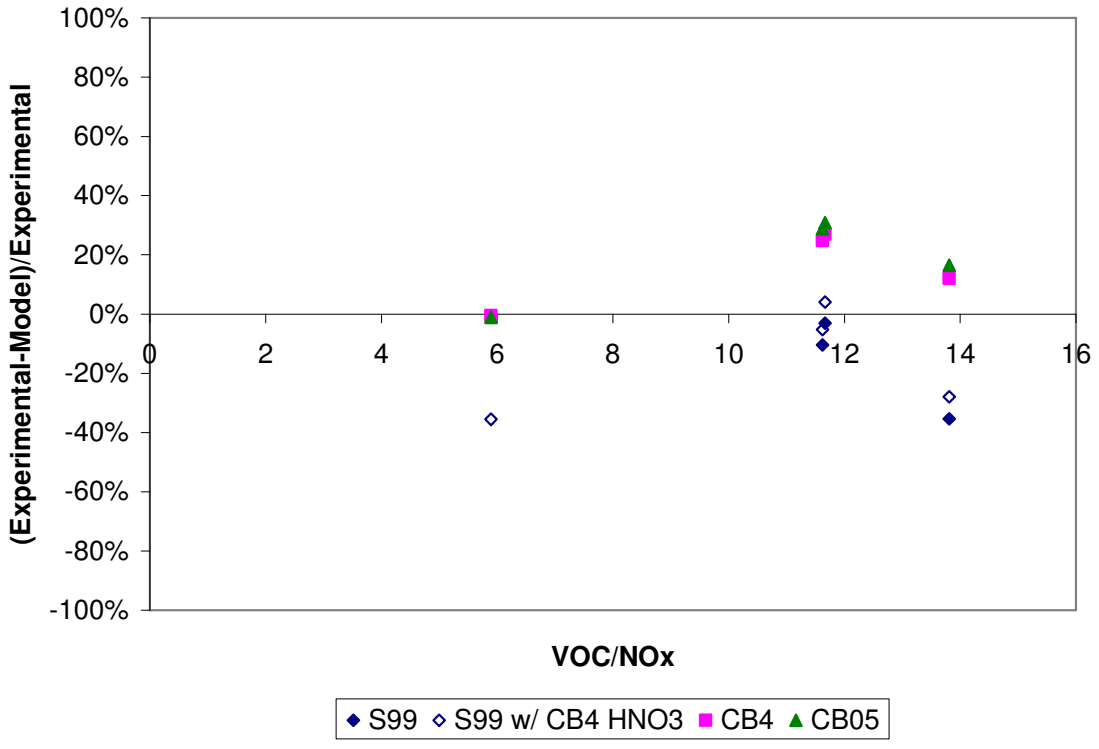

Figure 6-35. Model underprediction error for peak ozone in UNC chamber toluene experiments against VOC/NOx ratio.

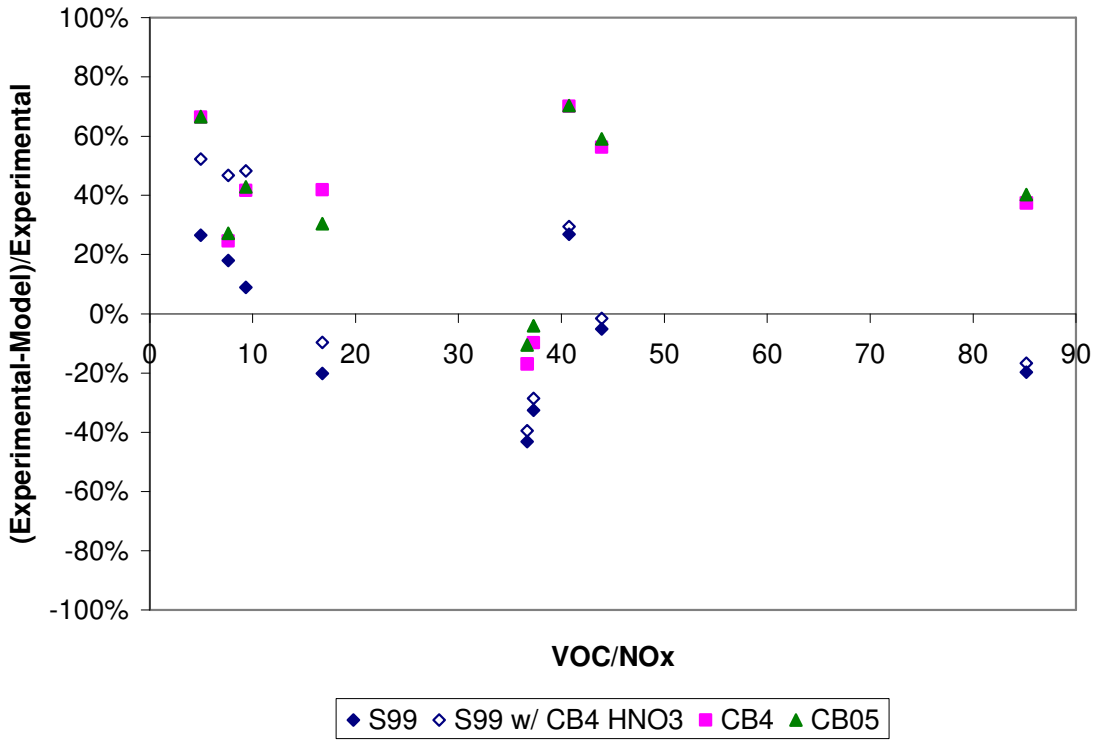

Figure 6-36. Model underprediction error for peak ozone in UCR chamber toluene experiments against VOC/NOx ratio.

6.5 Effect of the Cresol Yield in Simulations of Environmental Chamber Experiments for Aromatics

In CB-IV, toluene and other mono-substituted aromatics are represented as the lumped species TOL whereas in SAPRC99, toluene is lumped as ARO1. In SAPRC99, the species that are presumed to constitute ARO1 are specifically identified (Table 6-16), and the option of modeling the reactions of individual explicit hydrocarbons is available. Therefore, for further analysis of a toluene experiment, in particular the AU1788 chamber experiment with 4.93 ppmC toluene injection, the ARO1 + OH reaction in SAPRC99 was substituted with the explicit toluene + OH reaction as prescribed by Carter (2000) in the

explicit SAPRC99 mechanism. The toluene + OH reactions in CB-IV, CB05, fixed parameter SAPRC99, and explicit SAPRC99 are listed in Table 6-17. The effect of using the explicit toluene chemistry in SAPRC99 in simulations of UNC and UCR chamber experiments is illustrated in Sections 6.5.1 and 6.5.2, respectively.

Table 6-16. Compounds used to derive mechanisms for lumped parameter aromatics groups in fixed parameter SAPRC99 (Carter, 2000).

ARO1	Contribution	**ARO2**	Contribution
Toluene	70%	m-Xylene	22%
n-Propyl Benzene	10%	p-Xylene	22%
Ethyl Benzene	10%	o-Xylene	20%
Benzene	7%	1,3,5-Trimethyl Benzene	14%
s-Butyl Benzene	2%	1,2,3-Trimethyl Benzene	14%
Isopropyl Benzene	1%	1,2,4-Trimethyl Benzene	9%

Table 6-17. Reactions of toluene + OH in CB-IV in CAMx, CB05, and SAPRC99 in CAMx.

CB-IV
R[I63] = TOL + OH ----> 0.44*HO2 + 0.08*XO2 + 0.36*CRES + 0.56*TO2 @ 2.102E-12*EXP(322.0/TK);
CB05
R[I128] = TOL + OH ----> 0.44*HO2 + 0.08*XO2 + 0.36*CRES + 0.56*TO2 @ 1.8E-12*EXP(355./TK);
Fixed parameter SAPRC99
R[I202]= ARO1 + OH ----> 0.224* HO2 + 0.765*RO2R + 0.011*RO2N + 0.055*PROD + 0.118* GLY + 0.119*MGLY + 0.017*PHEN + 0.207*CRES + 0.059*BALD + 0.491*DCB1 + 0.108*DCB2 + 0.051*DCB3 @1.8105e-12*EXP(354.77/TK);
Explicit SAPRC99 (Carter, 2000)
R[I202]= TOL + OH ----> 0.234* HO2 + 0.758*RO2R + 0.008*RO2N + 0.116* GLY + 0.135*MGLY + 0.234*CRES + 0.085*BALD + 0.460*DCB1 + 0.156*DCB2 + 0.057*DCB3 @1.8105e-12*EXP(354.77/TK);
Explicit SAPRC99, enhancing cresol yield.
R[I202]= TOL + OH ----> 0.360* HO2 + 0.633*RO2R + 0.0067*RO2N + 0.0969* GLY + 0.1128*MGLY + 0.360*CRES + 0.0710*BALD + 0.384*DCB1 + 0.1303*DCB2 + 0.0476*DCB3 @1.8105e-12*EXP(354.77/TK);

Previous analyses in CAMx (Chapter 3) have indicated that differences in the aromatics chemistry, particularly mono-substituted aromatics, can be explained in part by differences in the branching ratio of ring-opening to ring-retaining products when the hydroxyl radical attacks the aromatic ring. In testing this hypothesis within the context of chamber simulations, the cresol yield in the explicit toluene + OH reaction in SAPRC99 was increased to the cresol yield assumed in CB-IV and CB05. Specifically, the cresol yield in this reaction was increased from 0.234 to 0.36. Subsequently, the yields of the remaining products of the explicit toluene + OH reaction were re-normalized to account

for the increase in the cresol yield. The net effect of this change is to yield more of the ring-retaining products and less of the more reactive ring-opening products. Table 6-17 illustrates this procedure for an explicit toluene + OH reaction derived by Dechapanya (2000).

Table 6-18. Explicit toluene + OH chemistry in SAPRC99 as derived by Dechapanya (2002).

Products	Original Yield	Percent Increase/Decrease	Modified Yield
CRES+HO_2	23.4%	12.6%	36.0%
BALD+RO_2R	11.0%	-1.8%	9.2%
NBEN+H_2O-NO_2 + XC	25.0%	-4.1%	20.9%
APTO1+RO_2R+GLY	23.8%	-3.9%	19.9%
APTO2+MGLY+RO_2R	16.7%	-2.8%	13.9%
Total Yield	100%	-	100%

The yields of the products of the explicit toluene + OH reaction prescribed by Carter (2000) in SAPRC99 and used in the CAMx version of the mechanism are provided in Table 6-19. The ratio of the renormalized yield to the original yield of the products in the explicit toluene + OH reaction proposed by Dechapanya (2002), except CRES and HO_2, (Table 6-18) was determined to be 0.835. The original yields of the products of the toluene + OH reaction prescribed by Carter (2000) were multiplied by this factor, except for the CRES and HO_2, to derive the re-normalized yields. As indicated in Table 6-19, the yield of the CRES and HO_2 products in the explicit toluene + OH chemistry in Carter (2000) was increased to 36% and the yield of the remaining products were renormalized using the renormalization factor of 0.835.

Table 6-19. Net explicit toluene + OH chemistry.

SAPRC99 in CAMx		
Products	Original Yield	Modified Yield
CRES	23.4%	36.0%
HO_2	23.4%	36.0%
BALD	8.50%	7.10%
RO_2-R	75.8%	63.3%
GLY	11.60%	9.69%
MGLY	13.50%	11.28%
DCB1	46.0%	38.4%
DCB2	15.60%	13.03%
DCB3	5.70%	4.76%
RO_2-N	0.800%	0.670%

6.5.1 Effect of the cresol yield in simulations of the UNC chamber experiments for aromatics

The effect of using the explicit toluene chemistry and increasing the yield of cresol in the explicit toluene+OH reaction in SAPRC99 to that of the CB mechanisms in simulations of the UNC chamber experiments for toluene are shown in Figures 6-37 to 6-40. The scenarios added to the simulations of the basecase are as follows:

- SAPRC99 with explicit toluene chemistry, labeled “S99 explicit tol”.
- SAPRC99 with explicit toluene chemistry and increased cresol yield to that of CB mechanisms, labeled “S99 explicit tol; CB cres”.

With the exception of ST1393 UNC experiment, the explicit toluene chemistry in SAPRC99 slightly reduces the peak ozone concentrations predicted with SAPRC99 relative to basecase SAPRC99. In the ST1393 experiment, however, the explicit

representation of toluene in SAPRC99 increases the peak ozone. In all the UNC toluene experiments but ST1393, increasing the cresol yield in the SAPRC99 explicit toluene significantly reduces peak ozone relative to basecase SAPRC99. In the ST1393 experiment, peak ozone is also reduced with the higher cresol yield, but to a much lesser extent.

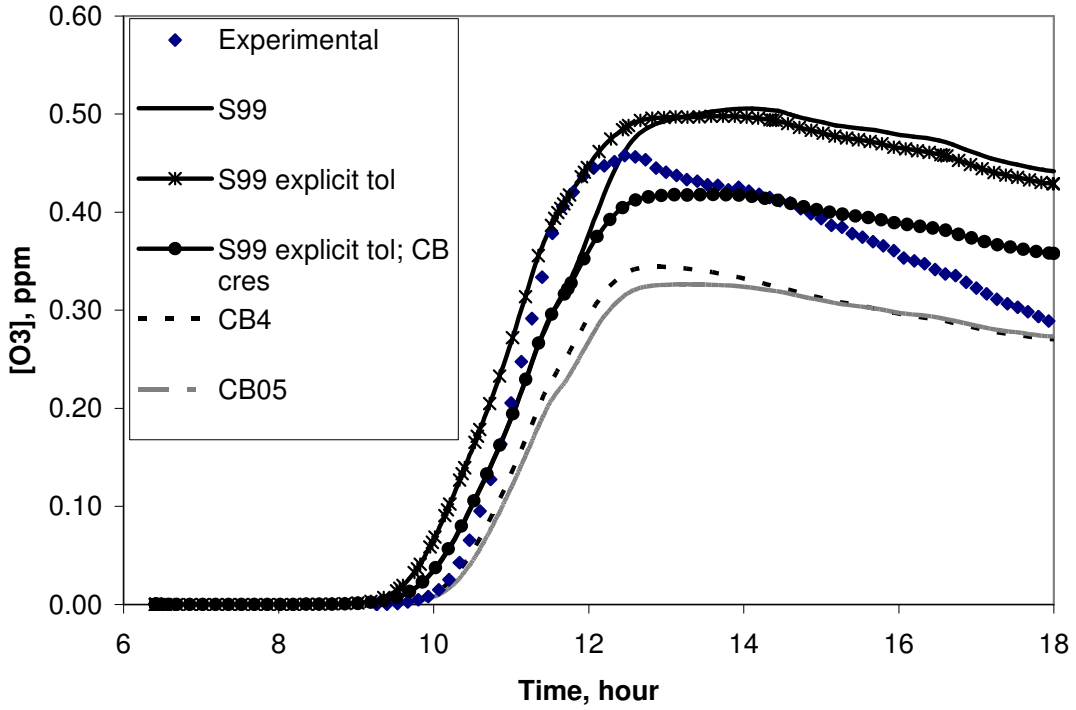

Figure 6-37. AU0183 UNC red chamber experiment with 4.59 ppmC toluene; explicit toluene chemistry in SAPRC99.

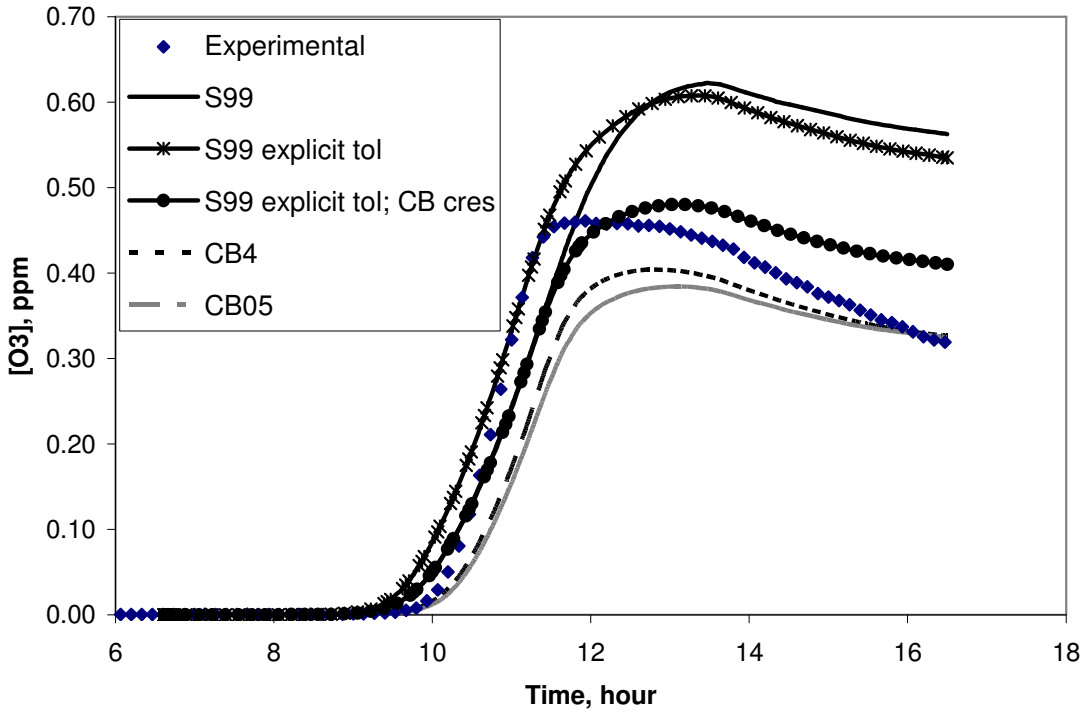

Figure 6-38. AU1788 UNC red chamber experiment with 4.93 ppmC toluene; explicit toluene chemistry in SAPRC99.

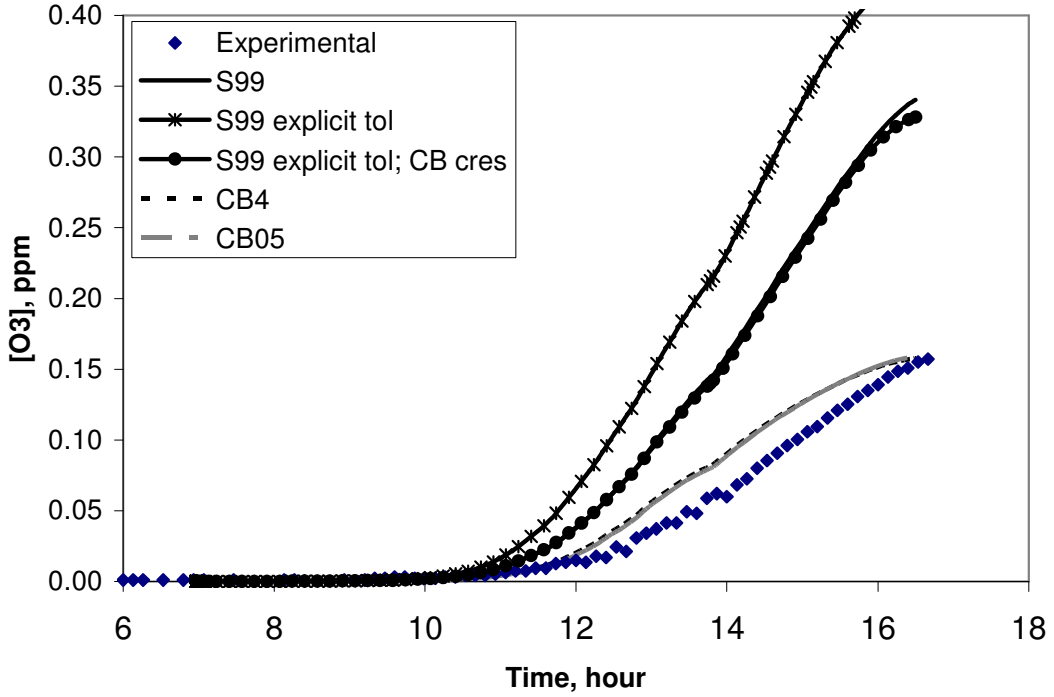

Figure 6-39. ST1393 UNC blue chamber experiment with 01.909 ppmC toluene; explicit toluene chemistry in SAPRC99.

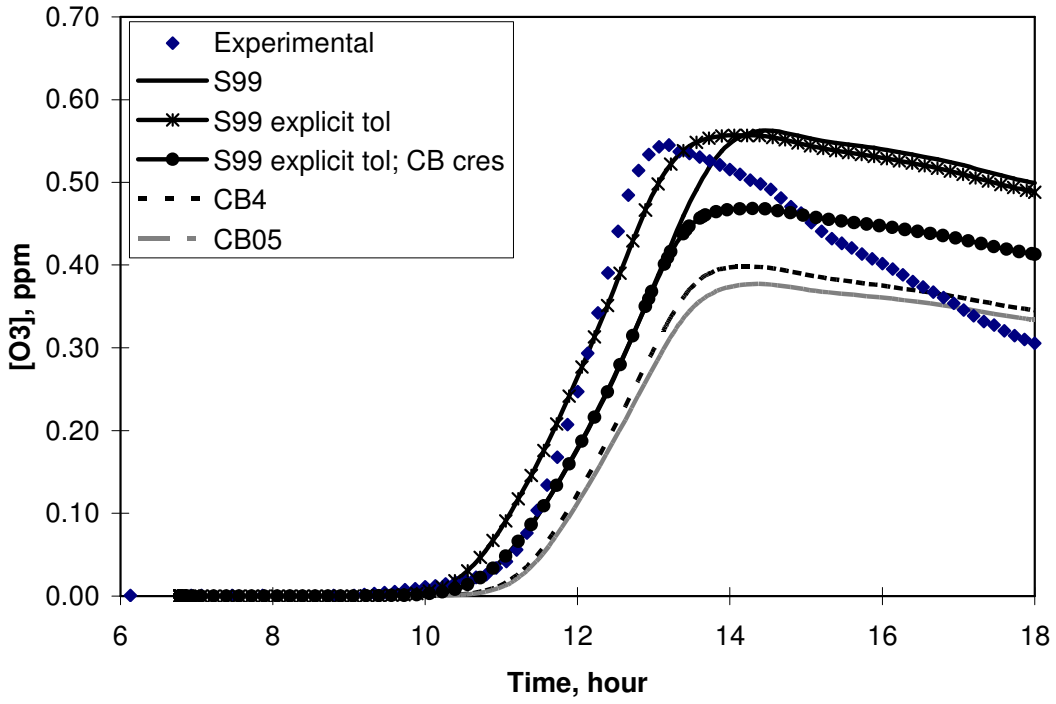

Figure 6-40. AU3095 UNC blue chamber experiment with 7.21 ppmC toluene; explicit toluene chemistry in SAPRC99.

6.5.2 Effect of the cresol yield in simulations of the UCR chamber experiments for aromatics

The effect of using the explicit toluene chemistry and increasing the yield of cresol in the explicit toluene+OH reaction in SAPRC99 to that of the CB mechanisms in simulations of the UCR chamber experiments for toluene are shown in Figures 6-41 and 6-42. Compared to the basecase scenario (Figure 6-12), the explicit toluene chemistry in SAPRC99 consistently increases the peak ozone concentrations in the UCR toluene experiments. A higher cresol yield in the explicit toluene chemistry of SAPRC99 (Figure 6-41) results in a lower peak ozone concentration relative to the basecase scenario (Figure 6-12).

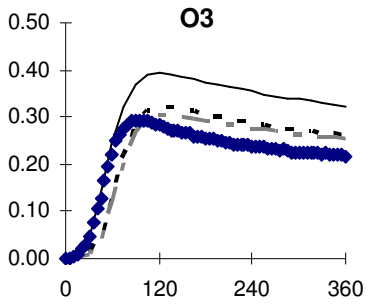

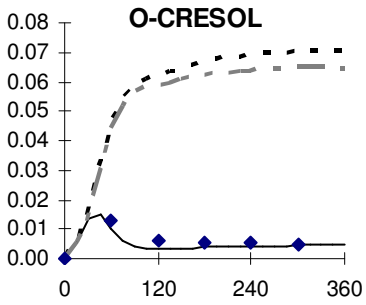

(a) EC271

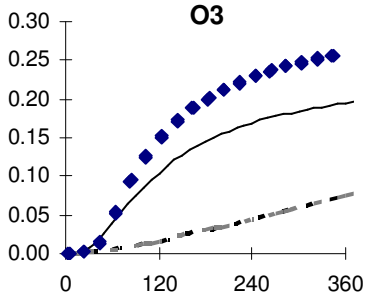

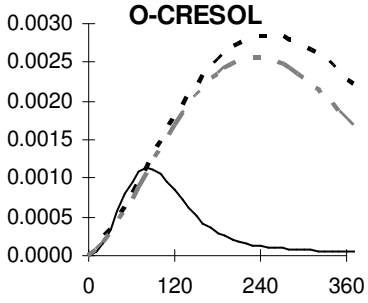

(b) EC273

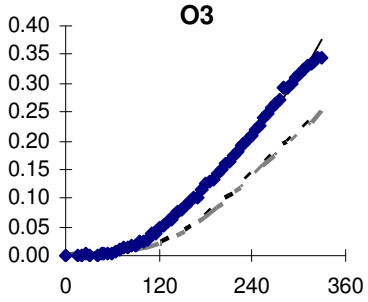

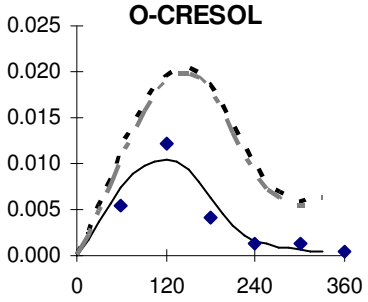

(c) EC340

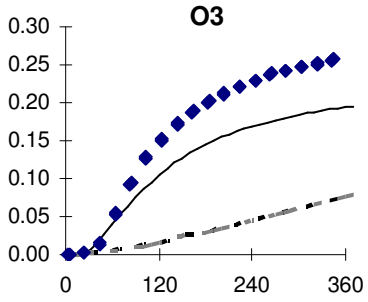

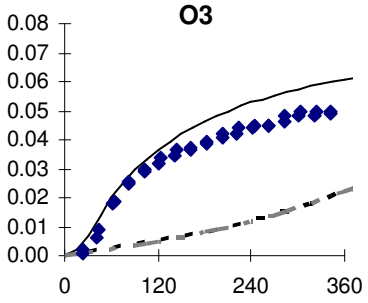

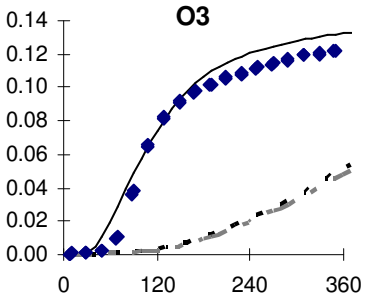

(d) EPA074B (e) EPA066B (f) EPA074A

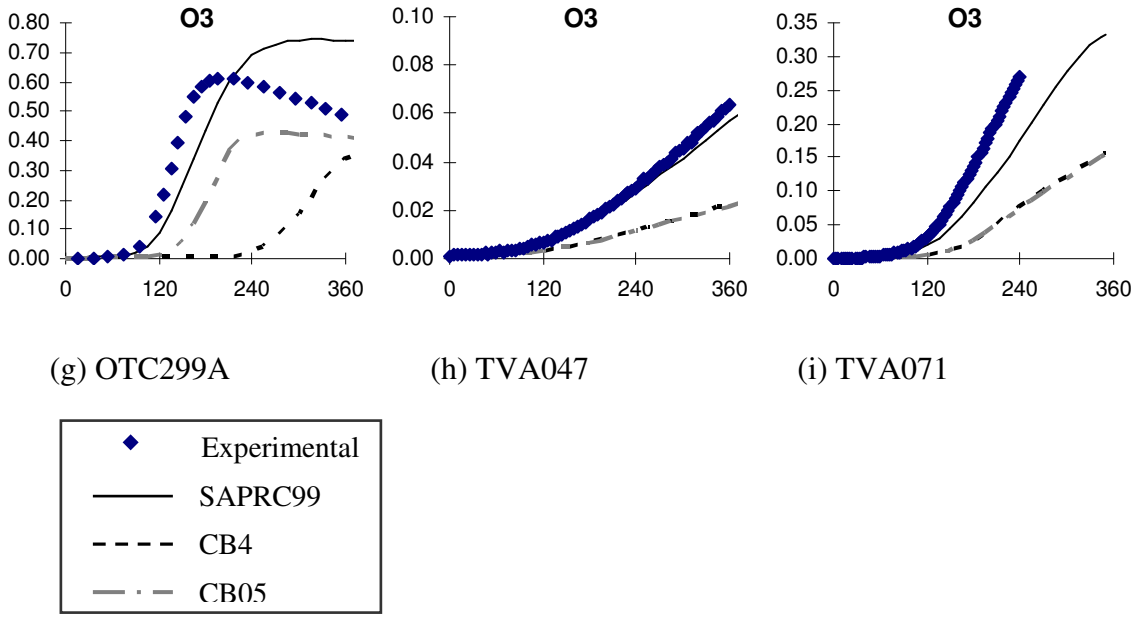

Figure 6-41. Concentrations of species in ppm as a function of time (minutes) in the toluene experiment at UCR; explicit toluene chemistry in SAPRC99.

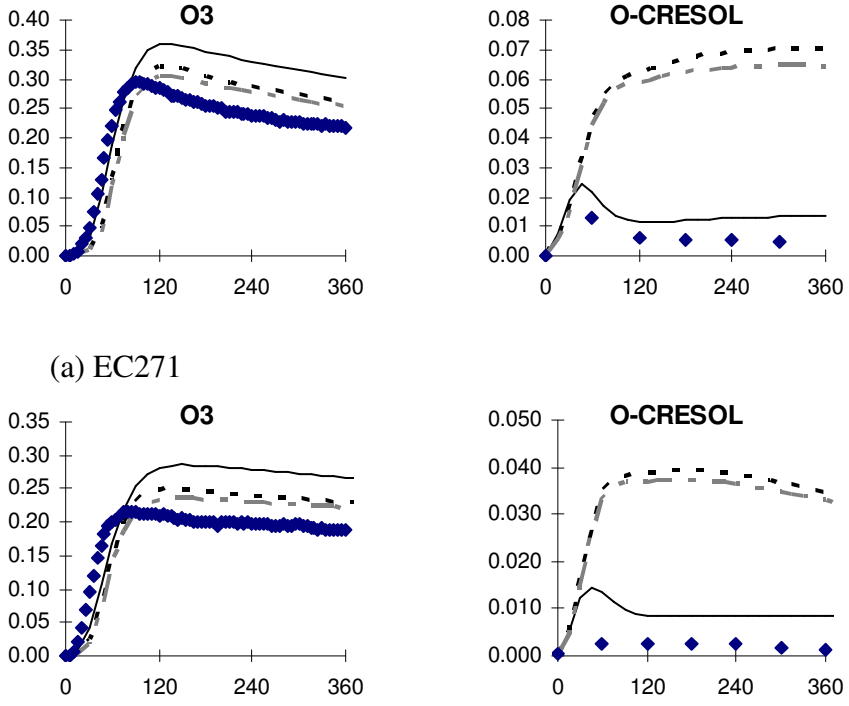

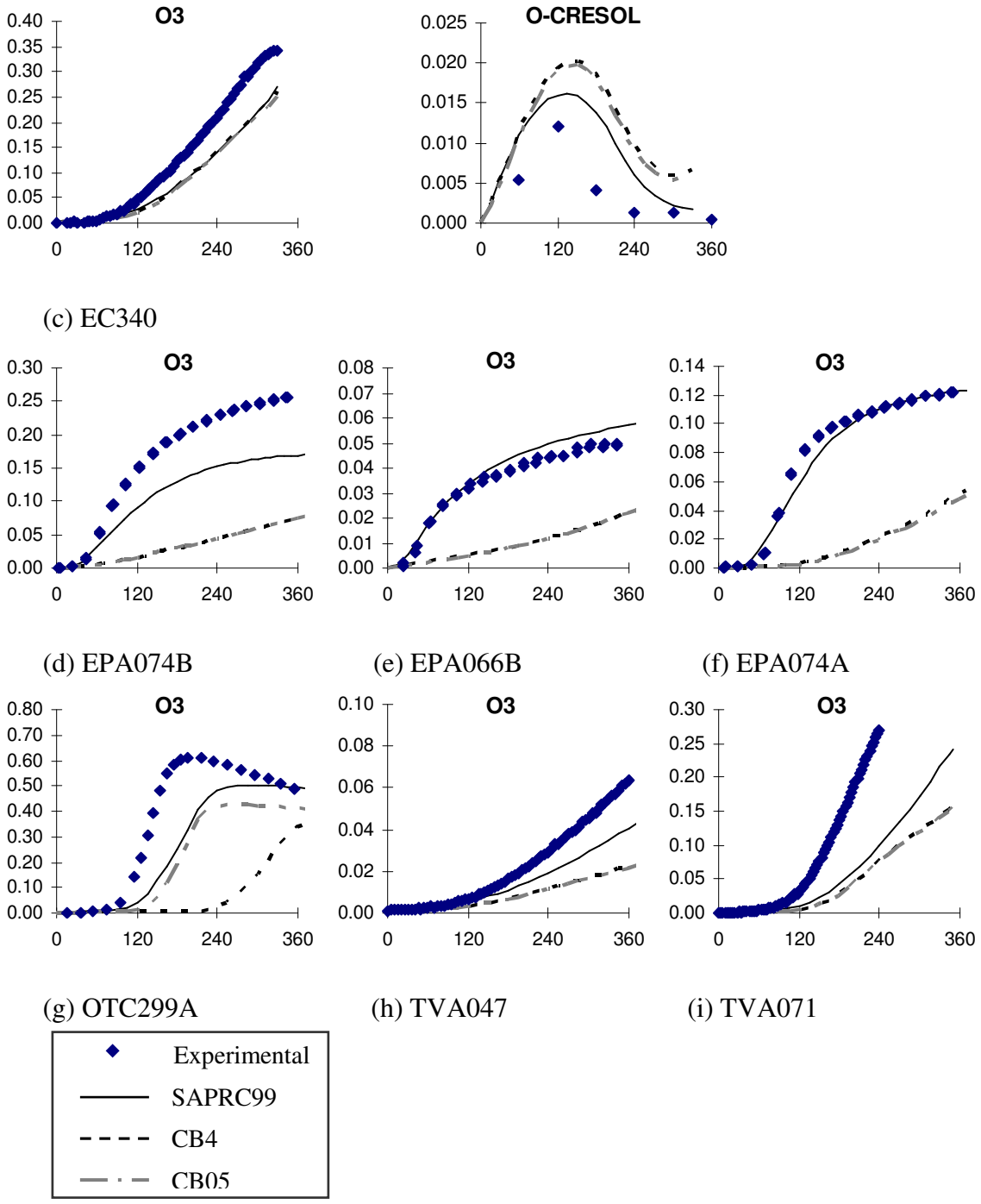

Figure 6-42 Concentrations of species in ppm as a function of time (minutes) in the toluene experiment at UCR; explicit toluene chemistry and increased cresol yield to that of CB in SAPRC99.

6.5.3 Comparison between simulations with modified cresol yield and UNC and UCR chamber data for aromatics

The relative bias of the SAPRC99 mechanism is reevaluated in the UNC and UCR chambers with addition of the SAPRC99 scenarios: explicit toluene chemistry and explicit toluene chemistry with increased cresol yield. In the UNC toluene experiments, Table 6-20, SAPRC99 generally shows less of an overprediction with the explicit toluene chemistry relative to basecase SAPRC99. With an increase in cresol yield, this affect is heightened, resulting in underpredictions with the SAPRC99 mechanism. In the UCR chambers (Table 6-21 and Figure 6-44), at very low VOC/NOx conditions, SAPRC99 with the explicit toluene mechanism shows a lower underprediction, tending towards an overprediction. At higher VOC/NOx conditions, the bias with SAPRC99 with explicit toluene is similar to the bias with basecase SAPRC99. When the cresol yield is increased in SAPRC99, in experiments where basecase SAPRC99 shows an underprediction, the simulation with the higher cresol yield leads to slightly more of an underprediction; in experiments where SAPRC99 basecase SAPRC99 shows an overprediction, the simulation with the higher cresol yields lead to slightly less of an overprediction.

Table 6-20. Comparison between the SAPRC99 and CB simulations and UNC chamber data for toluene; explicit toluene chemistry and increased cresol yield to that of CB in SAPRC99.

	Experiment	AU0183 Red	AU1788 Red	ST1393 Blue	AU3095 Blue
	VOC (ppmC)	4.590	4.930	1.909	7.210
	NOx (ppm)	0.395	0.357	0.324	0.618
	VOC/NOx	11.620	13.810	5.892	11.667
Peak Ozone (ppm)	SAPRC99	0.506	0.622	0.340	0.562
	S99 explicit toluene	0.498	0.608	0.428	0.557
	S99 explicit toluene w/ CB	0.418	0.480	0.328	0.468
	CB-IV	0.344	0.404	0.158	0.398
	CB05	0.326	0.384	0.159	0.377
	Experiment	0.458	0.460	0.157	0.545
(Experimental-Model) /Experimental	SAPRC99	-10.48%	-35.34%	-116.28%	-3.08%
	S99 explicit toluene	-8.73%	-32.29%	-172.26%	-2.16%
	S99 explicit toluene w/ CB	8.73%	-4.44%	-108.65%	14.16%
	CB-IV	24.89%	12.10%	-0.51%	27.00%
	CB05	28.82%	16.45%	-1.15%	30.85%
	MIR (g/g)	3.97	3.97	3.97	3.97
	MIR*VOC/NOx	46.1	54.8	23.4	46.3

Table 6-21. Comparison between the SAPRC99 and CB simulations and UCR chamber data toluene; explicit toluene chemistry and increased cresol yield to that of CB in SAPRC99.

	Experiment	EC271	EC273	EC340	EPA074B	EPA066B	EPA074A	OTC299A	TVA047	TVA071
	VOC (ppmC)	8.020	4.110	3.760	1.100	0.426	1.054	8.530	0.520	2.480
	NOx (ppm)	0.215	0.112	0.493	0.027	0.005	0.024	0.509	0.105	0.266
	VOC/NOx	37.302	36.696	7.627	40.741	85.200	43.917	16.758	4.952	9.323
Peak Ozone (ppm)	SAPRC99	0.390	0.306	0.281	0.191	0.069	0.130	0.734	0.069	0.246
	S99 explicit toluene	0.393	0.306	0.374	0.196	0.070	0.133	0.744	0.091	0.331
	S99 explicit toluene w/ CB	0.360	0.286	0.286	0.170	0.064	0.123	0.503	0.066	0.241
	CB-IV	0.323	0.250	0.259	0.078	0.036	0.054	0.356	0.032	0.157
	CB05	0.306	0.237	0.250	0.078	0.035	0.051	0.426	0.031	0.154
	Experiment	0.294	0.214	0.343	0.261	0.058	0.124	0.611	0.094	0.270
(Experimental-Model) /Experimental	SAPRC99	-32.52%	-43.13%	18.01%	26.92%	-19.76%	-5.17%	-20.07%	26.50%	8.97%
	S99 explicit toluene	-33.81%	-43.08%	-9.00%	25.09%	-20.28%	-7.51%	-21.66%	2.99%	-22.73%
	S99 explicit toluene w/ CB	-22.41%	-33.69%	16.55%	34.93%	-11.11%	0.40%	17.70%	29.38%	10.64%
	CB-IV	-9.80%	-16.92%	24.56%	70.13%	37.35%	56.22%	41.81%	66.35%	41.68%
	CB05	-4.05%	-10.51%	27.13%	70.24%	40.29%	59.05%	30.39%	66.56%	42.86%
	MIR (g/g)	3.97	3.97	3.97	3.97	3.97	3.97	3.97	3.97	3.97
	MIR*VOC/NOx	148.09	145.68	30.28	161.74	338.24	174.35	66.53	19.66	37.01

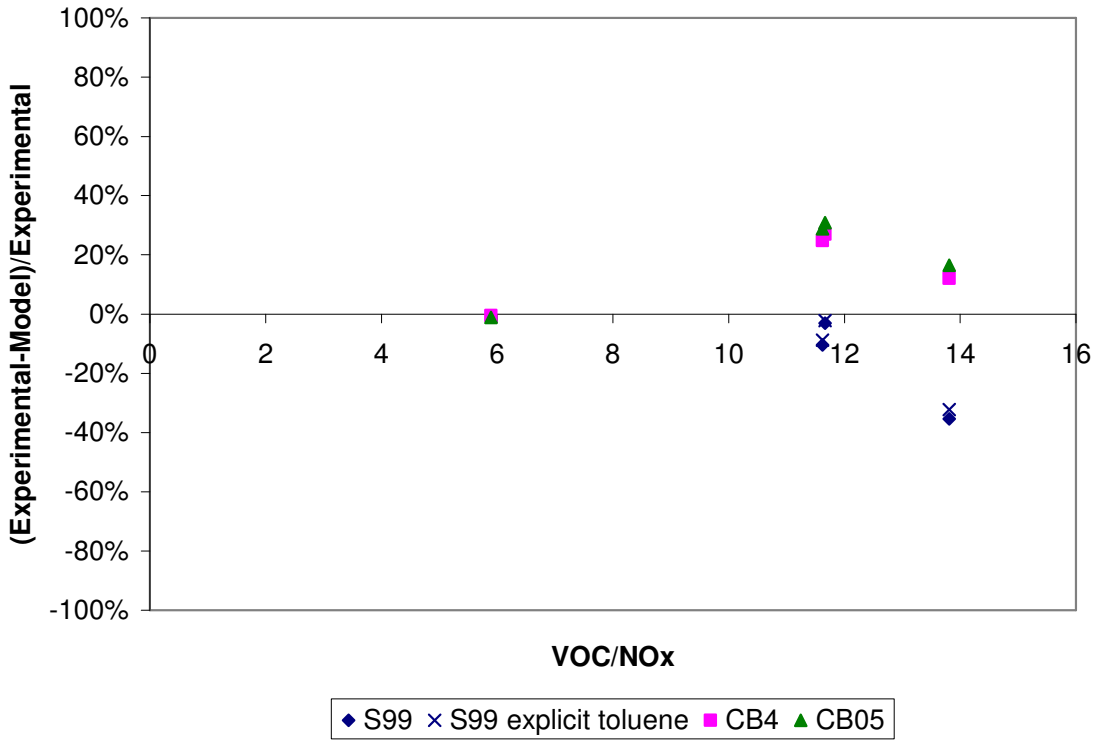
100%
80%
60%
40%
20%
0%
-20%
-40%
-60%
-80%
-100%
0
2
4
6
8
10
12
14
16
(Experimental-Model)/Experimental
VOC/NOx
S99
S99 explicit toluene
CB4
CB05

(a)

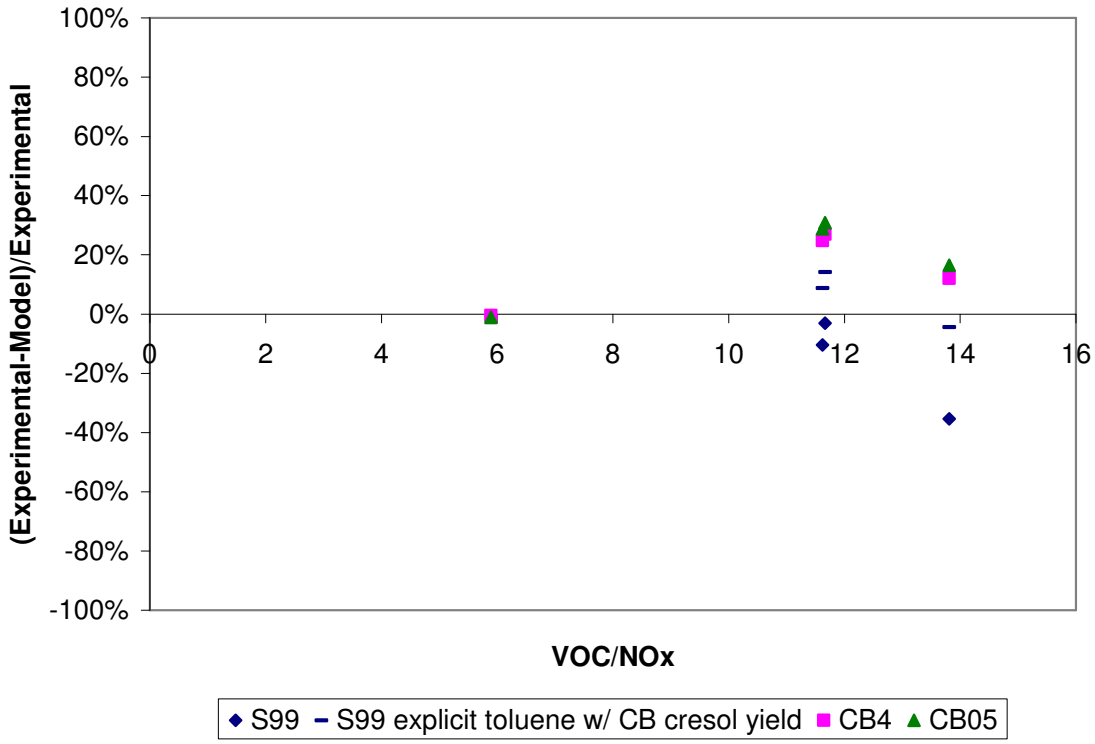

(b)

Figure 6-43. Model underprediction error for peak ozone in UNC chamber toluene experiments against VOC/NOx ratio; (a) explicit toluene chemistry in SAPRC99 and (b) increased cresol yield in explicit toluene chemistry to that of CB in SAPRC99.

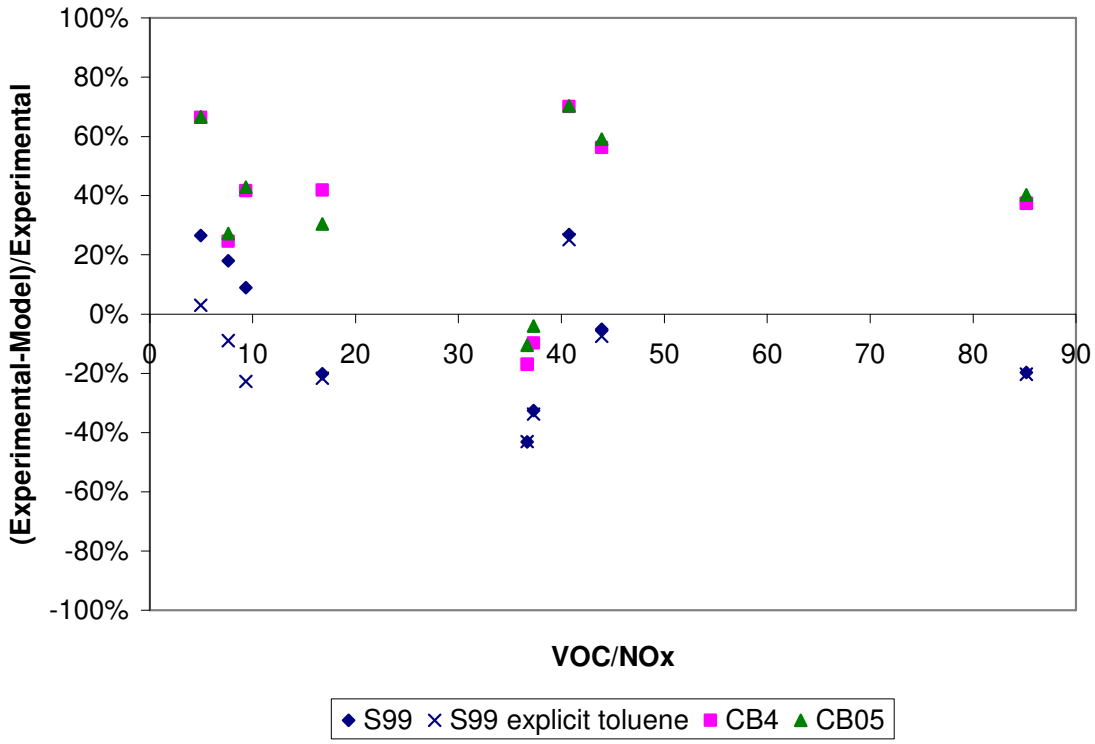
100%
80%
60%
40%
20%
0%
-20%
-40%
-60%
-80%
-100%
0
10
20
30
40
50
60
70
80
90
(Experimental-Model)/Experimental
VOC/NOx
S99
S99 explicit toluene
CB4
CB05

(a)

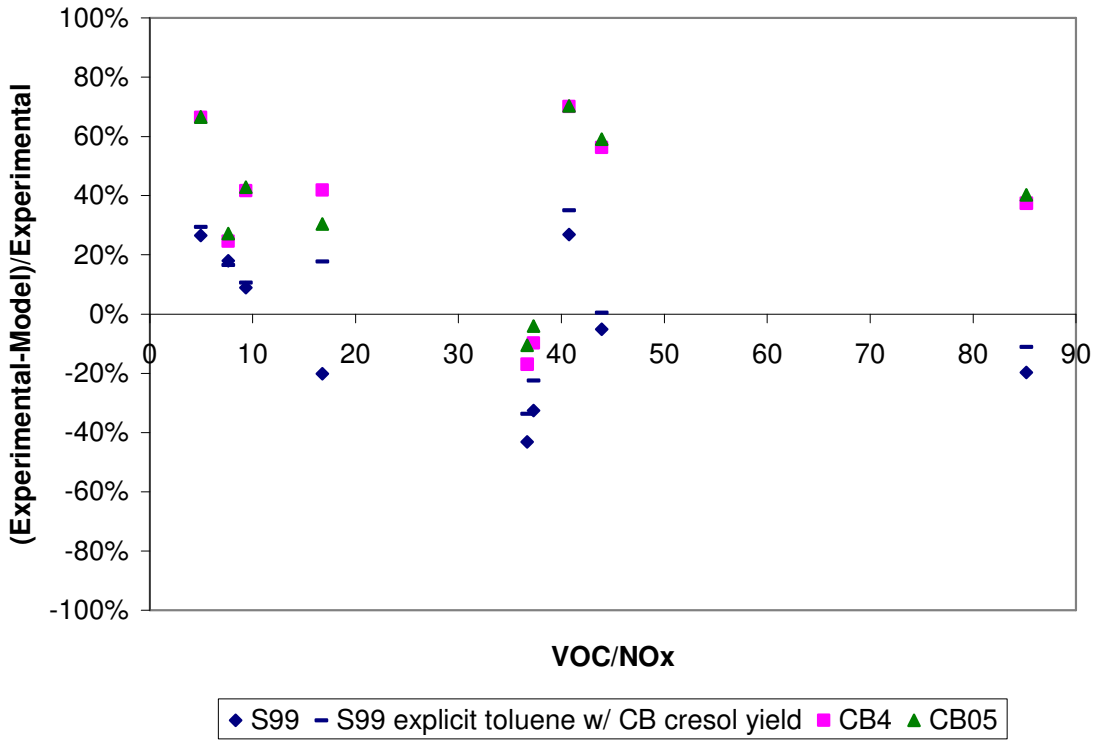

(b)

Figure 6-44. Model underprediction error for peak ozone in UCR chamber toluene experiments against VOC/NOx ratio; (a) explicit toluene chemistry in SAPRC99 and (b) increased cresol yield in explicit toluene chemistry to that of CB in SAPRC99.

6.6 COMBINED FFFECT OF THE $OH+NO_2$ RATE CONSTANT AND CRESOL YIELD IN SIMULATIONS OF ENVIRONMENTAL CHAMBER EXPERIMENTS FOR AROMATICS

A final sensitivity study for the chamber aromatics experiments involved assessing the combined effect of increasing the $OH+NO_2$ rate constant in SAPRC99 as well as increasing the cresol yield in the explicit toluene chemistry in SAPRC99. This simulation is denoted "S99 w/ CB4 HNO_3; explicit tol; CB cres" in the UNC chamber experiments below.

6.6.1 Combined effect of the OH+NO_2 rate constant and cresol yield in simulations of the UNC Chamber Experiments for aromatics

Figures 6-45 – 6–48 illustrate the combined effect of increasing the radical termination rate and the cresol yield from toluene + OH in SAPRC99 in the UNC toluene experiments. In the ST1393 experiment, this modification increased the peak ozone concentration simulated with SAPRC99 while in the other toluene experiments, it decreased the predicted peak ozone in SAPRC99 relative to the basecase.

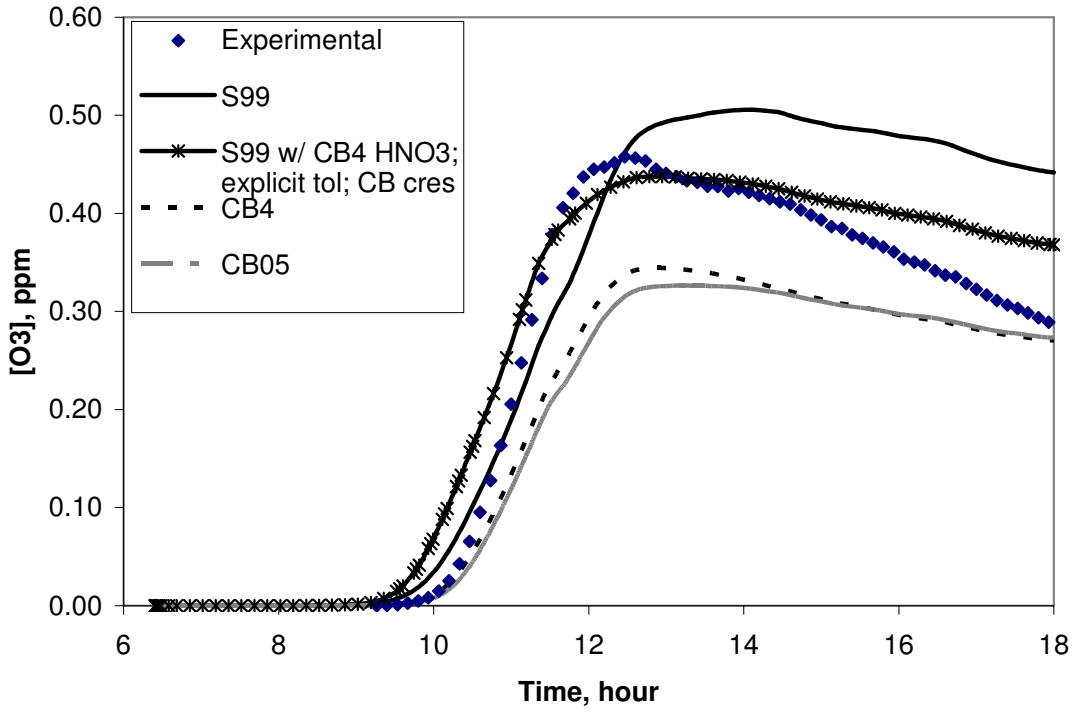

Figure 6-45. AU0183 UNC red chamber experiment with 4.59 ppmC toluene; OH+NO_2 rate in SAPRC99 increased to that of CB-IV and cresol yield in explicit toluene chemistry in SAPRC99 increased to that of CB.

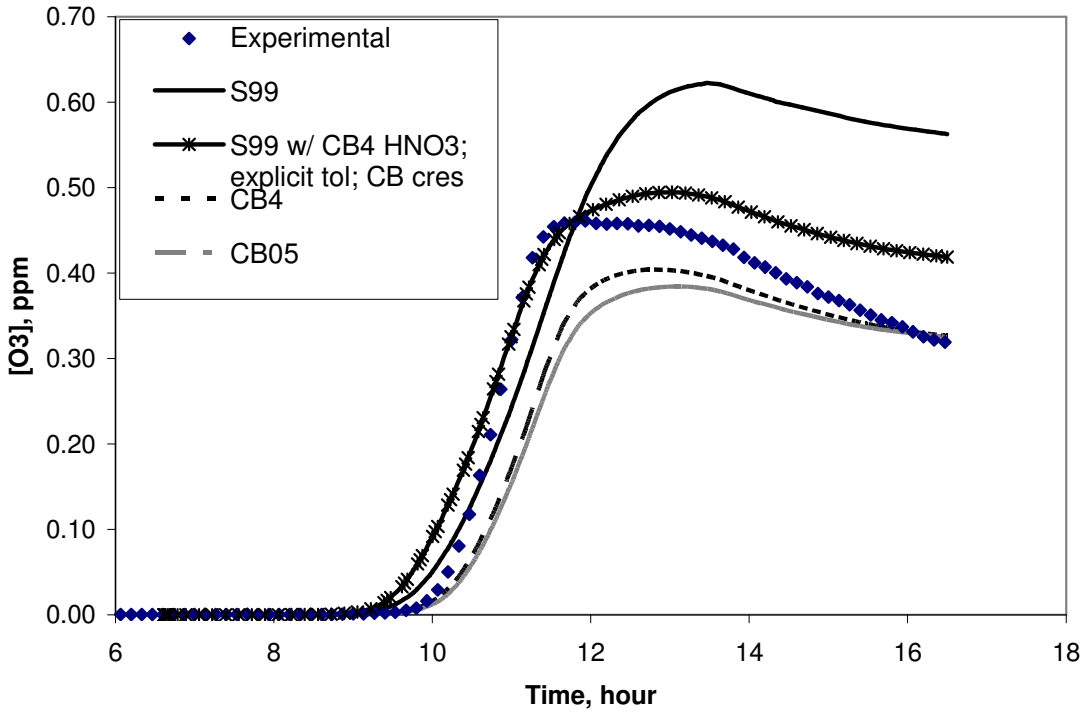

Figure 6-46. AU1788 UNC red chamber experiment with 4.93 ppmC toluene; OH+NO_2 rate in SAPRC99 increased to that of CB-IV and cresol yield in explicit toluene chemistry in SAPRC99 increased to that of CB.

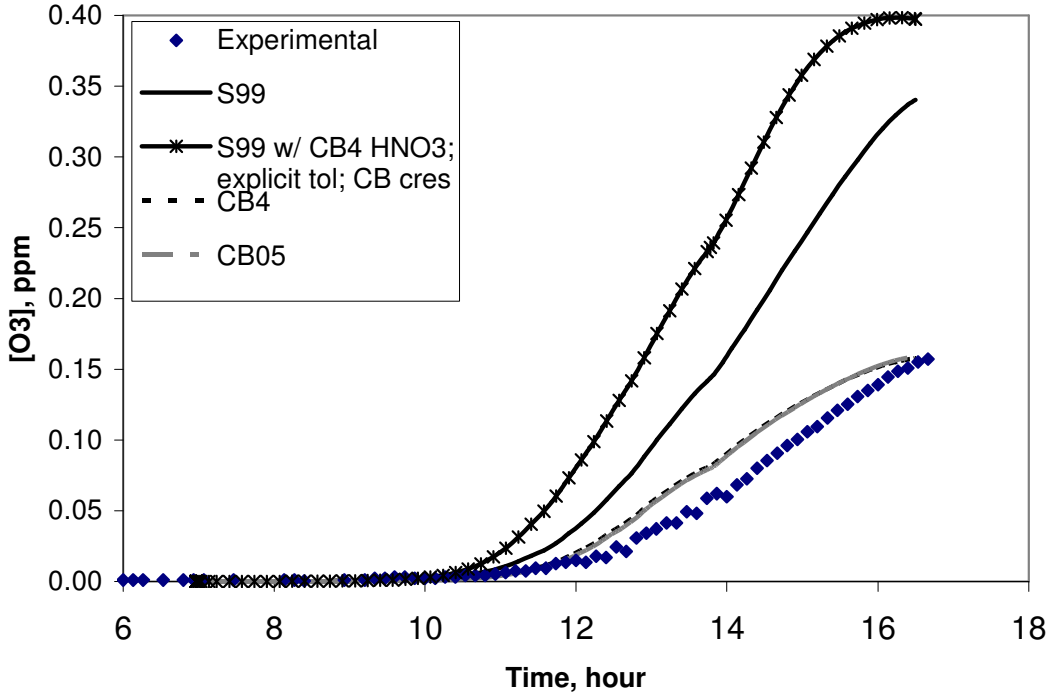

Figure 6-47 ST1393 UNC blue chamber experiment with 01.909 ppmC toluene; $OH+NO_2$ rate in SAPRC99 increased to that of CB-IV and cresol yield in explicit toluene chemistry in SAPRC99 increased to that of CB.

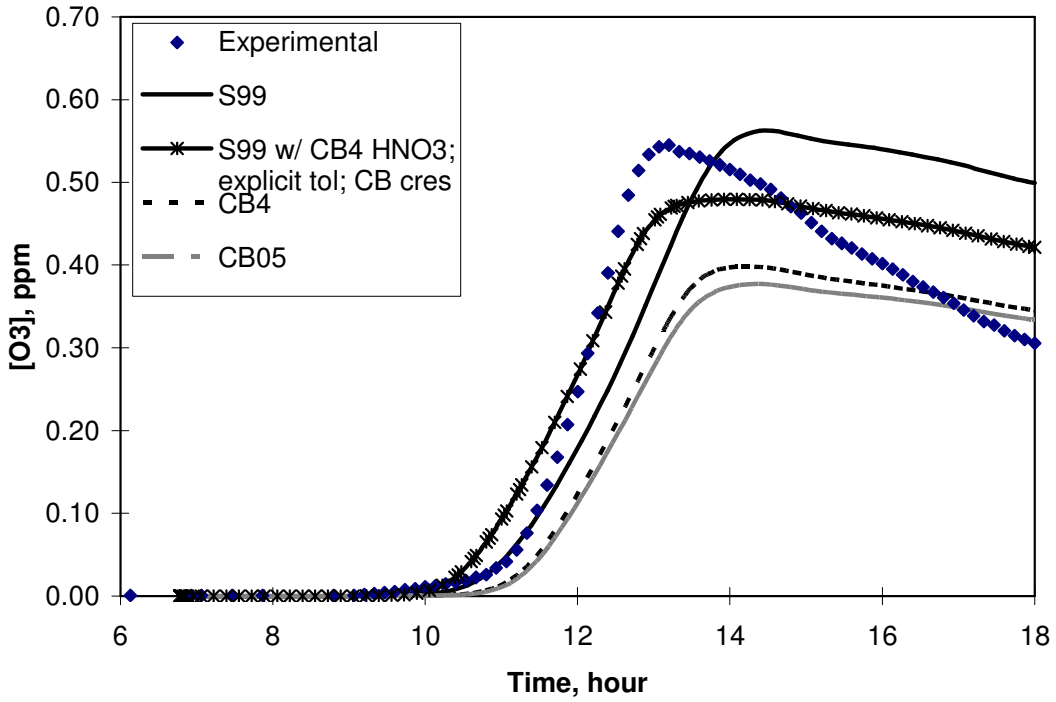

Figure 6-48. AU3095 UNC blue chamber experiment with 7.21 ppmC toluene; OH+NO_2 rate in SAPRC99 increased to that of CB-IV and cresol yield in explicit toluene chemistry in SAPRC99 increased to that of CB.

6.6.2 Combined effect of the OH+NO_2 rate constant and cresol yield in simulations of the UCR Chamber Experiments for aromatics

The combined effect of the radical termination rate and cresol yield from the toluene + OH reaction in SAPRC99 for the UCR chamber experiments is illustrated in Figure 6-49. Relative to basecase SAPRC99, Figure 6-12, the peak ozone predicted with the modified SAPRC99 is lower.

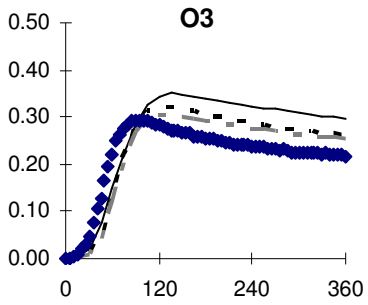

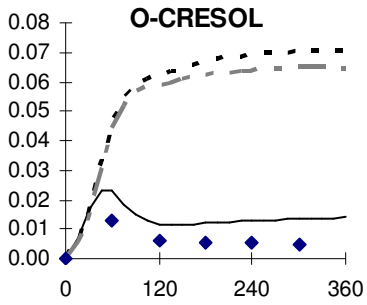

(a) EC271

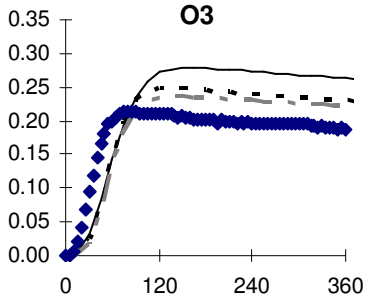

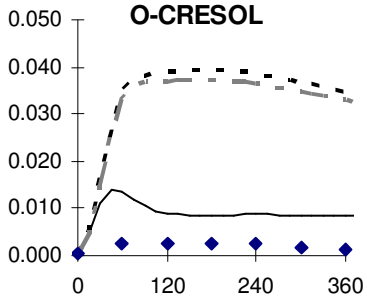

(b) EC273

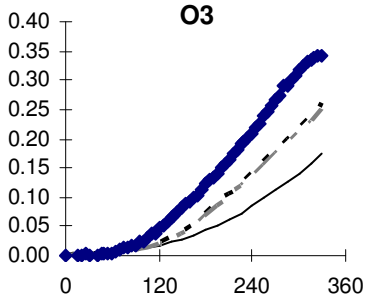

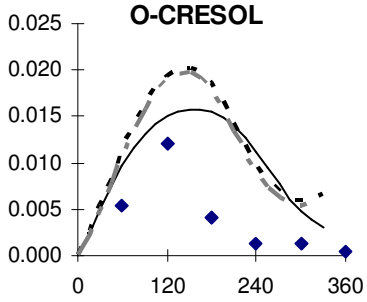

(c) EC340

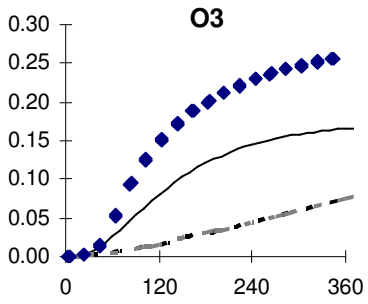

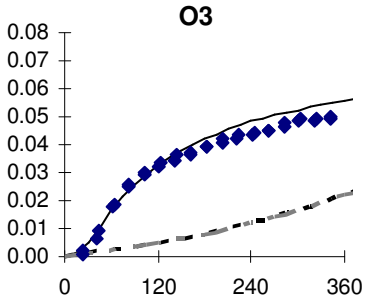

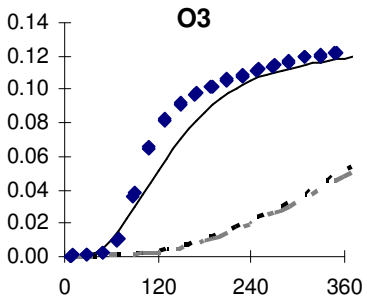

(d) EPA074B (e) EPA066B (f) EPA074A

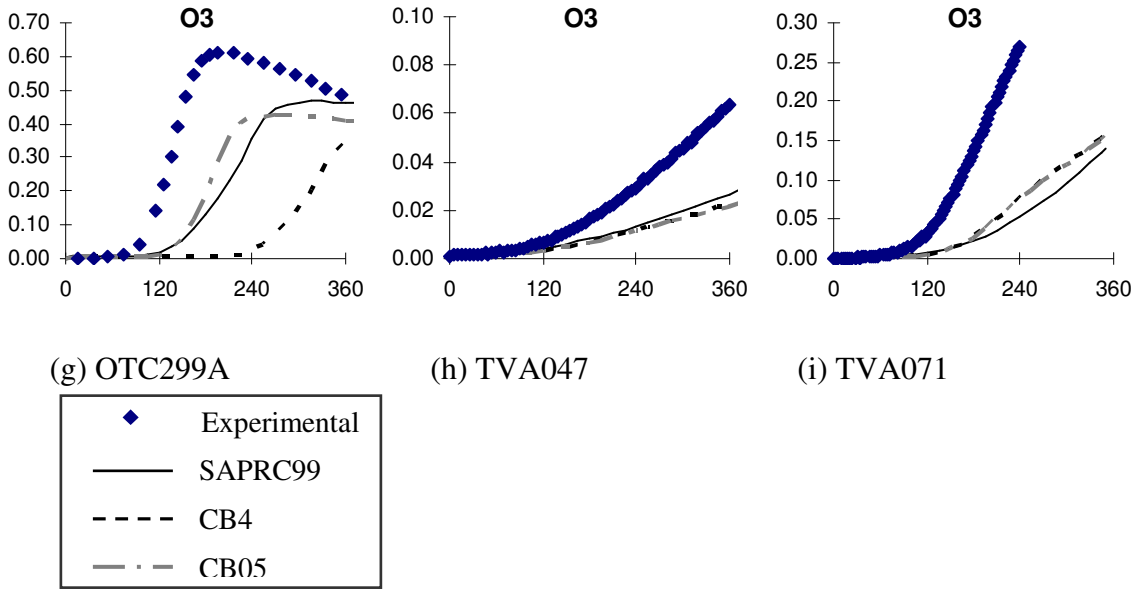

Figure 6-49. Concentrations of species in ppm as a function of time (minutes) in the toluene experiment at UCR; explicit toluene chemistry in SAPRC99; OH+NO_2 rate in SAPRC99 increased to that of CB-IV and cresol yield in explicit toluene chemistry in SAPRC99 increased to that of CB.

6.6.3 Comparison between simulations with modified OH+NO_2 rate constant and cresol yield and UNC and UCR Chamber data for aromatics

Table 6-22 and Figure 6-50 evaluate the bias with the modified SAPRC99 relative to the basecase SAPRC99 in the UNC chamber. Except for the ST1393 experiment, the combined modification to the SAPRC99 mechanism leads to less of an overprediction in SAPRC99, resulting in an overprediction in some experiments. Likewise, in the UCR chamber experiments, Table 6-23 and Figure 6-51, increasing the termination rate and cresol yield in SAPRC99 leads to less of an overprediction and more of an underprediction relative to the basecase.

Table 6-22. Comparison between the SAPRC99 and CB simulations and UNC chamber data for toluene; OH+NO_2 rate constant in SAPRC99 increased to that of CB-IV and explicit toluene chemistry in SAPRC99 with cresol yield increased to that of CB.

	Experiment	AU0183 Red	AU1788 Red	ST1393 Blue	AU3095 Blue
	VOC (ppmC)	4.590	4.930	1.909	7.210
	NOx (ppm)	0.395	0.357	0.324	0.618
	VOC/NOx	11.620	13.810	5.892	11.667
Peak Ozone (ppm)	SAPRC99	0.506	0.622	0.340	0.562
	S99 w/ CB4 HNO3 and explicit toluene w/ CB cresol yield	0.437	0.495	0.398	0.480
	CB-IV	0.344	0.404	0.158	0.398
	CB05	0.326	0.384	0.159	0.377
	Experiment	0.458	0.460	0.157	0.545
(Experimental-Model) /Experimental	SAPRC99	-10.48%	-35.34%	-116.28%	-3.08%
	S99 w/ CB4 HNO3 and explicit toluene w/ CB cresol yield	4.59%	-7.70%	-153.18%	11.96%
	CB-IV	24.89%	12.10%	-0.51%	27.00%
	CB05	28.82%	16.45%	-1.15%	30.85%
	MIR (g/g)	3.97	3.97	3.97	3.97
	MIR*VOC/NOx	46.1	54.8	23.4	46.3

Table 6-23. Comparison between the SAPRC99 and CB simulations and UCR chamber data toluene; $OH+NO_2$ rate constant in SAPRC99 increased to that of CB-IV and explicit toluene chemistry in SAPRC99 with cresol yield increased to that of CB.

	Experiment	EC271	EC273	EC340	EPA074B	EPA066B	EPA074A	OTC299A	TVA047	TVA071
	VOC (ppmC)	8.020	4.110	3.760	1.100	0.426	1.054	8.530	0.520	2.480
	NOx (ppm)	0.215	0.112	0.493	0.027	0.005	0.024	0.509	0.105	0.266
	VOC/NOx	37.302	36.696	7.627	40.741	85.200	43.917	16.758	4.952	9.323
Peak Ozone (ppm)	SAPRC99	0.390	0.306	0.281	0.191	0.069	0.130	0.734	0.069	0.246
	S99 w/ CB4 HNO3 and explicit toluene w/ CB cresol yield	0.350	0.279	0.174	0.166	0.063	0.119	0.466	0.044	0.140
	CB-IV	0.323	0.250	0.259	0.078	0.036	0.054	0.356	0.032	0.157
	CB05	0.306	0.237	0.250	0.078	0.035	0.051	0.426	0.031	0.154
	Experiment	0.294	0.214	0.343	0.261	0.058	0.124	0.611	0.094	0.270
(Experimental-Model) /Experimental	SAPRC99	-32.52%	-43.13%	18.01%	26.92%	-19.76%	-5.17%	-20.07%	26.50%	8.97%
	S99 explicit toluene w/ CB cresol yield and CB4 HNO3	-19.01%	-30.28%	49.42%	36.50%	-8.34%	3.80%	23.75%	53.31%	48.09%
	CB-IV	-9.80%	-16.92%	24.56%	70.13%	37.35%	56.22%	41.81%	66.35%	41.68%
	CB05	-4.05%	-10.51%	27.13%	70.24%	40.29%	59.05%	30.39%	66.56%	42.86%
	MIR (g/g)	3.97	3.97	3.97	3.97	3.97	3.97	3.97	3.97	3.97
	MIR*VOC/NOx	148.09	145.68	30.28	161.74	338.24	174.35	66.53	19.66	37.01

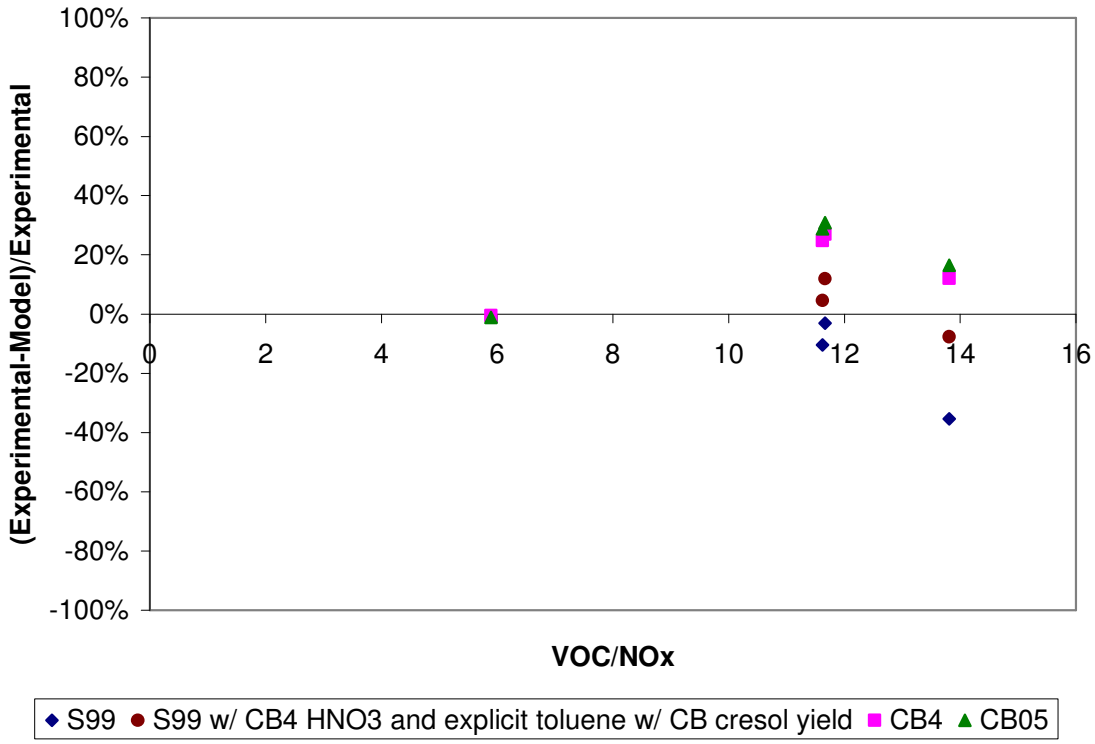

Figure 6-50. Model underprediction error for peak ozone in UNC chamber toluene experiments against VOC/NOx ratio; OH+NO_2 rate constant in SAPRC99 increased to that of CB-IV and explicit toluene chemistry in SAPRC99 with cresol yield increased to that of CB.

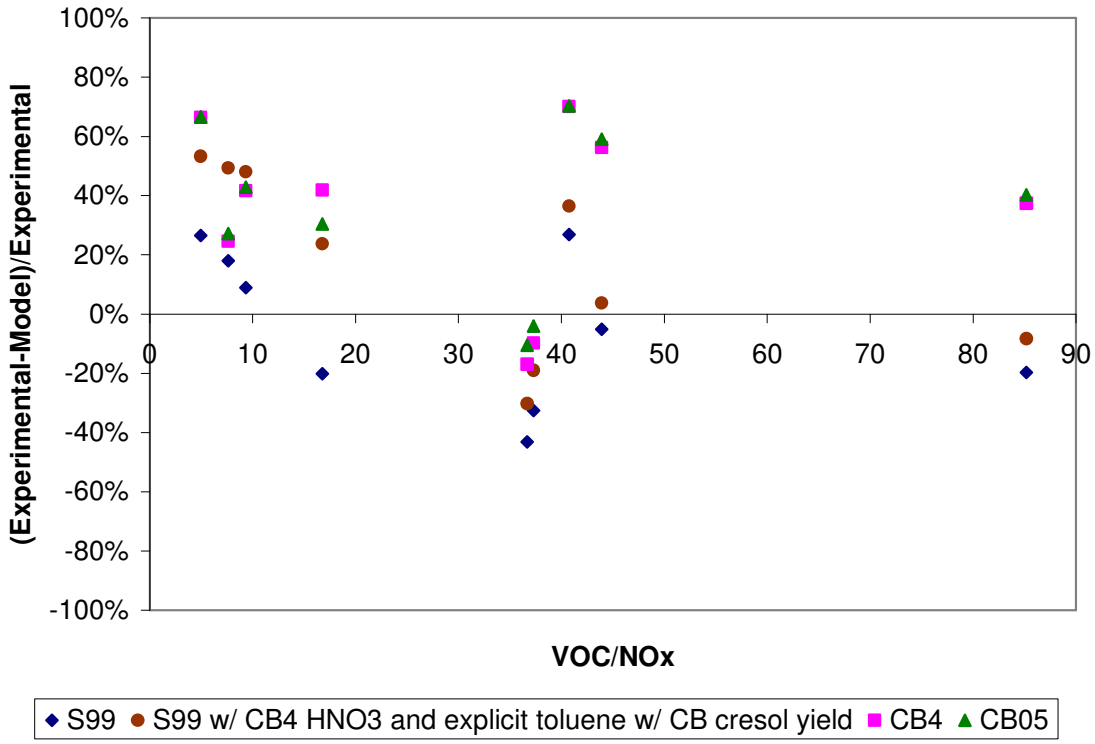

Figure 6-51. Model underprediction error for peak ozone in UCR chamber toluene experiments against VOC/NOx ratio; OH+NO_2 rate constant in SAPRC99 increased to that of CB-IV and explicit toluene chemistry in SAPRC99 with cresol yield increased to that of CB.

6.7 DIFFERENCE IN PEAK OZONE CEONCENTRATIONS BETWEEN SAPRC99 AND CB-IN UNC AND UCR CHAMBER EXPERIMENTS

Table 6-24 and 6-25 summarize the differences in peak ozone concentrations between the various simulations of SAPRC99 and basecase CB-IV for the UNC and UCR toluene experiments, respectively. The differences in peak ozone concentrations reported in these tables are illustrated in Figures 6-52 and 6-53. In the UNC experiment, with the exception of the ST1393 experiment, the SAPRC simulation with explicit toluene and a cresol yield equal to that of CB is closest in agreement with the CB mechanism in terms of peak ozone concentrations. In the ST1393 case, increasing the

$OH+NO_2$ rate constant in SAPRC99 substantially closes the gap in peak ozone between SAPRC99 and CB. The SAPRC99 simulation with increased termination rate and cresol yield also lessens the gap in peak ozone between SAPRC99 and CB, but not to the extent of increasing the cresol yield in SAPRC99 alone. However, for the ST1393 experiment, the combined modification to SAPRC99 lowers the discrepancy between SAPRC99 and CB-IV more than increasing the cresol yield in SAPRC99 alone. Furthermore, except for the ST1393 experiment, increasing the termination rate and the cresol yield in SAPRC simultaneously has more of an effect on closing the gap between SAPRC99 and CB-IV than increasing the termination rate in SAPRC99 alone.

In the UCR chamber experiments, simultaneusly increasing the termination rate and cresol yield in the SAPRC99 mechanism is more effective at reducing the discrepancy between SAPRC99 and CB-IV than increasing the termination rate and cresol yield in SAPRC99 separately.

Table 6-24. Differences in peak ozone concentrations in UNC toluene experiments.

	Difference in Peak Ozone (S99 - CB4 basecase) (ppm)				
UCR Toluene Experiment	S99 basecase	S99 w/ CB4 HNO3 rate	S99 explicit toluene	S99 explicit toluene w/ CB cres yield	S99 w/ CB4 HNO3 and explicit toluene w/ CB cresol yield
AU0183 Red	0.16200	0.13800	0.15400	0.07400	0.09300
AU1788 Red	0.21800	0.18400	0.20400	0.07600	0.09100
ST1393 Blue	0.18200	0.05500	0.27000	0.17000	0.24000
AU3095 Blue	0.16400	0.12500	0.15900	0.07000	0.08200

Table 6-25. Differences in peak ozone concentrations in UCR toluene experiments.

	Difference in Peak Ozone (S99 - CB4 basecase) (ppm)				
UCR Toluene Experiment	S99 basecase	S99 w/ CB4 HNO3 rate	S99 explicit toluene	S99 explicit toluene w/ CB cres yield	S99 w/ CB4 HNO3 and explicit toluene w/ CB cresol yield
EC271	0.06680	0.05530	0.07060	0.03710	0.02710
EC273	0.05610	0.04820	0.05600	0.03590	0.02860
EC340	0.02250	-0.07630	0.11520	0.02750	-0.08530
EPA074B	0.11280	0.10600	0.11760	0.09190	0.08780
EPA066B	0.03300	0.03120	0.03330	0.02800	0.02640
EPA074A	0.07600	0.07150	0.07890	0.06910	0.06490
OTC299A	0.37830	0.31520	0.38800	0.14740	0.11040
TVA047	0.03730	0.01320	0.05930	0.03460	0.01220
TVA071	0.08820	-0.01780	0.17370	0.08370	-0.01730

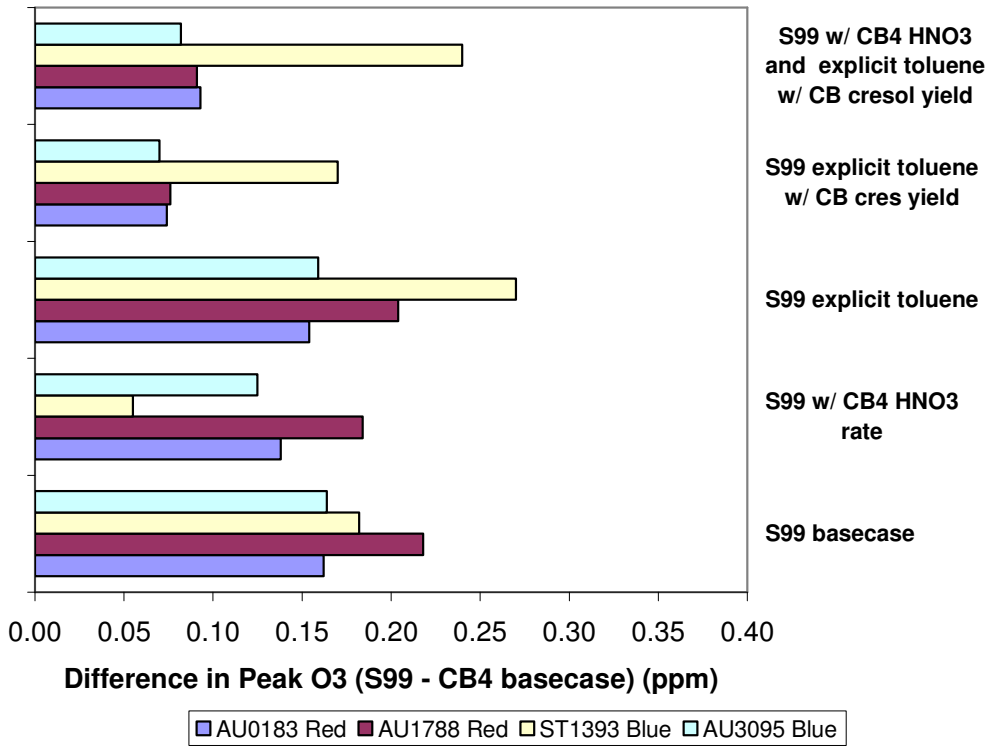

Figure 6-52. Differences in peak ozone concentrations in UNC toluene experiments.

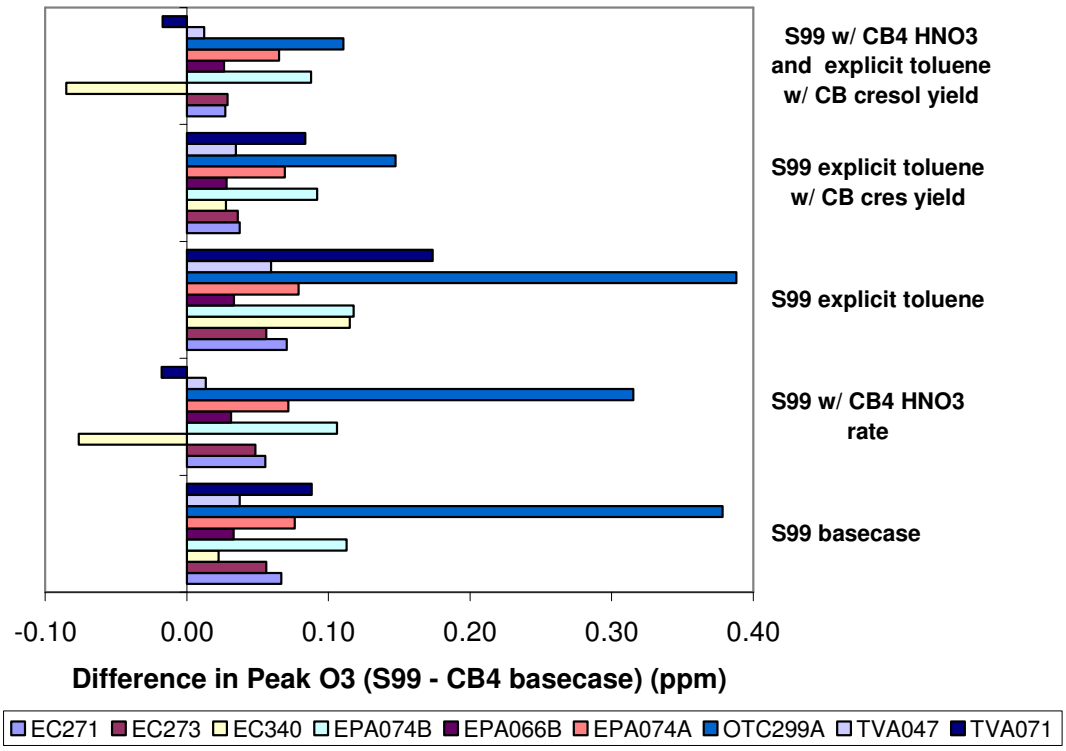

Figure 6-53. Differences in peak ozone concentrations in UCR toluene experiments.

6.8 SUMMARY

Predictions of SAPRC99, CB-IV and CB05 were compared to UNC and UCR environmental chamber experiments involving singly and multiply substituted aromatics. For aromatic generally, and mono-substituted aromatics specifically, the differences in predictions between the CB and SAPRC mechanisms are larger than for other compound classes.

The SAPRC99 mechanism performed better than the CB mechanisms in simulating some chamber experiments with toluene; the mechanism performances were more comparable for xylenes and other multiply substituted aromatics.

Sensitivity analyses indicate that the differences between the mechanisms decrease substantially if the yield for the lumped species CRES, and rate constant for the OH + NO_2 are made consistent between the two mechanisms. The lumped group referred to as CRES, is often referred to as cresol, and comparisons between chamber experiments and observed cresol concentrations are generally better for the SAPRC mechanism than for the CB mechanisms. However, in the CB mechanism, the CRES species is used to represent both cresol yields and other products (such as unsaturated dicarbonyls) that react rapidly with the nitrate radical. Therefore direct comparisons of CRES yields with cresol concentrations for the CB mechanisms are not appropriate.

While it is clear that there are substantial differences in predictions of aromatics chemistry between the CB and SAPRC mechanisms, much still remains unresolved about aromatics chemistry. To help address these uncertainties, future versions of lumped chemical mechanisms should seek to more clearly separate the yields of cresols from the NOx sinks in aromatics chemistry encountered at low NOx conditions.

6.9 REFERENCES

Calvert, J.G., R. Atkinson, K.H. Becker, R.M. Kamens, J.H. Seinfeld, T.J. Wallington, and G. Yarwood, (2002), *The Mechanisms of Atmospheric Oxidation of Aromatic Hydrocarbons*, Oxford University Press, 556 pages.

Carter, W. P. L. (2000). *Documentation of the SAPRC-99 chemical mechanism for VOC reactivity assessment*. Air Pollution Research Center and College of Engineering, Center for Environmental Research and Technology, University of California at Riverside, CA.

Carter, W. P. L. (2007, May). *Documentation of the SAPRC-07 chemical mechanism and updated ozone reactivity scales.* Draft Final Report to the California Air Resources Board, Sacramento, CA.

Dechapanya, W. (2002, May). *Kinetic and physic models of Secondary Organic Aerosol formation and their application to Houston condition*. Ph.D. Dissertation, Department of Chemical Engineering, The University of Texas at Austin, TX.

Gery, M. W., Whitten, G. Z., and Killus, J. P. (1989). A photochemical kinetics mechanism for urban and regional scale computer modeling. Journal of Geophysical Research, 20, 12,925-12,956.

Killus, J.P. and G.Z. Whitten (1982) "A Mechanism Describing the Photochemical Oxidation of Toluene in Smog," *Atmospheric Environment*, Vol. 16, pp 1973-1982.

Killus, J. P. and Whitten, G. Z. (1990). Background reactivity in smog chambers. *The International Journal of Chemical Kinetics*, 22, 547-575.

Killus, J.P. and G.Z. Whitten (1983) Comments on "Photochemical reactivity and ozone formation in 1-olefin–nitrogen oxide–air systems" , *Environ. Sci. Technol.*, Vol. 17, pp 760-762.

Zádor, J., Turányi, T., Wirtz, K., and Pilling, M.J. (2006). Measurement and investigation of chamber radical sources in the European Photoreactor (EUPHORE). *Journal of Atmospheric Chemistry*, 55, 147-166.

Chapter 7: Summary of Findings and Recommendations

Air quality planning in the United States relies on predictions of photochemical to assess the extent of emission reductions required and the relative effectiveness of various emission reduction strategies. In modeling an air pollution episodes for Houston, Texas, the work described in this thesis demonstrated that two chemical mechanisms, commonly used in photochemical models (SAPRC99 and CBIV) led to predictions of ozone concentrations and sensitivities to emission reductions that were substantially different. As described in this thesis, various modeling tools were used to diagnose the differences between SAPRC99 and CB-IV under the Houston-Galveston conditions, which exhibit high hydrocarbon reactivity as well as high NOx emission density. In addition, the performance of the SAPRC99, CB-IV, and CB05 mechanisms were evaluated in environmental chamber simulations. Key findings are summarized below, followed by recommendations for future work.

7.1 KEY FINDINGS

- Air quality modeling using CAMx for a 2000 episode in the Houston-Galveston revealed substantial differences in ozone concentrations between the predictions of SAPRC99 and CB-IV (1996 version). SAPRC99 predicts ozone concentrations that are 30-45 ppb higher than CB-IV. The differences in ozone predictions are greatest when predicted ozone concentrations are high.
- In sensitivity studies in CAMx with varying VOC and NOx emissions reductions, SAPRC99 showed more sensitivity to reductions in NOx emissions. Predictions of ozone concentrations in SAPRC99 and CB-IV converged when NOx emissions were substantially reduced.

- Sensitivity studies in CAMx show that differences between SAPRC99 and CB-IV under the conditions of Houston-Galveston can be attributed to the following:
    - Differences in the chemistry of aromatics, especially mono-subsituted aromatics (e.g., toluene). In CB-IV, the oxidation of mono-subsituted aromatics leads to higher ring-retaining products (e.g., cresol), which are less reactive than ring-opening products, relative to SAPRC99.
    - Differences in the rates of nitric acid formation, which is lower in SAPRC99 than CB-IV.
    - Differences in free radical formation pathways: Higher formation of higher aldehydes in SAPRC99 than CB-IV, which contribute to higher free radical production through photolysis.
- Equating the $OH+NO_2$ rate constants in SAPRC99, CB-IV, and CB05 in simulations of CO-NOx chamber experiments without modifications to account for wall effects caused the predicted ozone concentrations in the three mechanisms to converge. Therefore, in photochemical modeling simulations in which wall mechanisms are not applicable, a major reason for differences in the inorganic chemistry between the three mechanisms is the difference in the rate parameters for the $OH+NO_2$ reaction.
- Increasing or decreasing the radical concentrations in high reactivity chamber experiments involving olefins by equating the $OH+NO_2$ rate constants in SAPRC99 and CB-IV and by increasing the radical yield in olefin-zone reactions in SAPRC99, CB-IV, and CB05 had little impact on predicted ozone concentrations.
- Simulations of chamber experiments with olefins showed that the performance of the mechanisms in simulating olefins chemistry is improved by a more explicit

representation of internal olefin chemistry, which has recently been adopted in CB05.

- The performance of SAPRC99 was improved in some simulations of propylene experiments when the propylene was modeled explicitly, as opposed to being represented by a lumped chemical species.
- The SAPRC99 mechanism generally performed better than the CB mechanisms in simulating chamber experiments with toluene. The mechanism performances were relatively more comparable for the di- and multiply-substituted aromatics.
- Differences between SAPRC99 and CB-IV in simulating chamber experiments for mono-substituted aromatics was substantially reduced when the yield for the lumped species CRES and the $OH+NO_2$ rate constant were made consistent between the two mechanisms. However, the CRES species in CB-IV does not solely represent cresols, but other products that react rapidly with the nitrate radical, as well.

In conclusion, the analyses in CAMx and evaluations in chamber simulations indicate that major causes for the differences in SAPRC and CB mechanisms under conditions encountered in Houston-Galveston are the chemistry of aromatics, and to a lesser extent, radical termination rates. These differences are due to differences in both reaction rate parameters/stoichiometry and the condensation methods in the mechanisms

Based on the findings of this thesis, Carter (Faraji *et al*., 2007) performed simulations based on the EPA chamber experiments at UCR, in which ambient surrogate mixtures were used as reactants. Carter evaluated the simulations of these ambient surrogate mixtures which are composed of reactive organic gases (ROG) both with and without aromatics. Similar to the single-VOC experiments, injections of the ROGs and NOx vary from one experiment to another. The composition of the full surrogate mixtures and the

composition of the surrogate mixture without aromatics are listed in Table 7-1. The results (Figure 7-1a and 7-1b) show that all the mechanisms underpredict O_3 at low ROG/NOx ratios, with the bias decreasing as the ROG/NOx ratio increases. This problem is worse for CB-IV than for SAPRC99 and CB05, which perform similarly. Additionally, the results show that when the aromatics are removed from the surrogate mixture (Figure 7-1c), CB05 performs the best, and that SAPRC99 and CB-IV tend to underpredict O_3, with the biases being worse for CB-IV. Furthermore, the performance of the SAPRC99 mechanism improves considerably if compounds are modeled explicitly, rather than in lumped groups.

Table 7-1. Relative compositions of reactive organic gas surrogates used in the UCR EPA surrogate mixture - NO_x experiments

Compound	Surrogate Composition	
	Full	No Aromatics
n-Butane	90	125
n-Octane	22	37
Ethene	16	23
Propene	15	22
trans-2-Butene	14	23
Toluene	21	-
m-Xylene	20	-
Formaldehyde	20	-

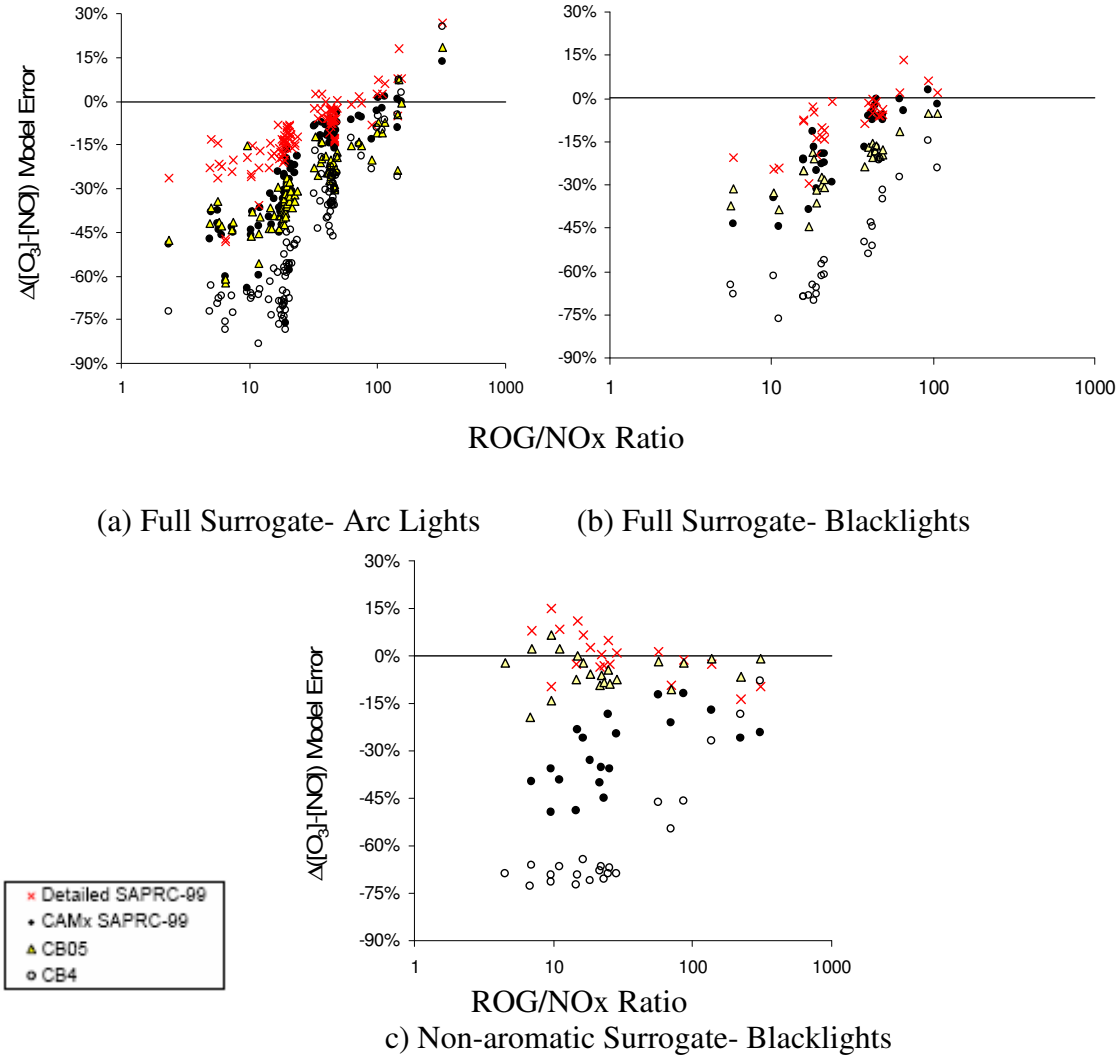

Figure 7-1. Model error Δ([O_3]-[NO]) in simulating O_3 formed and NOx oxidized for various UCR EPA Surrogate-NOx experiments.

7.2 RECOMMENDATIONS

In choosing a mechanism that will be most effective for conditions in eastern Texas, several guiding principles emerge. Over the past several decades, comprehensive updates to the CB and SAPRC chemical mechanisms have been released roughly every 5-10 years. These updates incorporate changes to the mechanisms that reflect evolving

knowledge about rate constants and key chemical pathways. For example, the rate parameters for the critical OH + NO_2 rate constant have been adjusted in CB05, as compared to CB-IV, and in SAPRC07, as compared to SAPRC99. These updates generally reflect more current knowledge, and, as a guiding principle, should be used when possible.

In addition, the updates often provide explicit representations of chemical species that have recently been identified as being especially critical. For example, explicit isoprene chemistry was incorporated into both SAPRC and CB mechanisms in the 1990s and the newly released CB05 incorporates internal olefins as an explicit compound class. Therefore, As new comprehensive updates to mechanisms are developed, more explicit representation of both key chemical pathways (e.g., the low NOx routes for aromatics) and key chemical species (propene, toluene, and possibly other aromatics) would likely make the mechanisms more useful in analyzing the complex industrial emission sources in the Houston area.

Finally, recognizing that it may be difficult to unambiguously define the most appropriate mechanism for use in Houston, the effectiveness of proposed control strategies should be evaluated using multiple chemical mechanisms.

Appendices

Appendix A: SAPRC and CB Chemical Mechanisms

A.1 SAPRC Chemical Mechanism

SAPRC90

Table A-1.1. List of reactions and rate constant parameters for the SAPRC90 mechanism (Carter, 1990)

Label*	Rate parameters† (A	E_a	B)	Reaction‡
Inorganic reactions				
A1	Phot Set = NO2			NO2 + HV = NO + O
A2	6.00E-34	0.0	-2.3	O + O2 + M = O3 + M
A3A	6.50E-12	-0.238	0.0	O + NO2 = NO + O2
A3B	See note 4			O + NO2 = NO3 + M
A4	2.00E-12	2.782	0.0	O3 + NO = NO2 + O2
A5	1.40E-13	4.968	0.0	O3 + NO2 = O2 + NO3
A6	1.70E-11	-0.298		NO + NO3 = #2 NO2
A7	3.30E-39	-1.050	0.0	NO + NO + O2 = #2 NO2
A8	See note 6			NO2 + NO3 = N2O5
A9	See note 7			N2O5 = NO2 + NO3
A10	1.00E-21	0.0	0.0	N2O5 + H2O = #2 HNO3
A11	2.50E-14	2.44	0.0	NO2 + NO3 = NO + NO2 + O2
A12A	Phot Set = NO3NO			NO3 + HV = NO + O2
A12B	Phot Set = NO3NO2			NO3 + HV = NO2 + O
A13A	Phot Set = O3O3P			O3 + HV = O + O2
A13B	Phot Set = O3O1D			O3 + HV = O*1D2 + O2
A14	2.20E-10	0.0	0.0	O*1D2 + H2O = #2 HO.
A15	1.92E-11	-0.251	0.0	O*1D2 + M = O + M
A16	See note 14			HO. + NO = HONO
A17	Phot Set = HONO			HONO + HV = HO. + NO
A18	See note 16			HO. + NO2 = HNO3
A19	6.45E-15	-1.652	0.0	HO. + HNO3 = H2O + NO3
A20	(Ignored)			HNO3 + HV = HO. + NO2
A21	2.40E-13	0.0	0.0	HO. + CO = HO2. + CO2
A22	1.60E-12	1.87	0.0	HO. + O3 = HO2. + O2
A23	3.70E-12	-0.48	0.0	HO2. + NO = HO. + NO2
A24	See note 20			HO2. + NO2 = HNO4
A25	See note 21			HNO4 = HO2. + NO2
A26	(Ignored)			HNO4 + HV = products
A27	1.30E-12	-0.755	0.0	HNO4 + HO. = H2O + NO2 + O2
A28	1.10E-14	0.994	0.0	HO2. + O3 = HO. + #2 O2
A29A	2.20E-13	-1.23	0.0	HO2. + HO2. = HO2H + O2
A29A	1.90E-33	-1.95	0.0	HO2. + HO2. + M = HO2H + O2 + M
A29C	3.10E-34	-5.60	0.0	HO2. + HO2. + H2O = HO2H + O2 + H2O
A29D	6.60E-35	-6.32	0.0	HO2. + HO2. + H2O = HO2H + O2 + H2O

Label*	Rate parameters† (A	E_a	B)	Reaction‡	N
A30A	Same *k* as A29A			NO3 + HO2. = HNO3 + O2	
A30B	Same *k* as A29B			NO3 + HO2. + M = HNO3 + O2 + M	
A30C	Same *k* as A29C			NO3 + HO2. + H2O = HNO3 + O2 + H2O	
A30A	Same *k* as A29D			NO3 + HO2. + H2O = HNO3 + O2 + H2O	
A31	Phot Set = H2O2			HO2H + HV = #2 HO.	
A32	3.30E–12	0.397	0.0	HO2H + HO. = HO2. + H2O	
A33	4.60E–11	−0.457	0.0	HO. + HO2. = H2O + O2	
Reactions of SO2					
SR1	See note 25			SO2 + HO. = HO2. + H2SO4	
SR2	2.30E–17	0.0	0.0	O3OL–SB + H2O =	
SR3	1.00E–13	0.0	0.0	O3OL–SB + SO2 = H2SO4	
Lumped alkyl and acyl peroxy radical reactions					
B1	4.20E–12	−0.360	0.0	RO2. + NO = NO	
B2	5.10E–12	−0.397	0.0	RCO3. + NO = NO	
B3	(Ignored)			RO2. + NO2 = NO2	
B4	See note 30			RCO3. + NO2 = NO2	
B5	3.40E–13	−1.590	0.0	RO2. + HO2. = HO2.	
B6	3.40E–13	−1.590	0.0	RCO3. + HO2. = HO2.	
B8	1.00E–15	0.0	0.0	RO2. + RO2. =	
B9	1.86E–12	−1.053	0.0	RO2. + RCO3. =	
B10	2.80E–12	−1.053	0.0	RCO3. + RCO3. =	
Reactions of other peroxy radical operators					
B11	Same *k* as B1			RO2–R. + NO = NO2 + HO2	
B12	Same *k* as B5			RO2–R. + HO2. = –OOH	
B13	Same *k* as B8			RO2–R. + RO2. = RO2. + #0.5 HO2.	
B14	Same *k* as B9			RO2–R. + RCO3. = RCO3. + #0.5 HO2.	
B19	Same *k* as B1			RO2–N. + NO = RNO3	
B20	Same *k* as B5			RO2–N. + HO2. = –OOH + MEK + #1.5–C	
B21	Same *k* as B8			RO2–N. + RO2. = RO2. + #0.5 HO2. + MEK + #1.5–C	
B22	Same *k* as B9			RO2–N. + RCO3. = RCO3. + #0.5 HO2. + MEK + #1.5–C	
G2	Same *k* as B1			RO2–NP. + NO = NPHE	
G3	Same *k* as B5			RO2–NP. + HO2. = –OOH + #6–C	
G4	Same *k* as B8			RO2–NP. + RO2. = RO2. + #0.5 HO2. + #6–C	
G5	Same *k* as B9			RO2–NP. + RCO3. = RCO3. + HO2. + #6–C	
B23	Same *k* as B1			RO2–XN. + NO = –N	
B24	Same *k* as B5			RO2–XN. + HO2. = –OOH	
B25	Same *k* as B8			RO2–XN. + RO2. = RO2. + #0.5 HO2.	
B26	Same *k* as B9			RO2–XN. + RCO3. = RCO3. + HO2.	
B15	Same *k* as B1			R2O2. + NO = NO2	
B16	Same *k* as B5			R2O2. + HO2. =	
B17	Same *k* as B8			R2O2. + RO2. = RO2.	
B18	Same *k* as B9			R2O2. + RCO3. = RCO3.	
Reactions of formaldehyde					
C1	Phot Set = HCHOAVGR			HCHO + HV = #2 HO2. + CO	
C2	Phot Set = HCHOAVGM			HCHO + HV = H2 + CO	
C3	1.13E–12	−1.288	2.0	HCHO + HO. = HO2. + CO + H2O	
C4	9.70E–15	−1.242	0.0	HCHO + HO2. = HOCOO.	
C4A	2.40E + 12	13.91	0.0	HOCOO. = HO2. + HCHO	
C4B	Same *k* as B1			HOCOO. + NO = –C + NO2 + HO2.	
C9	2.80E–12	5.00	0.0	HCHO + NO3 = HNO3 + HO2. + CO	
Reactions of acetaldehyde and PAN					
C10	5.55E–12	−0.618	0.0	CCHO + HO. = CCO–O2. + H2O + RCO3.	
C11A	Phot Set = CCHOR			CCHO + HV = CO + HO2. + HCHO + RO2–R. + RO2.	
C11B	(Ignored)			CCHO + HV = CH4 + CO	
C12	1.40E–12	3.696	0.0	CCHO + NO3 = HNO3 + CCO–O2. + RCO3.	
C13	Same *k* as B2			CCO–O2. + NO = CO2 + NO2 + HCHO + RO2–R. + RO2.	
C14	Same *k* as B4			CCO–O2. + NO2 = PAN	
C15	Same *k* as B6			CCO–O2. + HO2. = –OOH + CO2 + HCHO	
C16	Same *k* as B9			CCO–O2. + RO2. = RO2. + #0.5 HO2. + CO + HCHO	
C17	Same *k* as B10			CCO–O2. + RCO3. = RCO3. + HO2. + CO2 + HCHO	
C18	See note 47			PAN = CCO–O2. + NO2 + RCO3.	

Label*	Rate parameters† (A	E_a	B)	Reaction‡	No
Reactions of propionaldehyde and PPN (also used for lumped higher aldehydes and lumped higher acyl peroxy nitrates)					
C25	8.50E-12	−0.50	0.0	RCHO + HO. = C2CO-O2. + RCO3.	
C26	Phot Set = RCHO			RCHO + HV = CCHO + RO2-R. + RO2. + CO + HO2.	
C27	1.40E-12	3.696	0.0	NO3 + RCHO = HNO3 + C2CO-O2. + RCO3.	
C28	Same *k* as B2			C2CO-O2. + NO = CCHO + RO2-R. + CO2 + NO2 + RO2.	
C29	8.40E-12	0.0	0.0	C2CO-O2. + NO2 = PPN	
C30	Same *k* as B6			C2CO-O2. + HO2. = -OOH + CCHO + CO2	
C31	Same *k* as B9			C2CO-O2. + RO2. = RO2. + #0.5 HO2. + CCHO + CO2	
C32	Same *k* as B10			C2CO-O2. + RCO3. = RCO3. + HO2. + CCHO + CO2	
C33	1.60E+17	27.966	0.0	PPN = C2CO-O2. + NO2 + RCO3.	
Reactions of acetone					
C38	1.92E-13	−0.11	2.0	ACET + HO. = #0.8 "MGLY + RO2-R." + #0.2 "R2O2. + HCHO + CCO-O2. + RCO3." + RO2.	
C39	Phot Set = ACETONE			ACET + HV = CCO-O2. + HCHO + RO2-R. + RCO3. + RO2.	
Reactions of methyl ethyl ketone and lumped higher ketones					
C44	2.92E-13	−0.823	2.0	MEK + HO. = H2O + #0.5 "CCHO + HCHO + CCO-O2. + C2CO-O2." + RCO3. + #1.5 "R2O2. + RO2."	
C57	Phot Set = KETONE			MEK + HV = CCO-O2. + CCHO + RO2-R. + RCO3. + RO2.	
Reactions of the lumped alkyl nitrate					
C95	2.19E-11	1.408	0.0	RNO3 + HO. = NO2 + #0.155 MEK + #1.05 RCHO + #0.48 CCHO + #0.16 HCHO + #0.11 -C + #1.39 "R2O2. + RO2."	
Reactions of glyoxal and its PAN *analogue*					
C58A	Phot Set = GLYOXAL1			GLY + HV = #0.8 HO2. + #0.45 HCHO + #1.55 CO	
C58B	Phot Set = GLYOXAL2			GLY + HV = #0.13 HCHO + #1.87 CO	
C59	1.14E-11	0.0	0.0	GLY + HO. = #0.6 HO2. + #1.2 CO + #0.4 "HCOCO-O2. + RCO3."	
C60	Same *k* as C12			GLY + NO3 = HNO3 + #0.6 HO2. + #1.2 CO + #0.4 "HCOCO-O2. + RCO3."	
C62	Same *k* as B2			HCOCO-O2. + NO = NO2 + CO2 + CO + HO2.	
C63	Same *k* as B4			HCOCO-O2. + NO2 = GPAN	
C65	Same *k* as B6			HCOCO-O2. + HO2. = -OOH + CO2 + CO	
C66	Same *k* as B9			HCOCO-O2. + RO2. = RO2. + #0.5 HO2. + CO2 + CO	
C67	Same *k* as B10			HCOCO-O2. + RCO3. = RCO3. + HO2. + CO2 + CO	
C64	Same *k* as C18			GPAN = HCOCO-O2. + NO2 + RCO3.	
Reactions of methyl glyoxal					
C68A	Phot Set = MEGLYOX1			MGLY + HV = HO2. + CO + CCO-O2. + RCO3.	
C68B	Phot Set = MEGLYOX2			MGLY + HV = HO2. + CO + CCO-O2. + RCO3.	
C69	1.72E-11	0.0	0.0	MGLY + HO. = CO + CCO-O2. + RCO3.	
C70	Same *k* as C12			MGLY + NO3 = HNO3 + CO + CCO-O2. + RCO3.	
Reactions of phenol					
G46	2.63E-11	0.0	0.0	HO. + PHEN = #0.15 RO2-NP. + #0.85 RO2-R. + #0.2 GLY + #4.7 -C + RO2.	
G51	3.60E-12	0.0	0.0	NO3 + PHEN = HNO3 + BZ-O.	
Reaction of cresols and other alkylphenols					
G52	4.20E-11	0.0	0.0	HO. + CRES = #0.15 RO2-NP. + #0.85 RO2-R. + #0.2 MGLY + #5.5 -C + RO2.	
G57	2.10E-11	0.0	0.0	NO3 + CRES = HNO3 + BZ-O. + -C	
Reactions of benzaldehyde, PBzN *and analogous aromatic compounds*					
G30	1.29E-11	0.0	0.0	BALD + HO. = BZ-CO-O2. + RCO3.	
G31	Phot Set = BZCHO			BALD + HV = #7 -C	
G32	1.40E-12	3.747	0.0	BALD + NO3 = HNO3 + BZ-CO-O2. + RCO3.	
G33	Same *k* as B2			BZ-CO-O2. + NO = BZ-O. + CO2 + NO2 + R2O2. + RO2.	
G36	Same *k* as B6			BZ-CO-O2. + HO2. = -OOH + CO2 + PHEN	
G34	8.40E-12	0.0	0.0	BZ-CO-O2. + NO2 = PBZN	
G37	Same *k* as B9			BZ-CO-O2. + RO2. = RO2 + #0.5 HO2. + CO2 + PHEN	
G38	Same *k* as B10			BZ-CO-O2. + RCO3. = RCO3. + HO2. + CO2 + PHEN	
G35	1.60E+15	25.90	0.0	PBZN = BZ-CO-O2. + NO2 + RCO3.	

Label*	Rate parameters† (*A*	E_a	*B*)	Reaction‡	N
Reactions of phenoxy radicals and nitrophenols					
G43	1.30E-11	−0.596	0.0	BZ-O. + NO2 = NPHE	
G44	Same *k* as B5			BZ-O. + HO2. = PHEN	
G45	1.00E-3	0.0	0.0	BZ-O. = PHEN	
G58	3.60E-12	0.0	0.0	NPHE + NO3 = HNO3 + BZ(NO2)-O.	
G59	Same *k* as G43			BZ(NO2)-O. + NO2. = #2 -N + #6 -C	
G60	Same *k* as B5			BZ(NO2)-O. + HO2. = NPHE	
G61	Same *k* as G45			BZ(NO2)-O. = NPHE	
Reactions of the uncharacterized aromatic ring-opening product #1					
G7	1.14E-11	0.0	0.0	AFG1 = HCOCO-O2. + RCO3.	
G8	Phot Set = AROMUNK1			AFG1 + HV = HO2. + HCOCO-O2. + RCO3.	
Reactions of the uncharacterized aromatic ring-opening product #2					
G9	1.72E-11	0.0	0.0	HO. + AFG2 = C2CO-O2. + RCO3.	
G10	Phot Set = AROMUNK2			AFG2 + HV = HO2. + CO + CCO-O2. + RCO3.	
Reactions of the lumped hydroperoxide group					
B7	Phot Set = CO2H			-OOH + HV = HO2. + HO.	
B7A	1.18E-12	−0.254	0.0	HO. + -OOH = HO.	
B7B	1.79E-12	−0.435	0.0	HO. + -OOH = RO2-R. + RO2.	
Reactions of ethene					
D1	1.96E-12	−0.870	0.0	ETHE + HO. = #0.22 CCHO + #1.56 HCHO + RO2-R. + RO2.	
D6	1.20E-14	5.226	0.0	ETHE + O3 = HCHO + #0.37 O3OL-SB + #0.44 CO + #0.56 -C + #0.12 HO2.	
D8	1.04E-11	1.574	0.0	ETHE + O = HCHO + CO + HO2. + RO2-R. + RO2.	
D9	1.96E-12	5.413	0.0	ETHE + NO3 = NO2 + #2 HCHO + R2O2. + RO2.	
General alkane and aromatic reactions					
AnOH	See note 88			HO. + AARn = #AnRR RO2-R. + #AnNR RO2-N. + #AnXN RO2-XN. + #AnNP RO2-NP. + #AnRH HO2. + #AnR2 R2O2. + #AnRO2 RO2. + #AnA1 HCHO + #AnA2 CCHO + #AnA3 RCHO + #AnK3 ACET + #AnK4 MEK + #AnCO CO + #AnC2 CO2 + #AnPH PHEN + #AnCR CRES + #AnBZ BALD + #AnGL GLY + #AnMG MGLY + #AnU1 AFG1 + AnU2 AFG2 + #AnXC -C	
General alkene reactions					
OnOH	See note 89			OLEn + HO. = #OnP1R HCHO + #OnP2R CCHO + #OnP3R RCHO + #OnP4R ACET + #OnP5R MEK + #OnPR RO2-R. + #OnPN RO2-N. + RO2. + #OnOHXC -C	
OnO3	See note 89			OLEn + O3 = #OnO3A1 HCHO + #OnO3A2 CCHO + #OnO3A3 RCHO + #OnO3K3 ACET + #OnO3K4 MEK + #OnO3MG MGLY + #OnO3CO CO + #OnO3SB O3OL-SB + #OnO3P1 CCO-O2. + #OnO3P2 C2CO-O2. + #OnO3RH HO2. + #OnO3OH HO. + #OnO3RR RO2-R. + #OnO3R2 R2O2. + #OnO3RO2 RO2. + #OnO3PS RCO3. + #OnO3XC -C	
OnOA	See note 89			OLEn + O = #0.4 HO2. + #0.5 "MEK + RCHO" + #OnOAXC -C	
OnN3	See note 89			OLEn + NO3 = NO2 + #OnP1 HCHO + #OnP2 CCHO + #OnP3 RCHO + #OnP4 ACET + #OnP5 MEK + R2O2. + RO2. + #OnN3XC -C	

†Except as indicated otherwise, rate constants for reactions in this table are given by the expression
$k = A(T/300)^{B} \exp(- E_a/R T)$
where k and A are in cm, molecule, s units, T is the temperature in K and R is 0.0019872 kcaldeg $^{-1}$ mole $^{-1}$. If a note is
referenced which indicates that the "falloff expression" is used, then the rate constant is both temperature and pressure
dependent and is given by
$k=[(k_o \times M)/(I +[k_o \times M/k_\infty])] \times f^{g}$
where $g= 1/[1 +(\log 10[k_o \times M/k_\infty]/n)^2]$.
M is the pressure in molecules cm^{-3}. The notes for the reactions give the expressions for k_o and k_∞. Unless indicated otherwise
in the notes, f=0.6 and n = 1.
‡If a number or symbol preceded by a "#" appears in the list of reaction products, then that number or symbol is a product
yield coefficient. If no coefficient is given, then the yield is 1.0. If a product coefficient is given followed by a list of products
enclosed by double quotes, then that coefficient gives the yields of all the products given in the list.

Table A-1.2. List of species in the SAPRC90 mechanism (Carter, 1990).

No.	Name	Description
Active inorganic species*		
1	O3	Ozone
2	NO	Nitric oxide
3	NO2	Nitrogen dioxide
4	NO3	NO_3 radicals
5	N2O5	N_2O_5
6	HNO3	Nitric acid
7	HONO	Nitrous acid
8	HNO4	Peroxynitric acid
9	HO2.	HO_2 radicals
12	CO	Carbon monoxide
10	HO2H	Hydrogen peroxide
11	SO2	Sulphur dioxide
Active organic product species		
13	HCHO	Formaldehyde
14	CCHO	Acetaldehyde
15	PAN	Peroxy acetyl nitrate
16	RCHO	Propionaldehyde and lumped higher aldehydes
17	PPN	Peroxy propionyl nitrate and higher PAN analogues
18	ACET	Acetone
19	MEK	Methylethyl ketone and lumped higher ketones
20	RNO3	Lumped organic nitrates
21	GLY	Glyoxal
22	GPAN	PAN analogue formed from glyoxal
23	MGLY	Methyl glyoxal
24	PHEN	Phenol
25	CRES	Cresols and other alkyl phenols
26	BALD	Benzaldehyde and other aromatic aldehydes
27	PBZN	Peroxy benzoyl nitrate
28	NPHE	Nitrophenols and other aromatic nitro-compounds
29	AFG1	Unknown aromatic fragmentation product #1. (Formed from benzene, tetralin, and naphthalenes.)
30	AFG2	Unknown aromatic fragmentation product #2. (Formed from aromatics containing alkyl groups.)
31	–OOH	Chemical operator used to represent reactions at hydroperoxy groups
Active primary emitted species		
32	ETHE	Ethene
33+	AARn	*n*'th lumped group used to represent lumped alkanes and/or aromatics. (In general, there will be more than one such species.)
34+	OLEn	*n*'th lumped group used to represent lumped higher alkenes. (In general, there will be more than one such species.)
Active total peroxy radical species		
35	RO2.	Total alkyl peroxy radicals
36	RCO3.	Total peroxyacyl radicals
Product only species		
36	CO2	Carbon dioxide
37	H2SO4	Sulphuric acid
38	H2	Hydrogen
39	–C	"Lost carbon." Used to account for carbon balance.
40	–N	"Lost nitrogen." Used to account for nitrogen balance. (Primarily represents C_1–C_3 organic nitrates and dinitrophenols, whose reactions are neglected.)
Steady state† inorganic species		
41	HO.	Hydroxyl radicals
42	O	Ground state oxygen atoms
43	O*1D2	Excited oxygen atoms
Steady state organic radical species		
44	HOCOO.	Intermediate formed in the $HCHO + HO_2$ reaction
45	CCO–O2.	Peroxy acetyl radicals
46	C2CO–O2.	Higher peroxyacyl radicals
47	BZ–CO–O2.	Peroxy benzoyl radicals
48	HCOCO–O2.	Peroxyacyl radical formed from glyoxal

No.	Name	Description
49	BZ–O.	Phenoxy radicals
50	BZ(NO2)–O.	Phenoxy–type radicals containing nitro-groups
Steady state chemical "operators"		
51	O3OL–SB	Chemical operator used to account for the oxidation of SO_2 by ozone–alkene reaction intermediates (This is a product–only species if reactions of SO_2 are removed from the mechanism.)
52	RO2–R.	Chemical operator used to represent NO to NO_2 Conversion with generation of HO_2 radicals
53	RO2–X.	Chemical operator used to represent NO consumption and alkyl nitrate formation
54	RO2–NP.	Chemical operator used to represent NO consumption and nitrophenol formation
55	RO2–XN.	Chemical operator used to represent NO sink reactions
56	R2O2.	Chemical operator used to represent extra NO to NO_2 conversions
Constant species		
57	O2	Oxygen
58	M	Air
59	HV	Light factor (1.0 = normal intensity)
60	H2O	Water

*"Active" species are those which undergo chemical reaction and for which the steady state approximation is not applied.

†"Steady state" species are those where the steady state approximation can be employed.

SAPRC99

Table A-1.3. Listing of reactions in the base mechanism of SAPRC99 (Carter, 2000).

Label	Rate Parameters [a] k(298)	A	Ea	B	Refs & Notes [b]	Reaction and Products [c]
Inorganic Reactions						
1		Phot Set= NO2			1,2	NO2 + HV = NO + O3P
2	5.79e-34	5.68e-34	0.00	-2.8	3	O3P + O2 + M = O3 + M
3	7.96e-15	8.00e-12	4.09		4,5	O3P + O3 = #2 O2
4	1.01e-31	1.00e-31	0.00	-1.6	6,7,5	O3P + NO + M = NO2 + M
5	9.72e-12	6.50e-12	-0.24		4,5	O3P + NO2 = NO + O2
6	1.82e-12	Falloff, F=0.80			4,7,5,8	O3P + NO2 = NO3 + M
	0:	9.00e-32	0.00	-2.0		
	inf:	2.20e-11	0.00	0.0		
8	1.81e-14	1.80e-12	2.72		6	O3 + NO = NO2 + O2
9	3.52e-17	1.40e-13	4.91		6	O3 + NO2 = O2 + NO3
10	2.60e-11	1.80e-11	-0.22		6	NO + NO3 = #2 NO2
11	1.95e-38	3.30e-39	-1.05		6	NO + NO + O2 = #2 NO2
12	1.54e-12	Falloff, F=0.45			6,7	NO2 + NO3 = N2O5
	0:	2.80e-30	0.00	-3.5		
	inf:	2.00e-12	0.00	0.2		
13	5.28e-2	Falloff, F=0.45			6,7	N2O5 = NO2 + NO3
	0:	1.00e-3	21.86	-3.5		
	inf:	9.70e+14	22.02	0.1		
14	2.60e-22	2.60e-22			9	N2O5 + H2O = #2 HNO3
15		(Slow)			10	N2O5 + HV = NO3 + NO + O3P
16		(Slow)			10	N2O5 + HV = NO3 + NO2
17	6.56e-16	4.50e-14	2.50		11	NO2 + NO3 = NO + NO2 + O2
18		Phot Set= NO3NO			1,12,13	NO3 + HV = NO + O2
19		Phot Set= NO3NO2			1,12,13	NO3 + HV = NO2 + O3P
20		Phot Set= O3O3P			1,14,15	O3 + HV = O3P + O2
21		Phot Set= O3O1D			1,14,15	O3 + HV = O*1D2 + O2
22	2.20e-10	2.20e-10			4	O*1D2 + H2O = #2 HO.
23	2.87e-11	2.09e-11	-0.19		16	O*1D2 + M = O3P + M
24	7.41e-12	Falloff, F=0.60			17	HO. + NO = HONO
	0:	7.00e-31	0.00	-2.6		
	inf:	3.60e-11	0.00	-0.1		
25		Phot Set= HONO-NO			1,18,19	HONO + HV = HO. + NO
26		Phot Set= HONO-NO2			1,18,19	HONO + HV = HO2. + NO2
27	6.46e-12	2.70e-12	-0.52		6	HO. + HONO = H2O + NO2
28	8.98e-12	Falloff, F=0.60			20	HO. + NO2 = HNO3
	0:	2.43e-30	0.00	-3.1		
	inf:	1.67e-11	0.00	-2.1		
29	2.00e-11	2.00e-11			6,21	HO. + NO3 = HO2. + NO2
30	1.47e-13	k = k0+k3M/(1+k3M/k2)			22,23	HO. + HNO3 = H2O + NO3
	k0:	7.20e-15	-1.56	0.0		
	k2:	4.10e-16	-2.86	0.0		
	k3:	1.90e-33	-1.44	0.0		
31		Phot Set= HNO3			1,24	HNO3 + HV = HO. + NO2
32	2.09e-13	k = k1 + k2 [M]			25	HO. + CO = HO2. + CO2
	k1:	1.30e-13	0.00	0.0		
	k2:	3.19e-33	0.00	0.0		
33	6.63e-14	1.90e-12	1.99		6	HO. + O3 = HO2. + O2

Label	Rate Parameters [a] k(298)	A	Ea	B	Refs & Notes [b]	Reaction and Products [c]
34	8.41e-12	3.40e-12	-0.54		6	HO2. + NO = HO. + NO2
35	1.38e-12	Falloff, F=0.60			6	HO2. + NO2 = HNO4
	0:	1.80e-31	0.00	-3.2		
	inf:	4.70e-12	0.00	0.0		
36	7.55e-2	Falloff, F=0.50			6	HNO4 = HO2. + NO2
	0:	4.10e-5	21.16	0.0		
	inf:	5.70e+15	22.20	0.0		
37	Phot Set= HO2NO2				1,26	HNO4 + HV = #.61 {HO2. + NO2} + #.39 {HO. + NO3}
38	5.02e-12	1.50e-12	-0.72		6	HNO4 + HO. = H2O + NO2 + O2
39	1.87e-15	1.40e-14	1.19		6	HO2. + O3 = HO. + #2 O2
40A	2.87e-12	k = k1 + k2 [M]			27	HO2. + HO2. = HO2H + O2
	k1:	2.20e-13	-1.19	0.0		
	k2:	1.85e-33	-1.95	0.0		
40B	6.46e-30	k = k1 + k2 [M]			27	HO2. + HO2. + H2O = HO2H + O2 + H2O
	k1:	3.08e-34	-5.56	0.0		
	k2:	2.59e-54	-6.32	0.0		
41	4.00e-12	4.00e-12			28	NO3 + HO2. = #.8 {HO. + NO2 + O2} + #.2 {HNO3 + O2}
42	2.28e-16	8.50e-13	4.87		29	NO3 + NO3 = #2 NO2 + O2
43	Phot Set= H2O2				1,30	HO2H + HV = #2 HO.
44	1.70e-12	2.90e-12	0.32		6	HO2H + HO. = HO2. + H2O
45	1.11e-10	4.80e-11	-0.50		6	HO. + HO2. = H2O + O2
S2OH	9.77e-13	Falloff, F=0.45			6,31	HO. + SO2 = HO2. + SULF
	0:	4.00e-31	0.00	-3.3		
	inf:	2.00e-12	0.00	0.0		
H2OH	6.70e-15	7.70e-12	4.17		4	HO. + H2 = HO2. + H2O
Methyl peroxy and methoxy reactions						
MER1	7.29e-12	2.80e-12	-0.57		32,33	C-O2. + NO = NO2 + HCHO + HO2.
MER4	5.21e-12	3.80e-13	-1.55		32	C-O2. + HO2. = COOH + O2
MEN3	1.30e-12	1.30e-12			32	C-O2. + NO3 = HCHO + HO2. + NO2
MER5	2.65e-13	2.45e-14	-1.41		34	C-O2. + C-O2. = MEOH + HCHO + O2
MER6	1.07e-13	5.90e-13	1.01		34	C-O2. + C-O2. = #2 {HCHO + HO2.}
Peroxy Racical Operators						
RRNO	9.04e-12	2.70e-12	-0.72		35,36,33	RO2-R. + NO = NO2 + HO2.
RRH2	1.49e-11	1.90e-13	-2.58		36,37	RO2-R. + HO2. = ROOH + O2 + #-3 XC
RRN3	2.30e-12	2.30e-12			38,39	RO2-R. + NO3 = NO2 + O2 + HO2.
RRME	2.00e-13	2.00e-13			40,41	RO2-R. + C-O2. = HO2. + #.75 HCHO + #.25 MEOH
RRR2	3.50e-14	3.50e-14			42,41	RO2-R. + RO2-R. = HO2.
R2NO	Same k as rxn RRNO				43,44	R2O2. + NO = NO2
R2H2	Same k as rxn RRH2				43,44	R2O2. + HO2. = HO2.
R2N3	Same k as rxn RRN3				43,44	R2O2. + NO3 = NO2
R2ME	Same k as rxn RRME				43,44	R2O2. + C-O2. = C-O2.
R2RR	Same k as rxn RRR2				43,44,41	R2O2. + RO2-R. = RO2-R.
R2R3	Same k as rxn RRR2				43,44	R2O2. + R2O2. =
RNNO	Same k as rxn RRNO				43,45	RO2-N. + NO = RNO3
RNH2	Same k as rxn RRH2				43,45,46	RO2-N. + HO2. = ROOH + #3 XC

Label	Rate Parameters [a] k(298)	A	Ea	B	Refs & Notes [b]	Reaction and Products [c]
RNME	Same k as rxn RRME				43,45,47	RO2-N. + C-O2. = HO2. + #.25 MEOH + #.5 {MEK + PROD2} + #.75 HCHO + XC
RNN3	Same k as rxn RRN3				43,45,48	RO2-N. + NO3 = NO2 + O2 + HO2. + MEK + #2 XC
RNRR	Same k as rxn RRR2				43,45,47	RO2-N. + RO2-R. = HO2. + #.5 {MEK + PROD2} + O2 + XC
RNR2	Same k as rxn RRR2				43,44	RO2-N. + R2O2. = RO2-N.
RNRN	Same k as rxn RRR2				43,45,47	RO2-N. + RO2-N. = MEK + HO2. + PROD2 + O2 + #2 XC
Reactions of Acyl Peroxy Radicals, PAN, and PAN analogues						
APN2	1.05e-11	Falloff, F=0.30			49	CCO-O2. + NO2 = PAN
	0:	2.70e-28	0.00	-7.1		
	inf:	1.20e-11	0.00	-0.9		
DPAN	5.21e-4	Falloff, F=0.30			50	PAN = CCO-O2. + NO2
	0:	4.90e-3	24.05	0.0		
	inf:	4.00e+16	27.03	0.0		
APNO	2.13e-11	7.80e-12	-0.60		51	CCO-O2. + NO = C-O2. + CO2 + NO2
APH2	1.41e-11	4.30e-13	-2.07		52	CCO-O2. + HO2. = #.75 {CCO-OOH +O2} + #.25 {CCO-OH + O3}
APN3	4.00e-12	4.00e-12			53	CCO-O2. + NO3 = C-O2. + CO2 + NO2 + O2
APME	9.64e-12	1.80e-12	-0.99		54	CCO-O2. + C-O2. = CCO-OH + HCHO + O2
APRR	7.50e-12	7.50e-12			55,56	CCO-O2. + RO2-R. = CCO-OH
APR2	Same k as rxn APRR				43,44	CCO-O2. + R2O2. = CCO-O2.
APRN	Same k as rxn APRR				43,56,47	CCO-O2. + RO2-N. = CCO-OH + PROD2
APAP	1.55e-11	2.90e-12	-0.99		32	CCO-O2. + CCO-O2. = #2 {C-O2. + CO2} + O2
PPN2	1.21e-11	1.20e-11	0.00	-0.9	57,58	RCO-O2. + NO2 = PAN2
PAN2	4.43e-4	2.00e+15	25.44		59,58	PAN2 = RCO-O2. + NO2
PPNO	2.80e-11	1.25e-11	-0.48		60,58	RCO-O2. + NO = NO2 + CCHO + RO2-R. + CO2
PPH2	Same k as rxn APH2				61,58	RCO-O2. + HO2. = #.75 {RCO-OOH + O2} + #.25 {RCO-OH + O3}
PPN3	Same k as rxn APN3				61,58	RCO-O2. + NO3 = NO2 + CCHO + RO2-R. + CO2 + O2
PPME	Same k as rxn APME				61,58	RCO-O2. + C-O2. = RCO-OH + HCHO + O2
PPRR	Same k as rxn APRR				61,58	RCO-O2. + RO2-R. = RCO-OH + O2
PPR2	Same k as rxn APRR				61,44	RCO-O2. + R2O2. = RCO-O2.
PPRN	Same k as rxn APRR				61,47,58	RCO-O2. + RO2-N. = RCO-OH + PROD2 + O2
PPAP	Same k as rxn APAP				61,58	RCO-O2. + CCO-O2. = #2 CO2 + C-O2. + CCHO + RO2-R. + O2
PPPP	Same k as rxn APAP				61,58	RCO-O2. + RCO-O2. = #2 {CCHO + RO2-R. + CO2}
BPN2	1.37e-11	1.37e-11			62	BZCO-O2. + NO2 = PBZN
BPAN	3.12e-4	7.90e+16	27.82		63	PBZN = BZCO-O2. + NO2
BPNO	Same k as rxn PPNO				64,65	BZCO-O2. + NO = NO2 + CO2 + BZ-O. + R2O2.
BPH2	Same k as rxn APH2				64,65	BZCO-O2. + HO2. = #.75 {RCO-OOH + O2} + #.25 {RCO-OH + O3} + #4 XC
BPN3	Same k as rxn APN3				64,65	BZCO-O2. + NO3 = NO2 + CO2 + BZ-O. + R2O2. + O2
BPME	Same k as rxn APME				64,65	BZCO-O2. + C-O2. = RCO-OH + HCHO + O2 + #4 XC
BPRR	Same k as rxn APRR				64,65	BZCO-O2. + RO2-R. = RCO-OH + O2 + #4 XC
BPR2	Same k as rxn APRR				44,64	BZCO-O2. + R2O2. = BZCO-O2.

Label	Rate Parameters [a] k(298)	A	Ea	B	Refs & Notes [b]	Reaction and Products [c]
BPRN	Same k as rxn APRR				47,64,65	BZCO-O2. + RO2-N. = RCO-OH + PROD2 + O2 + #4 XC
BPAP	Same k as rxn APAP				64,65	BZCO-O2. + CCO-O2. = #2 CO2 + C-O2. + BZ-O. + R2O2.
BPPP	Same k as rxn APAP				64,58,65	BZCO-O2. + RCO-O2. = #2 CO2 + CCHO + RO2-R. + BZ-O. + R2O2.
BPBP	Same k as rxn APAP				64,65	BZCO-O2. + BZCO-O2. = #2 {BZ-O. + R2O2. + CO2}
MPN2	Same k as rxn PPN2				64,66	MA-RCO3. + NO2 = MA-PAN
MPPN	3.55e-4	1.60e+16	26.80		67	MA-PAN = MA-RCO3. + NO2
MPNO	Same k as rxn PPNO				64,66	MA-RCO3. + NO = NO2 + CO2 + HCHO + CCO-O2.
MPH2	Same k as rxn APH2				64,66	MA-RCO3. + HO2. = #.75 {RCO-OOH + O2} + #.25 {RCO-OH + O3} + XC
MPN3	Same k as rxn APN3				64,66	MA-RCO3. + NO3 = NO2 + CO2 + HCHO + CCO-O2. + O2
MPME	Same k as rxn APME				64,66	MA-RCO3. + C-O2. = RCO-OH + HCHO + XC + O2
MPRR	Same k as rxn APRR				64,66	MA-RCO3. + RO2-R. = RCO-OH + XC
MPR2	Same k as rxn APRR				44,64	MA-RCO3. + R2O2. = MA-RCO3.
MPRN	Same k as rxn APRR				64,66	MA-RCO3. + RO2-N. = #2 RCO-OH + O2 + #4 XC
MPAP	Same k as rxn APAP				64,66	MA-RCO3. + CCO-O2. = #2 CO2 + C-O2. + HCHO + CCO-O2. + O2
MPPP	Same k as rxn APAP				64,66	MA-RCO3. + RCO-O2. = HCHO + CCO-O2. + CCHO + RO2-R. + #2 CO2
MPBP	Same k as rxn APAP				64,66	MA-RCO3. + BZCO-O2. = HCHO + CCO-O2. + BZ-O. + R2O2. + #2 CO2
MPMP	Same k as rxn APAP				64,66	MA-RCO3. + MA-RCO3. = #2 {HCHO + CCO-O2. + CO2}
Other Organic Radical Species						
TBON	2.40e-11	2.40e-11			68,69	TBU-O. + NO2 = RNO3 + #-2 XC
TBOD	9.87e+2	7.50e+14	16.20		70,69	TBU-O. = ACET + C-O2.
BRN2	3.80e-11	2.30e-11	-0.30		71	BZ-O. + NO2 = NPHE
BRH2	Same k as rxn RRH2				72	BZ-O. + HO2. = PHEN
BRXX	1.00e-3	1.00e-3			73	BZ-O. = PHEN
BNN2	Same k as rxn BRN2				74	BZ(NO2)-O. + NO2 = #2 XN + #6 XC
BNH2	Same k as rxn RRH2				72	BZ(NO2)-O. + HO2. = NPHE
BNXX	Same k as rxn BRXX				73	BZ(NO2)-O. = NPHE
Explicit and Lumped Molecule Organic Products						
FAHV	Phot Set= HCHO_R				75	HCHO + HV = #2 HO2. + CO
FAVS	Phot Set= HCHO_M				75	HCHO + HV = H2 + CO
FAOH	9.20e-12	8.60e-12	-0.04		32	HCHO + HO. = HO2. + CO + H2O
FAH2	7.90e-14	9.70e-15	-1.24		32	HCHO + HO2. = HOCOO.
FAHR	1.51e+2	2.40e+12	13.91		32	HOCOO. = HO2. + HCHO
FAHN	Same k as rxn MER1				76	HOCOO. + NO = HCOOH + NO2 + HO2.
FAN3	5.74e-16	2.00e-12	4.83		77	HCHO + NO3 = HNO3 + HO2. + CO
AAOH	1.58e-11	5.60e-12	-0.62		32	CCHO + HO. = CCO-O2. + H2O
AAHV	Phot Set= CCHO_R				78	CCHO + HV = CO + HO2. + C-O2.
AAN3	2.73e-15	1.40e-12	3.70		79	CCHO + NO3 = HNO3 + CCO-O2.

Label	Rate Parameters [a] k(298)	A	Ea	B	Refs & Notes [b]	Reaction and Products [c]
PAOH	2.00e-11	2.00e-11			80,32,81, 82	RCHO + HO. = #.034 RO2-R. + #.001 RO2-N. + #.965 RCO-O2. + #.034 CO + #.034 CCHO + #-0.003 XC
PAHV	Phot Set= C2CHO				80,78	RCHO + HV = CCHO + RO2-R. + CO + HO2.
PAN3	3.67e-15	1.40e-12	3.52		80,83	RCHO + NO3 = HNO3 + RCO-O2.
K3OH	1.92e-13	1.10e-12	1.03		32,84	ACET + HO. = HCHO + CCO-O2. + R2O2.
K3HV	Phot Set= ACETONE				85	ACET + HV = CCO-O2. + C-O2.
K4OH	1.18e-12	1.30e-12	0.05	2.0	32,81,82	MEK + HO. = #.37 RO2-R. + #.042 RO2-N. + #.616 R2O2. + #.492 CCO-O2. + #.096 RCO-O2. + #.115 HCHO + #.482 CCHO + #.37 RCHO + #.287 XC
K4HV	Phot Set= KETONE, qy= 1.5e-1				86	MEK + HV = CCO-O2. + CCHO + RO2-R.
MeOH	9.14e-13	3.10e-12	0.72	2.0	87	MEOH + HO. = HCHO + HO2.
MER9	5.49e-12	2.90e-12	-0.38		88	COOH + HO. = H2O + #.35 {HCHO + HO.} + #.65 C-O2.
MERA	Phot Set= COOH				89	COOH + HV = HCHO + HO2. + HO.
LPR9	1.10e-11	1.10e-11			90,91	ROOH + HO. = H2O + RCHO + #.34 RO2-R. + #.66 HO.
LPRA	Phot Set= COOH				92	ROOH + HV = RCHO + HO2. + HO.
GLHV	Phot Set= GLY_R				93,94	GLY + HV = #2 {CO + HO2.}
GLVM	Phot Set= GLY_ABS, qy= 6.0e-3				93,95	GLY + HV = HCHO + CO
GLOH	1.10e-11	1.10e-11			32,96,97	GLY + HO. = #.63 HO2. + #1.26 CO + #.37 RCO-O2. + #-.37 XC
GLN3	9.63e-16	2.80e-12	4.72		97,98	GLY + NO3 = HNO3 + #.63 HO2. + #1.26 CO + #.37 RCO-O2. + #-.37 XC
MGHV	Phot Set= MGLY_ADJ				99	MGLY + HV = HO2. + CO + CCO-O2.
MGOH	1.50e-11	1.50e-11			32	MGLY + HO. = CO + CCO-O2.
MGN3	2.43e-15	1.40e-12	3.77		98	MGLY + NO3 = HNO3 + CO + CCO-O2.
BAHV	Phot Set= BACL_ADJ				100,101	BACL + HV = #2 CCO-O2.
PHOH	2.63e-11	2.63e-11			102,103	PHEN + HO. = #.24 BZ-O. + #.76 RO2-R. + #.23 GLY + #4.1 XC
PHN3	3.78e-12	3.78e-12			102,104	PHEN + NO3 = HNO3 + BZ-O.
CROH	4.20e-11	4.20e-11			102,105	CRES + HO. = #.24 BZ-O. + #.76 RO2-R. + #.23 MGLY + #4.87 XC
CRN3	1.37e-11	1.37e-11			102,104	CRES + NO3 = HNO3 + BZ-O. + XC
NPN3	Same k as rxn PHN3				106	NPHE + NO3 = HNO3 + BZ(NO2)-O.
BZOH	1.29e-11	1.29e-11			102	BALD + HO. = BZCO-O2.
BZHV	Phot Set= BZCHO, qy= 5.0e-2				107	BALD + HV = #7 XC
BZNT	2.62e-15	1.40e-12	3.72		108	BALD + NO3 = HNO3 + BZCO-O2.
MAOH	3.36e-11	1.86e-11	-0.35		109,82, 110	METHACRO + HO. = #.5 RO2-R. + #.416 CO + #.084 HCHO + #.416 MEK + #.084 MGLY + #.5 MA-RCO3. + #-0.416 XC
MAO3	1.13e-18	1.36e-15	4.20		109,111, 112,113	METHACRO + O3 = #.008 HO2. + #.1 RO2-R. + #.208 HO. + #.1 RCO-O2. + #.45 CO + #.117 CO2 + #.2 HCHO + #.9 MGLY + #.333 HCOOH + #-0.1 XC
MAN3	4.58e-15	1.50e-12	3.43		109,114, 82,115	METHACRO + NO3 = #.5 {HNO3 + RO2-R. + CO +MA-RCO3.} + #1.5 XC + #.5 XN

Label	Rate Parameters [a] k(298)	A	Ea	B	Refs & Notes [b]	Reaction and Products [c]
MAOP	6.34e-12	6.34e-12			116,5	METHACRO + O3P = RCHO + XC
MAHV	Phot Set= ACROLEIN, qy= 4.1e-3				109,117	METHACRO + HV = #.34 HO2. + #.33 RO2-R. + #.33 HO. + #.67 CCO-O2. + #.67 CO + #.67 HCHO + #.33 MA-RCO3. + #-0 XC
MVOH	1.89e-11	4.14e-12	-0.90		109,82	MVK + HO. = #.3 RO2-R. + #.025 RO2-N. + #.675 R2O2. + #.675 CCO-O2. + #.3 HCHO + #.675 RCHO + #.3 MGLY + #-0.725 XC
MVO3	4.58e-18	7.51e-16	3.02		109,111, 112,82 113	MVK + O3 = #.064 HO2. + #.05 RO2-R. + #.164 HO. + #.05 RCO-O2. + #.475 CO + #.124 CO2 + #.1 HCHO + #.95 MGLY + #.351 HCOOH + #-0.05 XC
MVN3		(Slow)			109	MVK + NO3 = #4 XC + XN
MVOP	4.32e-12	4.32e-12			116,5	MVK + O3P = #.45 RCHO + #.55 MEK + #.45 XC
MVHV	Phot Set= ACROLEIN, qy= 2.1e-3				109,117, 118	MVK + HV = #.3 C-O2. + #.7 CO + #.7 PROD2 + #.3 MA-RCO3. + #-2.4 XC
IPOH	6.19e-11	6.19e-11			119,109, 82	ISO-PROD + HO. = #.67 RO2-R. + #.041 RO2-N. + #.289 MA-RCO3. + #.336 CO + #.055 HCHO + #.129 CCHO + #.013 RCHO + #.15 MEK + #.332 PROD2 + #.15 GLY + #.174 MGLY + #-0.504 XC
IPO3	4.18e-18	4.18e-18			119,109, 82,120, 112,121, 113	ISO-PROD + O3 = #.4 HO2. + #.048 RO2-R. + #.048 RCO-O2. + #.285 HO. + #.498 CO + #.14 CO2 + #.125 HCHO + #.047 CCHO + #.21 MEK + #.023 GLY + #.742 MGLY + #.1 HCOOH + #.372 RCO-OH + #-.33 XC
IPN3	1.00e-13	1.00e-13			119,109, 82	ISO-PROD + NO3 = #.799 RO2-R. + #.051 RO2-N. + #.15 MA-RCO3. + #.572 CO + #.15 HNO3 + #.227 HCHO + #.218 RCHO + #.008 MGLY + #.572 RNO3 + #.28 XN + #-.815 XC
IPHV	Phot Set= ACROLEIN, qy= 4.1e-3				119,109, 82,122	ISO-PROD + HV = #1.233 HO2. + #.467 CCO-O2. + #.3 RCO-O2. + #1.233 CO + #.3 HCHO + #.467 CCHO + #.233 MEK + #-.233 XC
Lumped Parameter Organic Products						
K6OH	1.50e-11	1.50e-11			123	PROD2 + HO. = #.379 HO2. + #.473 RO2-R. + #.07 RO2-N. + #.029 CCO-O2. + #.049 RCO-O2. + #.213 HCHO + #.084 CCHO + #.558 RCHO + #.115 MEK + #.329 PROD2 + #.886 XC
K6HV	Phot Set= KETONE, qy= 2.0e-2				123,124	PROD2 + HV = #.96 RO2-R. + #.04 RO2-N. + #.515 R2O2. + #.667 CCO-O2. + #.333 RCO-O2. + #.506 HCHO + #.246 CCHO + #.71 RCHO + #.299 XC
RNOH	7.80e-12	7.80e-12			125	RNO3 + HO. = #.338 NO2 + #.113 HO2. + #.376 RO2-R. + #.173 RO2-N. + #.596 R2O2. + #.01 HCHO + #.439 CCHO + #.213 RCHO + #.006 ACET + #.177 MEK + #.048 PROD2 + #.31 RNO3 + #.351 XN + #.56 XC
RNHV	Phot Set= IC3ONO2				125,126	RNO3 + HV = NO2 + #.341 HO2. + #.564 RO2-R. + #.095 RO2-N. + #.152 R2O2. + #.134 HCHO + #.431 CCHO + #.147 RCHO + #.02 ACET + #.243 MEK + #.435 PROD2 + #.35 XC

Label	Rate Parameters [a] k(298)	A	Ea	B	Refs & Notes [b]	Reaction and Products [c]
Uncharacterized Reactive Aromatic Ring Fragmentation Products						
D1OH	5.00e-11	5.00e-11			127,128	DCB1 + HO. = RCHO + RO2-R. + CO
D1HV		(Slow)			127,129	DCB1 + HV = HO2. + #2 CO + RO2-R. + GLY + R2O2.
D1O3	2.00e-18	2.00e-18			127,130, 120	DCB1 + O3 = #1.5 HO2. + #.5 HO. + #1.5 CO + #.5 CO2 + GLY
D2OH	5.00e-11	5.00e-11			131,132	DCB2 + HO. = R2O2. + RCHO + CCO-O2.
D2HV	Phot Set= MGLY_ABS, qy= 3.7e-1				131,133	DCB2 + HV = RO2-R. + #.5 {CCO-O2. + HO2.} + CO + R2O2. + #.5 {GLY + MGLY + XC}
D3OH	5.00e-11	5.00e-11			131,132	DCB3 + HO. = R2O2. + RCHO + CCO-O2.
D3HV	Phot Set= ACROLEIN, qy= 7.3e+0				131,133	DCB3 + HV = RO2-R. + #.5 {CCO-O2. + HO2.} + CO + R2O2. + #.5 {GLY + MGLY + XC}

[a] Except as indicated, the rate constants are given by $k(T) = A \cdot (T/300)^{B} \cdot e^{-Ea/RT}$, where the units of k and A are $cm^3\ molec^{-1}\ s^{-1}$, Ea are kcal mol^{-1}, T is °K, and R=0.0019872 kcal $mol^{-1}\ deg^{-1}$. The following special rate constant expressions are used:

Phot Set = *name*: The absorption cross sections and quantum yields for the photolysis reaction are given in Table A-5, where "*name*" indicates the photolysis set used. If a "qy=*number*" notation is given, the number given is the overall quantum yield, which is assumed to be wavelength independent.

Falloff: The rate constant as a function of temperature and pressure is calculated using $k(T,M) = \{k0(T)\cdot[M]/[1 + k0(T)\cdot[M]/kinf(T)]\}\cdot F^{Z}$, where $Z = \{1 + [\log_{10}\{k0(T)\cdot[M])/kinf(T)\}]^2\}^{-1}$, [M] is the total pressure in molecules cm^{-3}, F is as indicated on the table, and the temperature dependences of k0 and kinf are as indicated on the table.

(Slow): The reaction is assumed to be negligible and is not included in the mechanism. It is shown on the listing for documentation purposes only.

k = k0+k3M(1+k3M/k2): The rate constant as a function of temperature and pressure is calculated using $k(T,M) = k0(T) + k3(T)\cdot[M] \cdot(1 + k3(T)\cdot[M]/k2(T))$, where [M] is the total bath gas (air) concentration in molecules cm^{-3}, and the temperature dependences for k0, k2 and k3 are as indicated on the table.

k = k1 + k2 [M]: The rate constant as a function of temperature and pressure is calculated using $k(T,M) = k1(T) + k2(T)\cdot[M]$, where [M] is the total bath gas (air) concentration in molecules cm^{-3}, and the temperature dependences for k1, and k2 are as indicated on the table.

Same k as Rxn *label*: The rate constant is the same as the reaction with the indicated label.

[c] Footnotes given in Table A-3.

[b] Format of reaction listing: "=" separates reactants from products; "#*number*" indicates stoichiometric coefficient, "#*coefficient* { *product list* }" means that the stoichiometric coefficient is applied to all the products listed.

Table A-1.4. Listing of reactions added to the SAPRC99 base mechanism to constitute the fixed parameter lumped mechanism (Carter, 2000).

Label	Rate Parameters [a] k(298)	A	Ea	B	Refs & Notes [a]	Reaction and Products [a]
Explicitly Represented Primary Organics						
c1OH	6.37e-15	2.15e-12	3.45		32	CH4 + HO. = H2O + C-O2.
etOH	8.52e-12	1.96e-12	-0.87		134	ETHENE + HO. = RO2-R. + #1.61 HCHO + #.195 CCHO
etO3	1.59e-18	9.14e-15	5.13		134	ETHENE + O3 = #.12 HO. + #.12 HO2. + #.5 CO + #.13 CO2 + HCHO + #.37 HCOOH
etN3	2.05e-16	4.39e-13	4.53	2.0	134	ETHENE + NO3 = RO2-R. + RCHO + #-1 XC + XN
etOA	7.29e-13	1.04e-11	1.57		134	ETHENE + O3P = #.5 HO2. + #.2 RO2-R. + #.3 C-O2. + #.491 CO + #.191 HCHO + #.25 CCHO + #.009 GLY + #.5 XC
isOH	9.82e-11	2.50e-11	-0.81		134,135	ISOPRENE + HO. = #.907 RO2-R. + #.093 RO2-N. + #.079 R2O2. + #.624 HCHO + #.23 METHACRO + #.32 MVK + #.357 ISO-PROD + #-0.167 XC
isO3	1.28e-17	7.86e-15	3.80		134,135	ISOPRENE + O3 = #.266 HO. + #.066 RO2-R. + #.008 RO2-N. + #.126 R2O2. + #.192 MA-RCO3. + #.275 CO + #.122 CO2 + #.592 HCHO + #.1 PROD2 + #.39 METHACRO + #.16 MVK + #.204 HCOOH + #.15 RCO-OH + #-0.259 XC
isN3	6.74e-13	3.03e-12	0.89		134,135	ISOPRENE + NO3 = #.187 NO2 + #.749 RO2-R. + #.064 RO2-N. + #.187 R2O2. + #.936 ISO-PROD + #-0.064 XC + #.813 XN
isOP	3.60e-11	3.60e-11			134,135	ISOPRENE + O3P = #.01 RO2-N. + #.24 R2O2. + #.25 C-O2. + #.24 MA-RCO3. + #.24 HCHO + #.75 PROD2 + #-1.01 XC
Lumped Terpenes (Based on estimated North America annual emissions rate of top 5 terpenes.)						
t1OH	8.27e-11	1.83e-11	-0.89		134,136	TERP + HO. = #.75 RO2-R. + #.25 RO2-N. + #.5 R2O2. + #.276 HCHO + #.474 RCHO + #.276 PROD2 + #5.146 XC
t1O3	6.88e-17	1.08e-15	1.63		134,136	TERP + O3 = #.567 HO. + #.033 HO2. + #.031 RO2-R. + #.18 RO2-N. + #.729 R2O2. + #.123 CCO-O2. + #.201 RCO-O2. + #.157 CO + #.037 CO2 + #.235 HCHO + #.205 RCHO + #.13 ACET + #.276 PROD2 + #.001 GLY + #.031 BACL + #.103 HCOOH + #.189 RCO-OH + #4.183 XC
t1N3	6.57e-12	3.66e-12	-0.35		134,136	TERP + NO3 = #.474 NO2 + #.276 RO2-R. + #.25 RO2-N. + #.75 R2O2. + #.474 RCHO + #.276 RNO3 + #5.421 XC + #.25 XN
t1OP	3.27e-11	3.27e-11			134,136	TERP + O3P = #.147 RCHO + #.853 PROD2 + #4.441 XC
Lumped Primary Organics (Based on base ROG mixture used in reactivity scenarios)						
a1OH	2.54e-13	1.37e-12	0.99	2.0	134,137	ALK1 + HO. = RO2-R. + CCHO
a2OH	1.04e-12	9.87e-12	1.33		134,138	ALK2 + HO. = #.246 HO. + #.121 HO2. + #.612 RO2-R. + #.021 RO2-N. + #.16 CO + #.039 HCHO + #.155 RCHO + #.417 ACET + #.248 GLY + #.121 HCOOH + #0.338 XC
a3OH	2.38e-12	1.02e-11	0.86		134,139	ALK3 + HO. = #.695 RO2-R. + #.07 RO2-N. + #.559 R2O2. + #.236 TBU-O. + #.026 HCHO + #.445 CCHO + #.122 RCHO + #.024 ACET + #.332 MEK + #-0.05 XC

Label	Rate Parameters [a]				Refs &	Reaction and Products [a]
	k(298)	A	Ea	B	Notes [a]	
a4OH	4.39e-12	5.95e-12	0.18		134,139	ALK4 + HO. = #.835 RO2-R. + #.143 RO2-N. + #.936 R2O2. + #.011 C-O2. + #.011 CCO-O2. + #.002 CO + #.024 HCHO + #.455 CCHO + #.244 RCHO + #.452 ACET + #.11 MEK + #.125 PROD2 + #-0.105 XC
a5OH	9.34e-12	1.11e-11	0.10		134,139	ALK5 + HO. = #.653 RO2-R. + #.347 RO2-N. + #.948 R2O2. + #.026 HCHO + #.099 CCHO + #.204 RCHO + #.072 ACET + #.089 MEK + #.417 PROD2 + #2.008 XC
b1OH	5.95e-12	1.81e-12	-0.71		134,140	ARO1 + HO. = #.224 HO2. + #.765 RO2-R. + #.011 RO2-N. + #.055 PROD2 + #.118 GLY + #.119 MGLY + #.017 PHEN + #.207 CRES + #.059 BALD + #.491 DCB1 + #.108 DCB2 + #.051 DCB3 + #1.288 XC
b2OH	2.64e-11	2.64e-11	0.00		134,139	ARO2 + HO. = #.187 HO2. + #.804 RO2-R. + #.009 RO2-N. + #.097 GLY + #.287 MGLY + #.087 BACL + #.187 CRES + #.05 BALD + #.561 DCB1 + #.099 DCB2 + #.093 DCB3 + #1.68 XC
o1OH	3.23e-11	7.10e-12	-0.90		134,139	OLE1 + HO. = #.91 RO2-R. + #.09 RO2-N. + #.205 R2O2. + #.732 HCHO + #.294 CCHO + #.497 RCHO + #.005 ACET + #.119 PROD2 + #.92 XC
o1O3	1.06e-17	2.62e-15	3.26		134,139	OLE1 + O3 = #.155 HO. + #.056 HO2. + #.022 RO2-R. + #.001 RO2-N. + #.076 C-O2. + #.345 CO + #.086 CO2 + #.5 HCHO + #.154 CCHO + #.363 RCHO + #.001 ACET + #.215 PROD2 + #.185 HCOOH + #.05 CCO-OH + #.119 RCO-OH + #.654 XC
o1N3	1.26e-14	4.45e-14	0.75		134,139	OLE1 + NO3 = #.824 RO2-R. + #.176 RO2-N. + #.488 R2O2. + #.009 CCHO + #.037 RCHO + #.024 ACET + #.511 RNO3 + #.677 XC + #.489 XN
o1OP	4.90e-12	1.07e-11	0.47		134,139	OLE1 + O3P = #.45 RCHO + #.437 MEK + #.113 PROD2 + #1.224 XC
o2OH	6.33e-11	1.74e-11	-0.76		134,139	OLE2 + HO. = #.918 RO2-R. + #.082 RO2-N. + #.001 R2O2. + #.244 HCHO + #.732 CCHO + #.511 RCHO + #.127 ACET + #.072 MEK + #.061 BALD + #.025 METHACRO + #.025 ISO-PROD + #-.054 XC
o2O3	1.07e-16	5.02e-16	0.92		134,139	OLE2 + O3 = #.378 HO. + #.003 HO2. + #.033 RO2-R. + #.002 RO2-N. + #.137 R2O2. + #.197 C-O2. + #.137 CCO-O2. + #.006 RCO-O2. + #.265 CO + #.07 CO2 + #.269 HCHO + #.456 CCHO + #.305 RCHO + #.045 ACET + #.026 MEK + #.006 PROD2 + #.042 BALD + #.026 METHACRO + #.073 HCOOH + #.129 CCO-OH + #.303 RCO-OH + #.155 XC
o2N3	7.27e-13	7.27e-13	0.00		134,139	OLE2 + NO3 = #.391 NO2 + #.442 RO2-R. + #.136 RO2-N. + #.711 R2O2. + #.03 C-O2. + #.079 HCHO + #.507 CCHO + #.151 RCHO + #.102 ACET + #.001 MEK + #.015 BALD + #.048 MVK + #.321 RNO3 + #.075 XC + #.288 XN
o2OP	2.09e-11	2.09e-11			134,139	OLE2 + O3P = #.013 HO2. + #.012 RO2-R. + #.001 RO2-N. + #.012 CO + #.069 RCHO + #.659 MEK + #.259 PROD2 + #.012 METHACRO + #.537 XC

Table A-1.5. Listing of model species used in the base and lumped mechanisms in SAPRC99 (Carter, 2000).

Type and Name	Description
	Species used in Base Mechanism
Constant Species.	
O2	Oxygen
M	Air
H2O	Water
H2	Hydrogen Molecules
HV	Light
Active Inorganic Species.	
O3	Ozone
NO	Nitric Oxide
NO2	Nitrogen Dioxide
NO3	Nitrate Radical
N2O5	Nitrogen Pentoxide
HONO	Nitrous Acid
HNO3	Nitric Acid
HNO4	Peroxynitric Acid
HO2H	Hydrogen Peroxide
CO	Carbon Monoxide
SO2	Sulfur Dioxide
Active Radical Species and Operators.	
HO.	Hydroxyl Radicals
HO2.	Hydroperoxide Radicals
C-O2.	Methyl Peroxy Radicals
RO2-R.	Peroxy Radical Operator representing NO to NO2 conversion with HO2 formation.
R2O2.	Peroxy Radical Operator representing NO to NO2 conversion without HO2 formation.
RO2-N.	Peroxy Radical Operator representing NO consumption with organic nitrate formation.
CCO-O2.	Acetyl Peroxy Radicals
RCO-O2.	Peroxy Propionyl and higher peroxy acyl Radicals
BZCO-O2.	Peroxyacyl radical formed from Aromatic Aldehydes
MA-RCO3.	Peroxyacyl radicals formed from methacrolein and other acroleins.
Steady State Radical Species	
O3P	Ground State Oxygen Atoms
O*1D2	Excited Oxygen Atoms
TBU-O.	t-Butoxy Radicals
BZ-O.	Phenoxy Radicals
BZ(NO2)-O.	Nitro-substituted Phenoxy Radical
HOCOO.	Radical formed when Formaldehyde reacts with HO2
PAN and PAN Analogues	
PAN	Peroxy Acetyl Nitrate
PAN2	PPN and other higher alkyl PAN analogues
PBZN	PAN analogues formed from Aromatic Aldehydes
MA-PAN	PAN analogue formed from Methacrolein

Type and Name	Description
Explicit and Lumped Molecule Reactive Organic Product Species	
HCHO	Formaldehyde
CCHO	Acetaldehyde
RCHO	Lumped C3+ Aldehydes
ACET	Acetone
MEK	Ketones and other non-aldehyde oxygenated products which react with OH radicals slower than 5 x 10^{-12} cm^3 $molec^{-2}$ sec^{-1}.
MEOH	Methanol
COOH	Methyl Hydroperoxide
ROOH	Lumped higher organic hydroperoxides
GLY	Glyoxal
MGLY	Methyl Glyoxal
BACL	Biacetyl
PHEN	Phenol
CRES	Cresols
NPHE	Nitrophenols
BALD	Aromatic aldehydes (e.g., benzaldehyde)
METHACRO	Methacrolein
MVK	Methyl Vinyl Ketone
ISO-PROD	Lumped isoprene product species
Lumped Parameter Products	
PROD2	Ketones and other non-aldehyde oxygenated products which react with OH radicals faster than 5 x 10^{-12} cm^3 $molec^{-2}$ sec^{-1}.
RNO3	Lumped Organic Nitrates
Uncharacterized Reactive Aromatic Ring Fragmentation Products	
DCB1	Reactive Aromatic Fragmentation Products that do not undergo signficant photodecomposition to radicals.
DCB2	Reactive Aromatic Fragmentation Products which photolyze with alpha-dicarbonyl-like action spectrum.
DCB3	Reactive Aromatic Fragmentation Products which photolyze with acrolein action spectrum.
Non-Reacting Species	
CO2	Carbon Dioxide
XC	Lost Carbon
XN	Lost Nitrogen
SULF	Sulfates (SO_3 or H_2SO_4)
Low Reactivity Compounds or Unknown Products Represented as Unreactive	
H2	Hydrogen
HCOOH	Formic Acid
CCO-OH	Acetic Acid
RCO-OH	Higher organic acids
CCO-OOH	Peroxy Acetic Acid
RCO-OOH	Higher organic peroxy acids
NROG	Unspecified Unreactive Carbon

Type and Name	Description
Species used in Lumped Mechanisms for Base Case and Ambient Simulations	
Primary Organics Represented explicitly	
CH4	Methane
ETHENE	Ethene
ISOPRENE	Isoprene
Lumped Parameter Species	
ALK1	Alkanes and other non-aromatic compounds that react only with OH, and have kOH < 5 x 10^2 ppm-1 min-1. (Primarily ethane)
ALK2	Alkanes and other non-aromatic compounds that react only with OH, and have kOH between 5 x 10^2 and 2.5 x 10^3 ppm-1 min-1. (Primarily propane and acetylene)
ALK3	Alkanes and other non-aromatic compounds that react only with OH, and have kOH between 2.5 x 10^3 and 5 x 10^3 ppm-1 min-1.
ALK4	Alkanes and other non-aromatic compounds that react only with OH, and have kOH between 5 x 10^3 and 1 x 10^4 ppm-1 min-1.
ALK5	Alkanes and other non-aromatic compounds that react only with OH, and have kOH greater than 1 x 10^4 ppm-1 min-1.
ARO1	Aromatics with kOH < 2x10^4 ppm-1 min-1.
ARO2	Aromatics with kOH > 2x10^4 ppm-1 min-1.
OLE1	Alkenes (other than ethene) with kOH < 7x10^4 ppm-1 min-1.
OLE2	Alkenes with kOH > 7x10^4 ppm-1 min-1.
TERP	Terpenes

SAPRC07

Table A-1.6. Listing of reactions and rate parameters in the base SAPRC07 mechanism (Carter, 2007).

Label	Reaction and Products [a]	Rate Parameters [b]			
		k(300)	A	Ea	B
Inorganic Reactions					
1	NO2 + HV = NO + O3P	Phot Set= NO2-06			
2	O3P + O2 + M = O3 + M	5.68e-34	5.68e-34	0.00	-2.60
3	O3P + O3 = #2 O2	8.34e-15	8.00e-12	4.09	
4	O3P + NO = NO2	1.64e-12	Falloff, F=0.60, N=1.00		
		0:	9.00e-32	0.00	-1.50
		inf:	3.00e-11	0.00	0.00
5	O3P + NO2 = NO + O2	1.03e-11	5.50e-12	-0.37	
6	O3P + NO2 = NO3	3.24e-12	Falloff, F=0.60, N=1.00		
		0:	2.50e-31	0.00	-1.80
		inf:	2.20e-11	0.00	-0.70
7	O3 + NO = NO2 + O2	2.02e-14	3.00e-12	2.98	
8	O3 + NO2 = O2 + NO3	3.72e-17	1.40e-13	4.91	
9	NO + NO3 = #2 NO2	2.60e-11	1.80e-11	-0.22	
10	NO + NO + O2 = #2 NO2	1.93e-38	3.30e-39	-1.05	
11	NO2 + NO3 = N2O5	1.24e-12	Falloff, F=0.35, N=1.33		

Label	Reaction and Products [a]	Rate Parameters [b]			
		k(300)	A	Ea	B
		0:	3.60e-30	0.00	-4.10
		inf:	1.90e-12	0.00	0.20
12	N2O5 = NO2 + NO3	5.69e-2	Falloff, F=0.35, N=1.33		
		0:	1.30e-3	21.86	-3.50
		inf:	9.70e+14	22.02	0.10
13	N2O5 + H2O = #2 HNO3	2.50e-22			
14	N2O5 + H2O + H2O = #2 HNO3 + H2O	1.80e-39			
	N2O5 + HV = NO3 + NO + O3P		(Slow)		
	N2O5 + HV = NO3 + NO2		(Slow)		
15	NO2 + NO3 = NO + NO2 + O2	6.75e-16	4.50e-14	2.50	
16	NO3 + HV = NO + O2		Phot Set= NO3NO-06		
17	NO3 + HV = NO2 + O3P		Phot Set= NO3NO2-6		
18	O3 + HV = O1D + O2		Phot Set= O3O1D-06		
19	O3 + HV = O3P + O2		Phot Set= O3O3P-06		
20	O1D + H2O = #2 OH	1.99e-10			
21	O1D + M = O3P + M	3.28e-11	2.38e-11	-0.19	
22	OH + NO = HONO	7.31e-12	Falloff, F=0.60, N=1.00		
		0:	7.00e-31	0.00	-2.60
		inf:	3.60e-11	0.00	-0.10
23	HONO + HV = OH + NO		Phot Set= HONO-06		
24	OH + HONO = H2O + NO2	5.95e-12	2.50e-12	-0.52	
25	OH + NO2 = HNO3	1.05e-11	Falloff, F=0.60, N=1.00		
		0:	1.80e-30	0.00	-3.00
		inf:	2.80e-11	0.00	0.00
26	OH + NO3 = HO2 + NO2	2.00e-11			
27	OH + HNO3 = H2O + NO3	1.51e-13	k = k0+k3M/(1+k3M/k2)		
		k0:	2.40e-14	-0.91	0.00
		k2:	2.70e-17	-4.37	0.00
		k3:	6.50e-34	-2.65	0.00
28	HNO3 + HV = OH + NO2		Phot Set= HNO3		
29	OH + CO = HO2 + CO2	2.28e-13	k = k1 + k2 [M]		
		k1:	1.44e-13	0.00	0.00
		k2:	3.43e-33	0.00	0.00
30	OH + O3 = HO2 + O2	7.41e-14	1.70e-12	1.87	
31	HO2 + NO = OH + NO2	8.85e-12	3.60e-12	-0.54	
32	HO2 + NO2 = HNO4	1.12e-12	Falloff, F=0.60, N=1.00		
		0:	2.00e-31	0.00	-3.40
		inf:	2.90e-12	0.00	-1.10
33	HNO4 = HO2 + NO2	1.07e-1	Falloff, F=0.60, N=1.00		
		0:	3.72e-5	21.16	-2.40
		inf:	5.42e+15	22.20	-2.30
34	HNO4 + HV = #.61 {HO2 + NO2} + #.39 {OH + NO3}		Phot Set= HNO4-06		
35	HNO4 + OH = H2O + NO2 + O2	4.61e-12	1.30e-12	-0.76	

Label	Reaction and Products [a]	Rate Parameters [b]			
		k(300)	A	Ea	B
36	HO2 + O3 = OH + #2 O2	1.69e-15	2.03e-16	-1.26	4.57
37	HO2 + HO2 = HO2H + O2	2.84e-12	k = k1 + k2 [M]		
		k1:	2.20e-13	-1.19	0.00
		k2:	1.90e-33	-1.95	0.00
38	HO2 + HO2 + H2O = HO2H + O2 + H2O	6.09e-30	k = k1 + k2 [M]		
		k1:	3.08e-34	-5.56	0.00
		k2:	2.66e-54	-6.32	0.00
39	NO3 + HO2 = #.8 {OH + NO2 + O2} + #.2 {HNO3 + O2}	4.00e-12			
40	NO3 + NO3 = #2 NO2 + O2	2.41e-16	8.50e-13	4.87	
41	HO2H + HV = #2 OH	Phot Set= H2O2			
42	HO2H + OH = HO2 + H2O	1.80e-12	1.80e-12	0.00	
43	OH + HO2 = H2O + O2	1.10e-10	4.80e-11	-0.50	
44	OH + SO2 = HO2 + SULF	9.49e-13	Falloff, F=0.60, N=1.00		
		0:	3.30e-31	0.00	-4.30
		inf:	1.60e-12	0.00	0.00
45	OH + H2 = HO2 + H2O	7.02e-15	7.70e-12	4.17	

Label	Reaction and Products [a]	Rate Parameters [b]			
		k(300)	A	Ea	B
Methyl peroxy and methoxy reactions					
BR01	MEO2 + NO = NO2 + HCHO + HO2	7.64e-12	2.30e-12	-0.72	
BR02	MEO2 + HO2 = COOH + O2	4.65e-12	3.46e-13	-1.55	0.36
BR03	MEO2 + HO2 = HCHO + O2 + H2O	4.50e-13	3.34e-14	-1.55	-3.53
BR04	MEO2 + NO3 = HCHO + HO2 + NO2	1.30e-12			
BR05	MEO2 + MEO2 = MEOH + HCHO + O2	2.16e-13	6.39e-14	-0.73	-1.80
BR06	MEO2 + MEO2 = #2 {HCHO + HO2}	1.31e-13	7.40e-13	1.03	
Active Peroxy Racical Operators					
BR07	RO2C + NO = NO2	9.23e-12	2.60e-12	-0.76	
BR08	RO2C + HO2 = HO2	7.63e-12	3.80e-13	-1.79	
BR09	RO2C + NO3 = NO2	2.30e-12			
BR10	RO2C + MEO2 = #.5 {RO2C + xHO2 + xHCHO + O2} + #.25 {HCHO + MEOH}	2.00e-13			
BR11	RO2C + RO2C =	3.50e-14			
BR12	RO2XC + NO = XN	Same k as rxn BR07			
BR13	RO2XC + HO2 = HO2	Same k as rxn BR08			
BR14	RO2XC + NO3 = NO2	Same k as rxn BR09			
BR15	RO2XC + MEO2 = #.5 {RO2C + xHO2 + xHCHO + O2} + #.25 {HCHO + MEOH}	Same k as rxn BR10			
BR16	RO2XC + RO2C =	Same k as rxn BR11			
BR17	RO2XC + RO2XC =	Same k as rxn BR11			
Reactions of Acyl Peroxy Radicals, PAN, and PAN analogues					
BR18	MECO3 + NO2 = PAN	9.37e-12	Falloff, F=0.30, N=1.41		
		0:	2.70e-28	0.00	-7.10
		inf:	1.21e-11	0.00	-0.90
BR19	PAN = MECO3 + NO2	6.27e-4	Falloff, F=0.30, N=1.41		
		0:	4.90e-3	24.05	0.00
		inf:	4.00e+16	27.03	0.00
BR20	PAN + HV = #.6 {MECO3 + NO2} + #.4 {MEO2 + CO2 + NO3}	Phot Set= PAN			
BR21	MECO3 + NO = MEO2 + CO2 + NO2	1.97e-11	7.50e-12	-0.58	
BR22	MECO3 + HO2 = CCOOH + #.7 O2 + #.3 O3	1.36e-11	5.20e-13	-1.95	
BR23	MECO3 + NO3 = MEO2 + CO2 + NO2 + O2	Same k as rxn BR09			
BR24	MECO3 + MEO2 = #.9 {CCOOH + HCHO + O2} + #.1 {HCHO + HO2 + MEO2 + CO2}	1.06e-11	2.00e-12	-0.99	
BR25	MECO3 + RO2C = CCOOH	1.56e-11	4.40e-13	-2.13	
BR26	MECO3 + RO2XC = CCOOH	Same k as rxn BR25			
BR27	MECO3 + MECO3 = #2 {MEO2 + CO2} + O2	1.54e-11	2.90e-12	-0.99	

Label	Reaction and Products [a]	Rate Parameters [b]			
		k(300)	A	Ea	B
BR28	RCO3 + NO2 = PAN2	1.21e-11	1.21e-11	0.00	-1.07
BR29	PAN2 = RCO3 + NO2	5.48e-4	8.30e+16	27.70	
BR30	RCO3 + NO = NO2 + RO2C + xHO2 + yROOH + xCCHO + CO2	2.08e-11	6.70e-12	-0.68	
BR31	RCO3 + HO2 = RCOOH + #.75 O2 + #.25 O3		Same k as rxn BR22		
BR32	RCO3 + NO3 = NO2 + RO2C + xHO2 + yROOH + xCCHO + CO2 + O2		Same k as rxn BR09		
BR33	RCO3 + MEO2 = RCOOH + HCHO + O2		Same k as rxn BR24		
BR34	RCO3 + RO2C = RCOOH + O2		Same k as rxn BR25		
BR35	RCO3 + RO2XC = RCOOH + O2		Same k as rxn BR25		
BR36	RCO3 + MECO3 = #2 CO2 + MEO2 + RO2C + xHO2 + yROOH + xCCHO + O2		Same k as rxn BR27		
BR37	RCO3 + RCO3 = #2 {RO2C + xHO2 + xCCHO + yROOH + CO2}		Same k as rxn BR27		
BR38	BZCO3 + NO2 = PBZN	1.37e-11			
BR39	PBZN = BZCO3 + NO2	4.27e-4	7.90e+16	27.82	
BR40	BZCO3 + NO = NO2 + CO2 + BZO + RO2C		Same k as rxn BR30		
BR41	BZCO3 + HO2 = RCOOH + #.75 O2 + #.25 O3 + #4 XC		Same k as rxn BR22		
BR42	BZCO3 + NO3 = NO2 + CO2 + BZO + RO2C + O2		Same k as rxn BR09		
BR43	BZCO3 + MEO2 = RCOOH + HCHO + O2 + #4 XC		Same k as rxn BR24		
BR44	BZCO3 + RO2C = RCOOH + O2 + #4 XC		Same k as rxn BR25		
BR45	BZCO3 + RO2XC = RCOOH + O2 + #4 XC		Same k as rxn BR25		
BR46	BZCO3 + MECO3 = #2 CO2 + MEO2 + BZO + RO2C		Same k as rxn BR27		
BR47	BZCO3 + RCO3 = #2 CO2 + RO2C + xHO2 + yROOH + xCCHO + BZO + RO2C		Same k as rxn BR27		
BR48	BZCO3 + BZCO3 = #2 {BZO + RO2C + CO2}		Same k as rxn BR27		
BR49	MACO3 + NO2 = MAPAN		Same k as rxn BR28		
BR50	MAPAN = MACO3 + NO2	4.79e-4	1.60e+16	26.80	
BR51	MACO3 + NO = NO2 + CO2 + HCHO + MECO3		Same k as rxn BR30		
BR52	MACO3 + HO2 = RCOOH + #.75 O2 + #.25 O3 + XC		Same k as rxn BR22		
BR53	MACO3 + NO3 = NO2 + CO2 + HCHO + MECO3 + O2		Same k as rxn BR09		
BR54	MACO3 + MEO2 = RCOOH + HCHO + XC + O2		Same k as rxn BR24		
BR55	MACO3 + RO2C = RCOOH + XC		Same k as rxn BR25		
BR56	MACO3 + RO2XC = RCOOH + O2 + XC		Same k as rxn BR25		
BR57	MACO3 + MECO3 = #2 CO2 + MEO2 + HCHO + MECO3 + O2		Same k as rxn BR27		
BR58	MACO3 + RCO3 = HCHO + MECO3 + RO2C + xHO2 + yROOH + xCCHO + #2 CO2		Same k as rxn BR27		
BR59	MACO3 + BZCO3 = HCHO + MECO3 + BZO + RO2C + #2 CO2		Same k as rxn BR27		

Label	Reaction and Products [a]	Rate Parameters [b]			
		k(300)	A	Ea	B
BR60	MACO3 + MACO3 = #2 {HCHO + MECO3 + CO2}	Same k as rxn BR27			
Other Organic Radical Species					
BR61	TBUO + NO2 = RNO3 + #-2 XC	2.40e-11			
BR62	TBUO = ACET + MEO2	1.18e+3	7.50e+14	16.20	
BR63	BZO + NO2 = NPHE	3.79e-11	2.30e-11	-0.30	
BR64	BZO + HO2 = CRES + #-1 XC	Same k as rxn BR08			
BR65	BZO = CRES + RO2C + xHO2 + #-1 XC	1.00e-3			
Explicit and Lumped Molecule Organic Products					
BP01	HCHO + HV = #2 HO2 + CO	Phot Set= HCHOR-06			
BP02	HCHO + HV = H2 + CO	Phot Set= HCHOM-06			
BP03	HCHO + OH = HO2 + CO + H2O	8.47e-12	5.40e-12	-0.27	
BP04	HCHO + HO2 = HOCOO	7.79e-14	9.70e-15	-1.24	
BP05	HOCOO = HO2 + HCHO	1.76e+2	2.40e+12	13.91	
BP06	HOCOO + NO = HCOOH + NO2 + HO2	Same k as rxn BR01			
BP07	HCHO + NO3 = HNO3 + HO2 + CO	6.06e-16	2.00e-12	4.83	
BP08	CCHO + OH = MECO3 + H2O	1.49e-11	4.40e-12	-0.73	
BP09	CCHO + HV = CO + HO2 + MEO2	Phot Set= CCHO_R			
BP10	CCHO + NO3 = HNO3 + MECO3	2.84e-15	1.40e-12	3.70	
BP11	RCHO + OH = #.965 RCO3 + #.035 {RO2C + xHO2 + xCO + xCCHO + yROOH}	1.97e-11	5.10e-12	-0.80	
BP12	RCHO + HV = RO2C + xHO2 + yROOH + xCCHO + CO + HO2	Phot Set= C2CHO			
BP13	RCHO + NO3 = HNO3 + RCO3	6.74e-15	1.40e-12	3.18	
BP14	ACET + OH = RO2C + xMECO3 + xHCHO + yROOH	1.91e-13	4.56e-14	-0.85	3.65
BP15	ACET + HV = #.62 MECO3 + #1.38 MEO2 + #.38 CO	Phot Set= ACET-06, qy= 0.5			
BP16	MEK + OH = #.967 RO2C + #.039 {RO2XC + zRNO3} + #.376 xHO2 + #.51 xMECO3 + #.074 xRCO3 + #.088 xHCHO + #.504 xCCHO + #.376 xRCHO + yROOH + #.3 XC	1.20e-12	1.30e-12	0.05	2.00
BP17	MEK + HV = MECO3 + RO2C + xHO2 + xCCHO + yROOH	Phot Set= MEK-06, qy= 0.175			
BP18	MEOH + OH = HCHO + HO2	9.02e-13	2.85e-12	0.69	
BP19	HCOOH + OH = HO2 + CO2	4.50e-13			
BP20	CCOOH + OH = #.509 MEO2 + #.491 RO2C + #.509 CO2 + #.491 xHO2 + #.491 xMGLY + #.491 yROOH + #-0.491 XC	7.26e-13	4.20e-14	-1.70	

Label	Reaction and Products [a]	Rate Parameters [b]			
		k(300)	A	Ea	B
BP21	RCOOH + OH = RO2C + #.08 CO2 + xHO2 + #.063 CO2 + #.142 xCCHO + #.4 xRCHO + #.457 xBACL + yROOH + #-0.455 XC	1.20e-12			
BP22	COOH + OH = H2O + #.35 {HCHO + OH} + #.65 MEO2	5.46e-12	2.90e-12	-0.38	
BP23	COOH + HV = HCHO + HO2 + OH		Phot Set= COOH		
BP24	ROOH + OH = #.659 OH + #.339 RO2C + #.003 RO2XC + #.003 zRNO3 + #.659 RCHO + #.045 xOH + #.293 xHO2 + #.046 xHCHO + #.045 xCCHO + #.168 xRCHO + #.125 xMEK + #.341 yROOH + #-0.135 XC	6.78e-12			
BP25	ROOH + HV = RCHO + HO2 + OH		Phot Set= COOH		
BP26	R6OOH + OH = #.691 OH + #.395 RO2C + #.046 {RO2XC + zRNO3} + #.691 PROD2 + #.151 xOH + #.112 xHO2 + #.062 xCCHO + #.235 xRCHO + #.112 xPROD2 + #.309 yR6OOH + #.077 XC	1.64e-11			
BP27	R6OOH + HV = OH + #.142 HO2 + #.782 RO2C + #.077 RO2XC + #.077 zRNO3 + #.085 RCHO + #.142 PROD2 + #.782 xHO2 + #.026 xCCHO + #.058 xRCHO + #.698 xPROD2 + #.858 yR6OOH + #.017 XC		Phot Set= COOH		
BP28	RAOOH + OH = #.045 OH + #.192 HO2 + #.630 RO2C + #.132 {RO2XC +zRNO3} + #.1 PROD2 + #.093 MGLY + #.045 IPRD + #.032 xOH + #.598 xHO2 + #.594 xRCHO + #.021 xMEK + #.205 xMGLY + #.021 xAFG1 + #.021 xAFG2 + #.763 yR6OOH + #3.413 XC	1.08e-10			
BP29	RAOOH + HV = OH + HO2 + #.5 {GLY + MGLY + AFG1 + AFG2} + #.5 XC		Phot Set= COOH		
BP30	GLY + HV = #2 {CO + HO2}		Phot Set= GLY-07R		
BP31	GLY + HV = HCHO + CO		Phot Set= GLY-07M		
BP32	GLY + OH = #.63 HO2 + #1.26 CO + #.37 RCO3 + #-.37 XC	1.10e-11			
BP33	GLY + NO3 = HNO3 + #.63 HO2 + #1.26 CO + #.37 RCO3 + #-.37 XC	1.02e-15	2.80e-12	4.72	
BP34	MGLY + HV = HO2 + CO + MECO3		Phot Set= MGLY-06		
BP35	MGLY + OH = CO + MECO3	1.50e-11			
BP36	MGLY + NO3 = HNO3 + CO + MECO3	2.53e-15	1.40e-12	3.77	
BP37	BACL + HV = #2 MECO3		Phot Set= BACL-07		
BP38	CRES + OH = #.2 BZO + #.8 {RO2C + xHO2 + yR6OOH} + #.25 xMGLY + #5.05 XC	4.03e-11	1.70e-12	-1.89	

Label	Reaction and Products [a]	Rate Parameters [b]			
		k(300)	A	Ea	B
BP39	CRES + NO3 = HNO3 + BZO + XC	1.40e-11			
BP40	NPHE + OH = BZO + XN	3.50e-12			
BP41	NPHE + HV = HONO + #6 XC	Phot Set= NO2-06, qy= 1.5e-3			
BP42	NPHE + HV = #6 XC + XN	Phot Set= NO2-06, qy= 1.5e-2			
BP43	BALD + OH = BZCO3	1.20e-11			
BP44	BALD + HV = #7 XC	Phot Set= BALD-06, qy= 0.06			
BP45	BALD + NO3 = HNO3 + BZCO3	2.73e-15	1.34e-12	3.70	
Lumped Unsaturated Aromatic Ring-Opening Products					
BP46	AFG1 + OH = #.217 MACO3 + #.723 RO2C + #.060 {RO2XC + zRNO3} + #.060 zRNO3 + #.521 xHO2 + #.201 xMECO3 + #.334 xCO + #.407 xRCHO + #.129 xMEK + #.107 xGLY + #.267 xMGLY + #.783 yR6OOH + #-.076 XC	7.40e-11			
BP47	AFG1 + O3 = #.826 OH + #.522 HO2 + #.652 RO2C + #.522 CO + #.174 CO2 + #.432 GLY + #.568 MGLY + #.652 xRCO3 + #.652 xHCHO + #.652 yR6OOH + #-.872 XC	9.66e-18			
BP48	AFG1 + HV = #1.023 HO2 + #.173 MEO2 + #.305 MECO3 + #.500 MACO3 + #.695 CO + #.195 GLY + #.305 MGLY + #.217 XC		Phot Set= AFG1		
BP49	AFG2 + OH = #.217 MACO3 + #.723 RO2C + #.060 {RO2XC + zRNO3} + #.060 zRNO3 + #.521 xHO2 + #.201 xMECO3 + #.334 xCO + #.407 xRCHO + #.129 xMEK + #.107 xGLY + #.267 xMGLY + #.783 yR6OOH + #-.076 XC	7.40e-11			
BP50	AFG2 + O3 = #.826 OH + #.522 HO2 + #.652 RO2C + #.522 CO + #.174 CO2 + #.432 GLY + #.568 MGLY + #.652 xRCO3 + #.652 xHCHO + #.652 yR6OOH + #-.872 XC	9.66e-18			
BP51	AFG2 + HV = PROD2 + #-1 XC		Phot Set= AFG1		
BP52	AFG3 + OH = #.206 MACO3 + #.733 RO2C + #.117 {RO2XC + zRNO3} + #.117 zRNO3 + #.561 xHO2 + #.117 xMECO3 + #.114 xCO + #.274 xGLY + #.153 xMGLY + #.019 xBACL + #.195 xAFG1 + #.195 xAFG2 + #.231 xIPRD + #.794 yR6OOH + #.236 XC	9.35e-11			

Label	Reaction and Products [a]	Rate Parameters [b]			
		k(300)	A	Ea	B
BP53	AFG3 + O3 = #.471 OH + #.554 HO2 + #.013 MECO3 + #.258 RO2C + #.007 {RO2XC + zRNO3} + #.007 zRNO3 + #.580 CO + #.190 CO2 + #.366 GLY + #.184 MGLY + #.350 AFG1 + #.350 AFG2 + #.139 AFG3 + #.003 MACR + #.004 MVK + #.003 IPRD + #.095 xHO2 + #.163 xRCO3 + #.163 xHCHO + #.095 xMGLY + #.264 yR6OOH + #-.617 XC	1.43e-17			
Isoprene product species					
BP54	MACR + OH = #.5 MACO3 + #.5 {RO2C + xHO2} + #.416 xCO + #.084 xHCHO + #.416 xMEK + #.084 xMGLY + #.5 yROOH + #-0.416 XC	2.84e-11	8.00e-12	-0.76	
BP55	MACR + O3 = #.208 OH + #.108 HO2 + #.1 RO2C + #.45 CO + #.117 CO2 + #.1 HCHO + #.9 MGLY + #.333 HCOOH + #.1 xRCO3 + #.1 xHCHO + #.1 yROOH + #-0.1 XC	1.28e-18	1.40e-15	4.17	
BP56	MACR + NO3 = #.5 {MACO3 + RO2C + HNO3 + xHO2 + xCO} + #.5 yROOH + #1.5 XC + #.5 XN	3.54e-15	1.50e-12	3.61	
BP57	MACR + O3P = RCHO + XC	6.34e-12			
BP58	MACR + HV = #.33 OH + #.67 HO2 + #.34 MECO3 + #.33 MACO3 + #.33 RO2C + #.67 CO + #.34 HCHO + #.33 xMECO3 + #.33 xHCHO + #.33 yROOH		Phot Set= MACR-06		
BP59	MVK + OH = #.975 RO2C + #.025 {RO2XC + zRNO3} + #.3 xHO2 + #.675 xMECO3 + #.3 xHCHO + #.675 xRCHO + #.3 xMGLY + yROOH + #-0.725 XC	1.99e-11	2.60e-12	-1.21	
BP60	MVK + O3 = #.164 OH + #.064 HO2 + #.05 {RO2C + xHO2} + #.475 CO + #.124 CO2 + #.05 HCHO + #.95 MGLY + #.351 HCOOH + #.05 xRCO3 + #.05 xHCHO + #.05 yROOH + #-0.05 XC	5.36e-18	8.50e-16	3.02	
BP61	MVK + NO3 = #4 XC + XN		(Slow)		
BP62	MVK + O3P = #.45 RCHO + #.55 MEK + #.45 XC	4.32e-12			
BP63	MVK + HV = #.4 MEO2 + #.6 CO + #.6 PROD2 + #.4 MACO3 + #-2.2 XC		Phot Set= MVK-06		
BP64	IPRD + OH = #.289 MACO3 + #.67 {RO2C + xHO2} + #.041 {RO2XC + zRNO3} + #.336 xCO + #.055 xHCHO + #.129 xCCHO + #.013 xRCHO + #.15 xMEK + #.332 xPROD2 + #.15 xGLY + #.174 xMGLY + #-0.504 XC + #.711 yR6OOH	6.19e-11			
BP65	IPRD + O3 = #.285 OH + #.4 HO2 + #.048 {RO2C + xRCO3} + #.498 CO + #.14 CO2 + #.124 HCHO + #.21 MEK + #.023 GLY + #.742 MGLY + #.1 HCOOH + #.372 RCOOH + #.047 xCCHO + #.001 xHCHO + #.048 yR6OOH + #-.329 XC	4.18e-18			

Label	Reaction and Products [a]	Rate Parameters [b]			
		k(300)	A	Ea	B
BP66	IPRD + NO3 = #.15 {MACO3 + HNO3} + #.799 {RO2C + xHO2} + #.051 {RO2XC + zRNO3} + #.572 xCO + #.227 xHCHO + #.218 xRCHO + #.008 xMGLY + #.572 xRNO3 + #.85 yR6OOH + #.278 XN + #-.815 XC	1.00e-13			
BP67	IPRD + HV = #1.233 HO2 + #.467 MECO3 + #.3 RCO3 + #1.233 CO + #.3 HCHO + #.467 CCHO + #.233 MEK + #-.233 XC	Phot Set= MACR-06			
Lumped Parameter Organic Products					
BP68	PROD2 + OH = #.472 HO2 + #.473 RO2C + #.070 RO2XC + #.070 zRNO3 + #.002 HCHO + #.001 CCHO + #.143 RCHO + #.329 PROD2 + #.379 xHO2 + #.029 xMECO3 + #.049 xRCO3 + #.211 xHCHO + #.083 xCCHO + #.402 xRCHO + #.115 xMEK + #.007 xPROD2 + #.528 yR6OOH + #.883 XC	1.55e-11			
BP69	PROD2 + HV = #.400 MECO3 + #.600 RCO3 + #1.590 RO2C + #.086 RO2XC + #.086 zRNO3 + #.914 xHO2 + #.303 xHCHO + #.163 xCCHO + #.780 xRCHO + yR6OOH + #-.085 XC	Phot Set= MEK-06, qy= 4.86e-3			
BP70	RNO3 + OH = #.019 NO2 + #.189 HO2 + #.976 RO2C + #.175 RO2XC + #.175 zRNO3 + #.001 RCHO + #.010 MEK + #.007 PROD2 + #.189 RNO3 + #.312 xNO2 + #.305 xHO2 + #.011 xHCHO + #.428 xCCHO + #.036 xRCHO + #.004 xACET + #.170 xMEK + #.030 xPROD2 + #.305 xRNO3 + #.792 yR6OOH + #.175 XN + #.054 XC	7.20e-12			
BP71	RNO3 + HV = NO2 + #.344 HO2 + #.721 RO2C + #.102 RO2XC + #.102 zRNO3 + #.074 HCHO + #.214 CCHO + #.074 RCHO + #.124 MEK + #.190 PROD2 + #.554 xHO2 + #.061 xHCHO + #.230 xCCHO + #.063 xRCHO + #.008 xACET + #.083 xMEK + #.261 xPROD2 + #.656 yR6OOH + #.396 XC	Phot Set= IC3ONO2			
Explicitly Represented Primary Organics					
BE01	CH4 + OH = H2O + MEO2	6.62e-15	1.85e-12	3.36	
BE02	ETHENE + OH = RO2C + xHO2 + #1.61 xHCHO + #.195 xCCHO + yROOH	8.15e-12	Falloff, F=0.60, N=1.00		
			0: 1.00e-28	0.00	-4.50
			inf: 8.80e-12	0.00	-0.85
BE03	ETHENE + O3 = #.16 OH + #.16 HO2 + #.51 CO + #.12 CO2 + HCHO + #.37 HCOOH	1.68e-18	9.14e-15	5.13	
BE04	ETHENE + NO3 = RO2C + xHO2 + xRCHO + yROOH + #-1 XC + XN	2.24e-16	3.30e-12	5.72	2.00
BE05	ETHENE + O3P = #.8 HO2 + #.51 MEO2 + #.29 RO2C + #.51 CO + #.1 CCHO + #.29 xHO2 + #.278 xCO + #.278 xHCHO + #.012 xGLY + #.29 yROOH + #.2 XC	7.43e-13	1.07e-11	1.59	

Label	Reaction and Products [a]	Rate Parameters [b]			
		k(300)	A	Ea	B
BE06	ISOPRENE + OH = #.986 RO2C + #.093 {RO2XC + zRNO3} + #.907 xHO2 + #.624 xHCHO + #.23 xMACR + #.32 xMVK + #.357 xIPRD + yR6OOH + #-0.167 XC	9.96e-11	2.54e-11	-0.81	
BE07	ISOPRENE + O3 = #.266 OH + #.066 HO2 + #.192 RO2C + #.008 {RO2XC + zRNO3} + #.275 CO + #.122 CO2 + #.4 HCHO + #.1 PROD2 + #.39 MACR + #.16 MVK + #.15 IPRD + #.204 HCOOH + #.192 {xMACO3 + xHCHO} + #.2 yR6OOH + #-0.559 XC	1.34e-17	7.86e-15	3.80	
BE08	ISOPRENE + NO3 = #.936 RO2C + #.064 {RO2XC + zRNO3} + #.749 xHO2 + #.187 xNO2 + #.936 xIPRD + yR6OOH + #-0.064 XC + #.813 XN	6.81e-13	3.03e-12	0.89	
BE09	ISOPRENE + O3P = #.25 MEO2 + #.24 RO2C + #.01 {RO2XC + zRNO3} + #.75 PROD2 + #.24 xMACO3 + #.24 xHCHO + #.25 yR6OOH + #-1.01 XC	3.50e-11			
BE10	ACETYLEN + OH = #.7 OH + #.3 HO2 + #.3 CO + #.7 GLY + #.3 HCOOH	7.56e-13	Falloff, F=0.60, N=1.00		
BE11	ACETYLEN + O3 = #.5 OH + #1.5 HO2 + #1.5 CO + #.5 CO2	1.16e-20	1.00e-14	8.15	
BE12	BENZENE + OH = #.116 OH + #.29 {RO2C + xHO2} + #.024 {RO2XC + zRNO3} + #.57 {HO2 + CRES} + #.116 AFG3 + #.290 xGLY + #.029 xAFG1 + #.261 xAFG2 + #.314 yRAOOH + #-.976 XC	1.22e-12	2.33e-12	0.38	

[a] Format of reaction listing: "=" separates reactants from products; "#number" indicates stoichiometric coefficient, "#coefficient { product list }" means that the stoichiometric coefficient is applied to all the products listed.

[b] Except as indicated, the rate constants are given by $k(T) = A \cdot (T/300)^{B} \cdot e^{-Ea/RT}$, where the units of k and A are cm^3 $molec^{-1}$ s^{-1}, Ea are kcal mol^{-1}, T is ^oK, and R=0.0019872 kcal mol^{-1} deg^{-1}. The following special rate constant expressions are used:

Phot Set = name: The absorption cross sections and (if applicable) quantum yields for the photolysis reaction are given in **Error! Reference source not found.**, where "name" indicates the photolysis set used. If a "qy=number" notation is given, the number given is the overall quantum yield, which is assumed to be wavelength independent.

Falloff: The rate constant as a function of temperature and pressure is calculated using $k(T,M) = \{k0(T)\cdot[M]/[1 + k0(T)\cdot[M]/kinf(T)]\}\cdot F^{Z}$, where $Z = \{1 + [\log10\{k0(T)\cdot[M])/kinf(T)\}/N]^2\ \}^{-1}$, [M] is the total pressure in molecules cm^{-3}, F and N are as indicated on the table, and the temperature dependences of k0 and kinf are as indicated on the table.

k = k0+k3M(1+k3M/k2): The rate constant as a function of temperature and pressure is calculated using $k(T,M) = k0(T) + k3(T)\cdot[M] \cdot(1 + k3(T)\cdot[M]/k2(T))$, where [M] is the total bath gas (air) concentration in molecules cm-3, and the temperature dependences for k0, k2 and k3 are as indicated on the table.

k = k1 + k2 [M]: The rate constant as a function of temperature and pressure is calculated using k(T,M) = k1(T) + k2(T)·[M], where [M] is the total bath gas (air) concentration in molecules cm-3, and the temperature dependences for k1, and k2 are as indicated on the table.

Same K as Rxn xx: Uses the same rate constant as the reaction in the base mechanism with the same label.

Table A-1.7. Listing of reactions and rate parameters used for the lumped model species in the fixed parameter version of the lumped SAPRC-07 mechanism (Carter, 2007).

Label	Reaction and Products [a]	Rate Parameters [b]		
		k(298)	A	Ea
Reactions Added to the Standard Base Mechanism				
BL01	ALK1 + OH = RO2C + xHO2 + xCCHO + yROOH	2.54e-13	1.34e-12	0.99
BL02	ALK2 + OH = #.965 RO2C + #.035 {RO2XC + zRNO3} + #.965 xHO2 + #.261 xRCHO + #.704 xACET + yROOH + #-.105 XC	1.11e-12	1.49e-12	0.17
BL03	ALK3 + OH = #1.253 RO2C + #.07 {RO2XC + zRNO3} + #.694 xHO2 + #.236 xTBUO + #.026 xHCHO + #.445 xCCHO + #.122 xRCHO + #.024 xACET + #.332 xMEK + yROOH + #-.046 XC	2.31e-12	1.51e-12	-0.25
BL04	ALK4 + OH = #1.773 RO2C + #.144 {RO2XC + zRNO3} + #.834 xHO2 + #.011 xMEO2 + #.011 xMECO3 + #.002 xCO + #.030 xHCHO + #.454 xCCHO + #.242 xRCHO + #.442 xACET + #.110 xMEK + #.128 xPROD2 + yR6OOH + #-.097 XC	4.26e-12	3.67e-12	-0.09
BL05	ALK5 + OH = #1.597 RO2C + #.348 {RO2XC + zRNO3} + #.652 xHO2 + #.037 xHCHO + #.099 xCCHO + #.199 xRCHO + #.066 xACET + #.080 xMEK + #.425 xPROD2 + yR6OOH + #2.012 XC	9.22e-12	2.65e-12	-0.74
BL06	OLE1 + OH = #1.138 RO2C + #.095 {RO2XC + zRNO3} + #.904 xHO2 + #.001 xMEO2 + #.700 xHCHO + #.301 xCCHO + #.470 xRCHO + #.005 xACET + #.119 xPROD2 + #.026 xMACR + #.008 xMVK + #.006 xIPRD + yROOH + #.822 XC	3.29e-11	6.18e-12	-1.00
BL07	OLE1 + O3 = #.193 OH + #.116 HO2 + #.104 MEO2 + #.063 RO2C + #.004 {RO2XC + zRNO3} + #.368 CO + #.125 CO2 + #.500 HCHO + #.147 CCHO + #.353 RCHO + #.006 MEK + #.189 PROD2 + #.185 HCOOH + #.022 CCOOH + #.112 RCOOH + #.040 xHO2 + #.007 xCCHO + #.031 xRCHO + #.002 xACET + #.044 yR6OOH + #.69 XC	1.09e-17	3.15e-15	3.38
BL08	OLE1 + NO3 = #1.312 RO2C + #.176 {RO2XC + zRNO3} + #.824 xHO2 + #.009 xCCHO + #.002 xRCHO + #.024 xACET + #.546 xRNO3 + yR6OOH + #.454 XN + #.572 XC	1.44e-14	4.73e-13	2.08
BL09	OLE1 + O3P = #.450 RCHO + #.437 MEK + #.113 PROD2 + #1.224 XC	5.02e-12	1.49e-11	0.65
BL10	OLE2 + OH = #.966 RO2C + #.086 {RO2XC + zRNO3} + #.914 xHO2 + #.209 xHCHO + #.787 xCCHO + #.483 xRCHO + #.136 xACET + #.076 xMEK + #.021 xPROD2 + #.027 xMACR + #.002 xMVK + #.037 xIPRD + yR6OOH + #.113 XC	6.41e-11	1.26e-11	-0.97

Label	Reaction and Products [a]	Rate Parameters [b]		
		k(298)	A	Ea
BL11	OLE2 + O3 = #.421 OH + #.093 HO2 + #.290 MEO2 + #.199 RO2C + #.003 {RO2XC + zRNO3} + #.296 CO + #.162 CO2 + #.152 HCHO + #.426 CCHO + #.316 RCHO + #.048 ACET + #.031 MEK + #.042 PROD2 + #.028 MACR + #.021 MVK + #.033 HCOOH + #.061 CCOOH + #.222 RCOOH + #.039 xHO2 + #.147 xMECO3 + #.007 xRCO3 + #.108 xHCHO + #.066 xCCHO + #.019 xRCHO + #.196 yR6OOH + #.133 XC	1.24e-16	8.15e-15	2.49
BL12	OLE2 + NO3 = #1.185 RO2C + #.136 {RO2XC + zRNO3} + #.409 xNO2 + #.423 xHO2 + #.033 xMEO2 + #.074 xHCHO + #.546 xCCHO + #.153 xRCHO + #.110 xACET + #.002 xMEK + #.026 xMVK + #.007 xIPRD + #.322 xRNO3 + yR6OOH + #.270 XN + #.117 XC	7.70e-13	2.15e-13	-0.76
BL13	OLE2 + O3P = #.014 HO2 + #.013 RO2C + #.074 RCHO + #.709 MEK + #.203 PROD2 + #.007 xHO2 + #.007 xMACO3 + #.006 xCO + #.006 xMACR + #.014 yR6OOH + #.666 XC	2.06e-11	1.43e-11	-0.22
BL14	ARO1 + OH = #.283 OH + #.166 HO2 + #.483 RO2C + #.068 {RO2XC + zRNO3} + #.166 CRES + #.283 AFG3 + #.483 xHO2 + #.217 xGLY + #.138 xMGLY + #.049 xBALD + #.079 xPROD2 + #.164 xAFG1 + #.192 xAFG2 + #.150 yR6OOH + #.402 yRAOOH+ #.004 XC	6.18e-12		
BL15	ARO2 + OH = #.199 OH + #.108 HO2 + #.582 RO2C + #.111 RO2XC + #.111 zRNO3 + #.108 CRES + #.199 AFG3 + #.582 xHO2 + #.111 xGLY + #.291 xMGLY + #.104 xBACL + #.033 xBALD + #.042 xPROD2 + #.223 xAFG1 + #.211 xAFG2 + #.074 xAFG3 + #.090 yR6OOH + #.603 yRAOOH+ #1.503 XC	2.20e-11		
BL16	TERP + OH = #1.147 RO2C + #.2 {RO2XC + zRNO3} + #.759 xHO2 + #.042 xRCO3 + #.002 xCO + #.264 xHCHO + #.533 xRCHO + #.036 xACET + #.005 xMEK + #.255 xPROD2 + #.009 xMGLY + #.014 xBACL + #.002 xMVK + #.001 xIPRD + yR6OOH + #5.055 XC	7.98e-11	1.87e-11	-0.86
BL17	TERP + O3 = #.585 OH + #.052 HO2 + #.875 RO2C + #.203 RO2XC + #.203 zRNO3 + #.166 CO + #.045 CO2 + #.079 HCHO + #.004 MEK + #.409 PROD2 + #.107 HCOOH + #.043 RCOOH + #.067 xHO2 + #.126 xMECO3 + #.149 xRCO3 + #.019 xCO + #.150 xHCHO + #.220 xRCHO + #.165 xACET + #.001 xGLY + #.002 xMGLY + #.055 xBACL + #.001 xMACR + #.001 xIPRD + #.545 yR6OOH + #3.526 XC	6.99e-17	1.02e-15	1.60
BL18	TERP + NO3 = #1.508 RO2C + #.397 RO2XC + #.397 zRNO3 + #.422 xNO2 + #.162 xHO2 + #.019 xRCO3 + #.010 xCO + #.017 xHCHO + #.001 xCCHO + #.509 xRCHO + #.174 xACET + #.001 xMGLY + #.003 xMACR + #.001 xMVK + #.002 xIPRD + #.163 xRNO3 + yR6OOH + #4.476 XC + #.415 XN	6.53e-12	1.28e-12	-0.97
BL19	TERP + O3P = #.147 RCHO + #.853 PROD2 + #4.441 XC	3.71e-11		
Reactions Added to the Base Mechanism with Chlorine Chemistry				
CL01	ALK1 + CL = HCL + RO2C + xHO2 + xCCHO + yROOH	5.95e-11	8.30e-11	0.20
CL02	ALK2 + CL = HCL + #.970 RO2C + #.030 RO2XC + #.030 zRNO3 + #.970 xHO2 + #.482 xRCHO + #.488 xACET + yROOH + #-.090 XC	1.37e-10	1.20e-10	-0.08

Label	Reaction and Products [a]	Rate Parameters [b]		
		k(298)	A	Ea
CL03	ALK3 + CL = HCL + #1.361 RO2C + #.07 {RO2XC + zRNO3} + #.836 xHO2 + #.094 xTBUO + #.078 xHCHO + #.341 xCCHO + #.343 xRCHO + #.075 xACET + #.253 xMEK + yROOH + #.178 XC	1.86e-10		
CL04	ALK4 + CL = HCL + #1.744 RO2C + #.161 {RO2XC + #.161 zRNO3} + #.831 xHO2 + #.004 xMEO2 + #.004 xMECO3 + #.002 xCO + #.036 xHCHO + #.297 xCCHO + #.421 xRCHO + #.256 xACET + #.078 xMEK + #.114 xPROD2 + yR6OOH + #.363 XC	2.58e-10		
CL05	ALK5 + CL = HCL + #1.538 RO2C + #.348 {RO2XC + zRNO3} + #.652 xHO2 + #.021 xHCHO + #.074 xCCHO + #.250 xRCHO + #.041 xACET + #.038 xMEK + #.392 xPROD2 + yR6OOH + #2.366 XC	4.19e-10		
CL06	OLE1 + CL = #.325 HCL + #1.462 RO2C + #.105 {RO2XC + zRNO3} + #.895 xHO2 + #.027 xHCHO + #.159 xCCHO + #.056 xRCHO + #.194 xMACR + #.015 xMVK + #.030 xIPRD + #.218 xCLCCHO + #.383 xCLACET + yR6OOH + #1.286 XC	3.64e-10		
CL07	OLE2 + CL = #.304 HCL + #1.536 RO2C + #.126 {RO2XC + zRNO3} + #.410 xHO2 + #.001 xMEO2 + #.463 xCL + #.082 xHCHO + #.573 xCCHO + #.463 xRCHO + #.062 xMVK + #.204 xIPRD + #.146 xCLACET + yR6OOH + #-.080 XC	3.89e-10		
CL08	ARO1 + CL = #.881 RO2C + #.119 {RO2XC + zRNO3} + #.881 xHO2 + #.671 xBALD + #.210 xPROD2 + yR6OOH+ #.329 XC	1.02e-10		
CL09	ARO2 + CL = #.842 RO2C + #.158 {RO2XC + zRNO3} + #.842 xHO2 + #.614 xBALD + #.227 xPROD2 + yR6OOH+ #2.392 XC	1.92e-10		
CL10	TERP + CL = #.548 HCL + #2.258 RO2C + #.582 RO2XC + #.582 zRNO3 + #.252 xHO2 + #.034 xMECO3 + #.050 xRCO3 + #.016 xMACO3 + #.068 xCL + #.035 xCO + #.158 xHCHO + #.185 xRCHO + #.274 xACET + #.007 xGLY + #.003 xBACL + #.006 xAFG1 + #.006 xAFG2 + #.003 xMVK + #.158 xIPRD + #.109 xCLCCHO + yROOH + #3.55 XC	5.97e-10		

[a] Format of reaction listing: "=" separates reactants from products; "#number" indicates stoichiometric coefficient, "#coefficient { product list }" means that the stoichiometric coefficient is applied to all the products listed.

[b] The rate constants are given by $k(T) = A \cdot e^{-Ea/RT}$, where the units of k and A are cm^3 $molec^{-1}$ s^{-1}, Ea are kcal mol^{-1}, T is ^oK, and R=0.0019872 kcal mol^{-1} deg^{-1}.

Table A-1.8. List of model species used in the SAPRC07 mechanism (Carter, 2007).

Name	Description
Constant Species.	
O2	Oxygen
M	Air
H2O	Water
H2	Hydrogen Molecules
HV	Light
Active Inorganic Species.	

Name	Description
O3	Ozone
NO	Nitric Oxide
NO2	Nitrogen Dioxide
NO3	Nitrate Radical
N2O5	Nitrogen Pentoxide
HONO	Nitrous Acid
HNO3	Nitric Acid
HNO4	Peroxynitric Acid
HO2H	Hydrogen Peroxide
CO	Carbon Monoxide
SO2	Sulfur Dioxide
H2	Hydrogen
Active Radical Species and Operators.	
OH	Hydroxyl Radicals
HO2	Hydroperoxide Radicals
MEO2	Methyl Peroxy Radicals
RO2C	Peroxy Radical Operator representing NO to NO_2 and NO_3 to NO_2 conversions, and the effects of peroxy radical reactions on acyl peroxy and other peroxy radicals.
RO2XC	Peroxy Radical Operator representing NO consumption (used in conjunction with organic nitrate formation), and the effects of peroxy radical reactions on NO_3, acyl peroxy radicals, and other peroxy radicals.
MECO3	Acetyl Peroxy Radicals
RCO3	Peroxy Propionyl and higher peroxy acyl Radicals
BZCO3	Peroxyacyl radical formed from Aromatic Aldehydes
MACO3	Peroxyacyl radicals formed from methacrolein and other acroleins.
Steady State Radical Species	
O3P	Ground State Oxygen Atoms
O1D	Excited Oxygen Atoms
TBUO	t-Butoxy Radicals
BZO	Phenoxy Radicals
HOCOO	Radical formed when Formaldehyde reacts with HO2
PAN and PAN Analogues	
PAN	Peroxy Acetyl Nitrate
PAN2	PPN and other higher alkyl PAN analogues
PBZN	PAN analogues formed from Aromatic Aldehydes
MAPAN	PAN analogue formed from Methacrolein
Explicit and Lumped Molecule Reactive Organic Product Species	
HCHO	Formaldehyde
CCHO	Acetaldehyde
RCHO	Lumped C3+ Aldehydes. Mechanism based on propionaldehyde
ACET	Acetone
MEK	Ketones and other non-aldehyde oxygenated products that react with OH radicals faster than 5×10^{-13} but slower than 5×10^{-12} cm^3 $molec^{-2}$ sec^{-1}. Mechanism based on methyl ethyl ketone.
MEOH	Methanol
HCOOH	Formic Acid
CCOOH	Acetic Acid. Also used for peroxyacetic acid.
RCOOH	Higher organic acids and peroxy acids. Mechanism based on propionic acid.
COOH	Methyl Hydroperoxide

Name	Description
ROOH	Lumped organic hydroperoxides with 2-4 carbons. Mechanism based n-propyl hydroperoxide.
R6OOH	Lumped organic hydroperoxides with 5 or more carbons (other than those formed following OH addition to aromatic rings, which are represented separately). Mechanism based on 3-hexyl hydroperoxide.
RAOOH	Organic hydroperoxides formed following OH addition to aromatic rings, which is represented separately because of their probable role in SOA formation. Mechanism based on two isomers expected to be formed in the m-xylene system.
GLY	Glyoxal
MGLY	Methyl Glyoxal
BACL	Biacetyl
CRES	Phenols and Cresols. Mechanism based on o-cresol.
NPHE	Nitrophenols
BALD	Aromatic aldehydes. Mechanism based on benzaldehyde
MACR	Methacrolein
MVK	Methyl Vinyl Ketone
IPRD	Lumped isoprene product species. Mechanism based on that of Carter and Atkinson (1996).
<u>Aromatic unsaturated ring fragmentation products</u> (see discussion of aromatic mechanisms)	
AFG1	Lumped photoreactive monounsaturated dicarbonyl aromatic fragmentation products that photolyze to form radicals.
AFG2	Lumped photoreactive monounsaturated dicarbonyl aromatic fragmentation products that photolyze to form non-radical products
AFG3	Lumped diunsaturatred dicarbonyl aromatic fragmentation product.
<u>Lumped Parameter Products</u>	
PROD2	Ketones and other non-aldehyde oxygenated products that react with OH radicals faster than 5 x 10^{-12} cm^3 $molec^{-2}$ sec^{-1}. Mechanism based on $CH_3C(O)CH_2CH_2CH_2OH$, $CH_3C(O)$-$CH_2CH(CH_3)CH_2OH$, $CH_3CH_2C(O)CH_2CH_2CH(CH_3)OH$, $CH_3CH_2C(O)CH_2CH_2CH(OH)$-$CH_2CH_3$, and $CH_3CH_2CH_2CH(OH)CH_2$-$CH_2C(O)CH_2CH_3$ (PROD2-1 through 5), each weighed equally.
RNO3	Lumped Organic Nitrates. Mechanism based on $CH_3CH_2CH(CH_3)ONO_2$, $CH_3CH(OH)CH_2$-$CH_2CH_2ONO_2$, $CH_3CH_2CH(CH_3)CH(CH_3)ONO_2$, $CH_3CH_2CH_2CH_2CH_2CH(ONO_2)CH_2OH$, $CH_3CH_2C(CH_3)(ONO_2)CH_2CH(CH_3)CH_3$, and $CH_3CH_2CH_2CH_2CH_2CH_2CH_2CH(ONO_2)$-$CH_2CH_3$ (RNO3-1 through 6), each weighed equally.
<u>Non-Reacting Species</u>	
CO2	Carbon Dioxide
SULF	Sulfates (SO_3 or H_2SO_4)
XC	Lost Carbon or carbon in unreactive products
XN	Lost Nitrogen or nitrogen in unreactive products
<u>Primary Organics Represented explicitly</u>	
CH4	Methane
ETHENE	Ethene
ISOPRENE	Isoprene
ACETYLEN	Acetylene
BENZENE	Benzene
<u>Lumped model species added to the base mechanism to represent various types of emitted species in the lumped mechanism for airshed models</u> (not part of the base mechanism)	
ALK1	Alkanes and other non-aromatic compounds that react only with OH, and have kOH (OH radical rate constant) between 2 and 5 x 10^2 ppm^{-1} min^{-1}. (Primarily ethane)

Name	Description
ALK2	Alkanes and other non-aromatic compounds that react only with OH, and have kOH between 5 x 10^2 and 2.5 x 10^3 ppm^{-1} min^{-1}. (Primarily propane)
ALK3	Alkanes and other non-aromatic compounds that react only with OH, and have kOH between 2.5 x 10^3 and 5 x 10^3 ppm^{-1} min^{-1}.
ALK4	Alkanes and other non-aromatic compounds that react only with OH, and have kOH between 5 x 10^3 and 1 x 10^4 ppm^{-1} min^{-1}.
ALK5	Alkanes and other non-aromatic compounds that react only with OH, and have kOH greater than 1 x 10^4 ppm-1 min-1.
ARO1	Aromatics with kOH < $2x10^4$ ppm^{-1} min^{-1}.
ARO2	Aromatics with kOH > $2x10^4$ ppm^{-1} min^{-1}.
OLE1	Alkenes (other than ethene) with kOH < $7x10^4$ ppm^{-1} min^{-1}.
OLE2	Alkenes with kOH > $7x10^4$ ppm^{-1} min^{-1}.
TERP	Terpenes

A.2 CB CHEMICAL MECHANISM

CB-IV96

Table A-2.1. Reactions and Rate Constants for the OTAG (1996) version of the CB-IV mechanism in CAMx (CAMx Mechanism 3) (Yarwood *et al*., 2005a).

Reaction Number	Reactants	Products	k_{298}^{1} (ppm^{-n} min^{-1})
1	NO2	NO + O	Photolysis
2	O	O3	4.323E+06
3	O3 + NO	NO2	2.664E+01
4	O + NO2	NO	1.375E+04
5	O + NO2	NO3	2.309E+03
6	O + NO	NO2	2.438E+03
7	NO2 + O3	NO3	4.731E-02
8	O3	O	Photolysis
9	O3	O1D	Photolysis
10	O1D	O	4.250E+10
11	O1D + H2O	2 OH	3.260E+05
12	O3 + OH	HO2	1.000E+02
13	O3 + HO2	OH	2.999E+00
14	NO3	0.89 NO2 + 0.89 O + 0.11 NO	Photolysis
15	NO3 + NO	2 NO2	4.417E+04
16	NO3 + NO2	NO + NO2	5.901E-01
17	NO3 + NO2	N2O5	1.853E+03
18	N2O5 + H2O	2 HNO3	1.900E-06
19	N2O5	NO3 + NO2	2.776E+00
20	NO + NO	2 NO2	1.539E-04
21	NO + NO2 + H2O	2 HONO	1.600E-11
22	NO + OH	HONO	9.799E+03
23	HONO	NO + OH	Photolysis
24	OH + HONO	NO2	9.770E+03
25	HONO + HONO	NO + NO2	1.500E-05
26	NO2 + OH	HNO3	1.682E+04
27	OH + HNO3	NO3	2.179E+02
28	HO2 + NO	OH + NO2	1.227E+04
29	HO2 + NO2	PNA	0.000E+00
30	PNA	HO2 + NO2	0.000E+00
31	OH + PNA	NO2	0.000E+00
32	HO2 + HO2	H2O2	4.144E+03
33	HO2 + HO2 + H2O	H2O2	2.181E-01
34	H2O2	2 OH	Photolysis
35	OH + H2O2	HO2	2.520E+03
36	OH + CO	HO2	3.220E+02
37	FORM + OH	HO2 + CO	1.500E+04
38	FORM	2 HO2 + CO	Photolysis
39	FORM	CO	Photolysis
40	FORM + O	OH + HO2 + CO	2.370E+02
41	FORM + NO3	HNO3 + HO2 + CO	9.300E-01
42	ALD2 + O	C2O3 + OH	6.360E+02

Reaction Number	Reactants	Products	k_{298}[1] (ppm^{-n} min^{-1})
43	ALD2 + OH	C2O3	2.400E+04
44	ALD2 + NO3	C2O3 + HNO3	3.700E+00
45	ALD2	FORM + 2 HO2 + CO + XO2	Photolysis
46	C2O3 + NO	FORM + NO2 + HO2 + XO2	2.820E+04
47	C2O3 + NO2	PAN	1.370E+04
48	PAN	C2O3 + NO2	2.540E-02
49	C2O3 + C2O3	2 FORM + 2 XO2 + 2 HO2	3.700E+03
50	C2O3 + HO2	0.79 FORM + 0.79 XO2 + 0.79 HO2 + 0.79 OH	9.600E+03
51[2]	OH	FORM + XO2 + HO2	2.100E+01
52	PAR + OH	0.87 XO2 + 0.13 XO2N + 0.11 HO2 + 0.11 ALD2 - 0.11 PAR + 0.76 ROR	1.203E+03
53	ROR	0.96 XO2 + 1.1 ALD2 + 0.94 HO2 - 2.1 PAR + 0.04 XO2N	1.371E+05
54	ROR	HO2	9.545E+04
55	ROR + NO2	NTR	2.200E+04
56	O + OLE	0.63 ALD2 + 0.38 HO2 + 0.28 XO2 + 0.3 CO + 0.2 FORM + 0.02 XO2N + 0.22 PAR + 0.2 OH	5.920E+03
57	OH + OLE	FORM + ALD2 - PAR + XO2 + HO2	4.200E+04
58	O3 + OLE	0.5 ALD2 + 0.74 FORM + 0.22 XO2 + 0.1 OH + 0.33 CO + 0.44 HO2 - PAR	1.800E-02
59	NO3 + OLE	0.91 XO2 + FORM + 0.09 XO2N + ALD2 + NO2 - PAR	1.135E+01
60	O + ETH	FORM + 1.7 HO2 + CO + 0.7 XO2 + 0.3 OH	1.080E+03
61	OH + ETH	XO2 + 1.56 FORM + 0.22 ALD2 + HO2	1.192E+04
62	O3 + ETH	FORM + 0.42 CO + 0.12 HO2	2.700E-03
63	TOL + OH	0.44 HO2 + 0.08 XO2 + 0.36 CRES + 0.56 TO2	9.150E+03
64	TO2 + NO	0.9 NO2 + 0.9 HO2 + 0.9 OPEN + 0.1 NTR	1.200E+04
65	TO2	CRES + HO2	2.500E+02
66	OH + CRES	0.4 CRO + 0.6 XO2 + 0.6 HO2 + 0.3 OPEN	6.100E+04
67	CRES + NO3	CRO + HNO3	3.250E+04
68	CRO + NO2	NTR	2.000E+04
69	OPEN	C2O3 + HO2 + CO	Photolysis
70	OPEN + OH	XO2 + 2 CO + 2 HO2 + C2O3 + FORM	4.400E+04
71	OPEN + O3	0.03 ALD2 + 0.62 C2O3 + 0.7 FORM + 0.03 XO2 + 0.69 CO + 0.08 OH + 0.76 HO2 + 0.2 MGLY	1.500E-02
72	OH + XYL	0.7 HO2 + 0.5 XO2 + 0.2 CRES + 0.8 MGLY + 1.1 PAR + 0.3 TO2	3.620E+04
73	OH + MGLY	XO2 + C2O3	2.600E+04
74	MGLY	C2O3 + HO2 + CO	Photolysis
75	O + ISOP	0.75 ISPD + 0.5 FORM + 0.25 XO2 + 0.25 HO2 + 0.25 C2O3 + 0.25 PAR	5.320E+04
76	OH + ISOP	0.912 ISPD + 0.629 FORM + 0.991 XO2 + 0.912 HO2 + 0.088 XO2N	1.476E+05
77	O3 + ISOP	0.65 ISPD + 0.6 FORM + 0.2 XO2 + 0.066 HO2 + 0.266 OH + 0.2 C2O3 + 0.15 ALD2 + 0.35 PAR + 0.066 CO	1.900E-02
78	NO3 + ISOP	0.2 ISPD + 0.8 NTR + XO2 + 0.8 HO2 + 0.2 NO2 + 0.8 ALD2 + 2.4 PAR	9.960E+02
79	XO2 + NO	NO2	1.200E+04
80	XO2 + XO2		2.000E+03
81	XO2N + NO	NTR	1.200E+04
82	SO2 + OH	SULF + HO2	1.110E+03
83	SO2	SULF	8.167E-05
84	MEOH + OH	FORM + HO2	1.600E+03
85	ETOH + OH	HO2 + ALD2	4.300E+03
86	XO2 + HO2		8.900E+03
87	XO2N + HO2		8.900E+03
88	XO2N + XO2N		2.000E+03
89	XO2 + XO2N		4.000E+03
90	OH + HO2		1.626E+05
91	CRO		2.778E-04
92	OH + ISPD	1.565 PAR + 0.167 FORM + 0.713 XO2 + 0.503 HO2 + 0.334 CO + 0.168 MGLY + 0.273 ALD2 + 0.498 C2O3	4.967E+04
93	O3 + ISPD	0.114 C2O3 + 0.15 FORM + 0.85 MGLY + 0.154 HO2 + 0.268 OH + 0.064 XO2 + 0.02 ALD2 + 0.36 PAR + 0.225 CO	1.050E-02
94	NO3 + ISPD	0.357 ALD2 + 0.282 FORM + 1.282 PAR + 0.925 HO2 + 0.643 CO + 0.85 NTR + 0.075 C2O3 + 0.075 XO2 + 0.15 HNO3	1.478E+00
95	ISPD	0.333 CO + 0.067 ALD2 + 0.9 FORM + 0.832 PAR + 1.033 HO2 + 0.7 XO2 + 0.967 C2O3	Photolysis
96	NO2 + ISOP	0.2 ISPD + 0.8 NTR + XO2 + 0.8 HO2 + 0.2 NO + 0.8 ALD2 + 2.4 PAR	2.200E-04

Notes:

[1] Rate constants are shown for 298 K and 1 atmosphere in units of ppm and minutes. See the CAMx chemistry parameters file (Section 5) for the temperature and pressure dependencies.

[2] Reaction 51 implicitly includes 1.85 ppm of methane in the rate constant.

Table A-2.2. Species names for the CB-IV mechanism (Yarwood *et al*., 2005a).

Species Name	Description
NO2	Nitrogen dioxide
NO	Nitric oxide
O	Oxygen atom in the $O^3(P)$ electronic state
O3	Ozone
NO3	Nitrate radical
O1D	Oxygen atom in the $O^1(D)$ electronic state
OH	Hydroxyl radical
HO2	Hydroperoxy radical
N2O5	Dinitrogen pentoxide
HNO3	Nitric acid
HONO	Nitrous acid
PNA	Peroxynitric acid (HNO_4)
H2O2	Hydrogen peroxide
CO	Carbon monoxide
FORM	Formaldehyde
ALD2	Higher aldehyde (based on acetaldehyde)
C2O3	Acylperoxy radical (based on acetylperoxy)
XO2	NO to NO2 conversion from alkylperoxy (RO_2) radical
PAN	Peroxyacyl nitrate (based on peroxyacetyl nitrate)
PAR	Paraffin carbon bond (C-C)
XO2N	NO to organic nitrate conversion from alkylperoxy (RO_2) radical
ROR	Secondary alkoxy radical
NTR	Organic nitrate (RNO_3)
OLE	Olefin carbon bond (C=C)
ETH	Ethene
TOL	Toluene and other monoalkyl aromatics
CRES	Cresol and higher molecular weight phenols
TO2	Toluene-hydroxyl radical adduct
OPEN	Aromatic ring opening product
CRO	Methylphenoxy radical
MGLY	Methylglyoxal and other aromatic products
XYL	Xylene and other polyalkyl aromatics
ISOP	Isoprene
ISPD	Isoprene product (lumped methacrolein, methyl vinyl ketone, etc.)
SO2	Sulfur dioxide
SULF	Sulfuric acid (gaseous)
MEOH	Methanol
ETOH	Ethanol

CB2002

Table A-2.3. Reactions and rate constant for the CB2002 mechanism (Yarwood *et al*., 2005a).

Reaction Number	Reactants	Products	k_{298}^{1} (ppm^{-n} min^{-1})
1	NO2	NO + O	photolysis
2	O + O2 + M	O3 + M	2.22E-05
3	O3 + NO	NO2 + O2	2.89E+01
4	O + NO2	NO + O2	1.51E+04
5	O + NO2	NO3 + O2	2.33E+03
6	O + NO	NO2	2.46E+03
7	NO + NO + O2	2.0*NO2	7.11E-10
8	O3 + NO2	NO3 + O2	4.77E-02
9	NO3	NO + O2	photolysis
10	NO3	NO2 + O	photolysis
11	NO3 + NO	2.0*NO2	3.92E+04
12	NO3 + NO2	NO + NO2 + O2	9.69E-01
13	NO3 + NO2	N2O5	1.74E+03
14	N2O5	NO3 + NO2	2.26E+00
15	N2O5 + H2O	2.0*HNO3	3.69E-07
16	N2O5 + H2O + H2O	2.0*HNO3 + H2O	6.55E-11
17	NO3 + OH	NO2 + HO2	3.25E+04
18	NO3 + HO2	HNO3 + O2	1.36E+03
19	NO3 + NO3	2.0*NO2 + O2	3.38E-01
20	O3	O + O2	photolysis
21	O3	O1D + O2	photolysis
22	O1D + O2	O + O2	5.98E+04
23	O1D + N2	O + N2	3.85E+04
24	O1D + H2O	2.0*OH	3.25E+05
25	O3 + OH	HO2 + O2	1.16E+02
26	O3 + HO2	OH + 2.0*O2	3.02E+00
27	O3 + O	2.0*O2	1.18E+01
28	NO + NO2 + H2O	2.0*HONO	1.60E-11
29	HONO + HONO	NO + NO2 + H2O	1.48E-05
30	OH + NO	HONO	1.09E+04
31	HONO	OH + NO	photolysis
32	HONO	HO2 + NO2	photolysis
33	OH + HONO	NO2 + H2O	7.18E+03
34	HO2 + NO	OH + NO2	1.20E+04
35	HO2 + NO2	PNA	2.05E+03
36	PNA	HO2 + NO2	5.17E+00
37	OH + PNA	NO2 + H2O + O2	6.87E+03
38	OH + NO2	HNO3	1.57E+04
39	OH + HNO3	NO3 + H2O	2.17E+02
40	HO2 + HO2	H2O2 + O2	4.29E+03

Reaction Number	Reactants	Products	k_{298}^{1} (ppm^{-n} min^{-1})
41	HO2 + HO2 + H2O	H2O2 + O2 + H2O	2.38E-01
42	H2O2	2.0*OH	photolysis
43	OH + H2O2	HO2 + H2O	2.50E+03
44	OH + HO2	O2 + H2O	1.64E+05
45	OH + CO	HO2 + CO2	3.55E+02
46	OH + CH4	XO2 + FORM + HO2	9.37E+00
47	FORM	2.0*HO2 + CO	photolysis
48	FORM	CO + H2	photolysis
49	FORM + O	OH + HO2 + CO	2.34E+02
50	FORM + OH	HO2 + CO	1.36E+04
51	FORM + NO3	HNO3 + HO2 + CO	8.49E-01
52	ALD2	XO2 + 2.0*HO2 + CO + FORM	photolysis
53	ALD2 + O	C2O3 + OH	6.63E+02
54	ALD2 + OH	C2O3 + H2O	2.05E+04
55	ALD2 + NO3	C2O3 + HNO3	4.03E+00
56	C2O3 + NO	NO2 + XO2 + FORM + HO2	2.62E+04
57	C2O3 + NO2	PAN	1.55E+04
58	PAN	C2O3 + NO2	2.76E-02
59	C2O3 + HO2	0.25*O3	2.08E+04
60	C2O3 + C2O3	2.0*XO2 + 2.0*FORM + 2.0*HO2	2.45E+04
61	OH + PAR	0.87*XO2 + 0.13*XO2N + 0.11*HO2 + 0.11*ALD2 + 0.76*ROR + -0.11*PAR	1.20E+03
62	ROR	1.1*ALD2 + 0.96*XO2 + 0.94*HO2 + -2.1*PAR + 0.04*XO2N + 0.02*ROR	1.32E+05
63	ROR	HO2	9.60E+04
64	ROR + NO2	RNO3	2.22E+04
65	O + ETH	0.49*FORM + 0.60*XO2 + 0.95*CO + 1.55*HO2 + 0.35*OH	1.08E+03
66	OH + ETH	XO2 + 1.56*FORM + HO2 + 0.22*ALD2	1.25E+04
67	O3 + ETH	1.03*FORM + 0.325*CO + 0.08*HO2 + 0.02*H2O2 + 0.08*OH	2.34E-03
68	O + OLE	0.519*ALD2 + 0.147*HO2 + 0.097*XO2 + 0.102*CO + 0.051*FORM + 0.005*XO2N + 0.809*PAR + 0.051*OH	1.63E+04
69	OH + OLE	FORM + ALD2 + XO2 + HO2 + -1.0*PAR	6.52E+04
70	O3 + OLE	0.150*HO2 + 0.085*OH + 0.130*CO + 0.485*FORM + 0.210*ALD2 + 0.044*XO2 + 0.001*XO2N + 0.966*PAR	1.66E-02
71	NO3 + OLE	0.7*XO2 + NO2 + FORM + ALD2 + 0.3*XO2N + -1.0*PAR	2.44E+02
72	O + ISOP	0.25*HO2 + 0.25*XO2 + 0.75*ISPD + 0.50*FORM + 0.25*PAR + 0.25*C2O3	5.32E+04
73	OH + ISOP	0.991*XO2 + 0.629*FORM + 0.912*HO2 + 0.088*XO2N + 0.912*ISPD	1.47E+05
74	O3 + ISOP	0.60*FORM + 0.15*ALD2 + 0.35*PAR + 0.066*CO + 0.066*HO2 + 0.266*OH + 0.20*C2O3 + 0.20*XO2 + 0.65*ISPD	1.90E-02
75	NO3 + ISOP	XO2 + 0.65*ISPD + 0.80*RNO3 + 0.80*HO2 + 0.20*NO2 + 0.80*ALD2 + 2.4*PAR	9.95E+02
76	NO2 + ISOP	0.80*ALD2 + 2.4*PAR + 0.80*RNO3 + XO2 + 0.80*HO2 + 0.20*ISPD + 0.20*NO	2.22E-04
77	ISPD + OH	1.565*PAR + 0.167*FORM + 0.713*XO2 + 0.503*HO2 + 0.334*CO + 0.168*MGLY + 0.273*ALD2 + 0.498*C2O3	4.96E+04
78	ISPD + O3	0.114*C2O3 + 0.15*FORM + 0.85*MGLY + 0.154*HO2 + 0.268*OH + 0.064*XO2 + 0.02*ALD2 + 0.36*PAR + 0.225*CO	1.05E-02
79	ISPD + NO3	0.357*ALD2 + 0.282*FORM + 1.282*PAR + 0.925*HO2 + 0.643*CO + 0.85*RNO3 + 0.075*C2O3 + 0.075*XO2 + 0.075*HNO3	1.48E+00
80	ISPD	0.333*CO + 0.067*ALD2 + 0.90*FORM + 0.832*PAR + 1.033*HO2 + 0.70*XO2 + 0.967*C2O3	photolysis
81	OH + TOL	0.08*XO2 + 0.44*HO2 + 0.36*CRES + 0.56*TO2	8.75E+03
82	TO2 + NO	0.90*NO2 + 0.9*HO2 + 0.9*OPEN + 0.1*RNO3	1.20E+04
83	TO2	CRES + HO2	2.52E+02
84	OH + CRES	0.40*CRO + 0.60*XO2 + 0.6*HO2 + 0.30*OPEN	6.06E+04
85	NO3 + CRES	CRO + HNO3	3.25E+04
86	CRO + NO2	RNO3	2.07E+04
87	OPEN	C2O3 + HO2 + CO	photolysis
88	OPEN + OH	XO2 + 2.0*CO + 2.0*HO2 + C2O3 + FORM	4.43E+04
89	OPEN + O3	0.03*ALD2 + 0.62*C2O3 + 0.70*FORM + 0.03*XO2 + 0.69*CO + 0.08*OH + 0.76*HO2 + 0.2*MGLY	1.49E-02
90	OH + XYL	0.70*HO2 + 0.10*XO2 + 1.10*PAR + 0.20*CRES + 0.30*TO2 + 0.80*MGLY	3.71E+04
91	MGLY	C2O3 + HO2 + CO	photolysis
92	OH + MGLY	XO2 + C2O3	2.51E+04
93	XO2 + NO	NO2	1.13E+04
94	XO2N + NO	RNO3	1.13E+04

Reaction Number	Reactants	Products	k_{298}[1] (ppm^{-n} min^{-1})
95	XO2 + XO2		6.99E+02
96	XO2 + HO2		8.22E+03
97	XO2N + HO2		8.22E+03
98	XO2N + XO2N		6.99E+02
99	XO2 + XO2N		1.40E+03

Notes:
[1] Rate constants are shown for 298 K and 1 atmosphere in units of ppm and minutes.

CB-IVxi

Table A-2.4. Reactions added in the CB-IVxi mechanism (Yarwood *et al.*, 2005a).

Number	Reaction
101	O1D + H2 = OH + HO2
102	OH + H2 = HO2
103	OH + O = HO2
104	OH + OH = O
105	OH + OH = H2O2
106	HO2 + O = OH
107	H2O2 + O = OH + HO2
108	NO3 + O = NO2
109	NO3 + OH = HO2 + NO2
110	NO3 + HO2 = HNO3
111	NO3 + O3 = NO2
112	NO3 + NO3 = 2 NO2
113	PAN = C2O3 + NO2
114	HNO3 = OH + NO2
115	N2O5 = NO2 + NO3
116	NTR = NO2 + XO2
117	PNA = 0.61 HO2 + 0.61 NO + 0.39 OH + 0.39 NO2

Table A-2.5. Rate constants for reactions added in the CB-IVxi mechanism (Yarwood *et al*., 2005a).

Reaction Number	k_{298} (ppm^{-1} min^{-1})	Temperature Effect E/R (K)
101	162600	
102	9.89	2000
103	48640	-120
104	41200	
105	9298	Fall off expression
106	86750	-200
107	2.5	2000
108	14780	
109	32500	
110	5200	
111	0.015	
112	0.34	2450
113	0.0014 x JHCHOr	
114	0.025 x JHCHOr	
115	0.006 x JNO2	
116	0.1 x JHCHOr	
117	0.00063 x JNO2	

CB05

Table A-2.6. Reactions in the CB05 core mechanism (Yarwood *et al*., 2005b).

Label	Reactants	Products	Rate Expression	Notes
R1	NO2	NO + O	1.0 x <NO2_SAPRC99>	20
R2	O+O2+M	O3 + M	6.0E–34^–2.4	1
R3	O3+NO	NO2	3.0E–12 @ 1500	1
R4	O+NO2	NO	5.6E–12 @ –180	1
R5	O+NO2	NO3	2.5E–31^–1.8 & 2.2E–11^–0.7	1
R6	O+NO	NO2	9.0E–32^–1.5 & 3.0E–11	1
R7	NO2+O3	NO3	1.2E–13 @ 2450	1
R8	O3	O	1.0 x <O3_O3P_IUPAC05>	2
R9	O3	O1D	1.0 x <O3_O1D_IUPAC05>	2
R10	O1D+M	O + M	2.1E–11 @ –102	1
R11	O1D+H2O	2*OH	2.20E–10	1
R12	O3+OH	HO2	1.7E–12 @ 940	1
R13	O3+HO2	OH	1.0E–14 @ 490	1
R14	NO3	NO2 + O	1.0 x <NO3NO2_SAPRC99>	20
R15	NO3	NO	1.0 x <NO3NO_SAPRC99>	20
R16	NO3+NO	2*NO2	1.5E–11 @ –170	1
R17	NO3+NO2	NO + NO2	4.5E–14 @ 1260	1
R18	NO3+NO2	N2O5	2.0E–30^–4.4 &	1

Label	Reactants	Products	Rate Expression	Notes
			1.4E–12^–0.7	
R19	N2O5+H2O	2*HNO3	2.50E–22	2
R20	N2O5+H2O+H2O	2*HNO3	1.80E–39	2
R21	N2O5	NO3 + NO2	1E–03^–3.5 @ 11000 & 9.7E14^0.1 @ 11080 & 0.45 & 1.0	2
R22	NO+NO+O2	2*NO2	3.3E–39 @ –530	2
R23	NO+NO2+H2O	2*HONO	5.00E–40	3
R24	NO+OH	HONO	7.0E–31^–2.6 & 3.6E–11^–0.1	1
R25	HONO	NO + OH	1.0 x <HONO_IUPAC05>	2
R26	OH+HONO	NO2	1.8E–11 @ 390	1
R27	HONO+HONO	NO + NO2	1.00E–20	4
R28	NO2+OH	HNO3	2.0E–30^–3.0 & 2.5E–11	1
R29	OH+HNO3	NO3	%2 2.4E–14 @ –460 & 2.7E–17 @ –2199 & 6.5E–34 @ –1335	1
R30	HO2+NO	OH + NO2	3.5E–12 @ –250	1
R31	HO2+NO2	PNA	1.8E–31^–3.2 & 4.7E–12 & 0.6	2
R32	PNA	HO2 + NO2	4.1E–5 @ 10650 & 4.8E15 @ 11170 & 0.6	2
R33	OH+PNA	NO2	1.3E–12 @ –380	1
R34	HO2+HO2	H2O2	%3 2.3E–13 @ –600 & 1.7E–33 @ –1000	1
R35	HO2+HO2+H2O	H2O2	%3 3.22E–34 @ –2800 & 2.38E–54 @ –3200	1
R36	H2O2	2*OH	1.0 x <H2O2_SAPRC99>	20
R37	OH+H2O2	HO2	2.9E–12 @ 160	1
R38	O1D+H2	OH + HO2	1.10E–10	1
R39	OH+H2	HO2	5.5E–12 @ 2000	1
R40	OH+O	HO2	2.2E–11 @ –120	1
R41	OH+OH	O	4.2E–12 @ 240	1
R42	OH+OH	H2O2	6.9E–31^–1.0 & 2.6E–11^0	1
R43	OH+HO2		4.8E–11 @ –250	1
R44	HO2+O	OH	3.0E–11 @ –200	1
R45	H2O2+O	OH + HO2	1.4E–12 @ 2000	1
R46	NO3+O	NO2	1.00E–11	1
R47	NO3+OH	HO2 + NO2	2.20E–11	1
R48	NO3+HO2	HNO3	3.50E–12	1
R49	NO3+O3	NO2	1.00E–17	5
R50	NO3+NO3	2*NO2	8.5E–13 @ 2450	1
R51	PNA	0.610*HO2 + 0.610*NO2 + 0.390*OH + 0.390*NO3	1.0 x <HO2NO2_IUPAC05>	2
R52	HNO3	OH + NO2	1.0 x <HNO3_IUPAC05>	2
R53	N2O5	NO2 + NO3	1.0 x <N2O5_IUPAC05>	2
R54	XO2+NO	NO2	2.6E–12 @ –365	6

Label	Reactants	Products	Rate Expression	Notes
R55	XO2N+NO	NTR	2.6E–12 @ –365	6
R56	XO2+HO2	ROOH	7.5E–13 @ –700	7
R57	XO2N+HO2	ROOH	7.5E–13 @ –700	7
R58	XO2+XO2		6.80E–14	8
R59	XO2N+XO2N		6.80E–14	8
R60	XO2+XO2N		6.80E–14	8
R61	NTR+OH	HNO3 + HO2 + 0.330*FORM + 0.330*ALD2 + 0.330*ALDX – 0.660*PAR	5.9E–13 @ 360	9
R62	NTR	NO2 + HO2 + 0.330*FORM + 0.330*ALD2 + 0.330*ALDX – 0.660*PAR	1.0 x <NTR_IUPAC05>	28
R63	ROOH+OH	XO2 + 0.500*ALD2 + 0.500*ALDX	3.01E–12 @ –190	1
R64	ROOH	OH + HO2 + 0.500*ALD2 + 0.500*ALDX	1.0 x <COOH_SAPRC99>	20
R65	OH+CO	HO2	%3 1.44E–13 @ 0.0 & 3.43E–33 @ 0.0	2
R66	OH+CH4	MEO2	2.45E–12 @ 1775	1
R67	MEO2+NO	FORM + HO2 + NO2	2.8E–12 @ –300	1
R68	MEO2+HO2	MEPX	4.1E–13 @ –750	1
R69	MEO2+MEO2	1.370*FORM + 0.740*HO2 + 0.630*MEOH	9.5E–14 @ –390	1
R70	MEPX+OH	0.700*MEO2 + 0.300*XO2 + 0.300*HO2	3.8E–12 @ –200	1
R71	MEPX	FORM + HO2 + OH	1.0 x <COOH_SAPRC99>	20
R72	MEOH+OH	FORM + HO2	7.3E–12 @ 620	1
R73	FORM+OH	HO2 + CO	9.00E–12	1
R74	FORM	2*HO2 + CO	1.0 x <HCHO_R_SAPRC99>	20
R75	FORM	CO	1.0 x <HCHO_M_SAPRC99>	20
R76	FORM+O	OH + HO2 + CO	3.4E–11 @ 1600	1
R77	FORM+NO3	HNO3 + HO2 + CO	5.80E–16	1
R78	FORM+HO2	HCO3	9.7E–15 @ –625	2
R79	HCO3	FORM + HO2	2.4E+12 @ 7000	1
R80	HCO3+NO	FACD + NO2 + HO2	5.60E–12	1
R81	HCO3+HO2	MEPX	5.6E–15 @ –2300	1
R82	FACD+OH	HO2	4.00E–13	1
R83	ALD2+O	C2O3 + OH	1.8E–11 @ 1100	1
R84	ALD2+OH	C2O3	5.6E–12 @ –270	1
R85	ALD2+NO3	C2O3 + HNO3	1.4E–12 @ 1900	1
R86	ALD2	MEO2 + CO + HO2	1.0 x <CCHO_R_SAPRC99>	20
R87	C2O3+NO	MEO2 + NO2	8.1E–12 @ –270	1
R88	C2O3+NO2	PAN	2.7E–28^–7.1 & 1.2E–11^–0.9 & 0.3	2
R89	PAN	C2O3 + NO2	4.9E–3 @ 12100 & 5.4E16 @ 13830 & 0.3	2
R90	PAN	C2O3 + NO2	1.0 x <PAN_IUPAC05>	2
R91	C2O3+HO2	0.800*PACD + 0.200*AACD + 0.200*O3	4.3E–13 @ –1040	1
R92	C2O3+MEO2	0.900*MEO2 + 0.900*HO2 + FORM + 0.100*AACD	2.0E–12 @ –500	1
R93	C2O3+XO2	0.900*MEO2 + 0.100*AACD	4.4E–13 @ –1070	2

Label	Reactants	Products	Rate Expression	Notes
R94	C2O3+C2O3	2*MEO2	2.9E–12 @ –500	1
R95	PACD+OH	C2O3	4.0E–13 @ –200	10
R96	PACD	MEO2 + OH	0.0 x <COOH_SAPRC99>	20
R97	AACD+OH	MEO2	4.0E–13 @ –200	1
R98	ALDX+O	CXO3 + OH	1.3E–11 @ 870	11
R99	ALDX+OH	CXO3	5.1E–12 @ –405	2
R100	ALDX+NO3	CXO3 + HNO3	6.50E–15	2
R101	ALDX	MEO2 + CO + HO2	1.0 x <C2CHO_SAPRC99>	20
R102	CXO3+NO	ALD2 + NO2 + HO2 + XO2	6.7E–12 @ –340	2
R103	CXO3+NO2	PANX	2.7E–28^–7.1 & 1.2E–11^–0.9 & 0.3	12
R104	PANX	CXO3 + NO2	4.9E–3 @ 12100 & 5.4E16 @ 13830 & 0.3	12
R105	PANX	CXO3 + NO2	1.0 x <PAN_IUPAC05>	2
R106	PANX+OH	ALD2 + NO2	3.00E–13	13
R107	CXO3+HO2	0.800*PACD + 0.200*AACD + 0.200*O3	4.3E–13 @ –1040	14
R108	CXO3+MEO2	0.900*ALD2 + 0.900*XO2 + HO2 + 0.100*AACD + 0.100*FORM	2.0E–12 @ –500	15
R109	CXO3+XO2	0.900*ALD2 + 0.100*AACD	4.4E–13 @ –1070	16
R110	CXO3+CXO3	2*ALD2 + 2*XO2 + 2*HO2	2.9E–12 @ –500	1
R111	CXO3+C2O3	MEO2 + XO2 + HO2 + ALD2	2.9E–12 @ –500	1
R112	PAR+OH	0.870*XO2 + 0.130*XO2N + 0.110*HO2 + 0.060*ALD2 – 0.110*PAR + 0.760*ROR + 0.050*ALDX	8.10E–13	17
R113	ROR	0.960*XO2 + 0.600*ALD2 + 0.940*HO2 – 2.100*PAR + 0.040*XO2N + 0.020*ROR + 0.500*ALDX	1.0E+15 @ 8000	17
R114	ROR	HO2	1.60E+03	17
R115	ROR+NO2	NTR	1.50E–11	17
R116	O+OLE	0.200*ALD2 + 0.300*ALDX + 0.300*HO2 + 0.200*XO2 + 0.200*CO + 0.200*FORM + 0.010*XO2N + 0.200*PAR + 0.100*OH	1.E–11 @ 280	18
R117	OH+OLE	0.800*FORM + 0.330*ALD2 + 0.620*ALDX + 0.800*XO2 + 0.950*HO2 – 0.700*PAR	3.20E–11	21
R118	O3+OLE	0.180*ALD2 + 0.740*FORM + 0.320*ALDX + 0.220*XO2 + 0.100*OH + 0.330*CO + 0.440*HO2 – PAR	6.5E–15 @ 1900	22
R119	NO3+OLE	NO2 + FORM + 0.910*XO2 + 0.090*XO2N + 0.560*ALDX + 0.350*ALD2 – PAR	7E–13 @ 2160	23
R120	O+ETH	FORM + 1.700*HO2 + CO + 0.700*XO2 + 0.300*OH	1.04E–11 @ 792	4
R121	OH+ETH	XO2 + 1.560*FORM + 0.220*ALDX + HO2	1.0E–28^–0.8 & 8.8E–12	1
R122	O3+ETH	FORM + 0.630*CO + 0.130*HO2 + 0.130*OH + 0.370*FACD	1.2E–14 @ 2630	1
R123	NO3+ETH	NO2 + XO2 + 2.0*FORM	3.3E–12 @ 2880	2
R124	IOLE+O	1.240*ALD2 + 0.660*ALDX + 0.100*HO2 + 0.100*XO2 + 0.100*CO + 0.100*PAR	2.3E–11	26
R125	IOLE+OH	1.300*ALD2 + 0.700*ALDX + HO2 + XO2	1.0E–11 @ –550	26
R126	IOLE+O3	0.650*ALD2 + 0.350*ALDX + 0.250*FORM + 0.250*CO + 0.500*O + 0.500*OH + 0.500*HO2	8.4E–15 @ 1100	26

Label	Reactants	Products	Rate Expression	Notes
R127	IOLE+NO3	1.180*ALD2 + 0.640*ALDX + HO2 + NO2	9.6E–13 @ 270	26
R128	TOL+OH	0.440*HO2 + 0.080*XO2 + 0.360*CRES + 0.560*TO2	1.8E–12 @ –355	24
R129	TO2+NO	0.900*NO2 + 0.900*HO2 + 0.900*OPEN + 0.100*NTR	8.10E–12	17
R130	TO2	CRES + HO2	4.2	17
R131	OH+CRES	0.400*CRO + 0.600*XO2 + 0.600*HO2 + 0.300*OPEN	4.10E–11	17
R132	CRES+NO3	CRO + HNO3	2.20E–11	17
R133	CRO+NO2	NTR	1.40E–11	17
R134	CRO+HO2	CRES	5.50E–12	25
R135	OPEN	C2O3 + HO2 + CO	9.0 x <HCHO_R_SAPRC99>	20
R137	OPEN+O3	0.030*ALDX + 0.620*C2O3 + 0.700*FORM + 0.030*XO2 + 0.690*CO + 0.080*OH + 0.760*HO2 + 0.200*MGLY	5.4E–17 @ 500	17
R138	OH+XYL	0.700*HO2 + 0.500*XO2 + 0.200*CRES + 0.800*MGLY + 1.100*PAR + 0.300*TO2	1.7E–11 @ –116	17
R139	OH+MGLY	XO2 + C2O3	1.7E–11	17
R140	MGLY	C2O3 + HO2 + CO	1.0 x <MGLY_IUPAC05>	2
R141	O+ISOP	0.750*ISPD + 0.500*FORM + 0.250*XO2 + 0.250*HO2 + 0.250*CXO3 + 0.250*PAR	3.60E–11	19
R142	OH+ISOP	0.912*ISPD + 0.629*FORM + 0.991*XO2 + 0.912*HO2 + 0.088*XO2N	2.54E–11 @ –407.6	19
R143	O3+ISOP	0.650*ISPD + 0.600*FORM + 0.200*XO2 + 0.066*HO2 + 0.266*OH + 0.200*CXO3 + 0.150*ALDX + 0.350*PAR + 0.066*CO	7.86E–15 @ 1912	19
R144	NO3+ISOP	0.200*ISPD + 0.800*NTR + XO2 + 0.800*HO2 + 0.200*NO2 + 0.800*ALDX + 2.400*PAR	3.03E–12 @ 448	19
R145	OH+ISPD	1.565*PAR + 0.167*FORM + 0.713*XO2 + 0.503*HO2 + 0.334*CO + 0.168*MGLY + 0.252*ALD2 + 0.210*C2O3 + 0.250*CXO3 + 0.120*ALDX	3.36E–11	19
R146	O3+ISPD	0.114*C2O3 + 0.150*FORM + 0.850*MGLY + 0.154*HO2 + 0.268*OH + 0.064*XO2 + 0.020*ALD2 + 0.360*PAR + 0.225*CO	7.10E–18	19
R147	NO3+ISPD	0.357*ALDX + 0.282*FORM + 1.282*PAR + 0.925*HO2 + 0.643*CO + 0.850*NTR + 0.075*CXO3 + 0.075*XO2 + 0.150*HNO3	1.00E–15	19
R148	ISPD	0.333*CO + 0.067*ALD2 + 0.900*FORM + 0.832*PAR + 1.033*HO2 + 0.700*XO2 + 0.967*C2O3	0.0036 x <ACROLEIN_SAPRC99>	20
R149	TERP+O	0.150*ALDX + 5.12*PAR	3.60E–11	20
R150	TERP+OH	0.750*HO2 + 1.250*XO2 + 0.250*XO2N + 0.280*FORM + 1.66*PAR + 0.470*ALDX	1.5E–11 @ –449	20
R151	TERP+O3	0.570*OH + 0.070*HO2 + 0.760*XO2 + 0.180*XO2N + 0.240*FORM + 0.001*CO + 7.000*PAR + 0.210*ALDX + 0.390*CXO3	1.2E–15 @ 821	20
R152	TERP+NO3	0.470*NO2 + 0.280*HO2 + 1.030*XO2 + 0.250*XO2N + 0.470*ALDX + 0.530*NTR	3.7E–12 @ –175	20
R153	SO2+OH	SULF + HO2	3.0E–31^–3.3 & 1.5E–12	1
R154	OH+ETOH	HO2 + 0.900*ALD2 + 0.050*ALDX + 0.100*FORM + 0.100*XO2	6.9E–12 @ 230	1
R155	OH+ETHA	0.991*ALD2 + 0.991*XO2 + 0.009*XO2N + HO2	8.7E–12 @ 1070	1

Label	Reactants	Products	Rate Expression	Notes
R156	NO2+ISOP	0.200*ISPD + 0.800*NTR + XO2 + 0.800*HO2 + 0.200*NO + 0.800*ALDX + 2.400*PAR	1.50E–19	19

Table Notes:

Rate constants are in units of molecules cm^{-3} and $seconds^{-1}$

Read rate expressions as follows:

A / <J_label>	k = A x j
A @ E	k = A x exp(–E/T)
A ^ B @ E	k = A x $(T/300)^B$ x exp(–E/T)
A^o ^ B^o @ E^o & A^∞ ^ B^∞ @ E^∞ & F & n	$k = \left[\frac{k^o[M]}{1+k^o[M]/k^\infty}\right]F^G$ where $G = \left[1+\left(\frac{\log(k^o[M]/k^\infty)}{n}\right)^{-2}\right]^{-1}$
%2 A^o @ E^o & A_2 @ E_2 & A_3 @ E_3	$k = k^o + \frac{k_3[M]}{1+k_3[M]/k_2}$
%3 A_1 @ E_1 & A_2 @ E_2	$k = k_1 + k_2[M]$

Table A-2.7. Species names for the CB05 core mechanism (Yarwood *et al*., 2005b).

Species Name	Description	Number of Carbons
NO	Nitric oxide	0
NO2	Nitrogen dioxide	0
O3	Ozone	0
O	Oxygen atom in the $O^3(P)$ electronic state	0
O1D	Oxygen atom in the $O^1(D)$ electronic state	0
OH	Hydroxyl radical	0
HO2	Hydroperoxy radical	0
H2O2	Hydrogen peroxide	0
NO3	Nitrate radical	0
N2O5	Dinitrogen pentoxide	0
HONO	Nitrous acid	0
HNO3	Nitric acid	0
PNA	Peroxynitric acid (HNO_4)	0
CO	Carbon monoxide	1
FORM	Formaldehyde	1
ALD2	Acetaldehyde	2
C2O3	Acetylperoxy radical	2
PAN	Peroxyacetyl nitrate	2
ALDX	Propionaldehyde and higher aldehydes	2
CXO3	C3 and higher acylperoxy radicals	2
PANX	C3 and higher peroxyacyl nitrates	2
XO2	NO to NO2 conversion from alkylperoxy (RO_2) radical	0
XO2N	NO to organic nitrate conversion from alkylperoxy (RO_2) radical	0
NTR	Organic nitrate (RNO_3)	1
ETOH	Ethanol	2

Species Name	Description	Number of Carbons
CH4	Methane	1
MEO2	Methylperoxy radical	1
MEOH	Methanol	1
MEPX	Methylhydroperoxide	1
FACD	Formic acid	1
ETHA	Ethane	2
ROOH	Higher organic peroxide	1
AACD	Acetic and higher carboxylic acids	2
PACD	Peroxyacetic and higher peroxycarboxylic acids	2
PAR	Paraffin carbon bond (C-C)	1
ROR	Secondary alkoxy radical	0
ETH	Ethene	2
OLE	Terminal olefin carbon bond (R-C=C)	2
IOLE	Internal olefin carbon bond (R-C=C-R)	4
ISOP	Isoprene	5
ISPD	Isoprene product (lumped methacrolein, methyl vinyl ketone, etc.)	4
TERP	Terpene	10
TOL	Toluene and other monoalkyl aromatics	7
XYL	Xylene and other polyalkyl aromatics	8
CRES	Cresol and higher molecular weight phenols	8
TO2	Toluene-hydroxyl radical adduct	7
OPEN	Aromatic ring opening product	4
CRO	Methylphenoxy radical	7
MGLY	Methylglyoxal and other aromatic products	3
SO2	Sulfur dioxide	0
SULF	Sulfuric acid (gaseous)	0

A.3 REFERENCES

Carter, W. P. L. (1990). A detailed mechanism for the gas-phase atmospheric reactions of organic compounds. Atmospheric Environment, 24A, 481-518.

Carter, W. P. L. (2007, May). *Documentation of the SAPRC-07 chemical mechanism and updated ozone reactivity scales.* Draft Final Report to the California Air Resources Board, Sacramento, CA.

Carter, W. P. L. (2000). *Documentation of the SAPRC-99 chemical mechanism for VOC reactivity assessment*. Air Pollution Research Center and College of Engineering, Center for Environmental Research and Technology, University of California at Riverside, CA.

Yarwood, G. and Rao, S. (2005b). *Updates to the Carbon Bond chemical mechanism: CB05*. Report to the U.S Environmental Protection Agency, Research Triangle Park, NC.

Yarwood, G., Whitten, G. Z., and Rao, S. (2005a). *Updates to the Carbon Bond 4 photochemical mechanism*. ENVIRON International Corporation. Report to the Lake Michigan Air Directors Consortium.

Appendix B: Comparison of the Carbon Bond and SAPRC photochemical mechanisms under conditions relevant to southeast Texas

B.1 Comparison of the SAPRC99, CB-IV96, and CB-IVXI Mechanisms for Various Emissions of VOCs and NOx

In order to identify the conditions, in terms of VOC/NOx ratios, under which the SAPRC and CB mechanisms diverge in ozone concentrations, the predictions of the mechanisms in scenarios with multiple NOx and VOC emission levels were evaluated. The mechanisms used in this evaluation are the SAPRC99, CB-IV96, and CB-IVxi mechanisms described below.

Carter (2000) provides a comprehensive documentation of the SAPRC99 mechanism. In this thesis, we use the SAPRC99 fixed parameter lumped mechanism. A list of reactions in the fixed parameter lumped mechanism of SAPRC99, followed by the species descriptions are provided in Tables A-1.4 to A-1.5 of Appendix A.

The version of CB-IV released in 1996, which occurred when the Ozone Transport Assessment Group (OTAG) commenced modeling (Yarwood *et al*., 2005). The 1996 version of CB-IV, referred to as the OTAG version of CB-IV, is the version of CB-IV used in this study. In this thesis, this version of the mechanism is termed CB-IV96. The list of reactions and rate constants for the 1996 version of CB-IV, followed by the species definitions, are provided in Tables A-2.1 and A-2.2 of Appendix A, respectively.

Yarwood *et al*. (2005) added seventeen inorganic reactions to the CB-IV96 mechanism described in Chapter 2 in order to describe additional relevant aspects of tropospheric chemistry. Since the reactions mostly involved the inorganic reaction set, the modification was referred to as the extended inorganic chemistry (CB-IVxi). The

reactions added in the CB-IVxi mechanism, followed by the rate constants for those reactions are included in Tables A-2.4 and A-2.5 of Appendix A, respectively.

A total of seventy five CAMx simulations were performed, twenty-five simulations using the CB-IV96 mechanism, twenty-five using the CB-IVxi mechanism (Yarwood et al., 2005) and twenty-five using the SAPRC99 mechanism. For each set of twenty-five runs, emission reductions considering all permutations of 0%, 25%, 50%, 75% and 100% anthropogenic VOC reductions and 0%, 25%, 50%, 75% and 100% NOx reductions were examined. The results are shown in Figures B-1 – B-3, in the form of ozone isopleth diagrams. To generate these isopleth diagrams, daily, area-wide ozone concentrations were determined for each of the 25 emission scenarios. These 25 points fill a rectangular grid in the isopleth diagrams. Lines of constant maximum ozone concentration, for varying degrees of VOC and NOx emission reductions were then interpolated from the 25 data points.

Figures B-1 – B-3 show isopleth diagrams for area-wide peak ozone concentrations on several days of the episode. On all of the days, both the CB-IV96 and SAPRC99 mechanisms lead to qualitatively similar relative reductions in maximum ozone concentrations. Both mechanisms predict NOx disincentives on August 25 and no NOx disincentives on the 31st and September 1. These two mechanisms converge in their predictions of absolute ozone concentrations as NOx is reduced by 80% or more from base case levels. On the other hand, CB-IVxi does not converge with the other two mechanisms at low NOx conditions.

The CB-IVxi mechanism shows similar qualitative responses to VOC and NOx emission reductions on August 25, but is much less responsive to VOC emission reductions on August 31 and September 1. Because the CB-IVxi mechanism is not widely used, and because it diverges from the other two mechanisms at low NOx

conditions, the focus in the main text of this thesis was on explaining differences between the CB-IV96 and the SAPRC99 mechanisms. The CAMx results shown in Figures B-1 – B-3 suggest that the differences in the ozone predictions for the CB-IV96 and SAPRC99 mechanisms occur under a wide variety of conditions.

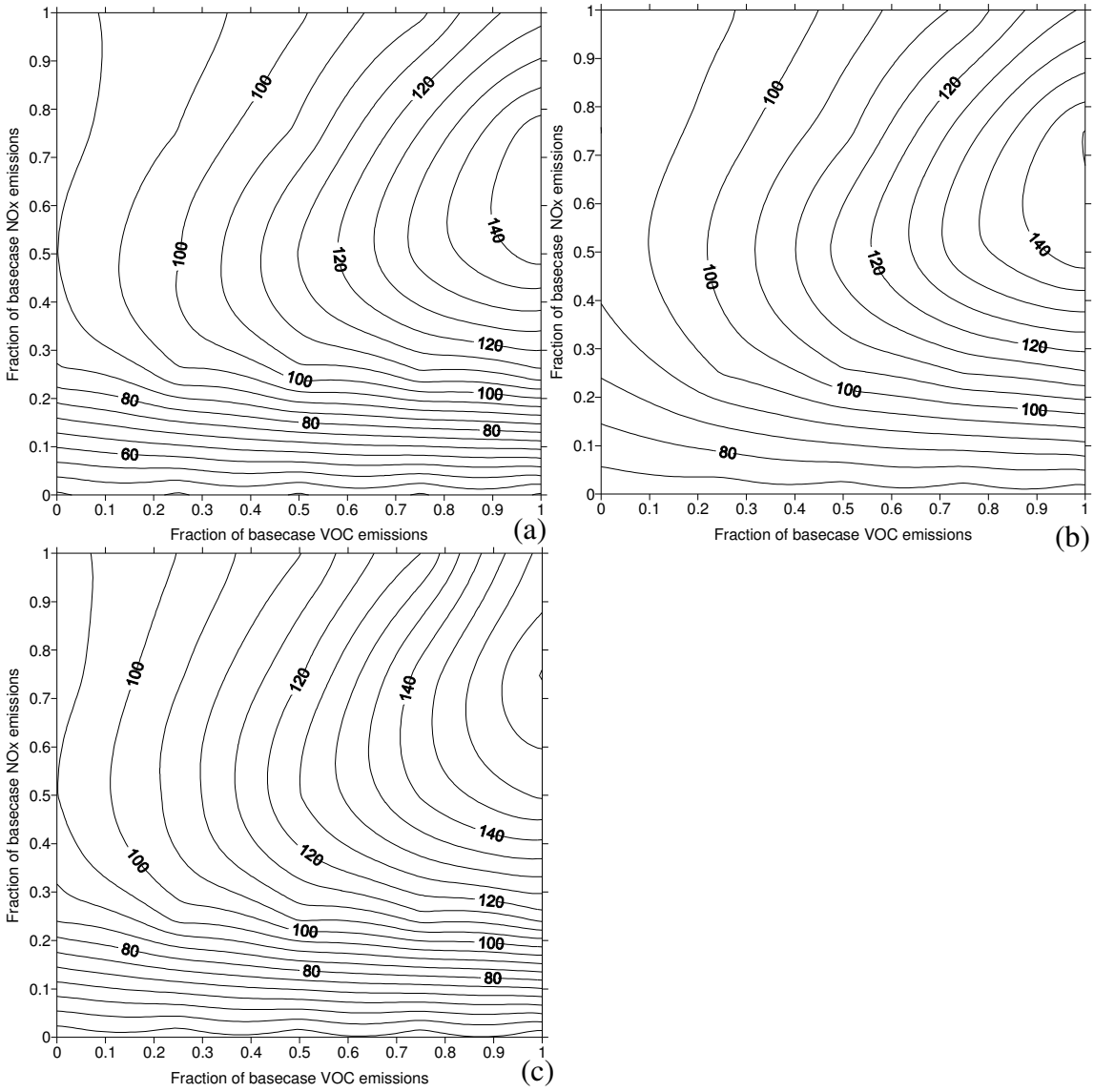

Figure B-1. Response of the area wide maximum ozone concentrations (ppb) on August 25 to VOC and NOx reductions using the (a) CB-IV96, (b)CB-IVxi, and (c) SAPRC99 mechanisms in CAMx.

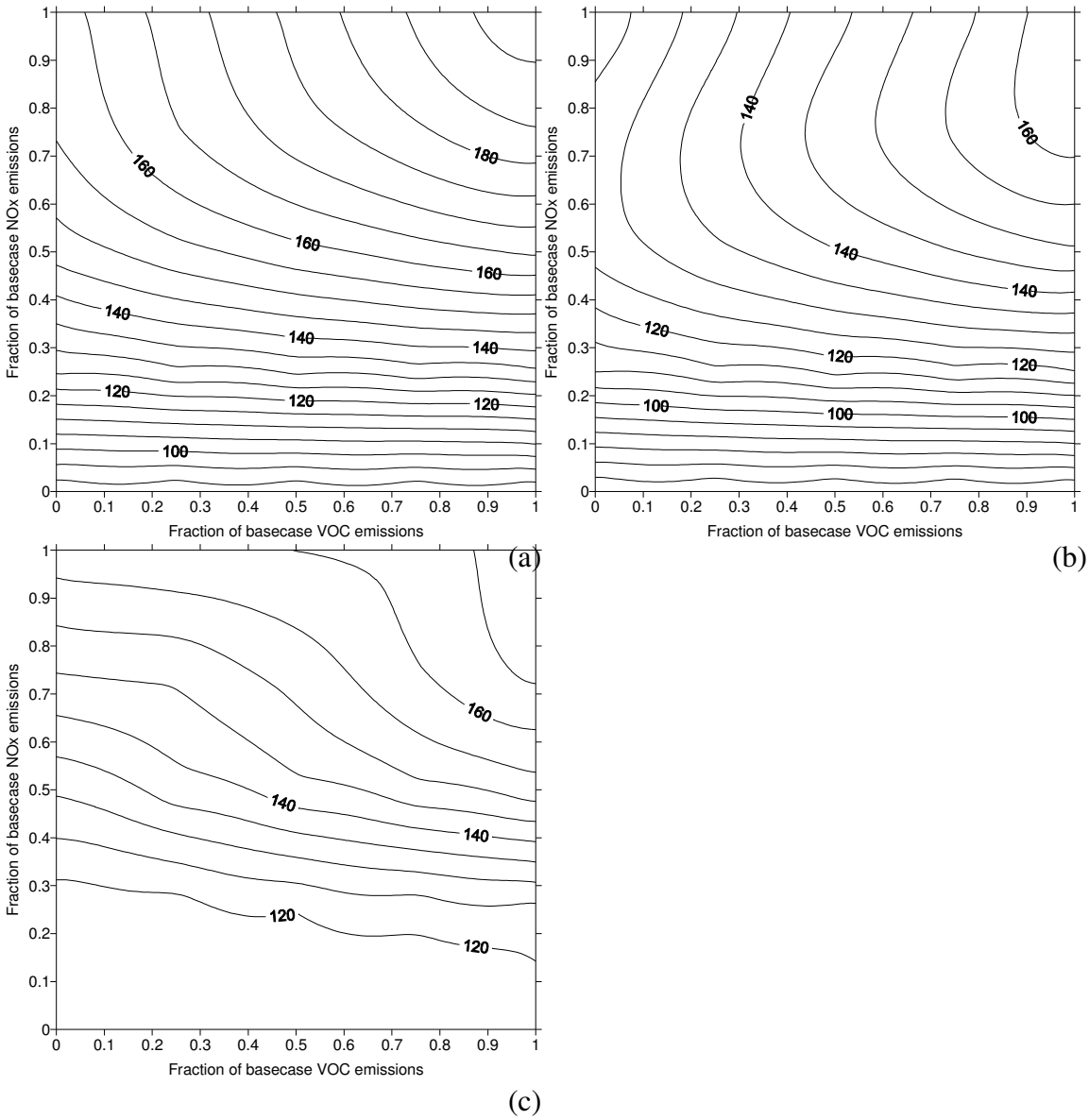

Figure B-2. Response of the area wide maximum ozone concentrations (ppb) on August 31 to VOC and NOx reductions using the (a) CB-IV96, (b) CB-IVxi, and (c) SAPRC99 mechanisms in CAMx.

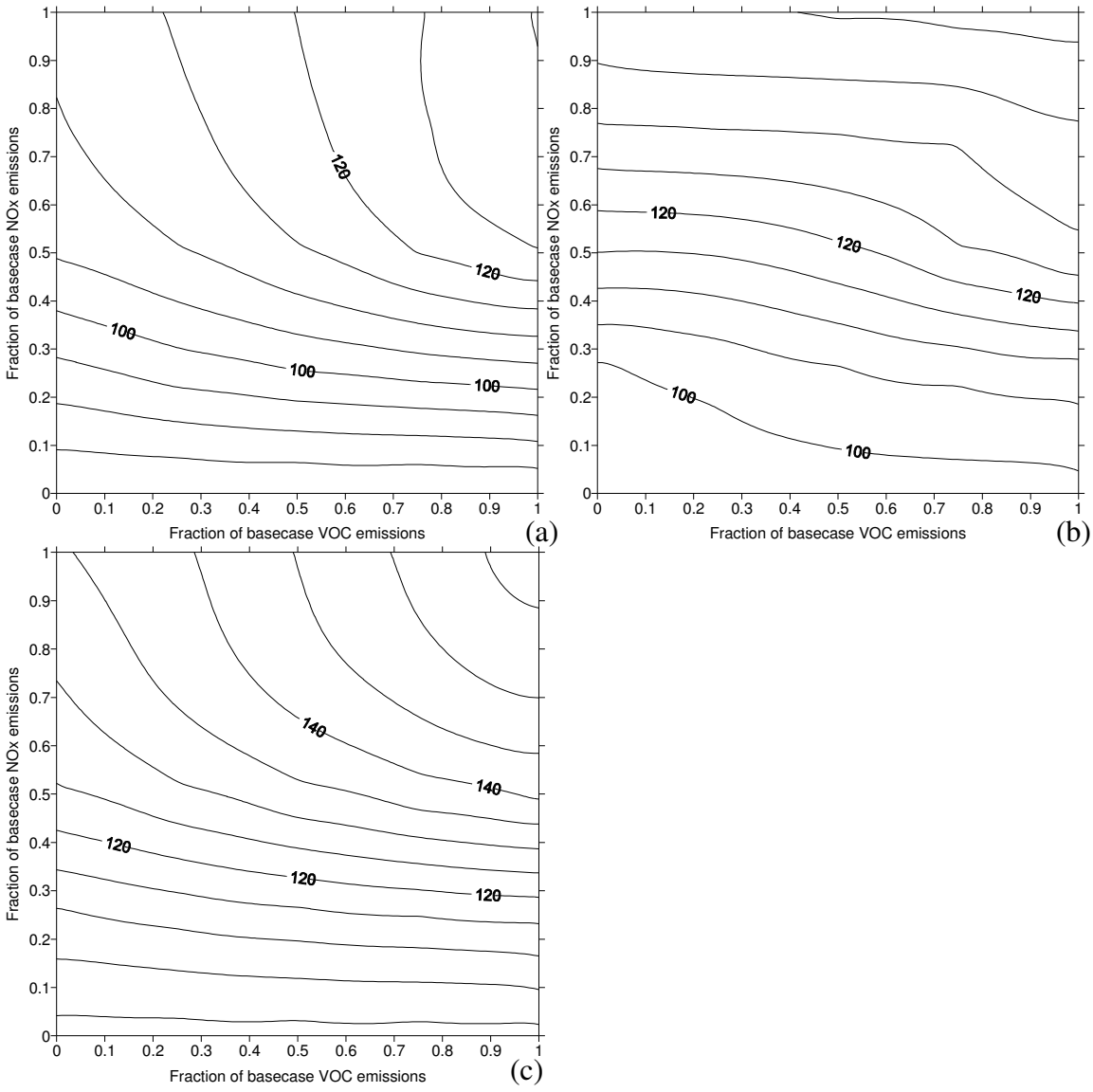

Figure B-3. Response of the area wide maximum ozone concentrations (ppb) on September 1 to VOC and NOx reductions using the (a) CB-IV96, (b)CB-IVxi, and (c) SAPRC99 mechanisms in CAMx.

B.2 POLICY IMPLICATIONS

In an attainment demonstration, to determine if emission reductions will lead to attainment at a monitor, a relative reduction factor (RRF) is estimated. An RRF is typically calculated between a future year and a base year. In this work, an RRF is

calculated between a base year (2000) and a base year (2000) with an applied emissions control. In this method, an RRF for an episode of interest is calculated for a monitoring station as follows:

$$RRF = \frac{\max 8\text{ hr avg } O_3 \text{ with emission controls}}{\max 8\text{ hr avg } O_3}$$

The maximum 8-hour averaged ozone for each monitor is calculated by averaging the daily maximum 8-hour ozone observed in a 7x7 array of cells (for a 4-km grid resolution) around each monitor that exceeds a certain threshold (e.g. 85 ppb), over the episode days. The percent relative reduction in ozone is calculated as follows:

% relative reduction in O_3 = (1 - RRF)*100%

Table B-1 lists the percentage relative reductions in 8-hour ozone concentrations as predicted by the SAPRC99 and CB-IV96 mechanisms in CAMx for monitoring stations located in three different regions of the Houston-Galveston area. The episode for which the RRF was calculated was the August 25-September 6, 2000 episode and the emissions control applied was a 75% reduction in NOx emissions. The emission reductions were applied to all source categories in the 8-county Houston-Galveston area. The Aldine site labeled in green is located in urban Houston, which is typically not impacted by plumes from the Ship Channel region. The Channel View, Deer Park, and Seabrook sites labeled in yellow are located in the Houston Ship Channel region which is characterized by high VOC emissions coemitted with NOx. The Bayland Park and Westhollow sites labeled in orange are located downwind from this source region. The percentage relative reductions for these sites were calculated as follows:

$$\%\ \text{relative reduction} = \left(1 - \frac{\text{max 8 hr avg } O_3 \text{ w/ 75\% NOx cut}}{\text{max 8 hr avg } O_3}\right) * 100\%$$

Table B-1. Relative reductions in 8-hour ozone after 75% NOx cut for selected monitors in the Houston-Galveston area.

Monitor	**SAPRC-99**	**CB-IV**	Difference from CB-IV
Aldine	23.2 %	22.3 %	4.0 %
Chnnlview	17.7 %	12.9 %	37.2 %
DeerPk	15.6 %	8.9 %	75.3 %
Seabrook	16.9 %	7.1 %	138.0 %
BaylandPk	16.2 %	13.6 %	19.1 %
Westhollow	17.8 %	12.0 %	48.3 %

While there is relatively good correspondence between CB-IV96 and SAPRC99 in their response for Aldine, the two mechanisms predict different responses for regions with the industrial source signature or regions downwind from industrial source region. The percentage relative reduction in 8-hour ozone concentrations for other monitoring stations in the Houston-Galveston area are listed in Table B-2, followed by a map of these monitoring stations in Figure B-4.

Table B-2. Relative reductions in 8-hour ozone after 75% NOx cut for monitors in the Houston-Galveston area.

Monitor	SAPRC-99	CB-IV	Difference from CB-IV
HouEast	18.00%	14.00%	28.57%
Aldine	23.20%	22.30%	4.04%
Chnnlview	17.70%	12.90%	37.21%
NWHarris	22.20%	24.10%	-7.88%
Galveston	14.40%	6.90%	108.70%
DeerPark	15.60%	8.90%	75.28%
Seabrook	16.90%	7.10%	138.03%
BaylandPk	16.20%	13.60%	19.12%
Conroe	23.90%	28.90%	-17.30%
HouRegOff	18.10%	14.20%	27.46%
ManvelCrx	22.60%	21.70%	4.15%
Clinton	17.40%	12.60%	38.10%
NWayside	19.30%	16.20%	19.14%
Monroe	17.80%	9.20%	93.48%
Lang	18.40%	15.70%	17.20%
Croquet	16.70%	15.30%	9.15%
Westhollow	17.80%	12.00%	48.33%
TexasAve	17.90%	15.40%	16.23%
HRM3	17.50%	13.30%	31.58%
Wllsville	19.90%	16.50%	20.61%
MustangB	20.20%	25.10%	-19.52%
TexasCity	14.20%	13.40%	5.97%
Lynchburg	15.70%	10.60%	48.11%
TexasCOld	14.10%	14.20%	-0.70%
ConroeOld	23.90%	28.90%	-17.30%

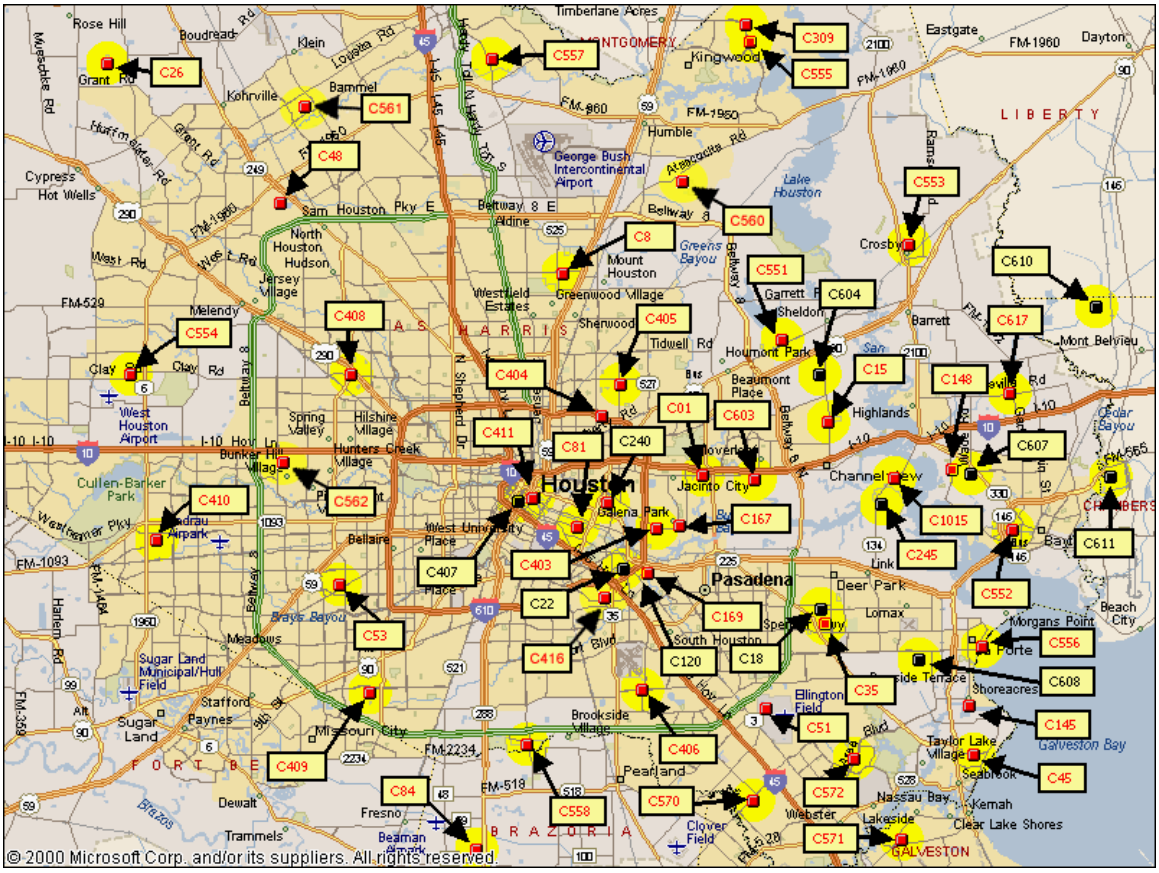

Figure B-4. Monitoring stations in the Houston-Galveston area.

The percentage relative reductions in 8-hour ozone as predicted by the mechanisms were compared to the percentage relative reduction in 8-hour ozone required for monitoring sites in the Ship Channel region and downwind of the Ship Channel region, Deer Park and Bayland Park, respectively, to be in attainment. As shown in Table B-3, SAPRC99 predicts that with a 75% reduction in NOx emissions, the two monitoring sites will bring the sites close to attainment of the 8-hour ozone standard of 85 ppb, while CB-IV96 does not. The relative reduction in 8-hour ozone required for a monitoring station is derived using the design value (DV) for a particular site. The DV is defined as the fourth highest maximum 8-hour averaged ozone concentration for each year,

averaged over three years. The average DVs for the Deer Park and Bayland Park sites were obtained for 2003-2005. The required relative reductions in 8-hour ozone for these two sites to be in attainment were calculated as follows:

$$\%\ \text{required relative reduction} = \left(1 - \frac{85\ \text{ppb}}{\text{DV (ppb)}}\right) * 100\%$$

Table B-3. Required versus predicted relative reductions in ozone with 75% NOx cut

		Relative Reductions in Ozone		
Monitor	Design Value*	Required for Attainment	Predicted with **SAPRC-99**	Predicted with **CB-IV**
DeerPk	101 ppb	15.8 %	15.6 %	8.9 %
BaylandPk	102 ppb	16.7 %	16.2 %	13.6 %

*The fourth highest daily maximum 8-hour averaged ozone concentration for each year averaged over 2003-2005

B.3 REFERENCES

Carter, W. P. L. (2000). *Documentation of the SAPRC-99 chemical mechanism for VOC reactivity assessment*. Air Pollution Research Center and College of Engineering, Center for Environmental Research and Technology, University of California at Riverside, CA.

Yarwood, G., Whitten, G. Z., and Rao, S. (2005). *Updates to the Carbon Bond 4 photochemical mechanism*. ENVIRON International Corporation. Report to the Lake Michigan Air Directors Consortium.

Appendix C:

C.1 PNA (HNO_4) CHEMISTRY IN SAPRC99 AND CB MECHANISMS

SAPRC99

```
HO2 + NO2          ---->          HNO4
                                       @ TROE(1.80E-31*T_300^-3.2, 4.70E-
                                       12*T_300^-0.0, b[M], 0.6);

HNO4               ---->          HO2 + NO2
                                       @ TROE(4.1E-5*EXP(-10650./TK),
                                       5.7E15*EXP(-11170./TK), b[M], 0.5);

HNO4               -hv->          0.610*HO2 + 0.610*NO2 + 0.390*OH
                                  + 0.390*NO3
                                       @j[PNA_to_HO2] ;

HNO4 + OH          ---->          NO2
                                       @ 1.50E-12*EXP(359.8/TK);
```

CB-IV and CB05

```
HO2  + NO2         -M-->          PNA
                                       @ TROE(1.80E-31*T_300^-3.2,
                                       4.70E-12*T_300^-0.0, b[M], 0.6);

PNA                -M-->          HO2 + NO2
                                       @ TROE(4.1E-5*EXP(-10650./TK),
                                       4.8E15*EXP(-11170./TK), b[M], 0.6);

PNA                -hv->           0.610*HO2 + 0.610*NO2 + 0.390*OH +
                                   0.390*NO3
                                       @ j[PNA_to_HO2];

OH   + PNA         ---->           NO2 + H2O + O2
                                       @ 1.30E-12*EXP(380.0/TK);
```

C.2 UNC UPDATED NOX WALL MECHANISM

```
#ifnot  UNCAUXNOXWALLSGZW_RXN_
#define UNCAUXNOXWALLSGZW_RXN_

/* Based on
```

```
 * $Log:
/MorphoModel/Mechanisms/Sources/stdinclude/UNCAuxNOxWalls01.rxn $
 *
 * Version by GZW for UT comparison study between CB4, CB05, and
SAPRC99
 * Completed on 13 July, 2007
 *
 */

/*****************************************************************
*                                                                *
*   UNC Chamber Dependent Inorganic Reactions (Walls)            *
*   Units are molecules/cc/secs ( 13 July, 2007, GZW)            *
*                                                                *
*****************************************************************/


/* ------------------------P a r t  O n e ----------------------- */


//
================================================================================
//                                                  NO2 wall reactions
//
SCALAR
 sf_depoNO2f  = 1.0,
 sf_depoNO2r  = 1.0,

#select
#case _S99_CAMx_
 sf_depoNO2f = 1.0,
#end

sf_WNO2WNO   = 1.0;

 R[DepoNO2f ] =                NO2      ---->  WNO2        @ 4.0E-06 *
sf_depoNO2f ;
 R[DepoNO2r ] =                WNO2     ---->  NO2         @ 3.5E-05 *
sf_depoNO2r ;

 R[DepoNOf ]  =                NO       ---->  WNO         @ 1.0E-05 *
sf_depoNO2f ;
 R[DepoNOr ]  =                WNO      ---->  NO          @ 3.5E-05 *
sf_depoNO2r ;

#select
#case _S99_CAMx_
 R[HNO4pWH2O] =     HNO4    +  WH2O     ---->  WHNO3               @
3.0E-17* sf_WNO2WNO ;
#case _CB05_
 R[PNApWH2O]  =     PNA     +  WH2O     ---->  WHNO3               @
3.0E-17* sf_WNO2WNO ;
#case _CB4_CAMx_
```

```
 R[PNApWH2O]  =     PNA     +  WH2O     ---->  WHNO3               @
3.0E-17* sf_WNO2WNO ;
#else
#message "check if mechanism is listed in UNCAuxNOxWallGZW, for PNA"
#end

 R[WNOpWNO2]=       WNO     +  WNO2     ---->  2.0*WHONO          @
1.0E-13* sf_WNO2WNO ;

//  Chamber wall water loss of N2O5
SCALARS
 sf_WH2OpN2O5 = 1.0;

 R[WH2ON2O5] = WH2O + N2O5    ----> 2.0*HNO3   @ 2.0E-17 * sf_WH2OpN2O5
;

// Chamber wall NOx production
// 1.0E-6 used before
 SCALARS
  sf_wall_NOx_src = 0.0;  // "scale factor", not rate

 R[WHNO3toNO2] =          WHNO3  -hv-> NO2                      @
sf_wall_NOx_src *

j[NO2_to_O3P];

//#end


#end   // UNCAUXNOXWALLS01_RXN_
```

C.3 UNC OLDER NOX WALL MECHANISM

```
#ifnot  UNCAUXNOXWALLSGZW_RXN_
#define UNCAUXNOXWALLSGZW_RXN_

/* Based on
 * $Log:
/MorphoModel/Mechanisms/Sources/stdinclude/UNCAuxNOxWalls01.rxn $
 *
 * 1     4/02/01 10:53a Jeffries
 * First version added
 *
 */

/*****************************************************************
*                                                                *
*   UNC Chamber Dependent Inorganic Reactions (Walls)            *
*   Units are molecules/cc/secs ( 3/10/99, HEJ )                 *
*                                                                *
*****************************************************************/
```

```
/* ------------------------P a r t  O n e ---------------------- */


//
=========================================================================
//                                                  NO2 wall water
reactions
//
SCALAR
 sf_depoNO2f  = 1.0,
 sf_depoNO2r  = 1.0,
 sf_WH2OpWNO2 = 1.0;

 R[DepoNO2f ] =     NO2     +  H2O      ---->  WNO2                @
1.0E-23* sf_depoNO2f;
 R[DepoNO2r ] =                WNO2     ---->  NO2                 @
1.0E-4 * sf_depoNO2r;

 R[DepoNOf ] =      NO      +  H2O      ---->  WNO                 @
1.5E-23* sf_depoNO2f;
 R[DepoNOr ] =                 WNO      ---->  NO                  @
1.0E-4 * sf_depoNO2r;

#select
#case _S99_CAMx_
 R[WNO2pWNO2] =     HNO4     +  WH2O     ---->  WHNO3               @
1.0E-16* sf_WH2OpWNO2;
#case _CB05_
 R[WNO2pWNO2] =     PNA     +  WH2O     ---->  WHNO3               @
1.0E-16* sf_WH2OpWNO2;
#case _CB4_CAMx_
 R[WNO2pWNO2] =     PNA     +  WH2O     ---->  WHNO3               @
1.0E-16* sf_WH2OpWNO2;
#else
#message "check if mechanism is listed in UNCAuxNOxWallGZW, for PNA"
#end
 R[WN2O4pWNO2] =               WHNO3    ---->  NO2                 @
5.0E-5 * sf_WH2OpWNO2;
 R[WH2OpWN2O4]=     WNO     +  WNO2     ---->  2.0*WHONO           @
2.0E-13* sf_WH2OpWNO2;


SCALARS
 sf_WHNO3pNOpNO2_src = 0.0;

 R[WHNO3pNOpNO2] = WHO2 + N2O5    ----> 2.0*HNO3   @ 5.0E-14 *
sf_WHNO3pNOpNO2_src;
```

```
#if _HONOJNO2_
//
=========================================================================
//                                                          WNO2 acid
reactions
//
// HONO production, independent of WHNO3
 SCALARS
  sf_HONO_wall_src = 1.0E-6;  // "scale factor", not rate

 R[WNO2hvHONO] =           NO2   -hv-> HONO                  @
sf_HONO_wall_src *

j[NO2_to_O3P];

#end


#end   // UNCAUXNOXWALLS01_RXN_
```

C.4 UNC WALL PARAMETERS ASSIGNED FOR OLEFINS EXPERIMENTS

```
  sf_WH2OpN2O5    = 9.0    // N2O5 + WH2O --> 2.0*WHNO3
  sf_depoNO2f     = 1.0    // NO2 + WH2O --> WHNO2
  sf_depoNO2r     = 1.0    // WNO2-->NO2
  sf_WH2OpWNO2    = 0.1    // WNO2-->WHONO
```

Appendix D: Effect of wall mechanism on chamber simulations in CO-NOx simulations

Three CO-NOx simulations, described in Table D-1, were prepared for use both in Morpho and in SAPRC software. Initial conditions for the simulations were generally based on experiment EPA326A in SARPC's smog chamber database, which had time independent light conditions, however these three simulations are not intended to reproduce any single experiment, and will not be compared to chamber data.

Table D-1. The initial conditions of three CO-NOx cases in Morpho and SAPRC*.

	CO(50)	CO(100)	CO(250)
NO	0.01533	0.01533	0.01533
NO_2	0.01002	0.01002	0.01002
HONO	5.00E-05	5.00E-05	5.00E-05
CO	**51**	**100**	**250**

*: The units of the initial concentrations are ppm. Time-independent air exchange of 0 hr^{-1}, air temperature of 305 K and humidity of 20,000 ppm (or 20.27 milli bar) were used.

As shown in Figures D-1 and D-2, activating PNA reactions in the CO-NOx simulations, decreased the ozone concentration (O_3 concentration at t =10 hours after the chamber injection) up to 6 % in the CO(100) simulation, and up to 8 ppb in the CO(250) simulation. In contrast, in the simulations using the UNC chamber model, including the wall reactions had a complex effect. For the CO(50) and CO (100) simulations, turning on the wall and PNA chemistry increased the ozone concentrations for both the SAPRC and CB chemical mechanisms; however, for the case of CO(250) simulation, turning on the wall mechanism decreased the ozone concentrations (Figure D-1). If the UCR chamber model is used, turning on the wall mechanism increased the ozone concentrations in all three simulations for all of the mechanisms, as shown in Figure D-2.

As quantitatively summarized in Table D-2, the modeling of wall effects in the UNC chamber model both increased and decreased ozone concentrations, while with the UCR chamber model, modeling wall effects consistently increased final ozone concentrations (O_3 at t = 10 hours).

Table D-2. Ozone concentrations (ppm) at 10 hr for CO-NOx simulations.

	UNC Chamber Model			UCR Chamber Model		
CO(50)	S99	CB4	CB05	S99	CB4	CB05
Wall(off)/PNA(off)	0.027	0.017	0.021	0.026	0.017	0.021
Wall(off)/PNA(on)	0.027	0.017	0.021	0.026	0.017	0.020
Wall(on)/PNA(on)	0.089	0.086	0.085	0.160	0.165	0.164
CO(100)	S99	CB4	CB05	S99	CB4	CB05
Wall(off)/PNA(off)	0.096	0.055	0.076	0.092	0.054	0.074
Wall(off)/PNA(on)	0.090	0.053	0.072	0.087	0.052	0.070
Wall(on)/PNA(on)	0.097	0.095	0.093	0.201	0.211	0.199
CO(250)	S99	CB4	CB05	S99	CB4	CB05
Wall(off)/PNA(off)	0.179	0.159	0.159	0.178	0.160	0.158
Wall(off)/PNA(on)	0.171	0.151	0.152	0.169	0.152	0.151
Wall(on)/PNA(on)	0.103	0.102	0.099	0.229	0.242	0.222

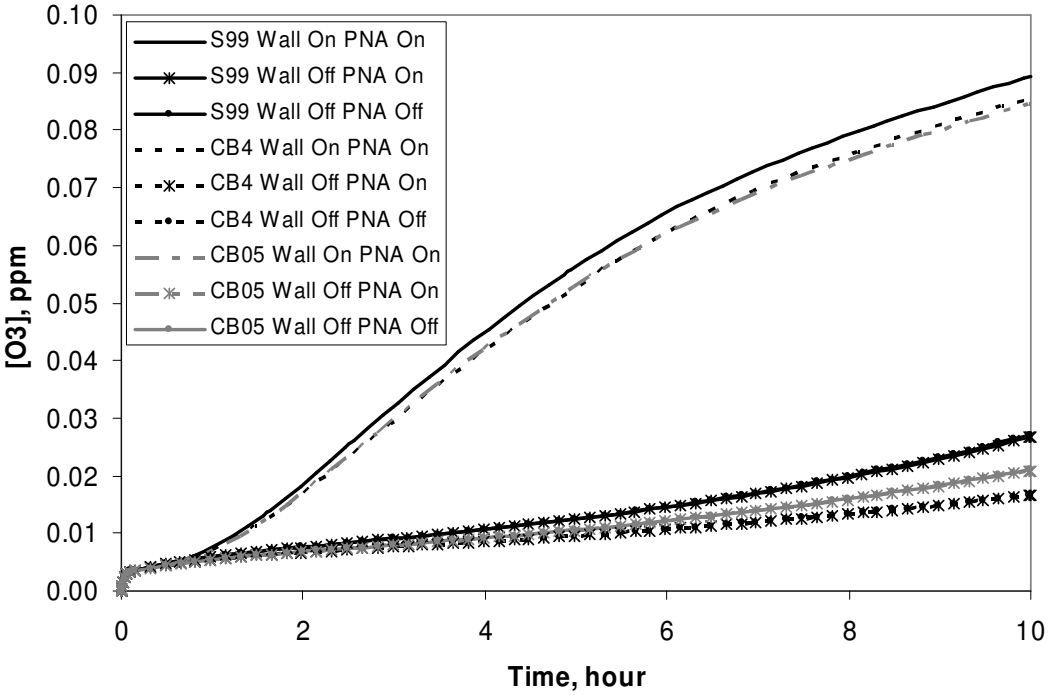

(a) Case CO(50) in Morpho

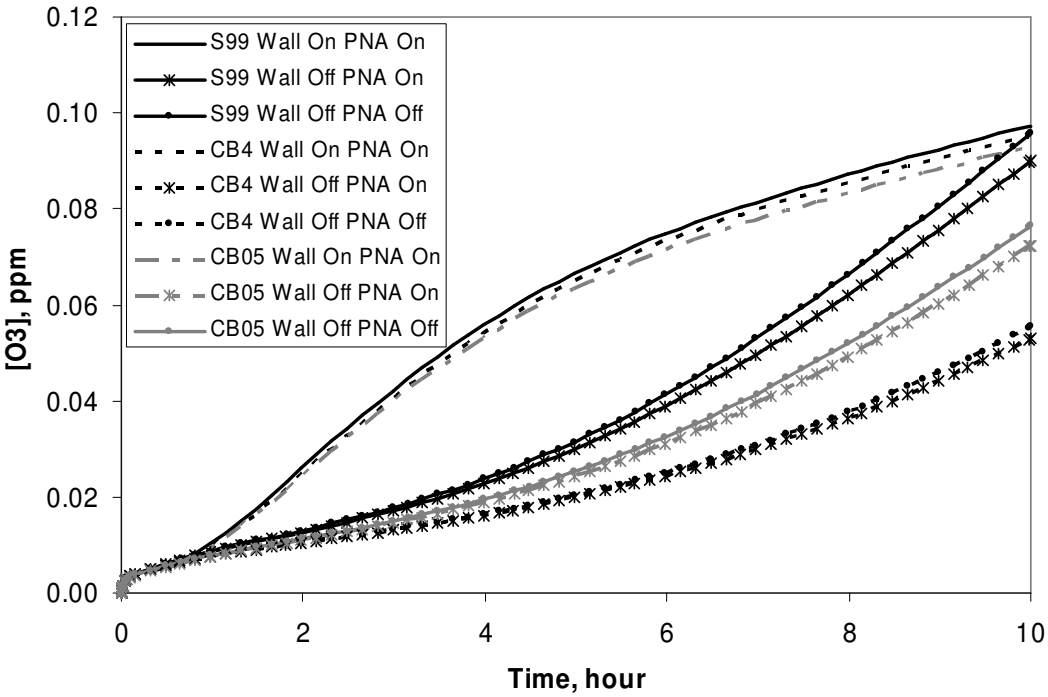

(b) Case CO(100) in Morpho

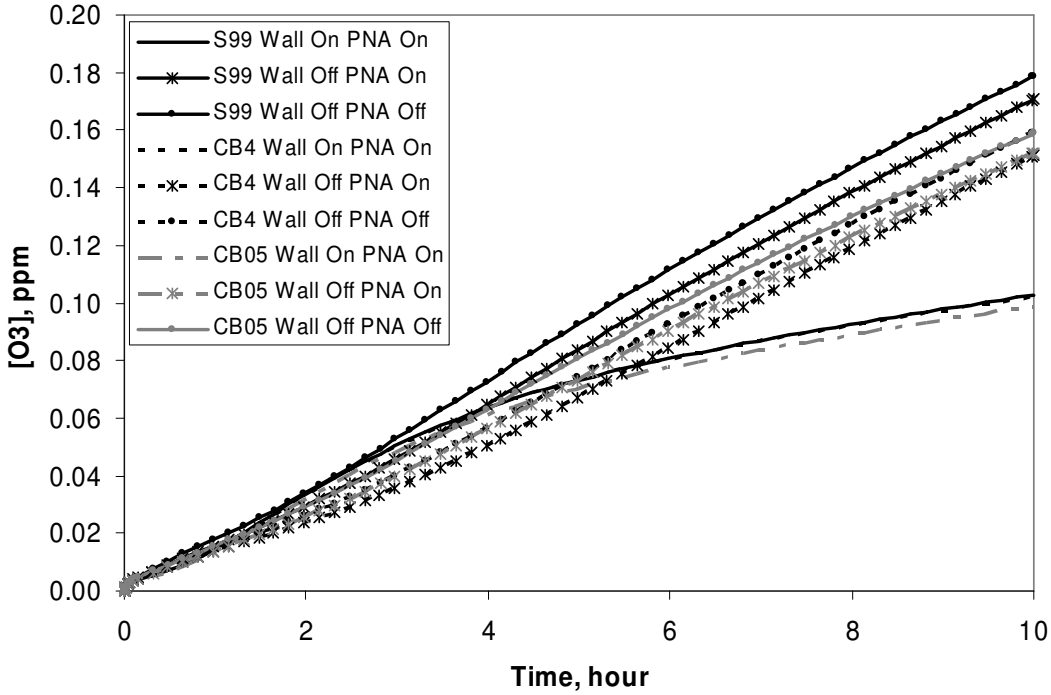

(c) Case CO(250) in Morpho

Figure D-1. Time series of the simulated O_3 concentrations in the three CO-NOx simulations in Morpho.

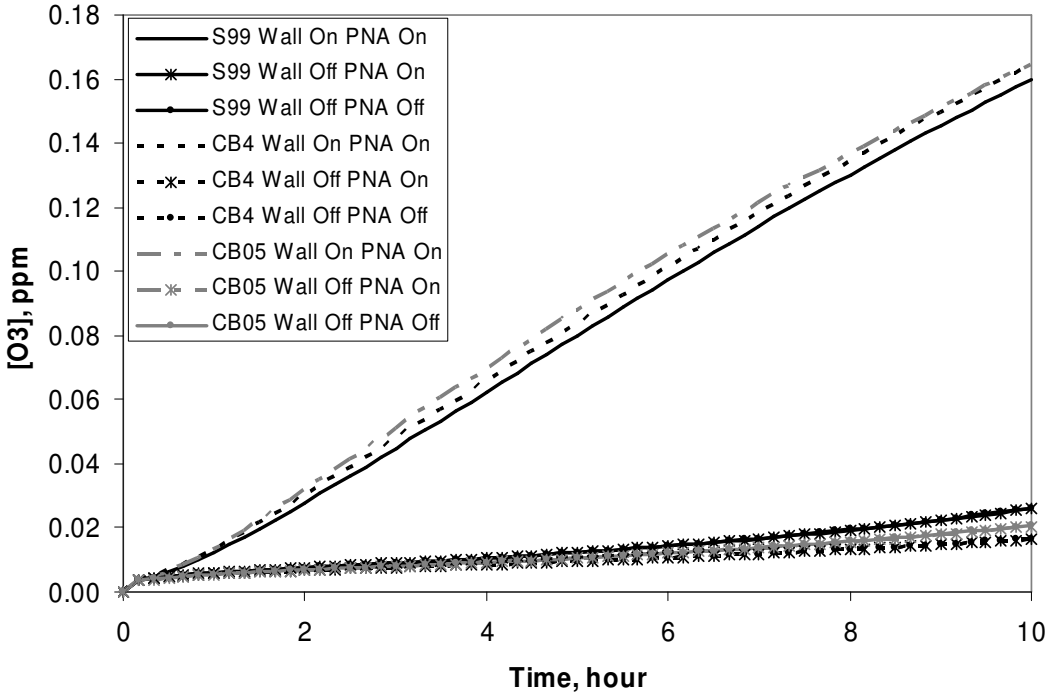

(a) Case CO(50) in SAPRC

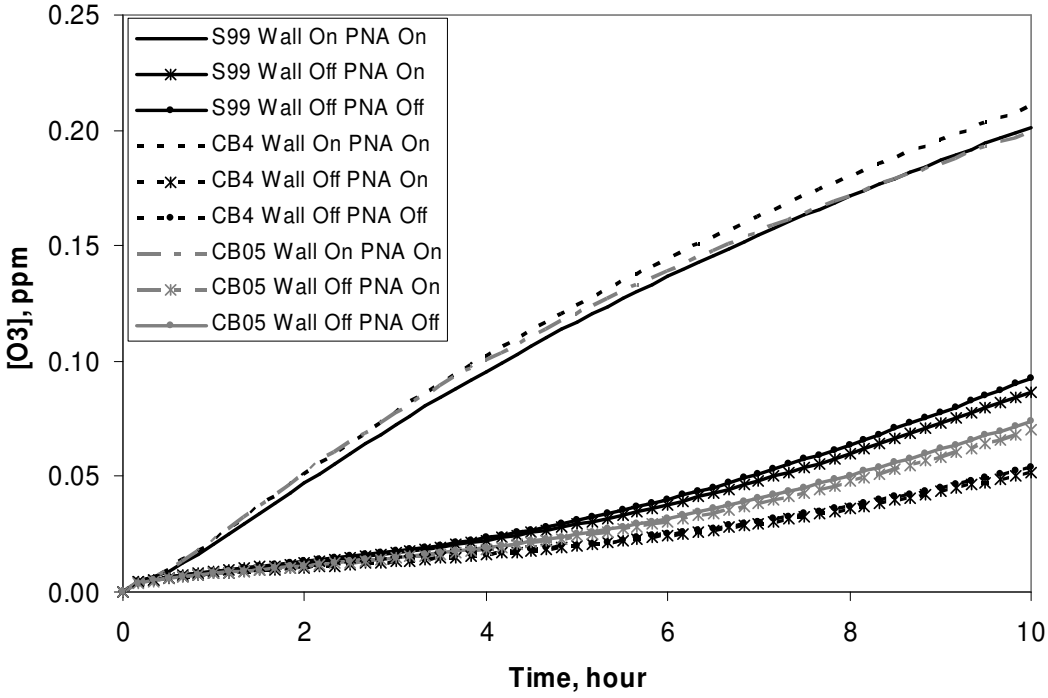

(b) Case CO(100) in SAPRC

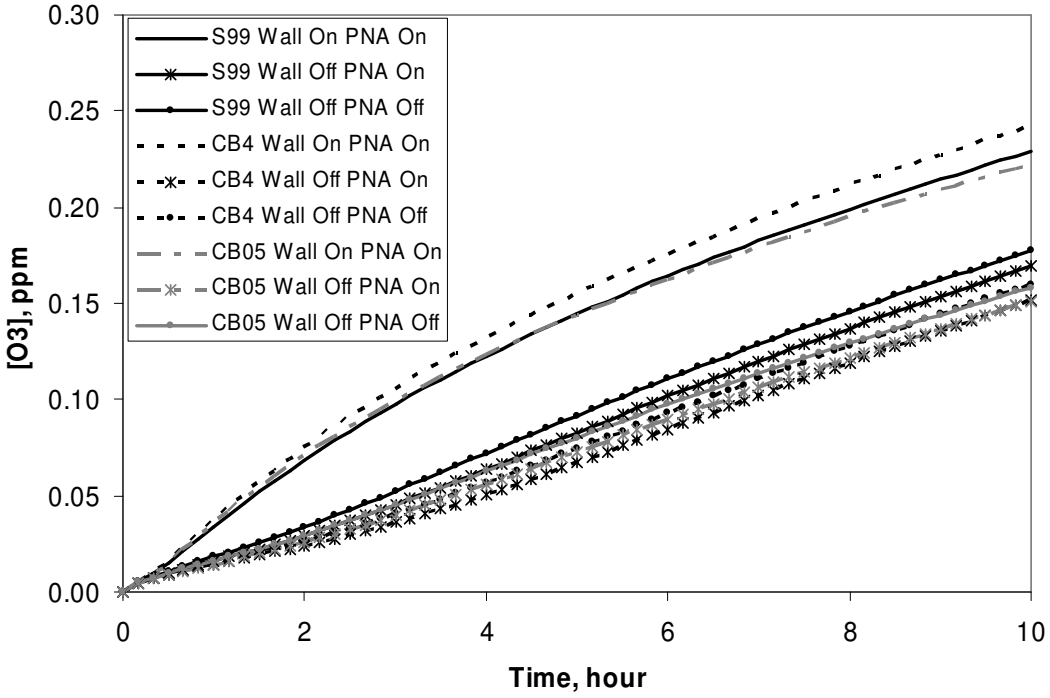

(c) Case CO(250) in SAPRC

Figure D-2. Time series of the simulated O_3 concentrations in the three CO-NOx simulations in SAPRC.

Turning on the wall mechanism (more correctly, the auxiliary mechanism for the chamber) activates several chamber-related processes such as NOx-to-HONO conversion at the wall surface (Carter *et al.*, 2005). The wall mechanism used in the UCR and TVA simulations also includes a wall reaction of HONO generation whose rate is independent of the NOx level (Equation 1 in Carter *et al.*, 2005). In the current wall mechanism for the University of North Carolina at Chapel Hill (UNC) outdoor chamber used in the Morpho simulations, there is no corresponding wall reaction independent of the NOx concentration.

When the wall mechanism was turned on in the UCR chamber model, the HONO, OH and HO_2 concentrations increased and the conversion rates of NO into NO_2 were accelerated in all three cases. Figure D-3 shows the changes in HONO, OH, HO_2, NO, NO_2, NOx, and NOy (in this study, NOy = NOx + HNO_3) associated with using the wall mechanism for the CO(250) simulation, which is typical of the other simulations in the UCR chamber model. The consistent increases in the radical concentrations, the faster oxidation rates of NO into NO_2, and the very limited depletions of NOx and NOy explain why the wall mechanism used for the UCR chamber consistently increased the simulated ozone concentrations in all three CO cases regardless of the amount of CO injection.

Figure D-4 shows the results of simulations performed using the UNC chamber model. In addition to using the wall mechanism reported in Appendix B.2 (developed by Whitten and used throughout this work), results using the original UNC chamber wall mechanism (used in studies such as Yarwood *et al.* (2005)) are reported. Both wall mechanisms increased O_3 in cases CO(50) and CO(100) and decreased O_3 in case CO(250), but to different extents.

Comparing the simulated O_3 and other key species concentrations gives some insights into the effects of the wall mechanism. In chamber simulations, NOx availability is important in determining the final O_3 concentration (Carter and Atkinson, 1987). Thus, changes in NO_2 (the major form of NOx in the later stages of the simulations) and NOy (an indicator showing the depletion of nitrogen-containing species) over time were investigated in the three CO-NOx simulations. As shown in Figures D-5 through D-7, the simulated NO_2, OH and HO_2 concentrations with the new wall mechanism (Appendix B.2) are consistently higher early in the simulation and lower later in the simulation than the NO_2, OH and HO_2 concentrations simulated with the earlier wall mechanism. The time series of NOy shows lower NOy availability in the simulations with the new wall mechanism.

It is not unexpected that the wall mechanisms for UNC and UCR chambers lead to different results. The UCR simulator and Morpho's wall reactions have been optimized to fit measured concentrations in very different chambers and under different humidity and light conditions. Thus, we should not conclude that simulation results are inconsistent between the two chambers, but the results do indicate that in going from chamber evaluations to CAMx simulations (without wall reactions), we will expect that mechanisms tuned to the two different chambers may respond differently.

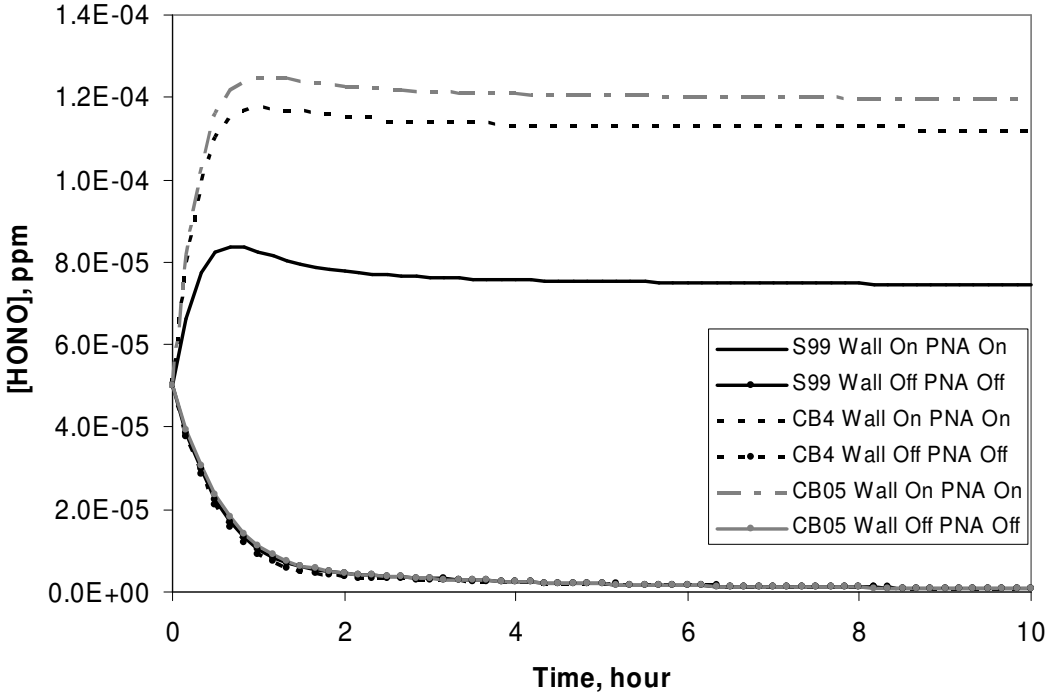

(a) HONO in CO(250)

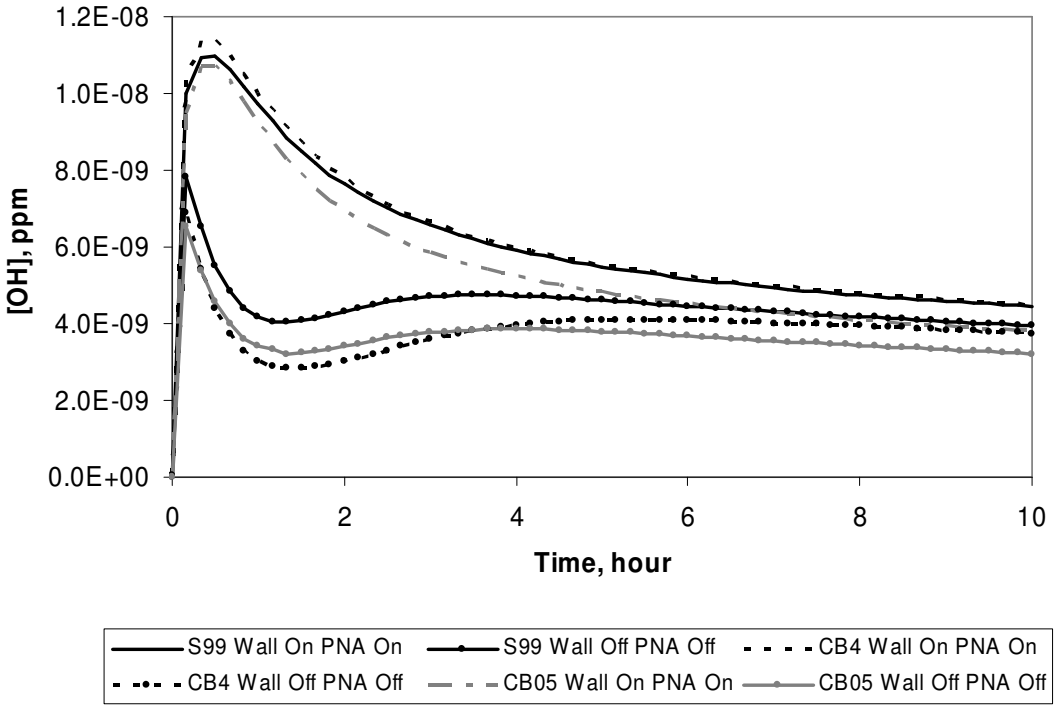
1.2E-08
1.0E-08
8.0E-09
6.0E-09
4.0E-09
2.0E-09
0.0E+00
[OH], ppm
0
2
4
6
8
10
Time, hour
S99 Wall On PNA On
S99 Wall Off PNA Off
CB4 Wall On PNA On
CB4 Wall Off PNA Off
CB05 Wall On PNA On
CB05 Wall Off PNA Off

(b) OH in CO(250)

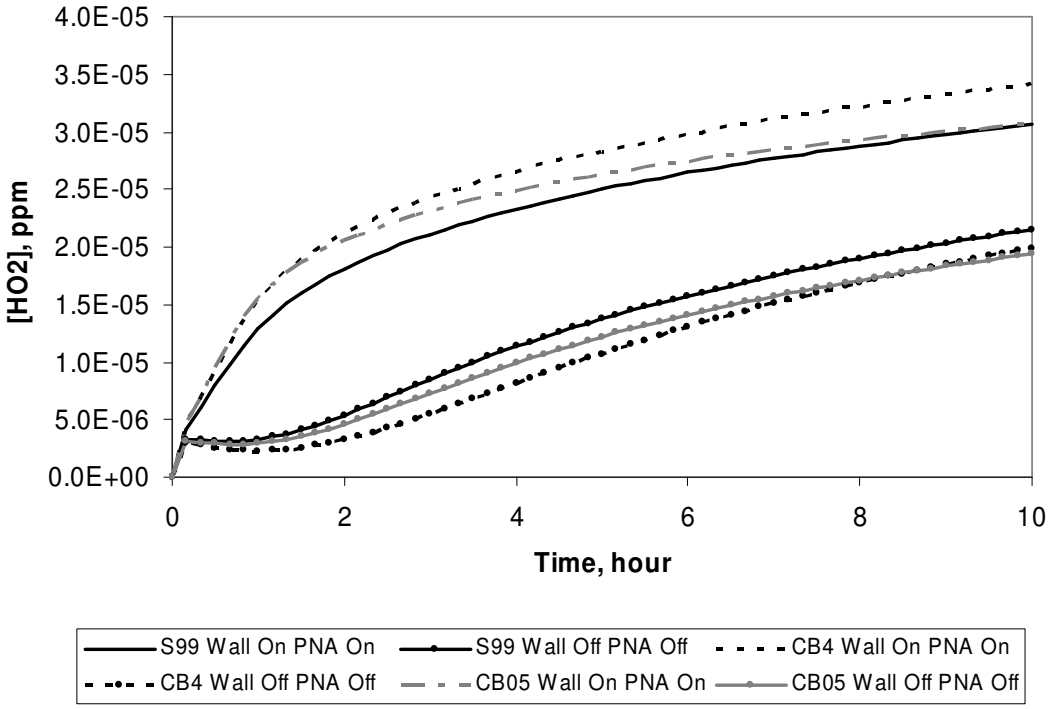

(c) HO_2 in CO(250)

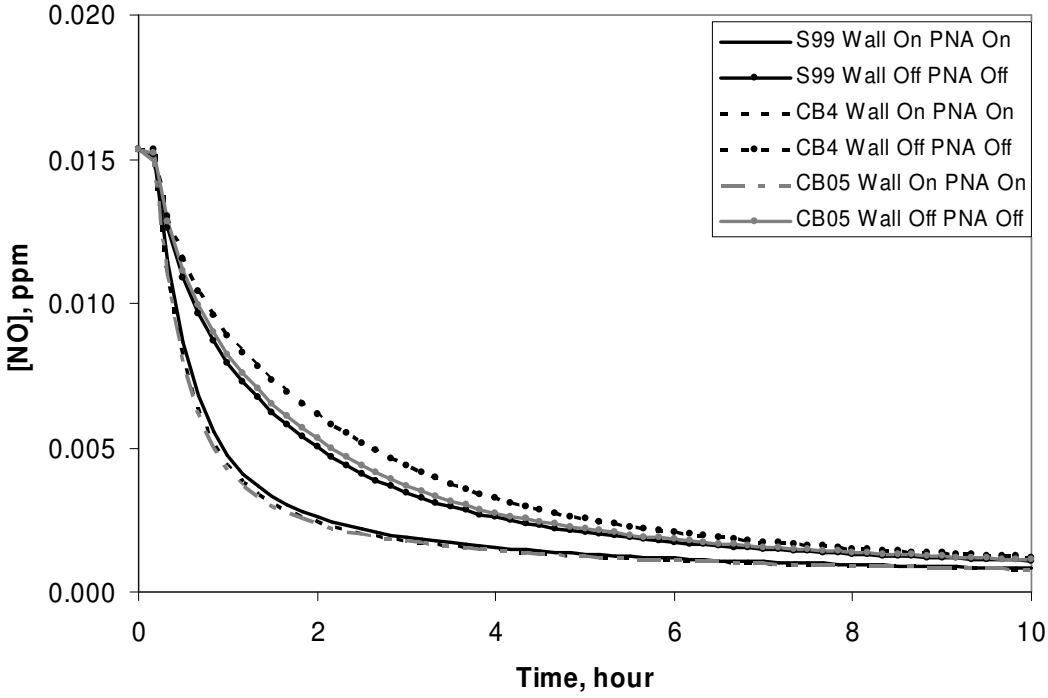
0.020
0.015
0.010
0.005
0.000
[NO], ppm
0
2
4
6
8
10
Time, hour
S99 Wall On PNA On
S99 Wall Off PNA Off
CB4 Wall On PNA On
CB4 Wall Off PNA Off
CB05 Wall On PNA On
CB05 Wall Off PNA Off

(d) NO in CO(250)

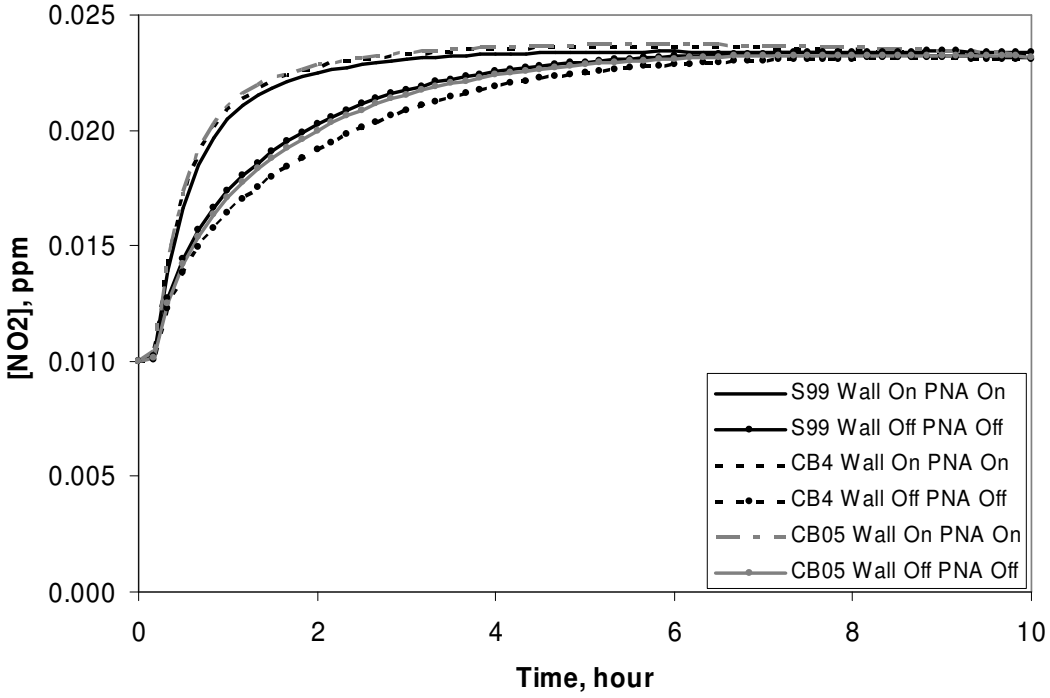

(e) NO_2 in CO(250)

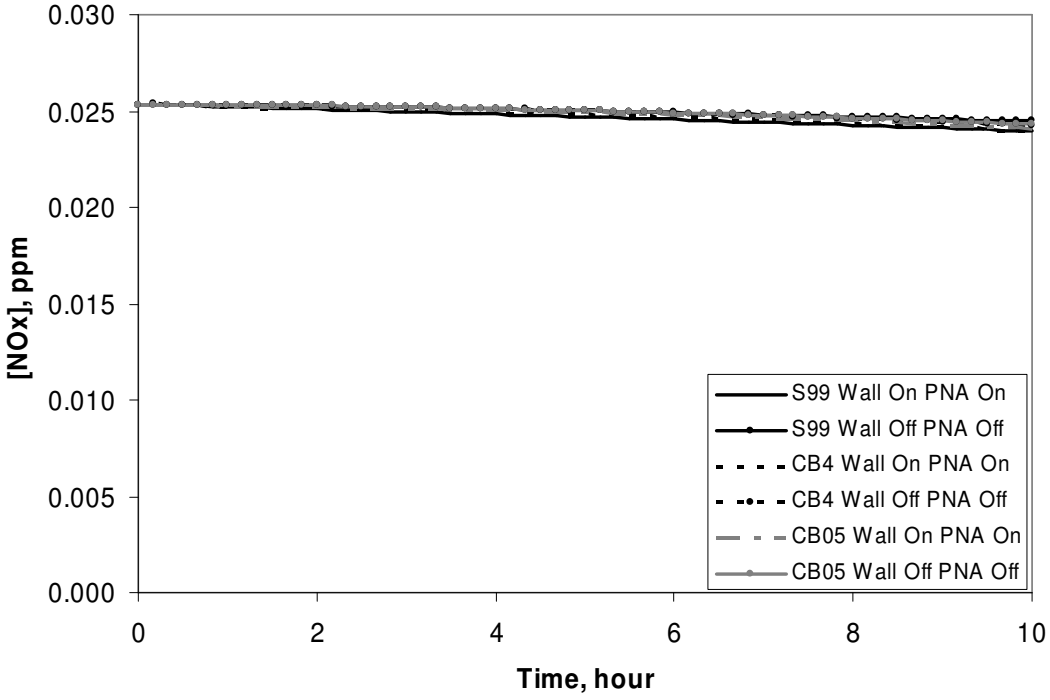

(f) NO_x in CO(250)

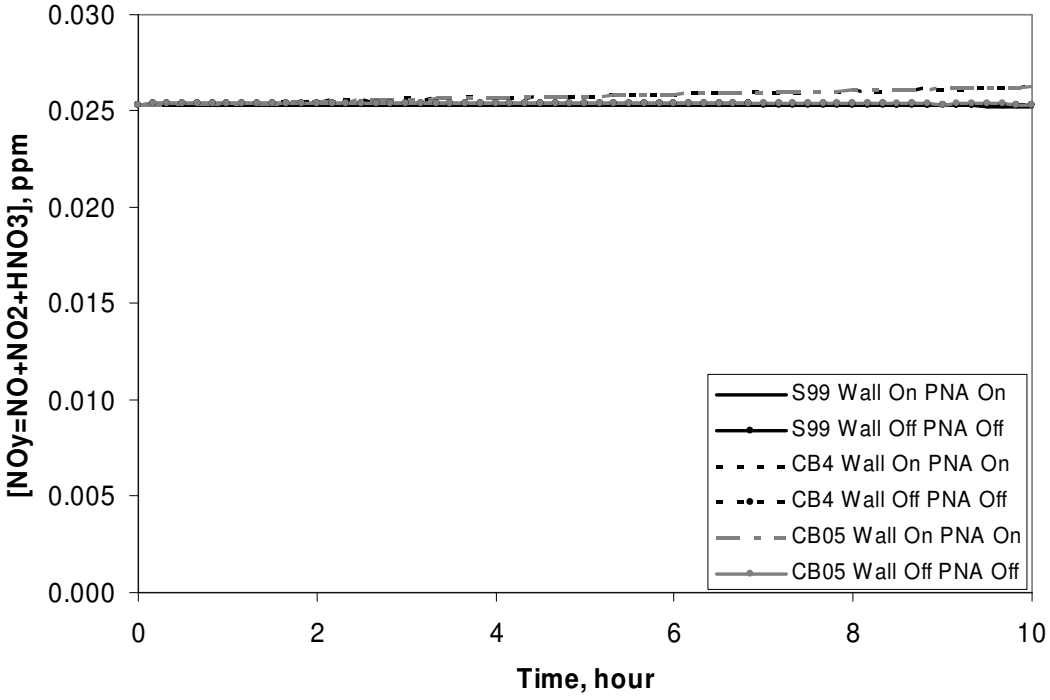

(g) NO_y in CO(250)

Figure D-3. Effects of the SAPRC wall mechanism on the simulated concentrations in case CO(250): (a) HONO, (b) OH, (c) HO_2, (d) NO, (e) NO_2, (f) NOx, and (g) NOy

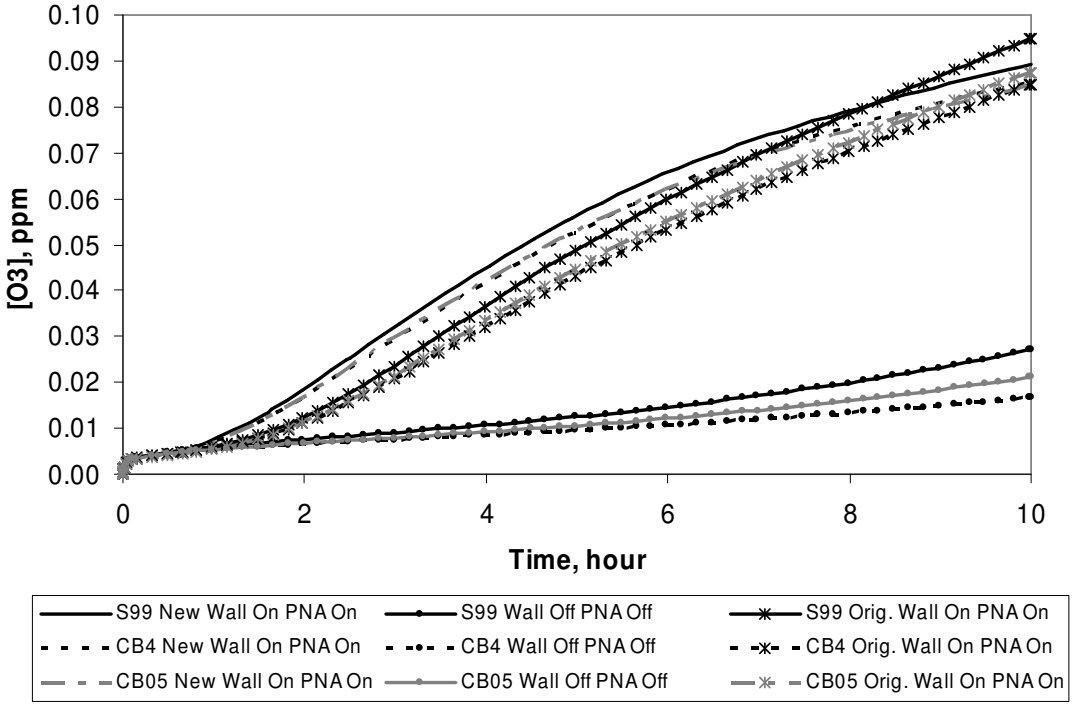

(a) Case CO(50) in Morpho

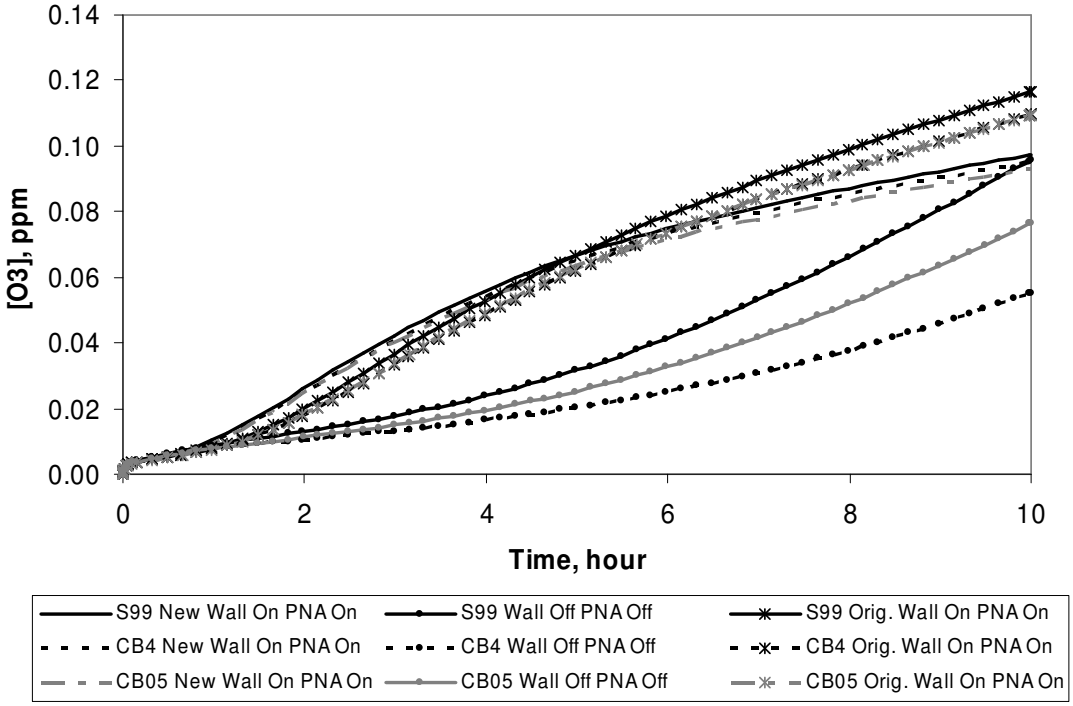

(b) Case CO(100) in Morpho

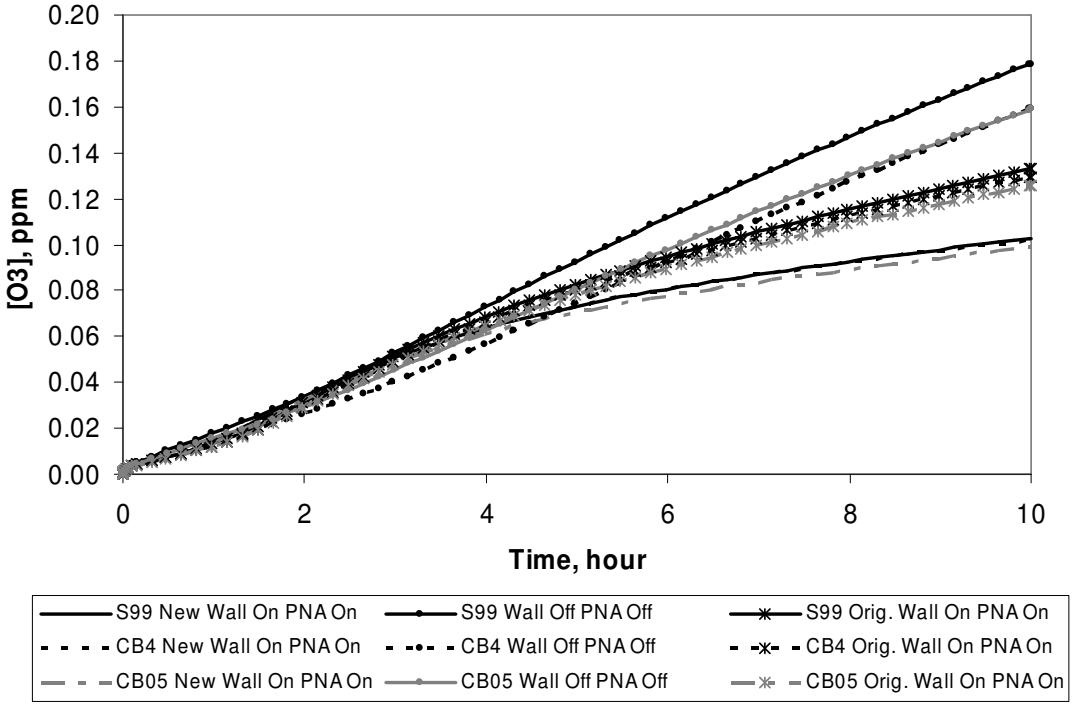

(c) Case CO(250) in Morpho

Figure D-4. Effects of two UNC wall mechanisms on the simulated O_3 concentrations.

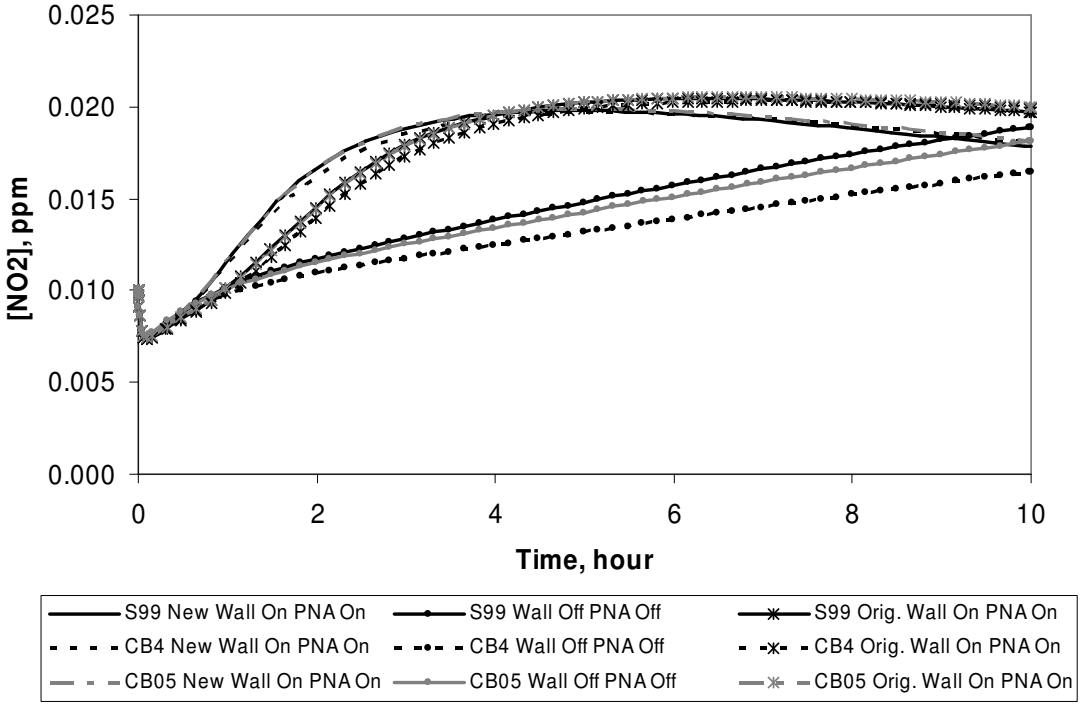
0.025
0.020
0.015
0.010
0.005
0.000
[NO2], ppm
0
2
4
6
8
10
Time, hour
S99 New Wall On PNA On
S99 Wall Off PNA Off
S99 Orig. Wall On PNA On
CB4 New Wall On PNA On
CB4 Wall Off PNA Off
CB4 Orig. Wall On PNA On
CB05 New Wall On PNA On
CB05 Wall Off PNA Off
CB05 Orig. Wall On PNA On

(a) NO_2 in CO(50)

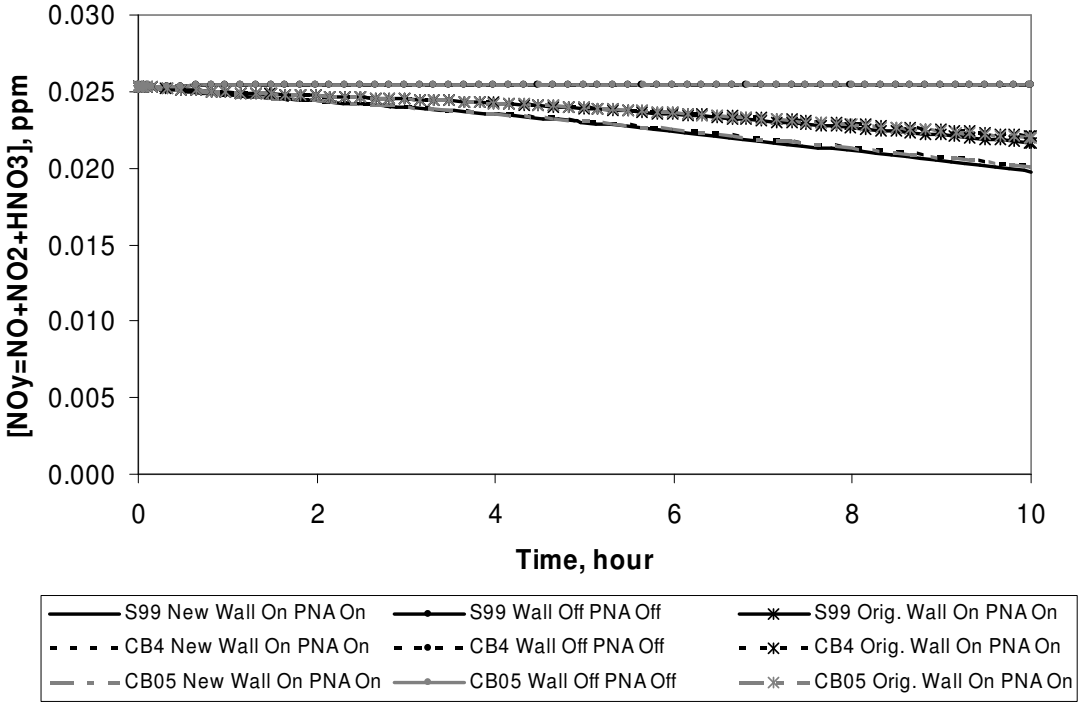
0.030
0.025
0.020
0.015
0.010
0.005
0.000
[NOy=NO+NO2+HNO3], ppm
0
2
4
6
8
10
Time, hour
S99 New Wall On PNA On
S99 Wall Off PNA Off
S99 Orig. Wall On PNA On
CB4 New Wall On PNA On
CB4 Wall Off PNA Off
CB4 Orig. Wall On PNA On
CB05 New Wall On PNA On
CB05 Wall Off PNA Off
CB05 Orig. Wall On PNA On

(b) NOy in CO(50)

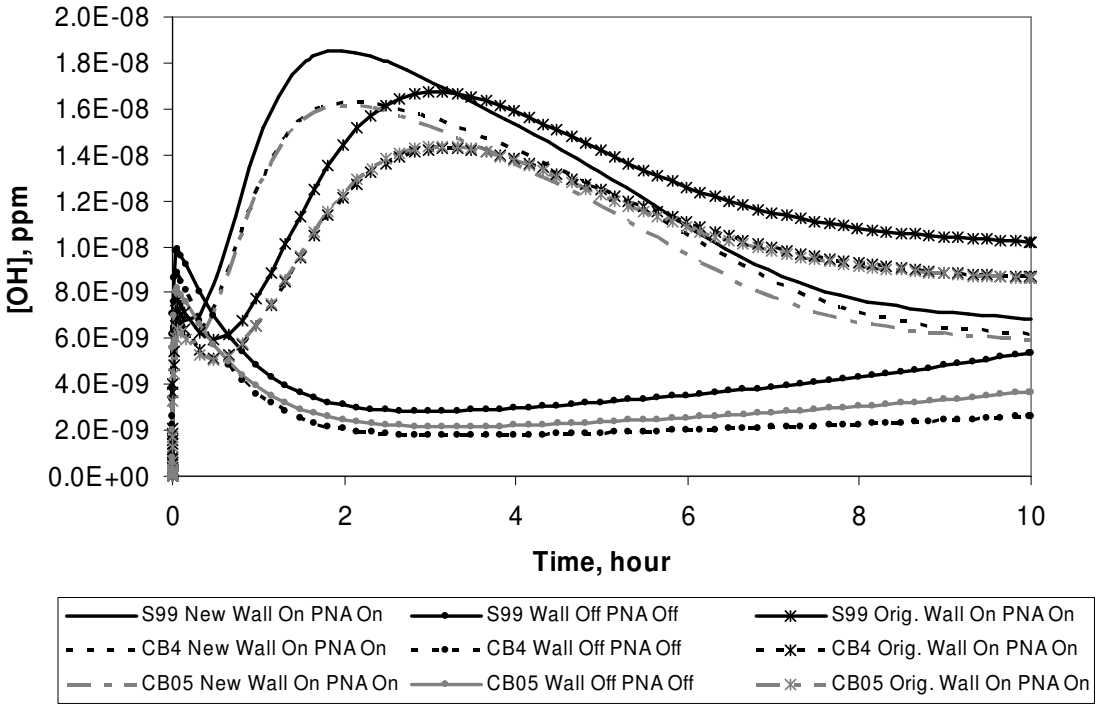
2.0E-08
1.8E-08
1.6E-08
1.4E-08
1.2E-08
1.0E-08
8.0E-09
6.0E-09
4.0E-09
2.0E-09
0.0E+00
[OH], ppm
0
2
4
6
8
10
Time, hour
S99 New Wall On PNA On
S99 Wall Off PNA Off
S99 Orig. Wall On PNA On
CB4 New Wall On PNA On
CB4 Wall Off PNA Off
CB4 Orig. Wall On PNA On
CB05 New Wall On PNA On
CB05 Wall Off PNA Off
CB05 Orig. Wall On PNA On

(c) OH in CO(50)

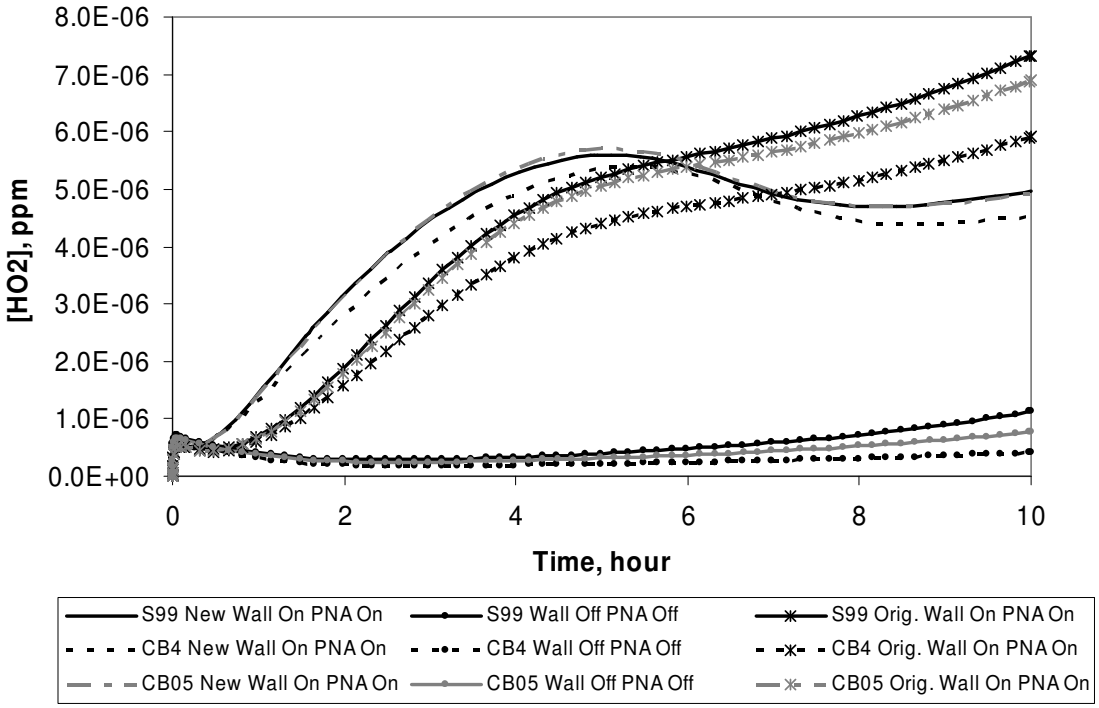

(d) HO_2 in CO(50)

Figure D-5. Effects of two UNC wall mechanisms on the simulated concentrations in case CO(50): (a) NO_2, (b) NOy, (c) OH, and (d) HO_2.

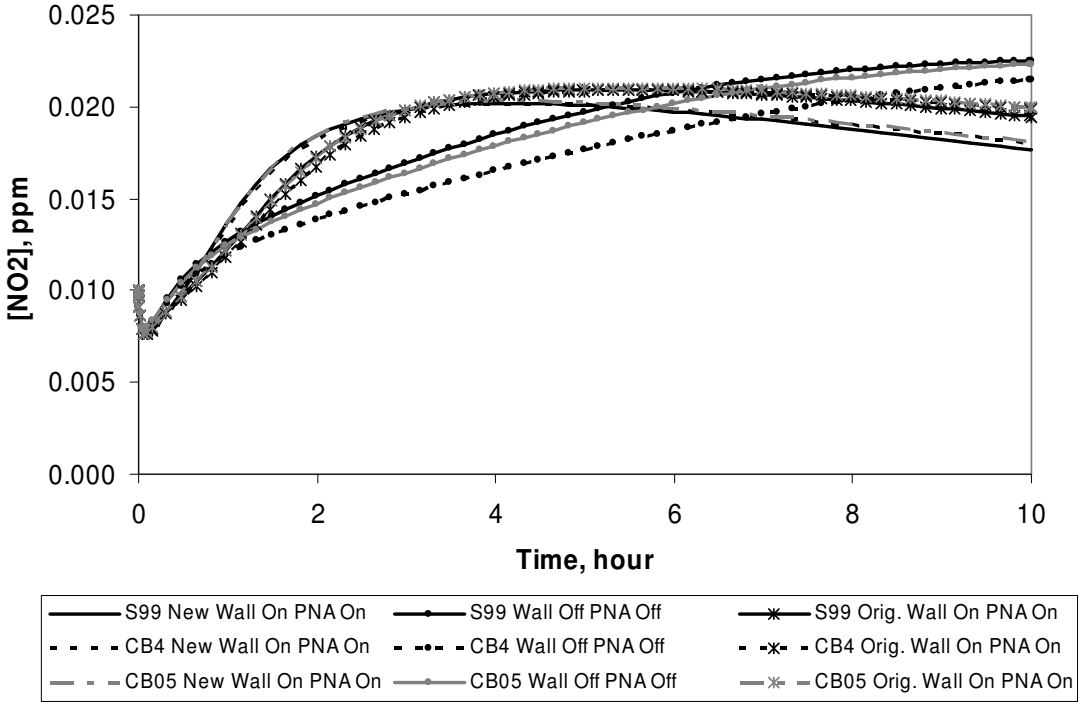

(a) NO_2 in CO(100)

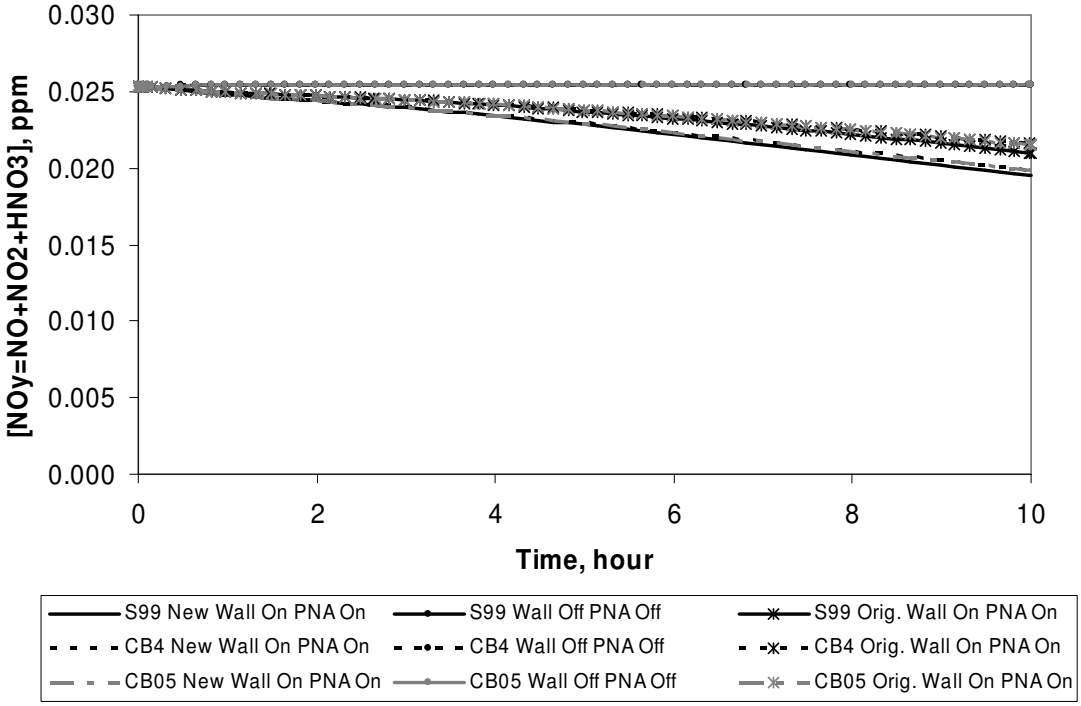

(b) NOy in CO(100)

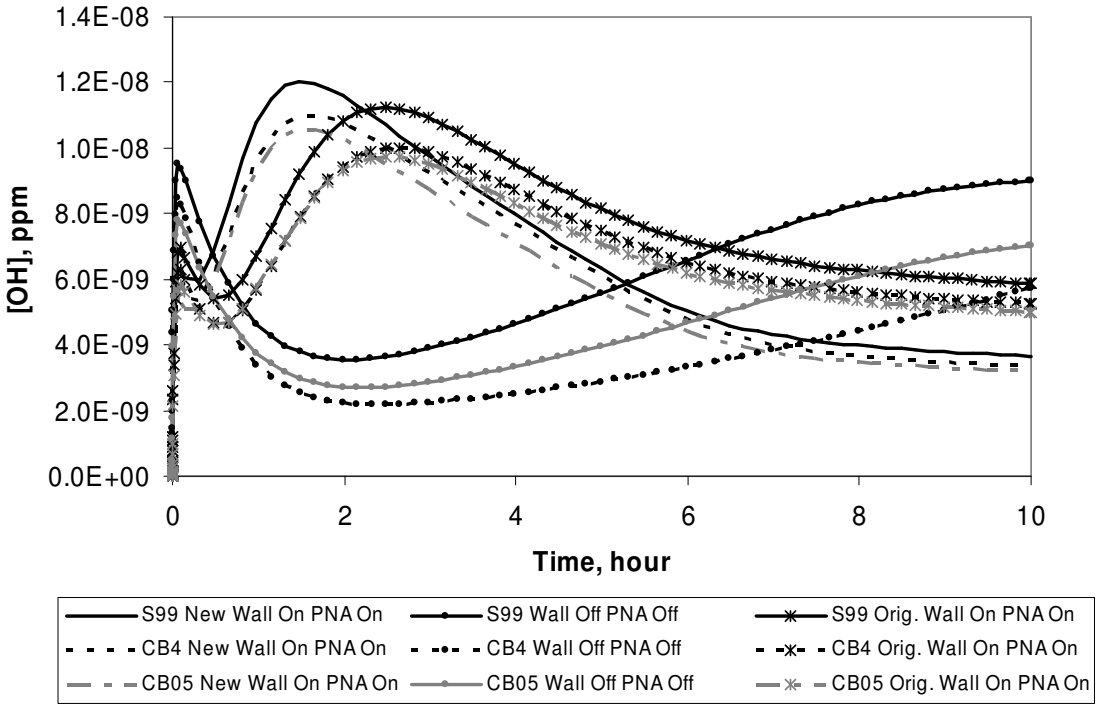
1.4E-08
1.2E-08
1.0E-08
8.0E-09
6.0E-09
4.0E-09
2.0E-09
0.0E+00
[OH], ppm
0
2
4
6
8
10
Time, hour
S99 New Wall On PNA On
S99 Wall Off PNA Off
S99 Orig. Wall On PNA On
CB4 New Wall On PNA On
CB4 Wall Off PNA Off
CB4 Orig. Wall On PNA On
CB05 New Wall On PNA On
CB05 Wall Off PNA Off
CB05 Orig. Wall On PNA On

(c) OH in CO(100)

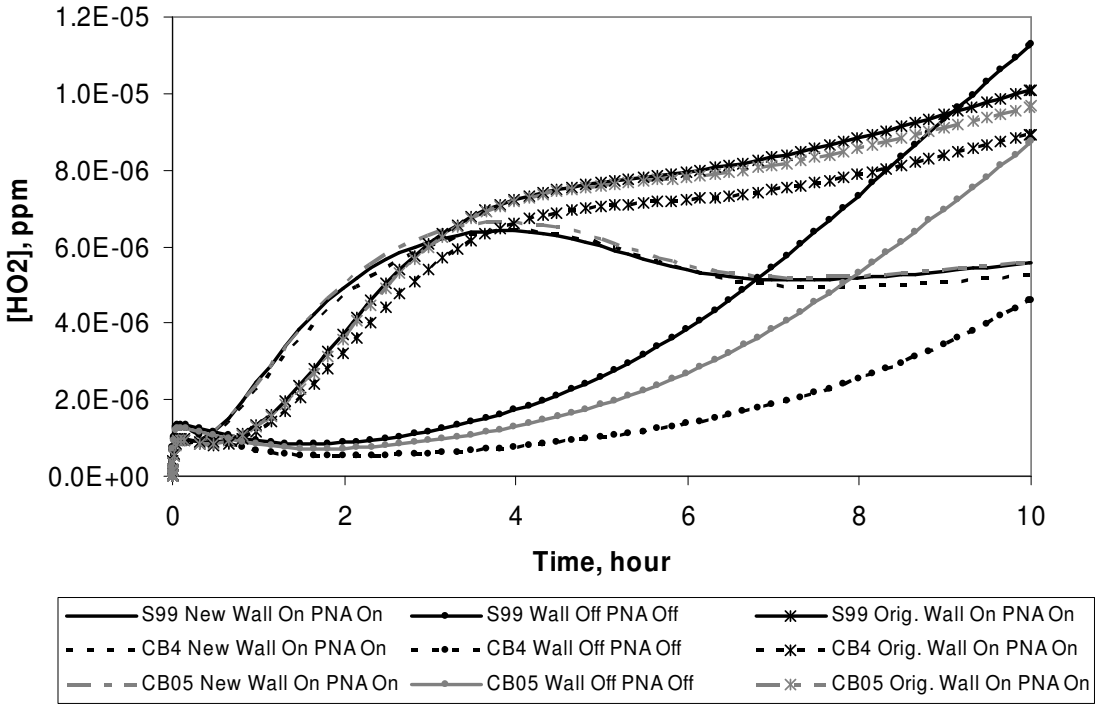

(d) HO_2 in CO(100)

Figure D-6. Effects of two UNC wall mechanisms on the simulated concentrations in case CO(100): (a) NO_2, (b) NOy, (c) OH, and (d) HO_2.

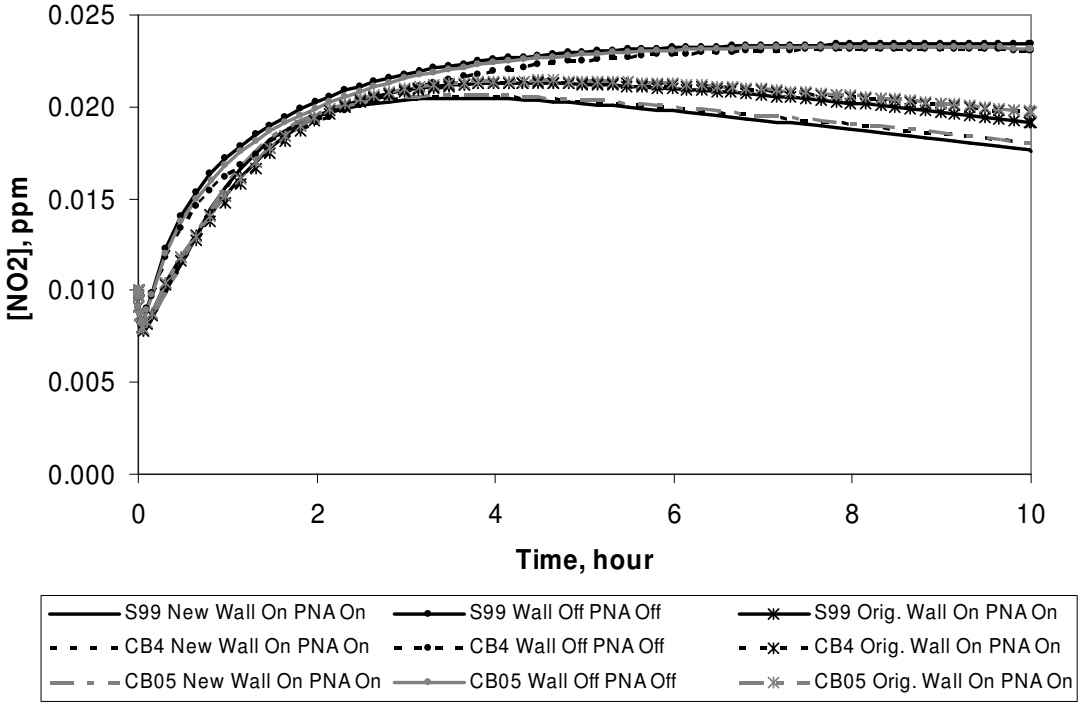

(a) NO_2 in CO(250)

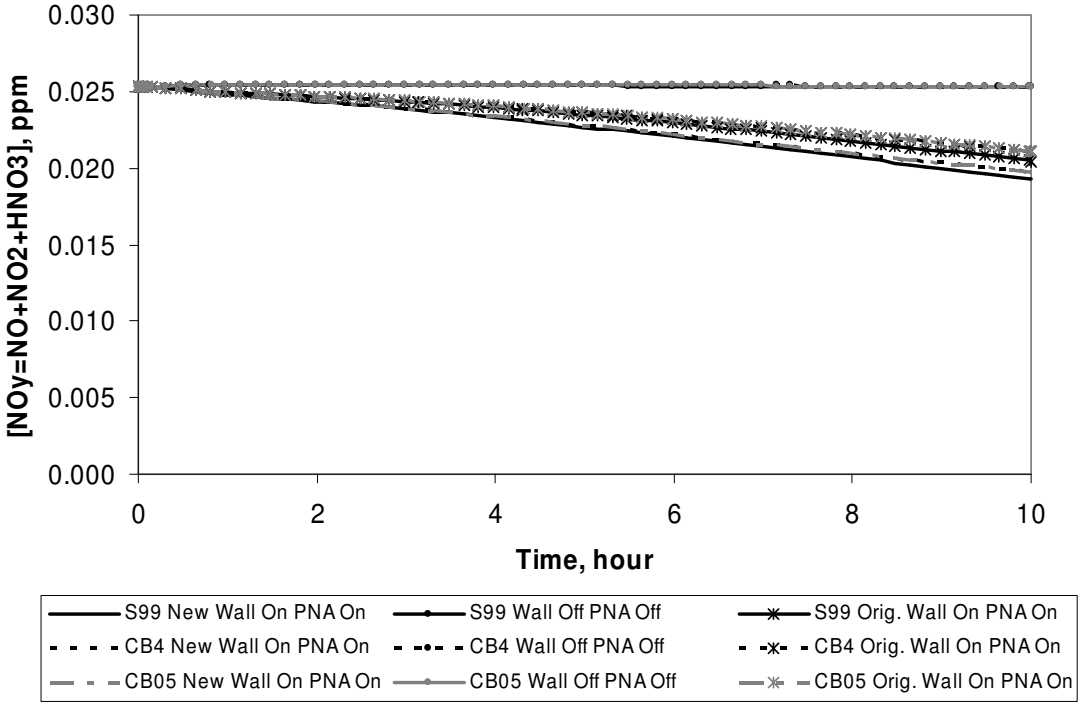

(b) NOy in CO(250)

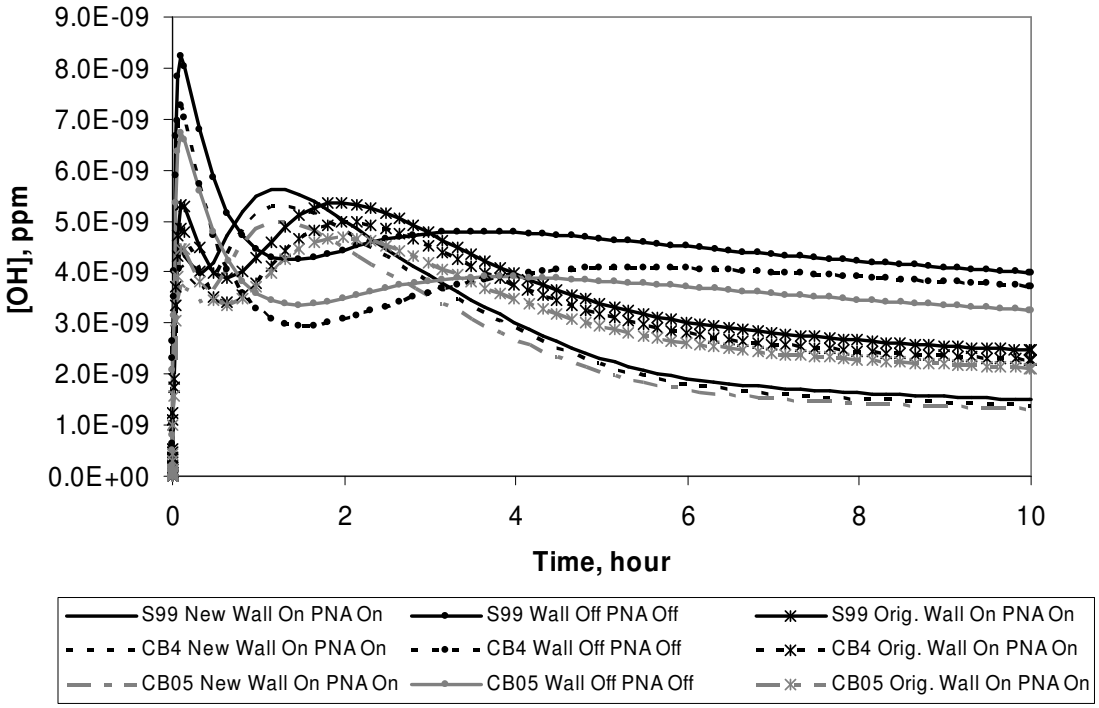
9.0E-09
8.0E-09
7.0E-09
6.0E-09
5.0E-09
4.0E-09
3.0E-09
2.0E-09
1.0E-09
0.0E+00
[OH], ppm
0
2
4
6
8
10
Time, hour
S99 New Wall On PNA On
S99 Wall Off PNA Off
S99 Orig. Wall On PNA On
CB4 New Wall On PNA On
CB4 Wall Off PNA Off
CB4 Orig. Wall On PNA On
CB05 New Wall On PNA On
CB05 Wall Off PNA Off
CB05 Orig. Wall On PNA On

(c) OH in CO(250)

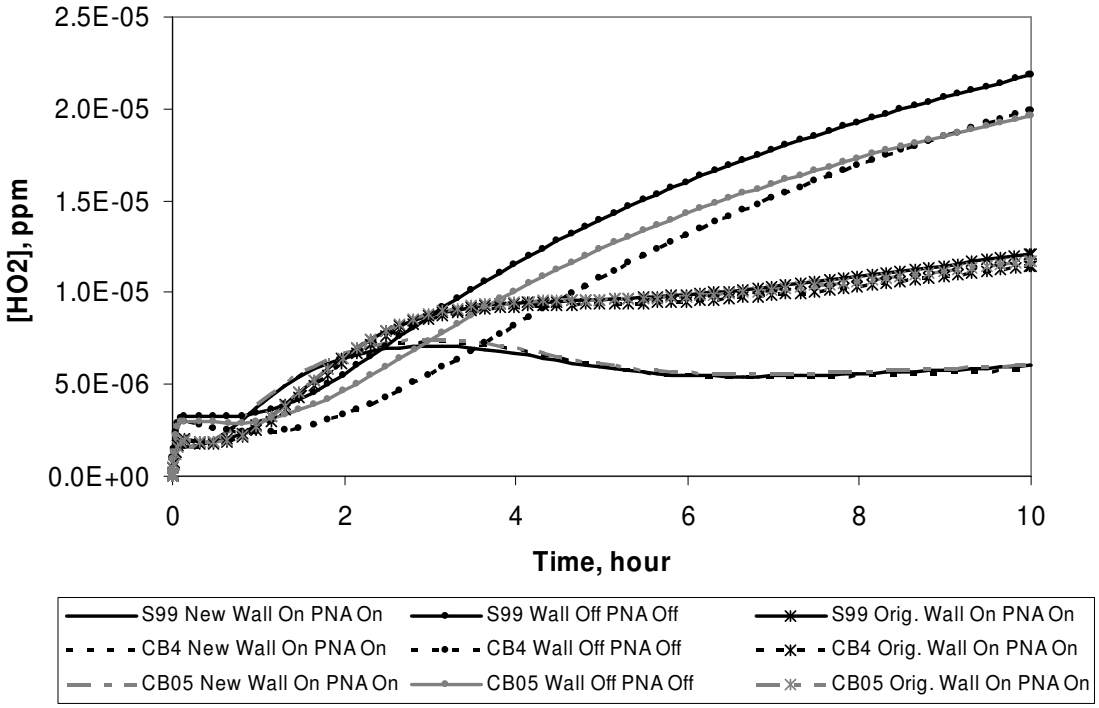

(d) HO_2 in CO(250)

Figure D-7. Effects of two UNC wall mechanisms on the simulated concentrations in case CO(250): (a) NO_2, (b) NOy, (c) OH, and (d) HO_2.

To summarize, the analyses presented above indicate that the SAPRC software used for the UCR and TVA simulations and the Morpho software used for the UNC simulations, predicted very similar ozone concentrations when nearly same initial conditions and environmental conditions were used and the wall mechanism was turned off. The effects of activating PNA chemistry in CB4, CB05 and SAPRC99 were very limited in the three CO-NOx simulations considered in this work, however, the effects of wall chemistry were much larger.

The simulations described to this point demonstrate that wall effects are large for low-reactivity systems, as expected (Killus and Whitten, 1990; *Hess et al.*, 1992; Carter *et al.*, 2005; Zádor *et al.*, 2006). Additional simulations were performed to assess the extent to which the wall mechanisms in the SAPRC software and the Morpho software correct the simulations for low-reactivity experiments. Table D-3 lists 12 UNC chamber experiments that were simulated in this work, and Table D-4 lists 53 UCR experiments that were previously simulated by Carter (2007). A summary of the data in Tables D-3 and D-4 is provided in Figures D-8 and D-9.

Table D-3. UNC chamber experiments involving CO.

Run ID	Start time	NO (ppm)	NO_2 (ppm)	CO (ppm)	CO/NOx (ppm/ppb)	[1]O_3 max	[2]O_3 at t = 6 hr: (model-exp)/exp			
							Exp.	S99	CB4	CB05
AU3093: RED	6:24	0.282	0.045	250	0.8	0.695	0.246	9%	-10%	-4%
AU3093: BLUE	6:24	0.282	0.039	100	0.3	0.306	0.056	2%	-40%	-28%
AU3096: RED	6:48	0.294	0.036	125	0.4	0.202	0.060	37%	-16%	2%
AU3096: BLUE	6:48	0.294	0.033	250	0.8	0.500	0.231	0%	-17%	-11%
JL0701: RED	5:12	0.588	0.057	170	0.3	0.015	0.002	285%	117%	164%
JL0701: BLUE	5:12	0.590	0.051	500	0.8	0.548	0.024	341%	248%	283%
JL2201: RED	5:12	0.200	0.016	400	1.9	0.884	0.194	-9%	-15%	-14%
JL2201: BLUE	5:12	0.600	0.047	400	0.6	0.176	0.007	1157%	735%	895%
OC0395: RED	7:13	0.251	0.065	250	0.8	0.568	0.350	-65%	-68%	-67%
OC0395: BLUE	7:13	0.256	0.053	250	0.8	0.580	0.436	-70%	-72%	-72%
ST2000: RED	6:07	0.230	0.080	250	0.8	0.372	0.103	97%	72%	82%
ST2000: BLUE	6:07	0.228	0.082	500	1.6	0.686	0.254	10%	6%	6%

1: "O_3 max" means the maximum ozone concentration measured during the chamber experiment;
2: O_3 concentrations at t = 6 hours after injection.

Table D-4. UCR chamber experiments involving CO.

	Run ID	[1]Light	NO (ppm)	NO2 (ppm)	CO (ppm)	CO/NOx (ppm/ppb)	[2]Final O_3	[2]Final D(O_3 - NO): (model-exp)/exp			
								Exp.	S99	CB4	CB05
1	EPA057A	A	0.054	0.002	81	1.5	0.028	0.067	-1%	1%	8%
2	EPA057B	A	0.048	0.002	82	1.7	0.031	0.067	2%	4%	11%
3	EPA058A	A	0.081	0.013	90	1.0	0.017	0.063	-11%	-9%	-3%
4	EPA058B	A	0.000	0.076	74	1.0	0.043	0.030	10%	6%	18%
5	EPA061A	A	0.007	0.000	86	11.8	0.066	0.072	1%	9%	4%
6	EPA061B	A	0.009	0.001	68	6.9	0.070	0.077	1%	9%	6%
7	EPA070A	A	0.025	0.001	87	3.3	0.065	0.088	-3%	1%	7%
8	EPA070B	A	0.026	0.001	77	2.9	0.050	0.074	7%	11%	18%
9	EPA071A	A	0.189	0.013	81	0.4	0.004	0.043	7%	13%	18%
10	EPA103A	A	0.016	0.010	46	1.8	0.101	0.114	-28%	-21%	-16%
11	EPA103B	A	0.018	0.009	46	1.7	0.077	0.091	-29%	-23%	-18%
12	EPA140A	A	0.014	0.009	44	1.9	0.071	0.083	2%	12%	18%
13	EPA140B	A	0.014	0.009	44	1.9	0.059	0.072	-6%	1%	8%
14	EPA174A	A	0.014	0.009	47	2.0	0.065	0.078	-32%	-29%	-23%
15	EPA174B	A	0.014	0.009	47	2.0	0.056	0.071	-24%	-21%	-15%
16	EPA214A	A	0.015	0.008	47	2.1	0.093	0.107	-23%	-17%	-13%
17	EPA214B	A	0.015	0.008	47	2.0	0.090	0.105	-37%	-34%	-29%
18	EPA228A	A	0.016	0.010	46	1.8	0.053	0.065	-21%	-18%	-11%
19	EPA228B	A	0.015	0.009	46	1.9	0.045	0.054	-3%	1%	8%
20	EPA234A	A	0.017	0.008	45	1.8	0.046	0.059	41%	54%	64%
21	EPA234B	A	0.017	0.009	45	1.7	0.036	0.048	35%	45%	56%
22	EPA306A	Bl	0.013	0.008	47	2.2	0.037	0.049	29%	39%	52%
23	EPA306B	Bl	0.014	0.009	47	2.1	0.024	0.034	50%	57%	74%
24	EPA326A	A	0.015	0.010	51	2.0	0.110	0.128	-30%	-23%	-19%
25	EPA326B	A	0.018	0.012	58	1.9	0.114	0.131	-45%	-42%	-37%
26	EPA345A	A	0.017	0.010	48	1.7	0.028	0.040	26%	31%	41%
27	EPA345B	A	0.017	0.010	48	1.7	0.023	0.035	42%	48%	59%
28	EPA346A	A	0.017	0.010	46	1.7	0.029	0.042	18%	22%	32%
29	EPA346B	A	0.017	0.010	48	1.8	0.027	0.041	24%	29%	39%
30	EPA362A	A	0.013	0.008	33	1.6	0.033	0.044	-15%	-11%	-4%
31	EPA362B	A	0.013	0.008	33	1.6	0.025	0.035	6%	11%	20%
32	EPA401A	Bl	0.017	0.011	49	1.7	0.022	0.034	-13%	-13%	-2%
33	EPA401B	Bl	0.017	0.012	50	1.7	0.018	0.031	11%	10%	24%
34	EPA411A	Bl	0.017	0.011	50	1.8	0.055	0.071	-50%	-50%	-44%
35	EPA411B	Bl	0.017	0.010	50	1.8	0.035	0.052	-42%	-42%	-35%
36	EPA437A	A	0.018	0.011	42	1.5	0.022	0.033	16%	21%	30%
37	EPA437B	A	0.018	0.011	42	1.5	0.017	0.026	45%	51%	62%
38	EPA585A	A	0.016	0.008	40	1.7	0.047	0.061	-11%	-5%	3%
39	EPA585B	A	0.016	0.008	40	1.6	0.053	0.068	-21%	-15%	-8%
1	CTC090A	A	0.192	0.070	92	0.4	0.014	0.093	-2%	8%	14%

2	CTC090B	A	0.191	0.070	92	0.4	0.012	0.124	-14%	-5%	1%
3	CTC224A	A	0.191	0.062	35	0.1	0.001	0.039	4%	11%	16%
4	CTC224B	A	0.191	0.058	35	0.1	0.001	0.038	-9%	-2%	1%
5	CTC031	A	0.206	0.058	89	0.3	0.009	0.142	-17%	-9%	-4%
6	CTC061	A	0.173	0.053	88	0.4	0.004	0.086	18%	32%	37%
1	DTC316A	Bl	0.127	0.049	42	0.2	0.030	0.133	-14%	-1%	5%
2	DTC316B	Bl	0.125	0.047	42	0.2	0.019	0.114	1%	17%	24%
3	DTC322A	Bl	0.137	0.048	44	0.2	0.008	0.084	-3%	2%	15%
4	DTC322B	Bl	0.136	0.050	44	0.2	0.007	0.081	-1%	4%	16%
5	DTC334A	Bl	0.153	0.052	44	0.2	0.006	0.083	-7%	-2%	10%
6	DTC334B	Bl	0.152	0.053	44	0.2	0.005	0.067	15%	20%	35%
7	DTC383A	Bl	0.068	0.010	46	0.6	0.046	0.105	15%	26%	41%
8	DTC383B	Bl	0.065	0.010	46	0.6	0.048	0.103	18%	29%	45%

1: Light source: A (arc light), Bl (black light); Carter (2007, June; worksheet C-1 in http://pah.cert.ucr.edu/~carter/SAPRC/saprc07.xls).

2: "Final" means at the hour of 6 or 5 (if the experiment was end before 6 hours after the injection). Linear interpolation was used to get the experimental concentration at hour of 6 (or 5) if there was not the measured concentration at the exact time (hour of 6).

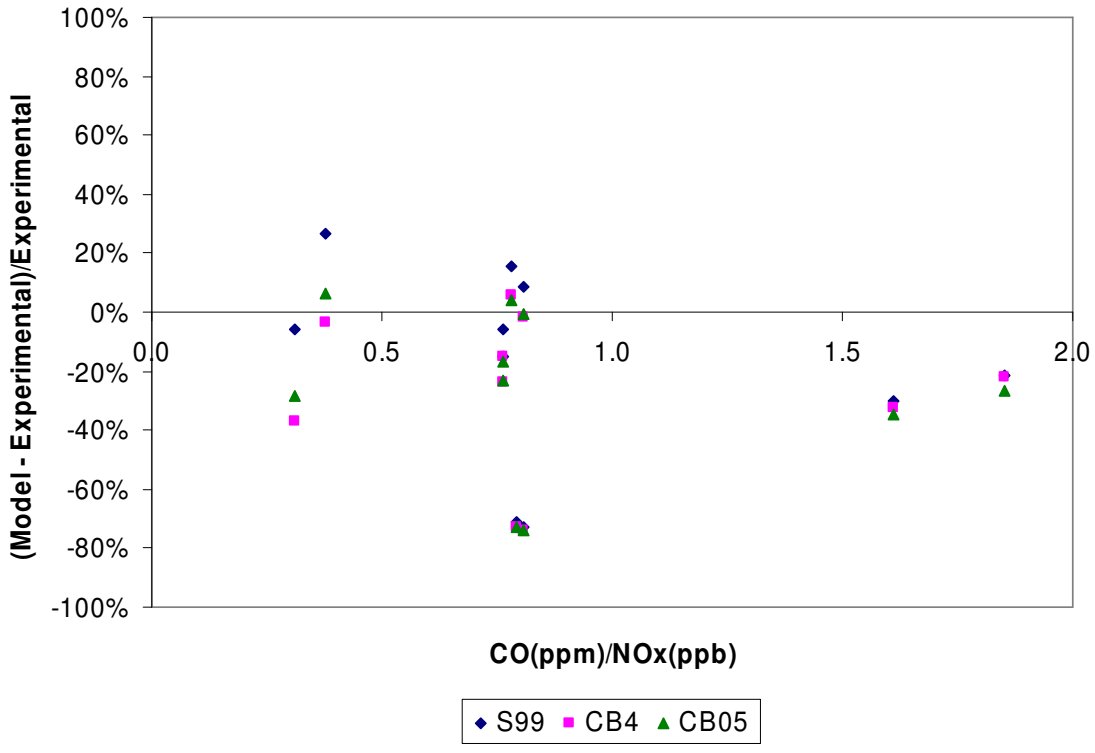

Figure D-8. The distributions of the model errors against CO/NOx ratio in simulating the UNC chamber experiments. (*Maximum O_3 concentrations were used for calculations)

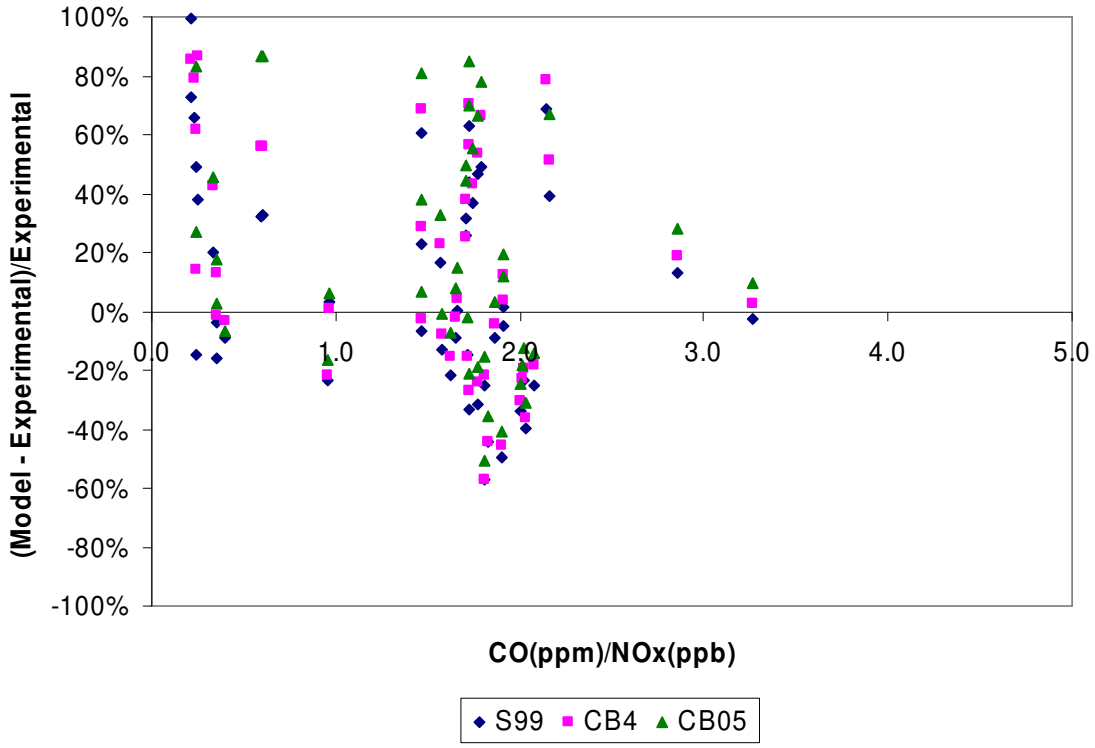

Figure D-9. The distributions of the model errors against CO/NOx ratio in simulating the UCR chamber experiments. (*O_3 concentrations at t = 6 hours (or 5 hours) after injection were used for calculations.)

REFERENCES

Carter, W. P. L. and Atkinson, R. (1987). An experimental study of incremental hydrocarbon reactivity. *Environmental Science & Technology*, 21, 670-679.

Carter, W. P. L, Crocker, D. R., Fitz, D. R., Malkina, I. L., Bumiller, K., Sauer, C. G., Pisano, J. T., Bufalino, C., and Song, C. (2005). *A new environmental chamber for evaluation of gas-phase chemical mechanisms and secondary aerosol formation*. Atmospheric Environment, 39, 7768-7788.

Killus, J. P. and Whitten, G. Z. (1990). Background reactivity in smog chambers. *The International Journal of Chemical Kinetics*, 22, 547-575.

Hess, G. D., Carnovale, F., Cope, M. E., and Johnson, G. M. (1992). The evaluation of some photochemical smog reaction mechanisms-I: temperature and initial composition effects. *Atmospheric Environment*, 26A, 625-641.

Appendix E: Olefins in the 8-county Houston-Galveston 2000 emissions inventory

An assessment of the mobile source emissions inventory for the 8-county Houston-Galveston area on August 30, 2000 was made for explicit olefins species. The mass emitted (tons/day) of each olefins species in the mobile source category on this day is reported in Table E-1. The methodology for deriving this table is also provided below. As reported in Table E-1, the terminal olefins dominating the mobile sources on this is ethylene, followed by isobutene and propylene.

Based on the evaluation of olefin species in the mobile source category of the emissions inventory for the 8-county Houston-Galveston area on August 30, 2000, the total daily mass of olefins amount to approximately 20.5 tons, which is approximately 12.6% of the total VOCs. The internal olefins at nearly 7 tons/day account for 32.7% of the total olefins and approximately 4% of the total VOCs. The dominant internal olefin in the mobile source category was 2-methyl-2-butene with a contribution of 1.732 tons/day. Trans-2-butene is emitted at 0.5993 tons/day.

Table E-1. Explicit olefin species in the mobile source category of the emission inventory for the 8-county Houston-Galveston area on August 30, 2000.

Chemical Species	Mass emitted (Tons/Day)	% of Total VOC	Internal Olefin?
ethylene	4.8989	3.0188	no
2-methylpropene (isobutene)	2.4187	1.4905	no
propylene	2.3053	1.4206	no
2-methyl-2-butene	1.7315	1.0670	yes
trans-2-pentene	1.4416	0.8884	yes
2-methyl-1-butene	1.0406	0.6412	no
cis-2-pentene	0.7558	0.4658	yes
1-pentene	0.6645	0.4095	no
trans-2-butene	0.5993	0.3693	yes
cis-2-butene	0.5955	0.3669	yes
1,3-butadiene	0.5365	0.3306	no
2-methyl-2-pentene	0.3513	0.2165	yes
trans-2-hexene	0.3476	0.2142	yes
1-butene	0.3400	0.2095	no
3-methyl-1-butene	0.3051	0.1880	no
isoprene	0.2811	0.1732	no
2-methyl-1-pentene	0.2682	0.1653	no
cyclopentene	0.2510	0.1546	yes
3-methyl-1-pentene	0.1958	0.1207	no
1-hexene	0.1916	0.1181	no
cis-2-hexene	0.1860	0.1146	yes
1-methylcyclopentene	0.1817	0.1119	yes
1-undecene	0.1312	0.0809	no
trans-3-heptene	0.1047	0.0645	yes
2,4,4-trimethyl-1-pentene	0.0790	0.0487	no
cis-2-heptene	0.0766	0.0472	yes
4-methyl-1-hexene	0.0392	0.0242	no
2,4-dimethyl-1-pentene	0.0350	0.0216	no
cis-2-octene	0.0276	0.0170	yes
trans-2-nonene	0.0177	0.0109	yes
normal pentene isomers	0.0130	0.0080	no
1-octene	0.0116	0.0072	no
c6 olefins (hexene isomers)	0.0110	0.0068	no
cb4 olefin bond	0.0110	0.0068	no
trans-2-octene	0.0093	0.0058	yes
cis-2-nonene	0.0089	0.0055	yes
3-methyl-trans-2-pentene	0.0035	0.0022	yes
4-methyl-1-pentene	0.0035	0.0022	no
heneicosane	0.0031	0.0019	no
cis-3-hexene	0.0028	0.0017	yes
1-heptene	0.0004	0.0002	no
methylhexenes	0.0004	0.0002	no

Total tons/day olefins	20.48	tons/day
tons/day internal olefins	6.69	tons/day
internal olefins/total olefins:	32.7%	
total olefins/total VOCs	12.62%	
internal olefins/total VOCs	4.12%	

The methodology for deriving Table E-1 is described below.

Table E-2. Eight counties in Houston-Galveston area with respective codes:

Brazoria	48039
Chambers	48071
Fort Bend	48157
Galveston	48167
Harris	48201
Liberty	48291
Montogmery	48339
Waller	48473

For on-road mobile EI, there are four profiles, retrieved from msg.chmspl.cb4 files. These profiles were assumed to be analogous to profiles Russell at UT Austin used in his xref file and hence to the profiles in the excel sheet **all_UT_spec_profiles_v2.xls**. Specifically, the U profiles in the "Tunnel" worksheet and the D201 profile in the "TCEQ" worksheet. Russell's xref files for the on-road mobile EI can be found in:

/Volumes/RAID/matt/matt_dissertation/TXAQS_EI/eps2/links/inputs

with the name:

chmprf.xref.voc.links.UT.gz

From msg.chmspl.cb4 files	From Russell's xref files
D201	D201
U2KGS	H2KGS
U2KGV	H2KGV
U2KWT	H2KWT

VOC tons/day for each profile was obtained for the 2000 Onroad Mobile Sources in the 8-County Houston area for a typical weekday, August 30th. These data were retrieved from **msg.chmspl.cb4.*48039*.0830** (for each county; located in folder: **msg.hga.0830\chmspl**) from the table "Output Criteria Emissions by Profile Code (English Tons)". The total VOC tons/day across the four profiles for each county is also available from the chmspl message files (Table D-3).

Table E-3. VOC totals (tons/day) for each of eight counties on August 30, 2000 reported in chmspl message files.

		VOC (tons/day)							
		Brazoria	**Chambers**	**Fort Bend**	**Galveston**	**Harris**	**Liberty**	**Mongtogmery**	**Waller**
Profile		**48039**	**48071**	**48157**	**48167**	**48201**	**48291**	**48339**	**48473**
D201	D201	0.174	0.0977	0.2294	0.2077	2.875	0.0618	0.2253	0.0482
H2KGS	U2KGS	0.8786	0.3803	0.9483	1.0068	13.6237	0.3789	1.1256	0.3595
H2KGV	U2KGV	1.1154	0.4842	1.2197	1.1448	17.0432	0.4859	1.473	0.4832
H2KWT	U2KWT	5.6861	2.2164	6.5109	6.5981	83.6041	2.2738	7.2169	2.1011
Total	162.2776	7.8541	3.1786	8.9083	8.9574	117.146	3.2004	10.0408	2.992

The VOC totals (tons/day) for each county for August 30, 2000 in the **chmspl** message files do not match with those obtained from the latest TCEQ SIP documentation shown in the table below. This is because the message files are from an earlier version of the EI.

Table E-4. VOC totals (tons/day) for each country for August 30, 2000, reported in TCEQ SIP documentation.

	NO_x	***VOC***	***CO***
Brazoria	13.95	6.78	101.33
Chambers	7.33	3.09	50.94
Fort Bend	18.61	8.73	124.41
Galveston	14.33	7.54	110.01
Harris	253.76	109.96	1,500.86
Liberty	6.20	2.89	42.34
Montgomery	21.62	8.98	137.53
Waller	5.98	2.55	40.89
8-County Total	341.78	150.52	2,108.31

***TCEQ HG SIP Documentation**

In **all_UT_spec_profiles_v2.xls**, in the "Tunnel" worksheet, there is a list of "Unique" numbers and corresponding Mass for the U profiles listed in the first column. In the "TCEQ" worksheet, for the D201 profile, there is a "SAROAD:TX" and corresponding Mass for the D201 profile listed in the first column. Both the "Unique" and "SAROAD:TX" numbers in the worksheets correspond to chemical species. The chemical species corresponding to the "SAROAD" and "Unique" numbers can be found in the emitdb.xls excel file in the "SAROAD Assignments" worksheet. The "Unique" numbers correspond to the "U.ID" column in that worksheet. We used the "Master List" in emitdb.xls to identify the chemical species corresponding to the Unique numbers. Each Unique (and SAROAD) number corresponding to a chemical species may be included in all, none, or some of the four mobile profiles. For each of the profiles that the chemical species is included in, there is a VOC Mass fraction. After the chemical species and their VOC mass fractions have been identified for each of the four onroad mobile source profiles, the type of hydrocarbons class of each were determined, e.g., aromatics, alkanes, alkenes, etc.. In addition, the surrogate species in which the individual chemical species are lumped in SAPRC and CB-IV were determined for each chemical species.

In order to determine the abundance of certain alkenes or olefins in the on-road mobile EI, all the chemical species classified as alkenes were extracted from the list of chemical species. The mass fraction of a chemical species contributing to an on-road mobile profile was multiplied by the total VOC tons/day for that profile available in Table 1. For each of the profiles, since the total mass fraction did not add up to exactly 1.0, the mass fractions were divided by the estimated mass fractions. For example, for the profile D201, the total mass fraction estimated was 0.9957. Hence, the mass fraction

of chemical species for that profile was all divided by 0.9957. Then, for each of the Houston's eight counties, the mass fraction of each species contributing to each of the profiles were multiplied by the total emissions of tons of VOC per day for a profile in that county and summed over all profiles. Furthermore, the contribution of individual chemical species emissions (tons/day) belonging to a particular hydrocarbon class in the non-road mobile source EI were summed over all eight counties. The total tons/day of each chemical species across the 4 source profiles and 8-counties were then divided by the total VOC tons/day across all profiles and counties to determine the percentage contribution of the chemical species relative to the total VOCs. However, in order to be able to divide by the total tons/day of VOCs, the chemical species (hydrocarbons) that are not considered VOCs by regulatory definitions should be extracted from the data set.

To distinguish the VOCs from non-VOCs from the list of compounds, the regulatory definition of a VOC was used. By regulatory definitions, a VOC is a compound whose rate of reaction with the hydroxyl radical is higher than the rate of reaction of Ethane with OH. Ethane rate of reaction with OH is 2.4E-13, which is considered negligibly reactive. The rates of reaction of the different compounds were estimated using estimation software downloaded from the EPA website, called EPI Suite. The "Aopwin" feature of this software, specifically, estimated the rate of the reaction of a compound with the OH radical with an input of the compound's CAS number. The list of compounds identified as alkenes in the on-road mobile EI were all classified as VOCs by regulatory definitions. The list of alkenes were then sorted in descending order of the percentage contribution of mass (tons/day) to the total mass of VOCs across all eight counties and all four profiles in the on-road mobile EI.

Appendix F: CO-NOx chemistry and Sensitivity of $OH+NO_2$ rate constant in CO-NOx systems

The CO and NOx (NO + NO_2) system illustrates many of the basic features of photochemical oxidant formation. CO molecules are slowly oxidized by OH radicals to generate HO_2 radicals. When NOx availability is sufficient, HO_2 in this CO-NOx system efficiently regenerates OH. This cycle involving OH and HO_2 forms NO_2 without consumption of O_3, and the subsequent photolysis of NO_2 into NO and O leads to net O_3.formation as shown in below reactions (R1 - R4). Formation of HNO_3 or H_2O_2 in reactions R5 and R6 lowers the efficiency of catalytic CO oxidation and O_3 formation in this system.

$$OH + CO\ (+O_2) \rightarrow HO_2\ (+ CO_2) \quad \text{(R1)}$$
$$HO_2 + NO \rightarrow OH + NO_2 \quad \text{(R2)}$$
$$NO_2 + h\nu \rightarrow NO + O(^3P) \quad \text{(R3)}$$
$$O(^3P) + O_2 \rightarrow O_3 \quad \text{(R4)}$$
$$OH + NO_2 \rightarrow HNO_3 \quad \text{(R5)}$$
$$HO_2 + HO_2 \rightarrow H_2O_2 \quad \text{(R6)}$$

Differences in reactions and integrated reaction rates within the CO-NOx system that might contribute to significant differences in predicted ozone concentrations between different chemical mechanisms were investigated. As shown in Table 5-1, SAPRC99 has an additional HONO photolysis reaction (R7) that is not included in CBIV and CB05:

$$HONO + h\nu \rightarrow HO_2 + NO_2 \quad \text{(R7)}$$

In addition, large differences exist between the mechanisms in the $OH+NO_2 \rightarrow HNO_3$ rate parameter as shown in Figure F-1. As a preliminary step, six sensitivity runs shown in Table F-2 were conducted to investigate the significance of these differences on predicted ozone concentrations. First, R7 in SAPRC99 was turned off to eliminate the

extra HONO photolysis reaction. Second, the rate constant of R5 in SAPRC99 was adjusted to have CBIV's rate constant or CB05's rate constant. Third, the rate constant of R5 in CBIV was adjusted to have S99's rate constant. The results of these preliminary studies indicated that the effects of adjusting the rate constant of R5 on peak predicted ozone concentrations were significantly larger than the impacts of inclusion of R7 in SAPRC99. Thus, further investigations presented in this Section focused on the effect of changing the $OH + NO_2 \rightarrow HNO_3$ rate parameter on predicted ozone concentrations using SAPRC99, CBIV and CB05. These differences were investigated with the three CO-NOx cases described in Table F-1 (shown below for reference). These simulations were conducted without the wall mechanisms as well as with the wall mechanism. The reason for running the comparisons without the wall mechanisms is to determine whether the mechanism predictions for CO-NOx chemistry would converge in regional photochemical modeling simulations (no wall effects) when R5 is equal between mechanisms.

As described in Chapter 4, sensitivity runs were conducted with the UNC and UCR chamber models for the CO-NOx system to examine the effects of the wall mechanism and, additionally, to evaluate the performance of the wall mechanism in simulations of several UNC and UCR chamber experiments. These studies demonstrated that under the low reactivity conditions of the CO system, the effects of the wall mechanism are large and that application of the wall mechanism improves agreement between simulations and chamber experiments.

Table F-1. Chemical reactions having different reaction rate parameters between CBIV, CB05 and SAPRC99 associated with the CO-NOx system[*].

Reaction	**Reaction Number in Morpho (CBIV | CB05 | S99)**	**Relative magnitude of the reaction constant**
$OH + NO_2 \rightarrow HNO_3$	I26 | I28 | I25	S99 < CB05 < CBIV
$OH + NO \rightarrow HONO$	I22 | I24 | I21	CBIV < S99 ≈ CB05
$HONO + h\nu \rightarrow OH + NO$	I23 | I25 | I22	CB05 < S99 ≈ CBIV
$O_3 + h\nu \rightarrow O^3P$	I8 | I8 | I17	S99 ≈ CBIV < CB05
$O^3P \rightarrow O_3$	I2 | I2 | I2	S99 < CB05 [1]
$HONO + h\nu \rightarrow HO_2 + NO_2$	** | ** | I23	[2]
$HO_2 + NO \rightarrow OH + NO_2$	I28 | I30 | I31	CB05 < CBIV ≈ S99
$HO_2 + HO_2 \rightarrow H_2O_2$	I32 | I34 | I37	CBIV ≤ S99 ≤ CB05
$HO_2 + HO_2 + H_2O \rightarrow H_2O_2$	I33 | I35 | I38	CBIV < S99 ≈ CB05
$OH + CO \rightarrow HO_2$	I36 | I65 | I29	S99 < CBIV < CB05
$O_3 + h\nu \rightarrow O^1D$	I9 | I9 | I18	CBIV ≤ CB05 ≈ S99
$O^1D \rightarrow O^3P$	I10 | I10 | I20	S99 ≤ CB05 [3]
$HO_2 + NO_3 \rightarrow HNO_3$ (CB05) $HO_2 + NO_3 \rightarrow 0.8(OH + NO_2) + 0.2HNO_3$ (S99)	* | I48 | I39	CB05 < S99

*: Two experiments included in Morpho's environmental chamber database, AU3093 and AU3096 were used in gathering the integrated reaction rates and relative magnitudes of the reactions listed;
**: No corresponding reaction exists in the chemical mechanism;
1: The order of reaction for S99 and CB05 is three, for CBIV, the order is one;
2: An extra HONO photolysis only in S99;
3: The order of reaction for S99 and CB05 is two, for CBIV, the order is one.

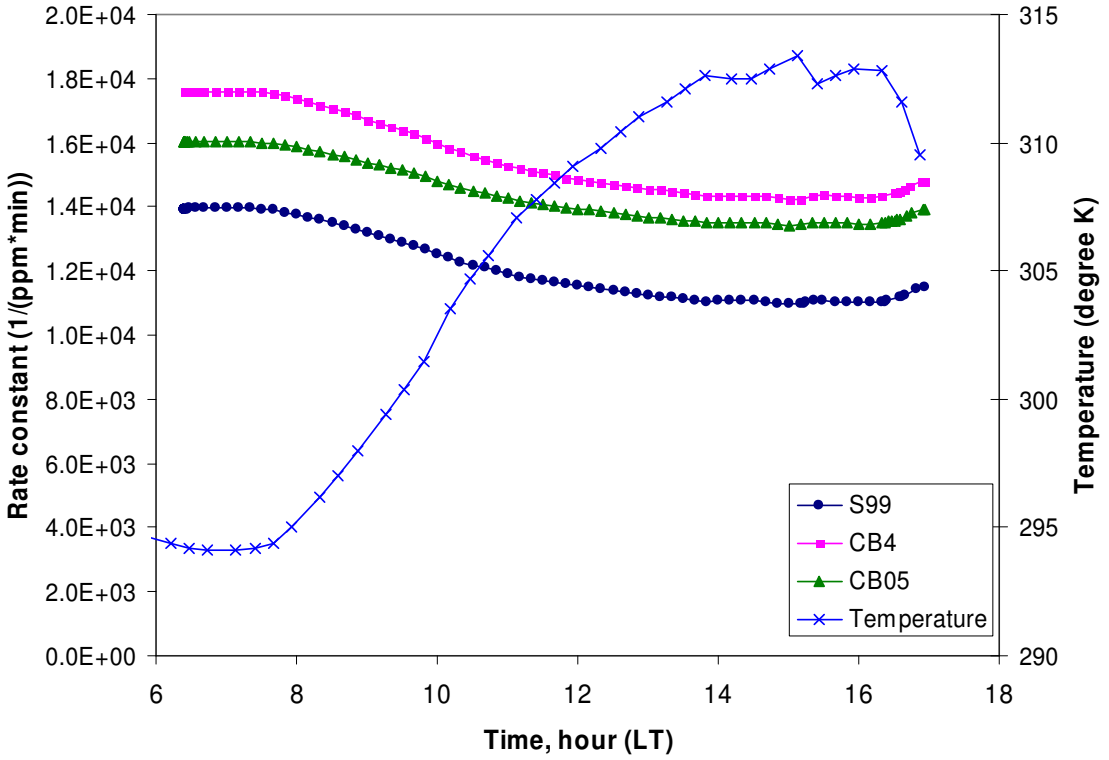

Figure F-1. The diurnal variations of air temperature and the reaction rate constant of R5 ($OH + NO_2 \rightarrow HNO_3$) for each mechanism in experiment AU3093 at the UNC smog chamber.

Table F-2. Preliminary sensitivity simulations associated with R5 and R7.

Mechanism	Adjustment(s)
SAPRC99	R7 in S99 turned off
SAPRC99	R5 in S99 adjusted to have CBIV's rate constant
SAPRC99	R7 in S99 turned off; R5 in S99 adjusted to have CBIV's rate constant
SAPRC99	R5 in S99 adjusted to have CB05's rate constant
SAPRC99	R7 in S99 turned off; R5 adjusted to have CB05's rate constant
CBIV	R5 in CBIV adjusted to have S99's rate constant

Table F-1 (repeated for reference). The initial conditions of three CO-NOx cases in Morpho and SAPRC*.

	CO(50)	CO(100)	CO(250)
NO	0.01533	0.01533	0.01533
NO_2	0.01002	0.01002	0.01002
HONO	5.00E-05	5.00E-05	5.00E-05
CO	**51**	**100**	**250**

*: The units of the initial concentrations are ppm. Time-independent air exchange of 0 hr^{-1}, air temperature of 305 K and humidity of 20,000 ppm (or 20.27 milli bar) were used.

SENSITIVITY STUDIES WITH THE WALL MECHANISM AND PNA CHEMISTRY

Sensitivity simulations on R5 without using the wall mechanism and the PNA chemistry were conducted only with the UNC chamber model because, as shown in Table F-2, the three mechanisms resulted in nearly the same ozone concentrations in Morpho and SAPRC when the same input data are supplied to both mechanism evaluation systems and when the wall mechanism is turned off. Figure F-2 shows predicted ozone concentrations for the three mechanisms for the Base Case and for cases with variations in the $OH+NO_2 \rightarrow HNO_3$. For the three CO-NOx cases under consideration, ozone concentrations for SAPRC99 (O_3 of S99 (Base Case)) are always higher than ozone concentration for both CBIV and CB05's (O_3 of CBIV (Base Case)) and O_3 of CB05 (Base Case)). When the rate constants of reaction R5 in each mechanism were set equal to each other, the differences in predicted O_3 between those mechanisms decreased significantly. For example, when the rate constant of R5 of SAPRC99 was changed to CBIV's corresponding rate constant, O_3 concentrations in Figure F-2 predicted for SAPRC99 and CBIV become very close regardless of the initial conditions. As shown in Figure F-3, the effects of changing the rate constant of R5 included modulating the concentrations of OH and HO_2 radicals and the NO to NO_2 conversion rate;

concentrations of NOx and NOy (where NOy = NOx + HNO_3) were nearly the same between all three Base Case runs and six sensitivity runs in each plot in Figure F-3.

When the wall mechanism and the PNA chemistry were turned on, the effects of changing the rate constants of R5 between mechanisms were limited (Figure F-4). Thus, for these three CO-NOx cases, the effects of turning on the wall mechanism, shown in Figures F-1 and F-2, were dominant relative to the changes in the R5 rate parameter described in Figure F-4.

Caution needs to be exercised in extrapolating these sensitivity study results, that include wall effects as well as conditions where high concentrations of CO dominate the atmospheric reactivity, to ambient air. However, the studies demonstrate that differences in the R5 rate parameter between CBIV, CB05 and SAPRC99 contribute to differences in predicted ozone concentrations between the three mechanisms.

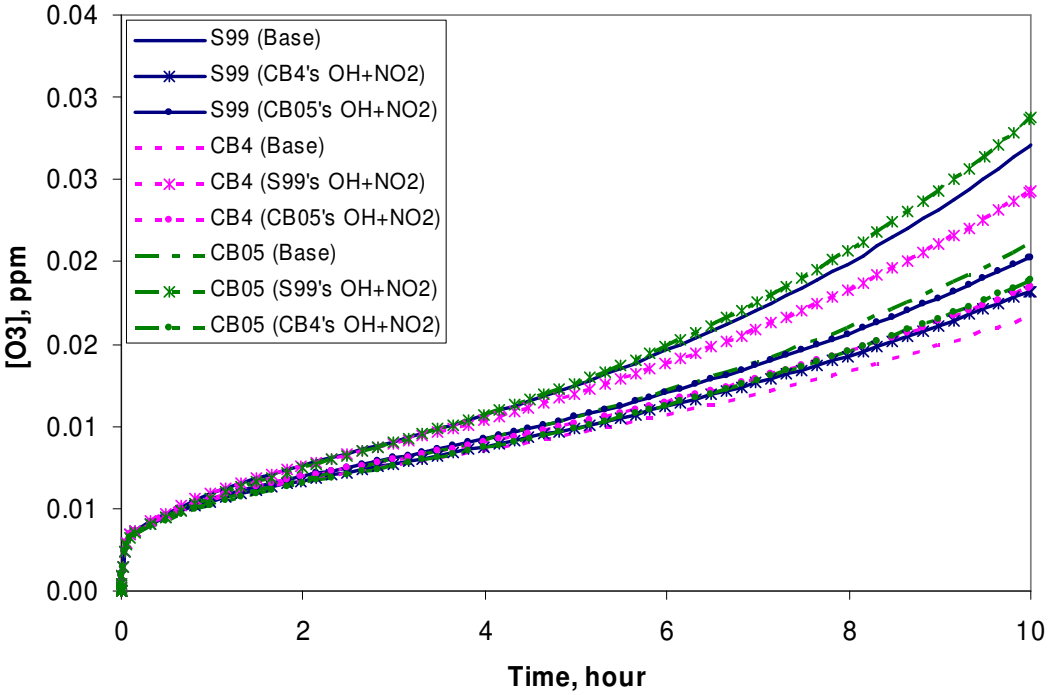

(a) Case CO(50) in Morpho

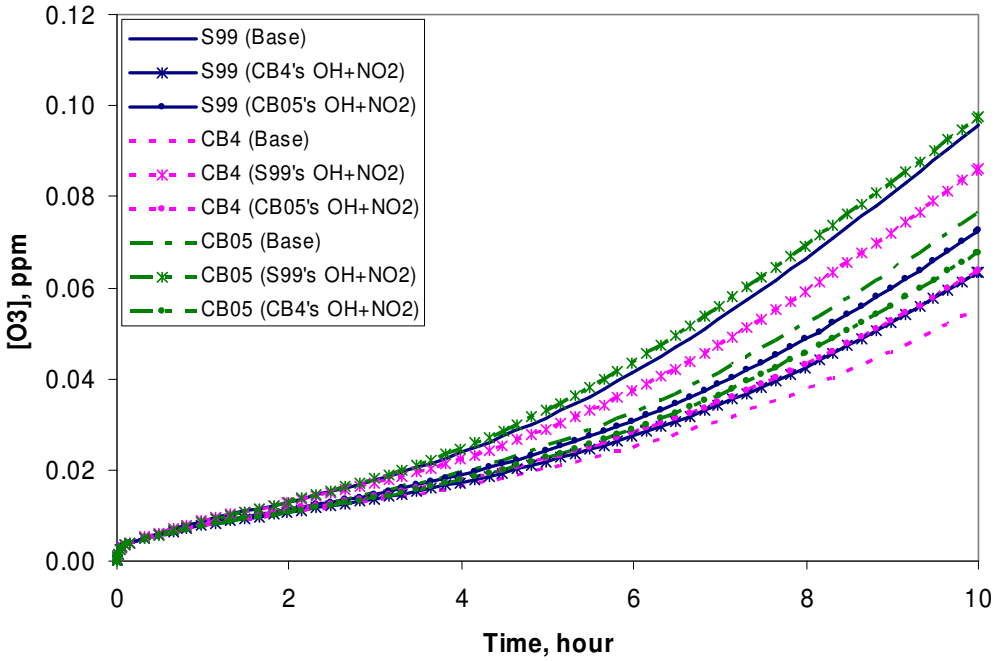

(b) Case CO(100) in Morpho

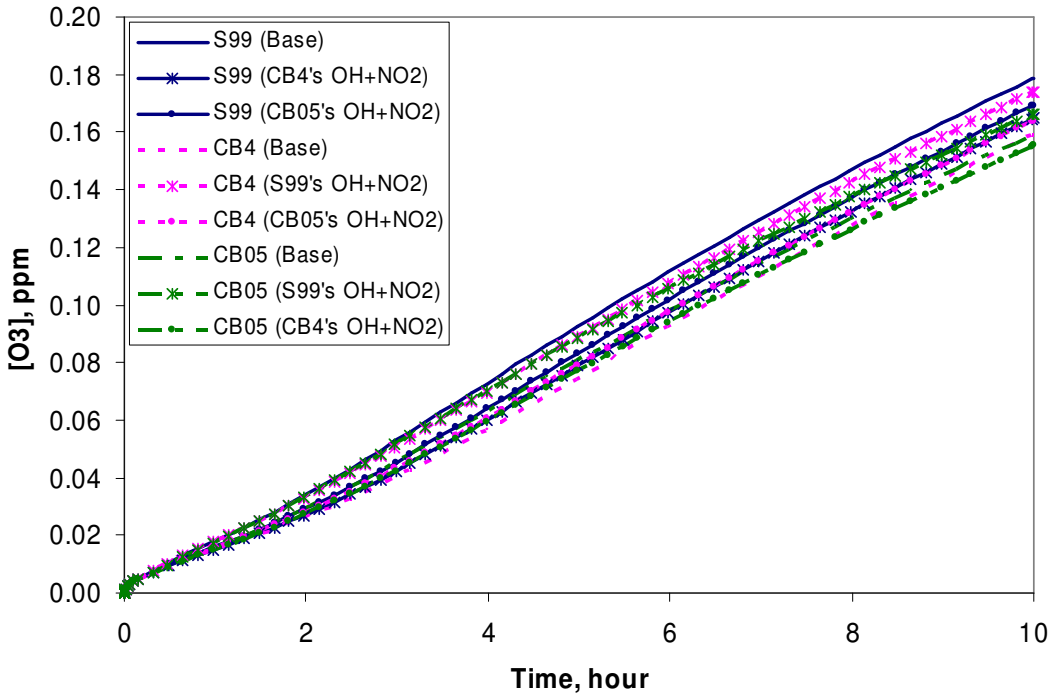

(c) Case CO(250) in Morpho

Figure F-2. Time series of predicted O_3 concentrations for the three CO-NOx cases (*All simulations were done without using the wall mechanism and the PNA chemistry for each mechanism. Table F-1 describes the three CO-NOx cases).

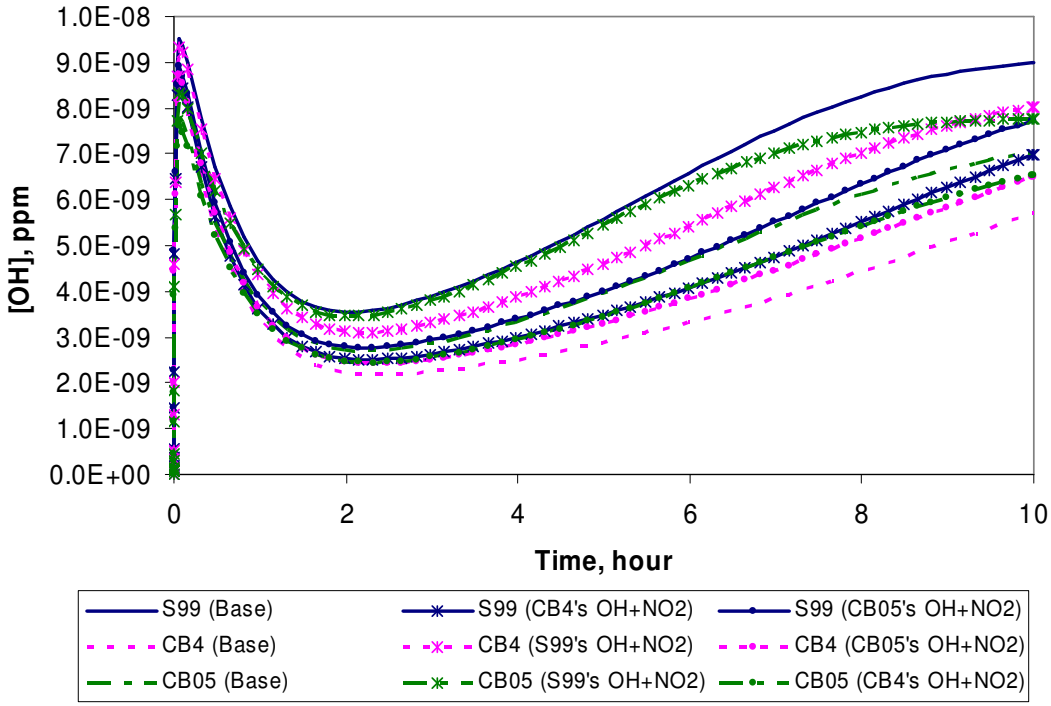

(a) OH in Case CO(100) in Morpho

(b)

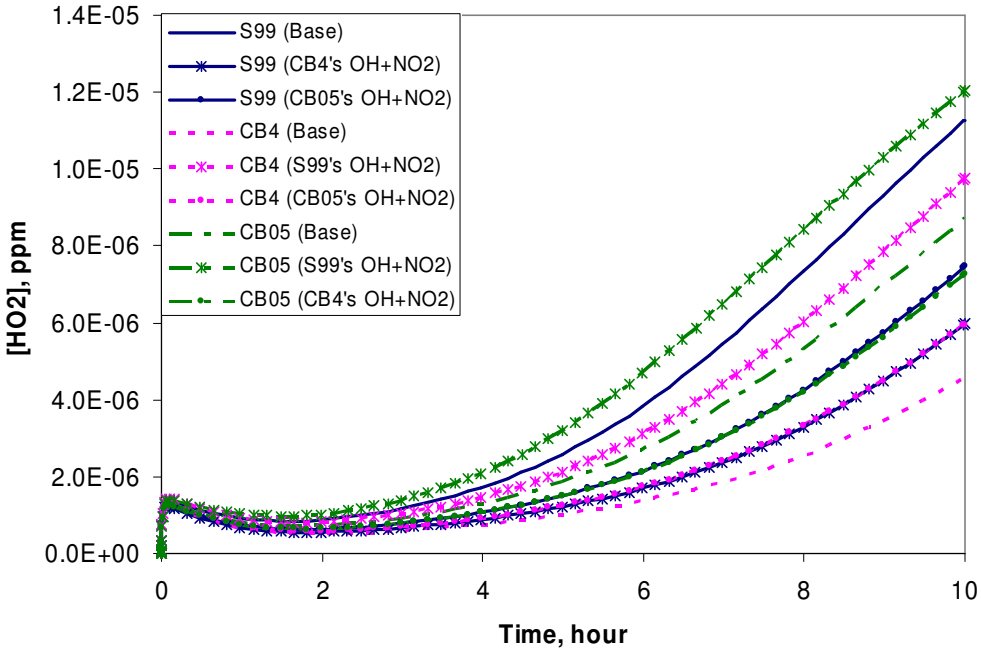

(c) HO_2 in Case CO(100) in Morpho

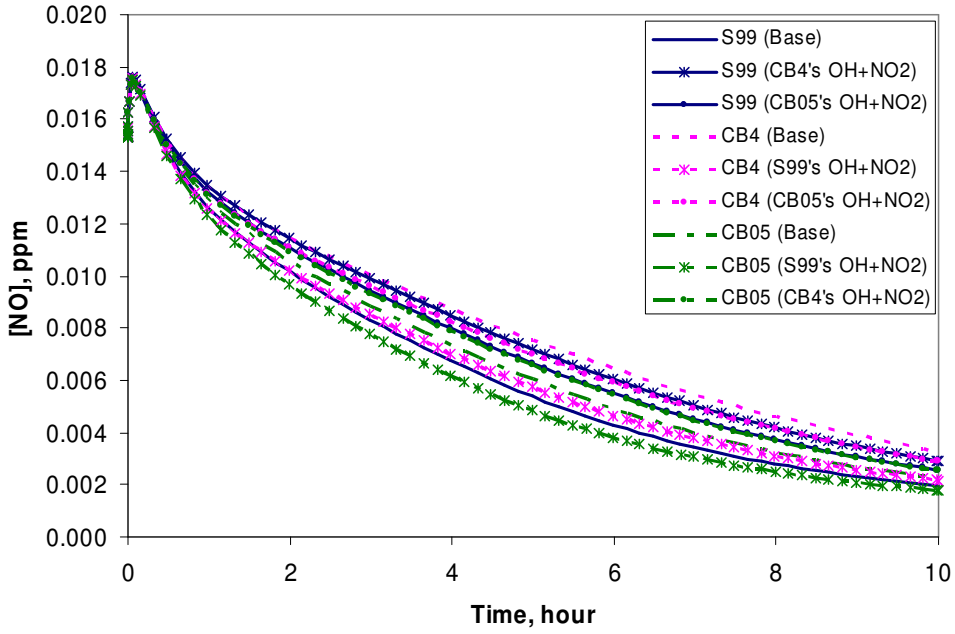

(c) NO in Case CO(100) in Morpho

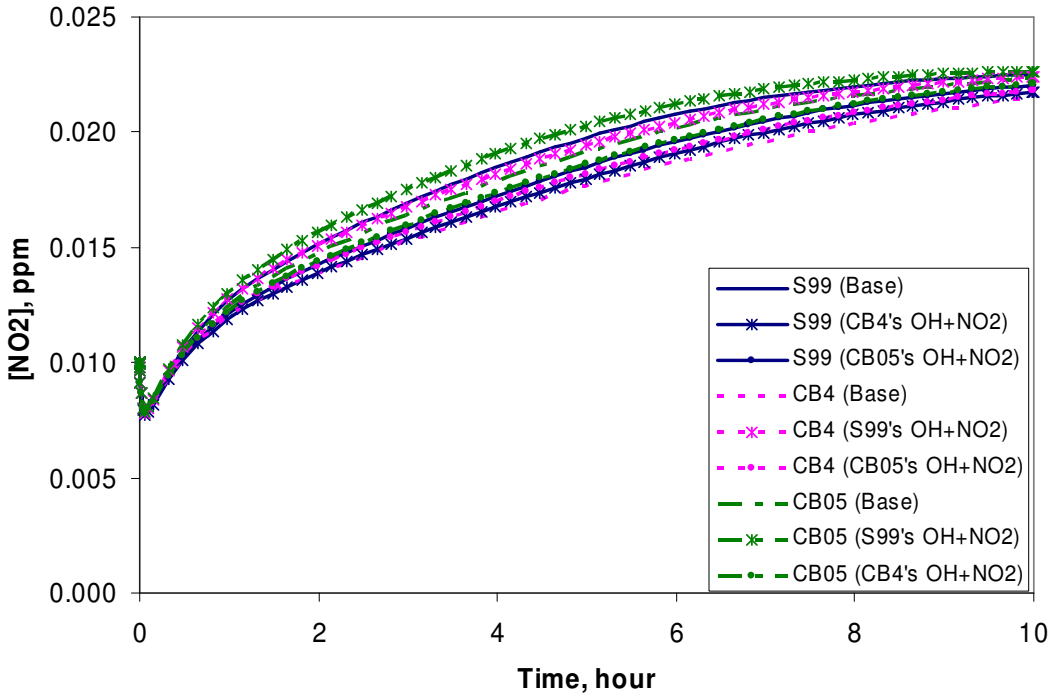

(d) NO_2 in Case CO(100) in Morpho

Figure F-3. Time series of the simulated concentrations in sensitivity runs in case CO(100): (a) OH, (b) HO_2, (c) NO, and (d) NO_2. (*All simulations were done without using the wall mechanism and the PNA chemistry for each mechanism.)

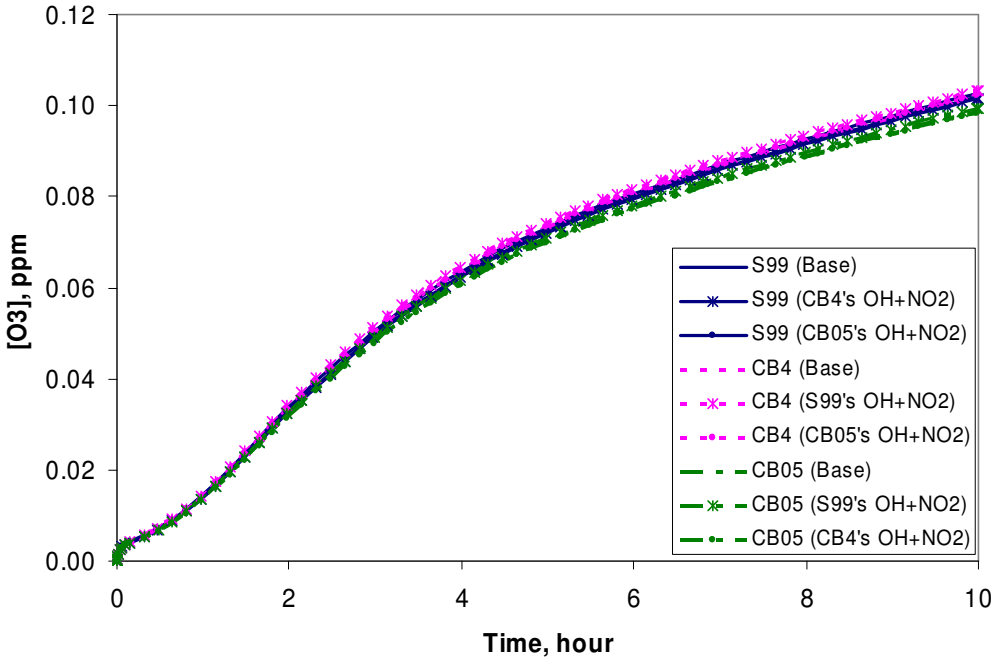

(a) O_3 in case CO(250) in Morpho

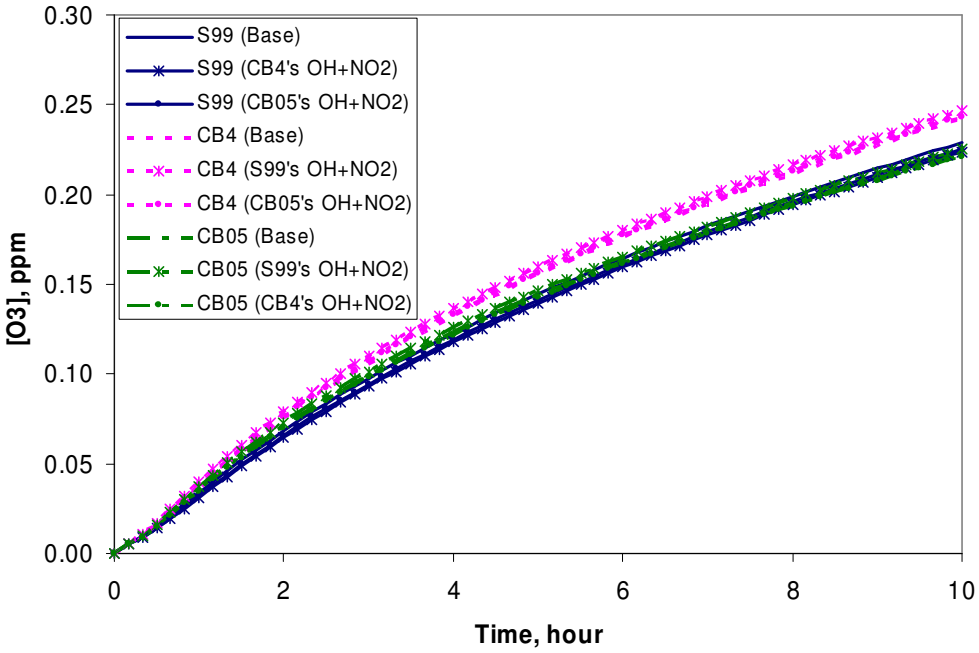

(b) O_3 in case CO(250) in SAPRC

Figure F-4. Time series of the simulated O_3 concentrations in sensitivity runs in case CO(250): (a) in the Morpho software (b) in the SAPRC software. (*All simulations were done with the wall mechanism and the PNA chemistry for each mechanism.)

SENSITIVITY STUDIES WITH THE $OH+NO_2$ RATE CONSTANT

Sensitivity runs on the R5 rate parameter were conducted only with the UNC chamber model for the four CO-NOx cases (AU3093[Red], AU3093[Blue], AU3096[Red] and AU3096[Blue]) included in Morpho's smog chamber database. As shown in Table F-3 and Figure F-5, making the R5 rate parameter equal between different mechanisms always decreased the differences in predicted O_3 concentrations between mechanisms. For the four cases in Morpho, O_3 and OH concentrations predicted for SAPRC99 are higher than those predicted for CBIV and CB05 (O_3 and OH of S99 (Base Case) in Figures F-5 and F-6, respectively). Thus, changing the rate parameters of

R5 in CBIV or CB05 with the rate parameter for SAPRC99 increased O_3 concentrations predicted using these mechanisms. Less removal of OH and NO_2 via HNO_3 in reaction R5 which leads to higher OH explains in part the increases in O_3 concentrations (Figure F-6). When the rate constant of SAPRC99 was set to the corresponding rate constant for CBIV, predicted O_3 concentrations decreased relative to the Base Case (Figures F-5 and F-6). These results were consistent with those for the three CO-NOx cases examined above: differences in the rate constant of reaction R5 between CBIV, CB05 and SAPRC99 have large impacts on differences in predicted ozone concentrations between mechanisms.

However, for the two selected cases (EPA306A and EPA306B) in SAPRC's smog chamber database, the effects are opposite to those observed with the Morpho database: instead of decreasing the differences between mechanisms, changes in the R5 rate parameter increased the differences in predicted O_3 concentrations as shown in Table F-4 and Figure F-7 (Data for Figure F-7 only available through hour 6). For EPA306A and ERPA 306B, O_3 concentrations predicted by SAPRC99 are lower than concentrations predicted by CBIV or CB05, and OH concentrations are nearly the same for the three mechanisms (CBIV (Base Case), CB05 (Base Case) and S99 (Base Case) in Figures F-7 and F-8). This is attributed to the fact that the main radical input parameter in the chamber model used in the SAPRC modeling database, which is the radical source parameter represented by the HONO input (RN), was adjusted separately for each mechanism to optimize model fits to experiments such as these. This compensates for differences in the OH + NO_2 rate constant among the mechanisms. Therefore forcing this rate constant to be the same without also forcing the RN parameters to be the same will

undo this compensation and causes the results of the simulations of these experiments to be different.

Table F-3. Model errors in the sensitivity runs with the 4 UNC chamber experiments*.

Run ID	Base Cases			
	S99	CBIV	CB05	Standard deviation in model error between mechanisms
AU3093:RED	-6%	-14%	-17%	6%
AU3093:BLUE	-5%	-35%	-26%	16%
AU3096:RED	29%	0%	9%	15%
AU3096:BLUE	-14%	-22%	-22%	5%
	All with S99 R5 rate constant			
Run ID	S99	CBIV	CB05	Standard deviation in model error between mechanisms
AU3093:RED	-6%	-3%	-10%	4%
AU3093:BLUE	-5%	-1%	-1%	2%
AU3096:RED	29%	35%	32%	3%
AU3096:BLUE	-14%	-12%	-15%	2%
	All with CBIV R5 rate constant			
Run ID	S99	CBIV	CB05	Standard deviation in model error between mechanisms
AU3093:RED	-17%	-14%	-19%	2%
AU3093:BLUE	-38%	-35%	-34%	2%
AU3096:RED	-5%	0%	-1%	3%
AU3096:BLUE	-25%	-22%	-25%	1%
	All with CB05 R5 rate constant			
Run ID	S99	CBIV	CB05	Standard deviation in model error between mechanisms
AU3093:RED	-13%	-11%	-17%	3%
AU3093:BLUE	-30%	-27%	-26%	2%
AU3096:RED	5%	11%	9%	3%
AU3096:BLUE	-21%	-19%	-22%	2%

*Model error = (modeled max O_3 – experimental max O_3)/experimental max O_3

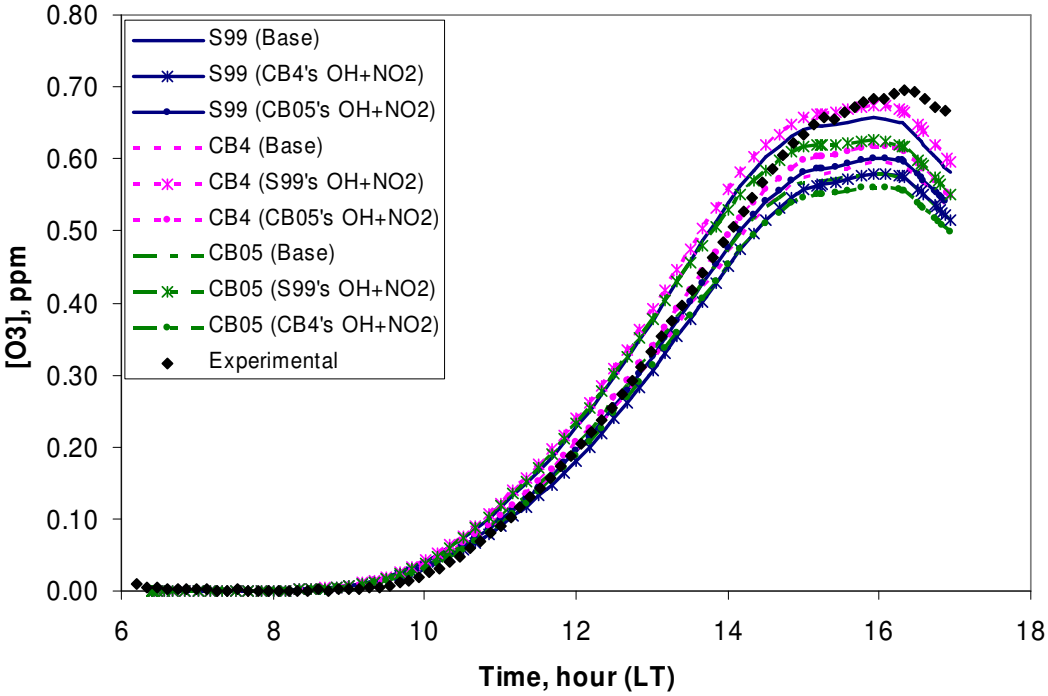
0.80
0.70
0.60
0.50
0.40
0.30
0.20
0.10
0.00
[O3], ppm
S99 (Base)
S99 (CB4's OH+NO2)
S99 (CB05's OH+NO2)
CB4 (Base)
CB4 (S99's OH+NO2)
CB4 (CB05's OH+NO2)
CB05 (Base)
CB05 (S99's OH+NO2)
CB05 (CB4's OH+NO2)
Experimental
6
8
10
12
14
16
18
Time, hour (LT)

(a) AU3093[Red]

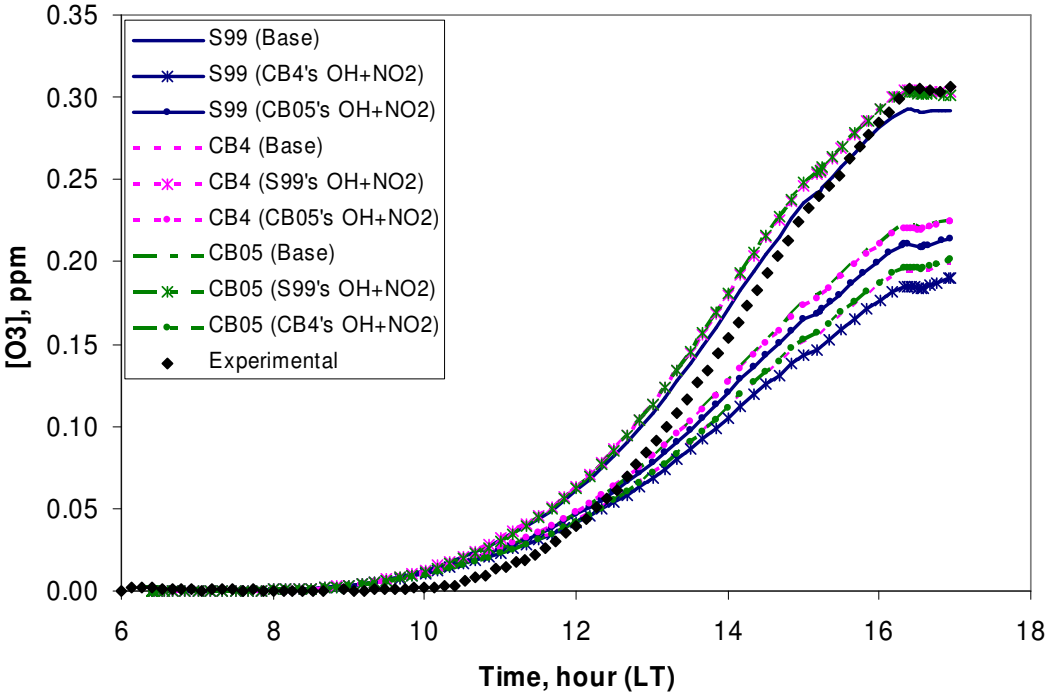

(b) AU3093[Blue]
(c)

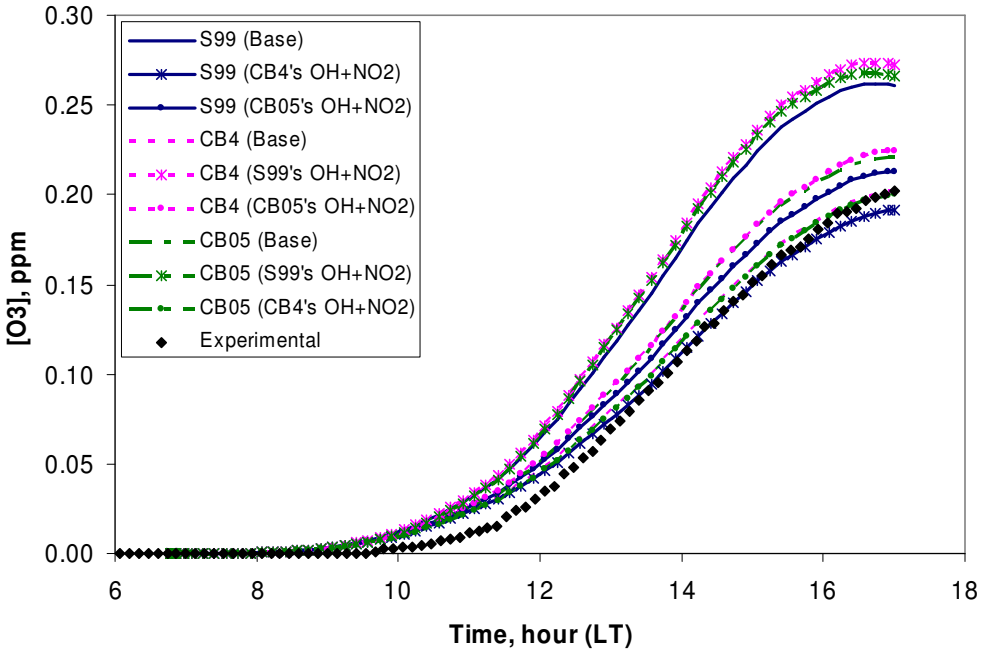
0.30
0.25
0.20
0.15
0.10
0.05
0.00
[O3], ppm
6
8
10
12
14
16
18
Time, hour (LT)
S99 (Base)
S99 (CB4's OH+NO2)
S99 (CB05's OH+NO2)
CB4 (Base)
CB4 (S99's OH+NO2)
CB4 (CB05's OH+NO2)
CB05 (Base)
CB05 (S99's OH+NO2)
CB05 (CB4's OH+NO2)
Experimental

(d) AU3096[Red]

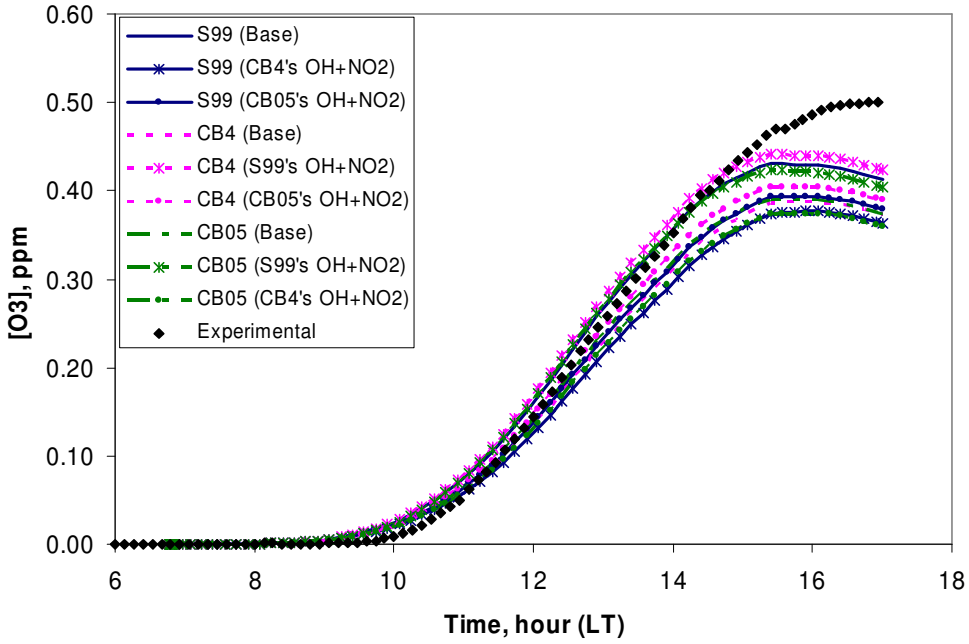

(d) AU3096[Blue].

Figure F-5. Time series of the simulated O_3 concentrations in sensitivity runs in Morpho with cases: (a) AU3093[Red], (b) AU3093[Blue], (c) AU3096[Red] and (d) AU3096[Blue]. (*All simulations were done using the wall mechanism and the PNA chemistry for each mechanism.)

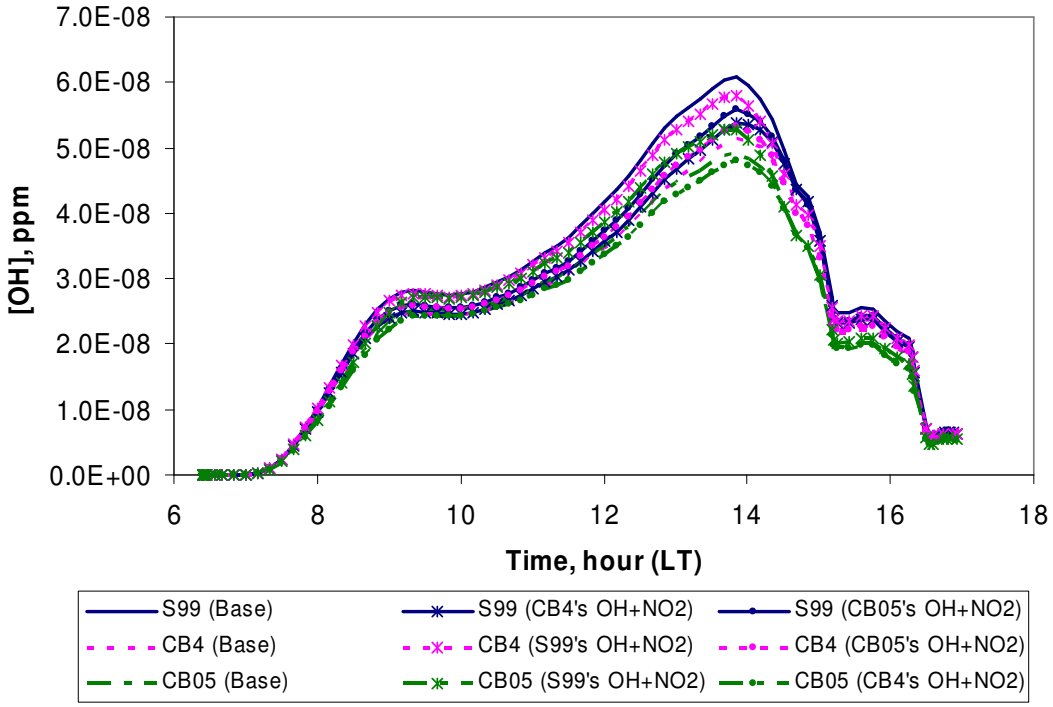
7.0E-08
6.0E-08
5.0E-08
4.0E-08
3.0E-08
2.0E-08
1.0E-08
0.0E+00
[OH], ppm
6
8
10
12
14
16
18
Time, hour (LT)
S99 (Base)
S99 (CB4's OH+NO2)
S99 (CB05's OH+NO2)
CB4 (Base)
CB4 (S99's OH+NO2)
CB4 (CB05's OH+NO2)
CB05 (Base)
CB05 (S99's OH+NO2)
CB05 (CB4's OH+NO2)

(a) AU3093[Red]

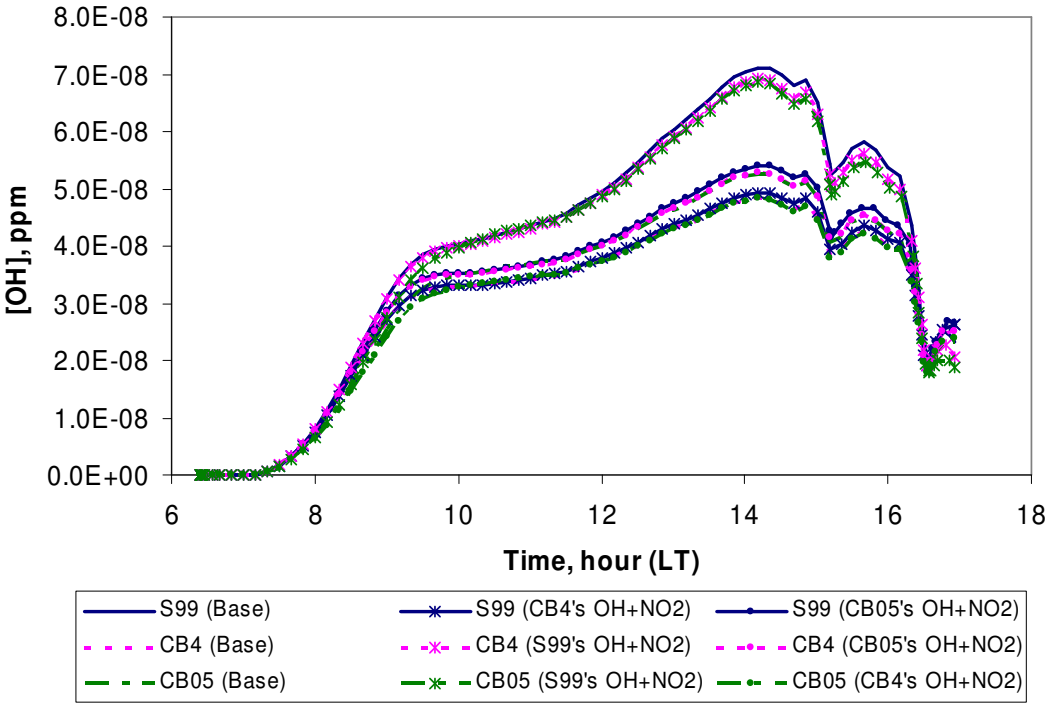

(b) AU3093[Blue]

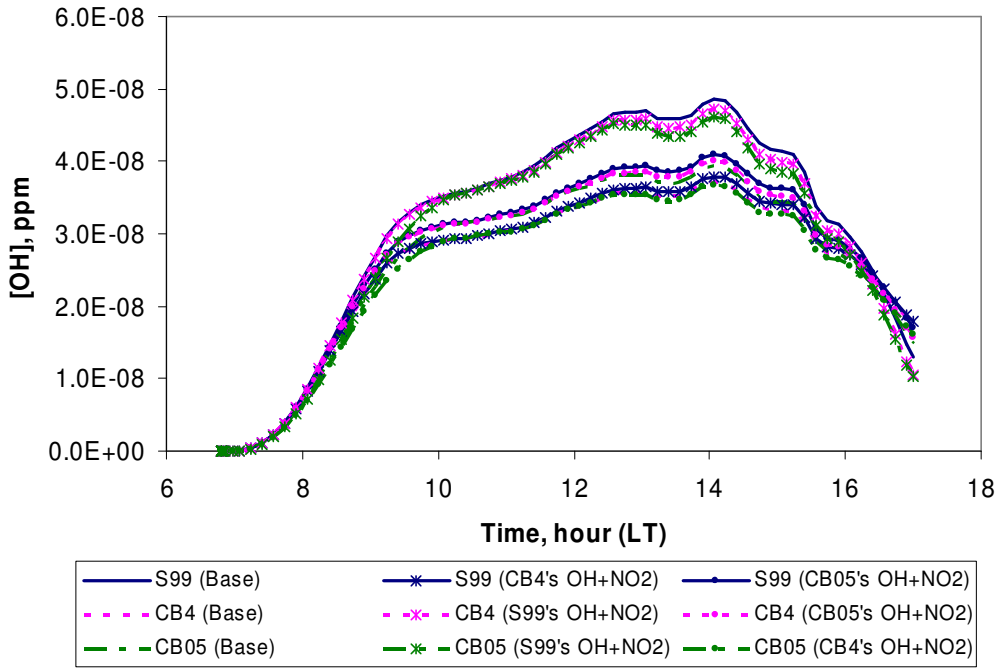
6.0E-08
5.0E-08
4.0E-08
3.0E-08
2.0E-08
1.0E-08
0.0E+00
[OH], ppm
6
8
10
12
14
16
18
Time, hour (LT)
S99 (Base)
S99 (CB4's OH+NO2)
S99 (CB05's OH+NO2)
CB4 (Base)
CB4 (S99's OH+NO2)
CB4 (CB05's OH+NO2)
CB05 (Base)
CB05 (S99's OH+NO2)
CB05 (CB4's OH+NO2)

(c) AU3096[Red]

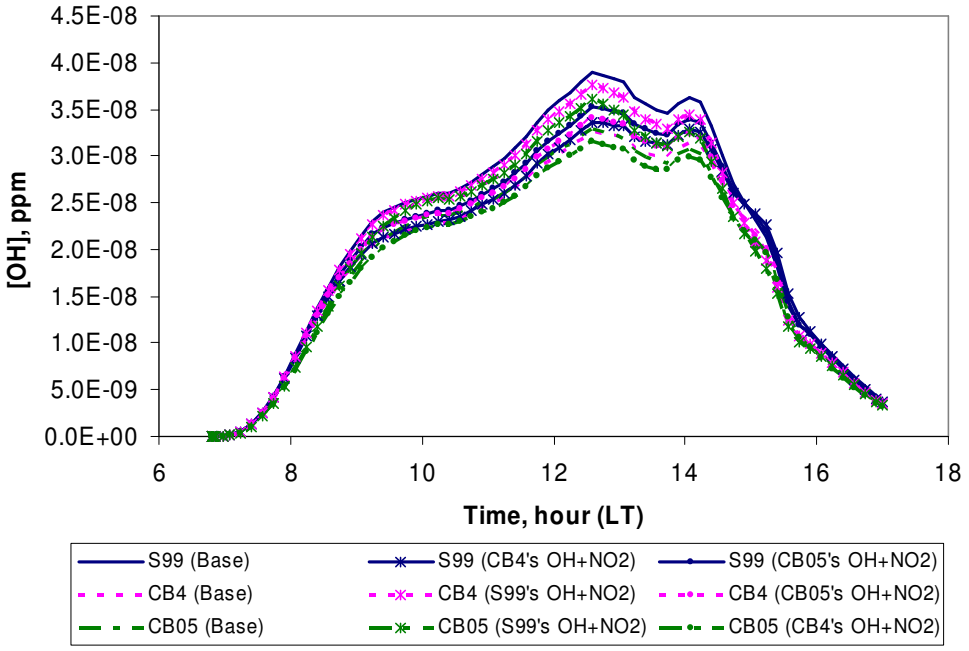

(d) AU3096[Blue].

Figure F-6. Time series of the simulated OH concentrations in sensitivity runs in Morpho with cases: (a) AU3093[Red], (b) AU3093[Blue], (c) AU3096[Red] and (d) AU3096[Blue]. (*All simulations were done using the wall mechanism and the PNA chemistry for each mechanism.)

Table F-4. Summary of the model errors in the sensitivity runs with the 2 UCR chamber experiments*.

Run ID	Base Cases			
	S99	CBIV	CB05	Standard deviation in model error between mechanisms
EPA306A	6%	16%	28%	11%
EPA306B	18%	25%	41%	12%
	All with S99 R5 rate constant			
Run ID	S99	CBIV	CB05	Standard deviation in model error between mechanisms
EPA306A	6%	37%	42%	19%
EPA306B	18%	52%	59%	22%
	All with CBIV R5 rate constant			
Run ID	S99	CBIV	CB05	Standard deviation in model error between mechanisms
EPA306A	-12%	16%	21%	18%
EPA306B	-4%	25%	32%	19%
	All with CB05 R5 rate constant			
Run ID	S99	CBIV	CB05	Standard deviation in model error between mechanisms
EPA306A	-6%	23%	28%	18%
EPA306B	3%	34%	41%	20%

*Model error = (modeled max O_3 – experimental max O_3)/experimental max O_3

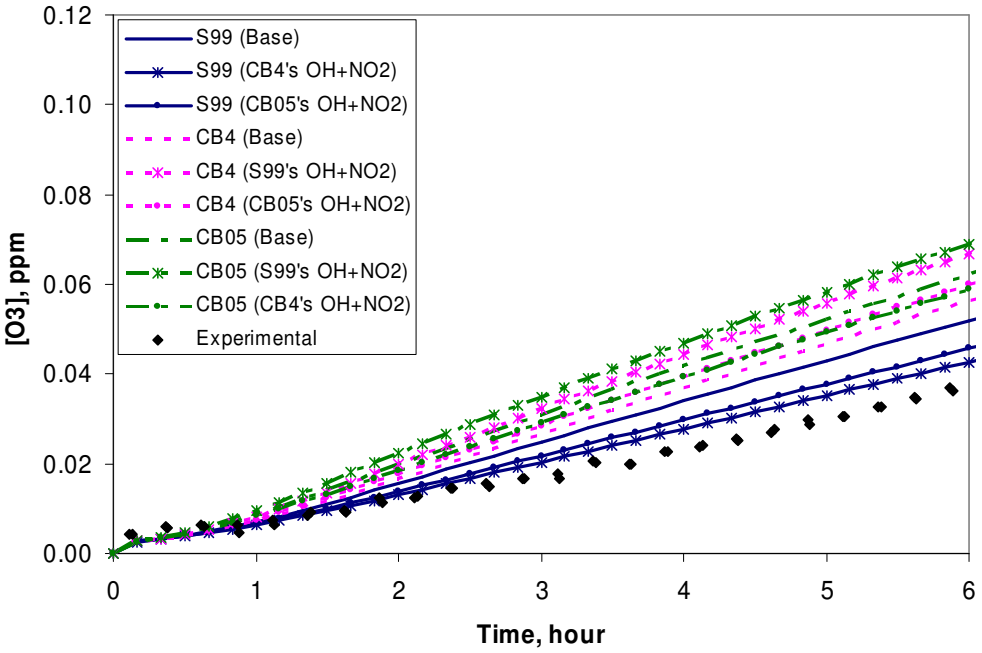

(a) EPA306A in SAPRC

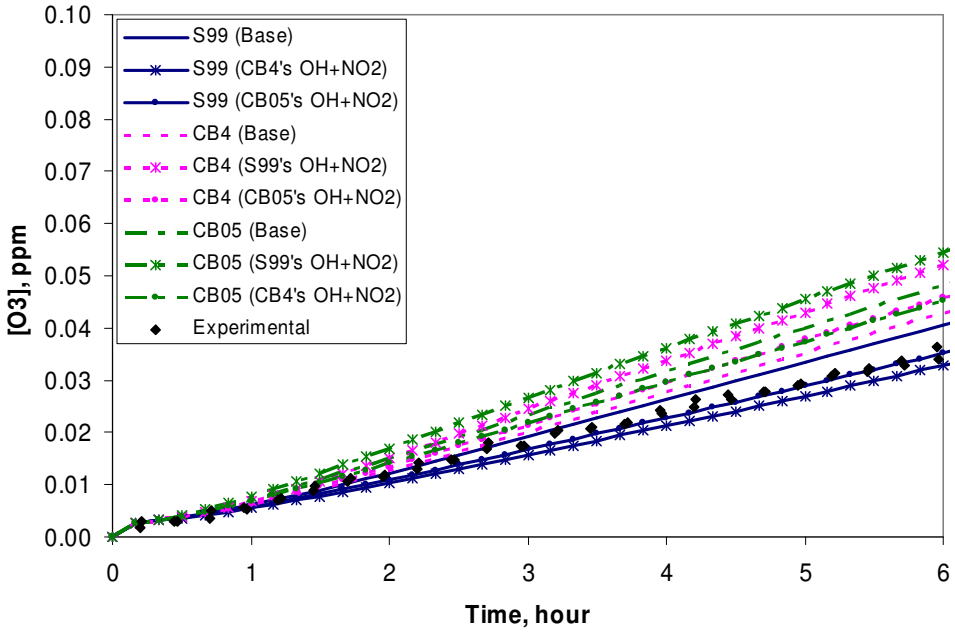

(b) EPA306B in SAPRC

Figure F-7. Time series of the simulated O_3 concentrations in sensitivity runs in SAPRC with cases: (a) EPA306A and (b) EPA306B. (*All simulations were done using the wall mechanism and the PNA chemistry for each mechanism.)

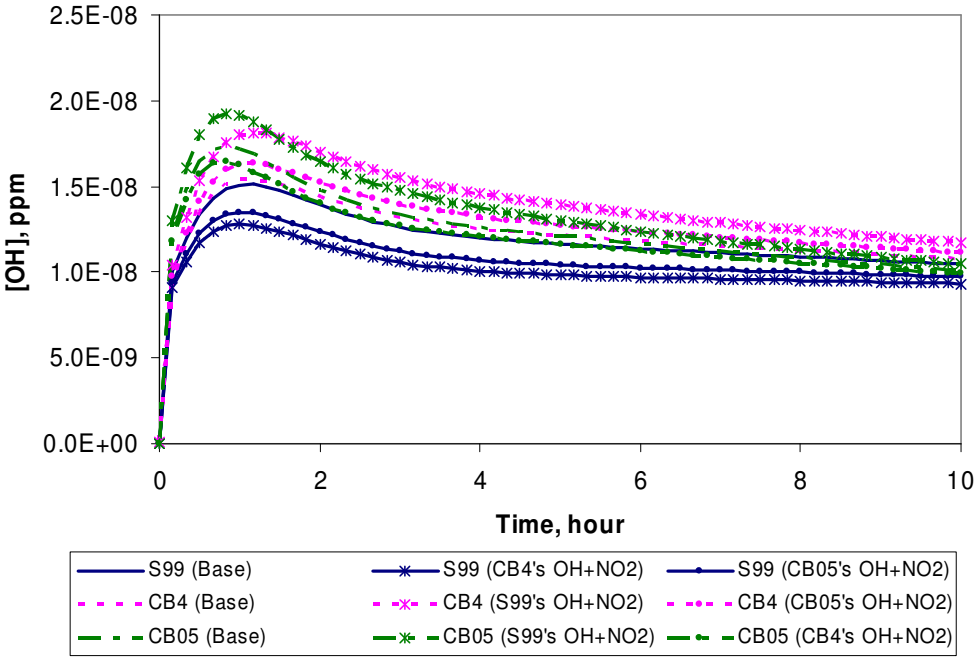

(a) EPA306A in SAPRC

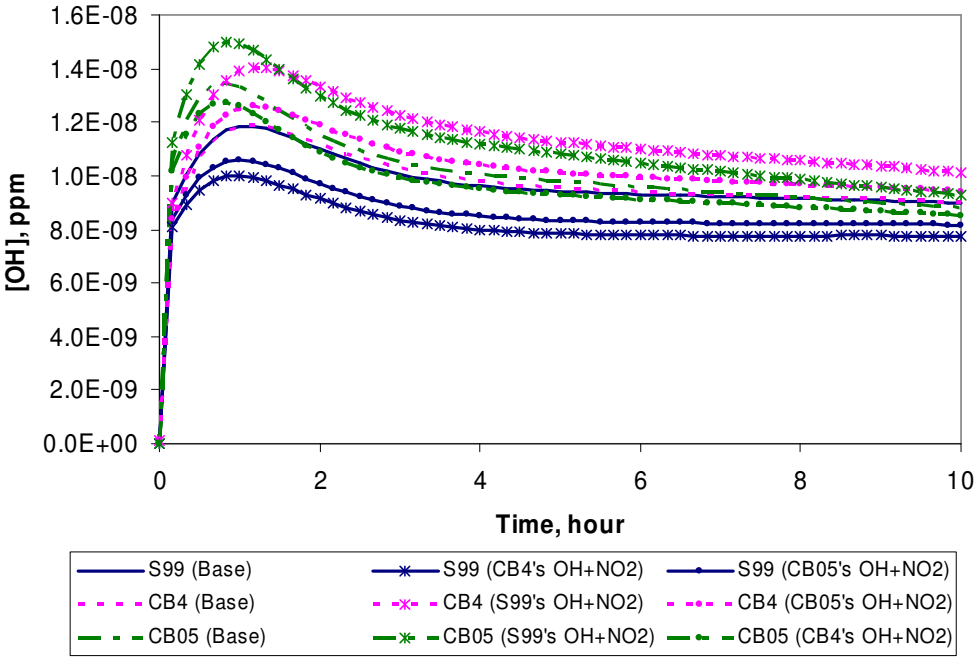

(b) EPA306B in SAPRC

Figure F-8. Time series of the simulated OH concentrations in sensitivity runs in SAPRC with cases: (a) EPA306A and (b) EPA306B. (*All simulations were done with using the wall mechanism and the PNA chemistry for each mechanism.)

Appendix G: Experiments of Aromatics in Environmental Chamber Experiments and Composition of Aromatics in Emissions Inventory

G.1 TOLUENE EXPERIMENTS AT UCR

The EC experiments included six toluene experiments in which concentrations of cresols were measured. These experiments are listed in Table G-1. The predictions of the SAPRC99, CB-IV, and CB05 mechanisms in simulating these experiments are shown in Figures G-1 - G-6. The x-axes are the concentrations of the designated species in ppm as a function of the simulation time in minutes.

Table G-1. List of toluene experiments with cresol measurements in EC chamber at UCR.

Experiment ID	VOC	NOx	Light Source
EC266	8.37 ppmC Toluene	440 ppb	Arc light solar simulator
EC269	3.96 ppmC Toluene	485 ppb	Arc light solar simulator
EC270	4.03 ppmC Toluene	466 ppb	Arc light solar simulator
EC271	8.02 ppmC Toluene	215 ppb	Arc light solar simulator
EC273	4.11 ppmC Toluene	112 ppb	Arc light solar simulator
EC340	3.76 ppmC Toluene	493 ppb	Arc light solar simulator

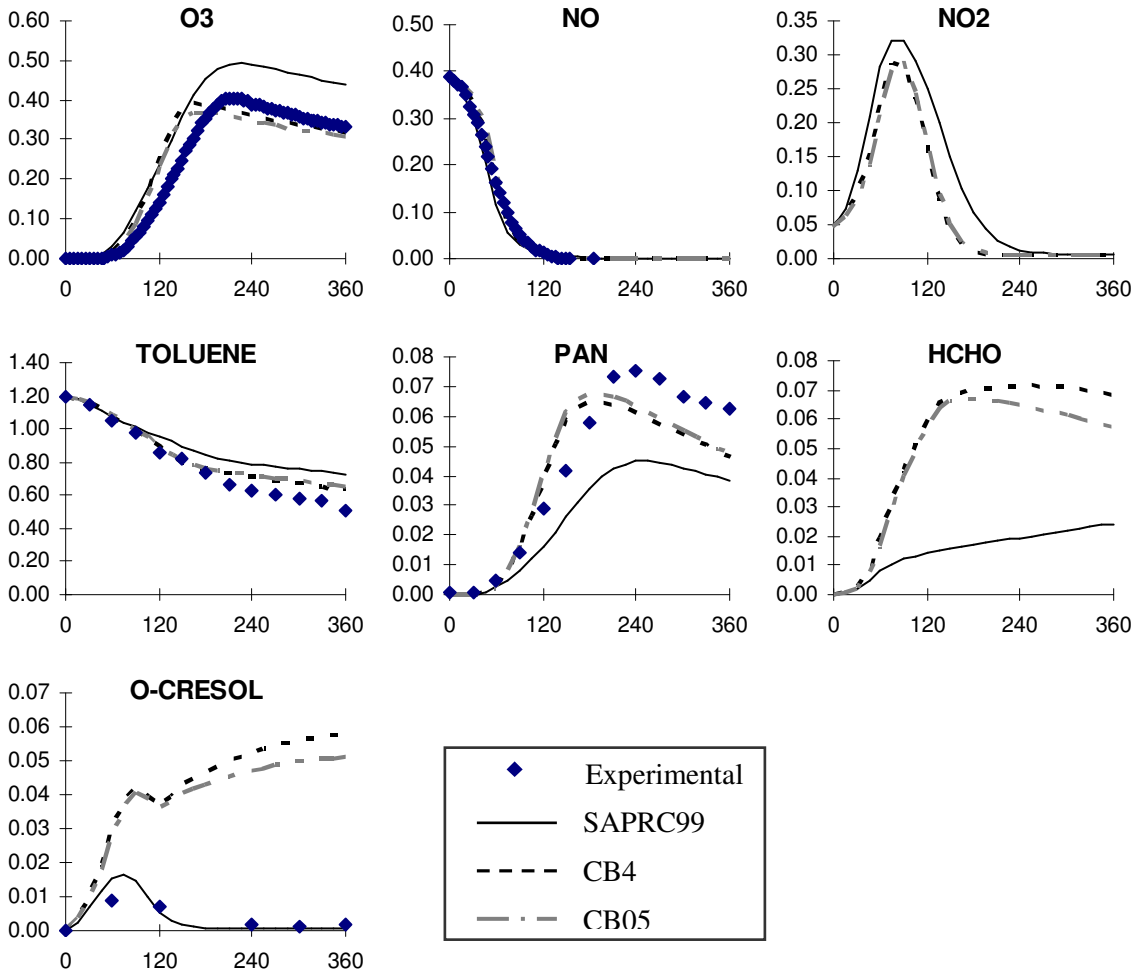

Figure G-1. Concentrations of species in ppm as a function of time (minutes) in the EC266 toluene experiment at UCR.

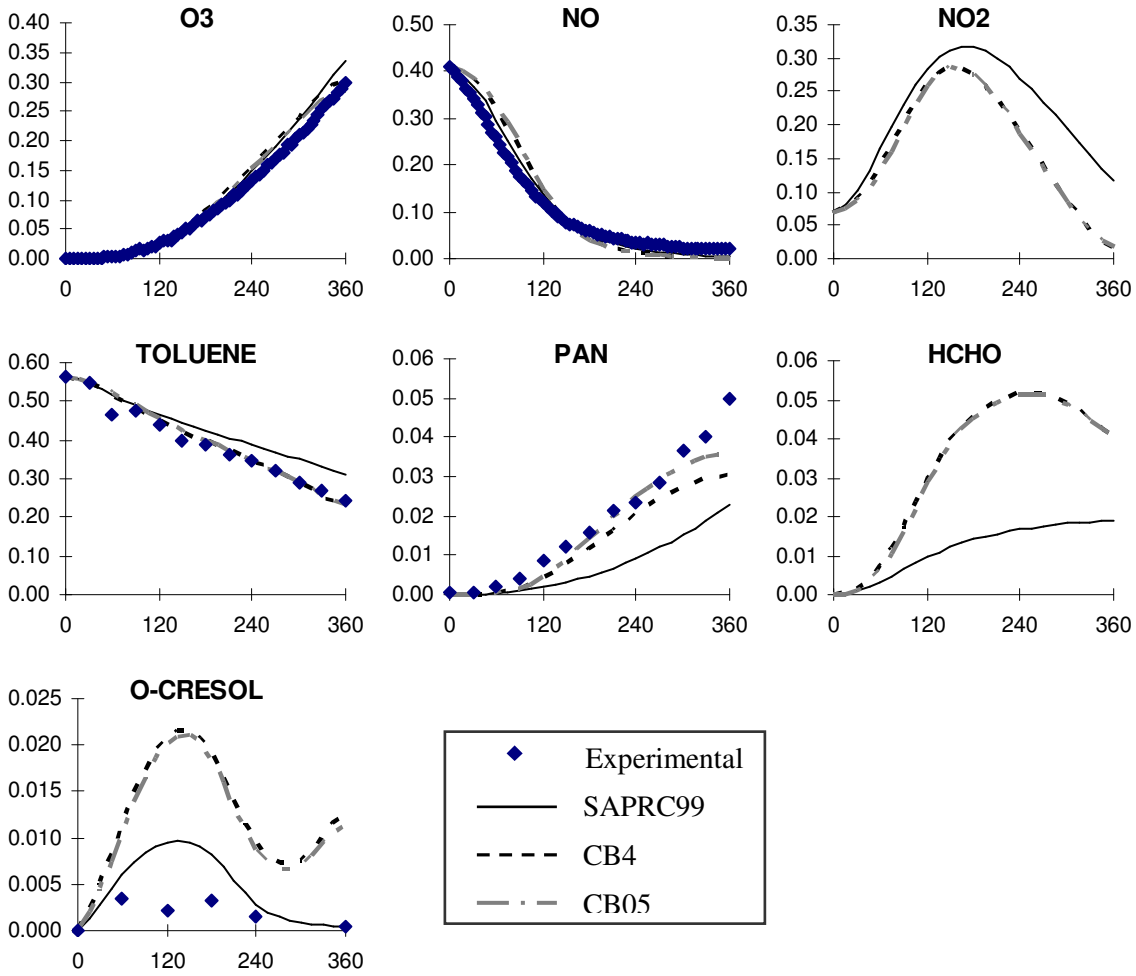

Figure G-2. Concentrations of species in ppm as a function of time (minutes) in the EC269 toluene experiment at UCR.

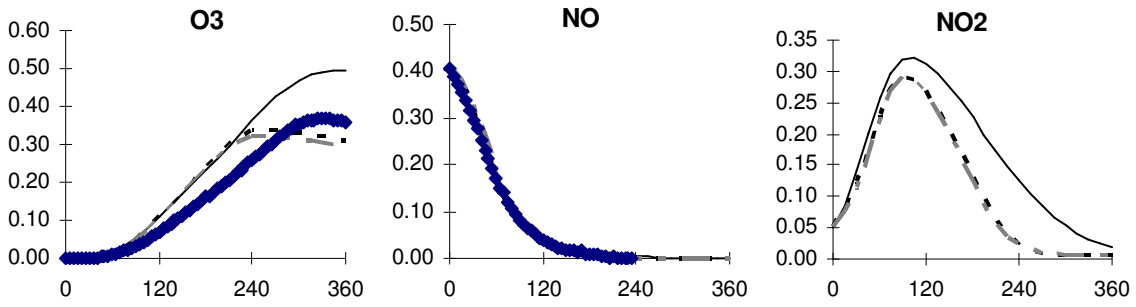

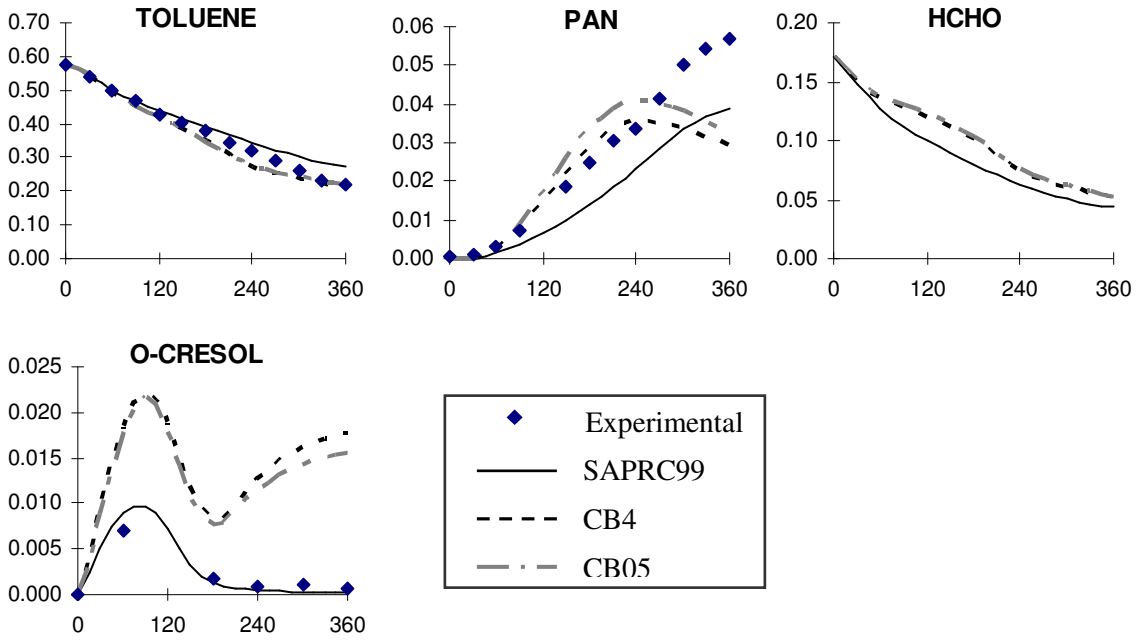

Figure G-3. Concentrations of species in ppm as a function of time (minutes) in the EC270 toluene experiment at UCR.

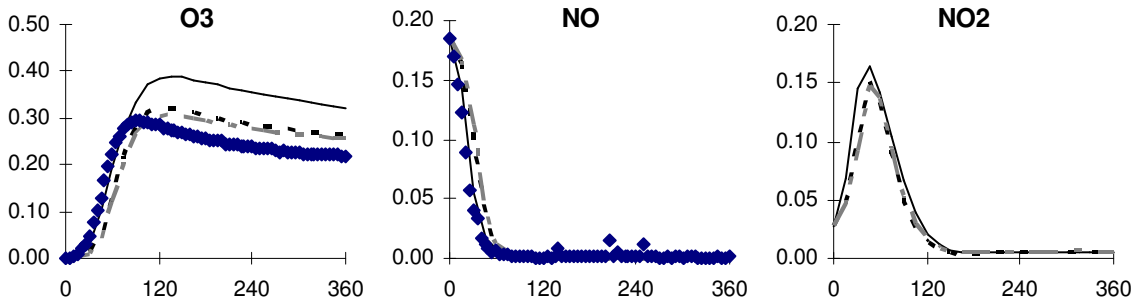

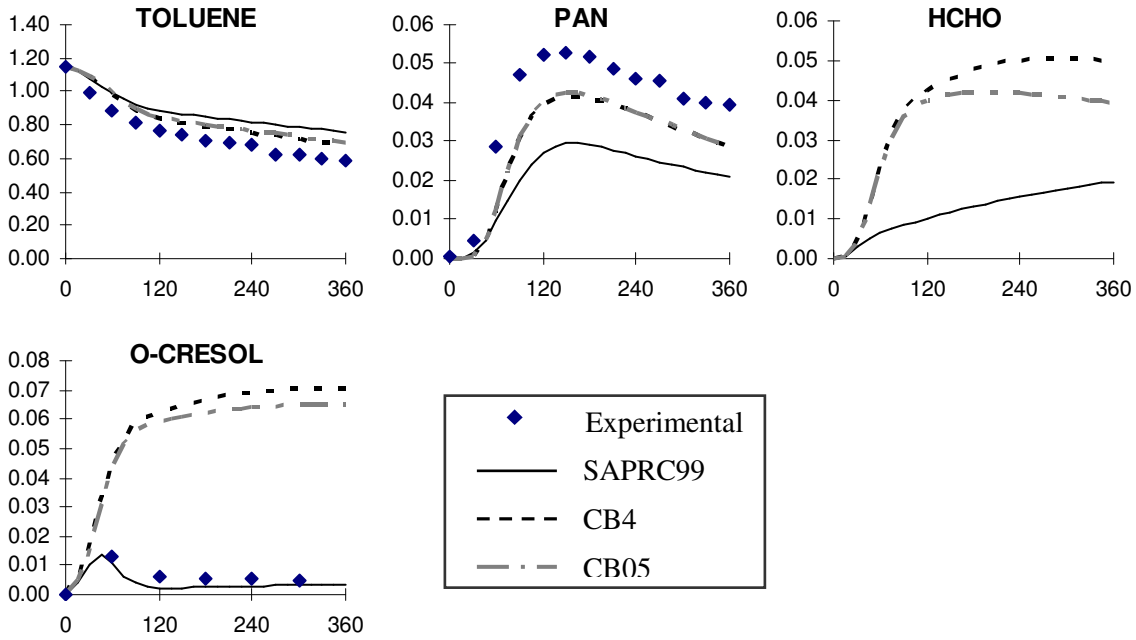

Figure G-4. Concentrations of species in ppm as a function of time (minutes) in the EC271 toluene experiment at UCR.

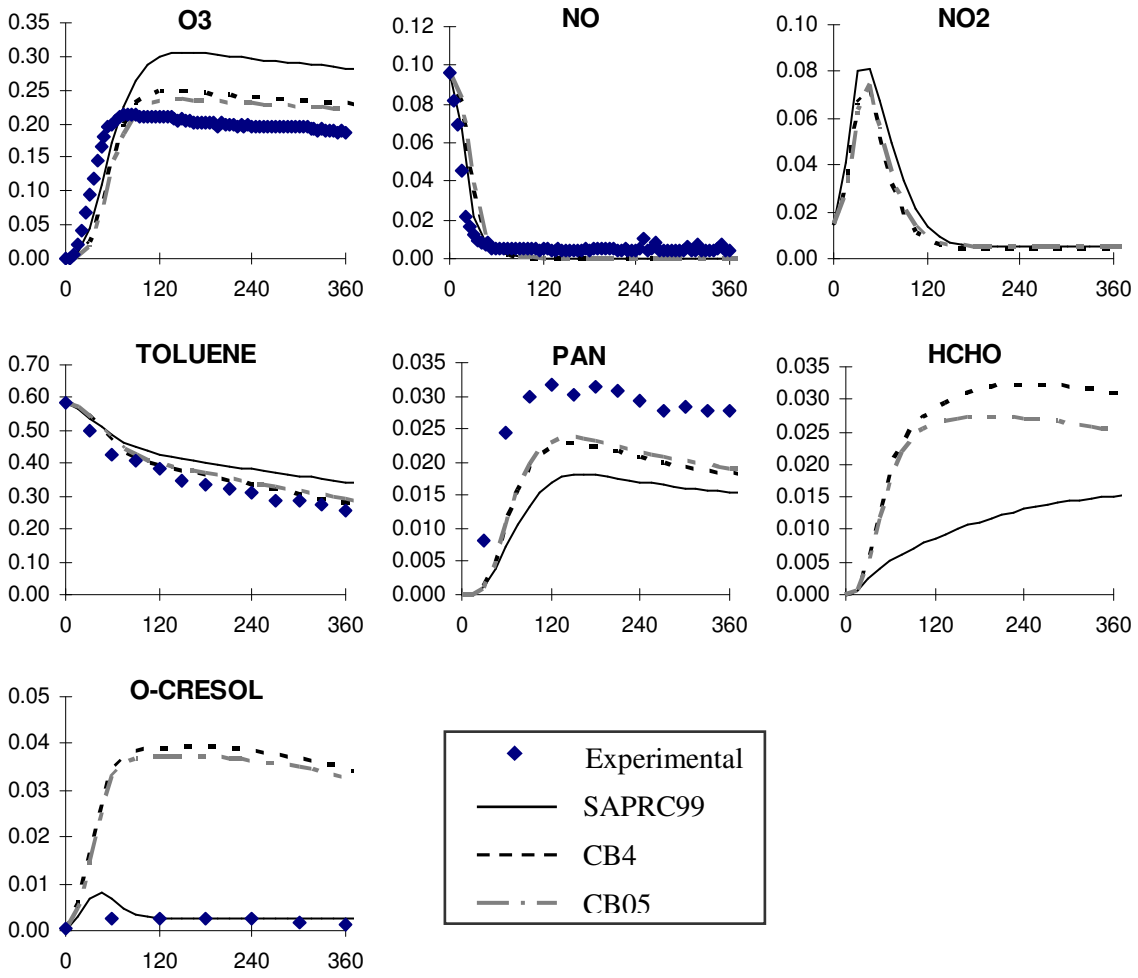

Figure G-5. Concentrations of species in ppm as a function of time (minutes) in the EC273 toluene experiment at UCR.

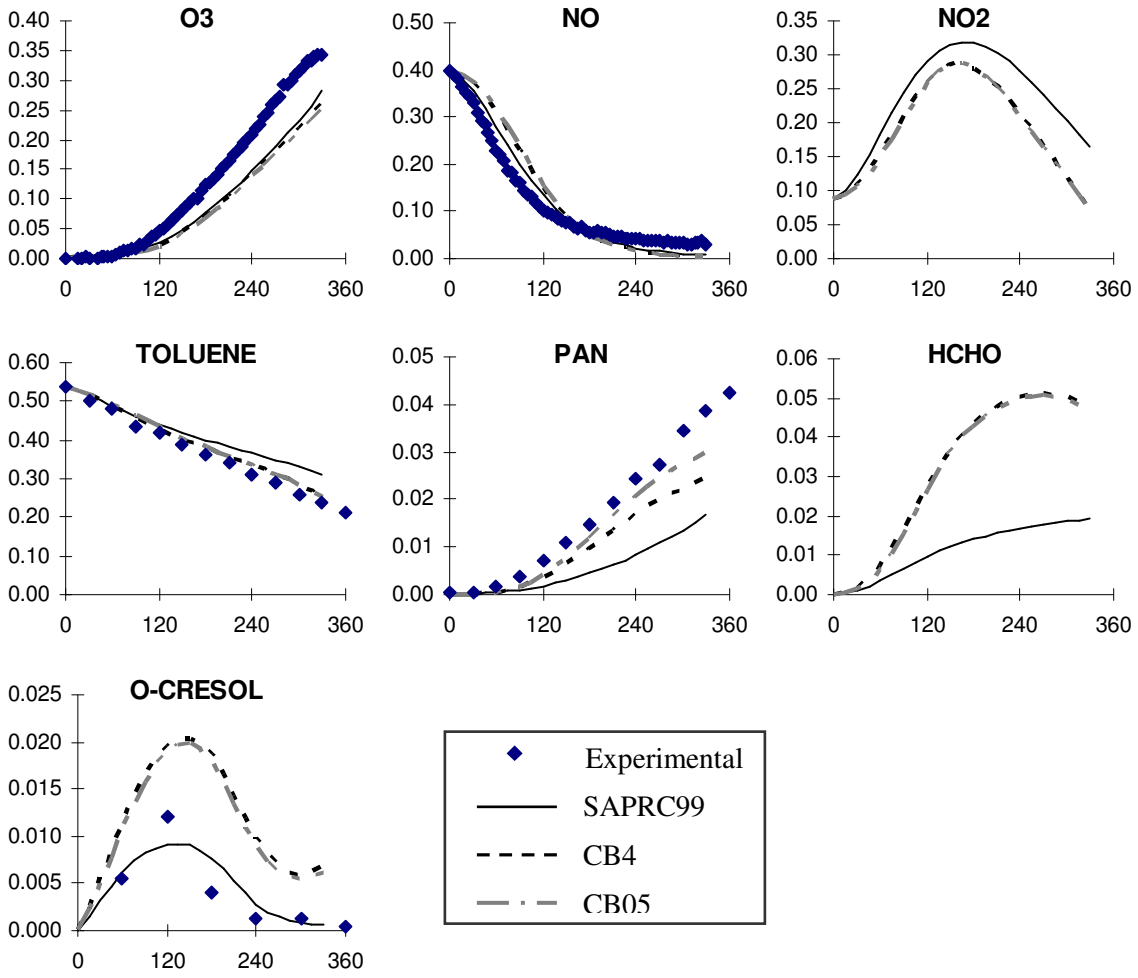

Figure G-6. Concentrations of species in ppm as a function of time (minutes) in the EC340 toluene experiment at UCR.

In addition to toluene experiments in the EC chamber at UCR, selected toluene experiments conducted with the EPA chamber at UCR were used to compare the performance of the mechanisms. These experiments are listed in Table G-2, followed by the results in Figures G-7 – G-14. These experiments are conducted at much lower levels of NOx relative to the experiments in the EC chamber.

Table G-2. List of toluene experiments at low NOx conditions in EPA chamber at UCR.

Experiment ID	VOC	NOx	Light Source
EPA074B	1.10 ppmC Toluene	27 ppb	Arc light solar simulator
EPA066B	0.425 ppmC Toluene	5 ppb	Arc light solar simulator
EPA074A	1.054 ppmC Toluene	24 ppb	Arc light solar simulator
EPA077A	1.065 ppmC Toluene	23 ppb	Arc light solar simulator
EPA210A	1.834 ppmC Toluene	42 ppb	Arc light solar simulator
EPA210B	1.842 ppmC Toluene	93 ppb	Arc light solar simulator
EPA443A	1.188 ppmC Toluene	31 ppb	Arc light solar simulator
EPA443B	2.552 ppmC Toluene	99 ppb	Arc light solar simulator

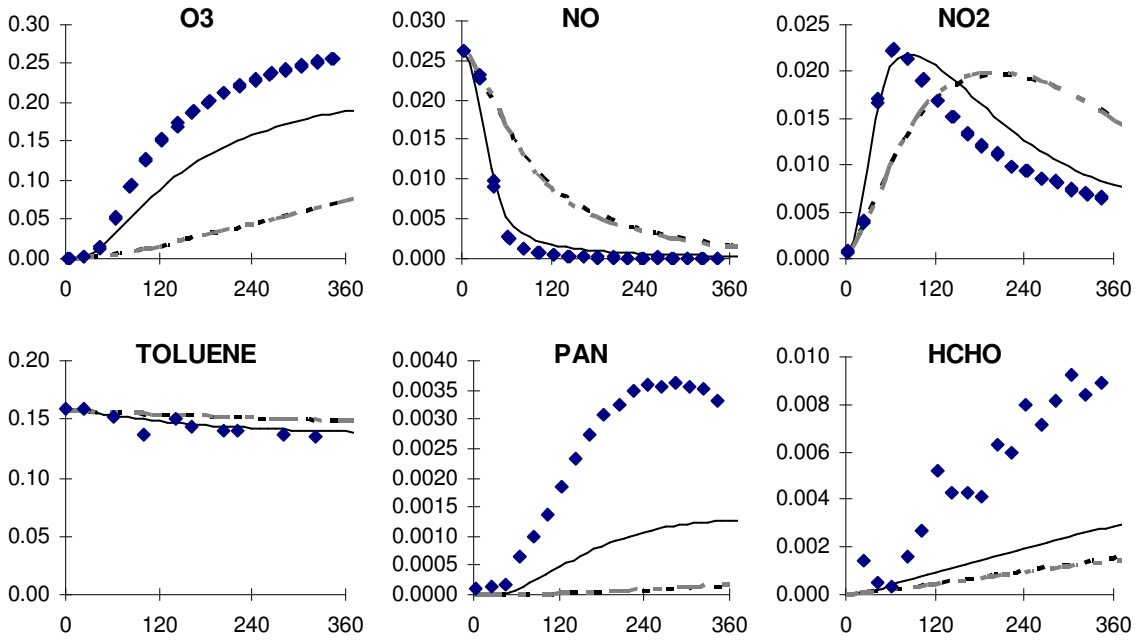

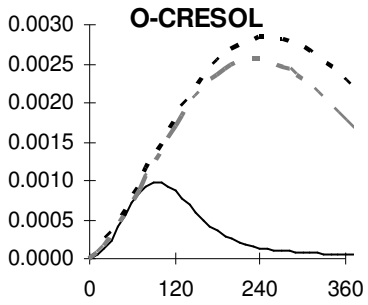

Figure G-7. Concentrations of species in ppm as a function of time (minutes) in the EPA074B toluene experiment at UCR.

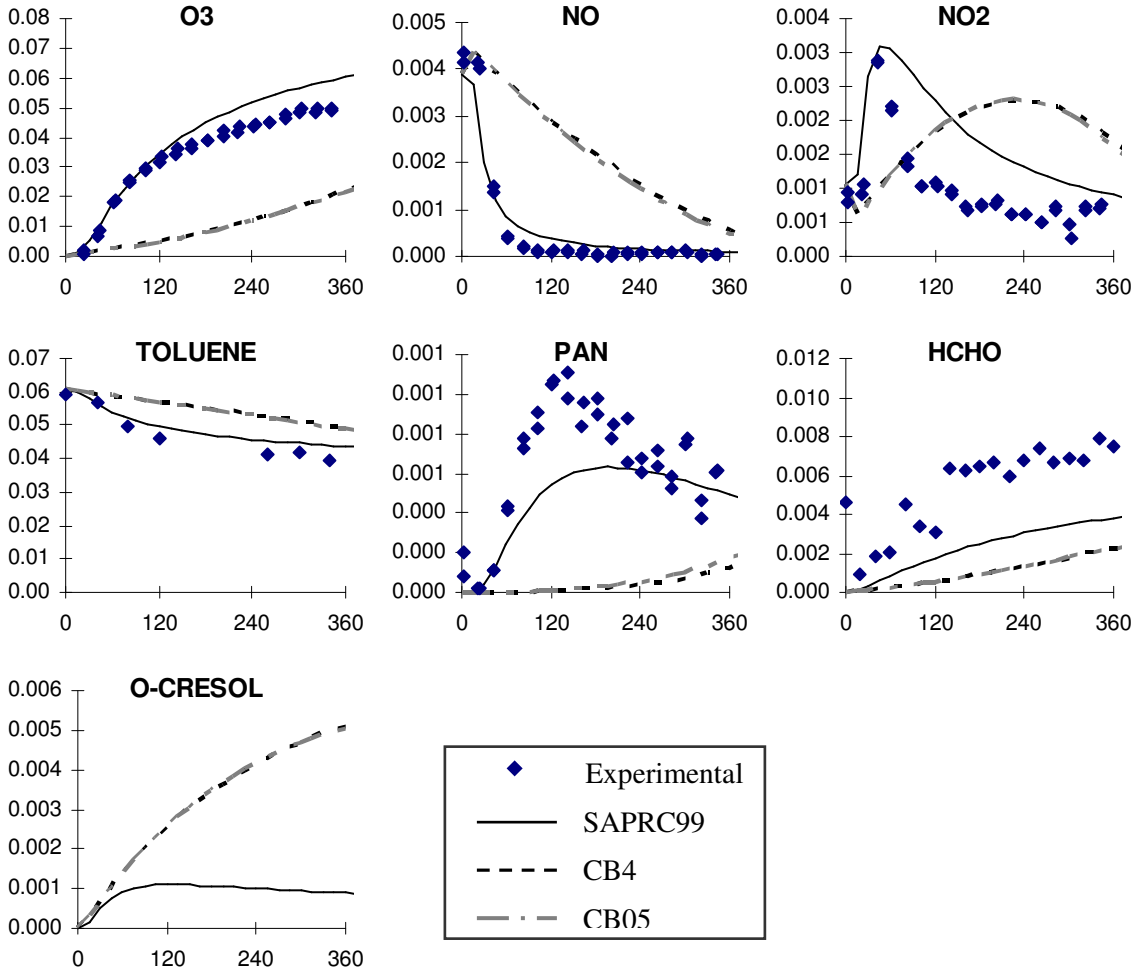

Figure G-8. Concentrations of species in ppm as a function of time (minutes) in the EPA066B toluene experiment at UCR.

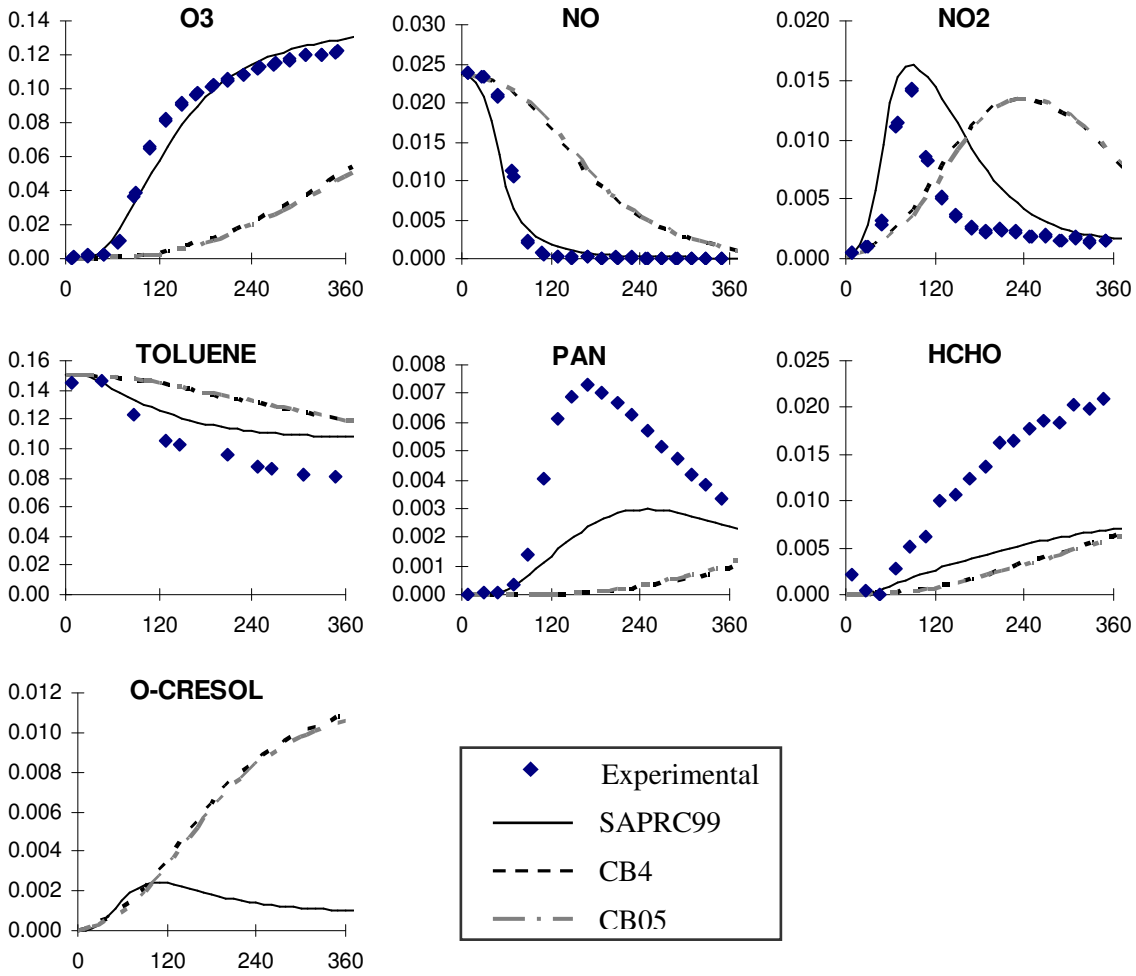

Figure G-9. Concentrations of species in ppm as a function of time (minutes) in the EPA074A toluene experiment at UCR.

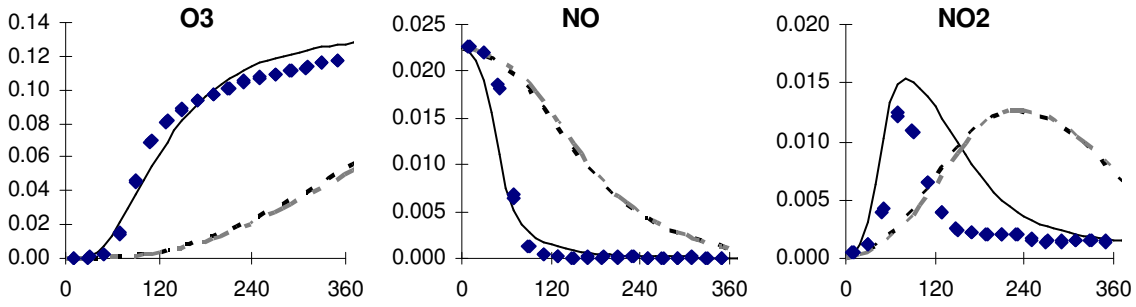

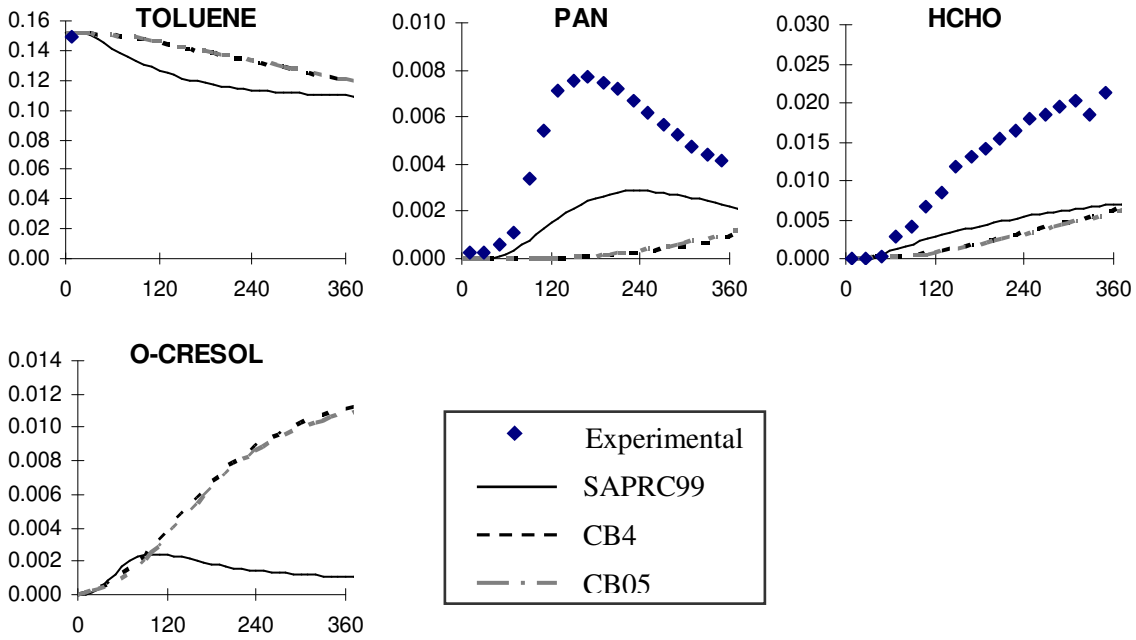

Figure G-10. Concentrations of species in ppm as a function of time (minutes) in the EPA077A toluene experiment at UCR.

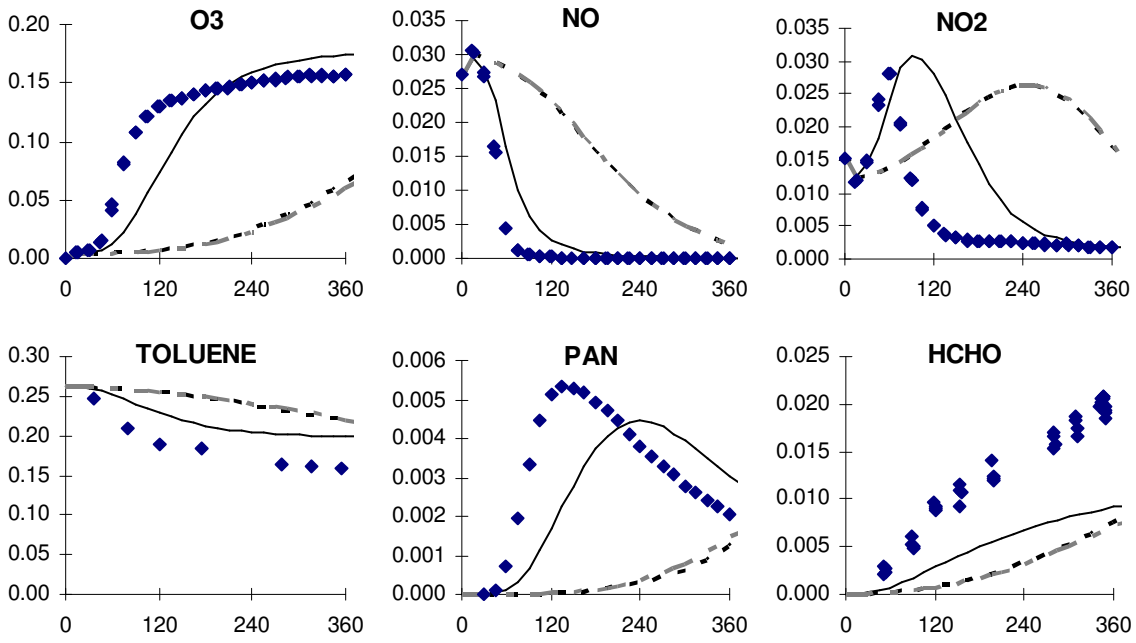

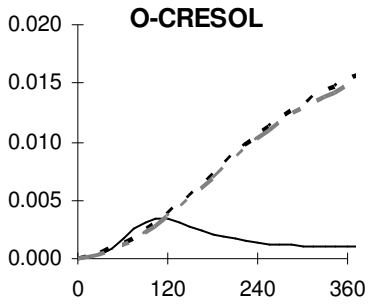

Figure G-11. Concentrations of species in ppm as a function of time (minutes) in the EPA210A toluene experiment at UCR.

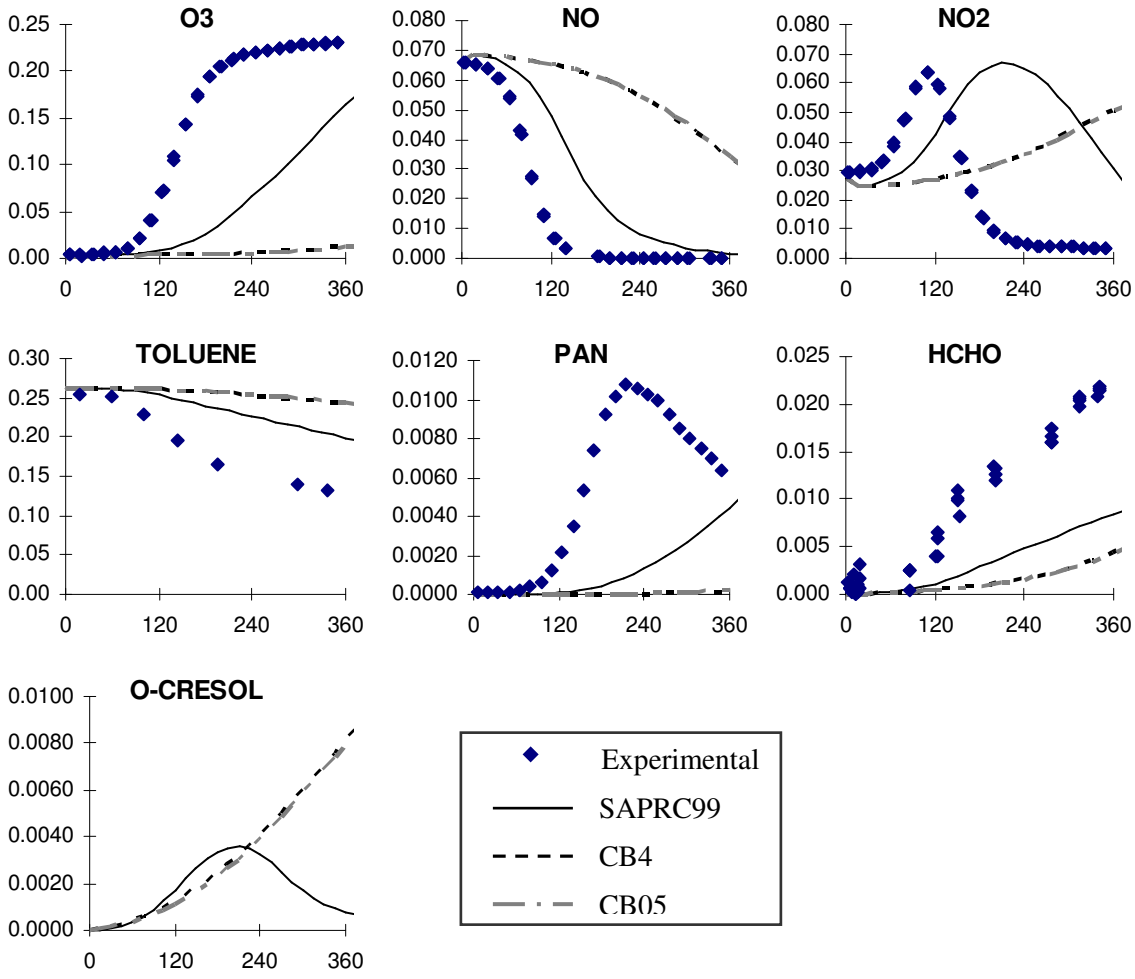

Figure G-12. Concentrations of species in ppm as a function of time (minutes) in the EPA210B toluene experiment at UCR.

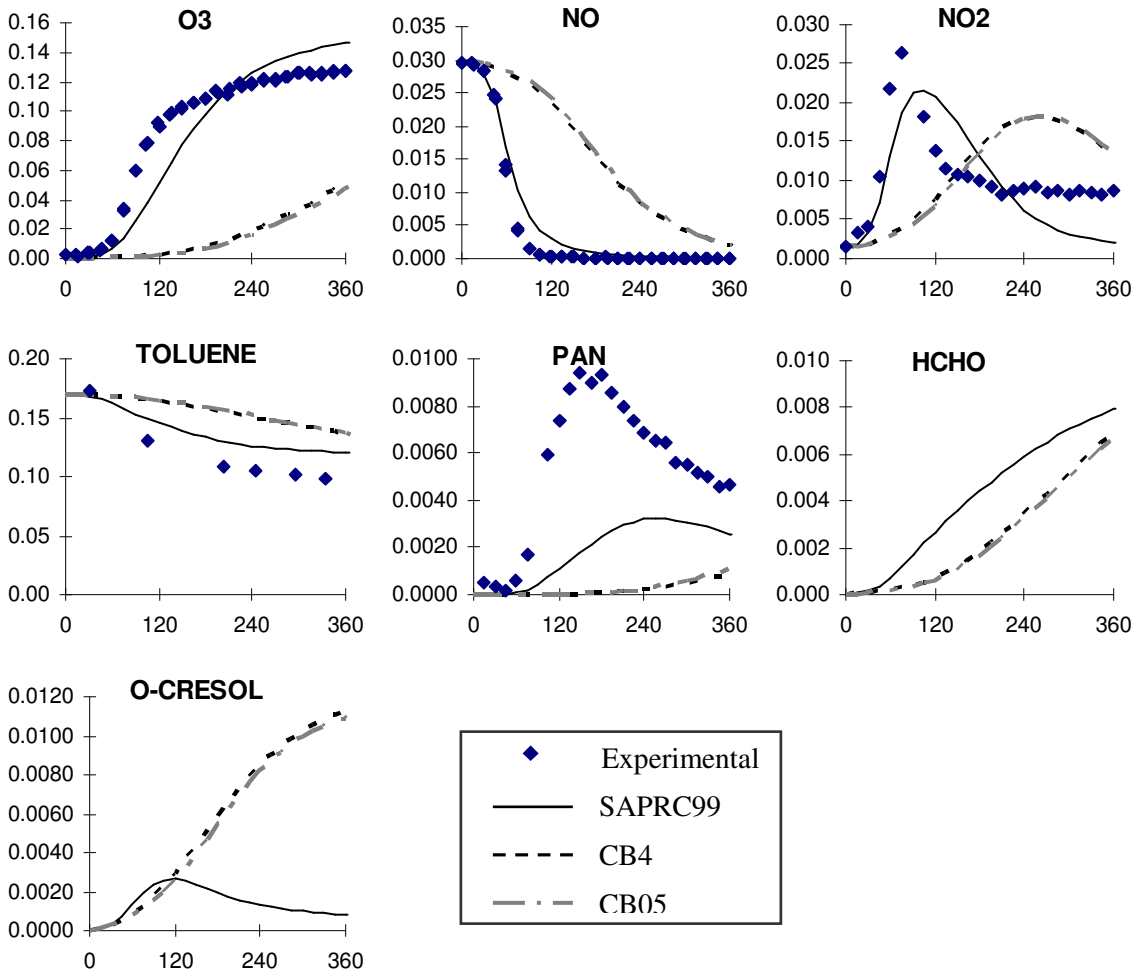

Figure G-13. Concentrations of species in ppm as a function of time (minutes) in the EPA443A toluene experiment at UCR.

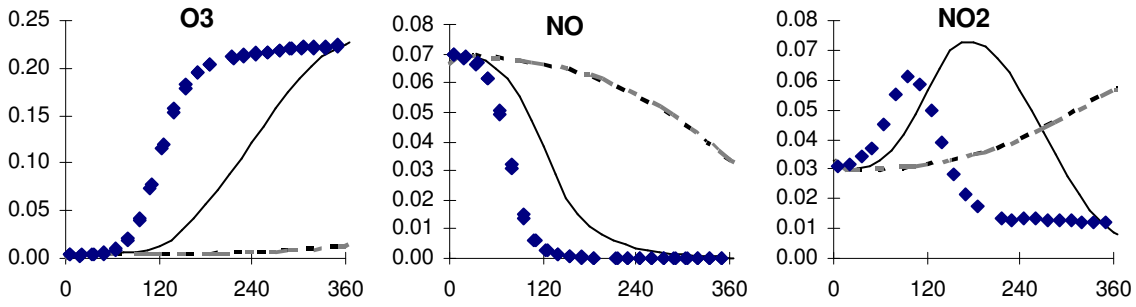

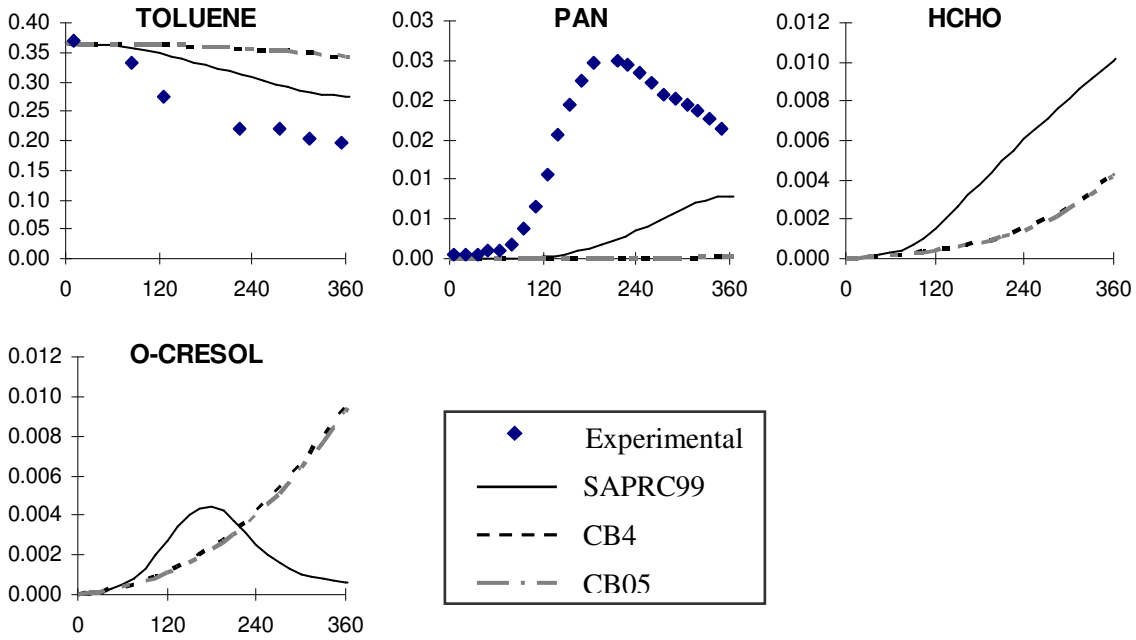

Figure G-14. Concentrations of species in ppm as a function of time (minutes) in the EPA443B toluene experiment at UCR.

In addition to the toluene experiments carried out at the EC and EPA chambers, toluene experiments at the OTC and TVA chambers were simulated with the SAPRC99, CB-IV and CB05 mechanisms. These experiments are listed in Table G-3 and the results are shown in Figures G-15 – G-21.

Table G-3. List of toluene experiments in the OTC and TVA chambers at UCR.

Experiment ID	VOC	NOx	Light Source
OTC299A	8.53 ppmC Toluene	509 ppb	Sunlight
OTC299B	3.56 ppmC Toluene	502 ppb	Sunlight
OTC300A	3.59 ppmC Toluene	521 ppb	Sunlight
OTC300B	3.56 ppmC Toluene	224 ppb	Sunlight
TVA047	0.52 ppmC Toluene	105 ppb	Blacklights + Sunlamps
TVA071	2.48 ppmC Toluene	266 ppb	Blacklights + Sunlamps
TVA080	0.41 ppmC Toluene	54 ppb	Blacklights + Sunlamps

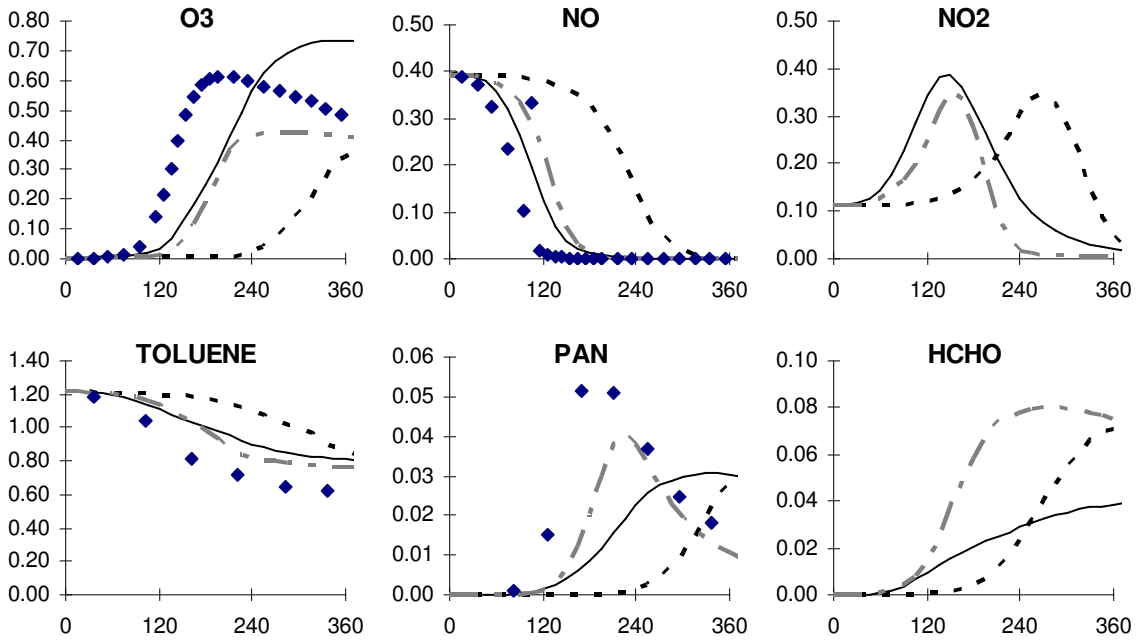

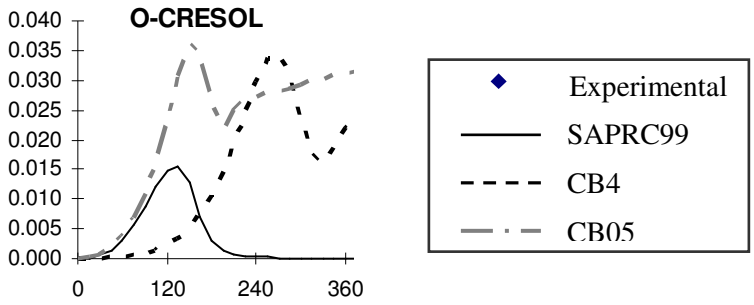

Figure G-15. Concentrations of species in ppm as a function of time (minutes) in the OTC299A toluene experiment at UCR.

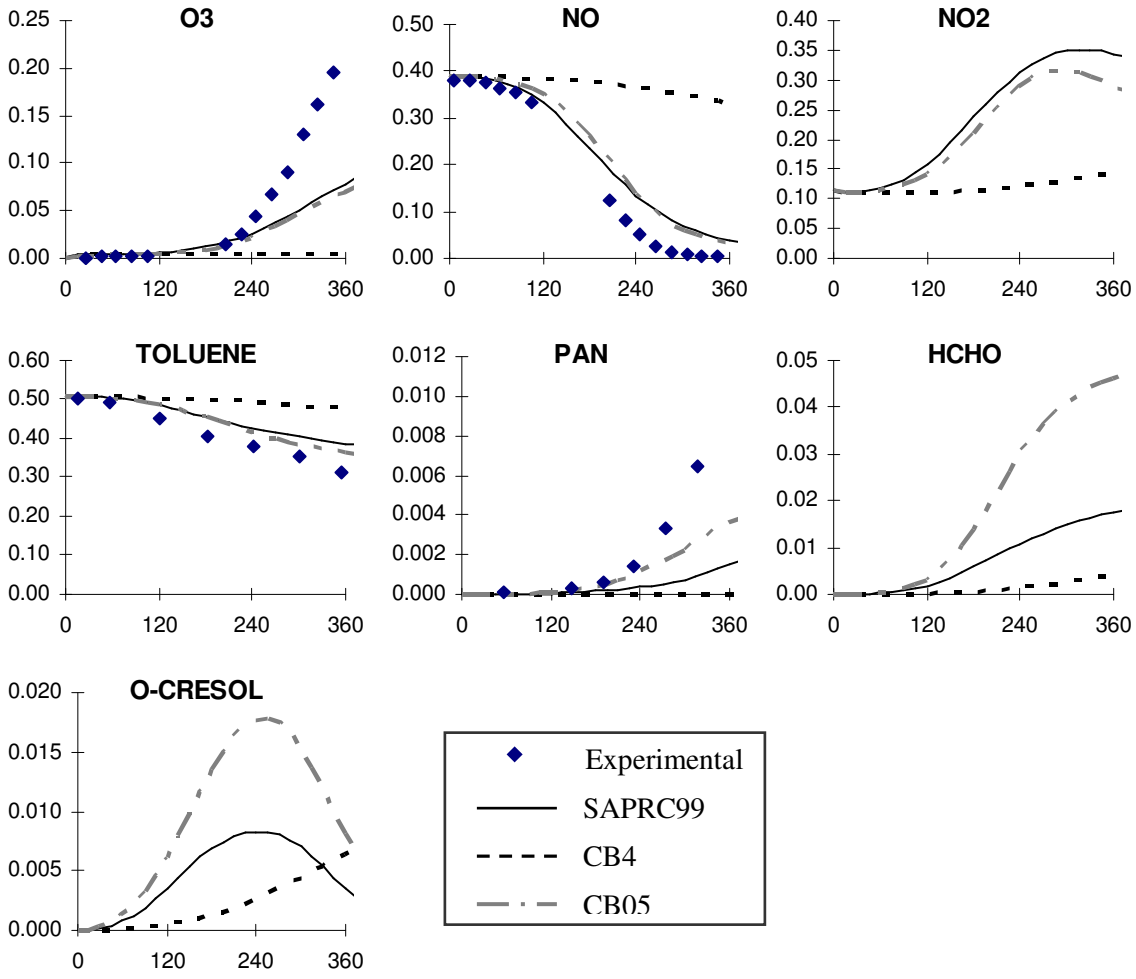

Figure G-16. Concentrations of species in ppm as a function of time (minutes) in the OTC299B toluene experiment at UCR.

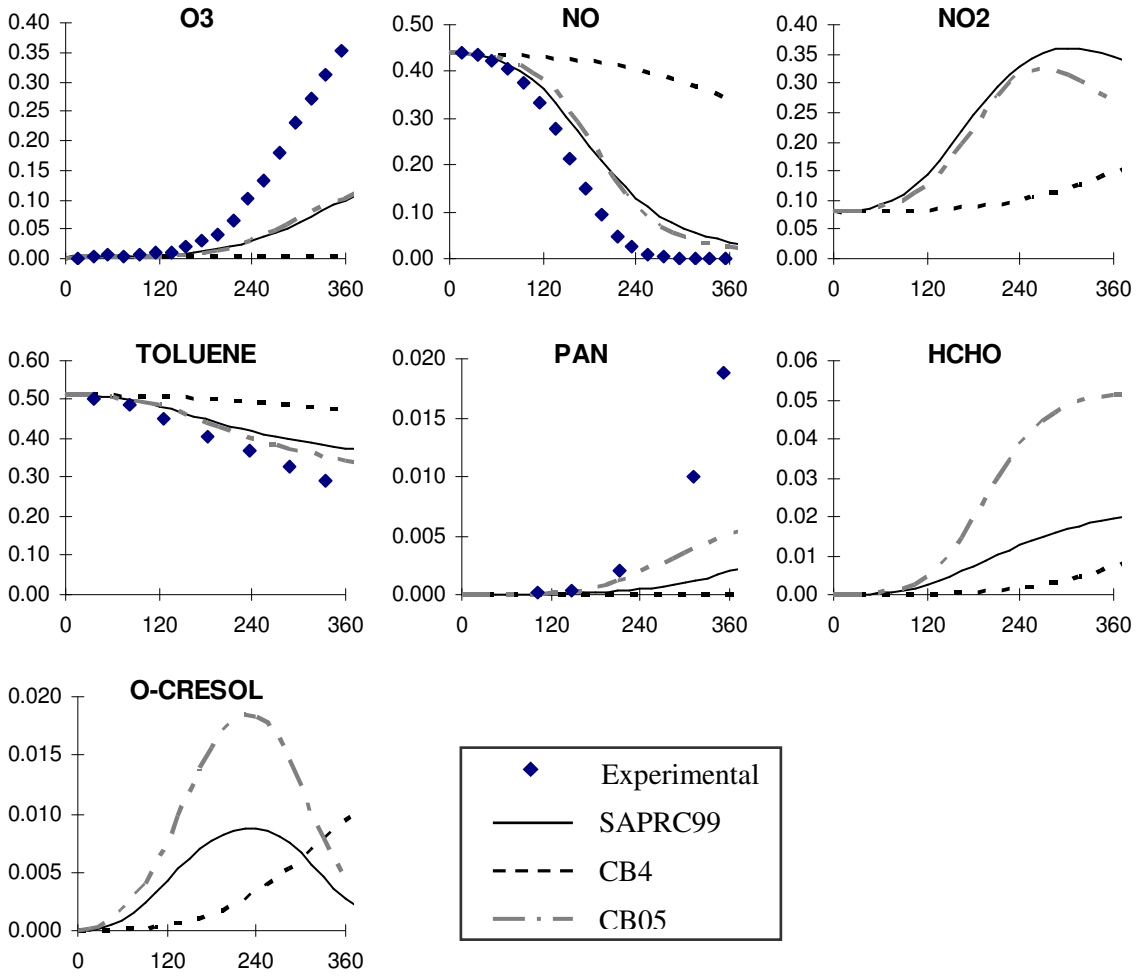

Figure G-17. Concentrations of species in ppm as a function of time (minutes) in the OTC300A toluene experiment at UCR.

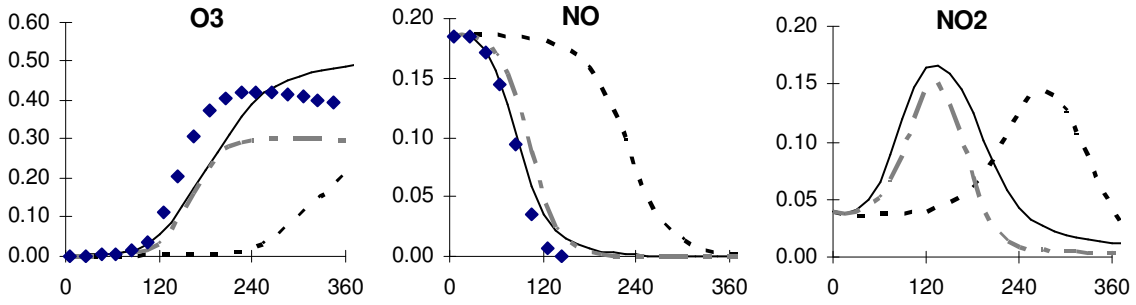

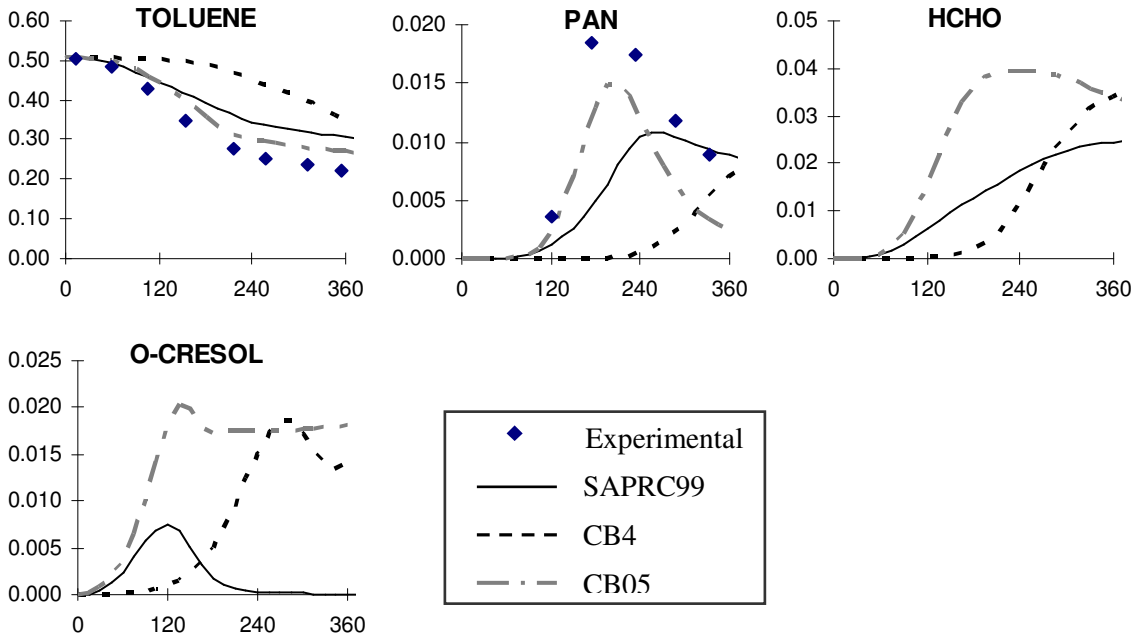

Figure G-18. Concentrations of species in ppm as a function of time (minutes) in the OTC300B toluene experiment at UCR.

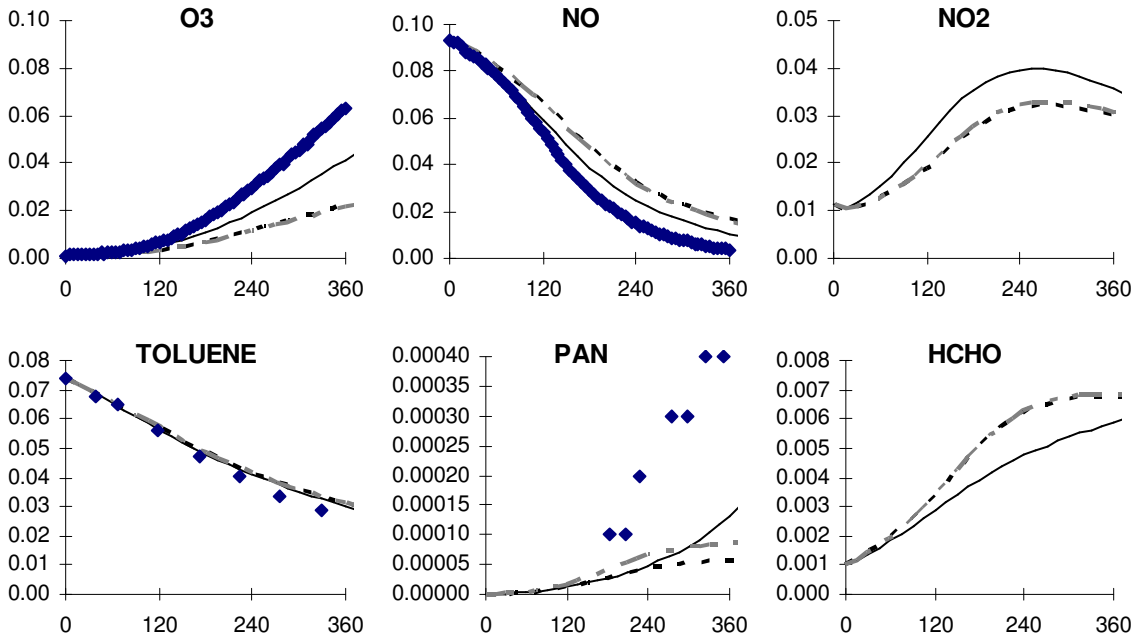

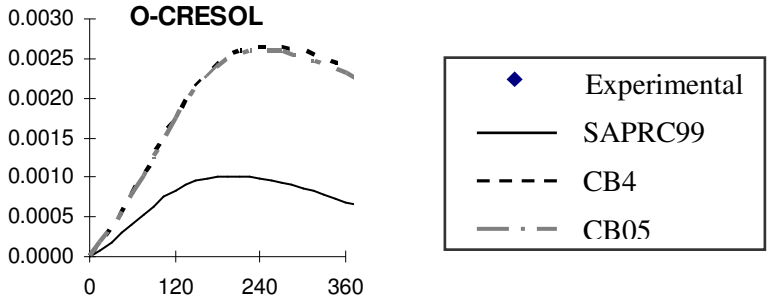

Figure G-19. Concentrations of species in ppm as a function of time (minutes) in the TVA047 toluene experiment at UCR.

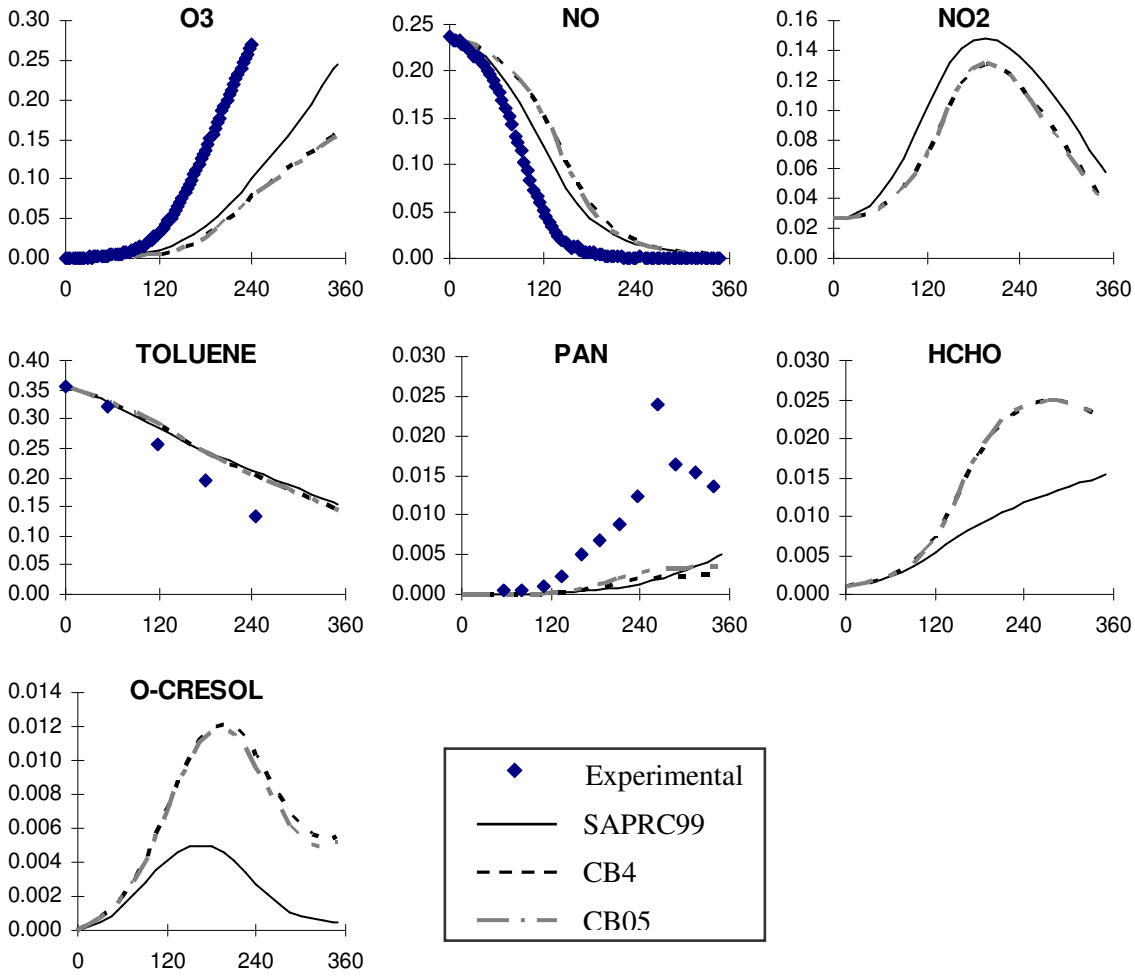

Figure G-20. Concentrations of species in ppm as a function of time (minutes) in the TVA071 toluene experiment at UCR.

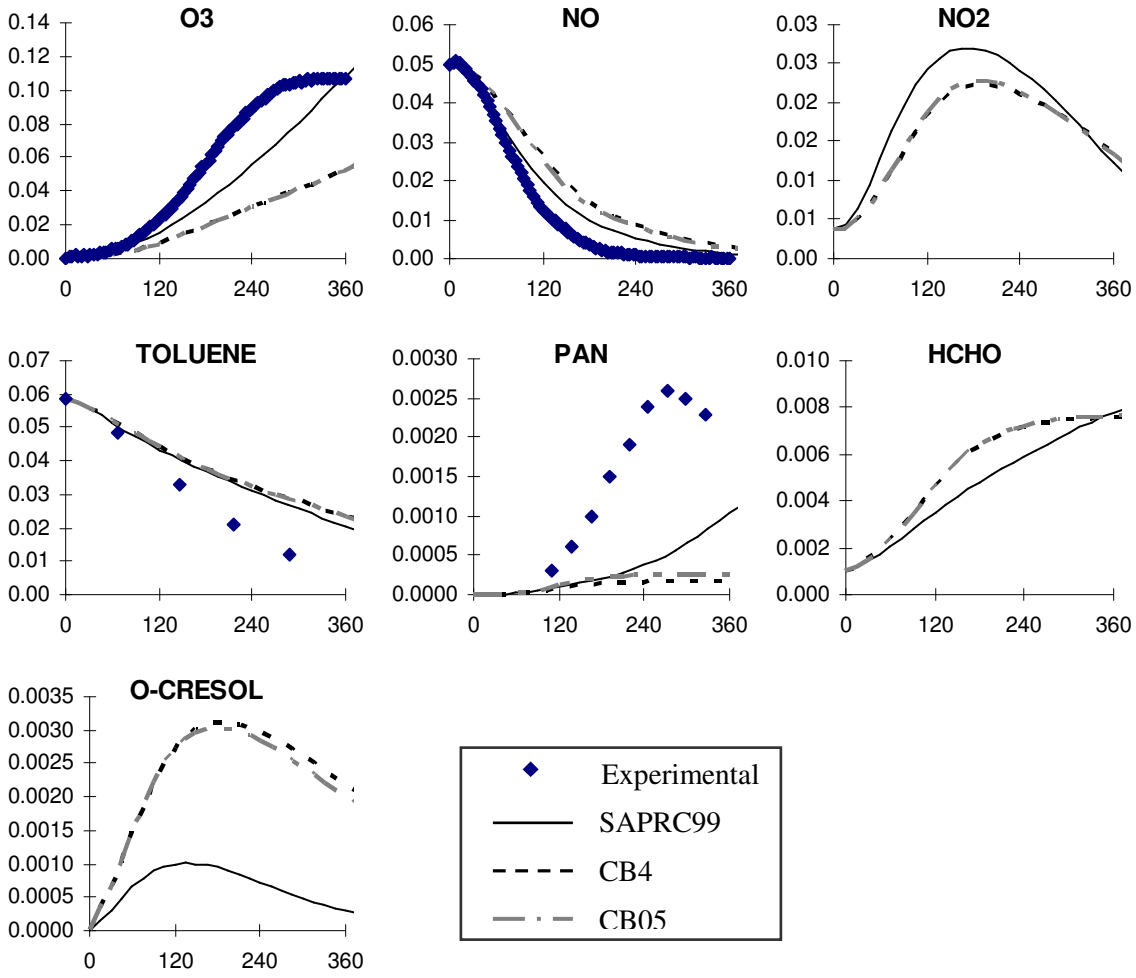

Figure G-21. Concentrations of species in ppm as a function of time (minutes) in the TVA080 toluene experiment at UCR.

Besides toluene experiments, other UCR experiments available for the mono-substituted aromatics are those of ethylbenzene. Table G-4 lists ethylbenzene experiments conducted in the CTC chamber, followed by the results in Figures G-22 – G-25.

Table G-4. List of ethylbenzene experiments in the CTC chambers at UCR.

Experiment ID	VOC	NOx	Light Source
CTC092A	8.22 ppmC Ethylbenzene	268 ppb	Arc light solar simulator
CTC092B	15.68 ppmC Ethylbenzene	270 ppb	Arc light solar simulator
CTC098B	15.01 ppmC Ethylbenzene	494 ppb	Arc light solar simulator
CTC057	16.22 ppmC Ethylbenzene	272 ppb	Arc light solar simulator

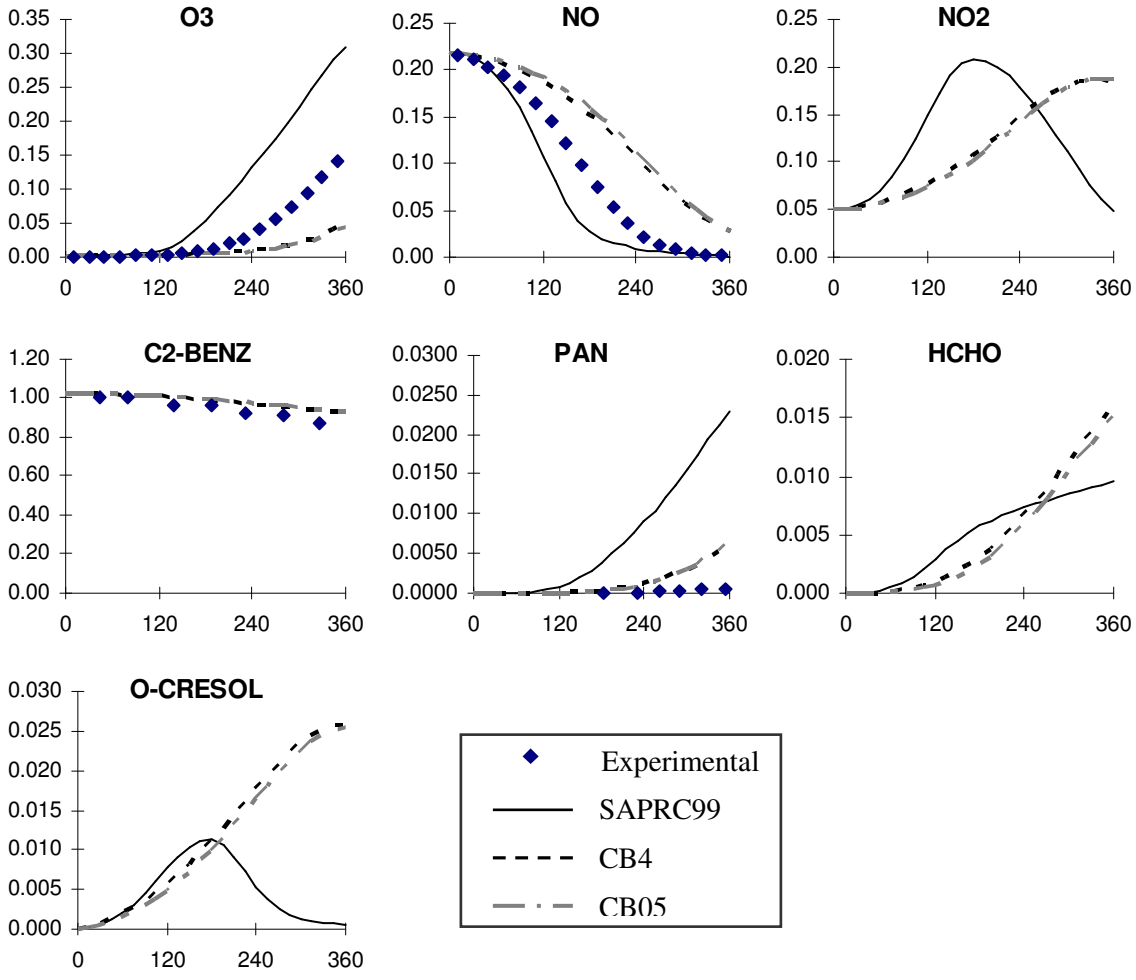

Figure G-22. Concentrations of species in ppm as a function of time (minutes) in the CTC092A ethylbenzene experiment at UCR.

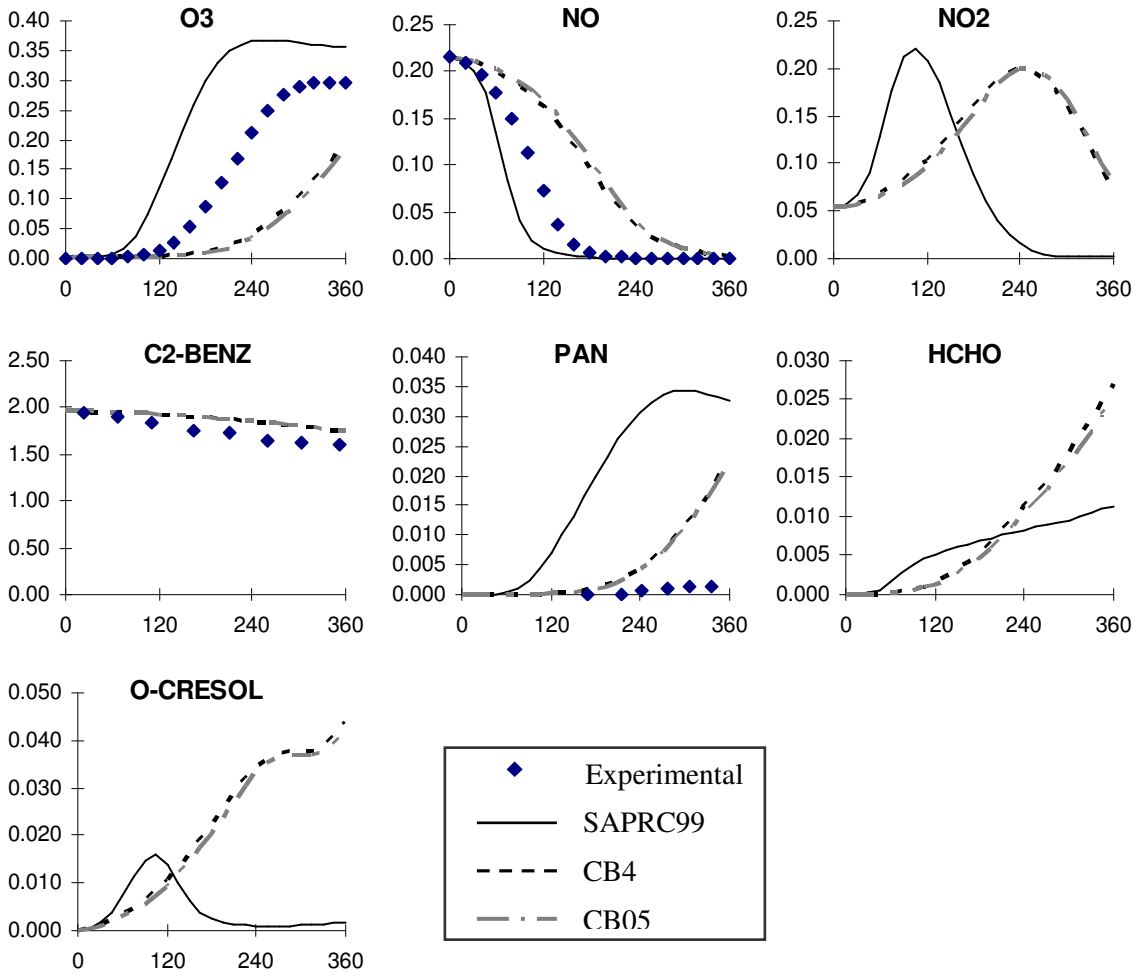

Figure G-23. Concentrations of species in ppm as a function of time (minutes) in the CTC092B ethylbenzene experiment at UCR.

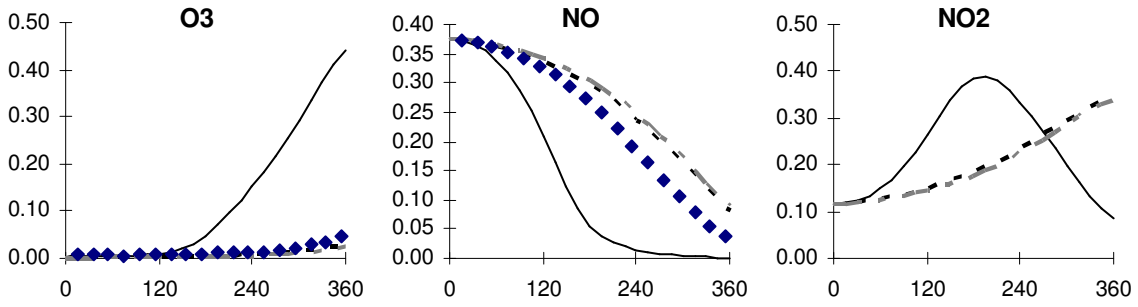

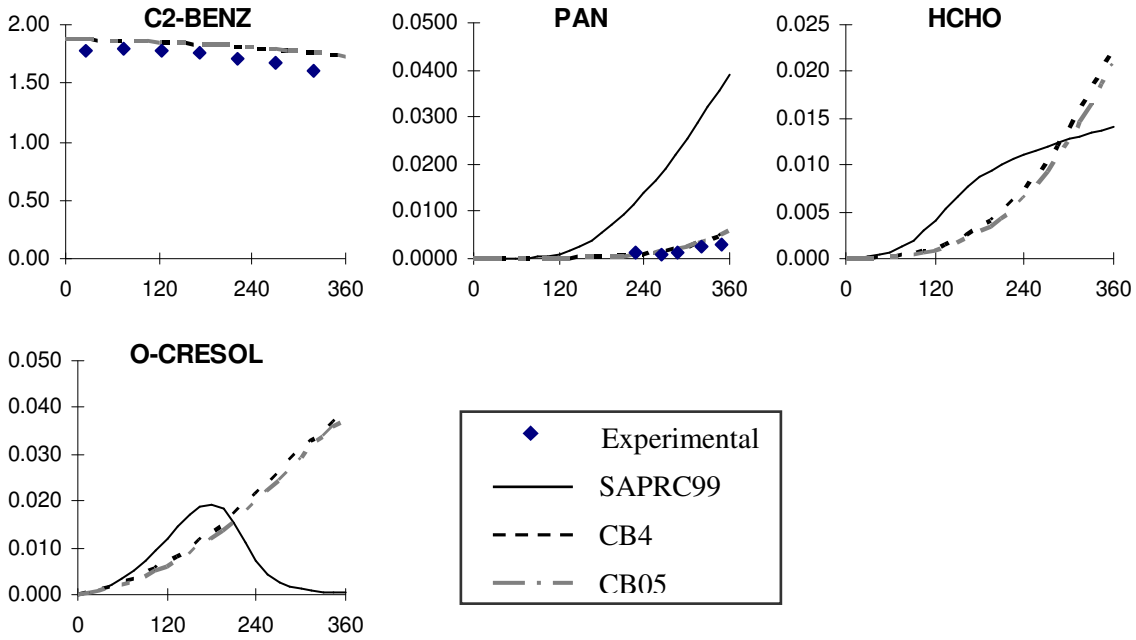

Figure G-24. Concentrations of species in ppm as a function of time (minutes) in the CTC098B ethylbenzene experiment at UCR.

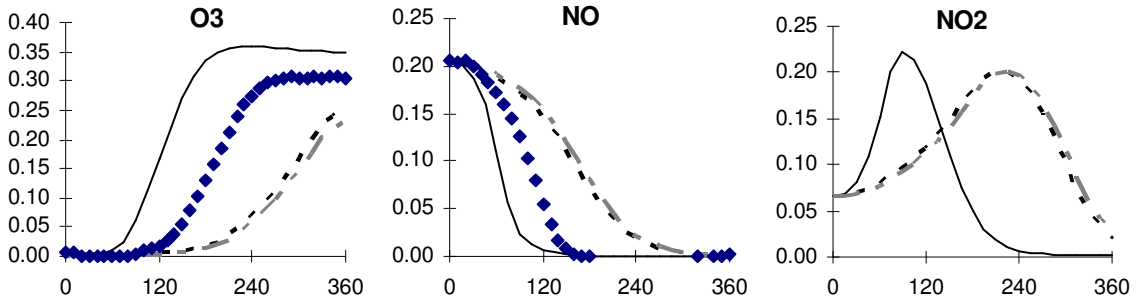

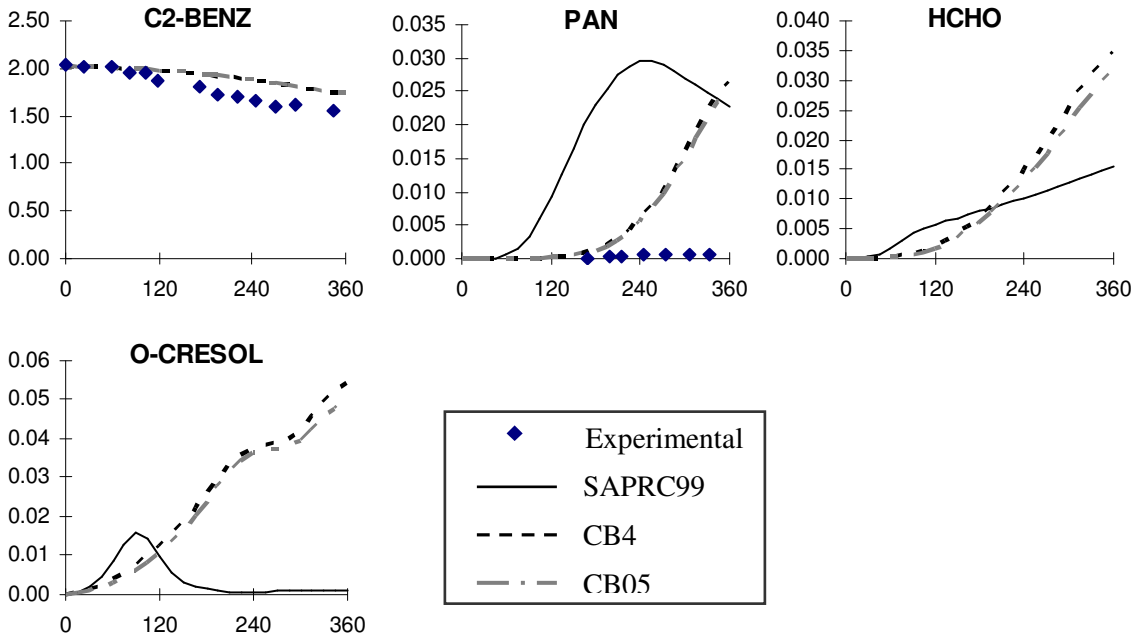

Figure G-25. Concentrations of species in ppm as a function of time (minutes) in the CTC057 ethylbenzene experiment at UCR.

G.2 SUMMARY OF AROMATICS SENSITIVITY STUDIES IN UNC AND UCR CHAMBERS

Table G-5. Summary of aromatics sensitivity studies in UNC chamber.

	Experiment	AU0183 Red	AU1788 Red	ST1393 Blue	AU3095 Blue
	VOC (ppmC)	4.590	4.930	1.909	7.210
	NOx (ppm)	0.395	0.357	0.324	0.618
	VOC/NOx	11.620	13.810	5.892	11.667
Peak Ozone (ppm)	SAPRC99	0.506	0.622	0.340	0.562
	S99 w/ CB4 HNO_3	0.482	0.588	0.213	0.523
	S99 explicit toluene	0.498	0.608	0.428	0.557
	S99 explicit toluene w/ CB cresol yield	0.418	0.480	0.328	0.468
	S99 w/ CB4 HNO3 and explicit toluene w/ CB cresol yield	0.437	0.495	0.398	0.480
	CB-IV	0.344	0.404	0.158	0.398
	CB05	0.326	0.384	0.159	0.377
	Experiment	0.458	0.460	0.157	0.545
(Experimental-Model)/Experimental	SAPRC99	-10.48%	-35.34%	-116.28%	-3.08%
	S99 w/ CB4 HNO_3	-5.24%	-27.94%	-35.50%	4.07%
	S99 explicit toluene	-8.73%	-32.29%	-172.26%	-2.16%
	S99 explicit toluene w/ CB cresol yield	8.73%	-4.44%	-108.65%	14.16%
	S99 w/ CB4 HNO3 and explicit toluene w/ CB cresol yield	4.59%	-7.70%	-153.18%	11.96%
	CB-IV	24.89%	12.10%	-0.51%	27.00%
	CB05	28.82%	16.45%	-1.15%	30.85%
	MIR (g/g)	3.97	3.97	3.97	3.97
	MIR*VOC/NOx	46.1	54.8	23.4	46.3

Table G-6. Summary of aromatics sensitivity studies in UCR chamber.

	Experiment	EC271	EC273	EC340	EPA074B	EPA066B	EPA074A	OTC299A	TVA047	TVA071
	VOC (ppmC)	8.020	4.110	3.760	1.100	0.426	1.054	8.530	0.520	2.480
	NOx (ppm)	0.215	0.112	0.493	0.027	0.005	0.024	0.509	0.105	0.266
	VOC/NOx	37.302	36.696	7.627	40.741	85.200	43.917	16.758	4.952	9.323
Peak Ozone (ppm)	SAPRC99	0.390	0.306	0.281	0.191	0.069	0.130	0.734	0.069	0.246
	S99 w/ CB4 HNO_3	0.378	0.298	0.183	0.184	0.067	0.126	0.671	0.045	0.140
	S99 explicit toluene	0.393	0.306	0.374	0.196	0.070	0.133	0.744	0.091	0.331
	S99 explicit toluene w/ CB cresol yield	0.360	0.286	0.286	0.170	0.064	0.123	0.503	0.066	0.241
	S99 w/ CB4 HNO3 and explicit toluene w/ CB cresol yield	0.350	0.279	0.174	0.166	0.063	0.119	0.466	0.044	0.140
	CB-IV	0.323	0.250	0.259	0.078	0.036	0.054	0.356	0.032	0.157
	CB05	0.306	0.237	0.250	0.078	0.035	0.051	0.426	0.031	0.154
	Experiment	0.294	0.214	0.343	0.261	0.058	0.124	0.611	0.094	0.270
(Experimental-Model)/Experimental	SAPRC99	-32.52%	-43.13%	18.01%	26.92%	-19.76%	-5.17%	-20.07%	26.50%	8.97%
	S99 w/ CB4 HNO_3	-28.61%	-39.44%	46.79%	29.53%	-16.65%	-1.53%	-9.75%	52.24%	48.28%
	S99 explicit toluene	-33.81%	-43.08%	-9.00%	25.09%	-20.28%	-7.51%	-21.66%	2.99%	-22.73%
	S99 explicit toluene w/ CB cresol yield	-22.41%	-33.69%	16.55%	34.93%	-11.11%	0.40%	17.70%	29.38%	10.64%
	S99 explicit toluene w/ CB cresol yield and CB4 HNO_3	-19.01%	-30.28%	49.42%	36.50%	-8.34%	3.80%	23.75%	53.31%	48.09%
	CB-IV	-9.80%	-16.92%	24.56%	70.13%	37.35%	56.22%	41.81%	66.35%	41.68%
	CB05	-4.05%	-10.51%	27.13%	70.24%	40.29%	59.05%	30.39%	66.56%	42.86%
	MIR (g/g)	3.97	3.97	3.97	3.97	3.97	3.97	3.97	3.97	3.97
	MIR*VOC/NOx	148.09	145.68	30.28	161.74	338.24	174.35	66.53	19.66	37.01

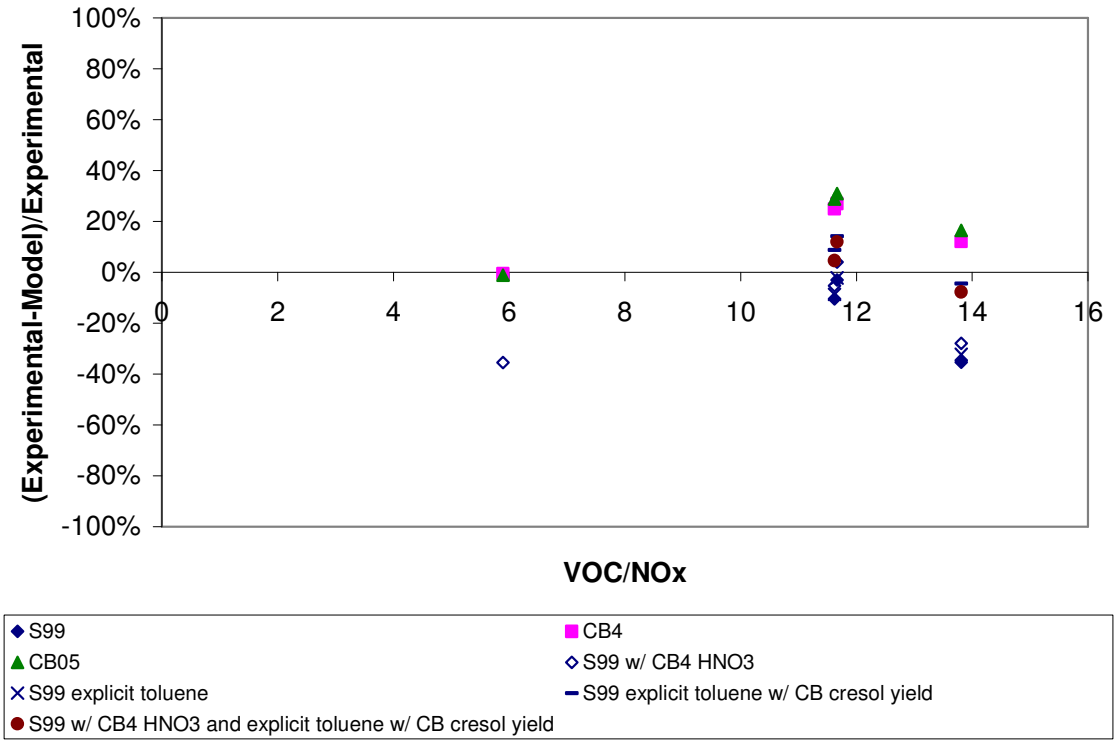

Figure G-25. Summary of aromatics sensitivity studies in UNC chamber.

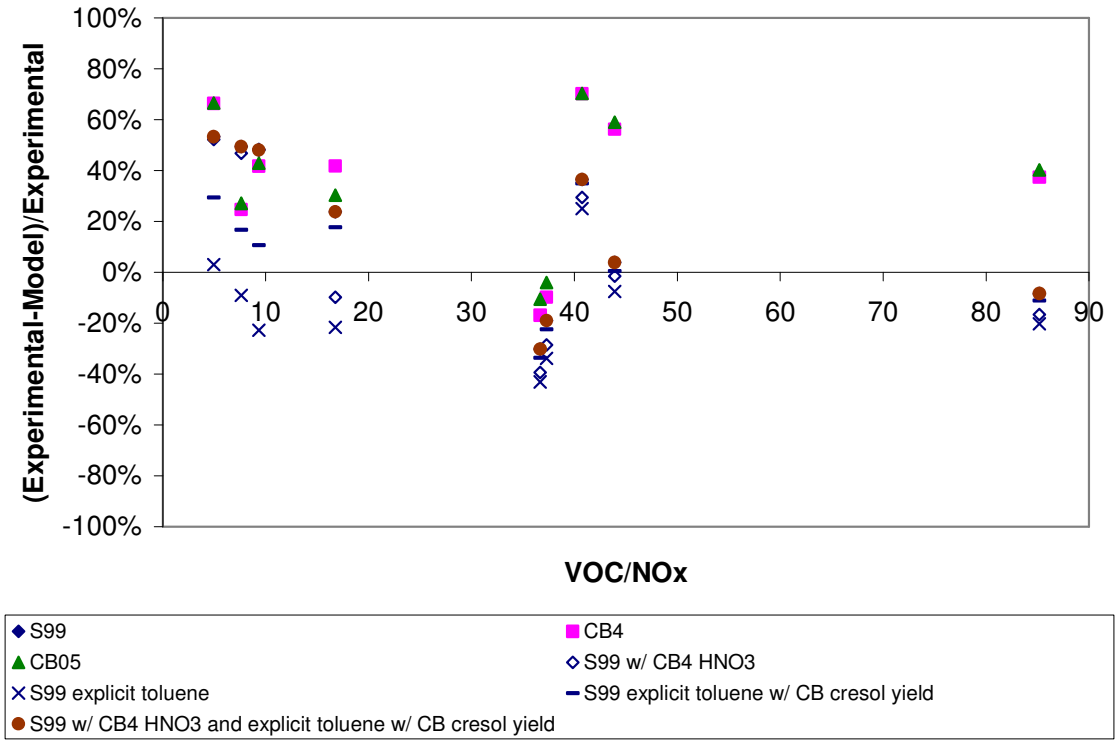

Figure G-26. Summary of aromatics sensitivity studies in UCR chamber.

G.3 COMPOSITION OF AROMATICS IN THE 8-COUNTY HOUSTON-GALVESTON AREA 2000 EMISSIONS INVENTORY

As shown in the following tables (Table G-7 to Table G-10), toluene is the dominant aromatics species across nearly all the source categories in the 8-county Houston-Galveston 2000 emissions inventory. In the mobile source category, toluene is emitted at 6.84 tons/day, comprising approximately 4.2 % of the total VOCs in this source category. In the area source category, toluene is emitted at 30.7 tons/day, which is about 20.7 % of the VOCs in the area source emissions. Toluene contributes 4.57 tons/day to the non-road mobile source emissions, which is 4.8 % of the VOCs emitted from this source category. Finally, in the point source emissions, toluene is the most

dominant species after benzene. It is at emitted at 4.48 %, comprising 3.0 % of the total VOCs from point source emissions.

Table G-7. Composition of aromatics in the mobile source category of the 8-county Houston-Galveston 2000 emissions inventory.

Compound Name	Sum of Species Emitted (tpd)	% by total VOCs
TOLUENE	6.840	4.2
M-XYLENE AND P-XYLENE	3.470	2.1
BENZENE	2.384	1.5
1,2,4-TRIMETHYLBENZENE	1.559	1.0
O-XYLENE	1.327	0.8
ETHYLBENZENE	1.138	0.7
M-ETHYLTOLUENE	1.124	0.7
1,3,5-TRIMETHYLBENZENE	0.604	0.4
P-ETHYLTOLUENE	0.478	0.3
NAPTHALENE	0.435	0.3
O-ETHYLTOLUENE	0.371	0.2
1,2,3-TRIMETHYLBENZENE	0.369	0.2
C7 ALKYLBENZENE	0.330	0.2
N-PROPYLBENZENE	0.301	0.2
C2 ALKYLNAPTHALENE	0.296	0.2
1,2-DIMETHYL-4-ETHYLBENZENE	0.294	0.2
1-METHYL-3-N-PROPYL	0.270	0.2
BUTYLBENZENE	0.243	0.2
1,4-DIETHYLBENZENE	0.243	0.2
INDANE	0.239	0.1
1-METHYL-2-PROPYLBENZENE	0.166	0.1
M-XYLENE AND P-XYLENE	0.163	0.1
1,4-DIMETHYL-2-ETHYLBENZENE	0.153	0.1
1,2,4,5-TETRAMETHYLBENZENE	0.142	0.1
CUMENE (ISOPROPYL BENZENE)	0.133	0.1
M-DIETHYLBENZENE	0.120	0.1
1,2,4-TRIMETHYLBENZENE	0.111	0.1
METHYLNAPHTHALENES	0.107	0.1
PENTYLBENZENE	0.105	0.1
1,2-dimethyl-3-ethylbenzene	0.083	0.1
NAPTHALENE	0.080	0.0
DI-ISO-PROPYLBENZENE	0.067	0.0
TOLUENE	0.067	0.0
1-METHYL-3-ISOPROPYLBENZENE	0.062	0.0
M-ETHYLTOLUENE	0.061	0.0
METHYLINDANS	0.055	0.0
O-XYLENE	0.055	0.0
TETRAMETHYLBENZENE	0.048	0.0
BENZENE	0.047	0.0
DIMETHYLNAPTHALENE	0.042	0.0
ETHYLBENZENE	0.042	0.0
P-ISOPROPYL TOLUENE	0.033	0.0
1,3,5-TRIMETHYLBENZENE	0.031	0.0
O-ETHYLTOLUENE	0.029	0.0
SEC-BUTYLBENZENE	0.029	0.0
ISOBUTYLBENZENE	0.029	0.0
trans-1-butyl-2-methylbenzene	0.027	0.0
1,2,3-TRIMETHYLBENZENE	0.025	0.0
1,3-DIMETHYL-2-ETHYLBENZENE	0.023	0.0
P-ETHYLTOLUENE	0.020	0.0
1,2,3,4-TETRAMETHYLBENZENE	0.018	0.0
ETHYLNAPHTALENE	0.017	0.0
N-PROPYLBENZENE	0.015	0.0
ETHYLDIMETHYLBENZENE	0.015	0.0
ACENAPHTHYLENE	0.013	0.0
BENZO(c)PHENANTHRENE	0.012	0.0
INDENE	0.011	0.0
PHENANTHRENE	0.009	0.0
INDANE	0.008	0.0
CUMENE (ISOPROPYL BENZENE)	0.005	0.0
SEC-BUTYLBENZENE	0.004	0.0
ISOBUTYLBENZENE	0.002	0.0
total Aromatics emission	**24.60**	-
total VOCs emission	**162.00**	-

Table G-8. Composition of aromatics in the area source category of the 8-county Houston-Galveston 2000 emissions inventory

Compound Name	Sum of Species Emitted (tpd)	% by total VOCs
TOLUENE	30.693	20.7
O-XYLENE	4.296	2.9
ISOMERS OF XYLENE	4.208	2.8
M-XYLENE AND P-XYLENE	2.935	2.0
TRIMETHYLBENZENE	1.394	0.9
BENZENE	1.225	0.8
ETHYLBENZENE	1.143	0.8
ISOMERS OF BUTYLBENZENE	0.919	0.6
ETHYLTOLUENE	0.684	0.5
METHYL NAPHTHALENES	0.632	0.4
C2 ALKYL INDAN	0.555	0.4
NAPTHALENE	0.518	0.3
MINERAL SPIRITS	0.372	0.3
C5-ALKYLBENZENES	0.310	0.2
ISOMERS OF PROPYLBENZENE	0.303	0.2
ETHYLDIMETHYLBENZENE	0.234	0.2
2,2 DICHLORONITROANILINE	0.195	0.1
TETRAMETHYLBENZENE	0.194	0.1
N-PROPYLBENZENE	0.185	0.1
ISOMERS OF ETHYLTOLUENE	0.135	0.1
BUTYLISOPROPYLPHTHALATE	0.111	0.1
METHYLINDANS	0.100	0.1
DIBUTYL PHTHALATE	0.087	0.1
INDANE	0.083	0.1
DIMETHYLINDANS	0.080	0.1
ISOPROPYLBENZENE	0.071	0.0
C6-ALKYLBENZENE	0.021	0.0
C2-ALKYLNAPHTHALENE	0.019	0.0
DIHYDRONAPTHALENE	0.011	0.0
TRIMETHYLINDAN	0.011	0.0
CHLOROBENZENE	0.011	0.0
METHYLDECALINS	0.009	0.0
C10H12	0.008	0.0
ETHYLINDAN	0.008	0.0
DIMETHYLBENZYLALCOHOL	0.005	0.0
ANILINE	0.004	0.0
ISOMERS OF DIETHYLBENZENE	0.004	0.0
P-DICHLOROBENZENE	0.004	0.0
PHTHALIC ANHYDRIDE	0.004	0.0
M-XYLENE	0.003	0.0
NAPHTHA	0.002	0.0
BENZYL CHLORIDE	0.002	0.0
TERT-BUTYLBENZENE	0.002	0.0
O-DICHLOROBENZENE	0.002	0.0
P-XYLENE	0.002	0.0
CRESOL	0.002	0.0
DIISOPROPYL BENZENE	0.002	0.0
2-FURFURAL	0.002	0.0
CREOSOTE	0.002	0.0
DIMETHYLINDENE	0.002	0.0
METHYLDIHYDRONAPHTHALENE	0.002	0.0
LACTOL SPIRITS	0.002	0.0
ISOMERS OF C11H20	0.002	0.0
NITROBENZENE	0.002	0.0
DIHYDROXYNAPTHALENEDIONE	0.001	0.0
BUTYL BENZOATE	0.001	0.0
CARYOPHYLLENE	0.001	0.0
C7-C16 PARAFFINS	0.001	0.0
PHENYL ISOCYANATE	0.001	0.0
BIPHENYL	0.001	0.0
BENZOTHIAZOLE	0.000	0.0
BENZOIC ACID	0.000	0.0
DIMETHYL PHTHALATE	0.000	0.0
PHENANTHRENE	0.000	0.0
DIMETHYLETHYLBENZOIC ACID	0.000	0.0
1,3,5-TRIMETHYLBENZENE	0.000	0.0
4-METHYLANILINE	0.000	0.0
C3/C4/C5 ALKYLBENZENES	0.000	0.0
M-ETHYLTOLUENE	0.000	0.0
ACENAPHTHYLENE	0.000	0.0
DICHLOROBENZENES	0.000	0.0
1,2,4-TRIMETHYLBENZENE	0.000	0.0
ANTHRAQUINONE	0.000	0.0
BROMODINITROBENZENE	0.000	0.0
C10 AROMATIC	0.000	0.0
CHRYSENE	0.000	0.0
ETHYL-PHENYL-PHENYL-ETHANE	0.000	0.0
FLUORANTHENE	0.000	0.0
FLUORENE	0.000	0.0
PYRENE	0.000	0.0
total Aromatics emission	**51.82**	**-**
total VOCs emission	**148.00**	**-**

Table G-9. Composition of aromatics in the non-road mobile source category of the 8-county Houston-Galveston 2000 emissions inventory

Compound Name	Sum of Species Emitted (tpd)	% by total VOCs
TOLUENE	4.568	4.8
P-XYLENE	2.142	2.2
1,2,4-TRIMETHYLBENZENE	2.047	2.1
C10 AROMATIC	1.690	1.8
1,3,5-TRIMETHYLBENZENE	1.664	1.7
O-XYLENE	1.385	1.4
BENZENE	1.362	1.4
M-ETHYLTOLUENE	0.903	0.9
ETHYLBENZENE	0.705	0.7
1,2,3-TRIMETHYLBENZENE	0.578	0.6
1,2 DIETHYLBENZENE	0.521	0.5
M-DIETHYLBENZENE	0.516	0.5
INDANE	0.464	0.5
ISOBUTYLBENZENE	0.459	0.5
N-PROPYLBENZENE	0.426	0.4
1-METHYL-3-ISOPROPYLBENZENE	0.319	0.3
O-ETHYLTOLUENE	0.178	0.2
1-METHYL-3-PROPYLBENZENE	0.154	0.2
M-XYLENE	0.154	0.2
S-BUTYLBENZENE	0.093	0.1
BUTYL BENZENE	0.025	0.0
4-PHENYL-1-BUTENE	0.022	0.0
T-1-PHENYLBUTENE	0.019	0.0
NAPTHALENE	0.016	0.0
METHYL NAPHTHALENES	0.014	0.0
C7-C16 PARAFFINS	0.009	0.0
M-XYLENE AND P-XYLENE	0.008	0.0
PENTYL BENZENE	0.006	0.0
Total aromatics emission	**20.44**	**-**
total VOCs emission	**96.00**	**-**

Table G-10. Composition of aromatics in the point source category of the 8-county Houston-Galveston 2000 emissions inventory

Compound Name	Sum of species emitted (tpd)	% by total VOCs
BENZENE	4.479	3.0
TOLUENE	3.090	2.1
ISOMERS OF XYLENE	1.900	1.3
ETHYLBENZENE	0.990	0.7
CHLOROBENZENE	0.639	0.4
M-XYLENE	0.556	0.4
CUMENE (ISOPROPYL BENZENE)	0.489	0.3
P-XYLENE	0.418	0.3
O-XYLENE	0.404	0.3
P-DICHLOROBENZENE	0.343	0.2
TRIMETHYLBENZENE	0.261	0.2
1,2,4-TRIMETHYLBENZENE	0.235	0.2
NAPTHALENE	0.187	0.1
C10H12	0.155	0.1
M-XYLENE AND P-XYLENE	0.135	0.1
PHTHALIC ANHYDRIDE	0.123	0.1
2-FURFURAL	0.092	0.1
CREOSOTE	0.091	0.1
O-DICHLOROBENZENE	0.084	0.1
1,3,5-TRIMETHYLBENZENE	0.076	0.1
MINERAL SPIRITS	0.066	0.0
ISOMERS OF BUTYLBENZENE	0.062	0.0
ETHYLTOLUENE	0.061	0.0
NAPHTHA	0.039	0.0
C7-C16	0.039	0.0
ISOMERS OF DIETHYLBENZENE	0.038	0.0
ETHYLDIMETHYLBENZENE	0.035	0.0
ANILINE	0.034	0.0
BENZYLCHLORIDE	0.033	0.0
1,2,3-TRIMETHYLBENZENE	0.028	0.0
PYRIDINE	0.024	0.0
CRESOL	0.022	0.0
ISOMERS OF PROPYLBENZENE	0.021	0.0
NITROBENZENE	0.020	0.0
DIISOPROPYLBENZENE	0.019	0.0
ISOMERS OF ETHYLTOLUENE	0.017	0.0
O-ETHYLTOLUENE	0.017	0.0
METHYLDECALINS	0.014	0.0
TETRAMETHYLBENZENE	0.014	0.0
C5 ALKYLBENZENES	0.011	0.0
METHYLNAPHTHALENES	0.010	0.0
BENZOIC ACID	0.010	0.0
METHYLINDANS	0.009	0.0
LACTOL SPIRITS	0.009	0.0
N-PROPYLBENZENE	0.009	0.0
BIPHENYL	0.008	0.0
DIPHENYLETHANE	0.008	0.0
INDENE	0.006	0.0
BENZYL ALCOHOL	0.006	0.0
C2 ALKYLINDAN	0.006	0.0
1-METHYL-3-N-PROPYLBENZENE	0.006	0.0
1-METHYL-3-ISOPROPYLBENZENE	0.006	0.0
P-ISOPROPYL TOLUENE	0.005	0.0
DICHLOROBENZENES	0.005	0.0
BUTYLBENZOATE	0.005	0.0
INDANE	0.004	0.0
1-METHYL-2-ETHYLBENZENE	0.004	0.0
PHENYLISOCYANATE	0.004	0.0
M-ETHYLTOLUENE	0.004	0.0
BENZOYL CHLORIDE	0.004	0.0
C3/C4/C5 ALKYLBENZENES	0.004	0.0
DIMETHYLPHTHALATE	0.004	0.0
C10 AROMATIC	0.003	0.0
ISOMERS OF C11H20	0.002	0.0
DIMETHYLINDANS	0.002	0.0
T-BUTYLBENZENE	0.002	0.0
M-DICHLOROBENZENE	0.002	0.0
2,2-DICHLORONITROANILINE	0.002	0.0
THIOPHENE	0.002	0.0
BUTYLBENZENE	0.001	0.0
BUTYLISOPROPYLPHTHALATE	0.001	0.0
DIMETHYLBENZYLALCOHOL	0.001	0.0
PHENANTHRENE	0.001	0.0
DIBUTYLPHTHALATE	0.001	0.0
4-METHYLANILINE	0.001	0.0
TEREPHTHALIC ACID	0.001	0.0
C6 ALKYLBENZENE	0.000	0.0
C2 ALKYLNAPTHALENE	0.000	0.0
BENZOTHIAZOLE	0.000	0.0
DIHYDRONAPTHALENE	0.000	0.0
TRIMETHYLINDAN	0.000	0.0
ACENAPHTHYLENE	0.000	0.0
FURFURYL ALCOHOL	0.000	0.0
ETHYLINDAN	0.000	0.0
ANTHRAQUINONE	0.000	0.0
BROMODINITROBENZENE	0.000	0.0
CHRYSENE	0.000	0.0
ETHYLPHENYLPHENYLETHANE	0.000	0.0
FLUORANTHENE	0.000	0.0
PYRENE	0.000	0.0
1-METHYL-3-ETHYLBENZENE	0.000	0.0
1,2-DIETHYLBENZENE	0.000	0.0
ISOBUTYLBENZENE	0.000	0.0
M-DIETHYLBENZENE	0.000	0.0
PENTYLBENZENE	0.000	0.0
Total Aromatics Emission	**15.52**	-
Total VOCs Emission	**148.60**	-

References

Adelman, Z. E. (1999). A *reevaluation of the carbon bond-IV photochemical mechan*ism. Master's Thesis, Department of Environmental Engineering, University of North Carolina at Chapel-Hill, NC.

Byun, D. W. (2002, October). *A study of photochemical processes of the Houston-Galveston metropolitan airshed with EPA CMAQ 2002*. Paper presented at the Model-3 User's Workshop, EPA, Research Triangle Park, NC.

Calvert, J.G., R. Atkinson, K.H. Becker, R.M. Kamens, J.H. Seinfeld, T.J. Wallington, and G. Yarwood, (2002), *The Mechanisms of Atmospheric Oxidation of Aromatic Hydrocarbons*, Oxford University Press, 556 pages.

Carter, W. P. L. (1990). A detailed mechanism for the gas-phase atmospheric reactions of organic compounds. *Atmospheric Environment*, 24A, 481-518.

Carter, W. P. L. (1995). Computer modeling of environmental chamber measurements of maximum incremental reactivities of Volatile Organic Compounds. *Atmospheric Environment*, 29, 2513-2517.

Carter, W. P. L. (1996). Condensed atmospheric photooxidation mechanism for isoprene. *Atmospheric Environment*, 30, 4275-4290.

Carter, W. P. L. (1994). Development of ozone reactivity scales for Volatile Organic Compounds. *Journal of Air* and *Waste Management Association*, 44, 881-899.

Carter, W. P. L. (2007, May). *Documentation of the SAPRC-07 chemical mechanism and updated ozone reactivity scales.* Draft Final Report to the California Air Resources Board, Sacramento, CA.

Carter, W. P. L. (2000). *Documentation of the SAPRC-99 chemical mechanism for VOC reactivity assessment*. Air Pollution Research Center and College of Engineering, Center for Environmental Research and Technology, University of California at Riverside, CA.

Carter, W.P.L. (2004, May). *Evaluation of a gas-phase atmospheric reaction mechanism for low NOx conditions*. Final Report to California Air Resources Board Contract No. 01-305. Available at http://www.cert.ucr.edu/□carter/absts.htm#lnoxrpt.

Carter, W. P. L, Crocker, D. R., Fitz, D. R., Malkina, I. L., Bumiller, K., Sauer, C. G., Pisano, J. T., Bufalino, C., and Song, C. (2005). *A new environmental chamber for evaluation of gas-phase chemical mechanisms and secondary aerosol formation*. Atmospheric Environment, 39, 7768-7788.

Carter, W. P. L., Luo, D., and Malkina, I. L. (1997, November). *Environmental chamber studies for development of an updated photochemical mechanism for VOC reactivity assessment*. Report to the California Air Resources Board, Contract 92-345, Coordinating Research Council Project M-9, and National Renewable Energy Laboratory Contract ZF-2-12252-07.

Carter, W. P. L., Luo, D., Malkina, I. L., and Fitz, D. (1993). *The University of California, Riverside environmental chamber data base for evaluating oxidant mechanisms: Indoor chamber experiments through 1993, Volumes I and II*. Report to the Environmental Protection Agency, Office of Research and Development, Research Triangle Park, NC.

Daum, P., Meagher, J., Allen, D. T., Durrenberger, C. (2002, November). Accelerated Science Evaluation of ozone formation n the Houston-Galveston area. Available at <http://www.utexas.edu/research/ceer/texaqsarchive/accelerated.htm>.

Dechapanya, W. (2002, May). *Kinetic and physic models of Secondary Organic Aerosol formation and their application to Houston condition*. Ph.D. Dissertation, Department of Chemical Engineering, The University of Texas at Austin, TX.

Dodge, M. (1989). A comparison of three photochemical oxidant mechanisms. *Journal of Geophysical Research*, 95(D4), 5121–5136.

ENVIRON International Corporation. (2004). *Users Guide to the Comprehensive Air Quality Model with Extensions (CAMx) version 4.03*. Available at http://www.camx.com.

Faraji, M. (2004). *Comparison of chemical mechanisms used in air quality models in Houston*. Master's Thesis, Department of Civil and Environmental Engineering, University of Texas at Austin, Austin, Texas.

Faraji, M., Heo, G., Kimura, Y., McDonald-Buller, E., Allen, D. T., Yarwood, G., Whitten, G., and Carter, W. P. L. (2007, August) *Comparison of the Carbon Bond and SAPRC photochemical mechanisms*. Draft Final Report to the Texas Commission on Environmental Quality.

Gery, M. W., Whitten, G. Z., and Killus, J. P. (1989). A photochemical kinetics mechanism for urban and regional scale computer modeling. *Journal of Geophysical Research*, 20, 12,925-12,956.

Jeffries, H., Fox, D., and Kamens, R. (1975). *Outdoor smog chamber studies: Effects of hydrocarbon reduction on nitrogen dioxide*. Report to the U.S. Environmental Protection Agency, Office of Research and Development, Washington, D.C..

Jeffries, H. E. and Tonnesen, S. (1994). A comparison of two photochemical reaction mechanisms using mass balance and process analysis. *Atmospheric Environment*, 28, 2991-3003.

Jeffries, H.J., Voicu, I., and Sexton, K. (2002, December). *Experimental Tests of Reactivity and Re-Evaluation of the Carbon Bond Four Photochemical Reaction Mechanism*. Report to the U.S. Environmental Protection Agency, Process Modeling Research Branch, Office of Research and Development, Research Triangle Park, NC.

Killus, J.P. and G.Z. Whitten (1982) "A Mechanism Describing the Photochemical Oxidation of Toluene in Smog," *Atmospheric Environment*, Vol. 16, pp 1973-1982.

Killus, J. P. and Whitten, G. Z. (1990). Background reactivity in smog chambers. *The International Journal of Chemical Kinetics*, 22, 547-575.

Killus, J.P. and G.Z. Whitten (1983) Comments on "Photochemical reactivity and ozone formation in 1-olefin–nitrogen oxide–air systems" , *Environ. Sci. Technol.*, Vol. 17, pp 760-762.

Kleinman, L. I., Daum, P. H., Imre D., Lee Y., Nunnermacker, L. J., and Springston, S. R. (2002). Ozone production and hydrocarbon reactivity in 5 urban areas: A cause of high ozone concentration in Houston, 2002. *Geophysical Research Letters*, 30 (12), 1639-1642.

Luecken, D., Phillips, S., Jang, C., and Possiel, N. (2006, December). *Effects of using the CB05 vs. SAPRC99 vs. CB4 chemical mechanisms on model predictions*. Presented at the International Conference on Chemical Mechanisms, The University of California at Davis, CA.

Luecken, D. and Sarwar, G. (2006). *Effects of using the CB05 versus the CB4 chemical mechanism on model predictions*. U.S. Environmental Protection Agency, Research Triangle Park, NC.

McGaughey, G. R., Desai, N.R., Allen, D.T., Seila, R.L., Lonneman, W.A., Fraser, M.P., Harley, R.A., Ivy, J.M., and Price, J.H., 2004. Analysis of Motor Vehicle Emissions in a Houston Tunnel during the Texas Air Quality Study 2000. Atmospheric Environment 38, 3363-3372.

National Research Council. (1999). *Ozone-forming potential of reformulated gasoline*. Washington, DC: National Academy Press.

Paulson, S., Chung, M.Y., and Hasson, A.S. (1999). OH radical formation from the gas-phase reaction of ozone with terminal alkenes and the relationship between structure and mechanism. *The Journal of Physical Chemistry A*, 103, 8125-8138.

Ryerson, T. R., Trainer, M., Angevine, W. M., Brock, C. A., Dissly, R. W., Fehsenfeld, F. C., Frost, G. J., Goldan, P. D., Holloway, J. S., Hubler, G., Jakoubek, R. O., Kuster, W. C., Neuman, J. A., D.K. Nicks Jr., D. K., Parrish, D. D., Roberts, J. M., and Sueper, D.T. (2003). Effect of petrochemical industrial emissions of reactive alkenes and NOx on tropospheric ozone formation in Houston, Texas. Journal of *Geophysical Research*, 108, 4249.

Russell, M. M. (2003). *Predicting secondary organic aerosol formation rates and concentrations in southeast Texas*. Ph.D. Dissertation, Department of Civil Engineering, University of Texas at Austin, Austin, Texas. Available at <http://www.lib.utexas.edu/etd/d/2003/russellmm039/russellmm039.pdf#page=3> .

Sexton, K. and Jeffries, H. (1999, July). UNC chamber data and model simulations using Morpho. Report to the Environmental Protection Agency from the University of North Carolina at Chapel Hill, NC.

Simonaitis, R., Meagher, J. F., and Bailey, E. M (1996). Evaluation of the condensed carbon bond (CB-IV) mechanism against smog chamber data at low VOC and NOx concentrations. *Atmospheric Environment*, 31, 27-43.

TexAQSI. *The Texas Air Quality Study 2000*. The University of Texas at Austin. Accessed 3 February 2002. <http://www.utexas.edu/research/ceer/texaqs/>.

Whitten, G. Z. (1983). The chemistry of smog formation: A review of current knowledge. *Environmental International*, 9, 447-463.

Yarwood, G., Stoeckenius, T. E., Heiken, J. G., and Dunker, A. M. (2003). Modeling weekday/weekend ozone differences in the Los Angeles region for 1997. *Journal of Air and Waste Management Association*, 53, 864-875.

Yarwood, G. and Rao, S. (2005b). *Updates to the Carbon Bond chemical mechanism: CB05*. Report to the U.S Environmental Protection Agency, Research Triangle Park, NC.

Yarwood, G., Whitten, G. Z., and Rao, S. (2005a). *Updates to the Carbon Bond 4 photochemical mechanism*. ENVIRON International Corporation. Report to the Lake Michigan Air Directors Consortium. Available at <http://www.camx.com/publ/pdfs/CB05_Final_Report_120805.pdf>.

Zádor, J., Turányi, T., Wirtz, K., and Pilling, M.J. (2006). Measurement and investigation of chamber radical sources in the European Photoreactor (EUPHORE). *Journal of Atmospheric Chemistry*, 55, 147-166.

Vita

Maedeh Faraji was born on December 30, 1981, in Tehran, Iran to Marzieh Mirghasemi and Hassan Faraji. She attended Austin High School and obtained her diploma in 1998. She graduated from the University of Texas at Austin on August 2002 with a major in Civil Engineering. In August 2004, she obtained her M.S.E. in Environmental and Water Resources Engineering from the University of Texas at Austin. She completed a Ph.D. in Civil Engineering at the University of Texas at Austin on September 2007. Maedeh worked as a research assistant at the Center for Energy and Environmental Resources at the University of Texas at Austin from May 2000 until September 2007. She is currently working as a data analyst in the Air Quality division at the Texas Commission for Environmental Quality.

Permanent address: 10100 Burnet Road, Bldg 133 Austin, Texas 78758

This dissertation was typed by the author.